



UNIVERSITAT ROVIRA I VIRGILI

EXCITATION OF ORGANOCATALYTIC INTERMEDIATES AND APPLICATION IN NEW RADICAL PROCESSES

Matteo Balletti

ADVERTIMENT. L'accés als continguts d'aquesta tesi doctoral i la seva utilització ha de respectar els drets de la persona autora. Pot ser utilitzada per a consulta o estudi personal, així com en activitats o materials d'investigació i docència en els termes establerts a l'art. 32 del Text Refós de la Llei de Propietat Intel·lectual (RDL 1/1996). Per altres utilitzacions es requereix l'autorització prèvia i expressa de la persona autora. En qualsevol cas, en la utilització dels seus continguts caldrà indicar de forma clara el nom i cognoms de la persona autora i el títol de la tesi doctoral. No s'autoritza la seva reproducció o altres formes d'explotació efectuades amb finalitats de lucre ni la seva comunicació pública des d'un lloc aliè al servei TDX. Tampoc s'autoritza la presentació del seu contingut en una finestra o marc aliè a TDX (framing). Aquesta reserva de drets afecta tant als continguts de la tesi com als seus resums i índexs.

ADVERTENCIA. El acceso a los contenidos de esta tesis doctoral y su utilización debe respetar los derechos de la persona autora. Puede ser utilizada para consulta o estudio personal, así como en actividades o materiales de investigación y docencia en los términos establecidos en el art. 32 del Texto Refundido de la Ley de Propiedad Intelectual (RDL 1/1996). Para otros usos se requiere la autorización previa y expresa de la persona autora. En cualquier caso, en la utilización de sus contenidos se deberá indicar de forma clara el nombre y apellidos de la persona autora y el título de la tesis doctoral. No se autoriza su reproducción u otras formas de explotación efectuadas con fines lucrativos ni su comunicación pública desde un sitio ajeno al servicio TDR. Tampoco se autoriza la presentación de su contenido en una ventana o marco ajeno a TDR (framing). Esta reserva de derechos afecta tanto al contenido de la tesis como a sus resúmenes e índices.

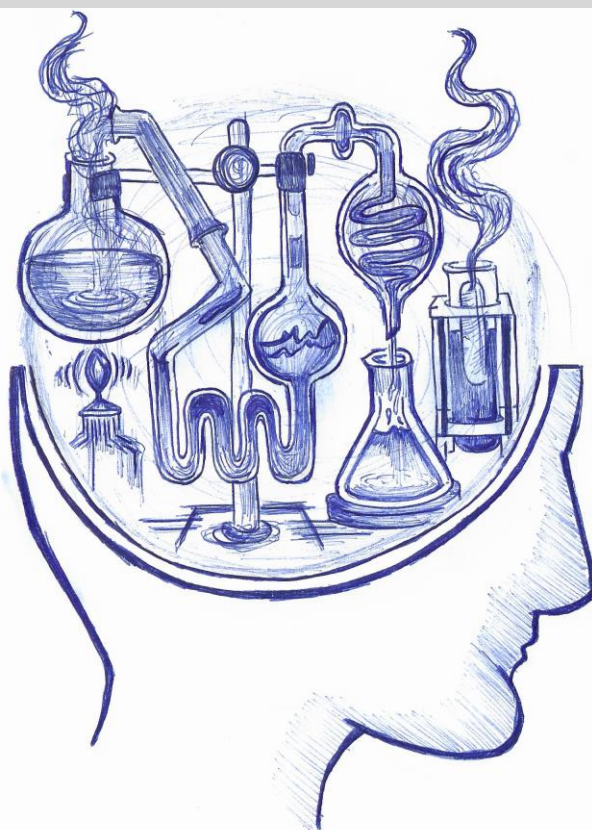
WARNING. Access to the contents of this doctoral thesis and its use must respect the rights of the author. It can be used for reference or private study, as well as research and learning activities or materials in the terms established by the 32nd article of the Spanish Consolidated Copyright Act (RDL 1/1996). Express and previous authorization of the author is required for any other uses. In any case, when using its content, full name of the author and title of the thesis must be clearly indicated. Reproduction or other forms of for profit use or public communication from outside TDX service is not allowed. Presentation of its content in a window or frame external to TDX (framing) is not authorized either. These rights affect both the content of the thesis and its abstracts and indexes.



UNIVERSITAT
ROVIRA i VIRGILI

Excitation of organocatalytic intermediates and application in new radical processes

Matteo Balletti



DOCTORAL THESIS
2022

UNIVERSITAT ROVIRA I VIRGILI

EXCITATION OF ORGANOCATALYTIC INTERMEDIATES AND APPLICATION IN NEW RADICAL PROCESSES

Matteo Balletti

UNIVERSITAT ROVIRA I VIRGILI

EXCITATION OF ORGANOCATALYTIC INTERMEDIATES AND APPLICATION IN NEW RADICAL PROCESSES

Matteo Balletti

Matteo Balletti

**Excitation of organocatalytic
intermediates and application in
new radical processes**

Doctoral Thesis

Supervised by Prof. Paolo Melchiorre

ICIQ – Institut Català d'Investigació Química



UNIVERSITAT
ROVIRA I VIRGILI



Tarragona

2022

UNIVERSITAT ROVIRA I VIRGILI

EXCITATION OF ORGANOCATALYTIC INTERMEDIATES AND APPLICATION IN NEW RADICAL PROCESSES

Matteo Balletti



UNIVERSITAT
ROVIRA i VIRGILI



Prof. Paolo Melchiorre, ICREA Research Professor & ICIQ Group Leader

I STATE that the present study, entitled “Excitation of organocatalytic intermediates and application in new radical processes”, presented by Matteo Balletti for the award of the degree of Doctor, has been carried out under my supervision at the Institut Català d’Investigació Química (ICIQ).

Tarragona, August 29th 2022

Doctoral Thesis Supervisor

Prof. Paolo Melchiorre

UNIVERSITAT ROVIRA I VIRGILI

EXCITATION OF ORGANOCATALYTIC INTERMEDIATES AND APPLICATION IN NEW RADICAL PROCESSES

Matteo Balletti

Acknowledgments

First and foremost, I would like to express my gratitude to *Prof. Paolo Melchiorre*, for giving me the opportunity to be part of his research group, for his support and for guiding me through this process of self-growth as a scientist and as a person.

I would like to thank all the members of the group for being such amazing people with who I shared amazing moments. All the people in the group helped me during my growth and thought me a lot and I will always be grateful for that. I would like to express a special thanks to *Daniele Mazzarella*, former PhD student of the group, for the amazing mentorship. I am also grateful to *Will Hartley* and *Martin Berger*, two amazing chemists which helped many times with precious suggestions and corrections. A special thanks goes to *Davide Spinnato* for the amazing and unforgettable moments passed together in the lab and outside of the lab. My gratitude goes also to *Andrea*, *Chiara* and *Julian* for the happiness and the suffering shared during these 3 years and for being amazing friends. Thanks to *Elena*, for the incredible run sessions and for designing my thesis cover image. Thanks to *Enrico* and *Tommy* for being such good project coworkers during their visiting periods.

I would also like to thank *Julia*, for the moments spent together and for being such a beautiful and lovely person while teaching me how to improve myself day by day.

I am also grateful to *Núria Planella*, for the administrative support. I thank the research support units at ICIQ, in particular I am indebted to the NMR-staff, the photophysical unit, the spectroscopy unit and the chromatography unit.

The final and most important thanks goes to my parents *Patrizia* and *Marcello* for being always by my side and giving me the strength in the darkest moments of the PhD. In the same way part of my success was due to my lifetime friends in Bologna, which as well, always stood by my side and helped me in so many moments.

I would also like to acknowledge the financial support from the Institute of Chemical Research of Catalonia (ICIQ), the Agencia Estatal de Investigación (PID2019-106278GB-I00) and the MCIN/AEI/10.13039/501100011033 (CEX2019-000925-S).



UNIVERSITAT ROVIRA I VIRGILI

EXCITATION OF ORGANOCATALYTIC INTERMEDIATES AND APPLICATION IN NEW RADICAL PROCESSES

Matteo Balletti

List of publications

Some of the results presented in this thesis have been published:

- de Pedro Beato, E.; Mazzarella, D.; Balletti, M.; Melchiorre, P. Photochemical Generation of Acyl and Carbamoyl Radicals Using a Nucleophilic Organic Catalyst: Applications and Mechanism Thereof. *Chem. Sci.* **2020**, *11*, 6312–6324.
- Balletti, M.; Marcantonio, E.; Melchiorre, P. “Photochemical organocatalytic enantioselective radical γ -functionalization of α -branched enals” *Chem. Commun.* **2022**, *58*, 6072–6075.

UNIVERSITAT ROVIRA I VIRGILI

EXCITATION OF ORGANOCATALYTIC INTERMEDIATES AND APPLICATION IN NEW RADICAL PROCESSES

Matteo Balletti

List of abbreviations

The abbreviations and acronyms used in my doctoral thesis are based on the recommendations of the ACS “guidelines for authors” and they can be found at <https://www.cas.org/support/documentation/references/cas-standard-abbreviations#listinga>.

*“Until you make the subconscious conscious,
it will direct your life and you will call it fate”*

C. G. Jung

UNIVERSITAT ROVIRA I VIRGILI

EXCITATION OF ORGANOCATALYTIC INTERMEDIATES AND APPLICATION IN NEW RADICAL PROCESSES

Matteo Balletti

Table of Contents

1. General Overview	1
1.1. Radical chemistry: new light on an established knowledge	1
1.2. Excitation of organocatalytic intermediates	6
1.2.1. Vinylogous radical chemistry	8
1.3. Excitation of dithiocarbamates intermediates	9
1.4. General Objectives and Summary	11
1.4.1. Photochemical generation of acyl and carbamoyl radicals using a nucleophilic organic catalyst	12
1.4.2. Photochemical organocatalytic enantioselective radical γ -functionalization of α -branched enals	13
1.4.3. Asymmetric γ -perfluoroalkylation of α -branched enals driven by the photoactivity of dienamine-based EDA complex	13
2. Photochemical generation of acyl and carbamoyl radicals using a nucleophilic organic catalyst	15
2.1. Introduction: early radical chemistry	15
2.2. Improving radical generation: thiocarbonyl compounds	16
2.3. Refining radical generation: photocatalytic manifolds	18
2.4. Shifting dithiocarbamates to a photocatalytic manifold	20
2.5. Strategies for the generation of carbamoyl radicals	22
2.5.1. Strategies based on the use of stoichiometric reagents	23
2.5.2. Catalytic strategies for the generation of carbamoyl radicals.....	27
2.6. Target of the project	30
2.6.1. Design Plan	30
2.7. Results and discussion	31
2.7.1. Reaction optimization.....	31
2.7.2. Reaction scope	35
2.7.3. Generation of acyl radicals	36
2.8. Mechanistic investigations	42
2.8.1. Generation and photolysis of the catalytic xanthyl anhydride.....	42
2.8.2. Fate and behavior of the xanthyl radical.....	45
2.8.3. Radical trap and ensuing process.....	50
2.8.4. Overall catalytic cycle	51
2.9. Conclusions	52
2.10. Experimental section	53
2.10.1. General information	53
2.10.2. Substrate synthesis	54

2.10.3.	Optimization studies.....	63
2.10.4.	General procedures and characterization of products	63
2.10.5.	Scale up reaction.....	84
2.10.6.	Mechanistic studies.....	94
3.	Photochemical organocatalytic enantioselective radical γ- functionalization of α-branched enal	118
3.1.	Introduction	118
3.2.	Enamine catalysis	121
3.3.	The principle of vinylogy.....	123
3.3.1.	General concept.....	123
3.3.2.	Vinylogous enamine catalysis	125
3.4.	Enamines as radical traps.....	126
3.5.	Target of the project	134
3.5.1.	Design plan.....	135
3.6.	Results and discussion.....	135
3.6.1.	Reaction optimization.....	135
3.6.2.	Reaction scope & product functionalization	140
3.6.3.	Mechanistic proposal	144
3.7.	Conclusions	146
3.8.	Experimental section	146
3.8.1.	General informations	146
3.8.2.	Substrate synthesis	148
3.8.3.	Catalyst synthesis.....	153
3.8.4.	General procedures and characterization of products	156
3.8.5.	Scaled up reaction	173
3.8.6.	Product derivatization	174
3.8.7.	Determination of the absolute configuration.....	178
3.8.8.	Failed substrates	179
4.	Asymmetric γ-perfluoroalkylation of α-branched enals driven by the photoactivity of dienamine-based EDA complex	180
4.1.	Introduction	181
4.2.	Electron donor-acceptor complexes	185
4.2.1.	General concepts	185
4.2.2.	Organocatalytic intermediates as EDA partners	188
4.3.	Enantioselective perfluoroalkylation of carbonyls	189
4.3.1.	Early approaches: chiral auxiliaries	190
4.3.2.	Improved routes: organocatalysis	191
4.4.	Target of the project	192
4.5.	Result and discussion	193

4.5.1.	Reaction optimization.....	193
4.5.2.	Reaction scope	197
4.5.3.	Mechanistic considerations	201
4.6.	Conclusions	202
4.7.	Experimental section	202
4.7.1.	General informations	202
4.7.2.	Experimental setup	203
4.7.3.	Substrate synthesis	205
4.7.4.	Catalyst synthesis	207
4.7.5.	General procedures	211
4.7.6.	Characterization of products.....	212
4.7.7.	Quantum yield measurements	222
4.7.8.	Crystal structure	225
4.7.9.	NMR traces	227
4.7.10.	UPC ² traces	267
5.	General conclusions	284

UNIVERSITAT ROVIRA I VIRGILI

EXCITATION OF ORGANOCATALYTIC INTERMEDIATES AND APPLICATION IN NEW RADICAL PROCESSES

Matteo Balletti

Chapter I

General Overview

The work developed in this thesis exploits the excitation of organocatalytic intermediates to provide novel strategies for the generation of radicals under mild conditions. The concept of photoexcitation led to the development of radical-based methodologies for asymmetric C-C bond formation.

1.1 Radical chemistry: new light on an established knowledge

Radicals contain an unpaired electron in their valence shell. The highly reactive, often transient nature of radicals is the reason why their chemistry was historically considered as “messy, unpredictable, [...] and essentially mysterious”.¹ For the same reason, radical reactivity has always taken a backseat respect to polar chemistry. Notwithstanding this, along the centuries chemists had learnt how to generate and control radicals to solve problems of paramount importance. Nowadays, we leverage on radical chemistry not only for the synthesis and discovery of pharmacologically active molecules,² but also in polymer manufacture.³

Within almost two centuries from the discovery of the first radical process,⁴ the methodologies we rely on for the generation of radicals evolved tremendously. The history of radical-based methodologies can be retraced by highlighting two main approaches to generate open-shell intermediates: 1) redox strategies (Figure 1.1a) and 2) homolytic strategies (Figure 1.1b). Redox strategies are based on the injection or removal of an electron from substrate **S** by means of reductants⁵ or oxidants,⁶ respectively. This *single-electron transfer* (SET) process leads to the formation of a charged radical species. The latter, when adorned with a suitable

¹ Walling, C. Some properties of radical reactions important in synthesis. *Tetrahedron* **1985**, *41*, 3887–3900.

² (a) Moir, M., Danon, J. J., Reekie, T. A. & Kassiou, An overview of late-stage functionalization in today's drug discovery. *Expert Opin. Drug Discov.* **2019**, *14*, 1137–1149. (b) Smith, J. M., Dixon, J. A., deGruyter, J. N. & Baran, P. S. Alkyl sulfonates: radical precursors enabling drug discovery. *J. Med. Chem.* **2019**, *62*, 2256–2264.

³ Matyjaszewski, K.; Xia, J. Atom Transfer Radical Polymerization. *Chem. Rev.* **2001**, *101*, 2921–2990. (b) Destarac, M. Controlled Radical Polymerization: Industrial Stakes, Obstacles and Achievements. *Macromol. React. Eng.* **2010**, *4*, 165–179.

⁴ Kolbe, H. Zersetzung der Valeriansäure durch den elektrischen Strom. *Ann. Chem. Pharm.* **1848**, *64*, 339–341.

⁵ (a) Molander, G. A. Reductions with Samarium(II) Iodide *Org. React.* **1994**, *46*, 211–256. (b) Szostack, M.; Spain, M.; Procter, D. Recent advances in the chemoselective reduction of functional groups mediated by samarium(II) iodide: a single electron transfer approach. *Chem. Soc. Rev.* **2013**, *42*, 9155–9183. (c) RajanBabu, T. V.; Nugent, W. A. Selective Generation of Free Radicals from Epoxides Using a Transition-Metal Radical. A Powerful New Tool for Organic Synthesis. *J. Am. Chem. Soc.* **1994**, *116*, 986–997.

⁶ (a) Nair, V.; Deepthi, A.; Cerium(IV) Ammonium Nitrate. A Versatile Single-Electron Oxidant. *Chem. Rev.* **2007**, *107*, 1862–1891. (b) Minisci, F. Free-radical additions to olefins in the presence of redox systems. *Acc. Chem. Res.* **1975**, *8*, 165–171.

leaving group (**Y**), evolves in the corresponding radical **I**, which can be used in further transformations (Figure 1.1a). Alternatively, such SET process can be achieved by electrochemical means. Whereas particularly intriguing, the electrochemical strategy reached its full maturity only in the last decade.⁷

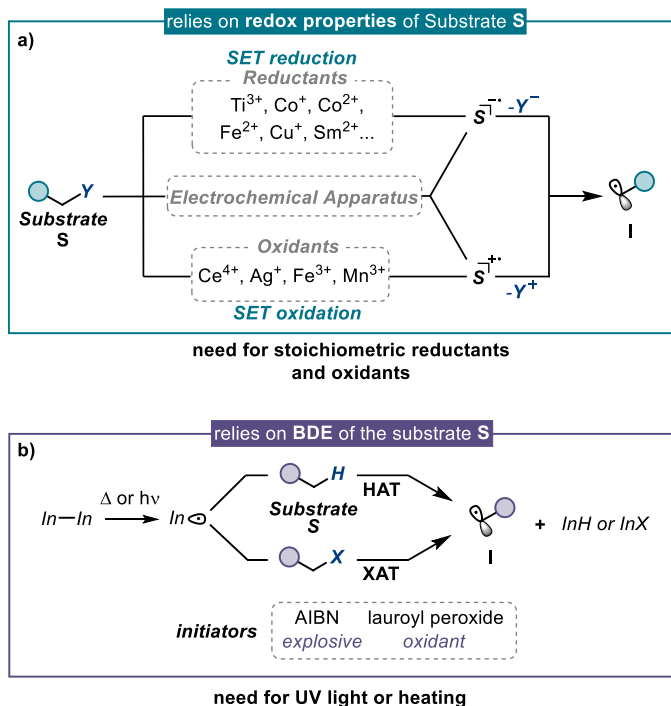


Figure 1.1. Classical strategies for the generation of radicals.

Another approach for the generation of radicals exploits the homolytic scission of a covalent bond (Figure 1.1b). Historically, this strategy relies on an initiator (*In-In*), a compound which contains one or several weak bonds with a bond-dissociation energy (BDE) in the range of 30-50 kcal/mol. Peroxides and diazo-compounds are the most representative examples of initiators.⁸ By absorbing energy in the form of heat or high-energy light, the weak bond can be homolitically cleaved generating a neutral radical intermediate $In\cdot$. The latter can further react with a substrate by hydrogen-atom transfer (HAT) or halogen-atom transfer (XAT) generating a radical **I** from a target substrate **S**.

⁷ (a) Yan, M.; Kawamata, Y.; Baran, P. S.; *Synthetic Organic Electrochemical Methods Since 2000: On the Verge of a Renaissance* *Chem. Rev.* **2017**, *117*, 13230–13319. (b) Horn, E. J.; Rosen, B. R.; Baran, P. S. *Synthetic Organic Electrochemistry: An Enabling and Innately Sustainable Method.* *ACS Cent. Sci.*, **2016**, *2*, 302–308. (c) Yan, M.; Kawamata, Y.; Baran, P. S. *Synthetic Organic Electrochemistry: Calling All Engineers* *Angew. Chem. Int. Ed.* **2017**, *57*, 4149–4155.

⁸ (a) Luo, Y., R. *Handbook of Bond Dissociation Energies in Organic Compounds*, CRC press, **2002**. (b) Lalevée, J.; Fouassier, J. P. Overview of Radical Initiation. In *Encyclopedia of Radicals in Chemistry, Biology and Materials*. Studer, A., Chatgililoglou, C., (Eds.); Wiley: New York, NY, USA, **2012**; Volume 1, chapter 2.

During the 20th century, radical chemistry showed promising potential and orthogonal reactivity respect to the classical polar pathways. However, the use of (super)stoichiometric amounts of redox agents, initiators, and drastic conditions (high temperatures, UV light) needed for their generation, dramatically affected the applicability of radicals for the development of new methodologies. For instance, the development of asymmetric radical reactions, especially in the seminal stage, struggled to flourish, mainly because of the drastic conditions (e.g. high temperature) affecting stereocontrol.⁹

During the last decade, the development of effective and mild radical generation strategies has experienced an increasing growth.¹⁰ This is mainly due to the outburst of *photoredox catalysis*, which shifted the paradigm by providing access to radical intermediates under mild conditions through a catalytic manifold.¹¹ A photocatalyst (**PC**) is a compound (transition-metal complexes¹² or organic dyes¹³) which can absorb visible-light irradiation to reach an excited state. Upon excitation, an electron from the higher occupied molecular orbital (HOMO) is promoted to the lower unoccupied molecular orbital (LUMO) (Figure 1.2a). In this new electronic configuration, the excited state **PC*** possesses new photophysical properties than in the ground state. Different events can take place to dissipate the energy surplus. Above them, the *photoinduced-electron transfer* (PET) process is the most exploited to generate radicals. The excitation of a photocatalyst enhances its redox properties making it both a better reductant and oxidant than in its ground state.¹⁴ This is possible because adding or removing an electron from such a half-filled electronic configuration becomes more favorable (Figure 1.2b). This visible-light mediated SET event has been used to effectively replace stoichiometric redox agents (Figure 1.1a) for the generation of radicals. Upon light absorption, **PC*** can enter an oxidative quenching cycle (Figure 1.2c), where **PC*** donates an electron to a suitable electron acceptor (**A**) via an SET. This event produces the radical anion **A^{•-}** and the oxidized form to the photocatalyst (**PC⁺**). A second SET can take place, this time

⁹ (a) Sibi, M. P.; Manyem, S.; Zimmerman, J. Enantioselective Radical Processes. *Chem. Rev.* **2003**, *103*, 3263–3296. (b) Zimmerman, J., Sibi, M. P. Enantioselective Radical Reactions. In *Radicals in Synthesis I. Topics in Current Chemistry*. Gansäuer, A. (Eds.) Springer: Berlin, Heidelberg, 2006

¹⁰ Studer, A.; Curran, D. P., Catalysis of Radical Reactions: A Radical Chemistry Perspective. *Angew. Chem. Int. Ed.* **2016**, *55*, 58-102.

¹¹ (a) Shaw, M. H.; Twilton, J.; MacMillan, D. W. C., Photoredox Catalysis in Organic Chemistry. *J. Org. Chem.* **2016**, *81*, 6898-6926. (b) Matsui, J. K.; Lang, S. B.; Heitz, D. R.; Molander, G. A., Photoredox-Mediated Routes to Radicals: The Value of Catalytic Radical Generation in Synthetic Methods Development. *ACS Catal.* **2017**, *7*, 2563-2575.

¹² (a) Prier, C. K.; Rankic, A. D.; MacMillan, D. W. C. Visible Light Photoredox Catalysis with Transition Metal Complexes: Applications in Organic Synthesis *Chem. Rev.* **2013**, *113*, 5322–5363. (b) Larsen, C. B.; Wegner, O. S. Photoredox Catalysis with Metal Complexes Made from Earth-Abundant Elements. *Chem. Eur. J.* **2017**, *24*, 2039-2058.

¹³ Nicewicz, D. A.; Nguyen, T. M. Recent Applications of Organic Dyes as Photoredox Catalysts in Organic Synthesis, *ACS Catal.* **2014**, *4*, 355-360.

¹⁴ Photochemistry and Photophysics: Concepts, Research, Applications. Photochemistry and Photophysics. Concepts, Research, Applications. **2014** Balzani, V.; Ceroni, P.; Juris, A. (Eds.) Wiley-VCH, Weinheim

between PC^{*+} and an electron donor (D), regenerating the PC and closing the photoredox catalytic cycle. Alternatively, the process may proceed through a reductive quenching cycle (Figure 1.2c), where PC^* firstly accepts one electron from a donor, affording the radical cation D^{*+} and a reduced form of photocatalyst ($PC^{\cdot-}$). Then, the latter reduces an acceptor (A) to regenerate the ground-state PC to close the cycle. All these redox events trigger the generation of radicals under very mild conditions and using weak visible light.

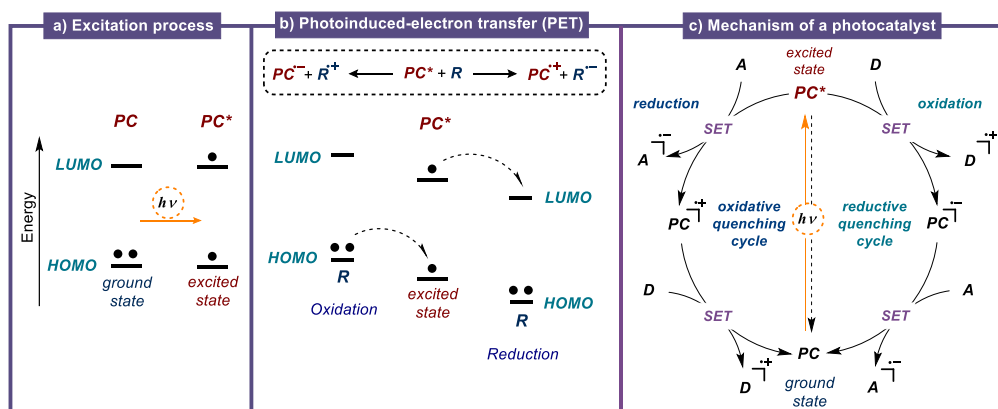


Figure 1.2. a) Excitation of a photocatalyst (PC) results in a different electronic configuration b) SET from the excited state PC^* to a reagent R becomes exergonic. c) General mechanism of action of a photocatalyst.

Whereas photoredox processes already sparked along the 20th century,¹⁵ it was thanks to the pioneering work of MacMillan and coworkers in 2008 that photocatalysis reached its maturity.¹⁶ The study highlighted how, through the aid of a photocatalyst, visible-light could be efficiently converted in a redox potential to generate radicals. The mild reaction conditions offered by the use of a photocatalyst allowed for the development of the elusive enantioselective α -alkylation of aldehydes with alkyl halides (Figure 1.3). Specifically, MacMillan and coworkers exploited a dual catalytic strategy which comprised an organocatalyst and a photocatalyst. Condensation of aldehyde **1** with the chiral aminocatalyst **3** delivered a catalytic amount of enamine **5**. Subsequent excitation of $[Ru(bpy)_3]^{2+}$ with a compact fluorescent lamp (CFL) generated the excited-state $^*[Ru(bpy)_3]^{2+}$, which engaged in an SET oxidation event with a sacrificial amount of enamine **5** (reductive quenching). This process led to the formation of $[Ru(bpy)_3]^+$ that behaved as a strong reductant. Subsequent SET with alkyl bromide **2** generated the radical **II** by reductive fragmentation. Trapping of

¹⁵ (a) Hedstrand, D.M.; Kruijzinga, W.H.; Kellogg, R.M. Light induced and dye accelerated reductions of phenacyl onium salts by 1,4-dihydropyridines *Tetrahedron Lett.*, **1978**, *19*, 1255 – 1258. (b) Cano-Yelo, H.; Deronzier, A. Photocatalysis of the Pschorr reaction by tris-(2,2'-bipyridyl)ruthenium(II) in the phenanthrene series. *J. Chem. Soc. Perkin Trans. 2*, **1984**, 1093-1098.

¹⁶ Nicewicz, D. A., MacMillan, D. W. C. Merging Photoredox Catalysis with Organocatalysis: the Direct Asymmetric Alkylation of Aldehydes. *Science* **2008**, *322*, 77-80.

the radical by the nucleophilic chiral enamine **5** allowed the formation of the C-C bond in a stereoselective fashion. The ensuing α -amino radical **III** underwent oxidation by the photoexcited Ru(II) complex forming the iminium ion **IV**, which was then hydrolyzed to afford the enantioenriched product **4** while regenerating **3**.

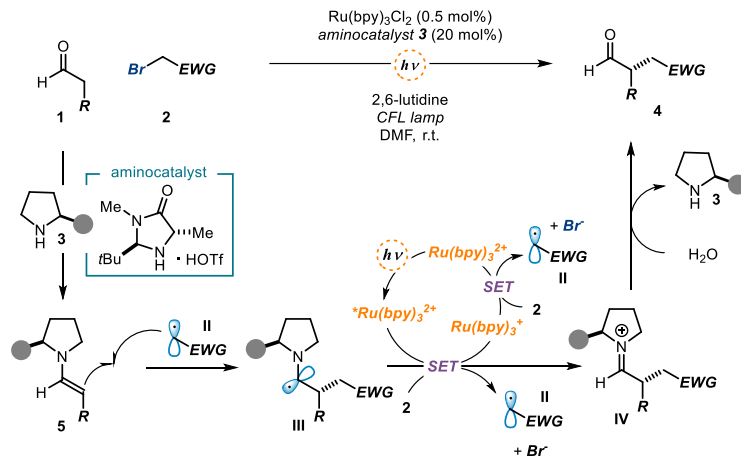


Figure 1.3. The pioneering work of MacMillan merging photoredox and organocatalysis: the enantioselective α -alkylation of aldehydes with activated alkyl bromides.

Overall, the photoredox catalyst converted visible-light energy into chemical energy available for redox manipulations. This work was eye-opening for several reasons. For the first time a general blueprint for the catalytic generation of radicals under mild reaction conditions was presented and rationalized. Furthermore, the group elegantly exemplified the possibility to couple radical processes with asymmetric organocatalysis, achieving exquisite levels of enantiocontrol. This work inspired a whole generation of chemists to explore deeply the potential offered by photoredox catalysis as a general catalytic platform for the generation of open-shell intermediates.

Nowadays, photocatalysis reached a complete maturity enabling access to a chemical space that was previously unimaginable.¹⁷ The mild conditions offered by visible light in the generation of radicals fostered the efficient coupling of photocatalysis with already developed catalytic systems (including organocatalysis, metal catalysis, and Lewis acid activation), showing remarkable results also in asymmetric synthesis.¹⁸

¹⁷ (a) Pitre, S. P.; Overman, L. E. Strategic Use of Visible-Light Photoredox Catalysis in Natural Product Synthesis *Chem. Rev.* **2022**, *122*, 1717-1751. (b) Marzo, L.; Pagire, S. K.; Reiser, O.; König, B. Visible-Light Photocatalysis: Does It Make a Difference in Organic Synthesis? *Angew. Chem. Int. Ed.* **2018**, *57*, 10034-10072.

¹⁸ (a) Skubi, K. L.; Blum, T. R.; Yoon, T. P. Dual Catalysis Strategies in Photochemical Synthesis *Chem. Rev.* **2016**, *116*, 10035-10074. (b) Twilton, J.; Le, C.; Zhang, P.; Shaw, M. H.; Evans, R. W.; MacMillan, D. W. C. The merger of transition metal and photocatalysis. *Nat. Chem. Rev.* **2017**, *1*, 0052. (c) Silvi, M.;

However, the organic chemist toolbox is not restricted to the use of an external photocatalyst to generate radicals. The recent advances in light-mediated radical processes resulted in interesting findings about the photoactivity of reaction intermediates. Of particular interest is the excitation of organocatalytic intermediates as radical-generating platforms.¹⁹ Melchiorre and coworkers recently reported how some organocatalytic adducts can reach an electronically excited state under visible-light irradiation. Analogously to a photocatalyst, the excitation leads to the generation of open-shell species through SET events. During my doctoral thesis, I exploited the enhanced redox properties acquired by some organocatalytic intermediates upon light excitation to develop new radical-based methodologies for the construction of chiral molecules.

1.2 Excitation of organocatalytic intermediates

In 2013, Melchiorre and coworkers found that, upon mixing the organocatalytic enamine **5** with the electron-poor benzyl bromides **2**, the color of the solution changed from colorless to bright yellow (Figure 1.4).²⁰ This observation was rationalized by a new ground-state association, called electron donor-acceptor (EDA) complex (orange box in Figure 1.4).²¹ This complex possesses new molecular orbitals and can be therefore regarded as a different molecule with new photophysical properties than the two individual progenitors. The main peculiarity is the appearance of a charge transfer band at longer wavelength of absorption, which makes it possible to selectively excite EDA complexes using visible light (460 nm) in the presence of the starting materials. The excitation is followed by an SET event that generates a radical ion **VI**, which eventually evolves in the radical **II**. The latter can be trapped by the chiral organocatalytic enamine **5** to give the enantioenriched product **4**. In this way, the organocatalytic intermediate is not just acting as a radical trap, but it also involved in the radical generation (through EDA complex formation). This photo-organocatalytic dichotomy offered a powerful approach to develop stereocontrolled radical-based methodologies without any external photocatalyst. The mild reaction conditions and the presence of a chiral

Melchiorre, P. Enhancing the potential of enantioselective organocatalysis with light. *Nature* **2018**, *554*, 41-49.

¹⁹ Also organometallic intermediates have shown to be prone to excitation. For representative examples see: (a) Silvi, M. Sandford, C.; Aggarwal, V. K. Merging Photoredox with 1,2-Metallate Rearrangements: The Photochemical Alkylation of Vinyl Boronate Complexes. *J. Am. Chem. Soc.* **2017**, *139*, 5736–5739. (b) Parasram, M. Gevorgian, V. Visible light-induced transition metal-catalyzed transformations: beyond conventional photosensitizers. *Chem. Soc. Rev.* **2017**, *46*, 6227–6240. (c) Crisenza, G.E.M.; Faraone, A.; Gandolfo, E.; Mazzarella, D.; Melchiorre, P. Catalytic Asymmetric C-C cross-coupling enabled by the photoexcitation of an allyl-iridium complex *Nat. Chem.* **2021**, *13*, 575–580.

²⁰ Arceo, E.; Jurberg, I. D.; Álvarez-Fernández, A.; Melchiorre, P. Photochemical Activity of a Key Donor–Acceptor Complex Can Drive Stereoselective Catalytic α -alkylation of Aldehydes. *Nature Chem.* **2013**, *5*, 750–756.

²¹ (a) Crisenza, G. E. M.; Mazzarella, D.; Melchiorre, P., Synthetic Methods Driven by the Photoactivity of Electron Donor–Acceptor Complexes. *J. Am. Chem. Soc.* **2020**, *142*, 5461–5476. (b) Lima, C. G. S.; Lima, T. M.; Duarte, M.; Jurberg, I. D.; Paixao, M. W. Organic Synthesis Enabled by Light-Irradiation of EDA Complexes: Theoretical Background and Synthetic Applications. *ACS Catal.* **2016**, *6*, 1389–1407

aminocatalyst allows the transformation to proceed with high efficiency and enantioselectivity.

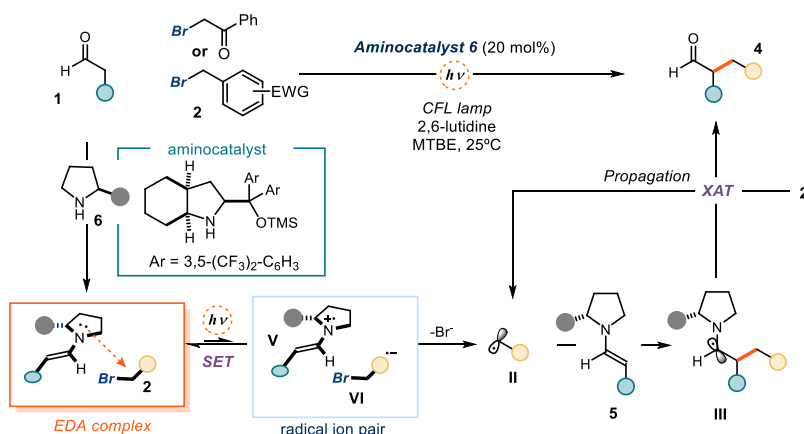


Figure 1.4. Photochemical stereoselective alkylation of aldehydes promoted by the photoactivity of enamine-based EDA complexes.

The EDA complex formation is strictly dependent on the physicochemical properties of the two partners, and therefore are not always formed. For example, when radical precursors different from **2** are employed, such association is not observed. Nevertheless, organocatalytic intermediates alone can be subjected to direct excitation processes. Our group also disclosed how, analogously to a photocatalyst, enamines **5** can be directly excited using a near UV light (390 nm, Figure 1.5).²² In the excited state, enamines behave as strong photoreductants (estimated $E_{\text{red}}^*(\text{VII}^+/\text{VII}^*) \sim -2.50$ V versus Ag/AgCl, NaCl sat.) and could therefore elicit the generation of radical **VI** upon reductive cleavage of bromomalonates **7**, which are not prone to EDA complex formation. Thanks to the chiral environment provided by the chiral aminocatalyst **8**, the C-C bond forming step proceeds with high degree of enantioselectivity. Overall, these photochemical manifolds, the EDA complex excitation and the direct excitation of organocatalytic intermediates, offer two powerful radical-generating strategies. The increasing knowledge in photo-mediated radical processes fostered the development of new stereocontrolled photocatalytic transformations previously unavailable using polar chemistry.²³ An interesting application is the radical functionalization of carbonyl substrates at remote positions by means of vinylogous enamines.

²² (a) Silvi, M.; Arceo, A.; Jurberg, I. D.; Cassani, C.; Melchiorre, P. Enantioselective Organocatalytic Alkylation of Aldehydes and Enals Driven by the Direct Photoexcitation of Enamines. *J. Am. Chem. Soc.* **2015**, *137*, 6120–6123. (b) Filippini, G.; Silvi, M.; Melchiorre, P. Enantioselective Formal α -Methylation and α -Benzoylation of Aldehydes by Means of Photo-organocatalysis *Angew. Chem. Int. Ed.* **2017**, *56*, 4447–4451.

²³ Silvi, M.; Melchiorre, P. Enhancing the potential of enantioselective organocatalysis with light. *Nature*, **2018**, *554*, 41–49.

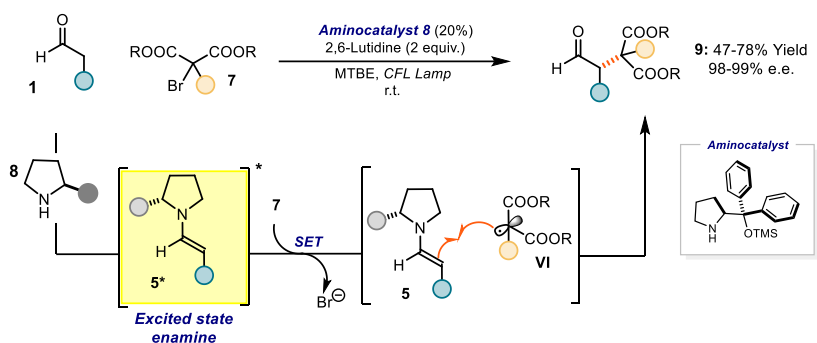


Figure 1.5. Photochemical stereoselective alkylation of aldehydes promoted by the direct excitation of enamines.

1.2.1 Vinylogous Radical Chemistry

During the first decade of the 21st century, enamine catalysis²⁴ was one of the most exploited method to functionalize carbonyls' α -positions using polar reactivity (Figure 1.6a). The recent advances in visible-light mediated processes greatly expanded the applications of enamine catalysis in radical chemistry. The methodologies for the asymmetric α -functionalization through enamine activation experienced a huge expansion after the advent of photoredox catalysis (Figure 1.6b).

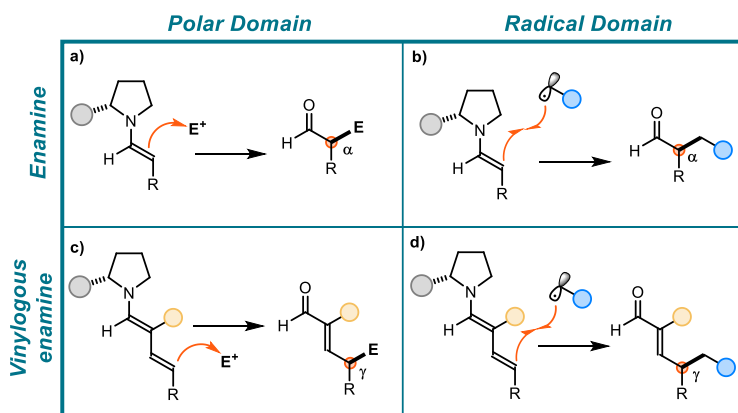


Figure 1.6. Functionalization of enamine intermediates through polar and radical chemistry.

In order to target stereocenters more remote from the catalyst's point of action, chemists became interested on vinylogous organocatalytic intermediates.²⁵ Already in 1935, Reynold

²⁴ a) Mukherjee, S.; Yang, J. H.; Hoffmann, S.; List, B. Asymmetric Enamine Catalysis. *Chem. Rev.* **2007**, *107*, 5471-5569. (b) List, B. "Enamine Catalysis Is a Powerful Strategy for the Catalytic Generation and Use of Carbanion Equivalents" *Acc. Chem. Res.* **2004**, *37*, 548-557.

²⁵ Jurberg, I. D.; Chatterjee, I.; Tannerta, R.; Melchiorre, P. When asymmetric aminocatalysis meets the vinylogous principle. *Chem. Commun.* **2013**, *49*, 4869-4883.

Fuson realized that the electronic effects of a functional group in a molecule are transmitted to a distal position through interposed conjugated double bonds.²⁶ This concept was termed “*vinylology*”, and it had been extensively applied in polar organocatalytic processes for the enantioselective functionalization of distal positions in a molecule (Figure 1.6c). Whereas the combination of organocatalysis and radical chemistry nowadays seems quite established, the analogous vinylologous radical reactivity is underdeveloped. The application of one-electron chemistry to vinyllogous enamines, for instance, has rarely been exploited to functionalize distal positions in an enantioselective fashion.²⁷ The group of Melchiorre showed that electrophilic radicals **VI**, generated by direct excitation of organocatalytic dienamines **XI**, could be trapped at the most remote γ -position with exquisite regio- and enantioselectivity (Figure 1.7).

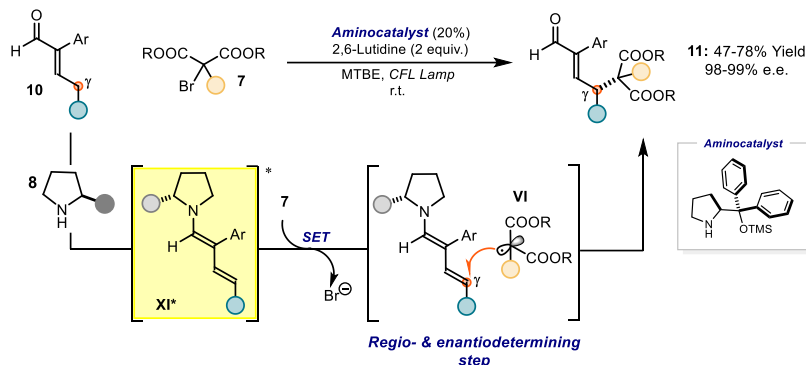


Figure 1.7. Direct enantioselective vinyllogous alkylation of enals.

This study offered the first example of vinyllogous radical reactivity in asymmetric catalysis, but the process was limited to tertiary malonyl radicals. In this thesis, I will show how the EDA complex activation strategy could be efficiently exploited to expand and refine the stereocontrolled radical γ -functionalization of enals **10**.

1.3 Excitation of dithiocarbamates intermediates

The most remarkable aspect of photoredox catalytic processes is the possibility to generate radicals under *catalytic* conditions. This feature unlocks transformations that would be challenging, if not impossible, to carry out under stoichiometric regime.²⁸ Xanthates

²⁶ Fuson, R. C. The principle of vinylology *Chem. Rev.* **1935**, *16*, 1-27.

²⁷ Silvi, M.; Arceo, E.; Jurberg, I. D.; Cassani, C.; Melchiorre, P. Enantioselective Organocatalytic Alkylation of Aldehydes and Enals Driven by the Direct Photoexcitation of Enamines *J. Am. Chem. Soc.* **2015**, *137*, 6120-6123.

²⁸ Matsui, J. K., Lang, S. B., Heitz, D. R.; Molander, G. A. Photoredoxmediated routes to radicals: the value of catalytic radical generation in synthetic methods development. *ACS Catal.* **2017**, *7*, 2563-2575.

chemistry, which is one of the main topics of my doctoral thesis, is a clear example of how visible-light excitation expanded the strategies available for radical generation allowing the development of new catalytic reactions. The groups of Barton and Zard were the first to pioneer the use of thiocarbonyl groups as radical precursors in a stoichiometric regime (Figure 1.8).²⁹ Xanthates **12** can be easily synthesized from the corresponding alkyl halides through S_N2 nucleophilic substitution. Compounds **12** possess a labile C-S bond that can be homolitically cleaved using an initiator. Following the mechanism depicted in Figure 1.8, the generation of the radical **XIII** proceeds through a chain mechanism. Capture of radical by a trap **13** generates a carbon-centered radical **XIV**, which undergoes a group transfer process with **12** to feed the radical chain.

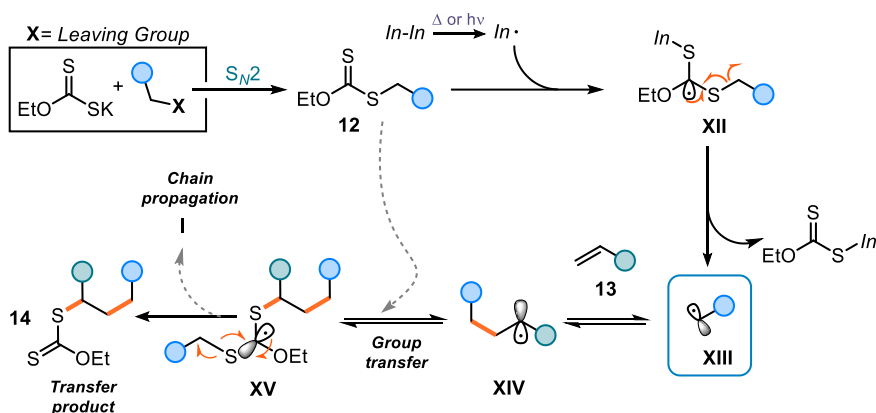


Figure 1.8. Mechanism of the degenerative xanthate transfer

Xanthates and dithiocarbamates (DTC) have found several applications in radical processes, including polymerizations.³⁰ During the 20th century, they constituted an exceptionally powerful tool to generate radicals, but they were used generally in stoichiometric amounts. This required the initial synthesis of stoichiometric thiocarbonyl derivatives followed by an additional step to remove or derivatize the final xanthate moiety in product **14**. Furthermore, the harsh conditions needed for the radical generation limited the applicability of these substrates.

In 2019, Melchiorre and coworkers showed that this radical generating strategy could be translated successfully into a catalytic regime (Figure 1.9).³¹ By exploiting a purposely designed dithiocarbamate **A**, it was possible to promote the *in situ* formation of a catalytic photoactive intermediate **16** from simple alkyl electrophiles **15**. Thanks to the photophysical

²⁹ Zard, S. Z.; On the Trail of Xanthates: Some New Chemistry from an Old Functional Group. *Angew. Chem. Int. Ed.* **1997**, *36*, 672-685.

³⁰ Poly, J.; Cabannes-Boue, B.; Hebing, L.; Mangin, R.; Sauvage, A.; Xiao, P.; Morlet-Savary, F.; Lalevee, J. Polymers synthesized by RAFT as versatile macrophotoinitiators. *Polym Chem* **2015**, *6*, 66-72.

³¹ Schweitzer-Chaput, B.; Horwitz, M. A.; de Pedro Beato, E.; Melchiorre, P. Photochemical generation of radicals from alkyl electrophiles using a nucleophilic organic catalyst. *Nat. Chem.* **2019**, *11*, 129-135.

properties of **A**, the intermediate **16** could absorb visible light and deliver the corresponding radical **XIII** upon excitation and subsequent C-S bond homolysis. After capture with a suitable radical trap **13**, the incipient radical **XIV** evolved to product **17** upon SET reduction. Crucial for the catalytic activity was the use of γ -terpinene, which served as both hydrogen donor and reductant to generate product **17** while providing an efficient catalyst turnover, respectively. This catalytic radical-generating strategy capitalized solely on the ability of the tailored dithiocarbamate (DTC) catalyst **A** to undergo S_N2 substitution with electrophiles. Importantly, this approach was suitable to activate substrates that are generally recalcitrant to SET processes due to their high redox potentials.

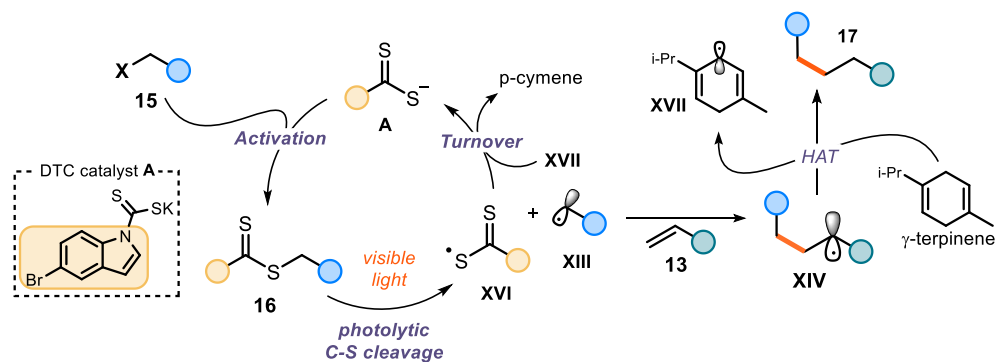


Figure 1.9. Radical generation platform based on a nucleophilic organic catalyst.

This catalytic platform was efficiently exploited to develop Giese-type additions, and also the alkylation of silyl enol ethers,³² a borylation process,³³ and three-component reactions.³⁴ In this doctoral thesis, I will describe how the DTC catalytic platform could be exploited to generate acyl and carbamoyl radicals. The mildness and selectivity of this radical-generating strategy led also to the development of a dual organocatalytic process for the asymmetric γ -alkylation of enals.

1.4 General objectives and summary

Traditionally, the generation of radicals involved the use of harsh conditions and stoichiometric redox agents or initiators, which often resulted in poor selectivity and challenging control over stereoselective bond formation. The main objective of this doctoral

³² Spinnato, D.; Schweitzer-Chapat, B.; Goti, G.; Oseka, M.; Melchiorre, P. A Photochemical Organocatalytic Strategy for the α -Alkylation of Ketones by Using Radicals. *Angew. Chem. Int. Ed.* **2020**, *59*, 9485-9490.

³³ Mazzarella, D.; Magagnano, G.; Schweitzer-Chapat, B.; Melchiorre, P. Photochemical Organocatalytic Borylation of Alkyl Chlorides, Bromides, and Sulfonates. *ACS Catal.* **2019**, *9*, 5876-5880.

³⁴ Cuadros, S.; Horwitz, M. A.; Schweitzer-Chapat, B.; Melchiorre, P. A visible-light mediated three component radical process using dithiocarbamate anion catalysis. *Chem. Sci.* **2019**, *10*, 5484-5488.

thesis was to study and develop organocatalytic platforms for the photochemical generation of radicals. Two of the three projects described in this doctoral thesis highlight how the mild conditions offered by the merger of light and organocatalysis were suitable for the regio- and stereoselective formation of new C-C bonds.

1.4.1 Photochemical generation of acyl and carbamoyl radicals using a nucleophilic organic catalyst

In Chapter II, the DTC catalytic platform originally used for the generation of alkyl radicals was expanded to form acyl and carbamoyl radicals. Leveraging on electrophilic acyl and carbamoyl chlorides **18**, the corresponding carbon-centered radicals **XVIII** could be generated and trapped efficiently (Figure 1.10).

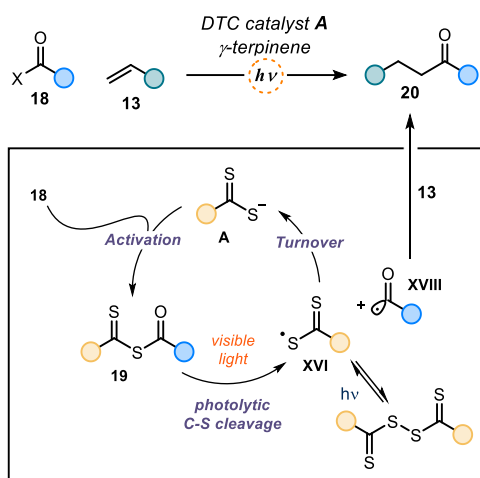


Figure 1.10. Photochemical generation of acyl radicals activated by a nucleophilic DTC organic catalyst.

The strategy used a commercially available nucleophilic organic catalyst **A** for the activation of the acyl and carbamoyl electrophiles **18**. The resulting radicals were trapped by a variety of electrophilic olefins in a Giese-type addition manifold. The chemistry required blue LEDs to activate precursors, which, due to their high reduction potential, were not readily prone to redox-based activation mechanisms. We also undertook an extensive mechanistic study, by means of transient absorption spectroscopy investigations, electrochemical studies, quantum yield measurements, and characterization of the key intermediates, to elucidate the light-regulated equilibria between the reactive radicals and the off-cycle intermediates. Furthermore, the nature of the turnover event for the catalyst regeneration was clarified.

1.4.2 Photochemical organocatalytic enantioselective radical γ -functionalization of α -branched enals

In Chapter III, the DTC catalytic platform was combined successfully with dienamine activation to develop the radical stereoselective γ -alkylation of α -branched enals **10** using simple and commercially available alkyl chlorides (and triflates) **15**, which are generally recalcitrant to SET activation.

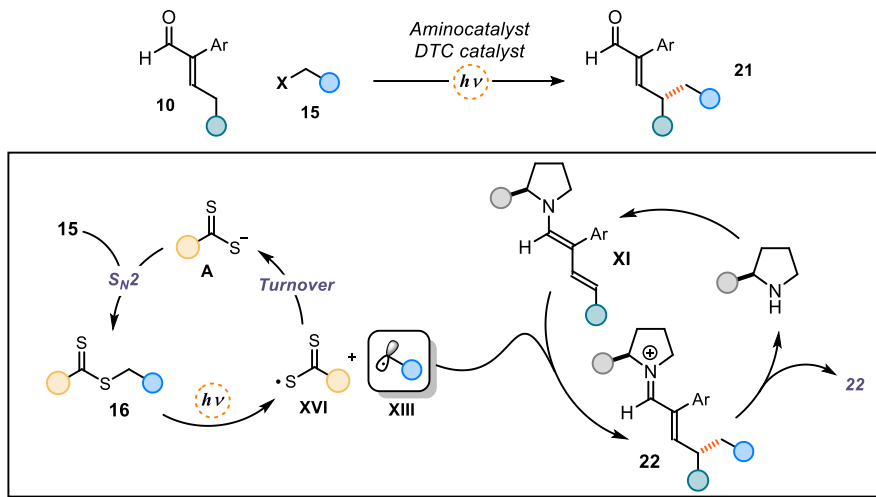


Figure 1.11. Dual photo-organocatalytic strategy for the γ -alkylation of enals.

The process required visible light and exploited the synergistic actions of two distinct organocatalysts. A secondary amine catalyst activated the α,β -unsaturated aldehyde, leading to a catalytic amount of dienamine **XI** in solution. Concomitantly, the DTC catalyst served to generate primary radicals **XIII** from simple alkyl electrophiles. Thanks to the mild reaction conditions, the radicals could be intercepted by the chiral dienamine generating products **21** in a stereoselective fashion and with exclusive γ -regioselectivity. The synthetic usefulness of the protocol was showcased by a user friendly scale-up reaction and subsequent manipulations of the chiral products bearing a remote stereocenter.

1.4.3 Stereoselective γ -fluoroalkylation of branched enals driven by photoexcitation of a dienamine-based EDA complex

In the last chapter of the thesis, the organocatalytic dienamine system was further exploited to realize a challenging stereoselective γ -perfluoroalkylation of enals (Figure 1.12).

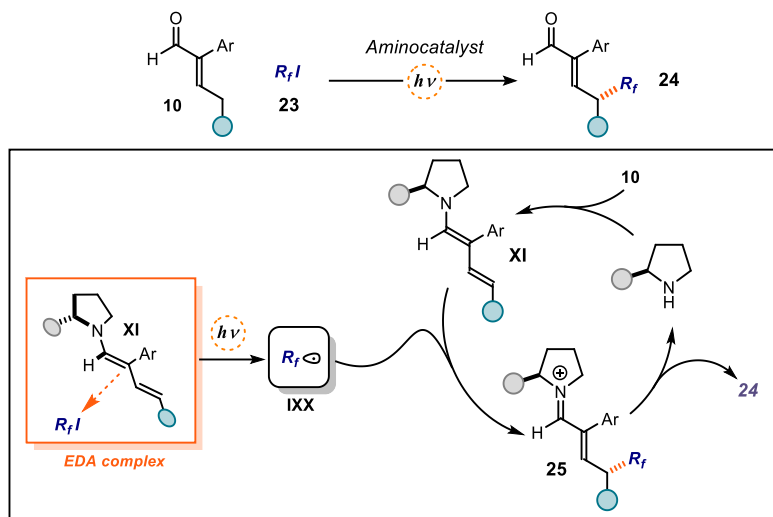


Figure 1.12. Asymmetric γ -perfluoroalkylation of enals using the photoactivity of a dienamine-based EDA complex.

Differently from the previous strategy, in this project we showed that chiral dienamines can elicit EDA complex formation with perfluoroalkyl iodides **23**. The excitation of this light-absorbing complex provided a suitable mechanism for the generation of fluoroalkyl radicals without the need of any external photocatalyst. The radicals were intercepted by the dienamine **XI** with high regio- and enantioselectivity. UV-Vis spectroscopic studies confirmed the formation of the EDA complex, while quantum yield measurements showed that the reaction proceeded through a radical chain manifold.

Chapter II

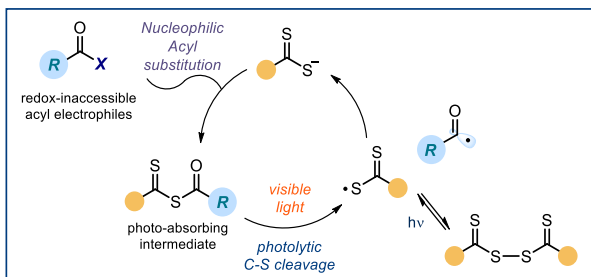
Photochemical generation of acyl and carbamoyl radicals using a nucleophilic organic catalyst

Target

Developing an organocatalytic photochemical strategy for the generation of carbamoyl and acyl radicals from easily accessible electrophilic reagents.

Tool

Exploiting the nucleophilic nature of an organic dithiocarbamate catalyst to activate electrophilic carbamoyl and acyl chlorides and generating the corresponding radicals by visible light excitation of the ensuing intermediate.³⁵



2.1 Introduction: early radical chemistry

Free radical chemistry occupies a prominent role not just in synthetic methodologies but also in life science and polymer manufacture.³⁶ One fascinating aspect of radical chemistry is the possibility to unlock divergent and orthogonal retrosynthetic disconnections with respect to the classical polar pathways;³⁷ this is why radicals also found elegant applications in total synthesis.³⁸ Traditionally, radical intermediates were prepared through methods requiring harsh conditions or toxic reagents, which limited the applicability of these processes.³⁹ One of the classical radical-generating strategies is based on the use of initiators, high-energy compounds which are intrinsically unstable and therefore undergo homolytic cleavage to generate radicals upon thermal or photochemical activation (Figure 2.1 left). The emerging

³⁵ The project conducted in this work has been published in collaboration with Dr. Eduardo de Pedro Beato & Dr. Daniele Mazzarella, who were involved in the discovery and optimization of the acylation and carbamoylation processes. I explored the scope of carbamoyl radicals and part of the mechanistic investigations. This work has been published, see: De Pedro Beato, E.; Mazzarella, D.; Balletti, M.; Melchiorre, P. Photochemical generation of acyl and carbamoyl radicals using a nucleophilic organic catalyst: applications and mechanism thereof. *Chem. Sci.* **2020**, *11*, 6312-6324.

³⁶ Renaud, P.; Sibi, M. P. "Radicals in Organic Synthesis. Eds.," **2001**, Wiley-VCH: Weinheim, Germany

³⁷ Yan, M.; Lo, J. C.; Edwards, J. T.; Baran, P. S. Radicals: Reactive Intermediates with Translational Potential. *J. Am. Chem. Soc.* **2016**, *138*, 12692-12714. (b) Smith, J. M.; Harwood, S. J.; Baram, P. S. Radical Retrosynthesis. *Acc. Chem. Res.* **2018**, *51*, 8, 1807-1817.

³⁸ Romero, K. J.; Galliher, M. S.; Pratt, D. A.; Stephenson C. R. J. Radicals in natural product synthesis. *Chem. Soc. Rev.* **2018**, *47*, 7851-7866.

³⁹ Baguley, P. A.; Walton, J. C. Flight from the Tyranny of Tin: The Quest for Practical Radical Sources Free from Metal Encumbrances. *Angew. Chem. Int. Ed.* **1998**, *37*, 3072-3082.

radicals are typically very reactive heteroatom-centered radicals, which can subsequently abstract an atom from the substrate (atom transfer manifold) delivering the target radical $R\cdot$.

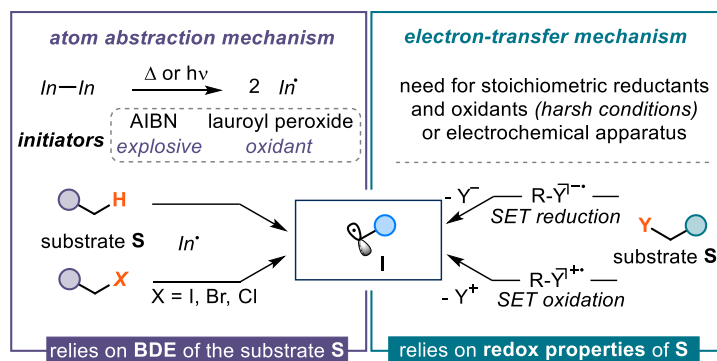


Figure 2.1. Classical strategies for the generation of radicals.

Another common strategy for accessing radical intermediates is by single-electron transfer (SET) manifold. In this case, stoichiometric redox agents (generally transition metals) are used to generate radical ions that can then undergo fragmentation to deliver the target radical $R\cdot$ (Figure 2.1 right).⁴⁰ These strategies have been extensively studied but generally their employment in organic synthesis is hampered by the need of relatively harsh conditions (hazardous and toxic reactants, high temperatures, UV-light irradiation).

2.2 Improving radical generation: thiocarbonyl compounds

A critical step towards the development of more selective and safer approaches for radical preparation has been the implementation of tailored sulfur-based radical precursors that can act as radical initiators and reagents. Seminal studies by Barton and Zard highlighted how thiocarbonyl compounds can serve to further expand the potential of synthetic radical chemistry.⁴¹

⁴⁰ Denisov, E. T.; Denisova, T. G.; Pokidova, T. S. *Handbook of Free Radical Initiators*. John Wiley & Sons, 2005.

⁴¹ Barton, D. H. R.; McCombie, S. W. A new method for the deoxygenation of secondary alcohols. *J. Chem. Soc., Perkin Trans. 1* **1975**, 1574-1585. (b) Barton, D. H. R.; Crich, D.; Motherwell, W. B. New and improved methods for the radical decarboxylation of acids. *J. Chem. Soc., Chem. Commun.* **1983**, 939-941. (c) Barton, D. H. R.; Zard, S. Z. Invention of new reactions useful in the chemistry of natural products. *Pure Appl. Chem.* **1986**, 58, 675-684. (d) Barton, D. H. R.; Crich, D.; Motherwell, W. B. The Invention of New Radical Chain Reactions. Part VII. Radical Chemistry of Thiohydroxamic Esters: A New Method for the Generation of Carbon Radicals from Carboxylic Acids. *Tetrahedron* **1985**, 41, 3901-3924.

Thiohydroxamic esters **1** (Figure 2.2) developed by Barton feature a very low N-O bond dissociation energy (~28 kcal/mol).⁴² Consequently, the absorption of energy by these compounds leads to the homolytic fragmentation of this bond.⁴³ For example, when an irradiation source of 360 nm is applied, an electronic transition promotes the excitation of the compound. From the excited state, homolytic scission of the N-O bond takes place leading to radicals **IIa** and **IIb**. The latter, upon decarboxylation, leads ultimately to radical **I**. The same process can take place when thermal energy is applied instead ($T > 62\text{ }^{\circ}\text{C}$).

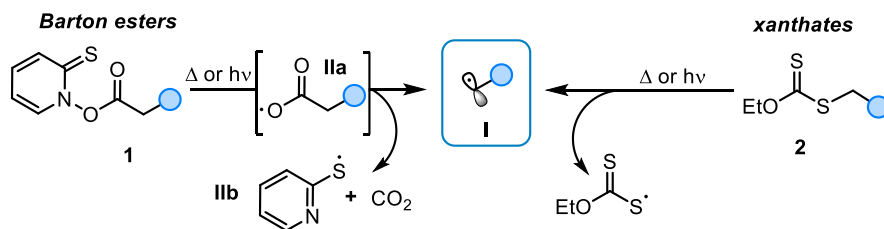


Figure 2.2. Thiocarbonyl compounds in the generation of radicals.

Analogously, xanthate (and dithiocarbamates) derivatives **2** were shown by Zard to react in a similar fashion.⁴⁴ Whereas they were mainly shown to generate a radical through the use of initiators, the labile C-S bond makes it possible to generate radicals by simple exposure to an energy source (light or heat). The application of whichever form of energy is a way to initiate a radical-chain mechanism known as *degenerative xanthate transfer*. This manifold is depicted in Figure 2.3 for the group transfer chemistry of xanthates. The mechanism starts with the generation of a first radical **I** by a catalytic initiator or by homolysis of the C-S bond. This radical can either be intercepted by a generic olefin **3**, which ultimately leads to the group transfer product, or by the progenitor xanthate **2** generating the more stabilized carbon-centered radical **II** which, through a reversible fragmentation mechanism, is in equilibrium with the radical **I**. This addition-fragmentation equilibrium controls the overall concentration of radical **I** in solution, circumventing alternative undesired pathways. This equilibrium has

⁴² Allonas, X.; Dietlin, C.; Fouassier, J.-P.; Casiraghi, A.; Visconti, M.; Norcini, G.; Bassi, G. Barton Esters as New Radical Photoinitiators for Flat Panel Display Applications *J. Photopolym. Sci. Technol.* **2008**, *21*, 505-509.

⁴³ (a) Barton, D. H. R.; Blundell, P.; Jaszberenyi, J. C. Quantum Yields in the Photochemically Induced Radical Chemistry of Acyl Derivatives of Thiohydroxamic Acids. *J. Am. Chem. Soc.* **1991**, *113*, 6937-6942. (b) Barton, D. H. R.; Jaszberenyi, J. C.; Tang, D. Photolytic Generation of Carbon Radicals from Barton Esters: Recent Developments. *Tetrahedron Lett.* **1993**, *34*, 3381-3384.

⁴⁴ (a) Delduc, P.; Tailhan, C.; Zard, S. Z., A convenient source of alkyl and acyl radicals. *J. Chem. Soc., Chem. Commun.* **1988**, 308-310. (b) Zard, S. Z., On the Trail of Xanthates: Some New Chemistry from an Old Functional Group. *Angew. Chem., Int. Ed.* **1997**, *36*, 672-685.

been extensively studied since it constitutes the base for the *reversible addition-fragmentation chain-transfer polymerization* (RAFT).⁴⁵

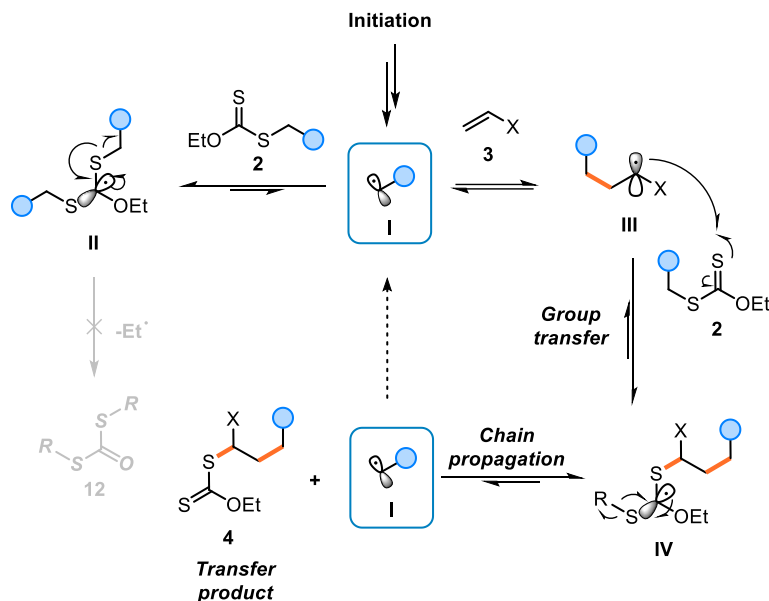


Figure 2.3. Mechanism of the degenerative xanthate transfer.

On the other hand, the capture of the radical by **3** generates a carbon-centered radical **III** which undergoes a group transfer process to feed the radical chain. It is noteworthy that all the steps in this scenario are equilibria, therefore the successful realization of a group transfer process is strictly depending on the relative stability of each intermediate. The most crucial requirement to fulfill this process is that radical **III** needs to be less stabilized than the initial radical **I**. This thermodynamic constraint ensures that radical **IV** will preferentially fragment in favor of product **4** sustaining the chain by concomitantly regenerating **I**.⁴⁶

2.3 Refining radical generation: photocatalytic manifolds

Albeit strategies based on group-transfer mechanism show promising potential in terms of accessibility and reactivity, their employment is plagued by the necessity to preform and

⁴⁵ Perrier, S. 50th Anniversary Perspective: RAFT Polymerization—A User Guide. *Macromolecules* **2017**, *50*, 7433-7447.

⁴⁶ For an elegant application of this concept see: Quiclet-Sire, B.; Zard, S. Z.; Radical Instability in Aid of Efficiency: A Powerful Route to Highly Functional MIDA Boronates. *J. Am. Chem. Soc.* **2015**, *137*, 6762-6765.

isolate purposely designed stoichiometric precursors. The application of photochemistry in modern organic synthesis led to the development of new *catalytic* methods for the generation of radicals under mild reaction conditions (Figure 2.4).⁴⁷

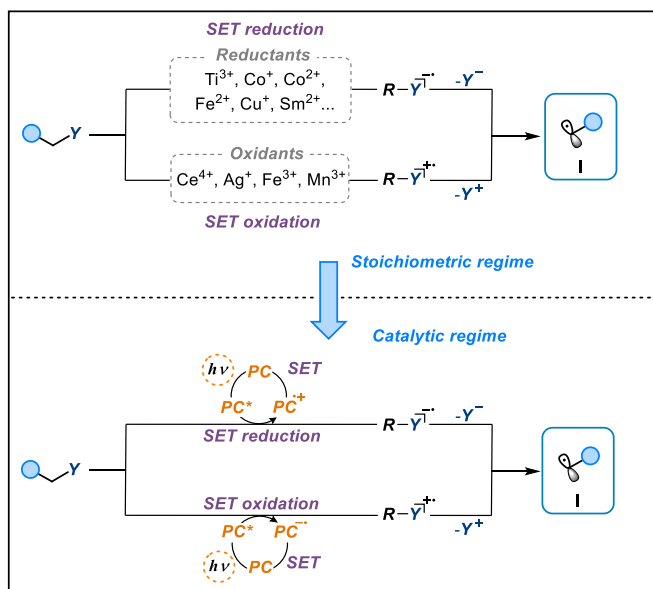


Figure 2.4. Shifting the SET strategies from a stoichiometric onto a catalytic manifold.

The earliest examples of radical generation strategies in the SET manifold were based on the use of stoichiometric amounts of metal salts (Fe^{3+} , Ag^+ , Ce^{4+} , Mn^{3+} , Sm^{2+} , Cu^+) as redox agents. Thanks to the massive investigation on photoredox catalysis⁴⁸, today we can leverage on the excitation of catalytic amounts of metal complexes⁴⁹ or organic dyes⁵⁰ to harness powerful oxidants and reductants for the generation of open-shell intermediates through SET events. At the same time, the excitation of a photocatalyst can promote the formation of high-energy excited states from which HAT processes can take place⁵¹, therefore replacing the previously initiator-based strategies which required hazardous reactants and harsh conditions

⁴⁷ Crespi, S.; Fagnoni, M. Generation of Alkyl Radicals: From the Tyranny of Tin to the Photon Democracy. *Chem. Rev.* **2020**, *120*, 9790-9833.

⁴⁸ Shaw, M. H.; Twilton, J.; MacMillan, D. W. C. Photoredox catalysis in Organic Chemistry. *J. Org. Chem.* **2016**, *81*, 6898-6926.

⁴⁹ Prier, C. K.; Rankic, D. A.; MacMillan, D. W. C. Visible Light Photoredox Catalysis with Transition Metal Complexes: Applications in Organic Synthesis. *Chem. Rev.* **2013**, *113*, 5322-5363.

⁵⁰ Nicewicz, D. A.; Nguyen, T. M. Recent Applications of Organic Dyes as Photoredox Catalysts in Organic Synthesis. *ACS Catal.* **2014**, *4*, 355-360.

⁵¹ (a) Capaldo, L.; Ravelli, D.; Fagnoni, M.; Direct Photocatalyzed Hydrogen Atom Transfer (HAT) for Aliphatic C-H Bonds Elaboration. *Chem. Rev.* **2022**, *122*, 1875-1924. (b) Capaldo, L.; Quadri, L. L.; Ravelli, D. Photocatalytic hydrogen atom transfer: the philosopher's stone for late-stage functionalization? *Green Chem.* **2020**, *22*, 3376-3396.

(Figure 2.5). The use of light and photocatalysts made therefore possible the shifting from the stoichiometric use of initiators and redox agents to the application of catalytic manifold to generate radicals under milder and safer conditions.

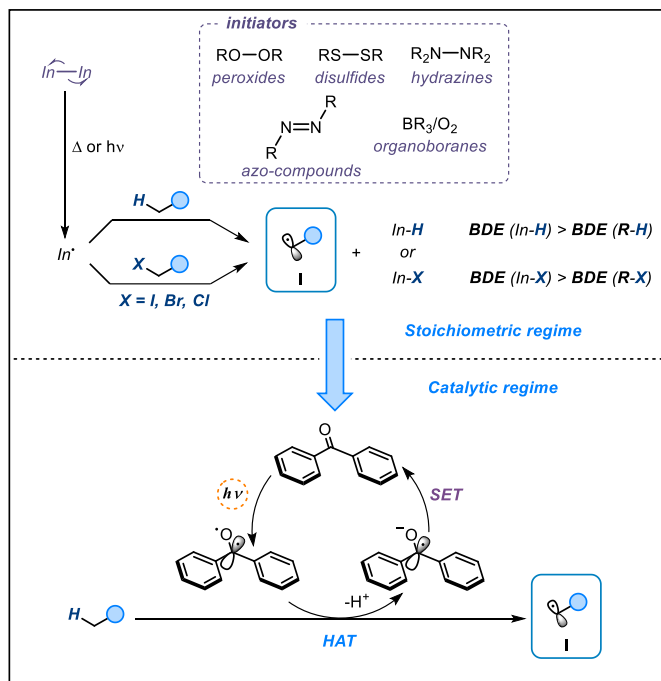


Figure 2.5. Shifting the HAT manifold from stoichiometric redox agents to photocatalysis.

2.4 Shifting dithiocarbamates to a photocatalytic manifold

The new opportunities offered by photocatalysis in the last decade allowed to apply classical radical generating strategies onto a catalytic regime.⁵² Yet, the need of matching the redox properties of the photocatalyst and the substrate (as well as matching BDEs in atom transfer processes) poses constraints in the design of new methodologies. To alleviate this restriction, our group recently developed a platform for the generation of radicals based on the use of dithiocarbonyl groups in a catalytic manifold.⁵³ Taking inspiration from the xanthates group transfer chemistry (Figure 2.3) our group wondered if it was possible to harness the

⁵² Matsui, J. K.; Lang, S. B.; Heitz, D. R.; Molander, G. A., Photoredox-Mediated Routes to Radicals: The Value of Catalytic Radical Generation in Synthetic Methods Development. *ACS Catal.* **2017**, *7*, 2563-2575.

⁵³ Schweitzer-Chaput, B.; Horvitz, M. A.; de Pedro Beato, E.; Melchiorre, P. Photochemical generation of radicals from alkyl electrophiles using a nucleophilic organic catalyst. *Nat. Chem.* **2019**, *11*, 129-135.

nucleophilic properties of xanthates and dithiocarbamates.⁵⁴ These organic catalysts, upon S_N2 activation of alkyl halides, could form *in situ* a catalytic photoactive intermediate able to absorb visible light and deliver radicals upon C-S homolysis. This strategy (Figure 2.6) capitalized solely on the ability of a newly-designed dithiocarbamate (DTC) catalyst **A** to undergo S_N2 substitution with a wide array of electrophiles, which are generally recalcitrant to undergo SET due to their high redox potentials.

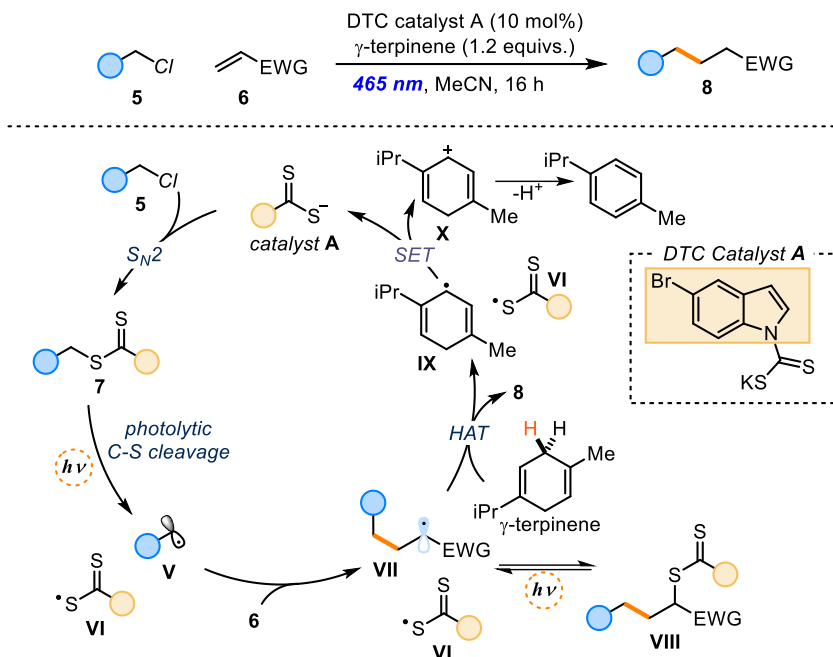


Figure 2.6. Dithiocarbamate anion catalysis for the activation of alkyl chlorides and the generation of radicals.

The key aspect of this strategy was the possibility to use visible light to generate a radical from intermediate **7**. We found that 5-bromoindole DTC catalyst **A** features a bathochromic shift in the absorption spectra with respect to classic aliphatic dithiocarbamates, opening the possibility to use visible light for the excitation of intermediate **7**. Analogously to the xanthate chemistry, the photoexcitation of the intermediate triggers the homolysis of the C-S bond, leading to the generation of the target radical **V** and the xanthyl radical **VI**. The former was shown to react with a variety of radical traps to forge new C-C and C-B bonds.⁵⁵ The ensuing

⁵⁴ Duan, X.; Maji, B.; Mayr, H. Characterization of the nucleophilic reactivities of thiocarboxylate, dithiocarbonate and dithiocarbamate anions. *Org. Biomol. Chem.*, **2011**, *9*, 8046-8050.

⁵⁵ (a) Cuadros, S.; Horwitz, M.A.; Schweitzer-Chaput B.; Melchiorre, P. A visible-light mediated three-component radical process using dithiocarbamate anion catalysis. *Chem. Sci.* **2019**, *10*, 5484-5488. (b)

radical **VII** would in turn abstract a hydrogen atom from γ -terpinene, used as sacrificial reductant, to afford the product and the cyclohexadienyl radical **IX**. In a simplified mechanistic picture, we proposed that a SET between **VI** ($E^0(\text{A}/\text{VI}) = +0.44 \text{ V vs Ag/AgCl}$ in CH_3CN)⁵⁶ and **IX** ($E_{\text{red}} = 0.05 \text{ V vs Ag/AgCl}$ in CH_3CN)⁵⁷ would provide the turnover event which closes the catalytic cycle. Overall, this radical-generating strategy demonstrated to be orthogonal to other approaches since it is not reliant on the redox properties of the radical precursor to generate the desired open-shell intermediate.

This chapter describes how this catalytic platform could be leveraged also for the generation of carbamoyl and acyl radicals. In addition, during the course of my investigation, several studies unraveled interesting mechanistic aspects, which were useful for expanding the potential of the catalyst platform. In the following sections, the state of the art in the generation of carbamoyl radicals will be highlighted so to define the context of this project.

2.5 Strategies for the generation of carbamoyl radicals

The synthetic importance of installing acyl and carbamoyl moieties lies in the possibility to directly prepare carbonyl-containing derivatives, which are useful building blocks and ubiquitous motifs in drug design. Whereas the introduction of such groups using classic polar chemistry is well documented, the generation of carbamoyl radicals is not straightforward.⁵⁸ Historically, the first strategies for the generation of such open-shell intermediates relied on the use of preformed carbamoyl chalcogen derivatives or stoichiometric oxidants in combination with thermal initiators or UV light irradiation. The recent advent of photocatalysis spurred the development of new methodologies⁵⁹ for the generation of acyl and carbamoyl radicals under a catalytic regime. Below I summarize briefly how the strategies for the generation of carbamoyl radicals evolved.

Mazzarella, D.; Magagnano, G.; Schweitzer-Chaput B.; Melchiorre, P. Photochemical Organocatalytic Borylation of Alkyl Chlorides, Bromides, and Sulfonates. *ACS Catal.* **2019**, 5876-5880. (c) Spinnato, D.; Schweitzer-Chaput, B.; Goti, G.; Ošeka, M. Melchiorre, P. A Photochemical Organocatalytic Strategy for the α -Alkylation of Ketones by using Radicals. *Angew. Chem. Int. Ed.* **2020**, 59, 9485-9490.

⁵⁶ Dag, Ö.; Yaman, S. Ö.; Önal, A. M.; İsci, H. Spectroelectrochemistry of Potassium Ethylxanthate, Bis(ethylxanthato)nickel(II) and Tetraethylammonium Tris(ethylxanthato)nickelate(II). *J. Chem. Soc., Dalton Trans.* **2001**, 2819-2824.

⁵⁷ Bahtia, K.; Schuler, R. H. Oxidation of Hydroxycyclohexadienyl Radical by Metal Ions. *J. Phys. Chem.* **1974**, 78, 2335-2338.

⁵⁸ Chatgililoglu, C.; Crich, D. Komatsu, M.; Ryu, I. The chemistry of acyl radicals. *Chem. Rev.* **1999**, 99, 1991-2070.

⁵⁹ Raviola, C.; Protti, S.; Ravelli, D.; Fagnoni, M. Photogenerated acyl/alkoxycarbonyl/carbamoyl radicals for sustainable synthesis. *Green Chem.* **2019**, 21, 748-764.

2.5.1 Strategies based on the use of stoichiometric reagents

One of the earliest approaches to access carbamoyl radicals used atom transfer processes (Figure 2.7). For example, formamides can serve as suitable substrates because of their low BDE of the C-H bond (87 kcal/mol). Already in 1964, the first acyl radical generation protocol was described by Friedman which used peroxides initiators and thermal energy to trigger the abstraction of the hydrogen atom from formamide **9**.⁶⁰ Differently from acyl radicals, carbamoyl radicals are not prone to decarbonylation, therefore they could be efficiently trapped with unbiased olefins **10**.

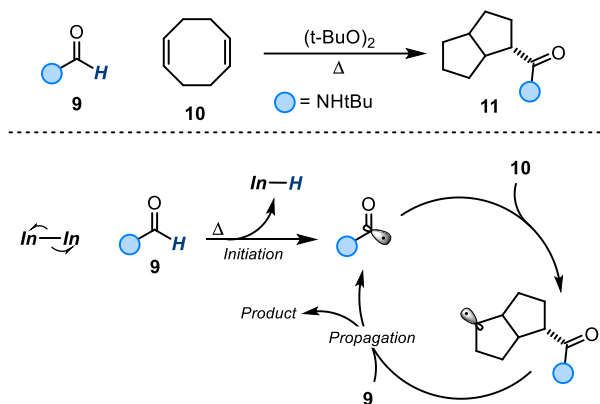


Figure 2.7. Generation of carbamoyl radicals from formamides using initiators.

Aldehydes and formamides were used as a source of radicals also by Minisci for the amidation of pyridines and quinolines under oxidative conditions (Figure 2.8).⁶¹ Using *tert*-butyl hydroperoxide as radical initiator, an alkoxy radical was generated. The latter performed HAT on the formamide **12** generating the nucleophilic acyl radical **XI**, which attacked the protonated quinoline H-**13**. A subsequent oxidation-deprotonation sequence involving the radical cation **XII** delivered the acylated product **14**. One of the main drawbacks of this protocol is the low selectivity of the reaction. The high BDE of the initiator promotes the HAT also on the aliphatic chain of the amide when bearing alkyl substituents, therefore leading to multiple alkylation processes.

⁶⁰ Friedman, L. 2-exo,cis-Bicyclo [3.3.0.] octane Derivatives via Free-Radical Additions to cis,cis-1,5-Cyclooctadiene. *J. Am. Chem. Soc.* **1964**, 86, 1885.

⁶¹ Minisci, F.; Gardini, G. P.; Galli, E.; Bertini, F. A New Selective Type of Aromatic Substitution: Homolytic Amidation. *Tetrahedron Lett.* **1970**, 11, 15-16.

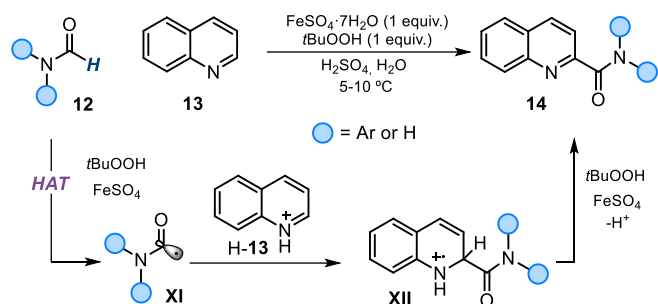


Figure 2.8. Generation of carbamoyl radicals from formamides using stoichiometric HAT reagents.

To address this issue, Minisci and coworkers developed a strategy based on a SET manifold (Figure 2.9).⁶² In this case, exploiting the ability of carboxyl radicals to undergo decarboxylative fragmentation upon oxidation, oxamic acid **15** was used as the substrate. SET oxidation of **15** by a mixture of sodium persulfate and silver nitrate led to the oxygen-centered radical **XIII**, which upon decarboxylation delivered the desired carbamoyl radical **XI** prone to the amidation of pyridines and quinolines.

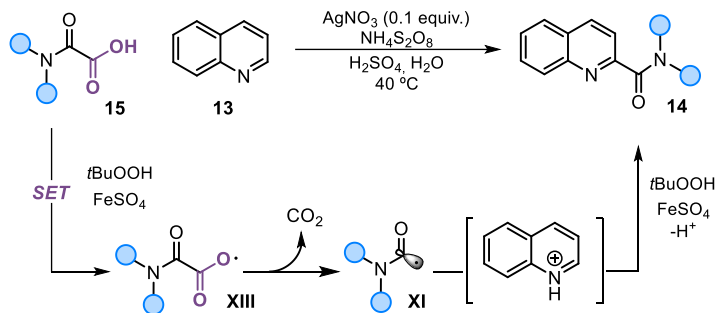


Figure 2.9. Generation of carbamoyl radicals from oxamic acids using stoichiometric SET oxidant.

Further progress in the field was spurred by the use of carbamoyl chalcogenides. These reagents can be easily prepared and stored for prolonged time. Another appealing property of these reagents is the low BDE of the C-X bond, which allows a relatively easy photolysis under exposition to UV-light. In 2001, the group of Kambe⁶³ reported the synthesis and use of carbamotelluroates **16** for the generation of carbamoyl radicals (Figure 2.10). Under

⁶² Minisci, F.; Citterio, A.; Vismara, E. Polar Effects in Free-Radical Reactions. New Synthetic Developments in the Functionalization of Heteroaromatic Bases by Nucleophilic Radicals. *Tetrahedron* **1985**, *41*, 4157-4170.

⁶³ Fujiwara, S.; Shimizu, Y.; Shinike, T.; Kambe, N. Photoinduced Group Transfer Radical Addition of Carbamotelluroates to Acetylenes. *Org. Lett.* **2001**, *3*, 2085-2088.

irradiation by a tungsten lamp, the C-Te bond underwent homolysis generating the carbamoyl radical. The latter was intercepted by terminal acetylenes **17** delivering the C(sp²)-centered radical **XIV**. This chain mechanism was then propagated by a group transfer mechanism which supplied the generation of the carbamoyl radical and the formation of the product **18**. Albeit straightforward, this process required the use of hazardous organotellurides, hampering the applicability of the process for preparative purposes.

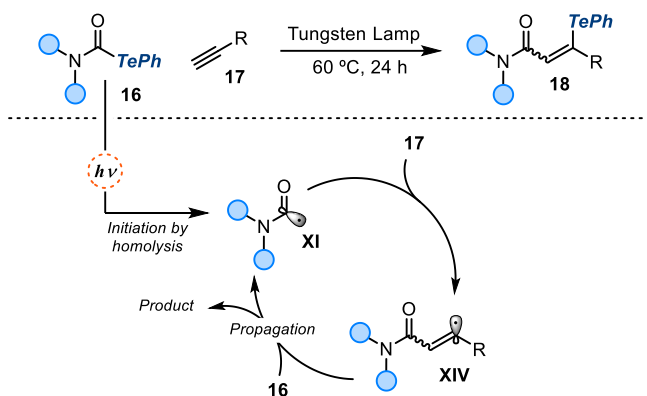


Figure 2.10. Generation of carbamoyl radicals from organotellurides.

A crucial step toward a greener and safer approach was achieved by Grainger and Innocenti.⁶⁴ Reminiscent of the xanthate group transfer chemistry, they developed a procedure for the generation of carbamoyl radicals using thiocarbonyl derivatives **19** as radical precursors (Figure 2.11). The low BDE of the C-S bond made the generation of carbamoyl radicals possible either by irradiation or by using an initiator. The carbamoyl radical **XV** then underwent cyclization into a pendant olefin. The ensuing alkyl radical **XVI** was then prone to a group transfer manifold to deliver the lactam products **20**.

⁶⁴ Grainger, R. S.; Innocenti, P. Dithiocarbamate Group Transfer Cyclization Reactions of Carbamoyl Radicals under “Tin-Free” Conditions. *Angew. Chem. Int. Ed.* **2004**, *43*, 3445-3448.

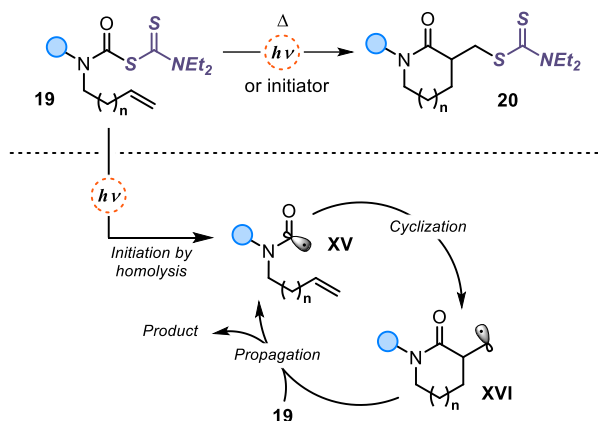


Figure 2.11. Generation of carbamoyl radicals using dithiocarbamates and a group transfer process.

Organocobalt Co(III) complexes are known to be photoactive and undergo photolytic scission delivering radicals.⁶⁵ As early as 1989, Pattenden and coworkers reported for the first time the possibility to use a stoichiometric amide salophen complex to generate a carbamoyl radical (Figure 2.12).⁶⁶ Upon visible light irradiation using a 300 W sunlamp, the Cobalt salophen complex **21** underwent homolytic cleavage releasing the carbamoyl radical **XV**. As a common feature with acyl chalcogenides, these cobalt species also have the tendency to undergo a group transfer process to release a product which still bears a Co(Salophen) moiety ready for further manipulation. Noteworthy, this chemistry worked also in intermolecular fashion without detrimental loss in yield.

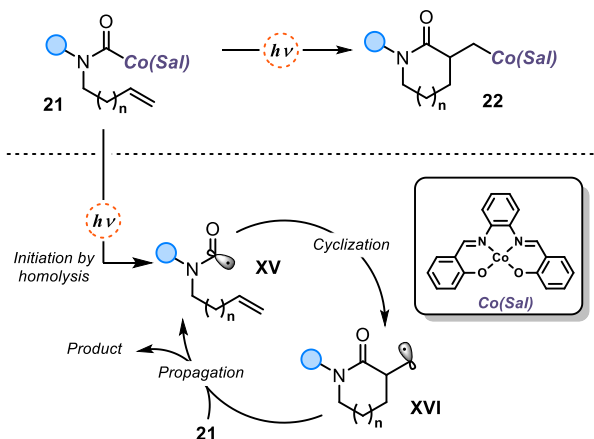


Figure 2.12. Generation of carbamoyl radicals using Co(salophen) group transfer manifold.

⁶⁵ Demartea, J.; Debuigne, A.; Detrembleur, C. Organocobalt Complexes as Sources of Carbon-Centered Radicals for Organic and Polymer Chemistries. *Chem. Rev.* **2019**, *119*, 6906-6955.

⁶⁶ Gill, G. B.; Pattenden, G.; Reynolds, S. J. Cobalt-Mediated Reactions. A New Synthetic Approach to β -, γ - and δ -Lactams. *Tetrahedron Lett.* **1989**, *30*, 3229-3232.

2.5.2 Catalytic strategies for the generation of carbamoyl radicals

The strategies previously described feature the use of stoichiometric redox agents or initiators. Also, the direct photolysis approach using chalcogen derivatives is somehow hampered by two factors: *i*) the need to preform a purposely designed radical precursor and *ii*) the limitation to achieve a group transfer product. The recent advent of photocatalysis and the application of modern photochemistry encouraged the development of novel catalytic methodologies for the generation of acyl and carbamoyl radicals.⁵⁹ In this context, polyoxometalates, especially tetrabutylammonium decatungstate (TBADT), found many applications for the generation of radicals.⁶⁷ By exposition to UV light irradiation, TBADT is directly excited to its singlet state. After intersystem crossing, the triplet state is reached. A recent study⁶⁸ demonstrated how the singly occupied molecular orbitals of the complex in the triplet state are mostly localized on the oxygen atoms, therefore leading to a highly electrophilic oxygen center with partial radical character.

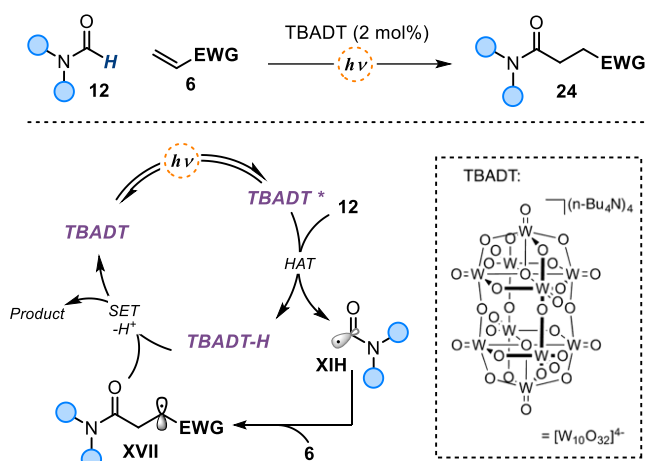


Figure 2.13. Generation of carbamoyl radicals using a catalytic HAT strategy.

The excited TBADT was shown to be highly prone to undergo HAT processes with a plethora of substrates, thus generating nucleophilic radicals. This process has been exploited by the group of Fagnoni and Ryu to generate carbamoyl radicals directly from formamides using catalytic amounts of TBADT (1-5 mol%, Figure 2.13). The nucleophilic carbamoyl radical

⁶⁷ (a) Ravelli, D.; Fagnoni, M.; Fukuyama, T.; Nishikawa, T.; Ryu, I. Site-Selective C–H Functionalization by Decatungstate Anion Photocatalysis: Synergistic Control by Polar and Steric Effects Expands the Reaction Scope. *ACS Catalysis*, **2018**, *8*, 701-713. (b) Tzirakis, M. D.; Lykakis, I. N.; Orfanopoulos, M., Decatungstate as an efficient photocatalyst in organic chemistry. *Chem. Soc. Rev.* **2009**, *38*, 2609-2621.

⁶⁸ De Waele, V.; Poizat, O.; Fagnoni, M.; Bagnò, A.; Ravelli, D. Unraveling the Key Features of the Reactive State of Decatungstate Anion in Hydrogen Atom Transfer (HAT) Photocatalysis. *ACS Catal.* **2016**, *6*, 7174-7182.

was reported to undergo Giese-type⁶⁹ addition or Minisci⁷⁰ alkylation with electron deficient heterocycles.

Photoredox catalysis can also offer an orthogonal approach for the generation of carbamoyl radicals based on the redox properties of the substrates. Similarly to Minisci' approach, the group of Feng exploited the ability of oxalic acid monoamides **25** to undergo oxidative decarboxylation (Figure 2.14).⁷¹ Reductive quenching of the excited iridium photocatalyst by SET with **25** generated the carboxyl radical, which fragmented to deliver the more stabilized carbamoyl radical **XI**. The latter is intercepted by an electron-poor olefin **6** in a Giese-type addition. Subsequent intramolecular homolytic aromatic substitution (HAS) delivered the cyclohexadienyl radical **IXX**, which was rapidly oxidized to furnish the aromatized product **26**. An interesting feature of this protocol is that ambient oxygen is used as external oxidant to close the photocatalytic cycle generating the superoxide ion, which promoted aromatization of **IXX** by HAT process.

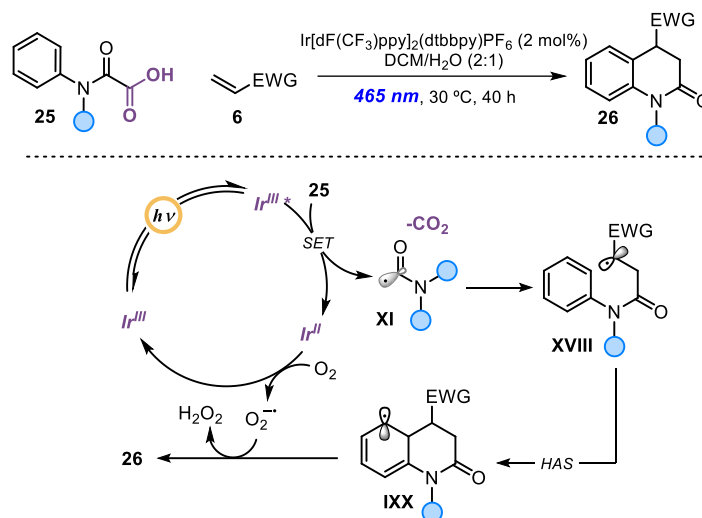


Figure 2.14. Generation of carbamoyl radicals using a catalytic oxidative SET strategy.

⁶⁹ Esposti, S.; Dondi, D.; Fagnoni, M.; Albini, A. Acylation of Electrophilic Olefins through Decatungstate-Photocatalyzed Activation of Aldehydes. *Angew. Chem., Int. Ed.*, **2007**, 46, 2531-2534.

⁷⁰ Quattrini, M. C.; Fujii, S.; Yamada, K.; Fukuyama, T.; Ravelli, D.; Fagnoni, M.; Ryu, I. Versatile cross-dehydrogenative coupling of heteroaromatics and hydrogen donors via decatungstate photocatalysis. *Chem. Commun.*, **2017**, 53, 2335-2338.

⁷¹ Bai, Q.-F.; Jin, C.; He, J.-Y.; Feng, G. Carbamoyl Radicals via Photoredox Decarboxylation of Oxamic Acids in Aqueous Media: Access to 3,4-Dihydroquinolin-2(1H)-ones. *Org. Lett.* **2018**, 20, 2172-2175.

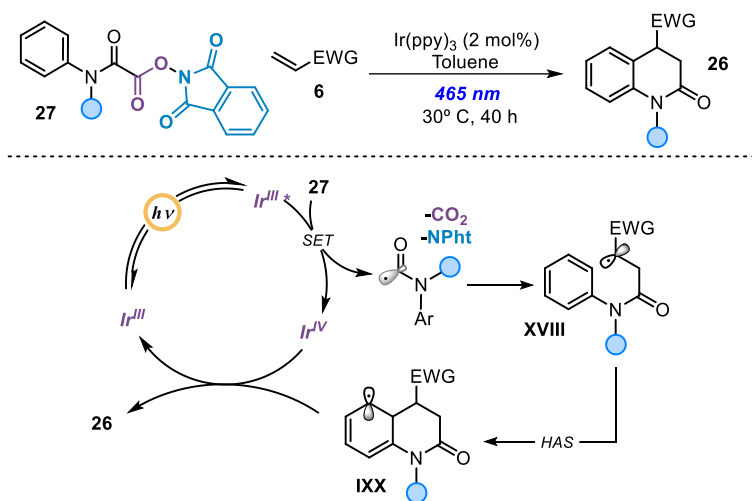


Figure 2.15. Generation of carbamoyl radicals using a catalytic reductive SET strategy.

The advancement of photoredox catalysis has been based also on the design of substrates purposely adorned with redox-active moieties prone to SET reductive processes to generate radicals. One prominent example is the use of redox active esters (RAEs). These bench-stable compounds are easily prepared in one step from carboxylic acids and *N*-hydroxy phthalimide. Whereas carboxylates deliver a radical $\text{R}\cdot$ upon SET oxidation (followed by CO_2 extrusion), the corresponding RAEs deliver the same radical $\text{R}\cdot$ upon SET reduction. This concept has been extensively used to generate a wide array of carbon-centered radicals in the photoredox regime.⁷² In the context of carbamoyl radicals, the group of Donald recently showed that it is indeed possible to use oxalic acid derived RAEs **27** for the generation of such radicals (Figure 2.15).⁷³ The excited $\text{Ir}(\text{ppy})_3$ complex underwent oxidative quenching with the RAE **27** promoting its fragmentation. The incipient carbamoyl radical was then trapped by a Michael acceptor followed by intramolecular HAS. The SET event between the oxidized Ir(IV) and the cyclohexadienyl radical **IXX** provided the turnover event for the catalyst regeneration along with the formation of the product.

⁷² Karmakar, S.; Silamkoti, A.; Meanwell, N. A.; Mathur, A.; Gupta, A. K. Utilization of $\text{C}(\text{sp}^3)$ -Carboxylic Acids and Their Redox-Active Esters in Decarboxylative Carbon–Carbon Bond Formation *Adv. Synth. Cat.* **2021**, 363, 15, 3693–3736.

⁷³ Petersen, W. F.; Taylor, R. J. K.; Donald, J. R. Photoredox-Catalyzed Reductive Carbamoyl Radical Generation: A Redox-Neutral Intermolecular Addition–Cyclization Approach to Functionalized 3,4-Dihydroquinolin-2-ones. *Org. Lett.* **2017**, 19, 874–877.

2.6 Target of the project

The target of this project was the development of a photocatalytic strategy for the generation of carbamoyl (and acyl) radicals using the DTC catalytic platform developed in our group for the activation of alkyl halides (discussed in section 2.4). Up to now, our strategy was limited to the activation of substrates prone to S_N2 displacement. In this study, we show that the potential of our catalytic platform can be expanded to include substrates amenable to nucleophilic acyl substitution, such as carbamoyl chlorides and anhydrides, generating valuable C(sp²)-centered radicals under mild conditions. Noteworthy, these substrates are not readily prone to SET activation due to their high reduction potentials, rendering this strategy orthogonal with respect to the ones based on photoredox manifolds.

2.6.1 Design plan

Figure 2.16 highlights our proposed strategy for the generation of carbamoyl radicals from the corresponding chlorides.

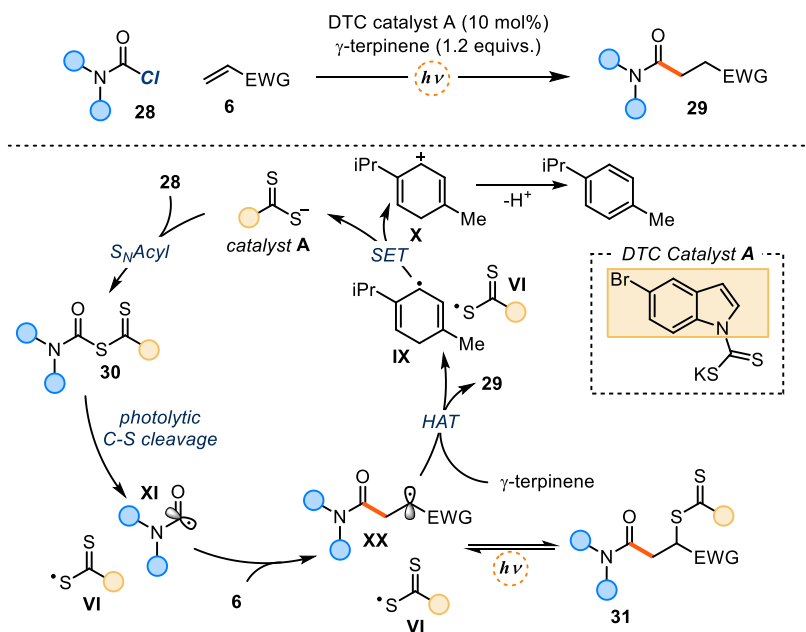


Figure 2.16. Design plan for the generation of carbamoyl radicals using DTC catalysis.

In analogy to the mechanism originally proposed for the DTC catalytic cycle, we envisioned that, upon nucleophilic acyl substitution, the nucleophilic dithiocarbamate catalyst would generate intermediate **30**. Thanks to the tailored absorption properties of our DTC catalyst, the visible-light irradiation of intermediate **30** would bring it into the excited state from which the homolytic cleavage of the C-S bond can take place. The ensuing nucleophilic carbamoyl

radical **XI** would be trapped in an inter- or intramolecular fashion to deliver a C(sp³)-centered radical **XX**, which should be able to abstract a hydrogen atom from γ -terpinene. Finally, SET reduction from the cyclohexadienyl radical **X** to the xanthyl radical **VI** would provide the turnover event responsible for catalyst regeneration (details on the feasibility of this turnover event are discussed in section 2.8).

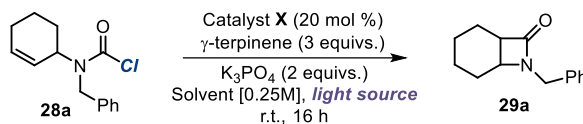
Taking inspiration from the work of Grainger and Innocenti,⁶⁴ we envisioned that an appealing application of this strategy could be found in the synthesis of lactams by translating this blueprint to an intramolecular version. This scaffold is ubiquitous in natural products and also in non-natural compounds exhibiting a broad spectrum of biological activities.⁷⁴

2.7 Results and discussion

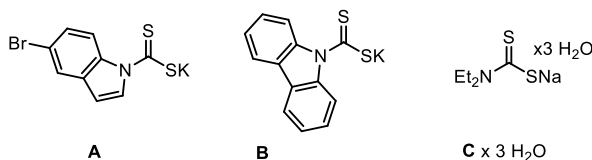
2.7.1 Reaction optimization

We started our investigation by studying the possibility to perform a radical cyclization using carbamoyl chloride **28a** as radical precursor. The initial conditions featured DCM as solvent, 2 equivalents of K₃PO₄ as basic additive to quench the HCl formed during the course of the reaction, and 3 equivalents of γ -terpinene as hydrogen donor. We firstly evaluated the performance of different DTC nucleophilic catalysts (20 mol%) under 465 nm irradiation (Table 2.1). Interestingly, the DTC catalyst **A** and **B**, which offered the best activities in the activation of alkyl halides, did not yield any of the desired product (entries 1 and 2). When the commercially available diethylamino catalyst **C** was used instead, product **29a** was detected in the reaction crude albeit in low yield (entry 3). In this case, the intermediate arising from the S_NAcyl between the catalyst and **28a** is not absorbing in the visible region. We therefore needed to switch the light wavelength from 465 nm to 405nm in order to achieve the excitation which leads to the desired reactivity.

⁷⁴ (a) Caruano, J.; Muccioli G. G.; Robiette, R. Biologically active γ -lactams: synthesis and natural sources. *Org. Biomol. Chem.* **2016**, *14*, 10134-10156. (b) Lima, L.M.; Silva, B.N.M.D.; Barbosa, G.; Barreiro, E. J. β -lactam antibiotics: An overview from a medicinal chemistry perspective. *Eur. J. Med. Chem.* **2020**, *208*, 112829-112850.

Table 2.1. Model reaction and optimization

catalysts used in this study



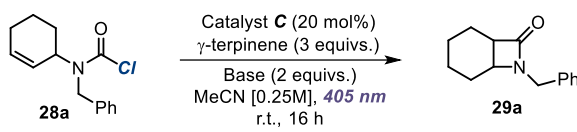
entry	catalyst	solvent	wavelength	yield 29a (%) ^a
1	A	DCM	465 nm	0
2	B	DCM	465 nm	0
3	C	DCM	405 nm	5
4	C	Acetonitrile	405 nm	28
5	C	Acetone	405 nm	26
6	C	AcOEt	405 nm	7
7	C	THF	405 nm	27
8	C	Toluene	405 nm	18
9	C	DMF	405 nm	10
10	C	DMA	405 nm	0

a) Reaction performed on a 0.2 mmol scale. Yields of **29a** determined by ¹H NMR analysis of the crude mixture using trichloroethylene as the internal standard.

This result prompted us to a more detailed screening of the reaction conditions. Evaluation of the reaction medium identified acetonitrile (entry 4) and THF (entry 7) as the best solvents, since they offered product **29a** with an increased yield to 28% and 27%, respectively. Other solvents with different dielectric constants (e.g. toluene and DMF) did not improve the yield of the reaction. Acetonitrile was therefore chosen as the optimal solvent for further optimization.

Next, we screened the effect of the base (Table 2.2.). The replacement of the counter-cation and the counter-anion in the inorganic base did not result in any increase in yield (entries 1 and 2). We also reasoned that a more soluble base could facilitate the process by increasing the penetration of the light in the media. However, the use of organic bases such as 1,8-diazabicyclo-7-undecene (DBU), tetramethylguanidine (TMG), and lutidine resulted in decreased yields (entries 3-5).

Table 2.2. Effect of the basic additive

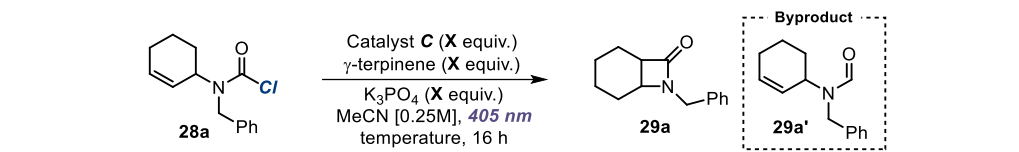


entry	base	yield 29a (%) ^a
1	Na ₂ PO ₃	18
2	K ₂ CO ₃	23
3	DBU	14
4	TMG	11
5	2,6-lutidine	7

a) Reaction performed on a 0.2 mmol scale. Yields of **29a** determined by ¹H NMR analysis of the crude mixture using trichloroethylene as the internal standard.

A final round of optimization was performed to evaluate the effect of the relative stoichiometry of the components and the temperature (Table 2.3). We began increasing the amount of the catalyst **C** to 40 mol% but it did not show any beneficial effect on the yield of the reaction (entry 1).

Table 2.3. Effect of the stoichiometry of the process



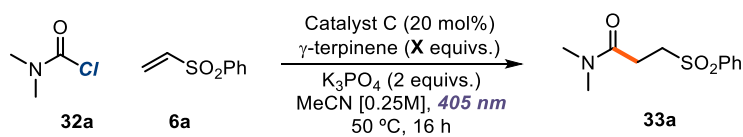
entry	catalyst	γ -terpinene	base	temperature	yield 29a (%) ^a
1	40 mol%	2 equiv.	2 equiv.	r.t.	30
2	20 mol%	2 equiv.	2 equiv.	r.t.	40
3	20 mol%	1.5 equiv.	2 equiv.	r.t.	51
4	20 mol%	1 equiv.	2 equiv.	r.t.	45
5	20 mol%	1.5 equiv.	1.5 equiv.	r.t.	35
6	20 mol%	1.5 equiv.	3 equiv.	r.t.	30
7	20 mol%	1.5 equiv.	2 equiv.	50 °C	67 (65)

a) Reaction performed on a 0.2 mmol scale. b) Yields of **29a** determined by ¹H NMR analysis of the crude mixture using trichloroethylene as the internal standard. The value shown in parentheses refers to the yield of isolated **29a** after chromatographic purification on silica gel.

Next, we screened the amount of hydrogen donor. During our investigation, we recognized the quenching of the carbamoyl radical prior to cyclization, generating the reduced formamide product **29a'**, as the main byproduct of the process. In light of this parasitic HAT process, we envisioned that a lower amount of hydrogen donor could facilitate the cyclization by

minimizing the direct hydrogen abstraction from the carbamoyl radical. Lowering the amount of γ -terpinene from 3 to 2 equivalents indeed increased the yield of product **29a** to 40% (entry 2). Further reduction to 1.5 equivalents revealed to be optimal (51% yield, entry 3), while using 1 equivalent offered slightly lower yield (entry 4). Modulating the amount of base did not increase the efficiency of the process (entries 5 and 6). Interestingly, when increasing the temperature to 50 °C, product **29a** was obtained in 65% yield (isolated compound, entry 7), probably due to a more effective nucleophilic acyl substitution from catalyst **C**. With the β -lactam product obtained in synthetically useful yields, we evaluated the feasibility of an intermolecular variant. This idea was tested by reacting dimethylamino carbamoyl chloride **32a** with vinyl sulfone **6a** using the optimized conditions (Table 2.3 entry 7).

Table 2.4. Optimization of the intermolecular variant



entry	H donor	Deviation	yield 33a (%) ^a
1	1.5	/	40
2	3	/	60
3	2	/	(60)
4	2	T = 25 °C	38
5	2	No catalyst C	0
6	2	No Light	0

a) Reaction performed on a 0.2 mmol scale. b) Yields of **33a** determined by ¹H NMR analysis of the crude mixture using trichloroethylene as the internal standard. The value shown in parentheses refers to the yield of isolated **33a** after chromatographic purification on silica gel.

Using the same conditions optimized so far, the reaction delivered product **33a** in 40% yield (Table 2.4, entry 1). We then evaluated if a modulation in the equivalents of γ -terpinene could impact the yield of the reaction. Using two equivalents of hydrogen donor proved optimal, increasing the yield of **33a** up to 60% (entries 2 and 3). Reducing the temperature was detrimental for reactivity (entry 4). Finally, control experiments showed that catalyst **C** and light were essential for the reaction to proceed (entries 5 and 6).

2.7.2 Reaction scope

With the optimized conditions for both the intramolecular (Table 2.3, entry 8) and the intermolecular variant (Table 2.2, entry 2), we evaluated the generality of the process.

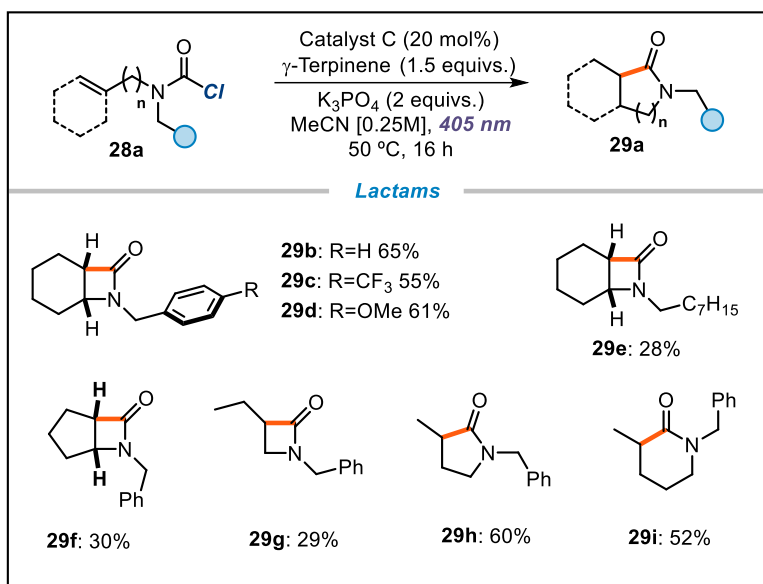


Figure 2.17. Scope of the intramolecular radical carbamoylation.

This methodology allowed the assembly of different substituted β -lactams (Figure 2.17). Both electron withdrawing and electron donating groups are tolerated on the pendant *N*-benzylic moiety, generating cyclohexane-fused β -lactams with good yields (products **29b**, **29c** and **29d**). It is also possible to install an aliphatic chain, albeit with some erosion in yield (adduct **29e**). This methodology allowed also the synthesis of cyclopentane-fused lactams (**29f**) and aliphatic α -branched lactams, albeit with less efficiency (**29g**). We also showed that γ - and δ -lactam backbones can be easily assembled with good to moderate yield (**29h** and **29i**).

Next, the scope of the intermolecular variant was assessed. Three dimethylamides derivatives could be prepared easily with good efficiency using different radical traps (products **33a**, **33b**, **33c**). To showcase the utility of the process, we assembled the Weinreb amide⁷⁵ derivative **33d** with an unconventional disconnection. Several carbocycles could be embedded on the amide side, bearing oxygen, sulfur and nitrogen moieties (adducts **33e**, **33f**, **33g**) or halogen atoms (**33h**, **33i**). We were pleased to find that the incorporation of a proline-derived backbone was tolerated in the product with no noticeable erosion in yield (**33j**). Additionally, our

⁷⁵ Nahm, S.; Weinreb, S. M. *N*-methoxy-*N*-methylamides as effective acylating agents. *Tetrahedron Lett.*, **1981**, 22, 3815-3818.

protocol allowed the late-stage derivatization of biologically-active *Paroxetine* scaffold (**33k**), albeit with moderate yield, showing an overall good functional group compatibility.

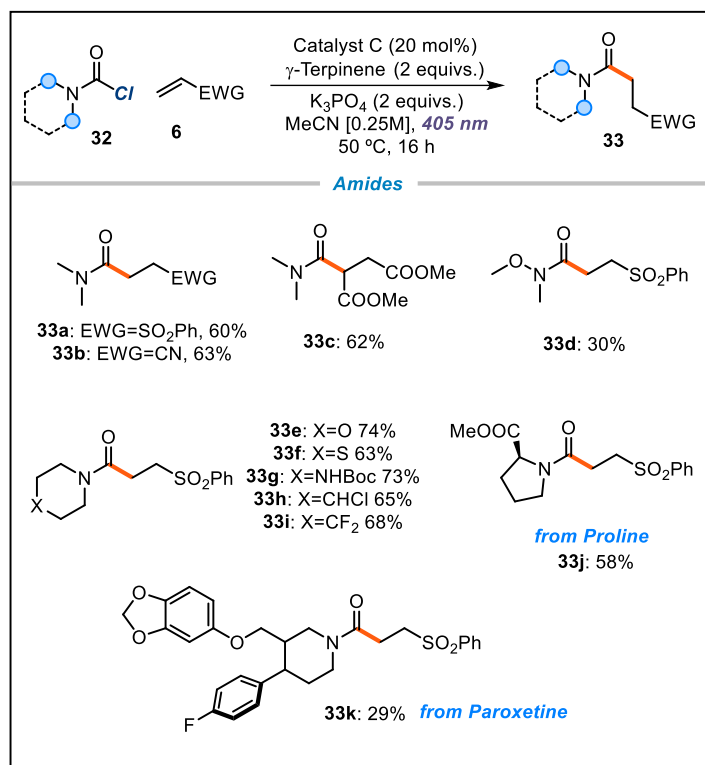


Figure 2.18. Scope of the intermolecular radical carbamoylation.

2.7.3 Generation of acyl radicals⁷⁶

The mechanistic blueprint of the radical carbamoylation was successfully extended to acyl derivatives, using redox-recalcitrant acyl chlorides and anhydrides as radical precursors.⁷⁷ In line with the carbamoyl radical generation mechanism described above, the catalytic intermediate **35** would be generated upon nucleophilic acyl substitution from our nucleophilic DTC catalyst **A**. The photon-absorbing intermediate **35** would, upon visible light excitation, fragment to deliver the acyl radical **XXI**, which would then be intercepted by an electron-poor olefin in a Giese-type addition. A HAT process from γ -terpinene, followed by SET, would reduce the ensuing radical **XXII** while regenerating the catalyst.

⁷⁶ This part of the publication was entirely conducted by Eduardo de Pedro Beato.

⁷⁷ For the redox potentials of Acyl chlorides and anhydrides see: Occhialini, D.; Daasbjerg, K.; Lund, H. Estimation of reduction and standard potentials of acyl radicals. *Acta Chem. Scand.* **1993**, *47*, 1100.

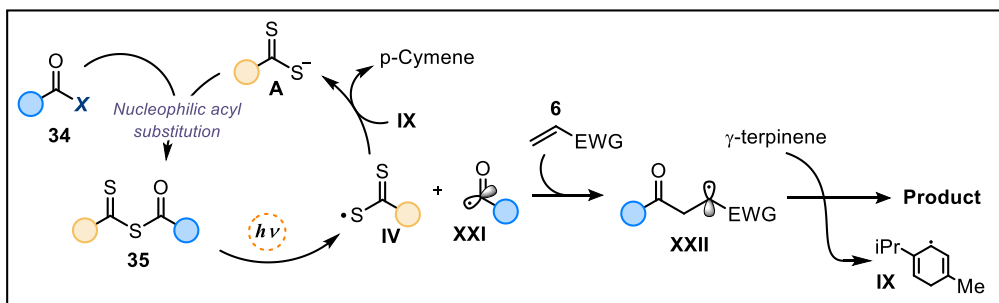


Figure 2.19. Blueprint for the intermolecular radical acylation.

To optimize this reaction, we started from the best conditions of the carbamoylation protocol. Since the catalytic intermediates deriving from acyl chlorides are yellow compounds, a blue light (using a 456 nm lamp) was sufficient for their effective excitation. After turning the solvent and the basic additive to DCM and K_3PO_4 , the effect of the DTC catalyst was evaluated (Table 2.5).

Table 2.5. Optimization of the intermolecular process

catalysts used in this study

catalyst A

catalyst C

catalyst D

entry	catalyst	deviation	yield 35a (%) ^a
1	A	none	7
2	D	none	83 (82) ^b
3	C · 3 H ₂ O	none	34
4	C	none	86
5	D	40 °C	40
6	D	under air	60
7	D	no light	0
8	none	none	0

Reactions performed on a 0.5 mmol scale at 60 °C for 16 h using 2.0 mL of DCM under illumination by a blue LED strip ($\lambda_{\text{max}} = 465 \text{ nm}$, 14 W) and using catalyst (10 mol%), 1.5 equiv. of **35a**, and 2 equiv. of Na_3PO_4 . ^aYield determined by ¹H NMR analysis of the crude mixture using trichloroethylene as the internal standard. ^bYield of the isolated product **35a**. LED: Light-emitting diode.

The 5-bromoindole DTC catalyst **A** showed poor efficiency, while the commercially available ethyl xanthogenate **D** showed excellent results delivering product **35a** in 82% yield (entry 2). While catalyst **C** trihydrate showed a lowered efficiency, the analogous anhydrous form offered an increased performance (entries 3 and 4). Since the latter is not commercially available, we decided to use catalyst **D** to perform further the optimization. The effect of the temperature showed to be of paramount importance, since decreasing the temperature from 60 to 40 °C clearly affected the reaction efficiency (entry 5). While the presence of air marginally reduced the yield (entry 6), control experiments showed that the action of the catalyst and the light is essential for reactivity (entries 7 and 8).

We then evaluated the use of anhydrides **36a** as acyl donors, instead of chloride **34a**. Using **36a** under the optimized conditions (table 2.5, entry 2), the reaction delivered the same product **35a** in 50% yield (Figure 2.20a). To increase the reactivity, we used different precursors, including the unsymmetrical anhydride **37a**, which can be prepared in one step from commercially available benzoic acid and ethyl chloroformate (Figure 2.20b). After simple filtration, anhydride **37a** was subjected to the reaction conditions; under these conditions, we could avoid the addition of sodium phosphate since the counteranion derived from the nucleophilic substitution could act as a base. We were pleased to find that this telescoped procedure produced the target product **35a** in 71% yield.

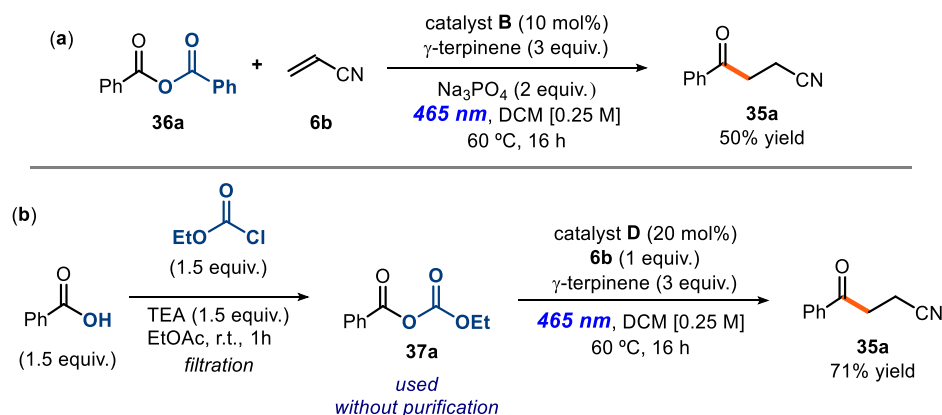


Figure 2.20. (a) Using an anhydride as the radical precursor. (b) Development of a telescoped procedure starting from the corresponding carboxylic acid

Inspired by the efficiency of this procedure, a similar protocol was developed to generate the acyl chloride *in situ* from the corresponding carboxylic acid (Figure 2.21). By treating the carboxylic acid with oxalyl chloride in the presence of substoichiometric amount of DMF, we could form the acyl chloride. Upon simple addition of the remaining reaction components, we could achieve an analogous reactivity as when using the preformed acyl chloride.

In situ formation of acyl chlorides

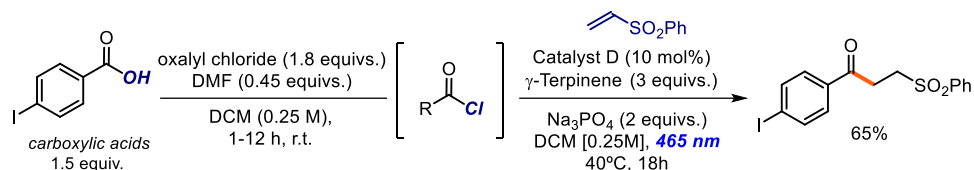
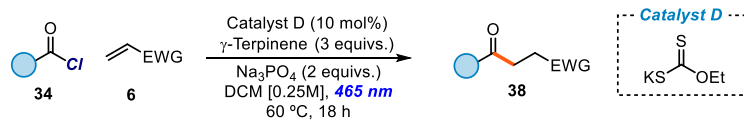
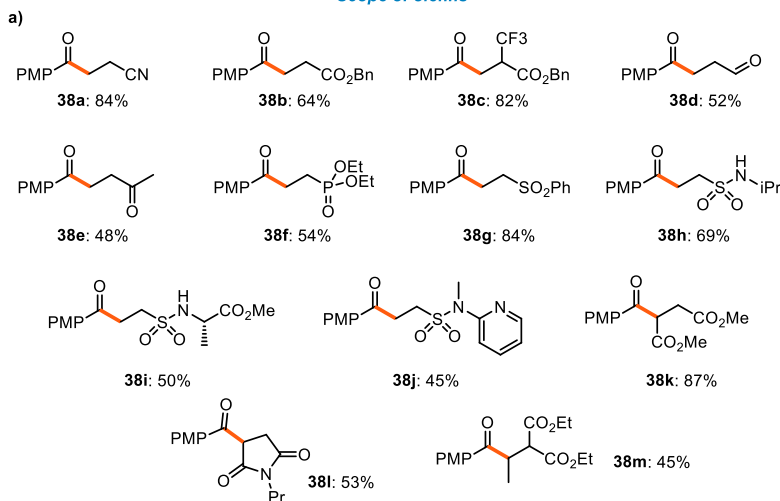


Figure 2.21. Protocol for the *in situ* formation of acyl chlorides starting from the corresponding carboxylic acid.

We focused on the evaluation of the reaction generality, subjecting a variety of electron-poor olefins to the optimized conditions (Figure 2.22a). The scope of the radical trap was quite broad: nitrile (product **38a**), ester (**38b** and **38c**), ketone (**38e**), sulfonate (**38f**) and phosphonate (**38g**) functionalities could be installed with good to moderate yields.



Scope of olefins



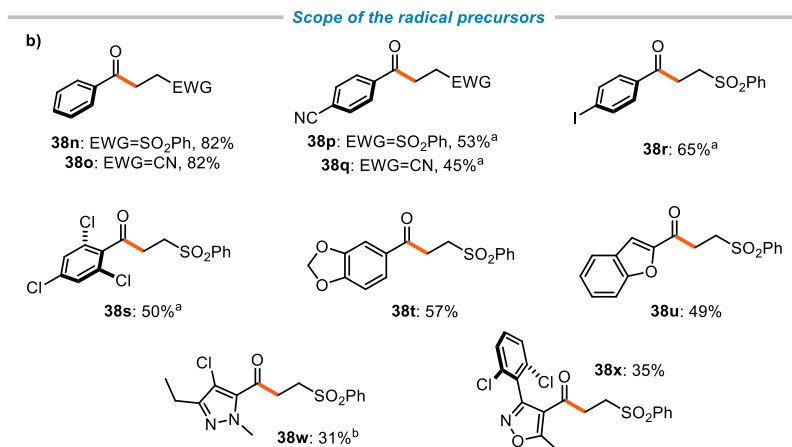


Figure 2.22. Photochemical catalytic generation of acyl radicals from the chloride precursors and their use in intermolecular Giese addition processes. Reaction performed on 0.5 mmol scale using 1.5 equivs of **34**
^aReaction time: 60 h. ^bAcyl chloride prepared from the acid and used without further purification, 20 mol% cataly. (a) Olefins **6** and (b) aroyl chlorides suitable for the process.

Importantly, an enal, which bears a labile aldehydic C-H bond, could also be used as radical trap (**38d**), showcasing the orthogonality of this acyl radical generation system with respect to a HAT-based process. Different sulfonamides were also tolerated, albeit with slightly diminished yields (adducts **38h**, **38i**, **38j**). Finally, also internal (**38k**, **38m**) and cyclic (**38l**) olefins proved valuable reaction partners. The flexibility of the aroyl radical precursor also showed to be quite broad (Figure 2.22b). Both electron-poor and electron-rich substituents could be installed on the benzene ring using different radical traps (**38n** – **38t**). Noteworthy, the presence of relatively complex heteroaromatic compounds, such as pyrazole and isoxazole, was tolerated well, as showcased by products **38w** and **38x**.

To expand the synthetic utility of the protocol, we tested aliphatic acyl chlorides (and anhydrides). The generation of aliphatic acyl radicals is historically hampered by the parasitic decarbonylation process which leads to the formation of the corresponding C(sp³)-centered radicals.⁷⁸ To reach the desired reactivity and reduce the amount of a decarbonylative fragmentation process, the reaction temperature was lowered to 40 °C. Several aliphatic acyl radicals reacted smoothly under these reaction conditions (Figure 2.23). Both linear (products **40a**, **40b**, **40c**, **40d**), branched (**40e**, **40f**), (hetero)cyclic (**40g**, **40h**, **40i**, **40l**, **40o**, **40p**, **40q**) and fluorinated (**40m**, **40n**) aliphatic acyl derivatives reacted smoothly with a wide array of electron-deficient olefins. Interestingly, the presence of heteroatoms was not a problem even when primary alkyl chlorides, which are prone to competitive S_N2 reaction, were embedded

⁷⁸ (a) Fisher, H.; Paul, H. Rate constants for some prototype radical reactions in liquids by kinetic electron spin resonance. *Acc. Chem. Res.* **1987**, *20*, 200-206. (b) Vollenweider, J.-K.; Paul, H. On the rates of decarbonylation of hydroxyacetyl and other acyl radicals. *Int. J. Chem. Kinet.* **1986**, *18*, 791-800.

in the scaffold (**40d**). Sterically demanding acyl radicals could also be efficiently installed in the product skeleton (adducts **40s**, **40t**, **40u**). Functionalization of *dehydrocholic acid* through a telescoped one-pot procedure showcased the possible late-stage functionalization of steroidal scaffolds (**40v**). Finally, the scalability of the process was illustrated by the facile synthesis of unsymmetrical ketone **40w** (1.14 grams) starting from simple and commercially available cyclohexane carboxylic acid.

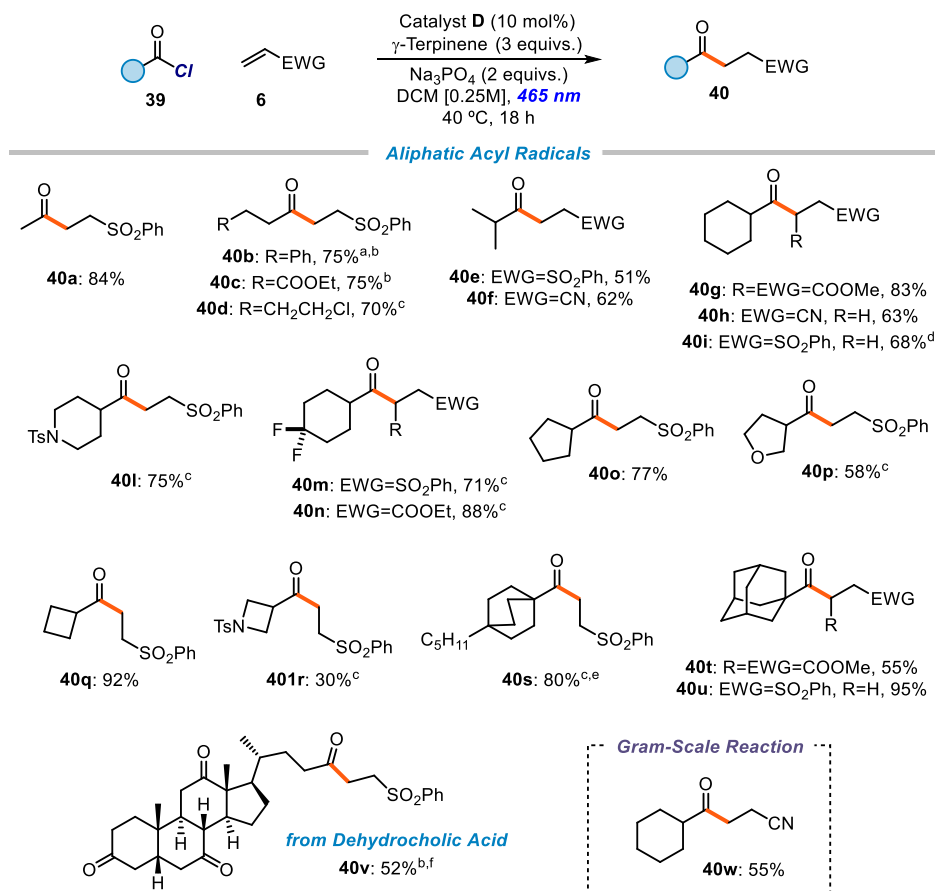


Figure 2.23. Table of aliphatic substrates. Reaction performed on 0.5 mmol scale using 1.5 equivs of **39**.
^aReaction time: 60 h. ^bReaction temperature: 60 °C. ^cAcid chloride prepared from the acid and used without further purification, 20 mol% catalyst. ^dProduct isolated as a 6:1 mixture with the olefin substrate, the corrected yield is reported. ^eYield measured by ¹H NMR analysis using trichloroethylene as the internal standard. ^fMixed anhydride prepared from the acid and used without further purification, 20 mol% catalyst.

2.8 Mechanistic investigations

The mechanistic picture of this transformation was based on the blueprint developed during our group's previous investigation on the catalytic DTC chemistry (Chapter 2.4). A simplified version of the catalytic cycle (Figure 2.24) involved four basic steps: 1) the nucleophilic acyl substitution of the substrate by the DTC catalyst; 2) photolysis of the ensuing catalytic intermediate **30**; 3) trapping of the resulting acyl radical **XI** and subsequent formation of the product; and 4) turnover of the catalyst by reduction of the S-centered radical **VI**. Importantly, the turnover event, which in our initial proposal involved a SET event between two fleeting radicals (Figure 2.16), is an unlikely scenario and needs therefore a deeper understanding.

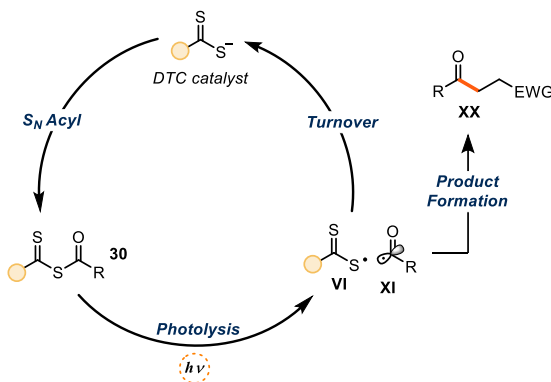


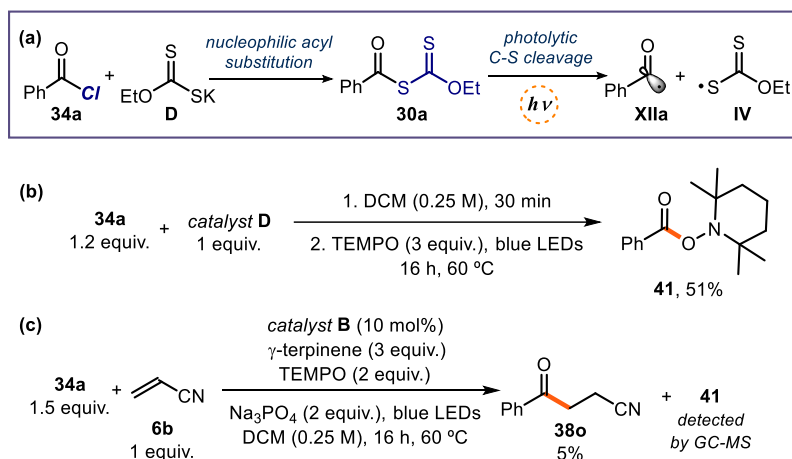
Figure 2.24. simplistic version of the mechanism

To get a better insight on the catalytic cycle and on the intermediates involved in this transformation, we decided to deconstruct the general catalytic cycle and characterize the key intermediates accountable for the reactivity. For this purpose, we selected the reaction between benzoyl chloride and acrylonitrile catalyzed by catalyst **D**.

2.8.1 Generation and photolysis of the catalytic xanthyl anhydride

We began our investigation by characterizing the active intermediate responsible of the generation of the radical (Figure 2.25a). We therefore synthesized intermediate **30a** by reacting aroyl chloride **34a** with stoichiometric amount of catalyst **D**. To prove that this intermediate (which appears as a yellow solid) could undergo direct photolysis, we submitted **30a** to blue LEDs irradiation in the presence of TEMPO as radical scavenger (Figure 2.25b). The TEMPO-trapped acyl radical adduct **41** was formed in 51% yield. Moreover, when TEMPO was added to our model reaction, the formation of the product was almost totally suppressed, while GC-MS analysis showed the presence of **41** in the reaction crude (Figure 2.25c).

The same experiments were additionally performed also for the carbamoyl radical using dimethylamino carbamoyl chloride and catalyst **D**, achieving similar results (see experimental section 3.9.10).



Scheme 2.25. The possible role of the acylxanthate **30a**. Mechanistic experiments to probe that a) **30a** is an active reaction intermediate; b) the benzoyl radical **XIIa** is generated during the process; and c) the model reaction is inhibited by a radical scavenger.

To prove and characterize the nature of the radicals originated from the photolysis of intermediate **30a**, we performed laser flash photolysis (LFP) and electron paramagnetic resonance (EPR) studies (Figure 2.26 left and right respectively). Previous LFP studies showed that the xanthyl radical displays a characteristic absorption band centered with a maximum at 620 nm.⁷⁹ When we subjected a sample of **30a** to a laser beam centered at 355 nm, we were pleased to observe the formation of a transient absorption band at 620 nm with a lifetime in the order of 0.1 ms, which is consistent with the reported spectra for the xanthyl radical **IV**. To further corroborate the generation of the xanthyl radical in our reaction conditions, we subjected intermediate **30a** to a 460 nm laser beam (the light used in our experiments), achieving similar results (See experimental section).

⁷⁹ Kaga, A.; Wu, X.; Lim, J. Y. J.; Hayashi, H.; Lu, Y.; Yeow E. K. L.; Chiba, S. Degenerative Xanthate Transfer to Olefins Under Visible-Light Photocatalysis. *Beilstein J. Org. Chem.* **2018**, *14*, 3047-3058.

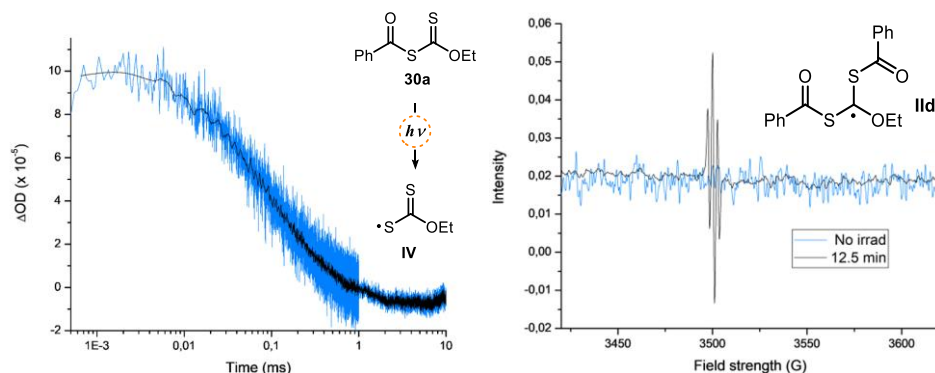


Figure 2.26. *left:* Absorption at 620 nm of the transient xanthyl radical **IVd** (blue line) generated upon 355 nm laser excitation of **30a** ($[30a]_0 = 3.00$ mM in MeCN). Note the logarithmic scale for time. Absorption decay (black line) processed through Savinsky Golay filter to facilitate lifetime measurement. ΔOD : optical density variation. *right:* EPR spectrum generated from **30a** ($[30a]_0 = 0.1$ M in toluene) at 298 K after 12.5 minutes (black line) of light irradiation by a 100 W mercury lamp.

We were also intrigued by the possibility to characterize the acyl radical produced from the photolysis of intermediate **30a**. We therefore analyzed a solution of **30a** in toluene by EPR spectroscopy under mercury lamp irradiation. Interestingly, the result was not coherent with the expected acyl radical spectrum, which should feature a singlet.⁸⁰ The sharp triplet that we observed was instead consistent with a more stabilized carbon-centered radical of type **II d** (Figure 2.26 right) which lies in proximity of two sulfur atoms and an ethoxy moiety.⁸¹ Reminiscent of the addition-fragmentation mechanism (Figure 2.3, section 2.2) which stands at the base of the RAFT polymerizations processes, we reasoned that the formation of radical **II d** is consistent with the high tendency of xanthates of type **30a**, and related thiocarbonyl congeners, to trap radical intermediates. As in the group transfer based processes, this equilibrium controls the overall concentration of reactive radicals, therefore, radical **II d** acts as a dynamic radical reservoir, enhancing the effective lifetime of the acyl radical **XII a** in solution (Figure 2.27).

⁸⁰ Bieszczad, B.; Perego, L. A.; Melchiorre, P. Photochemical C-H Hydroxyalkylation of Quinolines and Isoquinolines. *Angew. Chem. Int. Ed.* **2019**, *58*, 16878-16883.

⁸¹ Hawthorne, D. G.; Moad, G.; Rizzardo, E.; Thang, S. H. Living Radical Polymerization with Reversible Addition- Fragmentation Chain Transfer (RAFT): Direct ESR Observation of Intermediate Radicals. *Macromolecules* **1999**, *32*, 5457-5459.

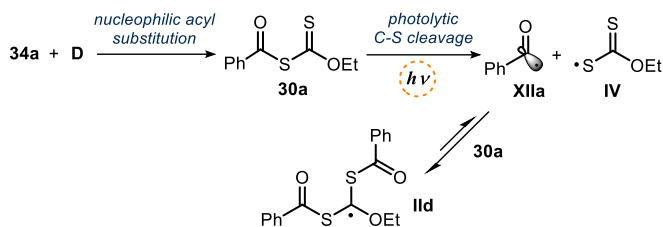


Figure 2.27. The reaction of the acyl radical **XIIa** with its precursor **30a** is reversible and imparts an increased lifetime to **XIIa**.

2.8.2 Fate and behavior of the xanthyl radical

One of the main mechanistic aspects to elucidate to the fate of the xanthyl radical and the related turnover event which, based on our original proposal, would require a SET between two fleeting radical species. During a previous investigation,^{22c} our group detected the formation of dimer **42a** which arises from the dimerization of the xanthyl radical **IVa**. Previous studies on the BDEs of such compounds revealed that the sulfur-sulfur bond is quite labile, showing that is actually possible to break this bond using simple light irradiation.⁸² We questioned whether this dimeric form of the catalyst could be catalytically competent in our photocatalytic process.

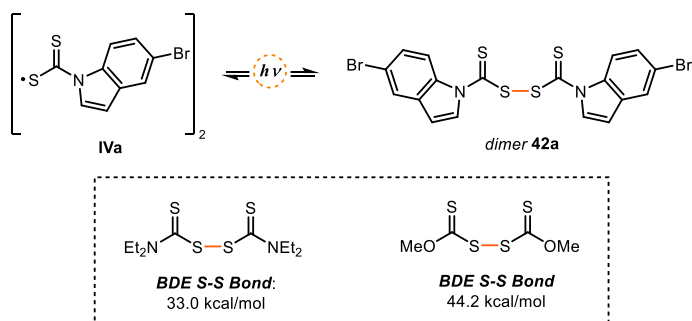


Figure 2.28. Dimerization of sulfur-centered radical **IVa** and photolysis equilibrium.

⁸² Degirmenci, I.; Coote, M. L. Effect of Substituents on the Stability of Sulfur-Centered Radicals. *J. Phys. Chem. A* **2016**, *120*, 7398-7403.

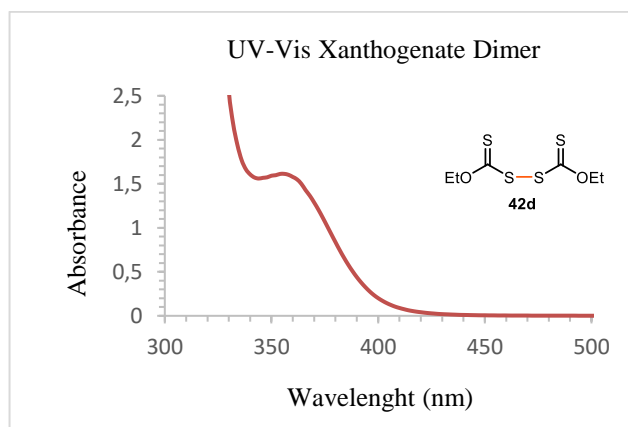


Figure 2.29. UV-Vis absorption of the dimer **42d** in MeCN (20 mM).

By synthesizing an authentic sample of the dimer **42a** from catalyst **D**, we confirmed that **42a** could actually absorb visible light up to 450 nm (Figure 2.29). Next, we evaluated the catalytic activity of dimer **42d** in the reaction with the acyl chloride (Figure 2.30). We could indeed detect product formation in good yields. These results are very informative of the reaction mechanism, since they imply that dimer **VIIa** is a photoactive species in equilibrium with the progenitor xanthyl radical **IIIa**. This dynamic equilibrium increases the lifetime of the xanthyl radical which can therefore be regarded as a persistent radical.

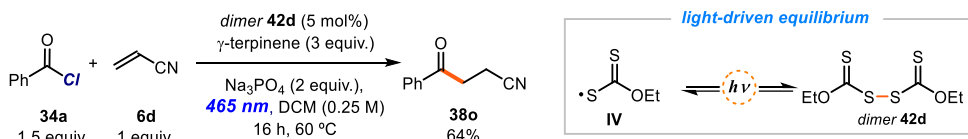


Figure 2.30. Model reaction catalyzed by dimer **42d** and the light-driven equilibrium between the xanthyl radical **IVd** and the dimer.

Overall, based on these experiments and on previous studies on persistent radical,⁸³ we believe that the proposed SET between the xanthyl radical and the cyclohexadienyl radical can be a reasonable turnover event. To further corroborate this proposal and clarify the possible turnover of the catalyst, we designed the experiment shown in Figure 2.31.

⁸³ Leifert, D.; Studer, A The persistent radical effect in organic synthesis. *Angew. Chem. Int. Ed.* **2020**, *59*, 74-108.

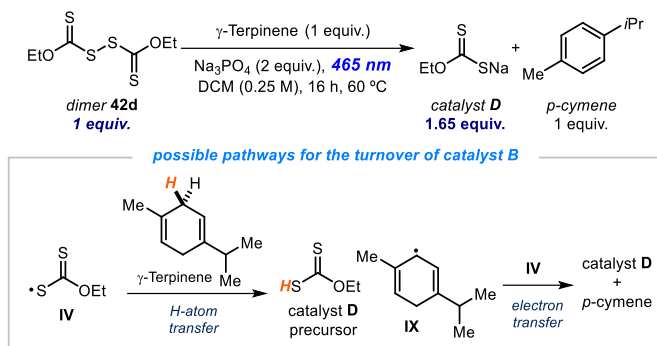


Figure 2.31. Experiment that probes the ability of γ -terpinene to reduce the xanthyl radical **IVd** via both a HAT and a SET manifold.

Exposing a solution of dimer **42d** and γ -terpinene (1:1 ratio) to blue light irradiation, we found that 1.65 equivalents of catalyst salt **D** were formed. This result provides compelling evidence to rationalize the mechanism of turnover of catalyst **D**. Importantly, considering the stoichiometry of the reaction in Scheme 3, it appears that γ -terpinene can provide two different pathways to reduce the xanthyl radical **IIIa**, namely an HAT process followed by an SET reduction from the ensuing cyclohexadienyl-type radical **V**.

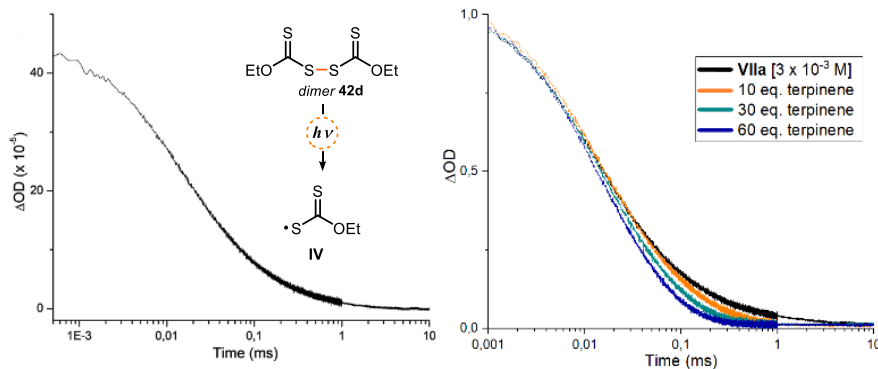


Figure 2.32. a) Absorption at 620 nm of the transient xanthyl radical **IV** generated upon 355 nm laser excitation of dimer **42d** ($[42d]_0 = 3 \times 10^{-3}$ M in acetonitrile). b) Decrease of the lifetime of **IV** upon addition of γ -terpinene. Note logarithmic scale for time; Δ OD: optical density variation. Absorption decays (orange, green, and blue lines) observed in the presence of increasing amounts of γ -terpinene. *Green line*: ratio **42d**/ γ -terpinene mimics the reaction conditions. Δ OD: optical density variation.

To further prove the generation of the xanthyl radical **IV** from the dimer **42d**, we subjected the dimer **42d** to LFP analysis using a laser beam centered at 355 nm. The transient observed is identical to the one achieved by exposition of the acylxanthate **30a** to the same analysis (Section 2.8.1), proving that the xanthyl radical **IV** is generated also from the photolysis of

the dimer **42d**. By adding increasing amounts γ -terpinene, we observed a decay of the lifetime of the xanthyl radical, which proves the interaction between the two species.

To highlight the direct correlation between the xanthate anion, its dimer, and the corresponding xanthyl radical, we performed cyclic voltammetry experiments. We started subjecting catalysts **D** to different electrochemical scans. When an increasingly reducing potential was applied to a solution of **D** (0 to -2.0 V Figure 2.33, left) no peak appeared, confirming that the xanthate anion could not undergo reduction. On the other hand, during the reversed scan (-2.0 to +1.5 V) an irreversible anodic peak appeared ($E_p^A = E_{ox} = 0.73$ V in CH_3CN vs Ag/AgCl). The latter can be ascribed to the oxidation of the xanthate catalyst **D** to form the xanthyl radical **IV** (orange dot). We then electrochemically analyzed catalyst **D** in the opposite order (Figure 2.33, right). As expected, during oxidation (0 to +2.0 V), we observed the same signal as in the previous experiment, which is congruent with the formation of radical **IV** upon SET oxidation of **D**. Noteworthy, following the ramp toward reductive potentials, we could observe the appearance of a second peak ($E_p^C = E_{red} = -1.40$ V in CH_3CN vs Ag/AgCl , blue dot) consonant with a reduction event.

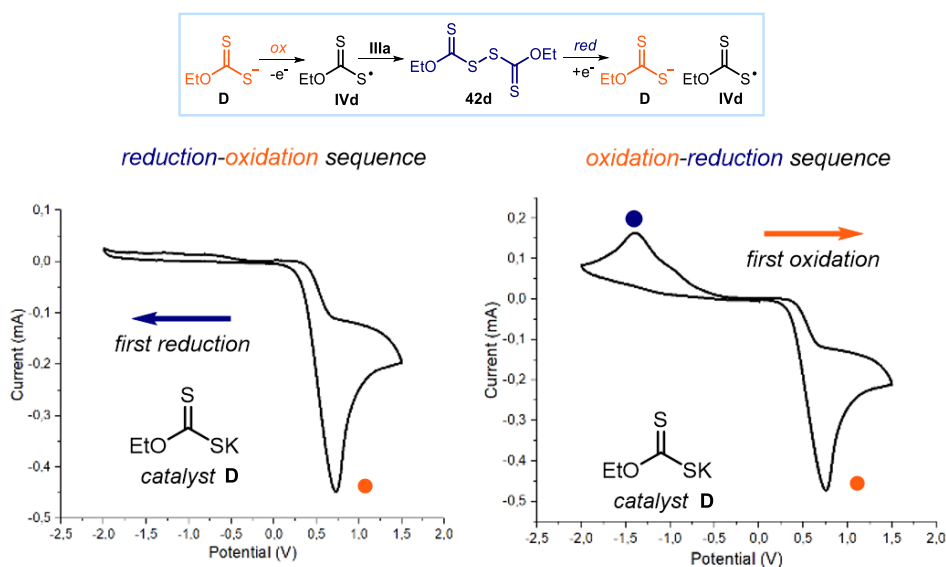


Figure 2.33. Cyclovoltammetric studies of catalyst **D** [0.02 M] in [0.1 M] TBAPF_6 in CH_3CN : reduction-oxidation scan sequence; oxidation-reduction scan sequence. The xanthyl radical **IVd**, which can be formed by SET reduction of **42d** and oxidation of **D**, is the link between catalyst **D** and dimer **42d**.

These results can be rationalized based on a fast dimerization of radical **IV**, generated during the forward oxidation scan, that forms dimer **42d**, which is prone to SET reduction. This proposal is consonant with the following observation: 1) the formation of the stable dimer makes the oxidation of catalyst **D** irreversible, since **IV** is rapidly sequestered in the form of

its dimer; 2) it is only in the cyclic voltammetric analysis that starts with oxidation that a reduction peak appears, which is ascribable to the reduction of dimer **42a**: this is because the dimer first requires the oxidation of catalyst **D** to be generated (Figure 2.33).

To confirm our mechanistic scenario, we reasoned that we should see the same reductive event when dimer **42d** is subjected to a similar electrochemical scan (Figure 2.34). When an original sample of dimer was subjected to an oxidation-reduction sequence, we didn't observe any peak during the application of positive potentials, while we could detect the previously observed peak during the reduction (blue dot, reduction of the dimer). Finally, we subjected **42d** to the reversed sequence. As expected, after applying a negative current to reduce the dimer, a second peak appeared during the positive scan ($E_p^A = E_{ox} = 0.53$ V in CH_3CN vs Ag/AgCl). This peak is consistent with the one previously detected (orange dot in Figure 2.33), and can be explained with the oxidation of the anion generated by the reduction of the dimer.

Collectively, these experiments highlight the redox properties of the catalyst and the subtle redox interplay between the three forms of the catalyst: the monomer, the dimer, and the xanthyl radical which can be regarded as the linking point between the latter.

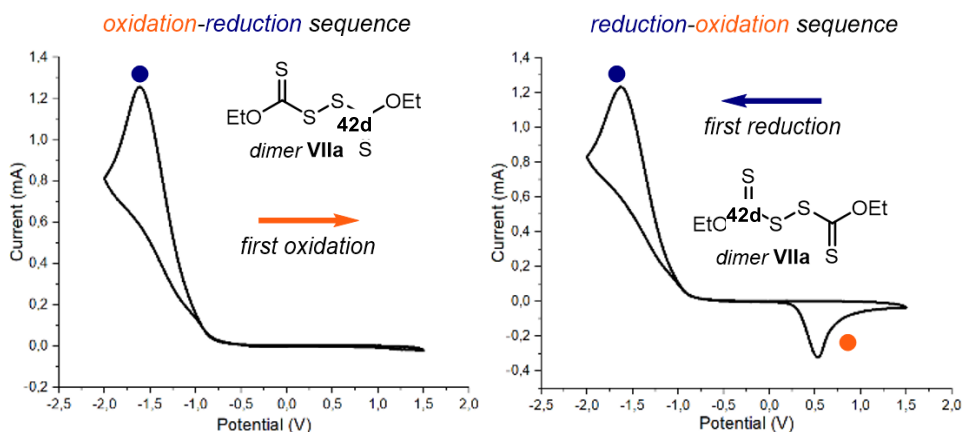


Figure 2.34. Cyclic voltammetric studies of dimer **42d** [0.02 M] in [0.1 M] TBAPF₆ in CH_3CN : oxidation-reduction scan sequence; reduction-oxidation scan sequence. Sweep rate: 500 mV/s. Pt electrode working electrode, Ag/AgCl (KCl 3.5 M) reference electrode, Pt wire auxiliary electrode.

2.8.3 Radical trap and ensuing process

The studies conducted so far allowed us to elucidate the generation of the radical and the possible turnover events of the catalyst. We then focused on the radical trapping process and the possibility of a group transfer manifold within our catalytic cycle (Figure 2.35).

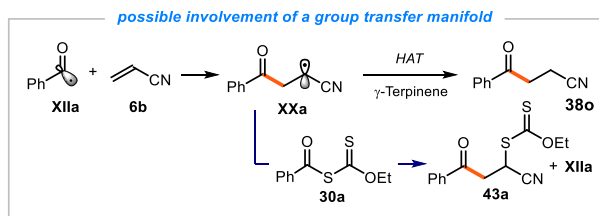


Figure 2.35. Focusing on the radical addition step and the ensuing product formation

A first experiment using a stoichiometric amount of catalyst **D** without γ -terpinene showed that the group transfer product is indeed formed under our reaction conditions in 35% yield (Figure 2.36a), while the Giese-type product could not be found, highlighting the importance of γ -terpinene in our catalytic cycle. On the other hand, under identical conditions but adding γ -terpinene (Figure 2.36b), the formation of group transfer product was suppressed, while the product **38o** was isolated in 23% yield. Interestingly, an increased amount of catalyst correlates with a decreased amount of product. This is probably because intermediate **30a**, which is now in higher amount, can also act as competitive radical trap, highjacking the acyl radical and lowering the efficiency of the Giese-type pathway. Finally, we decided to corroborate the presence of a group transfer manifold in our catalytic cycle and its direct evolution to the product by a possible light driven homolysis. Subjecting an original sample of group transfer product **43a** under standard conditions in the absence of the catalyst, afforded product **38o** in 35% yield (Figure 2.36c). Albeit we never observed this group transfer product under our catalytic conditions, this experiment shows that it might serve as an additional stabilizing out-of-cycle equilibrium.

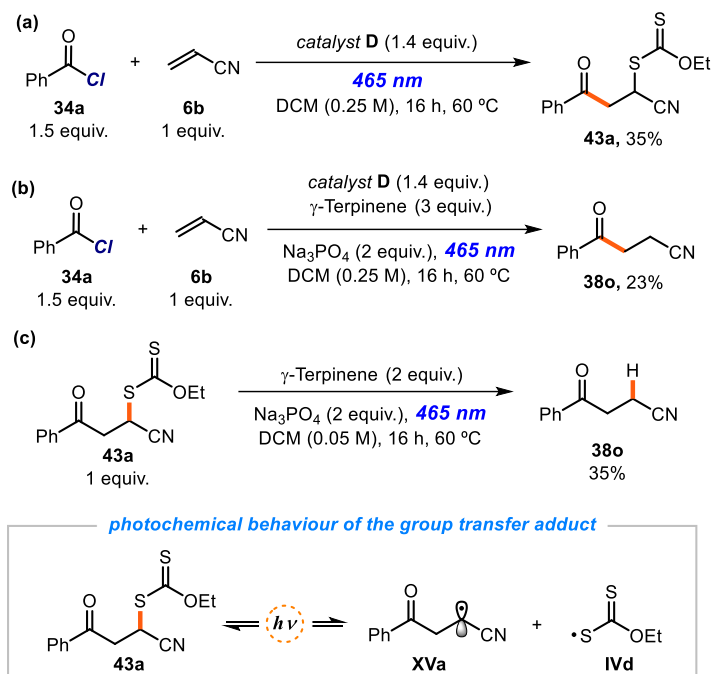


Figure 2.36. The model reaction in the presence of a stoichiometric amount of **B** and a) in the absence or b) in the presence of γ -terpinene (group transfer conditions). c) The behavior of group transfer product **43a** under the reaction conditions and upon blue light irradiation.

2.8.4 Overall catalytic cycle

These studies allowed us to uncover a mechanism more complex than originally thought (and discussed above). The real mechanistic picture (Figure 2.37) features different out-of-cycle equilibria which govern the catalytic cycle and are essential for stabilizing the open-shell intermediates and their concentration in solution. For example, the carbamoyl/acyl radical **XII** is subjected to a reversible addition-fragmentation equilibrium with **5a** leading to the stabilized radical **II**, which could be characterized through EPR experiments. The xanthyl radical ensuing from the homolysis is also involved in different processes, such as the light-driven dimerization equilibrium which lends a persistent character to **IV**. This finding clarified the possibility of a SET event between the two fleeting species **IV** and **IX** as a turnover event for the catalyst regeneration. Our studies also proved the existence of a photoactive group transfer product **43** which can also increase the lifetime of **XX** from which the product is generated.

Importantly, as corroborated by quantum yield experiments ($\phi = 0.034$, see the experimental section 2.10.6), a radical chain manifold ensuing from group transfer product or from SET between **XX** and **30**, is unlikely. The nucleophilicity of the DTC catalyst and the photocatalytic behaviour of **30** dictate the formation of every molecules of the product in a closed catalytic cycle.

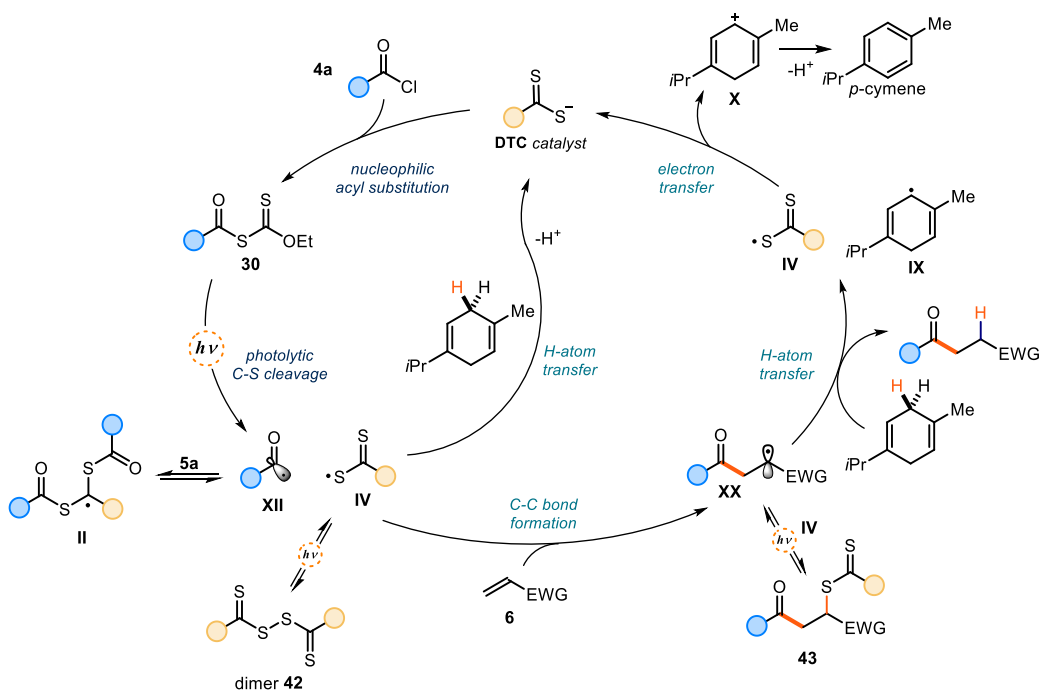


Figure 2.37. Detailed mechanistic picture including off-the-cycle equilibria

2.9 Conclusions

In summary, we exploited the DTC catalytic platform previously disclosed in our group to generate carbamoyl and acyl radicals from the corresponding chloride and anhydrides, substrates which are generally recalcitrant to SET manifolds. The protocol features mild conditions and broad generality towards a different array of radical traps and is scalable and operationally simple. Finally, a detailed mechanistic study was undertaken to elucidate the complex out-of-cycle equilibria, which govern the formation of the product and the turnover event for catalyst regeneration.

2.10 Experimental section

2.10.1 General information

The NMR spectra of the products and previously unreported starting materials are available in the published manuscript¹ and are not reported in the present dissertation.

The NMR spectra were recorded at 400 MHz and 500 MHz for ¹H and 100 or 125 MHz for ¹³C. The chemical shift (δ) for ¹H and ¹³C are given in ppm relative to residual signals of the solvents (CHCl₃ @ 7.26 ppm ¹H NMR and 77.16 ppm ¹³C NMR, and tetramethylsilane @ 0 ppm). Coupling constants are given in Hertz. The following abbreviations are used to indicate the multiplicity: s, singlet; d, doublet; q, quartet; m, multiplet; bs, broad signal; app, apparent. High resolution mass spectra (HRMS) were obtained from the ICIQ HRMS unit on MicroTOF Focus and Maxis Impact (Bruker Daltonics) with electrospray ionization. (ESI). UV-vis measurements were carried out on a Shimadzu UV-2401PC spectrophotometer equipped with photomultiplier detector, double beam optics and D₂ and W light sources or an Agilent Cary60 spectrophotometer. Emission spectra of light sources were recorded on Ocean Optics USB4000 fiber optic spectrometer. Yields of isolated compounds refer to materials of >95% purity as determined by ¹H NMR analysis.

General Procedures. All reactions were set up under an argon atmosphere in oven-dried glassware. Synthesis grade solvents were used as purchased, anhydrous solvents were taken from a commercial SPS solvent dispenser. Chromatographic purification of products was accomplished using forced-flow chromatography (FC) on silica gel (35-70 mesh). For thin layer chromatography (TLC) analysis throughout this work, Merck pre-coated TLC plates (silica gel 60 GF₂₅₄, 0.25 mm) were employed, using UV light as the visualizing agent and an acidic mixture of vanillin or basic aqueous potassium permanganate (KMnO₄) stain solutions, and heat as developing agents. Organic solutions were concentrated under reduced pressure on a Büchi rotatory evaporator.

Determination of Enantiomeric Purity. UPC² analysis on chiral stationary phase was performed on a Waters Acquity instrument using an ID3 chiral column. The exact conditions for the analyses are specified within the characterization section.

Materials. Most of the starting materials used in this study are commercial and were purchased in the highest purity available from Sigma-Aldrich, Fluka, Alfa Aesar, Fluorochem, and used as received, without further purifications.

The following substrates were synthesized according to reported procedures (Scheme 2.37).⁸⁴

⁸⁴ (a) Nyfeler, E.; Renaud, P. Decarboxylative Radical Azidation Using MPDOC and MMDOC Esters. *Org. Lett.* **2008**, *10*, 985-988. (b) Grainger, R. S.; Betou, M.; Male, L.; Pitak, M. B.; Coles, S. J. Semipinacol

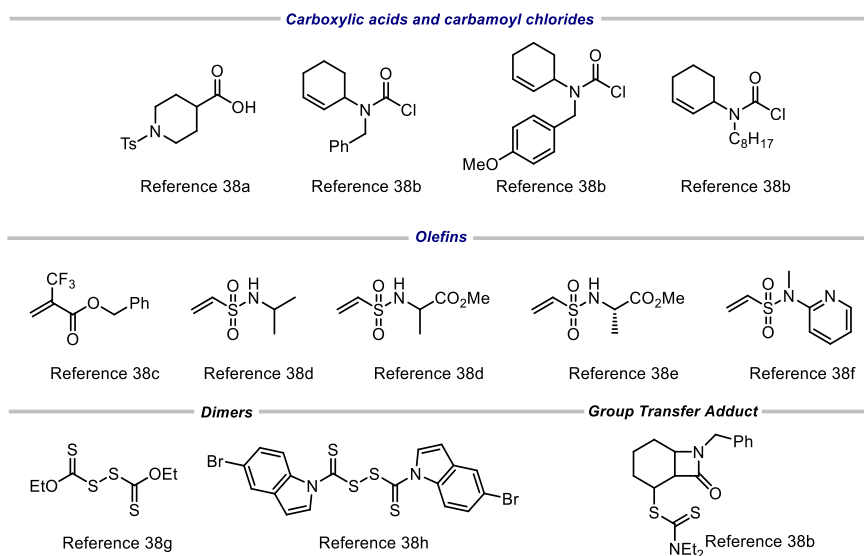
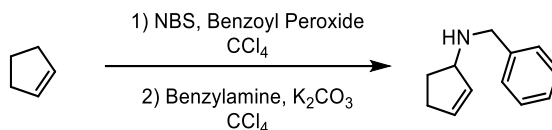


Figure 2.38. Starting materials synthesized according to known procedures.

2.10.2 Substrate synthesis

Synthesis of *N*-benzylcyclopent-2-en-1-amine:



A 2 M solution of cyclopentene (0.973 mL, 11 mmol) in CCl_4 (5.4 mL) was prepared and then *N*-bromosuccinimide (2.26 g, 10 mmol) and benzoic peroxyanhydride (36 mg, 0.15 mmol) were sequentially added. The solution was stirred at 40 °C for 4 hours, after which the reaction

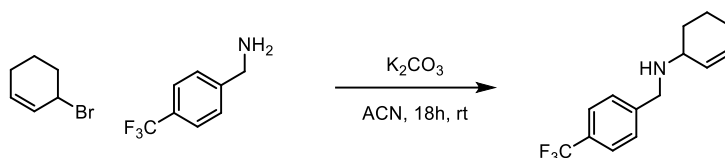
Rearrangement of Cis-Fused β -Lactam Diols into Keto-Bridged Bicyclic Lactams. *Org. Lett.* **2012**, *14*, 2234-2237. (c) Avenoz, A.; Busto, J. H.; Jiménez-Osés, G.; Peregrina, J. M. A Convenient Enantioselective Synthesis of (S)- α -Trifluoromethylisoserine. *J. Org. Chem.* **2005**, *70*, 5721-5724. (d) Wang, M.; Wang, Y.; Qi, X.; Xia, G.; Tong, K.; Tu, J.; Pittman, C. U.; Zhou, A. Selective Synthesis of Seven- and Eight-Membered Ring Sultams via Two Tandem Reaction Protocols from One Starting Material. *Org. Lett.* **2012**, *14*, 3700-3703. (e) Fenster, E.; Long, T. R.; Zang, Q.; Hill, D.; Neuenswander, B.; Lushington, G. H.; Zhou, A.; Santini, C.; Hanson, P. R. Automated Synthesis of a 184-Member Library of Thiadiazepan-1,1-dioxide-4-ones. *ACS Comb. Sci.* **2011**, *13*, 244-250. (f) Huang, R.; Li, Z.; Ren, P.; Chen, W.; Kuang, Y.; Chen, J.; Zhan, Y.; Chen, H.; Jiang, B. *N*-Phenyl-*N*-aceto-vinylsulfonamides as Efficient and Chemoselective Handles for *N*-Terminal Modification of Peptides and Proteins. *Eur. J. Org. Chem.* **2018**, *2018*, 829-836. (g) Jiang, S.; Li, Y.; Luo, X.; Huang, G.; Shao, Y.; Li, D.; Li, B. $\text{NH}_4\text{I}/\text{EtOCS}_2\text{K}$ promoted synthesis of substituted benzils from diphenylacetylene derivatives. *Tetrahedron Lett.* **2018**, *59*, 3249-3252.

was left at ambient temperature without stirring. After 2 hours, the floating materials were filtered off and washed with CCl_4 . The organic phase was then placed in a separatory funnel and washed with distilled water. The organic phase was collected, treated with MgSO_4 and subsequently filtered. At this stage, benzylamine (3.28 mL, 30 mmol) and K_2CO_3 (1.38 g, 10 mmol) were directly added to the solution. The reaction was stirred overnight at r.t and the resulting crude mixture was purified by silica gel chromatography (eluent: 9:1 hexane/AcOEt) to afford 234 mg of *N*-benzylcyclohex-2-en-1-amine (14% yield over 2 steps) as a yellow-orange oil.

$^1\text{H NMR}$ (400 MHz, CDCl_3) δ 7.39 – 7.24 (m, 5H), 5.89 (m, 2H), 3.93 (m, 1H), 3.84 (dd, J = 16.6, 12.9 Hz, 2H), 2.48 (m, 1H), 2.36 – 2.18 (m, 2H), 1.63 (m, 1H).

$^{13}\text{C NMR}$ (101 MHz, CDCl_3) δ 140.5, 133, 132.8, 128.4, 128.3, 126.9, 63.9, 51.8, 31.3, 30.8

Synthesis of *N*-(4-(trifluoromethyl)benzyl)cyclohex-2-en-1-amine:



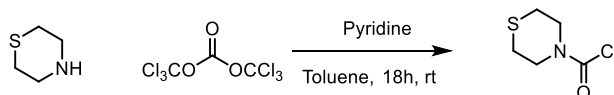
N-(4-(trifluoromethyl)benzyl)cyclohex-2-en-1-amine was prepared according to a reported procedure.^{38b} A solution of (4-(trifluoromethyl)phenyl)methanamine (1.314 g, 7.5 mmol) in CH_3CN (1.7 mL) was treated with 3-bromocyclohexene (0.288 mL, 2.5 mmol) and K_2CO_3 (346 mg, 2.5 mmol). After 2 hours at ambient temperature, the reaction mixture was quenched with H_2O (20 mL) and extracted with EtOAc (2 x 25 mL). The combined organic extracts were washed with brine (20 mL), dried over MgSO_4 , filtered, evaporated under reduced pressure, and purified by column chromatography (eluent: CH_2Cl_2 to $\text{CH}_2\text{Cl}_2/\text{EtOH}$ 9:1) to give the product (607 mg, 95 % yield) as a light-yellow oil.

$^1\text{H NMR}$ (400 MHz, CDCl_3) δ 7.57 (d, J = 8.1 Hz, 2H), 7.47 (d, J = 8.0 Hz, 2H), 5.82 – 5.76 (m, 1H), 5.75 – 5.62 (m, 1H), 3.90 (dd, J = 13.6, 3.3 Hz, 2H), 3.23 – 3.16 (m, 1H), 2.10 – 1.97 (m, 2H), 1.93 – 1.85 (m, 1H), 1.80 – 1.70 (m, 1H), 1.61 – 1.42 (m, 2H).

$^{13}\text{C NMR}$ (101 MHz, CDCl_3) δ 145.1, 129.8, 129.4, 129.3 (q, J = 32.7 Hz), 128.4, 125.4 (q, J = 3.7 Hz), 124.4 (q, J = 271.9 Hz), 52.6, 50.6, 29.6, 25.4, 20.3.

$^{19}\text{F NMR}$ (376 MHz, CDCl_3) δ -62.47.

Synthesis of thiomorpholine-4-carbonyl chloride:

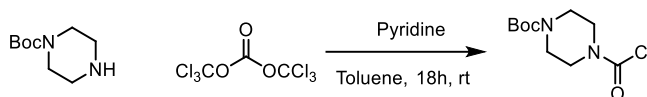


Thiomorpholine-4-carbonyl chloride was prepared according to a modification of a reported procedure.^{38b} To a solution of triphosgene (294 mg, 0.99 mmol) in toluene (15 mL) under N₂, pyridine (0.290 mL, 3.60 mmol) and subsequently a solution of thiomorpholine (310 mg, 3 mmol) in toluene (5 mL) were added. The reaction mixture was stirred for 18 hours at ambient temperature, quenched with NH₄Cl (20 mL of a saturated aq. solution) and extracted with Et₂O (2 x 30 mL). The combined organic extracts were washed sequentially with HCl (40 mL of a 0.25 M aq. solution), H₂O (40 mL) and brine (40 mL), dried over MgSO₄, filtered and evaporated under reduced pressure to afford Thiomorpholine-4-carbonyl chloride (310 mg, 75% yield) as a colorless oil.

¹H NMR (400 MHz, CDCl₃) δ 3.94 (dt, *J* = 38.9, 5.1 Hz, 1H), 2.72 – 2.64 (m, 1H).

¹³C NMR (101 MHz, CDCl₃) δ 148.5, 51.7, 49.3, 27.7, 27.3

Synthesis of tert-butyl 4-(chlorocarbonyl)piperazine-1-carboxylate:



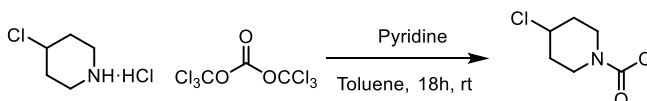
Tert-butyl 4-(chlorocarbonyl)piperazine-1-carboxylate was prepared according to a modification of a reported procedure.^{38b} To a solution of triphosgene (294 mg, 0.99 mmol) in toluene (15 mL) under N₂, pyridine (0.290 mL, 3.60 mmol) and subsequently a solution of *N*-Boc Piperazine (559 mg, 3 mmol) in toluene (5 mL) were sequentially added. The reaction mixture was stirred for 18 hours at ambient temperature, quenched with NH₄Cl (20 mL of a saturated aq. solution) and extracted with Et₂O (2 x 30 mL). The combined organic extracts were washed sequentially with HCl (40 mL of a 0.25 M aq. solution), H₂O (40 mL) and brine (40 mL), dried over MgSO₄, filtered and evaporated under reduced pressure to give Tert-butyl 4-(chlorocarbonyl)piperazine-1-carboxylate (597 mg, 82% yield) as a colorless oil.

¹H NMR (300 MHz, CDCl₃) δ 3.64 (m, 4H), 3.48 (d, *J* = 4.8 Hz, 4H), 1.46 (s, 9H).

¹³C NMR (101 MHz, CDCl₃) δ 154.3, 148.5, 80.7, 48.5, 46, 28.3.

HRMS (ESI pos): calculated for C₁₀H₁₇ClNaN₂O₃ (M+Na⁺): 271.0800, found: 271.0818.

Synthesis of 4-chloropiperidine-1-carbonyl chloride:



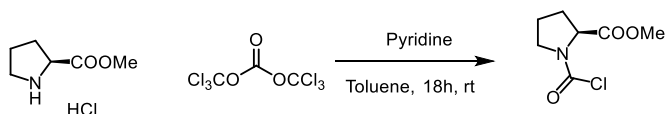
4-chloropiperidine-1-carbonyl chloride was prepared according to a modification of a reported procedure.^{38b} To a solution of triphosgene (259 mg, 0.872 mmol) in toluene (15 mL) under N₂, pyridine (0.498 mL, 6.15 mmol) and subsequently a solution of 4-chloropiperidine

hydrochloride (400 mg, 2.56 mmol) in toluene (5 mL) were sequentially added. The reaction mixture was stirred for 18 hours at ambient temperature, quenched with NH₄Cl (20 mL of a saturated aq. solution) and extracted with Et₂O (2 x 30 mL). The combined organic extracts were washed sequentially with HCl (40 mL of a 0.25 M aq. solution), H₂O (40 mL) and brine (40 mL), dried over MgSO₄, filtered and evaporated under reduced pressure to give 4-chloropiperidine-1-carbonyl chloride (420 mg, 90% yield) as a colorless oil.

¹H NMR (400 MHz, CDCl₃) δ 4.34 (tt, J = 6.5, 3.6 Hz, 1H), 4.01 – 3.64 (m, 4H), 2.18 – 2.03 (m, 2H), 2.00 – 1.86 (m, 2H).

¹³C NMR (101 MHz, CDCl₃) δ 148.4, 55.6, 45.6, 43.1, 34.7, 34.2.

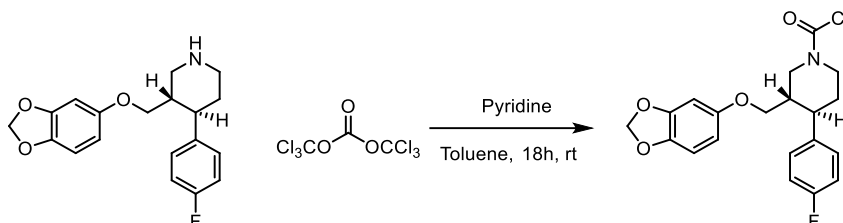
Synthesis of methyl (chlorocarbonyl)-L-prolinate:



Methyl (chlorocarbonyl)-L-prolinate was prepared according to a modification of a reported procedure.^{38b} To a solution of triphosgene (207 mg, 0.68 mmol) in toluene (15 mL) under N₂, pyridine (0.204 mL, 2.54 mmol) and subsequently a solution of L-methyl proline hydrochloride (350 mg, 2.13 mmol). The reaction mixture was stirred for 18 hours at ambient temperature, quenched with NH₄Cl (20 mL of a saturated aq. solution), and extracted with Et₂O (2 x 30 mL). The combined organic extracts were washed sequentially with HCl (40 mL of a 0.25 M aq. solution), H₂O (40 mL) and brine (40 mL), dried over MgSO₄, filtered and evaporated under reduced pressure to give methyl (chlorocarbonyl)-L-prolinate (275 mg, 68% yield) as a colorless oil.

¹H NMR (400 MHz, CDCl₃, 1:1 mixture of rotamers) δ: 4.57 – 4.46 (m, 1H), 3.85 - 3.55 (m, 2H), 3.77 (d, J = 12.4 Hz, 3H), 2.35 – 2.25 (m, 1H), 2.17 – 1.93 (m, 3H).

¹³C NMR (124 MHz, CDCl₃, 1:1 mixture of rotamers) δ: 171.8, 171.3, 147.8, 146.9, 62.4, 60.7, 52.9, 50.7, 49.2, 30.4, 30.3, 23.7, 23.6

Synthesis of compound Paroxetine-carbonyl chloride:

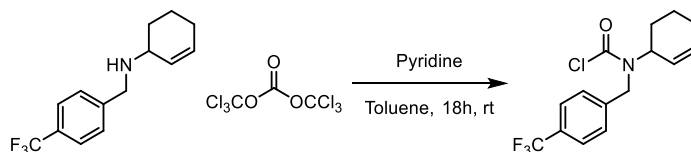
Paroxetine-carbonyl chloride was prepared according to a modification of a reported procedure.^{38b} To a solution of triphosgene (89 mg, 0.30 mmol) in toluene (3 mL) under N₂, pyridine (88 μL, 1 mmol) and subsequently a solution of Paroxetine (300 mg, 0.91 mmol) in toluene (6 mL), were added. The reaction mixture was stirred for 18 hours at ambient temperature, quenched with NH₄Cl (20 mL of a saturated aq. solution) and extracted with Et₂O (2 x 30 mL). The combined organic extracts were washed sequentially with HCl (40 mL of a 0.25 M aq. solution), H₂O (40 mL) and brine (40 mL), dried over MgSO₄, filtered and evaporated under reduced pressure to afford the target paroxetine derived carbamoyl chloride (130 mg, 36% yield) as a white crystal.

¹H NMR (500 MHz, CDCl₃) δ 7.14 (m, 2H), 7.00 (m, 2H), 6.64 (m, 1H), 6.36 (s, 1H), 6.14 (m, 1H), 5.89 (s, 2H), 4.63 (m, 1H), 4.49 (m, 1H), 3.63 (t, *J* = 8.7 Hz, 1H), 3.48 (dd, *J* = 9.6, 6.0 Hz, 1H), 3.20 (t, *J* = 12.9 Hz, 1H), 3.02 (m, 1H), 2.82 (m, 1H), 2.10 (m, 1H), 1.93 (m, 1H), 1.82 (qd, *J* = 12.9, 4.4 Hz, 1H)

¹³C NMR (126 MHz, CDCl₃) δ 162.9, 160.9, 154.0, 148.4, 142.0, 128.9, 115.8, 108.0, 105.8, 101.3, 98.1, 68.4, 52.2, 49.6, 47.0, 43.8, 42.3, 33.7

¹⁹F NMR (376 MHz, CDCl₃, proton decoupled) δ -115.51

HRMS (ESI pos): calculated for C₂₀H₁₉ClFNaNO₄ (M+Na⁺): 414.09, found 414.0884

Synthesis of cyclohex-2-en-1-yl(4-(trifluoromethyl)benzyl)carbamic chloride:

Cyclohex-2-en-1-yl(4-(trifluoromethyl)benzyl)carbamic chloride was prepared according to a modification of a reported procedure.^{38b} To a solution of triphosgene (252 mg, 0.848 mmol) in toluene (15 mL) under N₂, pyridine (0.242 mL, 2.99 mmol) and subsequently a solution of *N*-(4-(trifluoromethyl)benzyl)cyclohex-2-en-1-amine (637 mg, 2.5 mmol) in toluene (4 mL), were added. The reaction mixture was stirred for 18 hours at ambient temperature, quenched with NH₄Cl (20 mL of a saturated aq. solution) and extracted with Et₂O (2 x 30 mL). The combined organic extracts were washed sequentially with HCl (40 mL of a 0.25 M aq.

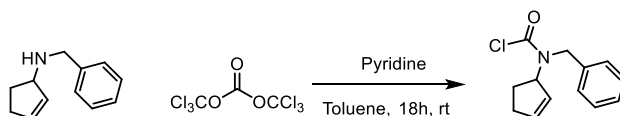
solution), H₂O (40 mL) and brine (40 mL), dried over MgSO₄, filtered and evaporated under reduced pressure to give desired carbamoyl chloride (722 mg, 91% yield) as a yellow oil.

¹H NMR (400 MHz, CDCl₃ mixture of rotamers) δ 7.60 (dd, *J* = 16.7, 8.1 Hz, 2H), 7.36 (d, *J* = 7.9 Hz, 2H), 5.85 – 6.00 (m, 1H), 5.55 – 5.41 (m, 1H), 5.10 – 4.90 (m, 1H), 4.82 – 4.49 (m, 2H), 2.08 – 1.94 (m, 3H), 1.85 – 1.40 (m, 3H).

¹³C NMR (101 MHz, CDCl₃ mixture of rotamers) δ 150.4, 150.3, 141.8, 141.4, 133.5, 133.4, 127.3, 126.5, 126.1, 126.1, 125.84 – 125.46 (m), 124.1 (q, *J* = 271.9 Hz) 58.7, 57.0, 50.4, 49.1, 28.5, 27.6, 24.5, 24.4, 21.2, 21.1.

¹⁹F NMR (376 MHz, CDCl₃ mixture of rotamers) δ -62.59, -62.63.

Synthesis of benzyl(cyclopent-2-en-1-yl)carbamic chloride:



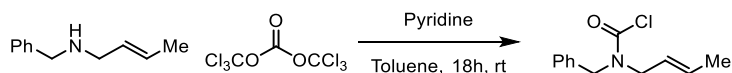
Benzyl(cyclopent-2-en-1-yl)carbamic chloride was prepared according to a modification of a reported procedure.^{38b} To a solution of triphosgene (134 mg, 0.44 mmol) in toluene (8 mL) under N₂, pyridine (0.129 mL, 1.6 mmol) and subsequently a solution of *N*-benzylcyclopent-2-en-1-amine (231 mg, 1.33 mmol) in toluene (2 mL). The reaction mixture was stirred for 18 hours at ambient temperature, quenched with NH₄Cl (20 mL of a saturated aq. solution) and extracted with Et₂O (2 x 30 mL). The combined organic extracts were washed sequentially with HCl (40 mL of a 0.25 M aq. solution), H₂O (40 mL) and brine (40 mL), dried over MgSO₄, filtered and evaporated under reduced pressure to give the target carbamoyl chloride (106 mg, 34% yield) as a yellowish oil.

¹H NMR (400 MHz, CDCl₃, mixture of rotamers) δ. 7.40 – 7.20 (m, 5H), 6.02 - 5.95 (m, 1H), 5.58 – 5.46 (m, 2H), 4.66 – 4.37 (m, 1H), 2.44 – 2.20 (m, 3H), 1.75 – 1.59 (m, 1H).

¹³C NMR (101 MHz, CDCl₃, mixture of rotamers) δ 150.1, 150, 137.3, 136.9, 136.4, 128.8, 128.7, 128.7, 128.6, 128.5, 127.3, 127.2, 126.2, 67.6, 66, 50.6, 48.9, 31.4, 31.3, 28.9, 28.4.

HRMS (ESI pos): calculated for C₁₃H₁₄ClNaNO (M+Na⁺) 258.07, found 258.0653.

Synthesis of (Z)-benzyl(but-2-en-1-yl)carbamic chloride:



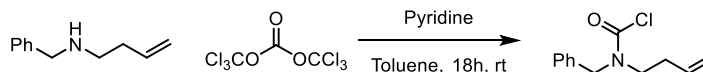
(*Z*)-benzyl(but-2-en-1-yl)carbamic chloride was prepared according to a modification of a reported procedure.^{38b} To a solution of triphosgene (250 mg, 0.843 mmol) in toluene (15 mL) under N₂, pyridine (0.241 mL, 2.98 mmol) and subsequently a solution of *N*-benzylbut-2-en-

1-amine (400 mg, 2.48 mmol) in toluene (4 mL), were added. The reaction mixture was stirred for 18 hours at ambient temperature, quenched with NH_4Cl (20 mL of a saturated aq. solution) and extracted with Et_2O (2 x 30 mL). The combined organic extracts were washed sequentially with HCl (40 mL of a 0.25 M aq. solution), H_2O (40 mL) and brine (40 mL), dried over MgSO_4 , filtered and evaporated under reduced pressure to give the target carbamoyl chloride (508 mg, 92% yield) as a yellow oil.

$^1\text{H NMR}$ (400 MHz, CDCl_3 , 1:1 mixture of rotamers) δ 7.42 – 7.30 (m, 3H), 7.29 – 7.24 (m, 2H), 5.75 – 5.54 (m, 1H), 5.53 – 5.34 (m, 1H), 4.68 (s, 1H), 4.55 (s, 1H), 3.90 (dd, $J = 15.6$, 6.3 Hz, 2H), 1.78 – 1.66 (m, 3H).

$^{13}\text{C NMR}$ (101 MHz, CDCl_3 , 1:1 mixture of rotamers) δ 150.2, 149.6, 135.8, 135.6, 131.3, 130.7, 129.0, 128.9, 128.4, 128.3, 128.1, 128.1, 127.3, 124.3, 124.0, 53.2, 51.9, 51.5, 50.5, 17.8.

Synthesis of benzyl(but-3-en-1-yl)carbamic chloride:

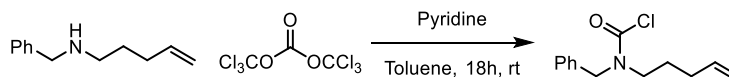


Benzyl(but-3-en-1-yl)carbamic chloride was prepared according to a modification of a reported procedure.^{38b} To a solution of triphosgene (252 mg, 0.85 mmol) in toluene (15 mL) under N_2 , pyridine (0.243 mL, 3.0 mmol) and subsequently a solution of *N*-benzylbut-3-en-1-amine (403 mg, 2.5 mmol) in toluene (4 mL), were added. The reaction mixture was stirred for 18 hours at ambient temperature, quenched with NH_4Cl (20 mL of a saturated aq. solution) and extracted with Et_2O (2 x 30 mL). The combined organic extracts were washed sequentially with HCl (40 mL of a 0.25 M aq. solution), H_2O (40 mL) and brine (40 mL), dried over MgSO_4 , filtered and evaporated under reduced pressure to give the target carbamoyl chloride (475 mg, 85% yield) as a yellow oil.

$^1\text{H NMR}$ (400 MHz, CDCl_3 , 1:1 mixture of rotamers) δ 7.41 – 7.31 (m, 3H), 7.30 – 7.24 (m, 2H), 5.80 – 5.67 (m, 1H), 5.16 – 5.04 (m, 2H), 4.72 (s, 1H), 4.59 (s, 1H), 3.53 – 3.35 (m, 2H), 2.42 – 2.30 (m, 2H).

$^{13}\text{C NMR}$ (101 MHz, CDCl_3 , 1:1 mixture of rotamers) δ 150.3, 149.6, 135.8, 135.6, 134.3, 134.0, 129.1, 129.0, 128.3, 128.2, 128.2, 127.2, 118.0, 117.8, 54.7, 52.7, 49.8, 48.9, 32.6, 31.7.

Synthesis of benzyl(pent-4-en-1-yl)carbamic chloride:



Benzyl(pent-4-en-1-yl)carbamic chloride was prepared according to a modification of a reported procedure.^{38b} To a solution of triphosgene (252 mg, 0.85 mmol) in toluene (15 mL) under N₂, pyridine (0.243 mL, 3.0 mmol) and subsequently a solution of *N*-benzylpent-4-en-1-amine (438 mg, 2.5 mmol) in toluene (4 mL), were added. The reaction mixture was stirred for 18 hours at ambient temperature, quenched with NH₄Cl (20 mL of a saturated aq. solution) and extracted with Et₂O (2 x 30 mL). The combined organic extracts were washed sequentially with HCl (40 mL of a 0.25 M aq. solution), H₂O (40 mL) and brine (40 mL), dried over MgSO₄, filtered and evaporated under reduced pressure to give the target carbamoyl chloride (553 mg, 93% yield) as a yellow oil.

¹H NMR (400 MHz, CDCl₃, 1:1 mixture of rotamers) δ 7.41 – 7.30 (m, 3H), 7.29 – 7.24 (m, 2H), 5.81 – 5.68 (m, 2H), 5.08 – 4.92 (m, 2H), 4.71 (s, 1H), 4.58 (s, 1H), 3.36 (dt, *J* = 13.6, 7.8 Hz, 2H), 2.05 (q, *J* = 7.5 Hz, 2H), 1.70 (app h, *J* = 7.6 Hz, 2H).

¹³C NMR (101 MHz, CDCl₃, 1:1 mixture of rotamers) δ 150.3, 149.6, 137.3, 137.1, 135.9, 135.7, 129.0, 129.0, 128.2, 127.2, 115.8, 115.6, 54.5, 52.6, 50.0, 49.1, 30.8, 30.8, 27.1, 26.3.

Reaction with aroyl chlorides

Experimental Setup

Our photoreactor consisted of a 12.5 cm diameter jar, fitted with 4 standard 29 sized ground glass joints arranged in a square and a central 29 sized joint. A commercial 1-meter LED strip was wrapped around the jar, followed by a layer of aluminium foil and cotton for insulation (Figure 3.7).

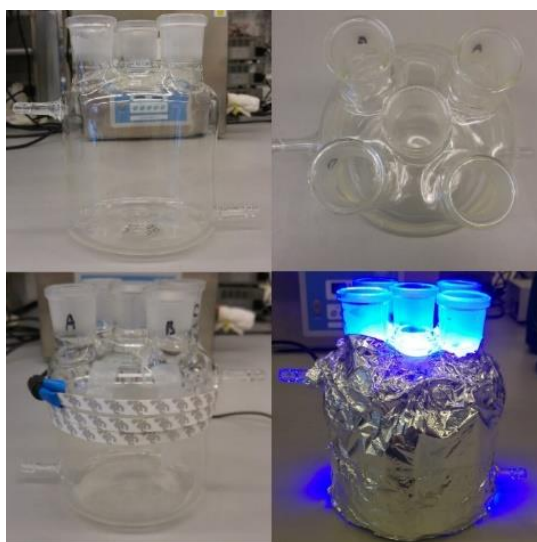


Figure 2.39. Photoreactor used for temperature-controlled reactions - pictures taken at different stages of the set-up assembly.

Each of the joints could be used to fit a standard 16 mm or 25 mm diameter Schlenk tube with a Teflon adaptor (Figure 3.8)



Figure 2.40. Teflon adaptors to use Schlenk tubes in the photoreactor.

An inlet and an outlet allow the circulation of liquid from a Huber Minichiller 300 inside the jar. This setup allows to perform reactions at temperatures ranging from $-20\text{ }^{\circ}\text{C}$ to $80\text{ }^{\circ}\text{C}$ with accurate control of the reaction temperature ($\pm 1\text{ }^{\circ}\text{C}$, Figure 3.9).

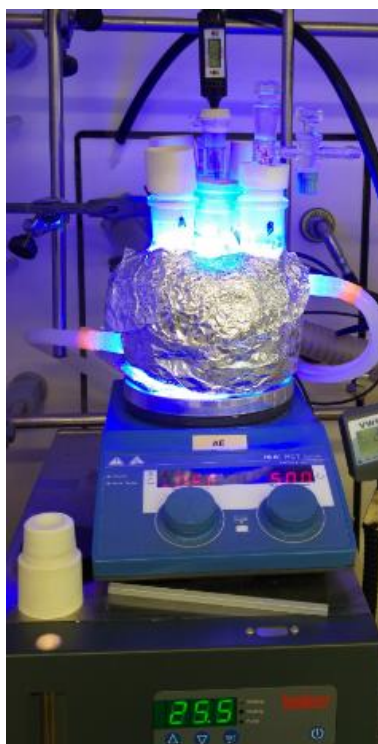
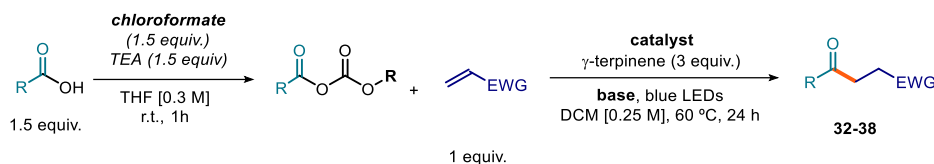


Figure 2.41. Fully assembled controlled temperature photoreactor in operation.

In order to maintain consistent illumination between different experiments, only the four external positions were used to perform reactions. The central position was used to monitor

the temperature inside a Schlenk tube identical to those used to perform reactions, ensuring that the reaction mixtures are at the desired temperature.

2.10.3 Optimization studies

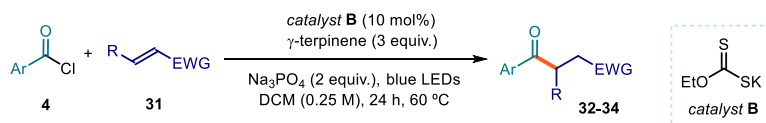


entry	acid	chloroformate	base	catalyst	acceptor	NMR yield (%)
1	Benzoic	Ethyl	Na ₃ PO ₄	10 mol% B	Acrylonitrile	50
2	Benzoic	Ethyl	Na ₃ PO ₄	10 mol% C	Acrylonitrile	55
3	Benzoic	Ethyl	Na ₃ PO ₄	20 mol% B	Acrylonitrile	60
4	Benzoic	Ethyl	Na ₃ PO ₄ (1 equiv.)	20 mol% B	Acrylonitrile	69
5	Benzoic	Ethyl	-	20 mol% B	Acrylonitrile	71
6	Benzoic	Methyl	-	20 mol% B	Acrylonitrile	61
7	Benzoic	Isobutyl	-	20 mol% B	Acrylonitrile	15
8	Cyclohexyl	Ethyl	-	20 mol% B	Vinyl sulfone	64
9	Cyclohexyl	Ethyl	-	20 mol% C	Vinyl sulfone	42
10	Cyclohexyl	Ethyl	-	30 mol% B	Vinyl sulfone	83
11	Cyclohexyl	Ethyl	-	50 mol% B	Vinyl sulfone	82

All reaction performed on 0.5 mmol scale; yield determined by ¹H NMR analysis of the crude reaction mixture using trichloroethylene as the internal standard.

2.10.4 General Procedures and characterization of products

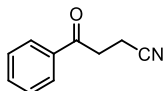
General Procedure A



In an oven dried tube of 15 mL (16 mm × 125 mm) with a Teflon septum screw cap, potassium ethyl xanthogenate **B** (8 mg, 0.05 mmol, 0.1 equiv.), sodium phosphate (164 mg, 1.00 mmol, 2 equiv.), acyl chloride **4** (0.75 mmol, 1.5 equiv.) and the electron-poor olefin **31** (0.5 mmol, 1 equiv., *if solid*), were dissolved in DCM (2 mL, HPLC grade). Then, γ -terpinene (240 μ L, 1.5 mmol, 3 equiv.) was added. The resulting yellow mixture was degassed with argon sparging for 60 seconds. When the electron-poor olefin **31** is *liquid*, it was added via syringe after the argon sparging. The reaction vessel was then placed in the temperature-controlled photoreactor (Figure 3.9) set at 60 °C (60–61 °C measured in the central well) and irradiated

for 16 hours upon stirring, if not otherwise specified. Then, the solvent was evaporated and the residue purified by column chromatography to afford the corresponding product in the stated yield with >95% purity according to ^1H NMR analysis.

2.10.4 Characterization of Products

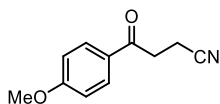


4-Oxo-4-phenylbutanenitrile (38o): Synthesized according to the general procedure A using benzoyl chloride (87 μL , 0.75 mmol, 1.5 equiv.) and acrylonitrile (33 μL , 0.5 mmol, 1 equiv.). The crude mixture was purified by flash column chromatography on silica gel (20% AcOEt in hexanes as eluent) to afford **38o** (65 mg, 82% yield) as a white solid.

^1H NMR (500 MHz, CDCl_3) δ 7.98 – 7.93 (m, 2H), 7.64 – 7.59 (m, 1H), 7.53 – 7.47 (m, 2H), 3.41 – 3.35 (m, 2H), 2.80 – 2.75 (m, 2H).

^{13}C NMR (126 MHz, CDCl_3) δ 195.4, 135.7, 134.0, 129.0, 128.1, 119.3, 34.4, 11.9

Matching reported literature data.⁸⁵

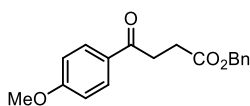


4-(4-methoxyphenyl)-4-oxobutanenitrile (38a): Synthesized according to the general procedure A using 4-methoxybenzoyl chloride (102 μL , 0.75 mmol, 1.5 equiv.) and acrylonitrile (33 μL , 0.5 mmol, 1 equiv.). The crude mixture was purified by flash column chromatography on silica gel (15% AcOEt in hexanes as eluent) to afford **38a** (80 mg, 84% yield) as a white solid.

^1H NMR (500 MHz, CDCl_3) δ 7.92 (app d, $J = 8.9$ Hz, 2H), 6.95 (app d, $J = 9.0$ Hz, 2H), 3.87 (s, 3H), 3.32 (t, $J = 7.3$ Hz, 2H), 2.75 (t, $J = 7.3$ Hz, 2H).

^{13}C NMR (126 MHz, CDCl_3) δ 193.9, 164.2, 130.4, 128.8, 119.5, 114.1, 55.7, 34.0, 12.0

Matching reported literature data.³⁹



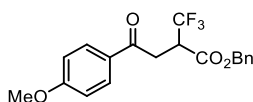
Benzyl 4-(4-methoxyphenyl)-4-oxobutanoate (38b): Synthesized according to the general procedure A using 4-methoxybenzoyl chloride (102 μL , 0.75 mmol, 1.5 equiv.) and benzyl acrylate (77 μL , 0.5 mmol, 1 equiv.). The crude mixture was purified by flash column chromatography on silica gel (15% AcOEt in hexanes as eluent), followed by a second purification (AcOEt/hexanes/toluene 1:6:6 as eluent) to afford **38b** (96 mg, 64% yield) as a yellow solid.

⁸⁵ Li, Y.; Shang, J.-Q.; Wang, X.-X.; Xia, W.-J.; Yang, T.; Xin, Y.; Li, Y.-M. Copper-Catalyzed Decarboxylative Oxyalkylation of Alkynyl Carboxylic Acids: Synthesis of γ -Diketones and γ -Ketonitriles. *Org. Lett.* **2019**, *21*, 2227- 2230.

¹H NMR (500 MHz, CDCl₃) δ 7.99 – 7.94 (m, 2H), 7.38 7.29 (m, 5H), 6.96 – 6.91 (m, 2H), 5.15 (s, 2H), 3.87 (s, 3H), 3.28 (t, *J* = 6.7 Hz, 2H), 2.81 (t, *J* = 6.7 Hz, 2H).

¹³C NMR (126 MHz, CDCl₃) δ 196.6, 173.0, 163.7, 136.1, 130.4, 129.8, 128.6, 128.3 (2C overlapping), 113.9, 66.6, 55.6, 33.1, 28.5.

HRMS (ESI pos): calculated for C₁₈H₁₈NaO₄ (M+Na⁺): 321.1097, found: 321.1091.



Benzyl 4-(4-methoxyphenyl)-4-oxo-2-(trifluoromethyl)butanoate (38c): Synthesized according to the general procedure A using 4-methoxybenzoyl chloride (102 μL, 0.75 mmol, 1.5 equiv.) and benzyl 2-(trifluoromethyl)acrylate (115 mg, 0.5 mmol, 1 equiv.).

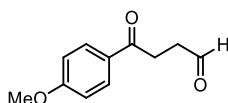
The crude mixture was purified by flash column chromatography on silica gel (10% AcOEt in hexanes as eluent). In order to remove traces of *p*-anisaldehyde formed as a byproduct during the reaction, after the chromatographic purification and solvent removal, the mixture was dissolved in 1.5 mL of MeOH, and 7.5 mL of saturated NaHSO₃ (aq) were added. Subsequently, the mixture was stirred for 30 s, diluted with 7.5 mL of H₂O, and extracted with 7.5 mL of 10% AcOEt in hexanes. The organic layer was dried with MgSO₄, filtered, and concentrated in vacuo⁸⁶ to afford **38c** (150 mg, 82% yield) as a colorless oil.

¹H NMR (400 MHz, CDCl₃) δ 7.99 – 7.91 (m, 2H), 7.42 – 7.29 (m, 5H), 6.99 – 6.91 (m, 2H), 5.24 (dd, *J* = 18.3; 12.3 Hz, 2H), 4.01 – 3.89 (m, 1H), 3.87 (s, 3H), 3.78 (dd, *J* = 17.7, 10.8 Hz, 1H), 3.32 (dd, *J* = 17.7, 3.1 Hz, 1H).

¹³C NMR (100 MHz, CDCl₃) δ 193.8, 166.9 (q, *J* = 2.9 Hz), 164.2, 135.2, 130.6 (2CH overlapping), 128.9, 128.7, 128.5, 128.1, 125.0 (q, *J* = 280.4 Hz), 114.0, 67.9, 55.6, 45.9 (q, *J* = 27.9 Hz), 34.9 (d, *J* = 1.4 Hz).

¹⁹F NMR (376 MHz, CDCl₃, proton decoupled) δ -67.51 (s, 3F).

HRMS (ESI pos): calculated for C₁₉H₁₇F₃NaO₄ (M+Na⁺): 389.0971, found: 389.0978.



4-(4-Methoxyphenyl)-4-oxobutanal (38d): Synthesized according to the general procedure A using 4-methoxybenzoyl chloride (102 μL, 0.75 mmol, 1.5 equiv.) and acrolein (33 μL, 0.5 mmol, 1 equiv.).

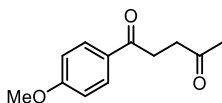
The crude mixture was purified by flash column chromatography on silica gel (20% AcOEt in hexanes as eluent), followed by a second purification (5:47:48 of Et₂O/DCM/hexanes as eluent) to afford **38d** (50 mg, 52% yield) as a yellow oil.

⁸⁶ Boucher, M. M.; Furigay, M. H.; Quach, P. K.; Brindle, C. S. Liquid–Liquid Extraction Protocol for the Removal of Aldehydes and Highly Reactive Ketones from Mixtures *Org. Process Res. Dev.* **2017**, *21*, 1394–1403.

¹H NMR (400 MHz, CDCl₃) δ 9.89 (s, 1H), 7.99 – 7.91 (m, 2H), 6.96 – 6.89 (m, 2H), 3.85 (s, 3H), 3.27 (app t, *J* = 6.4 Hz, 2H), 2.89 (app t, *J* = 6.5 Hz, 2H).

¹³C NMR (100 MHz, CDCl₃) δ 201.0, 196.4, 163.7, 130.4, 129.6, 113.9, 55.6, 37.8, 30.8

Matching reported literature data.⁸⁷



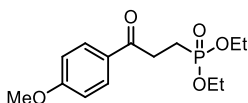
1-(4-Methoxyphenyl)pentane-1,4-dione (38e): Synthesized

according to the general procedure A using 4-methoxybenzoyl chloride (102 μL, 0.75 mmol, 1.5 equiv.) and methyl vinyl ketone (41 μL, 0.5 mmol, 1 equiv.). The crude mixture was purified by flash column chromatography on silica gel (20% AcOEt in hexanes as eluent), followed by a second one (10:45:45 of Et₂O/DCM/Hexanes as eluent) to afford **38e** (49 mg, 48% yield) white solid.

¹H NMR (400 MHz, CDCl₃) δ 7.98 – 7.91 (m, 2H), 6.95–6.89 (m, 2H), 3.85 (s, 3H), 3.25 – 3.18 (m, 2H), 2.88 – 2.82 (m, 2H), 2.24 (s, 3H).

¹³C NMR (100 MHz, CDCl₃) δ 207.6, 197.1, 164.6, 130.4, 129.9, 113.8, 55.6, 37.2, 32.2, 30.2.

Matching reported literature data.³⁹



Diethyl (3-(4-methoxyphenyl)-3-oxopropyl)phosphonate (38f):

Synthesized according to the general procedure A using 4-methoxybenzoyl chloride (102 μL, 0.75 mmol, 1.5 equiv.) and diethyl vinylphosphonate (77 μL, 0.5 mmol, 1 equiv.). Irradiations time: 24 hours. The crude mixture was purified by flash column chromatography on silica gel (20% AcOEt in hexanes as eluent) to afford **38f** (81 mg, 54% yield) as a white solid.

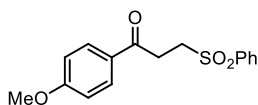
¹H NMR (400 MHz, CDCl₃) δ 7.91 (app d, *J* = 8.8 Hz, 2H), 6.89 (app d, *J* = 8.9 Hz, 2H), 4.20 – 3.96 (m, 4H), 3.82 (s, 3H), 3.28 – 3.12 (m, 2H), 2.22 – 2.04 (m, 2H), 1.28 (t, *J* = 7.0 Hz, 6H).

¹³C NMR (100 MHz, CDCl₃) δ 196.0 (d, *J* = 16.2 Hz), 163.7, 130.3, 129.4, 113.8, 61.7 (d, *J* = 6.6 Hz), 55.5, 31.3 (d, *J* = 2.9 Hz), 19.9 (d, *J* = 144.3 Hz), 6.5 (d, *J* = 6.5 Hz).

Matching reported literature data.⁸⁸

⁸⁷ Wang, J.; Huang, B.; Shi, C.; Yang, C.; Xia, W. Visible-Light-Mediated Ring-Opening Strategy for the Regiospecific Allylation/Formylation of Cycloalkanols *J. Org. Chem.* **2018**, *83*, 9696-9706.

⁸⁸ Yu, J.-W.; Huang, S. K. Synthesis of diethyl 3-aryl-3-oxopropylphosphonates. *Org. Prep. Proced. Int.* **1997**, *29*, 214-218.



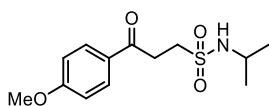
1-(4-Methoxyphenyl)-3-(phenylsulfonyl)propan-1-one (38g):

Synthesized according to the general procedure A using 4-methoxybenzoyl chloride (102 μ L, 0.75 mmol, 1.5 equiv.) and phenyl vinyl sulfone (84 mg, 0.5 mmol, 1 equiv.). Reaction time: 24 hours. The crude mixture was purified by flash column chromatography on silica gel (25% AcOEt in hexanes as eluent), followed by a second one (20% AcOEt in hexanes as eluent) to afford **38g** (128 mg, 84% yield) as a white solid.

$^1\text{H NMR}$ (500 MHz, CDCl_3) δ 7.96 – 7.93 (m, 2H), 7.91 – 7.87 (m, 2H), 7.69 – 7.63 (m, 1H), 7.60 – 7.54 (m, 2H), 6.95 – 6.90 (m, 2H), 3.86 (s, 3H), 3.57 – 3.51 (m, 2H), 3.46 – 3.40 (m, 2H).

$^{13}\text{C NMR}$ (126 MHz, CDCl_3) δ 193.9, 164.1, 139.3, 134.0, 130.5, 129.5, 129.0, 128.1, 114.1, 55.7, 51.3, 31.0.

Matching reported literature data.⁸⁹

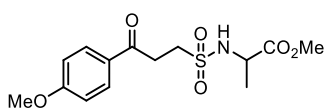


N-Isopropyl-3-(4-methoxyphenyl)-3-oxopropane-1-sulfonamide (38h): Synthesized according to the general procedure A using 4-methoxybenzoyl chloride (102 μ L, 0.75 mmol, 1.5 equiv.) and N-isopropylethanesulfonamide (75 mg, 0.5 mmol, 1 equiv.). Reaction time: 24 hours. The crude mixture was purified by flash column chromatography on silica gel (20% AcOEt in hexanes as eluent) to afford **38h** (98 mg, 69% yield) as a white solid.

$^1\text{H NMR}$ (400 MHz, CDCl_3) δ 7.98 – 7.91 (m, 2H), 6.97 – 6.90 (m, 2H), 4.35 (bs, 1H, NH), 3.87 (s, 3H), 3.74 – 3.58 (m, 1H), 3.54 – 3.38 (m, 4H), 1.24 (d, $J = 6.4$ Hz, 6H).

$^{13}\text{C NMR}$ (100 MHz, CDCl_3) δ 194.7, 164.1, 130.6, 129.2, 114.1, 55.7, 48.7, 46.5, 32.7, 24.4.

HRMS (ESI neg): calculated for $\text{C}_{13}\text{H}_{18}\text{NO}_4\text{S}$ (M^-): 284.0962, found 284.0974.



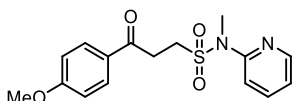
Methyl ((3-(4-methoxyphenyl)-3-oxopropyl)sulfonyl)alaninate (38i): Synthesized according to the general procedure A using 4-methoxybenzoyl chloride (102 μ L, 0.75 mmol, 1.5 equiv.) and methyl (vinylsulfonyl)alaninate (97 mg, 0.5 mmol, 1 equiv.). Reaction time: 24 hours. The crude mixture was purified by flash column chromatography on silica gel (35% AcOEt in hexanes as eluent), followed by a second one (20:40:40 of AcOEt/DCM/Hexanes as eluent) to afford **38i** (83 mg, 50% yield) as a colorless oil.

⁸⁹ Bhunia, A.; Yetra, S. R.; Bhojgude, S. S.; Biju, A. T. Efficient Synthesis of γ -Keto Sulfones by NHC-Catalyzed Intermolecular Stetter Reaction. *Org. Lett.* **2012**, *14*, 2830-2833.

¹H NMR (400 MHz, CDCl₃) δ 7.97 – 7.89 (m, 2H), 6.96 – 6.89 (m, 2H), 5.29 (d, *J* = 8.4 Hz, 2H), 4.25 – 4.14 (m, 1H), 3.85 (s, 3H), 3.73 (s, 3H), 3.53 – 3.40 (m, 4H), 1.45 (d, *J* = 7.15 Hz, 3H).

¹³C NMR (100 MHz, CDCl₃) δ 194.5, 173.2, 164.0, 130.5, 129.1, 114.0, 55.6, 52.9, 51.7, 48.4, 32.2, 19.9.

HRMS (ESI pos): calculated for C₁₄H₁₉NNaO₆S (M+Na⁺): 352.0825, found 352.0814.

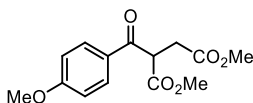


3-(4-Methoxyphenyl)-N-methyl-3-oxo-N-(pyridin-2-yl)propane-1-sulfonamide (38j): Synthesized according to the general procedure A using 4-methoxybenzoyl chloride (102 μL, 0.75 mmol, 1.5 equiv.) and N-methyl-N-(pyridin-2-yl)ethanesulfonamide (99 mg, 0.5 mmol, 1 equiv.). Reaction time: 24 hours. The crude mixture was purified by flash column chromatography on silica gel (20:20:60 of AcOEt/DCM/Hexanes as eluent), followed by a second one (20:20:60 of Et₂O/DCM/Hexanes as eluent) to afford **38j** (75 mg, 45% yield) as a yellowish oil.

¹H NMR (400 MHz, CDCl₃) δ 8.41 – 8.34 (m, 1H), 7.92 – 7.84 (m, 2H), 7.72 – 7.65 (m, 1H), 7.42 (app d, *J* = 8.3 Hz, 1H), 7.15 – 7.08 (m, 1H), 6.95 – 6.87 (m, 2H), 3.85 (s, 3H), 3.72 – 3.64 (m, 2H), 3.45 (s, 3H), 3.46 – 3.39 (m, 2H).

¹³C NMR (100 MHz, CDCl₃) δ 194.2, 164.0, 154.0, 148.3, 138.2, 130.5, 129.1, 121.0, 118.6, 114.0, 55.6, 46.3, 35.9, 31.8.

HRMS (ESI pos): calculated for C₁₆H₁₉N₂O₄S (M+H⁺): 335.1060, found 335.1043.



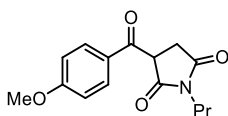
Dimethyl 2-(4-methoxybenzoyl)succinate (38k): Synthesized according to the general procedure A using 4-methoxybenzoyl chloride (102 μL, 0.75 mmol, 1.5 equiv.) and dimethyl fumarate (72 mg, 0.5 mmol, 1 equiv.). The crude mixture was purified by flash column chromatography on silica gel (20% AcOEt in hexanes as eluent) to afford **38k** (122 mg, 87% yield) as a colorless oil.

¹H NMR (500 MHz, CDCl₃) δ 8.03 – 7.98 (m, 2H), 6.96 – 6.92 (m, 2H), 4.82 (t, *J* = 7.1 Hz, 1H), 3.85 (s, 3H), 3.66 (s, 3H), 3.65 (s, 3H), 3.09 – 2.97 (m, 2H).

¹³C NMR (126 MHz, CDCl₃) δ 192.3, 171.9, 169.5, 164.2, 131.4, 128.8, 114.0, 129.0, 128.1, 114.1, 55.6, 52.8, 52.1, 33.2.

Matching reported literature data.⁹⁰

⁹⁰ Bonassi, F.; Ravelli, D.; Protti, S.; Fagnoni, M. Decatungstate Photocatalyzed Acylations and Alkylations in Flow via Hydrogen Atom Transfer. *Adv. Synth. Catal.* **2015**, *357*, 3687-3695.



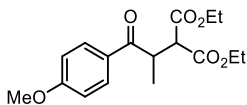
3-(4-Methoxybenzoyl)-1-propylpyrrolidine-2,5-dione (38l):

Synthesized according to the general procedure A using 4-methoxybenzoyl chloride (102 μL , 0.75 mmol, 1.5 equiv.) and 1-propyl-1H-pyrrole-2,5-dione (69.6 μL , 0.5 mmol, 1 equiv.). Chromatography on silica gel (20% AcOEt in hexanes as eluent) could not remove byproduct completely. Therefore, a further purification by semipreparative HPLC (Column SunFire C18, 60:40 Methanol/Water 6 min, up to 100% Methanol 1 min, 100% Methanol 4 min, 1 mL/min) was performed to obtain an analytical amount of the isolated product as a white solid. NMR yield (Trichloroethylene was used as internal standard): 53%.

$^1\text{H NMR}$ (500 MHz, CDCl_3) δ 8.12-8.07 (m, 2H), 7.02 – 6.97 (m, 2H), 4.78 (dd, $J = 8.3, 3.9$ Hz, 1H), 3.90 (s, 3H), 3.47 (t, $J = 7.3$ Hz, 2H), 3.37 (dd, $J = 18.1, 3.8$ Hz, 1H), 2.82 (dd, $J = 18.1, 8.8$ Hz, 1H), 1.64 – 1.54 (m, 2H, overlapping with water peak), 0.87 (t, $J = 7.4$ Hz, 3H).

$^{13}\text{C NMR}$ (126 MHz, CDCl_3) δ 190.9, 176.1, 173.4, 164.7, 132.4, 128.6, 114.2, 55.7, 48.2, 41.0, 31.8, 21.0, 11.3

HRMS (ESI pos): calculated for $\text{C}_{15}\text{H}_{17}\text{NNaO}_4$ ($\text{M}+\text{Na}^+$): 298.1050, found 298.1056.



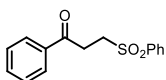
Diethyl 2-(1-(4-methoxyphenyl)-1-oxopropan-2-yl)malonate (38m):

Synthesized according to the general procedure A using 4-methoxybenzoyl chloride (102 μL , 0.75 mmol, 1.5 equiv.) and diethyl 2-ethylidenemalonate (93 μL , 0.5 mmol, 1 equiv.). The crude mixture was purified by flash column chromatography on silica gel (10% AcOEt in hexanes as eluent) to afford **38m** (60 mg, 37% yield) as a colorless oil.

$^1\text{H NMR}$ (400 MHz, CDCl_3) δ 8.03 – 7.96 (m, 2H), 6.98 – 6.93 (m, 2H), 4.31 – 4.21 (m, 2H) 4.20 – 4.02 (m, 3H), 3.97 (d, $J = 10.8$ Hz, 1H), 3.87 (s, 3H), 1.31 (t, $J = 7.0$ Hz, 3H), 1.19 (d, $J = 7.0$ Hz, 3H), 1.16 (t, $J = 7.1$ Hz, 3H).

$^{13}\text{C NMR}$ (100 MHz, CDCl_3) δ 200.2, 169.0, 168.5, 163.8, 131.0, 128.6, 114.0, 61.7, 55.6, 55.1, 40.3, 16.25, 14.3, 14.0.

HRMS (ESI pos): calculated for $\text{C}_{17}\text{H}_{22}\text{NaO}_6$ ($\text{M}+\text{Na}^+$): 345.1309, found 345.1306.



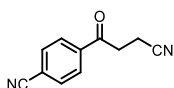
1-Phenyl-3-(phenylsulfonyl)propan-1-one (38n):

Synthesized according to the general procedure A using benzoyl chloride (87 μL , 0.75 mmol, 1.5 equiv.) and phenyl vinyl sulfone (84 mg, 0.5 mmol, 1 equiv.). The crude mixture was purified by flash column chromatography on silica gel (20% AcOEt in hexanes as eluent) to afford **38n** (112 mg, 82% yield) as a white solid.

$^1\text{H NMR}$ (400 MHz, CDCl_3) δ 7.99 – 7.88 (m, 4H), 7.70 – 7.63 (m, 1H), 7.63 – 7.54 (m, 3H), 7.51 – 7.43 (m, 2H), 3.60 – 3.53 (m, 2H), 3.53 – 3.46 (m, 2H).

$^{13}\text{C NMR}$ (100 MHz, CDCl_3) δ 195.5, 139.2, 135.9, 134.1, 133.9, 129.6, 128.9, 128.2, 128.1, 51.1, 31.5.

Matching reported literature data.⁴³



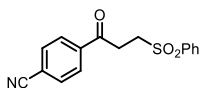
4-(3-Cyanopropanoyl)benzonitrile (38q): Synthesized according to the general procedure A using 4-cyanobenzoyl chloride (124 mg, 0.75 mmol, 1.5 equiv.) and acrylonitrile (33 μL , 0.5 mmol, 1 equiv.). In this

case the reaction was irradiated for 60 hours. The crude mixture was purified by flash column chromatography on silica gel (15% AcOEt in hexanes as eluent) to afford **38q** (92 mg, 45% yield) as a white solid.

$^1\text{H NMR}$ (500 MHz, CDCl_3) δ 8.04 (app d, $J = 8.2$ Hz, 2H), 7.80 (app d, $J = 8.2$ Hz, 2H), 3.39 (t, $J = 6.9$ Hz, 2H), 2.79 (t, $J = 7.0$ Hz, 2H).

$^{13}\text{C NMR}$ (126 MHz, CDCl_3) δ 194.3, 138.5, 132.8, 128.6, 118.8, 117.7, 117.3, 34.7, 11.8.

Matching reported literature data.³⁹



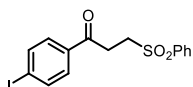
4-(3-(Phenylsulfonyl)propanoyl)benzonitrile (38p): Synthesized according to the general procedure A using 4-cyanobenzoyl chloride (124 mg, 0.75 mmol, 1.5 equiv.) and phenyl vinyl sulfone (84 mg, 0.5

mmol, 1 equiv.). In this case the reaction was irradiated for 60 hours. The crude mixture was purified by flash column chromatography on silica gel (25% AcOEt in hexanes as eluent) to afford **38p** (79 mg, 53% yield) as a white solid.

$^1\text{H NMR}$ (400 MHz, CDCl_3) δ 8.02 (app d, $J = 8.5$ Hz, 2H), 7.95 (app d, $J = 7.3$ Hz, 2H), 7.78 (app d, $J = 8.4$ Hz, 2H), 7.69 (app t, $J = 7.4$ Hz, 1H), 7.59 (app t, $J = 7.7$ Hz, 2H), 3.60 – 3.48 (m, 4H).

$^{13}\text{C NMR}$ (100 MHz, CDCl_3) δ 194.4, 139.1, 138.8, 134.2, 132.8, 129.6, 128.6, 128.1, 117.8, 117.2, 50.9, 31.8.

HRMS (ESI pos): calculated for $\text{C}_{16}\text{H}_{13}\text{NNaO}_3\text{S}$ ($\text{M}+\text{Na}^+$): 322.0508, found 322.0505.



1-(4-Iodophenyl)-3-(phenylsulfonyl)propan-1-one (38r):

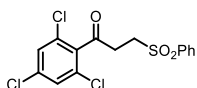
Synthesized according to the general procedure A using 4-iodobenzoyl chloride (200 mg, 0.75 mmol, 1.5 equiv.) and phenyl vinyl sulfone (84

mg, 0.5 mmol, 1 equiv.). In this case the reaction was irradiated for 60 hours. The crude mixture was purified by flash column chromatography on silica gel (20% AcOEt in hexanes as eluent) to afford **38r** (130 mg, 65% yield) as a white solid.

¹H NMR (500 MHz, CDCl₃) δ 7.99 – 7.92 (m, 2H), 7.87 – 7.82 (m, 2H), 7.70 – 7.65 (m, 1H), 7.65 – 7.61 (m, 2H), 7.61 – 7.56 (m, 2H), 3.58 – 3.51 (m, 2H) 3.49 – 3.42 (m, 2H).

¹³C NMR (126 MHz, CDCl₃) δ 194.9, 139.2, 138.3, 135.2, 134.1, 129.6, 129.5, 128.1, 102.1, 51.0, 31.4

HRMS (ESI pos): calculated for C₁₅H₁₃INaO₃S (M+Na⁺): 422.9522, found 422.9519.



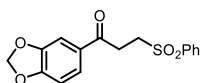
3-(Phenylsulfonyl)-1-(2,4,6-trichlorophenyl)propan-1-one (38s):

Synthesized according to the general procedure A using 2,4,6-trichlorobenzoyl chloride (183 mg, 0.75 mmol, 1.5 equiv.) and phenyl vinyl sulfone (84 mg, 0.5 mmol, 1 equiv.). In this case the reaction was irradiated for 60 hours. The crude mixture was purified by flash column chromatography on silica gel (25% AcOEt in hexanes as eluent) followed by a second one (5:25:70 of AcOEt/DCM/Hexanes as eluent) to afford **38s** (95 mg, 50% yield) as a white solid.

¹H NMR (400 MHz, CDCl₃) δ 7.98 – 7.92 (m, 2H), 7.72 – 7.65 (m, 1H), 7.63 – 7.56 (m, 2H), 7.36 (s, 2H), 3.58 – 3.50 (m, 2H), 3.33 – 3.25 (m, 2H).

¹³C NMR (100 MHz, CDCl₃) δ 197.2, 138.9, 137.0, 136.6, 134.2, 131.2, 129.6, 128.5, 128.1, 50.1, 36.5

HRMS (ESI pos): calculated for C₁₅H₁₁Cl₃NaO₃S (M+Na⁺): 398.9387, found 398.9390.



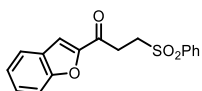
1-(Benzo[d][1,3]dioxol-5-yl)-3-(phenylsulfonyl)propan-1-one (38t):

Synthesized according to the general procedure A using benzo[d][1,3]dioxole-5-carbonyl chloride (138 mg, 0.75 mmol, 1.5 equiv.) and phenyl vinyl sulfone (84 mg, 0.5 mmol, 1 equiv.). Reaction time: 24 hours. The crude mixture was purified by flash column chromatography on silica gel (25% AcOEt in hexanes as eluent) to afford **38t** (90 mg, 57% yield) as a white solid.

¹H NMR (500 MHz, CDCl₃) δ 7.96 – 7.92 (m, 2H), 7.67 (tt, *J* = 7.3, 1.8 Hz, 1H), 7.60 – 7.55 (m, 2H), 7.52 (dd, *J* = 8.1, 1.8 Hz, 1H), 7.36 (d, *J* = 1.7 Hz, 1H), 6.84 (d, *J* = 8.1 Hz, 1H), 6.04 (s, 2H), 3.57 – 3.50 (m, 2H), 3.44 – 3.37 (m, 2H).

¹³C NMR (126 MHz, CDCl₃) δ 193.5, 152.5, 148.5, 139.2, 134.0, 130.8, 129.5, 128.1, 124.7, 108.2, 107.8, 102.2, 51.3, 31.2.

HRMS (ESI pos): calculated for C₁₆H₁₄NaO₅S (M+Na⁺): 341.0454, found 341.0452.



1-(Benzofuran-2-yl)-3-(phenylsulfonyl)propan-1-one (38u):

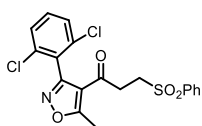
Synthesized according to the general procedure A using benzofuran-2-carbonyl chloride (135 mg, 0.75 mmol, 1.5 equiv.) and phenyl vinyl sulfone (84 mg, 0.5 mmol, 1 equiv.). Reaction time: 24 hours. The crude mixture was purified

by flash column chromatography on silica gel (25% AcOEt in hexanes as eluent) followed by a second one (20% AcOEt in hexanes as eluent) to afford **38u** (77 mg, 49% yield) as a yellowish solid.

¹H NMR (500 MHz, CDCl₃) δ 7.99 – 7.94 (m, 2H), 7.71 (app d, *J* = 7.8 Hz, 1H), 7.70 – 7.65 (m, 1H), 7.61 – 7.55 (app t, *J* = 8.0 Hz, 3H), 7.55 (s, 1H), 7.53 – 7.48 (m, 1H), 7.35 – 7.30 (m, 1H), 3.61 – 3.55 (m, 2H), 3.53 – 3.47 (m, 2H).

¹³C NMR (126 MHz, CDCl₃) δ 186.6, 155.9, 151.6, 139.0, 134.2, 129.6, 128.9, 128.2, 126.9, 124.3, 123.6, 113.7, 112.6, 50.6, 31.8

HRMS (ESI pos): calculated for C₁₇H₁₄NaO₄S (M+Na⁺): 337.0505, found 337.0504.



1-(3-(2,6-Dichlorophenyl)-5-methylisoxazol-4-yl)-3-

(phenylsulfonyl)propan-1-one (38x): Synthesized according to the general procedure A using 3-(2,6-dichlorophenyl)-5-methylisoxazole-

4-carbonyl chloride (218 mg, 0.75 mmol, 1.5 equiv.) and phenyl vinyl sulfone (84 mg, 0.5 mmol, 1 equiv.). Reaction time: 24 hours. The crude mixture was purified by flash column chromatography on silica gel (20% AcOEt in hexanes as eluent) to afford **38x** (75 mg, 35% yield) as a white solid.

¹H NMR (400 MHz, CDCl₃) δ 7.75 – 7.67 (m, 2H), 7.67 – 7.60 (m, 1H), 7.57 – 7.43 (m, 5H), 3.41 – 3.34 (m, 2H), 2.74 (s, 3H), 3.68 – 3.60 (m, 2H).

¹³C NMR (126 MHz, CDCl₃) δ 189.0, 176.5, 157.2, 138.6, 135.6, 134.0, 132.2, 129.5, 128.6, 128.0, 127.9, 116.1, 50.1, 34.3, 14.2.

HRMS (ESI pos): calculated for C₁₉H₁₅Cl₂NNaO₄S (M+Na⁺): 445.9991, found 445.9992.

Reaction with alkyl acyl chlorides

Experimental Setup



Figure 2.42. Photoreactor used for the reactions of aliphatic acyl chlorides.

Our 3D printed photoreactor consisted of a 9 cm diameter crystallizing dish with a 3D printed support of 6 positions, and a hole of 22 mm in the middle to allow ventilation. A commercial 1-meter LED strip was wrapped around the crystallizing dish. In order to control the temperature, a fan was used to cool down the reactor. Reaction temperature was measured, through a vial containing a thermometer, and it stayed between 35-40 °C (Figure 3.10). Each of the positions could be used to fit a standard 16 mm diameter vial with a Teflon screw cap. Experiments at 465 nm were conducted using a 1m strip, 14.4W “LEDXON MODULAR 9009083 LED, SINGLE 5050” purchased from Farnell, catalog number 9009083. The emission spectrum of these LEDs was recorded (Figure 3.11).

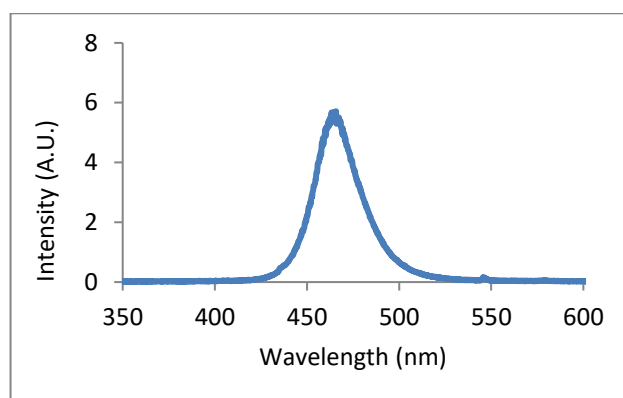
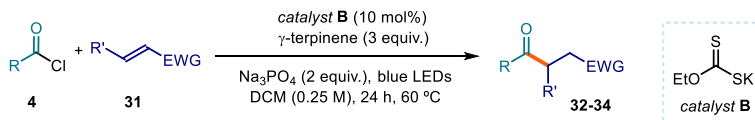


Figure 2.43. Emission spectrum of the 465 nm LED strip used in this study.

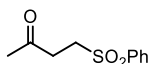
The emission maximum was determined as 465 nm with a spectral width of 30 nm (450-480 nm) at half peak intensity and a total spectral width of 120 nm (420-540 nm).

3.9.4.2 General Procedure B



In an oven dried tube of 15 mL (16 mm × 125 mm) with a Teflon septum screw cap, potassium ethyl xanthogenate **B** (8 mg, 0.05 mmol, 0.1 equiv.), sodium phosphate (164 mg, 1.00 mmol, 2 equiv.), acyl chloride **4** (0.75 mmol, 1.5 equiv.) and the electron-poor olefin **31** (0.5 mmol, 1 equiv., *if solid*), were dissolved in DCM (2 mL, HPLC grade). Then, γ -terpinene (240 μ L, 1.5 mmol, 3 equiv.) was added. The resulting yellow mixture was degassed with argon sparging for 60 seconds. When the electron-poor olefin **31** is *liquid*, it was added via syringe after the argon sparging. The vial was then placed in the 3D printed support photoreactor (Figure 3.10) and irradiated under stirring for 24 hours, if not otherwise specified. After this, the solvent was evaporated and the residue purified by column chromatography to afford the corresponding product in the stated yield with >95% purity according to $^1\text{H NMR}$ analysis.

3.9.4.3 Characterization of Products

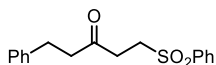


4-(Phenylsulfonyl)butan-2-one (40a): Synthesized according to the general procedure B using acetyl chloride (53 μ L, 0.75 mmol, 1.5 equiv.) and phenyl vinyl sulfone (84 mg, 0.5 mmol, 1 equiv.). The crude mixture was purified by flash column chromatography on silica gel (gradient from 25% to 100% AcOEt in hexanes as eluent): to afford product **40a** (70 mg 66% yield) as a colorless oil.

$^1\text{H NMR}$ (400 MHz, CDCl_3) δ 7.94 – 7.86 (m, 2H), 7.70 – 7.62 (m, 1H), 7.61 – 7.53 (m, 2H), 3.40 – 3.33 (m, 2H), 2.96 – 2.88 (m, 2H), 2.17 (s, 3H).

$^{13}\text{C NMR}$ (100 MHz, CDCl_3) δ 203.8, 139.1, 134.0, 129.6, 128.1, 50.6, 36.0, 30.0

Matching reported literature data.^{9b}



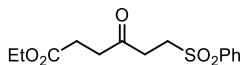
1-Phenyl-5-(phenylsulfonyl)pentan-3-one (40b): Synthesized according to the general procedure A using hydrocinnamoyl chloride

(111 μ L, 0.75 mmol, 1.5 equiv.) and phenyl vinyl sulfone (84 mg, 0.5 mmol, 1 equiv.). In this case the reaction was irradiated for 60 hours. The crude mixture was purified by two rounds of flash column chromatography on silica gel (25% AcOEt in hexanes as eluent): to afford **40b** (113 mg, 75% yield) as a white solid.

$^1\text{H NMR}$ (400 MHz, CDCl_3) δ 7.92 – 7.87 (m, 2H), 7.71 – 7.63 (m, 1H), 7.61 – 7.53 (m, 2H), 7.31 – 7.23 (m, 2H), 7.22 – 7.16 (m, 1H), 7.16 – 7.10 (m, 2H), 3.42 – 3.33 (m, 2H), 2.92 – 2.82 (m, 4H), 2.81 – 2.72 (m, 2H).

¹³C NMR (100MHz, CDCl₃) δ 205.3, 140.5, 139.1, 134.1, 129.5, 128.7, 128.4, 128.1, 126.5, 50.6, 44.4, 35.3, 29.7.

Matching reported literature data.⁹¹

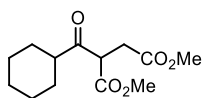


Ethyl 4-oxo-6-(phenylsulfonyl)hexanoate (40c): Synthesized according to the general procedure A using ethyl 4-chloro-4-oxobutanoate (107 μL, 0.75 mmol, 1.5 equiv.) and phenyl vinyl sulfone (84 mg, 0.5 mmol, 1 equiv.). Reaction time: 24 hours. The crude mixture was purified by flash column chromatography on silica gel (33% AcOEt in hexanes as eluent). Product was then dissolved in DCM, washed 3 times with a solution of CuSO₄ (5% in water), dried with MgSO₄ and evaporated under reduced pressure to afford **40c** (112 mg, 75% yield) as a white solid.

¹H NMR (400 MHz, CDCl₃) δ 7.92 – 7.87 (m, 2H), 7.69 – 7.63 (m, 1H), 7.61 – 7.53 (m, 2H), 4.09 (q, *J* = 7.1 Hz, 2H), 3.42 – 3.35 (m, 2H), 2.98 – 2.91 (m, 2H), 2.75 – 2.69 (m, 2H), 2.59 – 2.52 (m, 2H), 1.22 (t, *J* = 7.1 Hz, 3H).

¹³C NMR (126 MHz, CDCl₃) δ 204.5, 172.5, 139.1, 134.1, 129.5, 128.1, 60.9, 50.6, 37.2, 35.3, 28.0, 14.2

HRMS (ESI pos): calculated for C₁₄H₁₈NaO₅S (M+H⁺): 321.0767, found 321.0765.



Dimethyl 2-(cyclohexanecarbonyl)succinate (40g): Synthesized according to general procedure B using cyclohexanecarbonyl chloride (100 μL, 0.75 mmol, 1.5 equiv.) and dimethyl fumarate (72 mg, 0.5 mmol, 1 equiv.). The crude mixture was purified by flash column chromatography on silica gel (10% AcOEt in hexanes as eluent) to afford **40g** (107 mg, 83% yield) as a white solid.

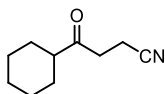
¹H NMR (500 MHz, CDCl₃) δ 4.14 (dd, *J* = 8.1, 6.2 Hz, 1H), 3.72 (s, 3H), 3.66 (s, 3H), 3.82 (s, 3H), 2.93 (dd, *J* = 17.5, 8.1 Hz, 1H), 2.81 (dd, *J* = 17.6, 6.5 Hz, 1H), 2.69 – 2.61 (m, 1H), 2.00 – 1.93 (m, 1H), 1.84 – 1.74 (m, 3H), 1.70 – 1.62 (m, 1H), 1.46 – 1.36 (m, 1H), 1.33 – 1.13 (m, 4H).

¹³C NMR (126 MHz, CDCl₃) δ 206.7, 171.9, 169.2, 52.8, 52.2, 52.1, 50.72, 32.4, 29.0, 28.1, 25.9, 25.8, 25.5.

Matching reported literature data.⁹²

⁹¹ Ravelli, D.; Montanaro, S.; Zema, M.; Fagnoni, M.; Albin, A. A Tin-Free, Radical Photocatalyzed Addition to Vinyl Sulfones. *Adv. Synth. Catal.* **2011**, *353*, 3295-3300.

⁹² Cartier, A.; Levernier, E.; Corcé, V.; Fukuyama, T.; Dhimane, A.-L.; Ollivier, C.; Ryu, I.; Fensterbank, L. Carbonylation of Alkyl Radicals Derived from Organosilicates through Visible-Light Photoredox Catalysis. *Angew. Chem. Int. Ed.* **2019**, *58*, 1789-1793.

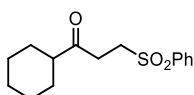


4-Cyclohexyl-4-oxobutanenitrile (40h): Synthesized according to the general procedure B using cyclohexanecarbonyl chloride (100 μL , 0.75 mmol, 1.5 equiv.) and acrylonitrile (33 μL , 0.5 mmol, 1 equiv.). The crude mixture was purified by flash column chromatography on silica gel (20% Et_2O in pentane as eluent) to afford **40h** (52 mg, 63% yield) as a colorless oil.

$^1\text{H NMR}$ (500 MHz, CDCl_3) δ 2.85-2.80 (m, 2H); 2.60-2.54 (m, 2H); 2.36 (tt, $J = 11.3$, 3.5 Hz, 1H); 1.89-1.82 (m, 2H); 1.82-1.75 (m, 2H); 1.71-1.64 (m, 1H); 1.40-1.15 (m, 5H).

$^{13}\text{C NMR}$ (126 MHz, CDCl_3) δ 209.4, 119.3, 50.6, 35.9, 28.5, 25.8, 25.6, 11.6.

Matching reported literature data.⁴⁶



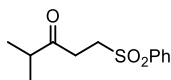
1-Cyclohexyl-3-(phenylsulfonyl)propan-1-one (40i): Synthesized according to the general procedure B using cyclohexanecarbonyl chloride (100 μL , 0.75 mmol, 1.5 equiv.) and phenyl vinyl sulfone (84 mg, 0.5 mmol, 1 equiv.). The crude mixture was purified by flash column chromatography on silica gel (20% AcOEt in hexanes as eluent) to afford **40i** (112 mg, 76% yield) as colorless oil.

A purity of 85% weight was determined $^1\text{H NMR}$ analysis (mixture with phenyl vinyl sulfone). Corrected yield: 68%.

$^1\text{H NMR}$ (400 MHz, CDCl_3) δ 7.93 – 7.86 (m, 2H), 7.69 – 7.62 (m, 1H), 7.62 – 7.50 (m, 2H), 3.39 – 3.32 (m, 2H), 2.97 – 2.89 (m, 2H), 2.39 – 2.25 (m, 1H), 1.88 – 1.58 (m, 5H), 1.38 – 1.08 (m, 5H).

$^{13}\text{C NMR}$ (100 MHz, CDCl_3) δ 193.9, 164.2, 130.4, 128.8, 119.5, 114.1, 55.7, 34.0, 12.0.

Matching reported literature data.⁹³



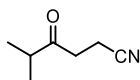
4-Methyl-1-(phenylsulfonyl)pentan-3-one (40e): Synthesized according to the general procedure B using isobutanoyl chloride (100 μL , 0.75 mmol, 1.5 equiv.) and phenyl vinyl sulfone (84 mg, 0.5 mmol, 1 equiv.). The crude mixture was purified by flash column chromatography on silica gel (20% AcOEt in hexanes as eluent), followed by a second one (15% AcOEt in hexanes as eluent) to afford **34h** (61 mg, 51% yield) as a colorless oil.

$^1\text{H NMR}$ (500 MHz, CDCl_3) δ 7.94 – 7.88 (m, 2H), 7.69 – 7.64 (m, 1H), 7.61 – 7.54 (m, 2H), 3.40 – 3.35 (m, 2H), 3.00 – 2.93 (m, 2H), 2.66 – 2.55 (m, 1H), 1.08 (d, $J = 7.0$ Hz, 6H).

$^{13}\text{C NMR}$ (126 MHz, CDCl_3) δ 210.0, 139.2, 134.0, 129.5, 128.1, 50.8, 41.1, 32.7, 18.3.

⁹³ Vu, M. D.; Das, M.; Liu, X.-W. Direct Aldehyde Csp²-H Functionalization through Visible-Light-Mediated Photoredox Catalysis. *Chem. Eur. J.* **2017**, *23*, 15899-15902.

HRMS (ESI pos): calculated for $C_{12}H_{16}NaO_3S$ ($M+Na^+$): 263.0712, found 263.0714.

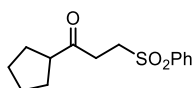


4-Cyclohexyl-4-oxobutanenitrile (40f): Synthesized according to the general procedure B using isobutanoyl chloride (100 μ L, 0.75 mmol, 1.5 equiv.) and acrylonitrile (33 μ L, 0.5 mmol, 1 equiv.). The crude mixture was purified by flash column chromatography on silica gel (20% Et₂O in pentane as eluent) to afford **40f** (39 mg, 62% yield) as a colorless oil.

¹H NMR (500 MHz, CDCl₃) δ 2.83 (t, J = 7.1 Hz, 2H), 2.66 – 2.56 (m, 1H), 2.57 (t, J = 7.2 Hz, 2H), 1.12 (d, J = 7.0 Hz, 6H).

¹³C NMR (126 MHz, CDCl₃) δ 210.0, 119.2, 40.7, 35.6, 18.2, 11.6

Matching reported literature data.⁹⁴

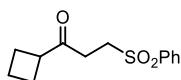


1-Cyclopentyl-3-(phenylsulfonyl)propan-1-one (40o): Synthesized according to the general procedure B using cyclopentanecarbonyl chloride (91 μ L, 0.75 mmol, 1.5 equiv.) and phenyl vinyl sulfone (84 mg, 0.5 mmol, 1 equiv.). The crude mixture was purified by flash column chromatography on silica gel (20% AcOEt in hexanes as eluent) to afford **40o** (102 mg, 77% yield) colorless oil.

¹H NMR (500 MHz, CDCl₃) δ 7.93 – 7.87 (m, 2H), 7.69 – 7.62 (m, 1H), 7.60 – 7.53 (m, 2H), 3.42 – 3.34 (m, 2H), 2.99 – 2.91 (m, 2H), 2.90 – 2.79 (m, 1H), 1.88 – 1.73 (m, 2H), 1.73 – 1.49 (m, 6H).

¹³C NMR (126 MHz, CDCl₃) δ 208.5, 139.2, 134.0, 129.5, 128.1, 51.5, 50.8, 34.0, 29.0, 26.0.

HRMS (ESI pos): calculated for $C_{14}H_{18}NaO_3S$ ($M+Na^+$): 289.0869, found 289.0873.



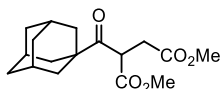
1-Cyclobutyl-3-(phenylsulfonyl)propan-1-one (40q): Synthesized according to the general procedure B using cyclobutanecarbonyl chloride (86 μ L, 0.75 mmol, 1.5 equiv.) and phenyl vinyl sulfone (84 mg, 0.5 mmol, 1 equiv.). The crude mixture was purified by flash column chromatography on silica gel (20% AcOEt in hexanes as eluent) to afford **40q** (116 mg, 92% yield) as a colorless oil.

¹H NMR (500 MHz, CDCl₃) δ 7.92 – 7.88 (m, 2H), 7.68 – 7.63 (m, 1H), 7.60 – 7.54 (m, 2H), 3.40 – 3.35 (m, 2H), 3.29 – 3.20 (m, 1H), 2.87 – 2.81 (m, 2H), 2.24 – 2.08 (m, 4H), 2.02 – 1.90 (m, 1H), 1.84 – 1.75 (m, 1H).

¹³C NMR (126 MHz, CDCl₃) δ 207.1, 139.2, 134.1, 129.5, 128.1, 50.6, 45.4, 32.3, 24.5, 17.9

HRMS (ESI pos): calculated for $C_{13}H_{15}NaO_6$ ($M+Na^+$): 275.0712, found 275.0716.

⁹⁴ Lee, W. Y.; Jang, S. Y.; Chae, W. K.; Park, O. S. A Total Synthesis of Isosolanone. *Synth. Commun.* **1993**, *23*, 3037-3046.

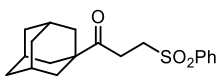
**Dimethyl 2-((3r,5r,7r)-adamantane-1-carbonyl)succinate (40t):**

Synthesized according to the general procedure B using 1-adamantanecarbonyl chloride (149 mg, 0.75 mmol, 1.5 equiv.) and dimethyl fumarate (72 mg, 0.5 mmol, 1 equiv.). The crude mixture was purified by flash column chromatography on silica gel (5% AcOEt in hexanes as eluent) to afford **40t** (85 mg, 55% yield) as a colorless oil.

$^1\text{H NMR}$ (500 MHz, CDCl_3) δ 4.37 (app t, $J = 7.2$ Hz, 1H), 3.67 (s, 3H), 3.64 (s, 3H), 2.79 (app d, $J = 7.2$ Hz, 2H), 2.03 (bs, 3H), 1.89 – 1.79 (m, 6H), 1.76 – 1.63 (m, 6H).

$^{13}\text{C NMR}$ (126 MHz, CDCl_3) δ 208.8, 171.7, 169.5, 52.7, 52.1, 47.7, 47.4, 38.0, 36.4, 33.5, 27.9

HRMS (ESI pos): calculated for $\text{C}_{17}\text{H}_{24}\text{NaO}_5$ ($\text{M}+\text{Na}^+$): 331.1516, found 331.1523.

**1-((3r,5r,7r)-Adamantan-1-yl)-3-(phenylsulfonyl)propan-1-one (40u):**

Synthesized according to the general procedure B using 1-adamantanecarbonyl chloride (149 mg, 0.75 mmol, 1.5 equiv.) and phenyl vinyl sulfone (84 mg, 0.5 mmol, 1 equiv.). The crude mixture was purified by flash column chromatography on silica gel (15% AcOEt in hexanes as eluent) to afford **40u** (165 mg, 95% yield) as a colorless oil.

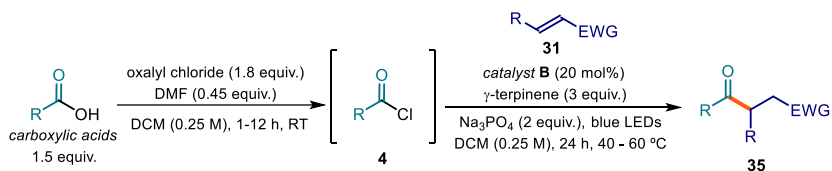
$^1\text{H NMR}$ (500 MHz, CDCl_3) δ 7.93 – 7.88 (m, 2H), 7.68 – 7.63 (m, 1H), 7.60 – 7.54 (m, 2H), 3.37 – 3.29 (m, 2H), 3.00–2.93 (m, 2H), 2.03 (bs, 3H), 1.79 – 1.70 (m, 9H), 1.66 (app d, $J = 12.2$ Hz, 3H).

$^{13}\text{C NMR}$ (126 MHz, CDCl_3) δ 211.2, 139.3, 133.9, 129.4, 128.0, 50.9, 46.5, 38.3, 36.5, 29.1, 27.9.

HRMS (ESI pos): calculated for $\text{C}_{19}\text{H}_{25}\text{O}_3\text{S}$ ($\text{M}+\text{H}^+$): 333.1519, found 333.1519.

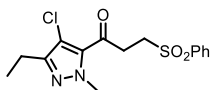
3.9.5 Reaction of carboxylic acids through acyl chloride formation

3.9.5.1 General Procedure C



In a round bottom flask, the carboxylic acid (0.75 mmol, 1.5 equiv) was dissolved in DCM (3 mL, HPLC grade). Then, oxalyl chloride (0.79 μL , 0.90 mmol, 1.8 equiv.) and DMF (17 μL , 0.22 mmol, 0.45 equiv.) were added at ambient temperature. The reaction was stirred at ambient temperature until complete consumption of the carboxylic acid was observed by

TLC. After that, the solvent was evaporated to dryness under vacuum at ambient temperature to obtain the crude acyl chloride, which was used without further purification in the next step. In an oven dried vial, with a Teflon septum screw cap, potassium ethyl xanthogenate **B** (16 mg, 0.10 mmol, 0.2 equiv.), sodium phosphate (164 mg, 1.00 mmol, 2 equiv.), and the electron-poor olefin **31** (0.5 mmol, 1 equiv.), were added. The crude acyl chloride was dissolved in DCM (2 mL, HPLC grade) and the solution was added to the vial, followed by γ -terpinene (240 μ L, 1.5 mmol, 3 equiv.). The resulting yellow mixture was degassed via argon sparging for 60 seconds. If the electron-poor olefin **31** was *liquid*, it was added via syringe after the argon sparging. The vial was then placed in the correspondent reactor (depending on the temperature used for the reaction) and irradiated for 24 hours. The solvent was evaporated and the residue purified by column chromatography to afford the corresponding product in the stated yield with >95% purity according to ^1H NMR analysis.

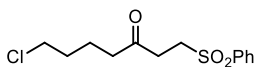


1-(4-Chloro-3-ethyl-1-methyl-1H-pyrazol-5-yl)-3-(phenylsulfonyl)propan-1-one (38w): Synthesized according to the general procedure C using 4-chloro-3-ethyl-1-methyl-1H-pyrazole-5-carboxylic acid (141 mg, 0.75 mmol, 1.5 equiv.) and phenyl vinyl sulfone (84 mg, 0.5 mmol, 1 equiv.). Acyl chloride formation was complete after 2 hours. The crude mixture was purified by flash column chromatography on silica gel (20% AcOEt in hexanes as eluent) to afford **38w** (52 mg, 31% yield) as a white solid.

$^1\text{H NMR}$ (500 MHz, CDCl_3) δ 7.98 – 7.92 (m, 2H), 7.71 – 7.64 (m, 1H), 7.62 – 7.54 (m, 2H), 3.98 (s, 3H), 3.57 – 3.51 (m, 2H), 3.49 – 3.42 (m, 2H), 2.63 (q, J = 7.6, 2H), 1.23 (t, J = 7.5, 2H).

$^{13}\text{C NMR}$ (126 MHz, CDCl_3) δ 186.6, 150.4, 139.0, 134.6, 134.1, 129.5, 128.3, 112.7, 50.6, 41.6, 35.5, 19.2, 12.9.

HRMS (ESI pos): calculated for $\text{C}_{15}\text{H}_{18}\text{ClN}_2\text{O}_3\text{S}$ ($\text{M}+\text{H}^+$): 341.0721, found 341.0709.

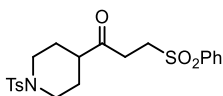


7-chloro-1-(phenylsulfonyl)heptan-3-one (40d): Synthesized according to the general procedure C using 5-chloropentanoic acid (72 μ L, 0.75 mmol, 1.5 equiv.) and dimethyl fumarate (72 mg, 0.5 mmol, 1 equiv.). Acyl chloride formation was complete after 3 hours. The crude mixture was purified by flash column chromatography on silica gel (20% AcOEt in hexanes as eluent). The product was then dissolved in DCM, washed 3 times with a solution of CuSO_4 (5% in water), dried with MgSO_4 and evaporated under reduced pressure to afford **40d** (108 mg, 70% yield) as a white solid.

¹H NMR (400 MHz, CDCl₃) δ 7.92 – 7.87 (m, 2H), 7.69 – 7.63 (m, 1H), 7.60 – 7.54 (m, 2H), 3.53 – 3.47 (m, 2H), 3.41 – 3.35 (m, 2H), 2.92 – 2.86 (m, 2H), 2.50 – 2.44 (m, 2H), 1.78 – 1.64 (m, 4H).

¹³C NMR (100 MHz, CDCl₃) δ 205.5, 139.1, 134.1, 129.5, 128.1, 50.6, 44.6, 41.9 35.0 31.8 20.9.

HRMS (ESI pos): calculated for C₁₃H₁₇ClNaO₃S (M+Na⁺): 311.0479, found 311.0477.



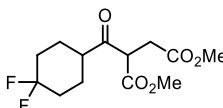
3-(Phenylsulfonyl)-1-(1-tosylpiperidin-4-yl)propan-1-one (40l):

Synthesized according to the general procedure C using 1-tosylpiperidine-4-carboxylic acid (213 mg, 0.75 mmol, 1.5 equiv.) and dimethyl fumarate (72 mg, 0.5 mmol, 1 equiv.). Acyl chloride formation was complete after 3 hours. In this case the reaction was irradiated for 36 hours. The crude mixture was purified by flash column chromatography on silica gel (40% AcOEt in hexanes as eluent) to afford **40l** (164 mg, 75% yield) as a white solid.

¹H NMR (500 MHz, CDCl₃) δ 7.90 – 7.85 (m, 2H), 7.69 – 7.64 (m, 1H), 7.64 – 7.60 (m, 2H), 7.60 – 7.54 (m, 2H), 7.32 (app d, *J* = 7.9 Hz, 2H), 3.71 (dt, *J* = 12.2, 3.5 Hz, 2H), 3.35 (app t, *J* = 7.4 Hz, 2H), 2.91 (app t, *J* = 7.4 Hz, 2H), 2.43 (s, 3H), 2.38 (td, *J* = 11.7, 2.5 Hz, 2H), 2.33 – 2.24 (m, 1H), 1.93 – 1.84 (m, 2H), 1.75 – 1.63 (m, 2H).

¹³C NMR (126 MHz, CDCl₃) δ 206.9, 143.8, 139.1, 134.2, 133.2, 129.9, 129.6, 128.0, 127.8, 50.6, 47.6, 45.5, 33.0, 27.0, 21.7.

HRMS (ESI pos): calculated for C₂₁H₂₆NO₅S₂ (M+H⁺): 436.1247, found 436.1251.



dimethyl 2-(4,4-difluorocyclohexane-1-carbonyl)succinate (40n):

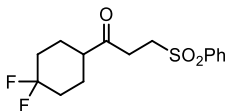
Synthesized according to the general procedure C using 4,4-difluorocyclohexane-1-carboxylic acid (123 mg, 0.75 mmol, 1.5 equiv.) and dimethyl fumarate (72 mg, 0.5 mmol, 1 equiv.). Acyl chloride formation was complete after 1 hour. The crude mixture was purified by flash column chromatography on silica gel (20% Et₂O in hexanes as eluent) to afford **40n** (128 mg, 88% yield) as a white solid.

¹H NMR (400 MHz, CDCl₃) δ 4.16 (dd, *J* = 9.1, 5.3 Hz, 1H), 3.73 (s, 3H), 3.67 (s, 3H), 3.03 (dd, *J* = 17.6, 9.3 Hz, 1H), 2.82 (dd, *J* = 17.5, 5.3 Hz, 1H), 2.83 – 2.74 (m, 1H), 2.22 – 2.02 (m, 3H), 1.98 – 1.65 (m, 5H).

¹³C NMR (100 MHz, CDCl₃) δ 205.6, 171.9, 168.8, 122.7 (dd, *J* = 241.6, 240.9 Hz), 53.0, 52.2, 52.1, 48.0, 32.7 (dd, *J* = 25.0 Hz), 25.2 (d, *J* = 9.0 Hz) 24.4 (d, *J* = 8.6 Hz)

¹⁹F NMR (376 MHz, CDCl₃, proton decoupled) δ -93.75 (d, *J* = 237.2 Hz, 1F); -100.48 (d, *J* = 238.2 Hz, 1F).

HRMS (ESI pos): calculated for $C_{13}H_{18}F_2NaO_5$ ($M+Na^+$): 315.1015, found 315.1017.



1-(4,4-Difluorocyclohexyl)-3-(phenylsulfonyl)propan-1-one (40m):

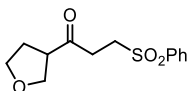
Synthesized according to the general procedure C using 4,4-difluorocyclohexane-1-carboxylic acid (123 mg, 0.75 mmol, 1.5 equiv.) and dimethyl fumarate (72 mg, 0.5 mmol, 1 equiv.). Acyl chloride formation was complete after 1 hour. The crude mixture was purified by flash column chromatography on silica gel (30% AcOEt in hexanes as eluent) to afford **40m** (112 mg, 71% yield) as a white solid.

1H NMR (400 MHz, $CDCl_3$) δ 7.93 – 7.88 (m, 2H), 7.70 – 7.64 (m, 1H), 7.61 – 7.55 (m, 2H), 3.41 – 3.35 (m, 2H), 3.01 – 2.94 (m, 2H), 2.52 – 2.39 (m, 1H), 2.18 – 2.04 (m, 2H), 1.99 – 1.86 (m, 2H), 1.85 – 1.64 (m, 4H).

^{13}C NMR (100 MHz, $CDCl_3$) δ 207.4, 139.2, 134.1, 129.6, 128.0, 122.5 (dd, $J = 241.6, 240.7$ Hz) 50.6, 48.1, 33.2, 32.7 (dd, $J = 24.4, 24.2$ Hz), 24.7 (d, $J = 9.5$ Hz).

^{19}F NMR (376 MHz, $CDCl_3$, proton decoupled) δ -93.72 (dd, $J = 237.6$ Hz); -100.82 (d, $J = 237.7$ Hz).

HRMS (ESI pos): calculated for $C_{15}H_{18}F_2NaO_3S$ ($M+Na^+$): 339.0837, found 339.0840.



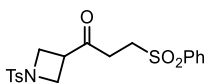
3-(Phenylsulfonyl)-1-(tetrahydrofuran-3-yl)propan-1-one (40p):

Synthesized according to the general procedure C using tetrahydrofuran-3-carboxylic acid (72 μ L, 0.75 mmol, 1.5 equiv.) and dimethyl fumarate (72 mg, 0.5 mmol, 1 equiv.). Acyl chloride formation was complete after 1 hour. The crude mixture was purified by flash column chromatography on silica gel (50% AcOEt in hexanes as eluent). The product was then dissolved in DCM, washed 3 times with a solution of $CuSO_4$ (5% in water), dried with $MgSO_4$ and evaporated under reduced pressure to afford **40p** (78 mg, 58% yield) as a colorless oil.

1H NMR (500 MHz, $CDCl_3$) δ 7.94 – 7.87 (m, 2H), 7.71 – 7.64 (m, 1H), 7.62 – 7.54 (m, 2H), 3.94 – 3.73 (m, 4H), 3.47 – 3.34 (m, 2H), 3.26 – 3.17 (m, 1H), 3.07 – 2.89 (m, 2H), 3.16 – 2.01 (m, 2H).

^{13}C NMR (126 MHz, $CDCl_3$) δ 205.6, 139.1, 134.1, 129.6, 128.1, 69.3, 68.4, 51.1, 50.6, 34.4, 29.1.

HRMS (ESI pos): calculated for $C_{13}H_{16}NaO_4S$ ($M+Na^+$): 291.0662, found 291.0665.



3-(Phenylsulfonyl)-1-(1-tosylazetididin-3-yl)propan-1-one (40r):

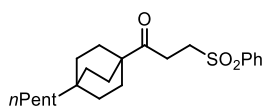
Synthesized according to the general procedure C using 1-tosylazetididine-3-carboxylic acid (191 mg, 0.75 mmol, 1.5 equiv.) and dimethyl fumarate (72

mg, 0.5 mmol, 1 equiv.). Acyl chloride formation was complete after 2 hours. In this case the reaction was irradiated for 36 hours. The crude mixture was purified by flash column chromatography on silica gel (40% AcOEt in hexanes as eluent) to afford **40r** (63 mg, 31% yield) as a white solid.

¹H NMR (400 MHz, CDCl₃) δ 7.88 – 7.82 (m, 2H), 7.74 – 7.63 (m, 3H), 7.60 – 7.53 (m, 2H), 7.40 – 7.33 (m, 2H), 3.92 – 3.88 (m, 2H), 3.88 – 3.81 (m, 2H), 3.41 – 3.28 (m, 3H), 2.79 (app t, *J* = 7.3 Hz, 2H), 2.44 (s, 3H).

¹³C NMR (100 MHz, CDCl₃) δ 202.1, 144.6, 138.9, 134.2, 131.3, 130.0, 129.6, 128.5, 128.0, 51.8, 50.3, 38.1, 33.1, 21.7.

HRMS (ESI pos): calculated for C₁₉H₂₁NNaO₅S₂ (M+Na⁺): 430.0753, found 430.0748.



1-(4-Pentylbicyclo[2.2.2]octan-1-yl)-3-(phenylsulfonyl)propan-1-one (40s): Synthesized according to the general procedure C using 4-pentylbicyclo[2.2.2]octane-1-

carboxylic acid (168 mg, 0.75 mmol, 1.5 equiv.) and phenyl vinyl sulfone (84 mg, 0.5 mmol, 1 equiv.). Acyl chloride formation was complete after 2 hours. Chromatography on silica gel (10% AcOEt in hexanes as eluent) could not remove byproducts completely. Purification by semipreparative HPLC (IC column, 60:40 Hexane/Ethanol, 1 mL/min) was performed to obtain an analytical amount of product **40s** as a white solid. NMR yield (Trichloroethylene was used as internal standard): 80%.

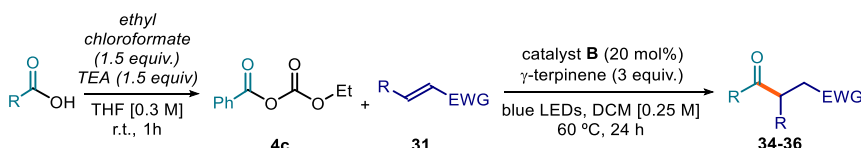
¹H NMR (500 MHz, CDCl₃) δ 7.93 – 7.87 (m, 2H), 7.69 – 7.63 (m, 1H), 7.61 – 7.54 (m, 2H), 3.36 – 3.29 (m, 2H), 2.97 – 2.90 (m, 2H), 1.69 – 1.61 (m, 6H), 1.43 – 1.34 (m, 6H), 1.31 – 1.24 (m, 2H), 1.24 – 1.12 (m, 4H), 1.11 – 1.04 (m, 2H), 0.87 (t, *J* = 7.3 Hz, 3H).

¹³C NMR (126 MHz, CDCl₃) δ 211.6, 139.4, 134.0, 129.5, 128.1, 51.0, 45.3, 41.3, 32.9, 30.8, 30.5, 30.1, 28.2, 23.5, 22.8, 14.2.

HRMS (ESI pos): calculated for C₂₂H₃₂NaO₃S (M+Na⁺): 399.1964, found 399.1951.

Reaction of carboxylic acids through anhydride formation

General Procedure D1



In a round bottom flask or vial, the carboxylic acid (0.75 mmol, 1.5 equiv) was dissolved in THF (2.5 mL, HPLC grade). Then, triethylamine (TEA, 105 μL, 0.75 mmol, 1.5 equiv.) and ethyl chloroformate (72 μL, 0.75 mmol, 1.5 equiv.) were added at ambient temperature. The reaction was stirred at ambient temperature for 1 hour. After that, it was filtered and the

remaining solid was washed with diethyl ether. The organic layers were concentrated to dryness under reduced pressure to obtain the crude anhydride, which was used without further purification in the next step. (When the carboxylic acid is not completely soluble in 2.5 mL of THF, follow the general procedure D2 detailed below).

In an oven dried tube or a vial, with a Teflon septum screw cap, potassium ethyl xanthogenate **B** (16 mg, 0.10 mmol, 0.2 equiv.) and the electron-poor olefin **31** (0.5 mmol, 1 equiv., *if solid*), were added. The crude anhydride was dissolved in DCM (2 mL, HPLC grade) and the solution was added to the vial, followed by γ -terpinene (240 μ L, 1.5 mmol, 3 equiv.). The resulting yellow mixture was degassed with argon sparging for 60 seconds. If the electron-poor olefin **31** was *liquid*, it was added via syringe after the argon sparging. The vial was then placed in the correspondent photoreactor (depending on the temperature used for the reaction) and irradiated for 24 hours. The solvent was evaporated and the residue purified by column chromatography to afford the corresponding product in the stated yield with >95% purity, according to ^1H NMR analysis.

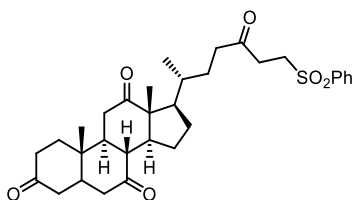
This procedure was employed for the optimization of the catalytic reaction with anhydride as radical precursor and for the scale-up process, as indicated below.

Note: Filtration of the triethylammonium salt is crucial for the reaction to work. Therefore, attempts to perform the reaction one-pot without removal of the ammonium salt were unsuccessful.

General Procedure D2

In a round bottom flask or vial, the carboxylic acid (0.75 mmol, 1.5 equiv.) was dissolved in THF (10 mL, HPLC grade). Then, triethylamine (105 μ L, 0.75 mmol, 1.5 equiv.) and ethyl chloroformate (72 μ L, 0.75 mmol, 1.5 equiv.) were added at ambient temperature. The reaction was stirred for 1 hour. The reaction crude was washed with water and NaHCO_3 saturated solution, dried over MgSO_4 , filtered and the organic layers concentrated to dryness under vacuum. The crude carbonate was used without further purification in the next step.

In an oven dried tube of 15 mL (16 mm \times 12.5 mm) or a vial, with a Teflon septum screw cap, potassium ethyl xanthogenate (16.02 mg, 0.10 mmol, 0.2 equiv.) and the electron-poor olefin **31** (0.5 mmol, 1 equiv. *if solid*), were added. The crude carbonate was dissolved in DCM (2 mL, HPLC grade) and the solution was added to the vial, followed by γ -terpinene (240 μ L, 1.5 mmol, 3 equiv.). The resulting yellow mixture was degassed with argon sparging for 60 seconds. If the electron-poor olefin **31** was *liquid*, it was added via syringe after the argon sparging. The vial was then placed in the correspondent photoreactor and irradiated for 24 hours. After cooling to ambient temperature, the solvent was evaporated and the residue purified by column chromatography to afford the corresponding product in the stated yield with >95% purity according to ^1H NMR analysis.



(8R,9S,10S,13R,14S,17R)-10,13-dimethyl-17-((R)-5-oxo-7-(phenylsulfonyl)heptan-2-yl)dodecahydro-3H-cyclopenta[a]phenanthrene-3,7,12(2H,4H)-trione

(40v): Synthesized according to the general procedure **D2** using dehydrocholic acid (302 μL , 0.75 mmol, 1.5 equiv.) and phenyl vinyl sulfone (84 mg, 0.5 mmol, 1 equiv.).

The crude mixture was purified by flash column chromatography on silica gel (33% acetone in hexanes as eluent), followed by a second purification (20% AcOEt in DCM as eluent) to afford **40v** (145 mg, 52% yield) as a colorless oil.

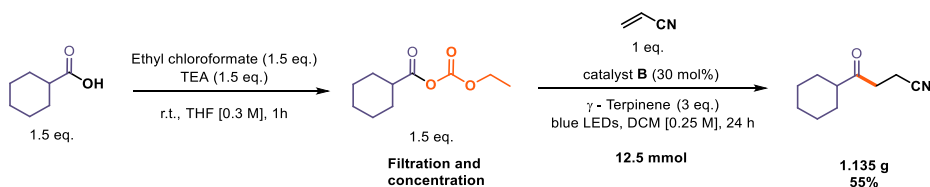
$^1\text{H NMR}$ (500 MHz, CDCl_3) δ 7.93 – 7.88 (m, 2H), 7.70 – 7.64 (m, 1H), 7.61 – 7.55 (m, 2H), 3.44 – 3.32 (m, 2H), 2.95 – 2.79 (m, 5H), 2.54 – 2.44 (m, 1H), 2.44 – 2.10 (m, 9H), 2.07 – 1.90 (m, 4H), 1.89 – 1.80 (m, 1H), 1.80 – 1.70 (m, 1H), 1.67 – 1.56 (m, 1H), 1.39 (s, 3H), 1.36 – 1.20 (m, 4H), 1.05 (s, 3H), 0.81 (d, $J = 6.5$ Hz, 3H).

$^{13}\text{C NMR}$ (126 MHz, CDCl_3) δ 212.0, 209.1, 208.8, 206.5, 139.2, 134.1, 129.6, 128.1, 57.0, 51.9, 50.6, 49.1, 47.0, 45.7, 45.7, 45.1, 42.9, 40.0, 38.8, 36.6, 36.1, 35.4, 35.4, 35.1, 29.1, 27.8, 25.2, 22.0, 18.9, 12.0.

HRMS (ESI pos): calculated for $\text{C}_{32}\text{H}_{42}\text{NaO}_6\text{S}$ ($\text{M}+\text{Na}^+$): 577.2594, found 577.2607.

2.10.5 Scale-up reaction

Experimental Setup and Procedure



In a 100 mL round bottom flask, cyclohexanecarboxylic acid (2.34 mL, 18.75 mmol, 1.5 equiv.) was dissolved in THF (60 mL, HPLC grade). Then, triethylamine (2.61 mL, 18.75 mmol, 1.5 equiv.) and ethyl chloroformate (1.80 mL, 18.75 mmol, 1.5 equiv.) were added at ambient temperature. The reaction was stirred at ambient temperature for 1 hour. Then, it was filtered into a 100 mL reaction flask that will be used as reaction vessel for the next step (the remaining solid was carefully washed with diethyl ether). The organic phase was concentrated to dryness under vacuum to obtain the crude carbonate, which was used without further purification in the next step.

In the same 100 mL round bottom flask with a Teflon septum, the crude carbonate was dissolved in DCM (50 mL, HPLC grade). Potassium ethyl xanthogenate **B** (601 mg, 3.75 mmol, 0.3 equiv.) and γ -terpinene (6.01 mL, 37.5 mmol, 3 equiv.) were added to the solution. The resulting yellow mixture was degassed with Nitrogen sparging for 2 minutes. Finally,

acrylonitrile (0.819 mL, 12.5 mmol, 1 equiv.) was added via syringe. The round bottom flask was then irradiated for 20 hours with a one meter 14W blue LED strip and cooled with a fan to keep the temperature between 30 and 35 °C (see Figure 3.12). After 24 hours, complete conversion of acrylonitrile was inferred by ^1H NMR analysis. The mixture was transferred to an extraction funnel, water was added and the organic layer was extracted with DCM. The organic layer was dried (MgSO_4) and concentrated to dryness. The product was then purified by chromatography on silica gel (10% AcOEt in hexanes) to afford 1.130 g of product **34e** (6.87 mmol, 55% yield) as a yellowish oil. NMR analysis was consistent with product synthesized in the small scale process.

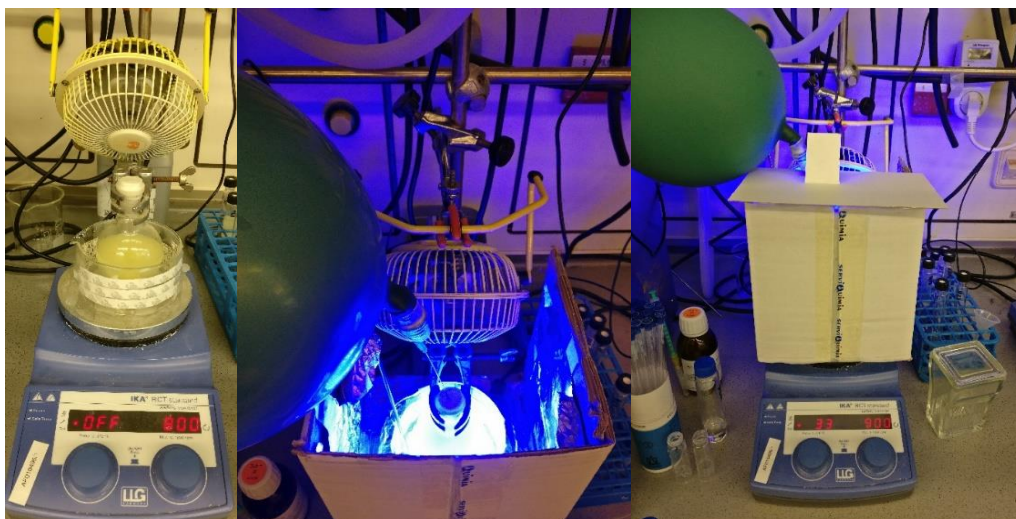


Figure 2.44. Experimental setup used for the large scale set up. (Left) Before irradiation. (Middle) Reaction set up from above. (Right) Reaction set up from the front.

Reaction of Carbamoyl Chlorides

Experimental Setup

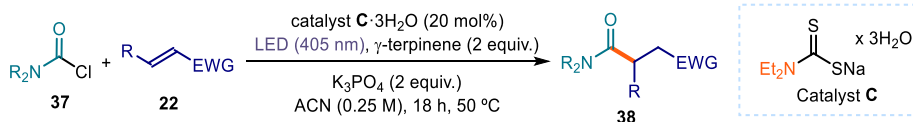
For the generation of carbamoyl radicals, we used the Hepatochem PhotoRedOx Box equipped with an EvoluChem LED 18 W light source at 405 nm, supplied by Hepatochem.



Figure 2.45. Photoreactor used for the reaction with the carbamoyl chlorides

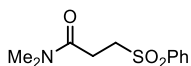
The reactor was connected to a Huber Minichiller 300 in order to perform reactions at 50 °C with accurate control of the reaction temperature ($\pm 1^\circ\text{C}$, Figure 3.13).

General Procedure for the intermolecular Giese addition (General Procedure E)



An oven-dried 15 mL Schlenk tube was charged with a mixture of carbamoyl chloride **37** (0.4 mmol, 2 equiv.), catalyst **C** trihydrate (9 mg, 0.04 mmol, 0.2 equiv.), alkene **31** (0.2 mmol, 1 equiv.), γ -terpinene (64 μL , 0.4 mmol, 2 equiv.) and K_3PO_4 (85 mg, 0.4 mmol, 2 equiv.) in acetonitrile (0.8 mL, 0.25 M). The reaction mixture was placed under an atmosphere of argon, cooled to -78°C , degassed *via* vacuum evacuation (5 minutes), backfilled with argon and, ultimately, warmed to ambient temperature. This freeze-pump-thaw cycle was repeated four times, and then the Schlenk tube was sealed with Parafilm and put into the Hepatochem PhotoRedOx Box equipped with a 405 nm EvoluChem LED 18 W light source at 50 °C (Figure 3.13). After 18 hours stirring, the reaction was cooled down to ambient temperature, water was added and the mixture was extracted with ethyl acetate (2x15 mL). The combined layers were dried over magnesium sulfate, filtered, and concentrated. The resulting crude mixture was purified by column chromatography on silica gel to give the corresponding product **38** in the stated yield.

Characterization of Products

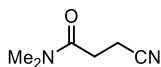


***N,N*-Dimethyl-3-(phenylsulfonyl)propanamide (33a)**: Synthesized according to general procedure E using dimethylcarbamic chloride (37 μL , 0.4 mmol, 2.0 equiv.) and phenyl vinyl sulfone (34 mg, 0.2 mmol). The crude mixture was purified by flash column chromatography on silica gel (gradient from hexane 100% to ethyl acetate 100%) to afford product **33a** (29 mg, 60% yield) as a pale-yellow oil.

$^1\text{H NMR}$ (400 MHz, CDCl_3) δ 7.95 – 7.88 (m, 2H), 7.69 – 7.62 (m, 1H), 7.61 – 7.52 (m, 2H), 3.53 – 3.33 (m, 2H), 2.99 (s, 3H), 2.89 (s, 3H), 2.85 – 2.73 (m, 2H).

$^{13}\text{C NMR}$ (100 MHz, CDCl_3) δ 168.8, 139.2, 134.0, 129.5, 128.1, 52.2, 37.2, 35.7, 26.2.

HRMS (ESI pos): calculated for $\text{C}_{11}\text{H}_{15}\text{NNaO}_3\text{S}$ ($\text{M}+\text{Na}^+$): 264.0665, found 264.0653.

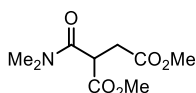


3-Cyano-*N,N*-dimethylpropanamide (33b): Synthesized according to general procedure E using dimethylcarbamic chloride (37 μL , 0.4 mmol, 2.0 equiv.) and acrylonitrile (13 μL , 0.2 mmol). The crude mixture was purified by flash column chromatography on silica gel (gradient from hexane 100% to ethyl acetate 100%) to afford product **33b** (16 mg, 63% yield) as a pale-yellow oil.

$^1\text{H NMR}$ (400 MHz, CDCl_3) δ 3.01 (s, 3H), 2.97 (s, 3H), 2.68 (s, 4H).

$^{13}\text{C NMR}$ (100 MHz, CDCl_3) δ 168.8, 119.6, 37.0, 35.7, 29.5, 13.1.

HRMS (ESI pos): calculated for $\text{C}_6\text{H}_{11}\text{N}_2\text{O}$ ($\text{M}+\text{H}^+$): 127.0866, found: 127.0869.

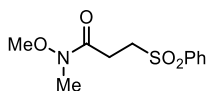


dimethyl 2-(dimethylcarbamoyl)succinate (33c): Synthesized according to general procedure E using dimethylcarbamic chloride (37 μL , 0.4 mmol, 2.0 equiv.) and dimethyl fumarate (29 mg, 0.2 mmol). The crude mixture was purified by flash column chromatography on silica gel (gradient from hexane 100% to ethyl acetate 100%) to afford product **33c** (27 mg, 62% yield) as a pale-yellow oil.

$^1\text{H NMR}$ (400 MHz, CDCl_3) δ 4.14 (dd, $J = 8.3, 6.0$ Hz, 1H), 3.72 (s, 3H), 3.67 (s, 3H), 3.16 (s, 3H), 3.11 – 2.80 (m, 6H).

$^{13}\text{C NMR}$ (100 MHz, CDCl_3) δ 172.4, 169.5, 167.9, 53.0, 52.2, 44.6, 38.0, 36.4, 33.6.

HRMS (ESI pos): calculated for $\text{C}_9\text{H}_{15}\text{NNaO}_5$ ($\text{M}+\text{Na}^+$): 240.0842, found: 240.0844.



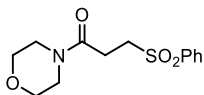
***N*-Methoxy-*N*-methyl-3-(phenylsulfonyl)propanamide (33d)**: Synthesized according to general procedure E using methoxy(methyl)carbamic chloride (41 μL , 0.4 mmol, 2.0 equiv.) and phenyl vinyl sulfone (34 mg, 0.2 mmol). The crude mixture was purified by flash column

chromatography on silica gel (gradient from hexane 100% to hexane 50% : 50% ethyl acetate) to afford product **33d** (16 mg, 30% yield) as a pale yellow oil.

$^1\text{H NMR}$ (400 MHz, CDCl_3) δ 7.97 – 7.90 (m, 2H), 7.75 – 7.63 (m, 1H), 7.63 – 7.54 (m, 2H), 3.69 (s, 3H), 3.52 – 3.37 (m, 2H), 3.14 (s, 3H), 2.97 – 2.92 (m, 2H).

$^{13}\text{C NMR}$ (101 MHz, CDCl_3) 170.4, 139.2, 134.0, 129.5, 128.2, 61.6, 51.5, 32.3, 25.4.

HRMS (ESI pos): calculated for $\text{C}_9\text{H}_{15}\text{NNaO}_5$ ($\text{M}+\text{Na}^+$): 240.0842, found: 240.0844.

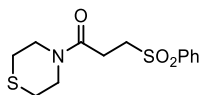


1-Morpholino-3-(phenylsulfonyl)propan-1-one (33e): Synthesized according to general procedure E using morpholine-4-carbonyl chloride (47 μL , 0.4 mmol, 2.0 equiv.) and phenyl vinyl sulfone (34 mg, 0.2 mmol). The crude mixture was purified by flash column chromatography on silica gel (gradient from hexane 100% to ethyl acetate 100%) to afford product **33e** (42 mg, 74% yield) as a pale-yellow oil.

$^1\text{H NMR}$ (400 MHz, CDCl_3) δ 8.00 – 7.85 (m, 2H), 7.71 – 7.62 (m, 1H), 7.62 – 7.51 (m, 1H), 3.76 – 3.58 (m, 5H), 3.55 – 3.49 (m, 2H), 3.47 – 3.42 (m, 3H), 2.94 – 2.74 (m, 2H).

$^{13}\text{C NMR}$ (100 MHz, CDCl_3) δ 167.5, 139.1, 134.0, 129.5, 128.0, 66.7, 66.5, 52.0, 45.8, 42.3, 25.9.

HRMS (ESI pos): calculated for $\text{C}_{13}\text{H}_{17}\text{NNaO}_4\text{S}$ ($\text{M}+\text{Na}^+$): 306.0770, found: 306.0762.

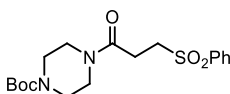


3-(Phenylsulfonyl)-1-thiomorpholinopropan-1-one (33f): synthesized according the general procedure E using thiomorpholine-4-carbonyl chloride **8f** (99 mg, 0.4 mmol, 2 eq.) and phenyl vinyl sulfone (34 mg, 0.2 mmol, 1 eq.). The crude mixture was purified by flash column chromatography on silica gel (5% AcOEt in hexane), followed by a second one (50% AcOEt in Hexane as eluent) to afford **33f** (37.8 mg, 63% yield) as a colorless oil.

$^1\text{H NMR}$ (400 MHz, CDCl_3) δ 7.96 (m, 2H) 7.70 (m, 1H) 7.61 (m, 2H) 3.85 (m, 2H), 3.76 (m, 1H), 3.65 (m, 1H), 3.50 (m, 1H), 2.86, (m, 2H), 2.64 (m, 6H).

$^{13}\text{C NMR}$ (126 MHz, CDCl_3) δ 167.3, 139.3, 134.1, 129.5, 128.1, 52.2, 48.3, 44.8, 27.9, 27.4, 26.2

HRMS (ESI pos): calculated for $\text{C}_{13}\text{H}_{17}\text{NaNO}_3\text{S}_2$ ($\text{M}+\text{Na}^+$): 322.05, found: 322.0533.



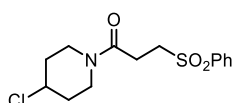
tert-Butyl 4-(3-(phenylsulfonyl)propanoyl)piperazine-1-carboxylate (33g): synthesized according general procedure E using tert-butyl 4-(chlorocarbonyl)piperazine-1-carboxylate (99 mg, 0.4 mmol, 2 eq.) and phenyl vinyl sulfone (34 mg, 0.2 mmol, 1 eq.). The crude mixture was purified by flash column chromatography on silica gel (5% AcOEt in hexane), followed by a

second purification (50% AcOEt in hexane as eluent) to afford **33g** (55 mg, 73% yield) as a white solid.

$^1\text{H NMR}$ (400 MHz, CDCl_3) δ 7.91 (m, 2H), 7.66 (m, 1H), 7.57 (m, 2H), 3.42 (m, 4H) 3.21 (m, 6H), 2.83 (t, $J = 7.8$ Hz, 2H), 1.45 (s, 9H)

$^{13}\text{C NMR}$ (126 MHz, CDCl_3) δ 167.6, 154.6, 139.3, 134.1, 129.6, 128.1, 80.7, 52.1, 45.4, 41.9, 28.5, 26.1

HRMS (ESI pos): calculated for $\text{C}_{18}\text{H}_{26}\text{NaN}_2\text{O}_5\text{S}$ ($\text{M}+\text{Na}^+$): 405.15, found 405.1455.



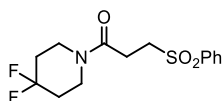
1-(4-Chloropiperidin-1-yl)-3-(phenylsulfonyl)propan-1-one

(33h): Synthesized according to general procedure E using 4-chloropiperidine-1-carbonyl chloride (73 mg, 0.4 mmol, 2 equiv.) and phenyl vinyl sulfone (34 mg, 0.2 mmol). The crude mixture was purified by flash column chromatography on silica gel (gradient from hexane 100% to ethyl acetate 100%) to afford product **33h** (41 mg, 65% yield) as a pale-yellow oil.

$^1\text{H NMR}$ (400 MHz, CDCl_3) δ 7.96 – 7.87 (m, 2H), 7.72 – 7.62 (m, 1H), 7.60 – 7.53 (m, 2H), 4.27 (tt, $J = 7.0, 3.6$ Hz, 1H), 3.68 (tdt, $J = 11.7, 8.2, 3.5$ Hz, 2H), 3.58 (ddd, $J = 13.6, 6.9, 4.0$ Hz, 1H), 3.49 – 3.42 (m, 2H), 3.38 (ddd, $J = 13.9, 7.0, 3.7$ Hz, 1H), 2.83 (td, $J = 7.1, 1.9$ Hz, 2H), 2.16 – 1.93 (m, 2H), 1.90 – 1.72 (m, 2H).

$^{13}\text{C NMR}$ (100 MHz, CDCl_3) δ 167.2, 139.2, 134.0, 129.5, 128.0, 56.1, 52.1, 42.5, 39.1, 35.1, 34.4, 25.9.

HRMS (ESI pos): calculated for $\text{C}_{14}\text{H}_{19}\text{ClNO}_3\text{S}$ ($\text{M}+\text{H}^+$): 316.0769, found: 316.0773.



1-(4,4-Difluoropiperidin-1-yl)-3-(phenylsulfonyl)propan-1-one

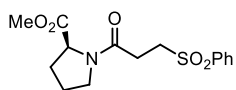
(33i): Synthesized according to general procedure E using 4,4-difluoropiperidine-1-carbonyl chloride (73 mg, 0.4 mmol, 2 equiv.) and phenyl vinyl sulfone (34 mg, 0.2 mmol). The crude mixture was purified by flash column chromatography on silica gel (gradient from hexane 100% to 1:1 hexane/ethyl acetate) to afford product **33i** (43 mg, 68% yield) as an off-white solid.

$^1\text{H NMR}$ (400 MHz, CDCl_3) δ 7.96 – 7.88 (m, 2H), 7.71 – 7.63 (m, 1H), 7.61 – 7.54 (m, 2H), 3.61 (dt, $J = 43.9, 6.0$ Hz, 4H), 3.51 – 3.43 (m, 2H), 2.92 – 2.83 (m, 2H), 2.13 – 1.84 (m, 4H).

$^{13}\text{C NMR}$ (100 MHz, CDCl_3) δ 167.4, 139.2, 134.1, 129.5, 128.0, 121.3 (t, $J = 242.4$ Hz), 52.1, 40.7 (dt, $J = 330.8, 5.4$ Hz), 34.1 (dt, $J = 78.0, 23.6$ Hz), 25.9.

$^{19}\text{F NMR}$ (376 MHz, CDCl_3) δ -98.22 (p, $J = 13.5$ Hz).

HRMS (ESI pos): calculated for $\text{C}_{18}\text{H}_{18}\text{F}_2\text{NaNO}_4$ ($\text{M}+\text{Na}^+$): 340.0789, found: 340.0785.



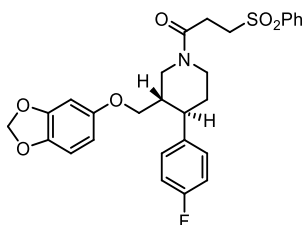
Methyl (3-(phenylsulfonyl)propanoyl)-L-prolinate (33j):

synthesized according the general procedure E using methyl (chlorocarbonyl)-L-prolinate (77 mg, 0.4 mmol, 2 eq.) and phenyl vinyl sulfone (34 mg, 0.2 mmol, 1 eq.). The crude mixture was purified by flash column chromatography on silica gel (5% AcOEt in hexane) to afford **38j** (46 mg, 58% yield) as a yellowish oil.

$^1\text{H NMR}$ (400 MHz, CDCl_3) δ 7.95 – 7.89 (m, 2H), 7.69 – 7.64 (m, 1H), 7.61 – 7.53 (m, 2H), 4.42 (dd, $J = 8.4, 3.5$ Hz, 1H), 3.70 (s, 3H), 3.68 – 3.59 (m, 1H), 3.56 – 3.38 (m, 3H), 2.83 (dt, $J = 9.7, 5.6$ Hz, 2H), 2.11 – 1.94 (m, 4H).

$^{13}\text{C NMR}$ (126 MHz, CDCl_3) δ 172.6, 167.8, 139.2, 134, 129.5, 128.1, 58.9, 52.4, 51.7, 47.1, 29.3, 27.4, 24.8.

HRMS (ESI pos): calculated for $\text{C}_{15}\text{H}_{19}\text{NaNO}_5\text{S}$ ($\text{M}+\text{Na}^+$): 326.10, found: 326.1063.



1-(3-((Benzo[d][1,3]dioxol-5-yloxy)methyl)-4-(4-fluorophenyl)piperidin-1-yl)-3-(phenylsulfonyl)propan-1-one (33k):

synthesized according the general procedure E using 3-((benzo[d][1,3]dioxol-5-yloxy)methyl)-4-(4-fluorophenyl)piperidine-1-carbonyl chloride **37k** (157 mg, 0.4 mmol, 2 eq.) and phenyl vinyl sulfone (34 mg, 0.2 mmol,

1 eq.). The crude mixture was purified by flash column chromatography on silica gel (gradient from hexane 100% to hexane 50:50 ethyl acetate) to afford product **33k** (46 mg, 29% yield) as a yellowish oil.

$^1\text{H NMR}$ (400 MHz, CDCl_3) δ 7.98 (m, 2H), 7.71 (m, 1H), 7.65 – 7.58 (m, 2H), 7.17 – 7.11 (m, 2H), 7.01 (m, 2H), 6.66 (dd, $J = 17.8, 8.4$ Hz, 1H), 6.38 (dd, $J = 11.9, 2.5$ Hz, 1H), 6.17 (ddd, $J = 15.1, 8.5, 2.5$ Hz, 1H), 5.92 (d, $J = 13.5$ Hz, 2H), 4.79 (dd, $J = 55.2, 13.1$ Hz, 1H), 4.07 (dd, $J = 69.6, 13.5$ Hz, 1H), 3.68 – 3.60 (m, 1H), 3.59 – 3.45 (m, 3H), 3.17 (m, 1H), 3.03 – 2.80 (m, 2H), 2.80 – 2.62 (m, 1H), 1.92 (m, 1H), 1.81 – 1.53 (m, 3H).

$^{13}\text{C NMR}$ (126 MHz, CDCl_3) δ 167.5, 154.5, 148.7, 142.3, 139.6, 138.4, 134.3, 129.7, 129.1, 128.3, 115.7, 115.8, 108.2, 106.0, 101.5, 98.4, 68.9, 52.5, 49.2, 46.4, 44.5, 42.2, 34.6, 33.8, 30.1, 26.3.

$^{19}\text{F NMR}$ (376 MHz, CDCl_3 , proton decoupled) δ – 115.58

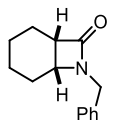
HRMS (ESI pos): calculated for $\text{C}_{28}\text{H}_{29}\text{FNO}_6\text{S}$ ($\text{M}+\text{H}^+$): 526.16, found: 526.1702.

General Procedure for the intramolecular cyclization (General Procedure F)



An oven-dried 15 mL Schlenk tube was charged with a mixture of carbamoyl chloride **28a** (0.2 mmol, 1 equiv.), catalyst **C** trihydrate (9 mg, 0.04 mmol, 0.2 equiv.), γ -terpinene (48 μ L, 0.3 mmol, 1.5 equiv.) and K₃PO₄ (85 mg, 0.4 mmol, 2 equiv.) in acetonitrile (0.8 mL, 0.25 M). The reaction mixture was placed under an atmosphere of argon, cooled to -78 °C, degassed *via* vacuum evacuation (5 minutes), backfilled with argon and, ultimately, warmed to ambient temperature. This freeze-pump-thaw cycle was repeated four times, and then the Schlenk tube was sealed with Parafilm and put into the Hepatochem PhotoRedOx Box equipped with a 405 nm EvoluChem LED 18 W light source at 50 °C (Figure 3.13). After 18 hours, the reaction vessel was cooled down to ambient temperature, water was added and the mixture was extracted with ethyl acetate (2x15 mL). The combined layers were dried over magnesium sulfate, filtered, and concentrated. The resulting crude mixture was purified by column chromatography on silica gel to give the corresponding product **29** in the stated yield.

Characterization of Products

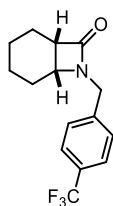


7-Benzyl-7-azabicyclo[4.2.0]octan-8-one (29b): Synthesized according to the general procedure F using benzyl(cyclohex-2-en-1-yl)carbamic chloride (50 mg, 0.2 mmol). The crude mixture was purified by flash column chromatography on silica gel (10% AcOEt in hexanes as eluent) to afford product **29b** (26 mg, 60% yield) as a pale-yellow oil.

¹H NMR (500 MHz, CDCl₃) δ 7.35 – 7.29 (m, 2H), 7.29 – 7.22 (m, 3H), 4.57 (d, J = 15.1 Hz, 1H), 4.08 (d, J = 15.1 Hz, 1H), 3.62 (ddd, J = 5.4, 4.2, 3.1 Hz, 1H), 3.20 – 3.15 (m, 1H), 1.89 – 1.80 (m, 1H), 1.74 – 1.49 (m, 5H), 1.49 – 1.33 (m, 2H).

¹³C NMR (126 MHz, CDCl₃) δ 171.1, 136.4, 128.9, 128.5, 127.8, 50.3, 47.1, 44.6, 23.0, 19.8, 19.1, 17.0.

HRMS (ESI pos): calculated for C₁₈H₁₈NaO₄ (M+H⁺): 216.1383, found: 216.1374.

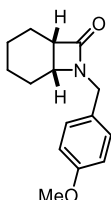


7-(4-(Trifluoromethyl)benzyl)-7-azabicyclo[4.2.0]octan-8-one (29c): Synthesized according to general procedure F using cyclohex-2-en-1-yl(4-(trifluoromethyl)benzyl)carbamic chloride (64 mg, 0.2 mmol). The crude mixture was purified by flash column chromatography on silica gel (5% AcOEt in hexanes as eluent) to afford product **29c** (31 mg, 55% yield) as a yellow oil.

¹H NMR (400 MHz, CDCl₃) δ 7.59 (d, *J* = 8.0 Hz, 2H), 7.39 (d, *J* = 8.0 Hz, 2H), 4.62 (d, *J* = 15.4 Hz, 1H), 4.16 (d, *J* = 15.4 Hz, 1H), 3.66 (dt, *J* = 5.1, 3.6 Hz, 1H), 3.23 (dt, *J* = 6.8, 4.6 Hz, 1H), 1.92 – 1.83 (m, 1H), 1.77 – 1.55 (m, 5H), 1.50 – 1.34 (m, 2H).

¹³C NMR (126 MHz, CDCl₃) δ 171.1, 140.5, 130.1 (q, *J* = 32.6 Hz), 128.6, 125.9 (q, *J* = 3.8 Hz), 124.2 (q, *J* = 272.1 Hz), 50.5, 47.3, 44.1, 23.0, 19.7, 19.0, 16.9.

HRMS (ESI pos): calculated for C₁₅H₁₇F₃NO (M+H⁺): 284.1257, found: 284.1258.

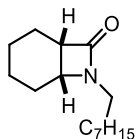


7-(4-Methoxybenzyl)-7-azabicyclo[4.2.0]octan-8-one (29d): Synthesized according to general procedure F using cyclohex-2-en-1-yl(4-methoxybenzyl)carbamic chloride (56 mg, 0.2 mmol). The crude mixture was purified by flash column chromatography on silica gel (15% AcOEt in hexanes as eluent) to afford product **29d** (30 mg, 61% yield) as a yellow oil.

¹H NMR (400 MHz, CDCl₃) δ 7.23 – 7.14 (m, 2H), 6.91 – 6.80 (m, 2H), 4.51 (d, *J* = 14.9 Hz, 1H), 4.04 (d, *J* = 14.9 Hz, 1H), 3.80 (s, 3H), 3.61 (ddd, *J* = 5.4, 4.1, 3.2 Hz, 1H), 3.17 (dt, *J* = 6.9, 4.6 Hz, 1H), 1.93 – 1.79 (m, 1H), 1.74 – 1.50 (m, 4H), 1.49 – 1.31 (m, 3H).

¹³C NMR (100 MHz, CDCl₃) δ 170.9, 159.2, 129.7, 128.4, 114.2, 55.4, 50.0, 46.9, 43.9, 23.0, 19.7, 19.0, 16.9.

HRMS (ESI pos): calculated for C₁₅H₁₉NNaO₂ (M+Na⁺): 268.1308, found: 268.1304.



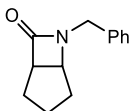
7-Octyl-7-azabicyclo[4.2.0]octan-8-one (29e): synthesized according the general procedure F using cyclohex-1-en-1-yl(octyl)carbamic chloride (54 mg, 0.2 mmol, 1 eq.). The crude mixture was purified by flash column chromatography on silica gel (5% AcOEt in Hexane) to afford **29e** (13 mg,

28% yield) as a colorless oil.

¹H NMR (400 MHz, CDCl₃) δ: 3.72 (ddd, *J* = 5.3, 4.2, 3.2 Hz, 1H), 3.33 (dt, *J* = 13.9, 7.6 Hz, 1H), 3.20 – 3.11 (m, 1H), 2.94 (ddd, *J* = 14.0, 7.9, 6.2 Hz, 1H), 1.94 – 1.39 (m, 10H), 1.35 – 1.20 (m, 9H), 1.00 – 0.81 (m, 3H).

¹³C NMR (101 MHz, CDCl₃) δ 171, 50.2, 46.6, 40.3, 31.9, 29.4, 29.3, 28.2, 27.3, 23.3, 22.8, 19.7, 19, 17.1, 14.2.

HRMS (ESI pos): calculated for C₁₅H₂₇NO (M+H⁺): 238,21 found: 238,2157

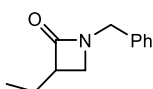


6-Benzyl-6-azabicyclo[3.2.0]heptan-7-one (29f): synthesized according the general procedure F using benzyl(cyclopent-2-en-1-yl)carbamic chloride (47 mg, 0.2 mmol, 1 eq.). The crude mixture was purified by flash column chromatography on silica gel (5% AcOEt in hexane) to afford **29f** (11 mg, 30% yield) as a yellowish oil.

¹H NMR (400 MHz, CDCl₃) δ 7.54 – 7.08 (m, 5H), 4.50 (d, *J* = 15.1 Hz, 1H), 4.08 (d, *J* = 15.1 Hz, 1H), 3.91 (t, *J* = 4.1 Hz, 1H), 3.47 (dd, *J* = 8.0, 3.6 Hz, 1H), 2.05 (dd, *J* = 13.2, 6.3 Hz, 1H), 1.83 – 1.70 (m, 2H), 1.58 (m, 1H), 1.47 – 1.30 (m, 1H), 1.18 (m, 1H).

¹³C NMR (126 MHz, CDCl₃) δ 169.6, 136.3, 128.8, 128.4, 127.8, 57.6, 55.1, 44.2, 27, 25.1, 22.8.

HRMS (ESI pos): calculated for C₁₃H₁₅NaNO (M+Na⁺): 224.11 found: 224.1041

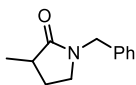


1-Benzyl-3-ethylazetidin-2-one (29g): synthesized according the general procedure F using benzyl(but-2-en-1-yl)carbamic chloride (47 mg, 0.2 mmol, 1 eq.). The crude mixture was purified by flash column chromatography on silica gel (5% AcOEt in hexane) to afford **29g** (11 mg, 29% yield) as a yellowish oil.

¹H NMR (500 MHz, CDCl₃) δ 7.37 – 7.26 (m, 5H), 4.46 (s, 2H), 3.60 – 3.52 (m, 2H), 3.18 – 3.10 (m, 1H), 1.72 – 1.65 (m, 2H), 0.93 (t, *J* = 7.3 Hz, 3H)

¹³C NMR (126 MHz, CDCl₃) δ: 171.9 (C), 136.3 (C), 128.9 (CH), 128.3 (CH), 127.9 (CH), 53.6 (CH₂), 48.7 (CH₂), 44 (CH), 29 (CH₂), 11.9 (CH₃).

Matching reported literature data.⁹⁵

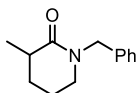


1-Benzyl-3-methylpyrrolidin-2-one (29h): Synthesized according to the general procedure F using benzyl(but-3-en-1-yl)carbamic chloride (48 mg, 0.2 mmol). The crude mixture was purified by flash column chromatography on silica gel (10% AcOEt in hexanes as eluent) to afford product **29h** (23 mg, 60% yield) as a yellow oil.

¹H NMR (500 MHz, CDCl₃) δ 7.37 – 7.30 (m, 2H), 7.29 – 7.24 (m, 1H), 7.24 – 7.20 (m, 2H), 4.49 – 4.40 (m, 2H), 3.22 – 3.09 (m, 2H), 2.51 (ddt, *J* = 15.8, 8.7, 7.2 Hz, 1H), 2.21 (dddd, *J* = 12.9, 8.7, 6.5, 4.4 Hz, 1H), 1.59 (dq, *J* = 12.6, 8.5 Hz, 1H), 1.24 (d, *J* = 7.1 Hz, 3H).

¹³C NMR (126 MHz, CDCl₃) δ 177.5, 136.8, 128.8, 128.2, 127.6, 46.9, 44.8, 36.9, 27.2, 16.5.

HRMS (ESI pos): calculated for C₁₂H₁₆NO (M+H⁺): 190.1226, found: 190.1228.



1-Benzyl-3-methylpiperidin-2-one (29i): Synthesized according to the general procedure F using benzyl(pent-4-en-1-yl)carbamic chloride (48 mg, 0.2 mmol). The crude mixture was purified by flash column chromatography

⁹⁵ Franco Bella, A.; Jackson, L. V.; Walton, J. C. Preparation of β- and γ-lactams *via* ring closures of unsaturated carbamoyl radicals derived from 1-carbamoyl-1-methylcyclohexa-2,5-dienes. *Org. Biomol. Chem.* **2004**, *2*, 421-428.

on silica gel (10% AcOEt in hexanes as eluent) to afford product **29i** (21 mg, 52% yield) as a yellow oil.

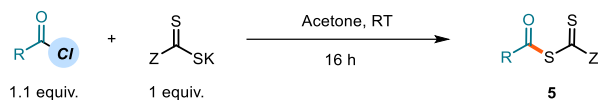
$^1\text{H NMR}$ (400 MHz, CDCl_3) δ 7.36 – 7.28 (m, 2H), 7.28 – 7.21 (m, 3H), 4.66 (d, $J = 14.6$ Hz, 1H), 4.50 (d, $J = 14.6$ Hz, 1H), 3.20 (dd, $J = 7.2, 5.1$ Hz, 2H), 2.56 – 2.42 (m, 1H), 1.96 (dtd, $J = 12.8, 6.2, 3.4$ Hz, 1H), 1.84 (ddtd, $J = 13.5, 6.6, 5.0, 3.4$ Hz, 1H), 1.78 – 1.66 (m, 1H), 1.53 (dddd, $J = 12.8, 10.4, 9.1, 3.4$ Hz, 1H), 1.30 (d, $J = 7.2$ Hz, 3H).

$^{13}\text{C NMR}$ (101 MHz, CDCl_3) δ 173.5, 137.7, 128.7, 128.1, 127.4, 50.4, 47.7, 36.8, 29.7, 21.8, 18.2.

HRMS (ESI pos): calculated for $\text{C}_{13}\text{H}_{18}\text{NO}$ ($\text{M}+\text{H}^+$): 204.1383, found: 204.1376.

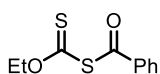
3.9.10 Mechanistic studies

General procedure for the synthesis of acyl xanthate intermediates (general procedure G)



In a round bottom flask, acyl chloride (1.1 equiv.) was dissolved in acetone (0.1 M) and cooled to 0 °C. The dithiocarbamate anion or the xanthate salts (1 equiv.) was then added and the resulting reaction mixture was stirred for 1 hour at 0 °C. The solvent was removed under reduced pressure at ambient temperature. The residue was then dissolved in DCM and washed with distilled water, NaHCO_3 solution and brine. The combined organic fractions were dried over MgSO_4 and concentrated to dryness to obtain the desired product.

Characterization of the Intermediates



Benzoic (O-ethyl carbonothioic) thioanhydride (**30a**).

Prepared according to the general procedure G using potassium ethyl xanthogenate **D** (1 mmol, 160 mg) and benzoyl chloride (1.1 mmol, 128 μL) in 10 mL of acetone. After work-up, the product **30a** (226 mg, 99% yield) was obtained as a yellow oil.

$^1\text{H NMR}$ (300 MHz, CDCl_3) δ 7.87 (app d, $J = 7.7$ Hz, 2 H); 7.64-7.54 (m, 1H); 7.49-7.39 (m, 2H); 4.69 (q, $J = 7.1$ Hz, 2H); 1.45 (t, $J = 7.1$ Hz, 3H).

$^{13}\text{C NMR}$ (75 MHz, CDCl_3) δ 203.4, 185.0, 135.7, 134.4, 129.0, 127.9, 71.1, 13.5.

Matching reported literature data.⁹⁶

⁹⁶ Ajayaghosh, A.; Das, S.; George, M. V. S-benzoyl O-ethyl xanthate as a new photoinitiator: Photopolymerization and laser flash photolysis studies. *J. Polym. Sci., Part A: Polym. Chem.* **1993**, *31*, 653-659.

Benzoic diethylcarbamothioic thioanhydride (30c).
CCN(C)C(=S)SC(=O)c1ccccc1 Prepared according to the general procedure G using sodium diethylcarbamodithioate trihydrate **C** (1.05 mmol, 237 mg) and benzoyl chloride (1 mmol, 116 μ L) in 10 mL of acetone. After work-up, the product **30c** was obtained as a yellow oil (220 mg, 87% yield).

$^1\text{H NMR}$ (300 MHz, CDCl_3) δ 7.95-7.88 (m, 2 H); 7.64-7.56 (m, 1H); 7.52-7.42 (m, 2H); 4.07-3.86 (m, 2H); 1.36 (t, $J = 7.1$ Hz, 3H).

Matching reported literature data.⁹⁷

UV-Vis Characterization of the Intermediates

CCOC(=S)SC(=O)c1ccccc1
5a

CCN(C)C(=S)SC(=O)c1ccccc1
5b

CCOC(=S)SC(=O)C1CCCCC1
5c

CCN(C)C(=S)SC(=O)N(C)C
5d

Intermediate	λ max	tail of absorption
5a	397 nm	490 nm
5b	400 nm	490 nm
5c	400 nm	490 nm
5d	343 nm	500 nm

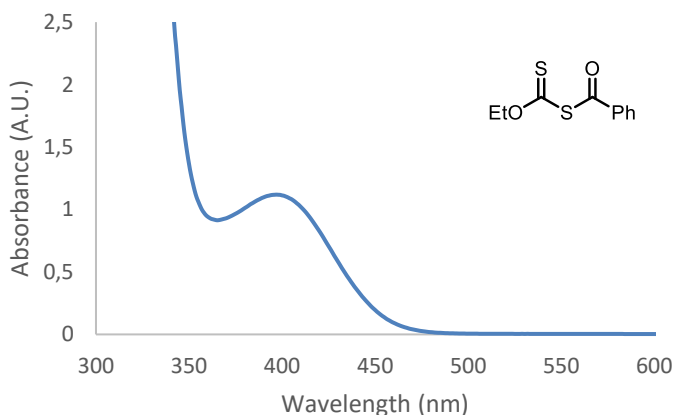


Figure 2.46. UV-Vis absorption spectrum of **5a** recorded at $1 \cdot 10^{-2}$ M concentration in acetonitrile.

⁹⁷ Azizi, N.; Alipour, M. Synthesis of carboxylic dithiocarbamic anhydride and substituted thiourea derivatives in water. *Environ. Chem. Lett.* **2018**, *16*, 1415-1421.

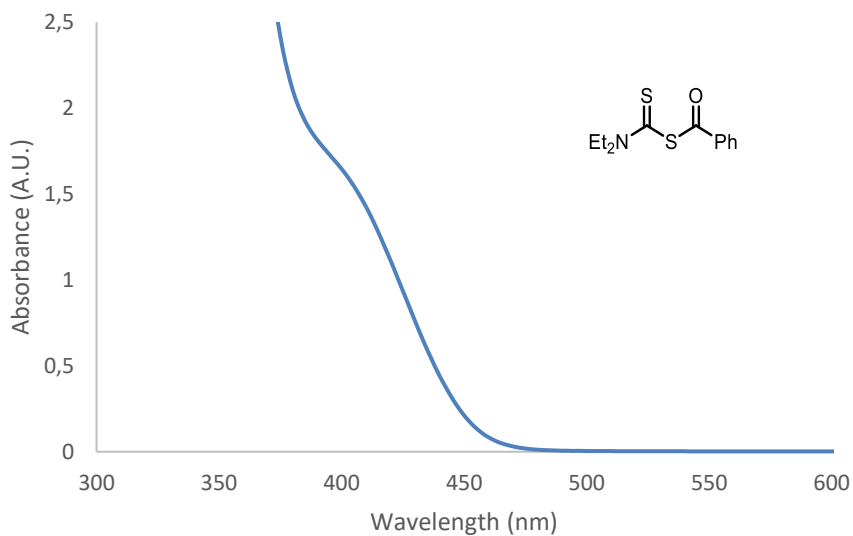


Figure 2.47. UV-Vis absorption spectrum of **5b** recorded at $1 \cdot 10^{-2}$ M concentration in acetonitrile.

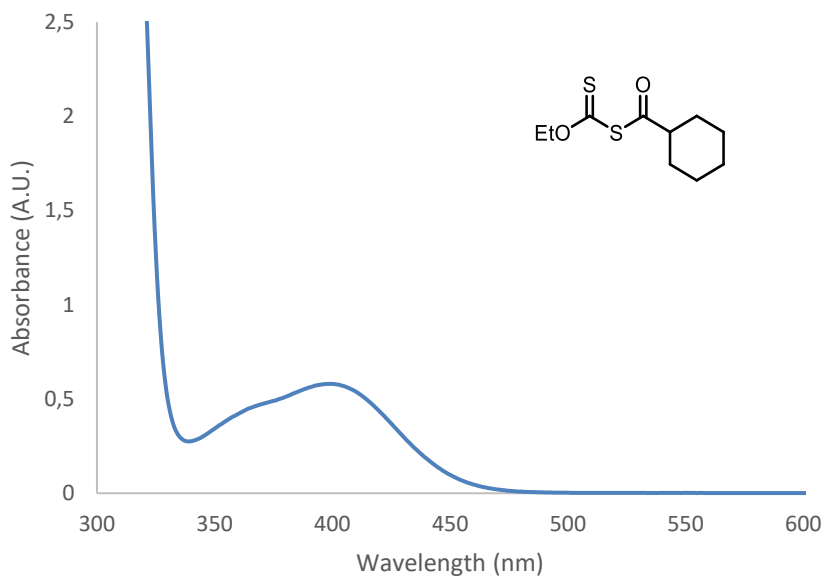


Figure 2.48. UV-Vis absorption spectrum of **5c** recorded at $2 \cdot 10^{-2}$ M concentration in acetonitrile.

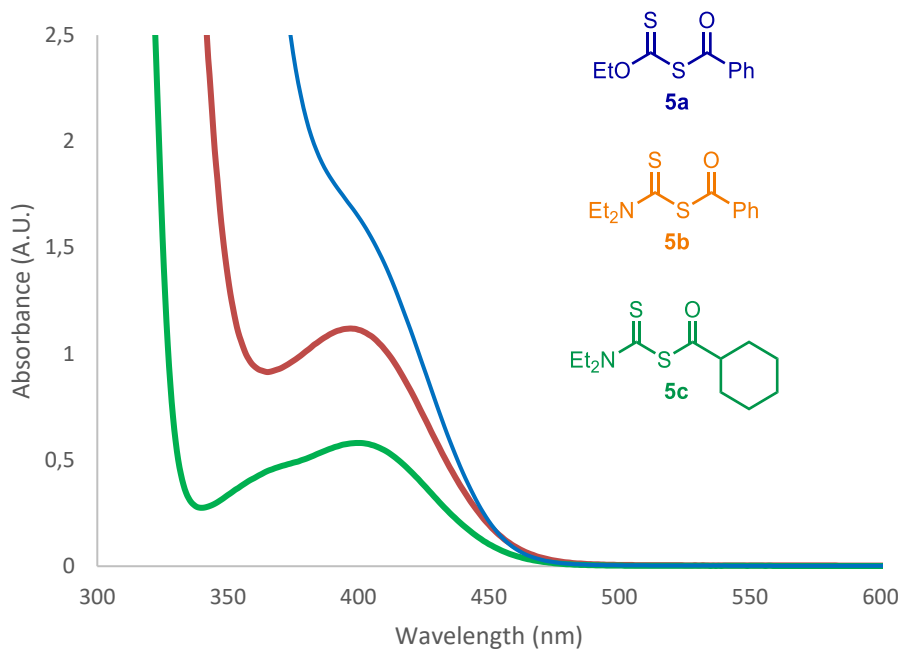


Figure 2.49. Superposition of the absorption spectra of the different acyl xanthates and acyl dithiocarbamate intermediates at the same concentration ($2 \cdot 10^{-2}$ M in acetonitrile).

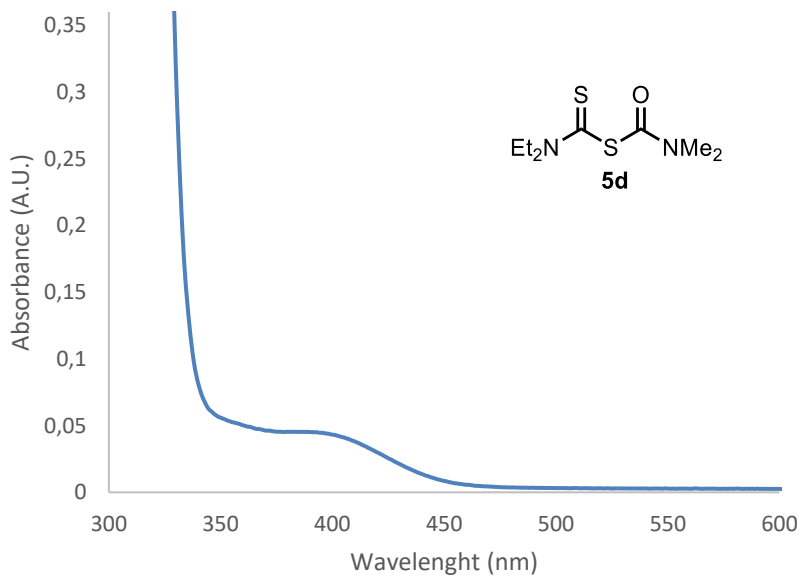


Figure 2.50. UV-Vis absorption spectrum of intermediate 5d recorded at $2 \cdot 10^{-3}$ M concentration in acetonitrile.

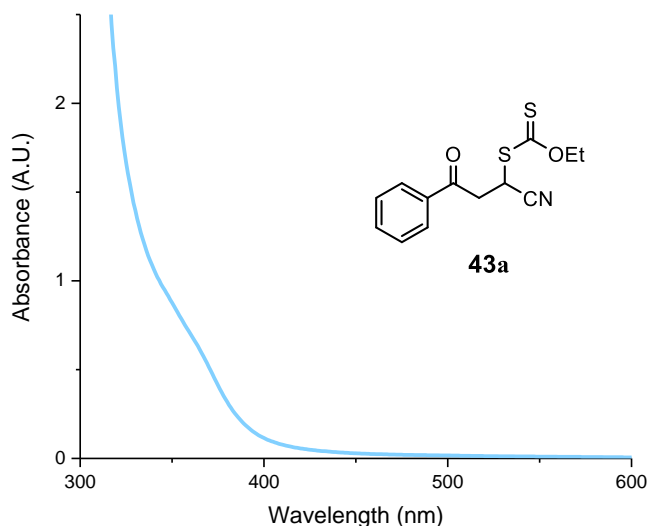
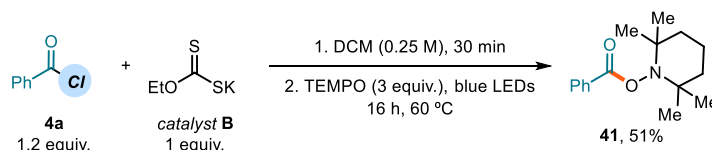


Figure 2.51. UV-Vis absorption spectrum of **43a** recorded at $1 \cdot 10^{-2}$ M in acetonitrile.

TEMPO Trapping Experiments

Stoichiometric reaction between TEMPO and in-situ acyl xanthate intermediate



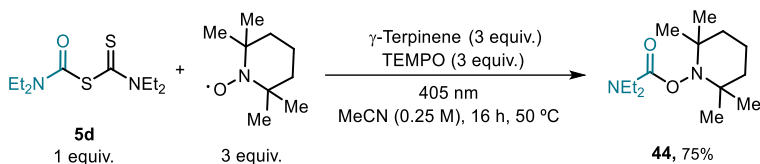
In an oven dried tube of 15 mL (16 mm × 125 mm) with a Teflon septum screw cap, potassium ethyl xanthogenate **D** (80.1 mg, 0.5 mmol, 1 equiv.) was suspended in DCM (2 mL, HPLC grade). Then, benzoyl chloride (69.6 μ L, 0.6 mmol, 1.2 equiv.) was added and the mixture was stirred at ambient temperature for 30 minutes. Then, TEMPO (234.4 mg, 1.5 mmol, 3 equiv.) was added and the resulting yellow solution was degassed with argon sparging for 60 seconds. The tube was then placed in the temperature controlled photoreactor set at a temperature of 60 °C (60-61°C measured in the central well) and irradiated for 16 hours. Chromatography on silica gel (5% AcOEt in hexanes as eluent) afforded adduct **41** (66 mg, yellow oil, 51% yield).

$^1\text{H NMR}$ (500 MHz, CDCl_3) δ 8.35 (d, $J = 6.9$ Hz, 2H), 7.83 (m, 1H), 7.74 (m, 2H), 2.12 – 1.70 (m, 6H), 1.55 (s, 6H), 1.40 (s, 6H).

$^{13}\text{C NMR}$ (126 MHz, CDCl_3) δ 161.45, 128.17, 124.89, 124.74, 123.78, 55.52, 34.28, 27.19, 16.09, 12.26.

Matching reported literature data.⁹⁸

Stoichiometric reaction between TEMPO and dithiocarbamate intermediate **Id**

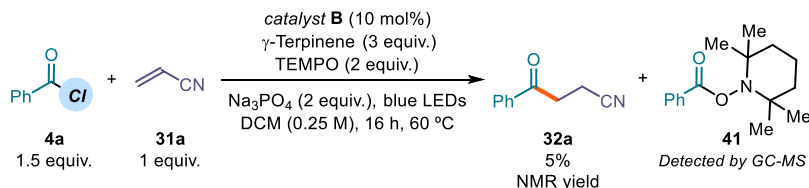


In an oven-dried 15 mL Schlenk tube was added a 0.25 M solution of the dithiocarbamate intermediate **30c** (28 mg, 127 μ mol, 1 equiv.) and TEMPO (60 mg, 0.38 mmol, 3 equiv.) in acetonitrile (0.5 mL). The reaction mixture was placed under an atmosphere of argon, cooled to -78 °C, degassed *via* vacuum evacuation (5 minutes), backfilled with argon and, ultimately, warmed to ambient temperature. This freeze-pump-thaw cycle was repeated four times, and then the Schlenk tube was sealed with Parafilm and put into the Hepatochem PhotoRedOx Box equipped with a 405 nm EvoluChem LED 18 W light source at 50 °C. After 18 hours, the reaction vessel was cooled down to ambient temperature, water was added and the mixture was extracted with ethyl acetate (2x15 mL). The combined layers were dried over $MgSO_4$, filtered, and concentrated. The resulting crude mixture was purified by column chromatography on silica gel (5% to 30% AcOEt in hexane) to give the corresponding product **44** (21 mg, 75% yield).

¹H NMR (400 MHz, $CDCl_3$) δ 2.96 (s, 6H), 1.73 – 1.48 (m, 6H), 3.06 (s, 3H), 1.13 (d, J = 17.6 Hz, 1H)

¹³C NMR (101 MHz, $CDCl_3$) δ 157.8, 60.2, 50.1, 39.1, 31.9, 21.1, 17.2.

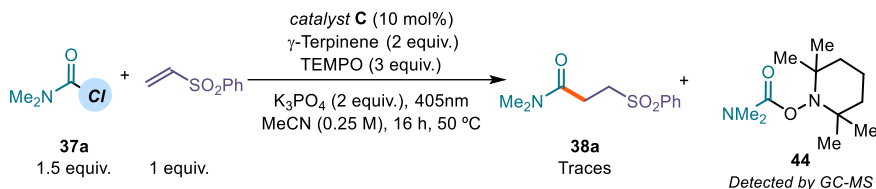
TEMPO inhibition of the model reactions



Reaction performed according to the general procedure A using benzoyl chloride (87 μ L, 0.75 mmol, 1.5 equiv.) and acrylonitrile (33 μ L, 0.5 mmol, 1 equiv.) and adding TEMPO (156.3 mg, 1 mmol, 2 equiv.) before the degassing step. The crude mixture was analyzed by ¹H NMR analysis after 16 hours using trichloroethylene (45 μ L, 0.5 mmol, 1 equiv.) as internal

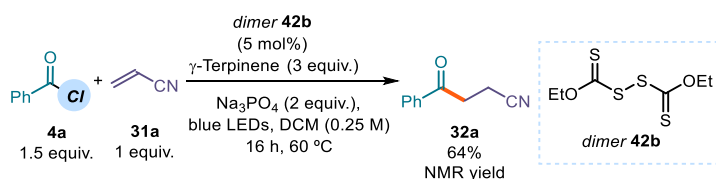
⁹⁸ He, X.-K.; Cai, B.-G.; Yang, Q.-Q.; Wang, L.; Xuan, J. Visible-Light-Promoted Cascade Radical Cyclization: Synthesis of 1,4-Diketones Containing Chroman-4-One Skeletons. *Chem. Asian J.* **2019**, *14*, 3269-3273.

standard, and by GC-MS. NMR yield: 5%. Traces of the TEMPO adduct **41** were detected by GC-MS analysis.



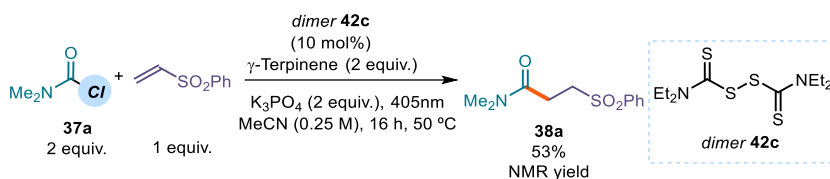
Reaction performed according to the general procedure E using dimethylcarbamyl chloride (37 μ L, 0.4 mmol, 2 equiv.) and phenyl vinyl sulfone (34 mg, 0.2 mmol, 1 equiv.) and adding TEMPO (62 mg, 0.4 mmol, 2 equiv.) before the degassing step.

Model reaction with catalyst dimer **42b** – Acylation



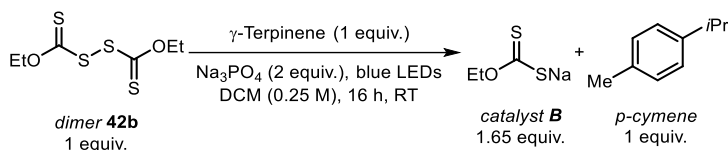
Reaction performed according to the general procedure A using benzoyl chloride (87 μ L, 0.75 mmol, 1.5 equiv.) and acrylonitrile (33 μ L, 0.5 mmol, 1 equiv.) while replacing *catalyst D* with *dimer 42d* (6 mg, 0.025 mmol, 0.05 equiv.). The crude reaction mixture was analyzed by 1H NMR analysis using trichloroethylene as internal standard. NMR yield: 64%.

Model reaction with dimer catalyst **42c** - Carbamoylation



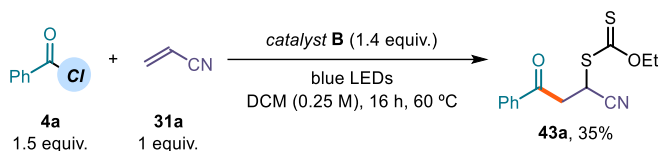
Reaction performed according to general procedure E using dimethylcarbamyl chloride (37 μ L, 0.4 mmol, 2.0 equiv.) and phenyl vinyl sulfone (34 mg, 0.2 mmol, 1 equiv.) while replacing *catalyst C* with *dimer 42c* (6 mg, 0.02 mmol, 0.1 equiv.). The crude reaction mixture was analyzed by 1H NMR analysis using trichloroethylene as internal standard. NMR yield: 53%.

Turn-over experiment with dimer catalyst **B** and terpinene



In an oven dried vial (16 mm \times 50 mm) with a Teflon septum screw cap, **dimer 42b** (60.6 mg, 0.25 mmol, 1 equiv.) and sodium phosphate (82 mg, 0.5 mmol, 2 equiv.) were dissolved in DCM (2 mL, HPLC grade). Then, γ -terpinene (40 μL , 0.25 mmol, 1 equiv.) was added. The resulting yellow mixture was degassed with argon, sparging for 60 seconds. The vial was then placed in the 3D-printed support photoreactor (Figure S6) and irradiated for 24 hours. Trichloroethylene was added as internal standard and a sample of the crude mixture was diluted in d_6 -DMSO to record the NMR yield.

Stoichiometric group transfer reaction with in-situ acyl xanthate intermediate

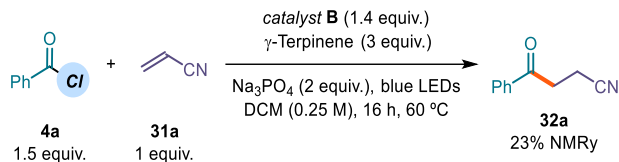


In an oven dried tube of 15 mL (16 mm \times 125 mm) with a Teflon septum screw cap, potassium ethyl xanthogenate **B** (112 mg, 0.7 mmol, 1.4 equiv.) was suspended in DCM (2 mL, HPLC grade). Then, benzoyl chloride (87 μL , 0.75 mmol, 1.5 equiv.) was added and the mixture was stirred at ambient temperature for 30 min. The reaction mixture was then degassed with argon, sparging for 60 seconds. Finally, acrylonitrile (33 μL , 0.5 mmol, 1 equiv.) was added via syringe. The tube was then placed in the temperature controlled photoreactor (Figure 3.7) set at a temperature of 60 $^\circ\text{C}$ (60-61 $^\circ\text{C}$ measured in the central well) and irradiated for 16 hours. The crude mixture was purified by flash column chromatography on silica gel (5% to 10% AcOEt in hexanes as eluent) to afford **43a** (50 mg, 35% yield) as a yellow oil.

$^1\text{H NMR}$ (400 MHz, CDCl_3) δ 7.97 – 7.89 (m, 2H), 7.69 – 7.58 (m, 1H), 7.50 (app t, J = 7.5 Hz, 2H), 5.08 (t, J = 6.2 Hz, 1H), 4.72 (q, J = 7.1 Hz, 2H), 3.70 (d, J = 6.3 Hz, 2H), 1.47 (t, J = 7.1 Hz, 3H).

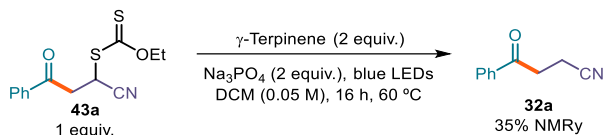
$^{13}\text{C NMR}$ (101 MHz, CDCl_3) δ 209.05, 193.54, 135.35, 134.39, 129.09, 128.30, 117.96, 71.54, 40.67, 32.49, 13.84.

Stoichiometric group transfer reaction with in-situ acyl xanthate intermediate in the presence of γ -terpinene



In an oven dried tube of 15 mL (16 mm \times 125 mm) with a Teflon septum screw cap, potassium ethyl xanthogenate (112 mg, 0.7 mmol, 1.4 equiv.) and sodium phosphate (164 mg, 1.0 mmol, 2 equiv) were dissolved in DCM (2 mL, HPLC grade). Benzoyl chloride (87 μL , 0.75 mmol, 1.5 equiv.) was added and the mixture was stirred at ambient temperature for 30 min. Then, γ -terpinene (240 μL , 1.5 mmol, 3 equiv.) was added. The mixture was degassed via argon sparging for 60 seconds. Finally, acrylonitrile (33 μL , 0.5 mmol, 1 equiv.) was added via syringe. The tube was then placed in the temperature controlled photoreactor (Figure 3.7) set at a temperature of 60 °C (60-61 °C measured in the central well) and irradiated for 16 hours. Trichloroethylene was added as internal standard, and a sample of the crude mixture was diluted in CDCl_3 to record the NMR yield. *No group transfer product 43a was observed.*

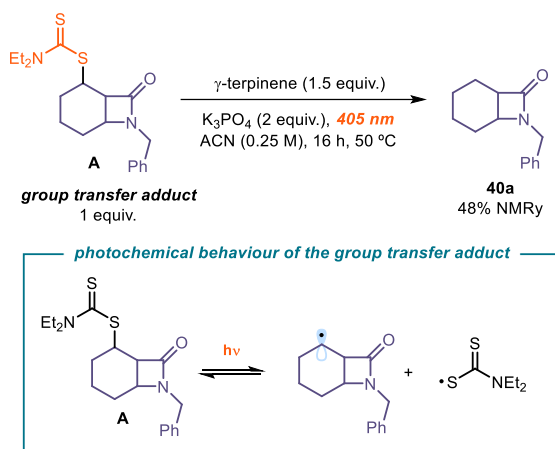
Direct photolysis of the group transfer product under reaction conditions



In an oven dried tube of 15 mL (16 mm \times 125 mm) with a Teflon septum screw cap, the group transfer product **43a** (28.01 mg, 0.1 mmol, 1 equiv.) and sodium phosphate (33 mg, 0.2 mmol, 2 equiv) were dissolved in DCM (2 mL, HPLC grade). Then, γ -terpinene (33 μL , 0.2 mmol, 2 equiv.) was added. The reaction mixture was degassed with Argon sparging for 60 seconds. The tube was then placed in the temperature controlled photoreactor (Figure 3.7) set at a temperature of 60 °C (60-61 °C measured in the central well) and irradiated for 16 hours.

Trichloroethylene was added as internal standard and a sample of the crude mixture was diluted in CDCl_3 to record the NMR yield – product **32a** was formed in 35%.

Direct photolysis of the group transfer product for the intramolecular reaction



An oven-dried 15 mL Schlenk tube was charged with an authentic sample of the group transfer adduct **A**, prepared according to Ref. 38b, γ -terpinene (48 μ L, 0.3 mmol, 1.5 equiv.) and K₃PO₄ (85 mg, 0.4 mmol, 2 equiv.) in acetonitrile (0.8 mL, 0.25 M). The reaction mixture was placed under an atmosphere of argon, cooled to -78 °C, degassed *via* vacuum evacuation (5 minutes), backfilled with argon and, ultimately, warmed to ambient temperature. This freeze-pump-thaw cycle was repeated four times, and then the Schlenk tube was sealed with Parafilm and put into the Hepatochem PhotoRedOx Box equipped with a 405 nm EvoluChem LED 18 W light source at 50 °C (Figure 3.13). After 18 hours stirring, the reaction was cooled down to ambient temperature, trichloroethylene was added as internal standard and a sample of the crude mixture was diluted in CDCl₃ to record the NMR of the crude - product **40a** was formed in 48%.

Cyclic Voltammetry Measurements

For the cyclic voltammetry (CV) measurements, a glassy carbon disk electrode (diameter: 3 mm) was used as a working electrode. A silver wire coated with AgCl immersed in a 3.5 M aqueous solution of KCl and separated from the analyte by a fritted glass disk was employed as the reference electrode. A Pt wire counter-electrode completed the electrochemical setup. The scan rate of used in each CV experiment is indicated case by case.

Potentials are quoted with the following notation: E_p^C refers to the cathodic peak potential, E_p^A refers to the anodic peak potential, while the E_{red} value describes the electrochemical properties of the referred compound.

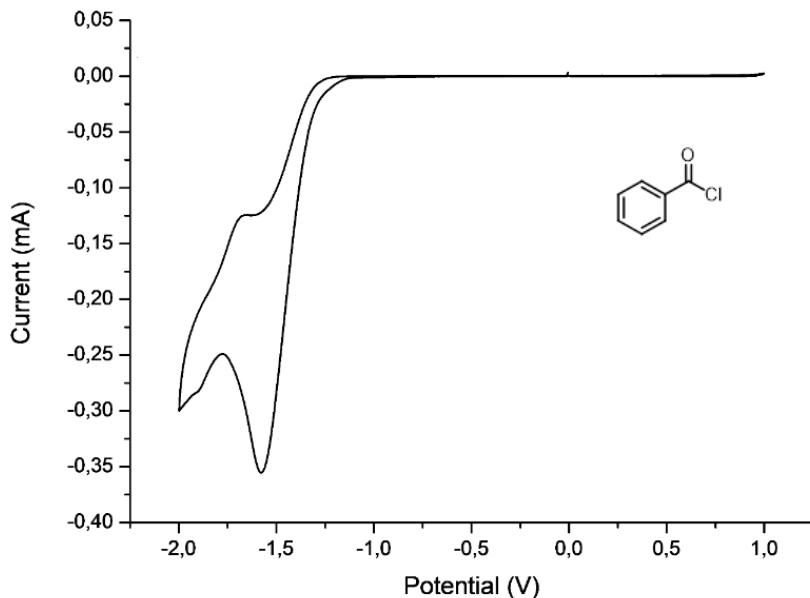


Figure 2.52. Cyclic voltammogram of benzoyl chloride **4a** [0.02 M] in [0.1 M] TBAPF₆ in CH₃CN. Sweep rate: 100 mV/s. Glassy carbon electrode working electrode, Ag/AgCl (KCl 3.5 M) reference electrode, Pt wire auxiliary electrode. Irreversible reduction, $E_p^C = E_{red}(4a/4a^{\cdot-}) = -1.57$ V.

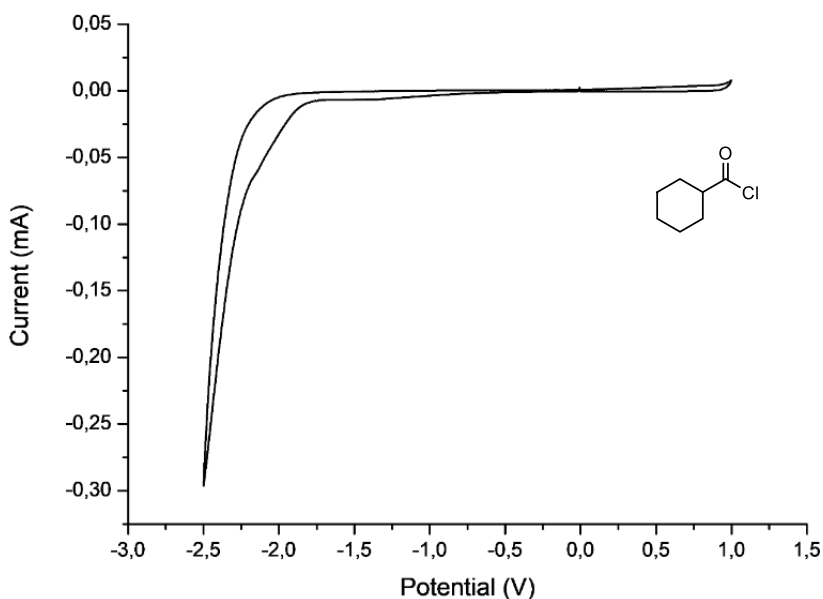


Figure 2.53. Cyclic voltammogram of cyclohexanecarbonyl chloride [0.02 M] in [0.1 M] TBAPF₆ in CH₃CN. Sweep rate: 100 mV/s. Glassy carbon electrode working electrode, Ag/AgCl (KCl 3.5 M) reference electrode, Pt wire auxiliary electrode. Reduction of cyclohexanecarbonyl chloride was not observed in the registered potential window (from 0 to -2.50 V).

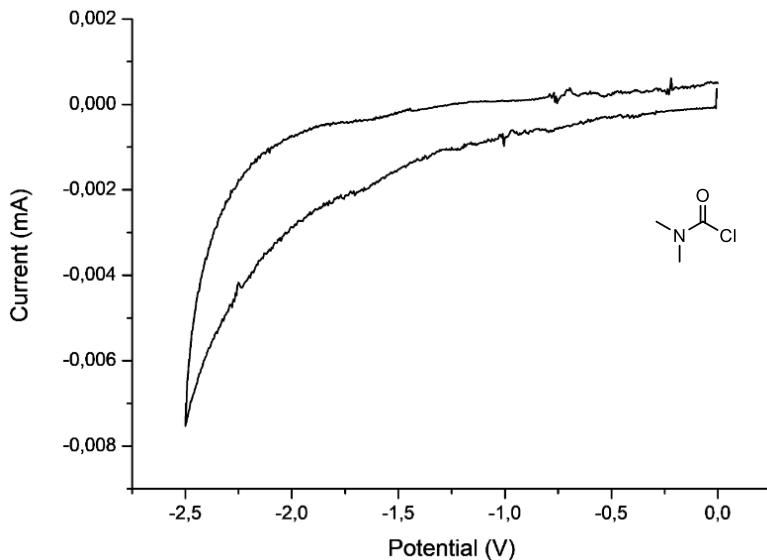


Figure 2.54. Cyclic voltammogram for **37a** [0.02M] in [0.1 M] TBAPF₆ in CH₃CN. Sweep rate: 50 mV/s. Glassy carbon electrode working electrode, Ag/AgCl (KCl 3.5 M) reference electrode, Pt wire auxiliary electrode. Reduction of **37a** was not observed in the registered potential window (from 0 to -2.50 V).

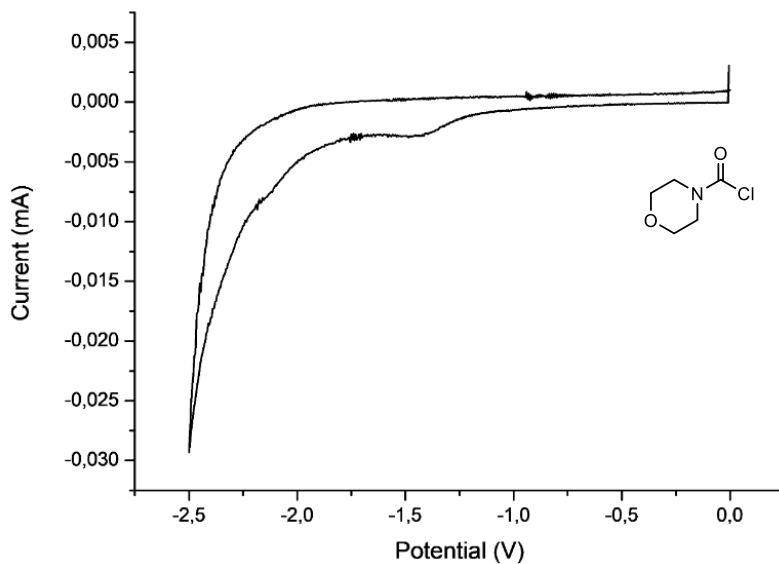


Figure 2.55. Cyclic voltammogram for **37e** [0.02M] in [0.1 M] TBAPF₆ in CH₃CN. Sweep rate: 100 mV/s. Glassy carbon electrode working electrode, Ag/AgCl (KCl 3.5 M) reference electrode, Pt wire auxiliary electrode. Reduction of **37e** was not observed in the registered potential window (from 0 to -2.50 V).

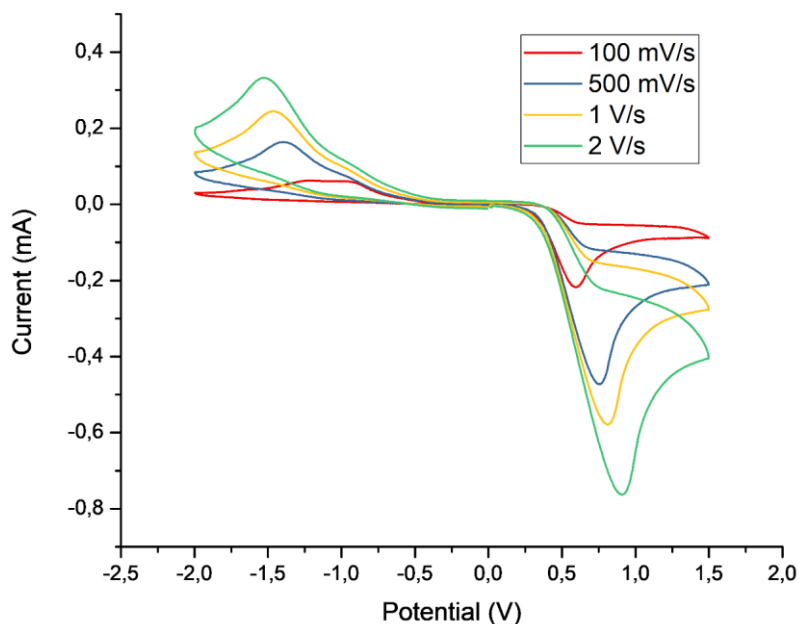


Figure 2.56. Cyclic voltammogram for catalyst **B** [0.02 M] in [0.1 M] TBAPF₆ in CH₃CN. Measurement started by oxidation from 0 to +1.5 V, followed by reduction from +1.5 V to -2.0 V, and finishing at 0 V. Glassy carbon electrode working electrode, Ag/AgCl (KCl 3.5 M) reference electrode, Pt wire auxiliary electrode. Two irreversible peaks observed increasing with sweep rate.

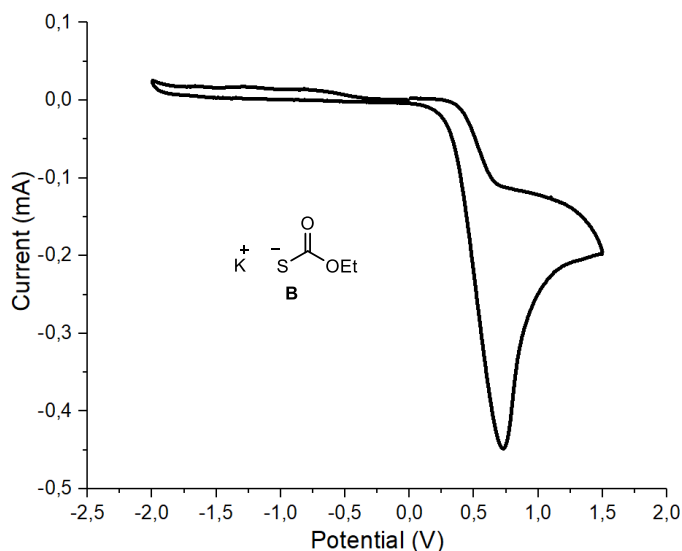


Figure 2.57. Cyclic voltammogram for catalyst **B** [0.02M] in [0.1 M] TBAPF₆ in CH₃CN. Measurement started by reduction from 0 to -2.0 V, followed by oxidation from -2.0 V to +1.5 V, and finishing at 0 V. Glassy carbon electrode working electrode, Ag/AgCl (KCl 3.5 M) reference electrode, Pt wire auxiliary electrode. Only one irreversible peak observed. Sweep rate: 500 mV/s.

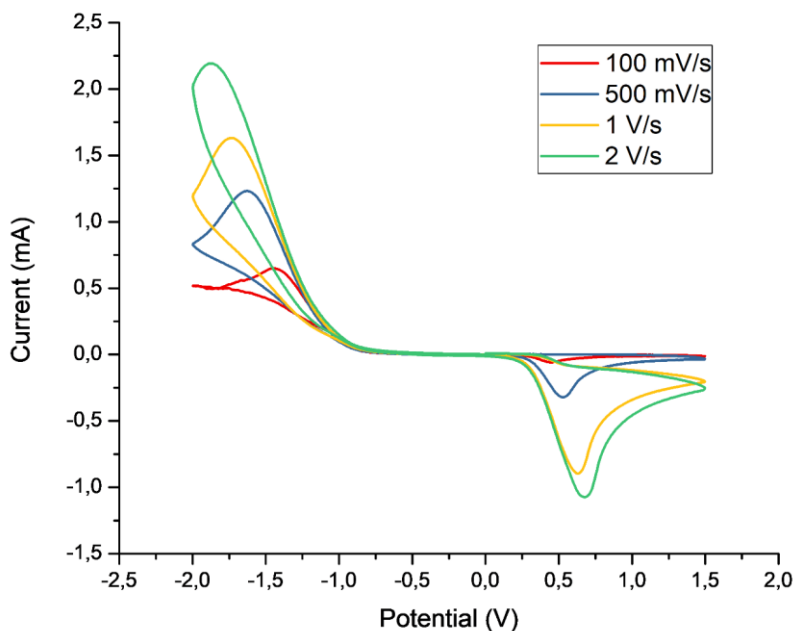


Figure 2.58. Cyclic voltammogram for dimer **42b** [0.02 M] in [0.1 M] TBAPF₆ in CH₃CN. Measurement started by reduction from 0 to -2.0 V, followed by oxidation from -2.0 V to +1.5 V, and finishing at 0 V. Glassy carbon electrode working electrode, Ag/AgCl (KCl 3.5 M) reference electrode, Pt wire auxiliary electrode. Two irreversible peaks observed increasing with sweep rate.

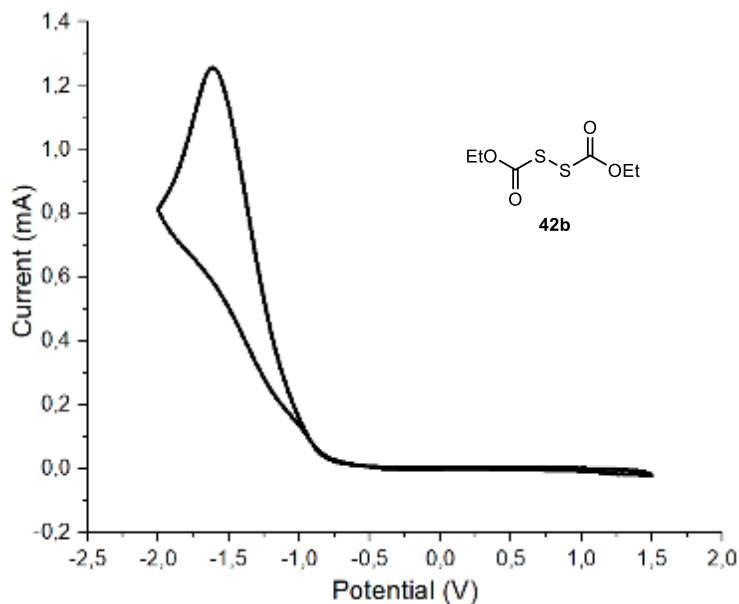


Figure 2.59. Cyclic voltammogram for dimer **42b** [0.02 M] in [0.1 M] TBAPF₆ in CH₃CN. Measurement started by oxidation from 0 to +1.5 V, followed by reduction from +1.5 V to -2.0 V, and finishing at 0 V. Glassy carbon electrode working electrode, Ag/AgCl (KCl 3.5 M) reference electrode, Pt wire auxiliary electrode. Two irreversible peaks observed increasing with sweep rate.

Transient Absorption Spectroscopy (TAS)

Studies with microsecond transient absorption spectroscopy (TAS) were performed using an excitation source of NdYAG (neodymium-doped yttrium aluminium garnet) Opolette laser with an optical parametric oscillator (OPO) system that allows variable wavelength excitation from 400 -1800 nm, pulse width of 6 ns, up to 2 mJ of energy from OPO output with fiber optic coupled, and high energy output from direct NdYAG harmonics 355 (20 mJ, 5 ns) and 532 (45mJ, 6 ns). The system is completed with 150 W tungsten lamp as probe; 2 monochromators Minuteman MM151; Si amplified photodetector module for VIS; DSPDAU high speed data rate recorder and interface software from RAMDSP. Laser intensities for each wavelength were the following: 355 nm – 1.30 mJ; 420 nm– 1.20 mJ; 460 nm – 1.95 mJ.

Several studies with different wavelengths and laser intensities were carried out, each of the conditions are indicated in a case by case bases. We selected a logarithmic time scale suitable for clearly showing the decay of the transient species in the samples. The characteristics of the detected transient species match literature data.³³

In a typical transient absorption spectroscopy experiment, solutions in acetonitrile of each of the substrates were prepared under an argon atmosphere and transferred into a screw-top 3.0 mL quartz cuvette for measurement. Upon irradiation with the appropriated wavelength, the decay of absorption at 620 nm of the transient xanthyl radical **IVb** was recorded.

Acyloxanthate **30a**

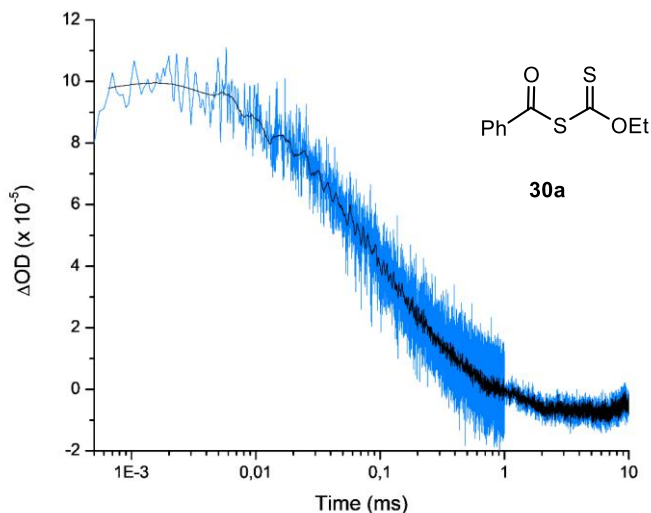


Figure 2.60. Absorption at 620 nm of the transient xanthyl radical **IVd** (blue line) generated upon 355 nm laser excitation of Acyloxanthate **30a** ($[30a] = 3$ mM in acetonitrile). Note logarithmic scale for time. Absorption decay (black line) processed through Savitsky Golay filter to facilitate lifetime measurement. ΔOD : optical density variation.

Compound **30a** was also measured upon 460 nm excitation in order to mimic the conditions of photolysis under catalytic conditions. Since photolysis of **30a** is less efficient at longer wavelengths, a higher concentration of **30a** was needed to obtain a comparable scale signal.

Note that changes in concentration of both **30a** and transient **IV** generated upon photolytic cleavage directly affects the lifetime of the detected species.

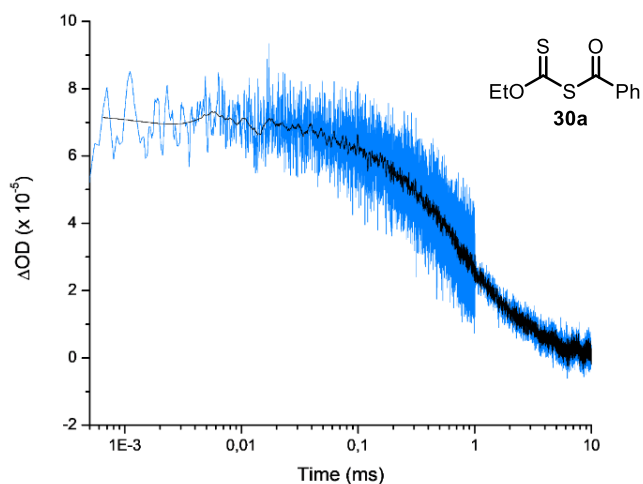


Figure 2.61. Absorption at 620 nm of the transient xanthyl radical **IV** (blue line) generated upon 460 nm laser excitation of acylxanthate **42d** ($[42d] = 300$ mM in acetonitrile). Note logarithmic scale for time. Absorption decay (black line) processed through Savinsky Golay filter to facilitate lifetime measurement. ΔOD : optical density variation.

Dimer 42d

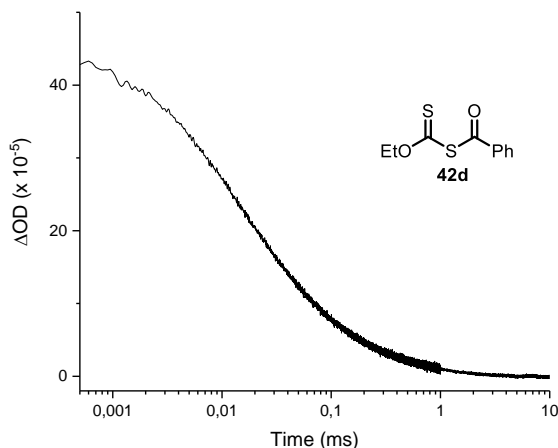


Figure 2.62. Absorption at 620 nm of the transient xanthyl radical **IV** (black line) generated upon 355 nm laser excitation of dimer **42d** ($[42d] = 3$ mM in acetonitrile). Note logarithmic scale for time. ΔOD : optical density variation.

Dimer **42d** was also measured upon 420 nm and 460 nm irradiation in order to support photolysis under the reaction conditions. A higher concentration of **42d** was used to ensure comparable scale signal.

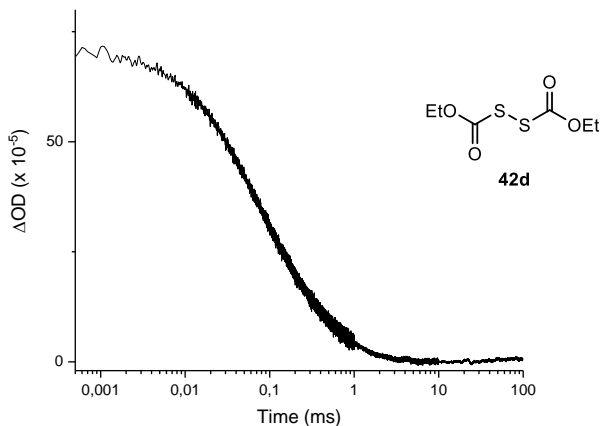


Figure 2.63. Absorption at 620 nm of the transient xanthyl radical **IV** (black line) generated upon 420 nm laser excitation of dimer **42d** ($[42d] = 300$ mM in acetonitrile). Note logarithmic scale for time. ΔOD : optical density variation.

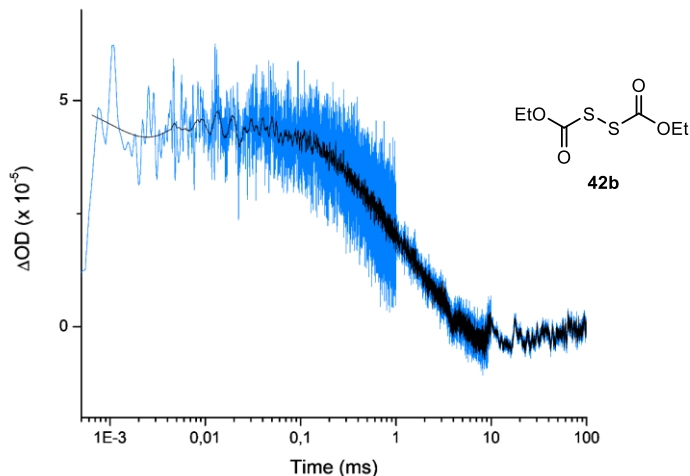


Figure 2.64. Absorption at 620 nm of the transient xanthyl radical **IV** (blue line) generated upon 460 nm laser excitation of dimer **42d** ($[42d] = 300$ mM in acetonitrile). Note logarithmic scale for time. Absorption decay (black line) processed through Savinsky Golay filter to facilitate lifetime measurement. ΔOD : optical density variation.

In order to perform the quenching experiment, increasing amounts of pure γ -terpinene was added while observing the effect on the absorption at 620 nm of the transient **IV**, which was recorded after every addition. Increasing amounts of pure γ -terpinene (up to 60 equivalents, 60 μ L) were added sequentially to a 2 mL solution of **42d** (3 mM in acetonitrile) in a screw-

top quartz cuvette, providing a final concentration of 2.91 mM. A decay of absorption of the transient xanthy radical, and therefore a shorter lifetime, was observed upon addition of γ -terpinene (Figure 3.33), which is consonant with a reaction between the two species. Turquoise line: ratio **42d**/ γ -terpinene mimics the reaction conditions. Note that precipitation of a solid, associated to ethyl xanthogenate, was observed upon addition and irradiation of the sample.

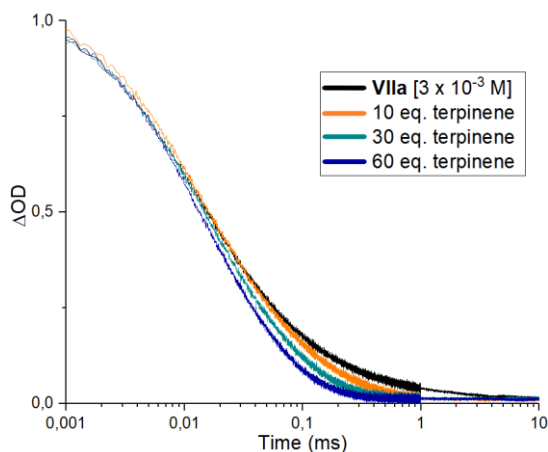


Figure 2.65. Absorption at 620 nm of the transient xanthy radical **IV** (black line) generated upon 355 nm laser excitation of dimer **42d** ($[42d]_0 = 3$ mM in acetonitrile) and subsequent decay of the absorption upon addition of 10 (orange line), 30 (green line, mimics proportions under reaction conditions) and 60 (blue line) equivalents of γ -terpinene, respectively. Note logarithmic scale for time. Absorption decay was normalized to 1. ΔOD : normalized optical density variation.

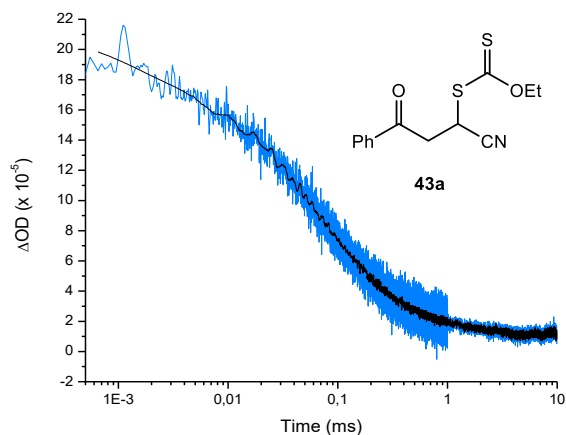


Figure 2.66. Absorption at 620 nm of the transient xanthy radical **IV** (blue line) generated upon 355 nm laser excitation of **43a** ($[43a] = 3$ mM in acetonitrile). Note logarithmic scale for time. Absorption decay (black line) processed through Savinsky Golay filter to facilitate lifetime measurement. ΔOD : optical density variation.

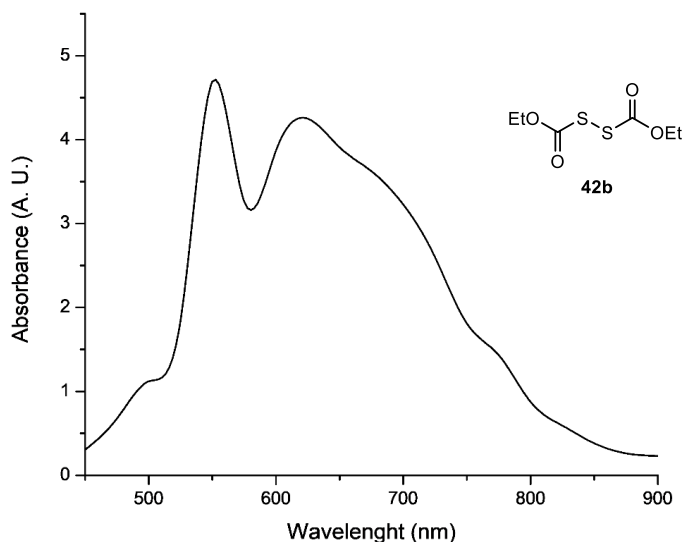


Figure 2.67. Absorption spectra of the transient xanthyl radical **IV** generated upon 355 nm laser excitation of Dimer **42d** ($[42d] = 3 \text{ mM}$ in acetonitrile) at $1 \mu\text{s}$ time of irradiation. Maximum characteristic from xanthyl radical can be observed around 625 nm.

Electron paramagnetic resonance (EPR)

EPR spectra were acquired on a Bruker EMX X-band EPR spectrometer with an ER 4116 HS cavity (9.86 GHz at room temperature) using 100 kHz field modulation (modulation amplitude: 1 G). Individual EPR tubes were filled with $\sim 0.7 \text{ mL}$ of the solution and were placed at the same position of the resonant cavity for EPR spectral acquisition. The spectral data were collected at 298 K with the following spectrometer settings: microwave power = 2.020 mW; center field = 3518 G, sweep width = 200 G, sweep time = 30 s, modulation frequency = 100 KHz, modulation amplitude = 1 G, power attenuation = 20 dB, time constant = 0.01 ms.

A fresh solution of acylxanthate **30a** 0.10 M in Toluene was prepared under air and measured without further precautions to remove oxygen from the solution. As expected, no signal was observed before of irradiation (note that **30a** decomposes rapidly, and a sample older than one day did show signals appearing before irradiation, due to decomposition); on the other hand, upon irradiation of the sample, appearance of a triplet at 3505 G was observed with a g-value of 2.00272 and a hyperfine splitting value a_{H} (2.6, 2H, $\gamma\text{-H}$). This signal reaches a maximum of intensity after 12.5 minutes of irradiation. The calculated EPR spectrum for the carbon radical of type **II**, which lies in proximity of two sulfur atoms and an ethoxy moiety, is shown in the Figure below.

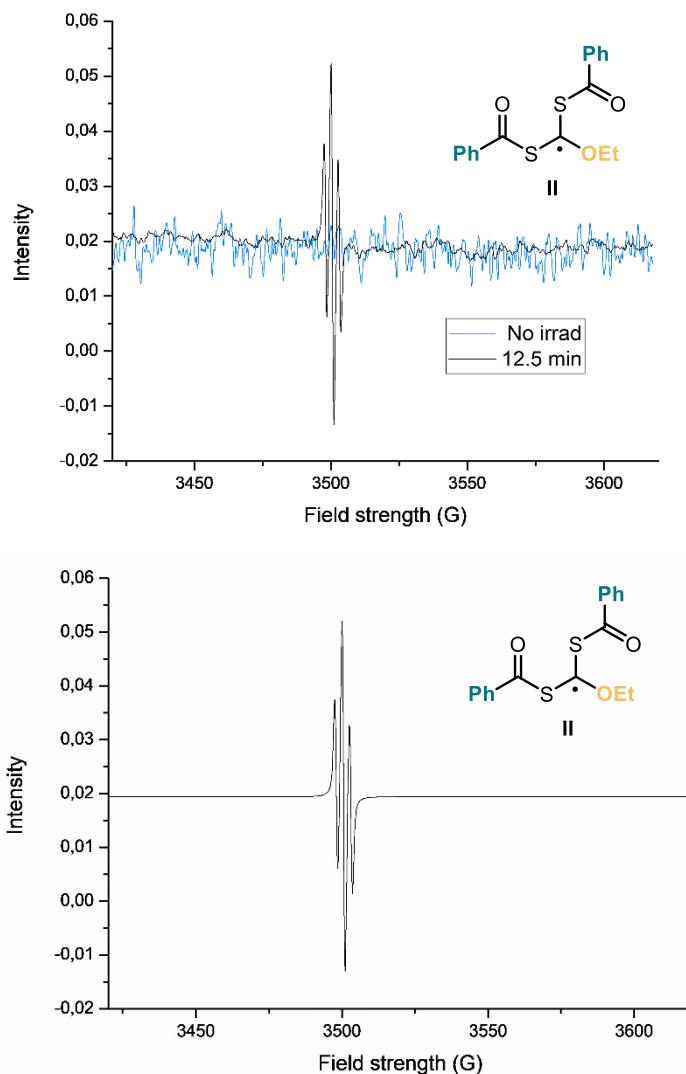


Figure 2.68. Comparison between (top) EPR spectra of acylxanthate **30** (0.1 M in toluene) before irradiation (blue line) and after irradiation with a LSB610 100W mercury lamp during 12.5 min (black line). Open-shell species was detected by appearance of a new signal centered at 3505 G (triplet); and (bottom) calculated EPR spectrum for intermediate **II** for a hyperfine coupling with two equivalent nuclei of spin $\frac{1}{2}$.

Quantum Yield Determination

A ferrioxalate actinometer solution was prepared by following the Hammond variation of the Hatchard and Parker⁹⁹ procedure outlined in the Handbook of Photochemistry.¹⁰⁰ The ferrioxalate actinometer solution measures the decomposition of ferric ions to ferrous ions, which are complexed by 1,10-phenanthroline and monitored by UV/Vis absorbance at 510

⁹⁹ Hatchard, C. G.; Parker, C. A. A new sensitive chemical actinometer II. Potassium ferrioxalate as a standard chemical actinometer. *Proc. R. Soc. Lond. A* **1956**, 518-536.

¹⁰⁰ Murov, S. L. *Handbook of Photochemistry* **1973**, Marcel Dekker Inc.

nm. The moles of iron-phenanthroline complex formed are related to moles of photons absorbed. The following solutions were prepared and stored in a dark laboratory (red light):

1. Potassium ferrioxalate solution: 294.8 mg of potassium ferrioxalate (commercially available from Alfa Aesar) and 139 μL of sulfuric acid (96%) were added to a 50 mL volumetric flask, and filled to the mark with water (HPLC grade).
2. Phenanthroline solution: 0.2% by weight of 1,10-phenanthroline in water (100 mg in 50 mL volumetric flask).
3. Buffer solution: 2.47 g of NaOAc and 0.5 mL of sulfuric acid (96%) were added to a 50 mL volumetric flask, and filled to the mark with water (HPLC grade).

The actinometry measurements were done as follows:

1. 1 mL of the actinometer solution was added to a screw-cap vial and placed on a single HP LED 1.5 cm away from the light source. The solution was irradiated at 460 nm (irradiance 40 mW/cm^2). This procedure was repeated 4 times, quenching the solutions after different time intervals: 10 s, 15 s, 20 s, and 25 s.
2. After irradiation, the actinometer solutions were removed and placed in a 10 mL volumetric flask containing 0.5 mL of 1,10-phenanthroline solution and 2 mL of buffer solution. These flasks were filled to the mark with water (HPLC grade).
3. The UV-Vis spectra of the complexed actinometer samples were recorded for each time interval. The absorbance of the complexed actinometer solution was monitored at 510 nm.

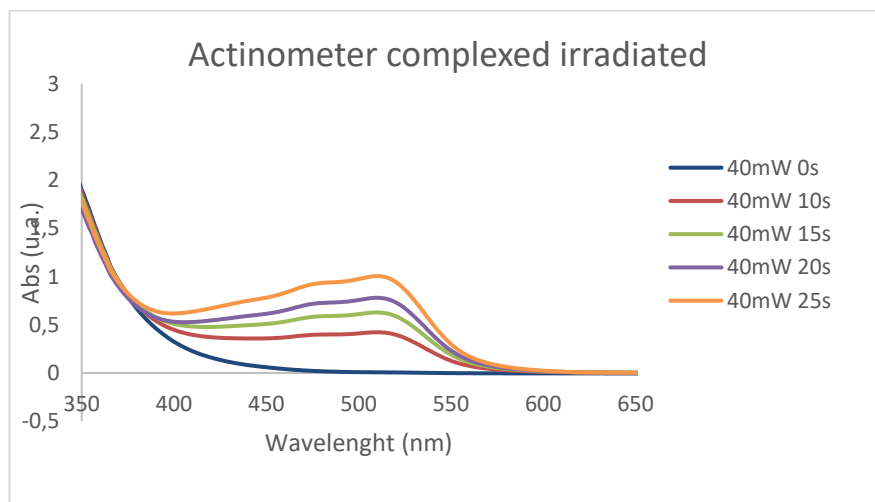


Figure 2.69. Absorbance of the complexed actinometer solutions.

The moles of Fe^{2+} formed for each sample is determined using Beers' Law (Eq. 1):

$$\text{Mols of Fe(II)} = V_1 \times V_3 \times \Delta A(510 \text{ nm})/10^3 \times V_2 \times l \times \varepsilon(510 \text{ nm}) \text{ (Eq. 1)}$$

where V_1 is the irradiated volume (1 mL), V_2 is the aliquot of the irradiated solution taken for the determination of the ferrous ions (1 mL), V_3 is the final volume after complexation with phenanthroline (10 mL), l is the optical path-length of the irradiation cell (1 cm), $\Delta A(510 \text{ nm})$ is the optical difference in absorbance between the irradiated solution and the one stored in the dark, $\varepsilon(510 \text{ nm})$ is the extinction coefficient the complex Fe(phen)_3^{2+} at 510 nm ($11100 \text{ L mol}^{-1} \text{ cm}^{-1}$). The moles of Fe^{2+} formed (x) are plotted as a function of time (t). The slope of this line was correlated to the moles of incident photons by unit of time ($q_{n,p}^0$) by the use of the following Equation 2:

$$\Phi(\lambda) = dx/dt q_{n,p}^0 [1 - 10^{-A(\lambda)}] \text{ (Eq. 2)}$$

where dx/dt is the rate of change of a measurable quantity (spectral or any other property), the quantum yield (Φ) for Fe^{2+} at 458 nm is 1.1,¹⁰¹ $[1 - 10^{-A(\lambda)}]$ is the ratio of absorbed photons by the solution, and $A(\lambda)$ is the absorbance of the actinometer at the wavelength used to carry out the experiments (460 nm). The absorbance at 460 nm $A(460)$ was measured using a Shimadzu 2401PC UV-Vis spectrophotometer in a 1 cm path quartz cuvette, obtaining an absorbance of 0.158.

$q_{n,p}^0$, which is the photon flux, was determined to be $1.048 \times 10^{-7} \text{ einstein s}^{-1}$.

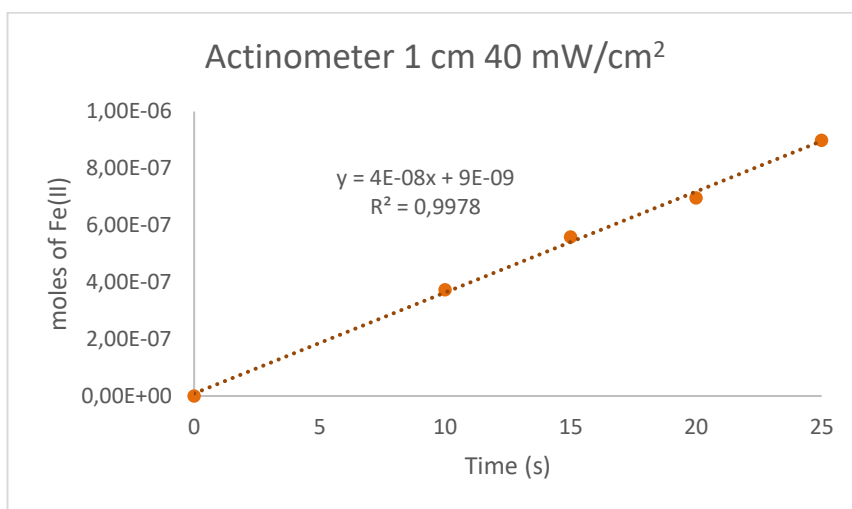


Figure 2.70. Determination of photon flux by linear representation of mols of Fe(II) with respect to irradiation time.

Consequently, the model reactions were performed.

¹⁰¹ Holubov, C. A.; Langford, C. H. Wavelength and Temperature Dependence in the Photolysis of the Chemical Actinometer, Potassium trisoxalatoferate(III), at Longer Wavelengths. *Inorganica Chim. Acta* **1981**, 53, 59-60.

The reactions were prepared on a screw-cap vial with stir bar. Cyclohexanecarbonyl chloride (50 μL , 0.375 mmol, 1.5 equiv.), γ -terpinene (120 μL , 0.75 mmol, 3 equiv.), and lutidine (58 μL , 0.5 mmol, 2 equiv.), were added to a solution of catalyst **D** (4 mg, 0.1 equiv.) in acetonitrile (1 mL). After degassing by bubbling Argon for 30 s, acrylonitrile **31a** (16 μL , 0.25 mmol) was added and the tube was sealed with parafilm and put in the HP-LED 460 nm at 1 cm distance at ambient temperature (reaction reaches around 35 $^{\circ}\text{C}$) with irradiance of 40 mW/cm^2 . Four different reactions were setup and irradiated for different times: 60 min, 80 min, 100 min and 120 min.

The moles of product **34a** formed for the model reaction were determined by GC measurement (FID detector) using 1,3,5-trimethoxybenzene as internal standard. The moles of product per unit of time are related to the number of photons absorbed. The photons absorbed are correlated to the number of incident photons by the use of Equation 1. According to this, plotting the moles of product (x) versus the moles of incident photons ($qn, 0\text{-}dt$), the slope is equal to: $\Phi \cdot (1 - 10^{-A(\lambda)(460\text{ nm})})$, where Φ is the quantum yield to be determined and $A(460\text{ nm})$ is the absorption of the reaction under study. $A(460\text{ nm})$ was measured using a Shimadzu 2401PC UV-Vis spectrophotometer in 10 mm path quartz. An absorbance of 0.103 was determined for the model reaction mixture. The quantum yield (Φ) of the photochemical transformation was measured to be 0.0338. The procedure was repeated a second time to provide a similar value: quantum yield (Φ) at 460 nm of 0.0332.

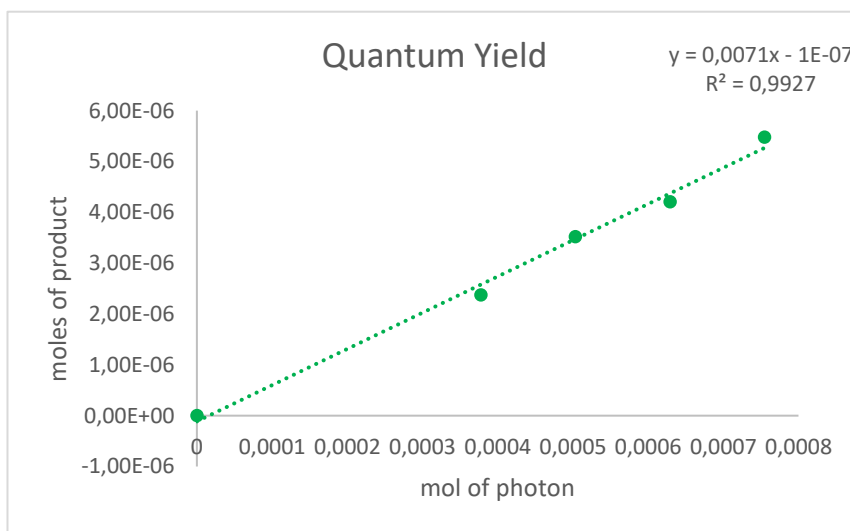


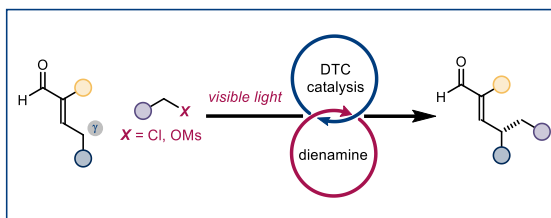
Figure 2.71. Determination of quantum yield by linear representation of mols of product with respect to indicent mol of photons on the reaction

Chapter III

Photochemical organocatalytic enantioselective radical γ -functionalization of α -branched enals

Target

To develop an organocatalytic photochemical strategy for the regio- and enantioselective γ -functionalization of α -branched enals.



Tool

Harnessing the photochemical properties of a nucleophilic dithiocarbamate catalyst to generate electrophilic radicals and a catalytic chiral dienamine intermediate to stereoselectively trap them.¹⁰²

3.1 Introduction

Most chemical transformations occur at the site, or in close proximity, of a functional group. For example, the deprotonation of a ketone with a base occurs adjacent to the carbonyl (C=O) functionality, which in turn permits a reaction to take place at the α -carbon. The concept of remote functionalization comprises the activation of a distal C-H bond that is not adjacent to a functional group.¹⁰³ This strategy has had a dramatic impact on the way chemists can construct a retrosynthetic plan for the synthesis of complex molecules. While the most straightforward and widely-used approach to disconnections and functional group interconversions is based on the manipulation of reactive functional groups,¹⁰⁴ the remote functionalization approach offers the possibility to use simple feedstock materials to functionalize generally inactive positions. Early examples of remote activation featured the use of metal ions to elicit desaturation reactions in a distal position to a chelating functionality (Figure 3.1a).¹⁰⁵ The ability of transition metals was further exploited in cross-coupling

¹⁰² The project discussed in this Chapter has been conducted in collaboration with Enrico Marcantonio, who performed part of the reaction scope. I was involved in the discovery of the reaction, its optimization, and evaluation of part of the reaction scope. This work has been published, see: Balletti, M.; Marcantonio, E.; Melchiorre, P. Photochemical organocatalytic enantioselective radical γ -functionalization of α -branched enals. *Chem. Commun.* **2022**, *58*, 6072-6075.

¹⁰³ (a) Sommer, H.; Julia-Hernandez, F.; Martin, R.; Marek, I. Walking metals for remote functionalization. *ACS Cent. Sci.*, **2018**, *4*, 153-165. (b) Vasseur, A.; Bruffaerts, J.; Marek, I.; Remote functionalization through alkene isomerization. *Nat. Chem.*, **2016**, *8*, 209-219. (c) Franzoni B.; Mazet, C.; Recent trends in Pd-catalyzed remote functionalization of carbonyl compounds. *Org. Biomol. Chem.* **2014**, *12*, 233-241.

¹⁰⁴ Warren, S. G.; Wyatt, P.; *The Disconnection Approach*; 2nd Ed.; John Wiley & Sons; Chichester, UK; **2008**.

¹⁰⁵ Schwartz, H. Remote functionalization of C-H and C-C bonds by "naked" transition-metal ions (Cosi Fan Tutte). *Acc. Chem. Res.* **1989**, *22*, 282-287.

technologies to derivatize C-H positions in arenes (Figure 3.1b)¹⁰⁶ and in simple aliphatic chains through “chain-walking” processes (Figure 3.1c).¹⁰⁷ Noteworthy, the recent advances in radical chemistry fostered the development of methodologies which allow the remote functionalization of aliphatic chains through the use of *N*-centered radicals, which readily undergo intramolecular 1,5-HAT (hydrogen atom transfer) to activate distal positions towards radical reactivity (Figure 3.1d).¹⁰⁸

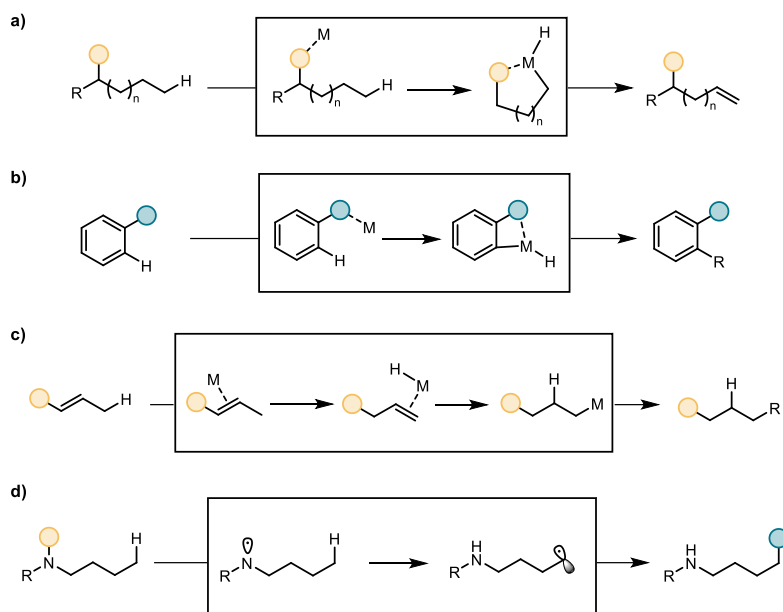


Figure 3.1. Strategies for remote functionalization

Despite the synthetic potential of remote functionalization, translating this concept to an asymmetric catalytic manifold is underdeveloped.¹⁰⁹ This is particularly true for acyclic systems because their flexibility challenges the catalyst’s ability to infer remote stereocontrol.

¹⁰⁶ Glorius, F.; Wencel-Delord, J.; Mild metal-catalyzed C–H activation: examples and concepts. *Chem. Soc. Rev.* **2016**, *45*, 2900-2936.

¹⁰⁷ Janssen-Müller, D.; Sahoo, B.; Sun, S.; Martin, R. Tackling Remote sp³ C–H Functionalization via Ni-Catalyzed chain-walking Reactions. *Isr. J. Chem.* **2020**, *60*, 195-206.

¹⁰⁸ (a) Sarkar, S.; Shing Cheung, K. P.; Gevorgian, V. C–H functionalization reactions enabled by hydrogen atom transfer to carbon-centered radicals. *Chem. Sci.* **2020**, *11*, 12974-12993. (b) Kumar, G.; Pradhan, S.; Chatterjee, I. N-Centered Radical Directed Remote C-H Bond Functionalization via Hydrogen Atom Transfer. *Chem. Asian J.* **2020**, *15*, 651-672.

¹⁰⁹ (a) Oiari, M.; Palomo, C.; Extended Enolates: Versatile Intermediates for Asymmetric C-H Functionalization via Noncovalent Catalysis. *Chem. Eur. J.*, **2021**, *27*, 10226-10246. For selected examples: (b) Patel, H. H.; Sigman, M.; Palladium-Catalyzed Enantioselective Heck Alkenylation of Acyclic Alkenols Using a Redox-Relay Strategy. *J. Am. Chem. Soc.*, **2015**, *137*, 3462-3465; (c) Chen, G.; Gong, W.; Zhuang, Z.; Andra, M. S.; Chen, Y.; Hong, X.; Yang, F.; Liu, T.; Houk, K. N.; Yu, J. Pd(II)-catalyzed Enantioselective Methylene C(sp³)-H Bond Activation *Science*, **2016**, *53*, 1023-1027; (d) Meng, F.; Li, X.; Torker, S.; Shi, Y.; Shen X.; Hoveyda, A. H. Catalytic enantioselective 1,6-conjugate additions of propargyl and allyl groups. *Nature*, **2016**, *537*, 387-393.

One effective strategy exploits the activation of enals with a chiral amine organocatalyst (Figure 3.2a). The resulting extended enamine (*dienamine*), which is characterized by a *vinyllogous* nucleophilicity, can be harnessed to perform functionalization at the more distal γ -carbon of carbonyl substrates. While the vast majority of protocols exploited the nucleophilicity of dienamines in polar manifolds to forge remote stereocenters, very few reports highlighted how these properties could be applied in radical chemistry.¹¹⁰ This stands in contrast with the well-known tendency of chiral enamines to trap electrophilic radicals at the α -position.¹¹¹ In this chapter, I will describe the implementation of an organocatalytic protocol for the radical γ -functionalization of branched enals using dienamine activation. By exploiting the nucleophilic properties of the dithiocarbamate (DTC) catalyst highlighted in chapter II, we generated radicals from simple alkyl chlorides using visible light irradiation. We envisioned that, even though the stereodirecting group of the aminocatalyst within the dienamine intermediate is distant from the γ -position, the radical-trapping step would take place in a stereocontrolled fashion, generating an enantioenriched γ -alkylated enal as product (Figure 3.2b).

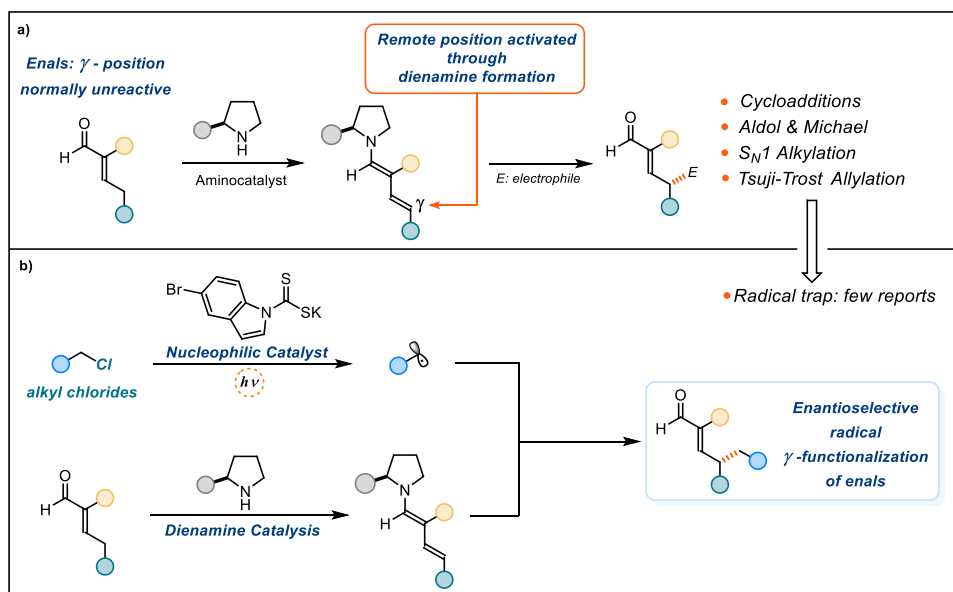


Figure 3.2. Idea of the project: enantioselective radical γ -functionalization of branched enals combining dienamine activation and DTC catalysis

¹¹⁰ M. Silvi, E. Arceo, I. Jurberg, C. Cassani and P. Melchiorre, Enantioselective Organocatalytic Alkylation of Aldehydes and Enals Driven by the Direct Photoexcitation of Enamines. *J. Am. Chem. Soc.*, **2015**, *137*, 6120-6123.

¹¹¹ Arceo, E.; Jurberg, I. D.; Alvarez-Fernandez, A.; Melchiorre, P. Photochemical activity of a key donor-acceptor complex can drive stereoselective catalytic α -alkylation of aldehydes. *Nat. Chem.* **2013**, *5*, 750-756.

3.2 Enamine Catalysis

During the last 20 years, organocatalysis has established itself as one of the most powerful tools to activate small molecules and drive unprecedented reactivity under mild reaction conditions.¹¹² Within the framework of organocatalysis, aminocatalysis, and in particular enamine catalysis,¹¹³ stood as the most exploited and efficient. The basis of this catalytic manifold is the reversible generation of an enamine from the condensation of a secondary (or primary) amine (**1**) with a carbonyl compound (Figure 3.3 left).

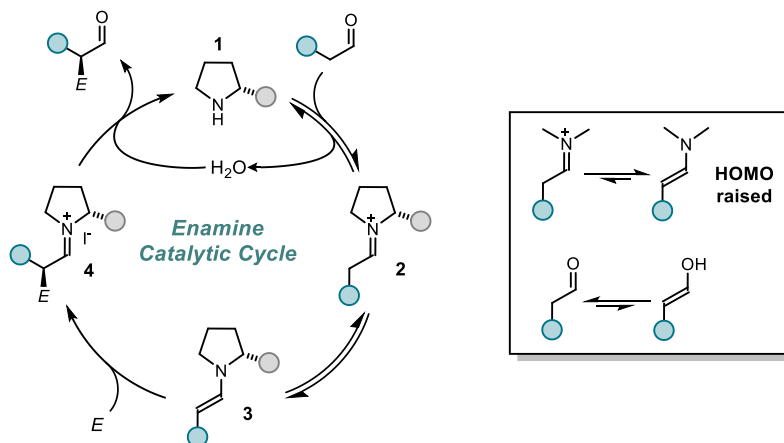


Figure 3.3. *left:* Schematic enamine catalytic cycle.

Right: Comparison between the enamine's and the enol's nucleophilicity

The initial formation of the iminium ion **2**, which is characterized by an increased α -proton acidity, drives the formation of the corresponding enamine **3**. This catalytic intermediate features an increased energy of the highest occupied molecular orbital (HOMO) compared to the corresponding enol counterpart (Figure 3.3 right) and can therefore react with several electrophiles (**E**) in solution.¹¹⁴ Since the electrophile can attack the two prochiral faces of the enamine, the role of chiral element on the scaffold of the aminocatalyst is to control the formation of the new C–E bond. The rational use of chiral amines as catalysts allowed for the construction of stereogenic centers with high degrees of enantiocontrol.¹¹⁵

¹¹² (a) Dalko, P. I. (ed.) *Comprehensive Enantioselective Organocatalysis: Catalysts, Reactions and applications*. Wiley-VCH, **2013**. (b) Xiang, S.; Tan, B. *Advances in asymmetric organocatalysis over the last 10 years* *Nat. Commun.* **2020**, *11*, 3786.

¹¹³ (a) Mukherjee, S.; Yang, J. H.; Hoffmann, S.; List, B. *Asymmetric Enamine Catalysis*. *Chem. Rev.* **2007**, *107*, 5471 – 5569. (b) List, B. "Enamine Catalysis Is a Powerful Strategy for the Catalytic Generation and Use of Carbanion Equivalents" *Acc. Chem. Res.* **2004**, *37*, 548-557.

¹¹⁴ Nielsen, D. Worgull, T. Zweifel, B. Gschwend, S. Bertelsen, K. A. Jørgensen *Mechanisms in aminocatalysis*. *Chem. Commun.* **2011**, *47*, 632-649.

¹¹⁵ C. F. Barbas III *Organocatalysis Lost: Modern Chemistry, Ancient Chemistry, and an Unseen Biosynthetic Apparatus*. *Angew. Chem. Int. Ed.* **2008**, *47*, 42-47.

The first example of enantioselective enamine catalysis dates back to 1970 when Hajos and Parrish reported that naturally-occurring proline could catalyze the intramolecular aldol reaction of **5** (Figure 3.4a).¹¹⁶ To explain the stereochemical outcome of the reaction and the high level of enantioselectivity, a model featuring H-bonding interaction between the proline's carboxylic acid and the carbonyl moieties was invoked for the first time. Despite this reaction's utility, particularly for the synthesis of steroidal motifs such as **6**, its mechanism remained unclear, and proline was not appreciated as a broadly applicable catalyst. Almost 30 years later, an important breakthrough made by List, Lerner, and Barbas who, based on previous studies of class I aldolase enzymes,¹¹⁷ exploited the same amino acid (proline) to perform the first enantioselective *intermolecular* aldol reaction between aryl aldehydes **7** and acetone (Figure 3.4b).¹¹⁸

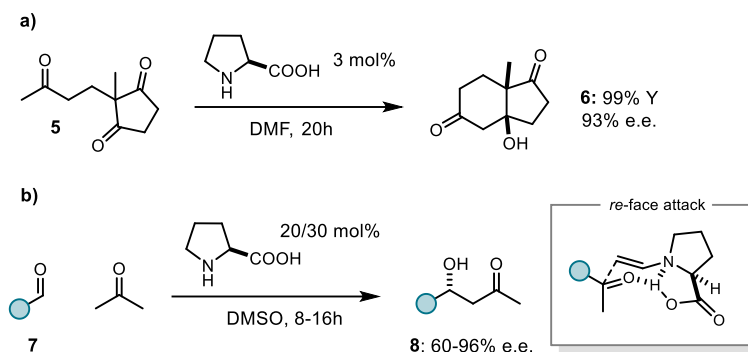


Figure 3.4. Early examples of Proline catalyzed aldol condensation by a) Hajos and Parrish (1970) and b) List & Barbas (2000)

A metal-free version of the Zimmerman-Traxler transition state, featuring a tricyclic hydrogen bonded framework, served to rationalize the enantiofacial selectivity.¹¹⁸ These studies prompted increased attention toward the use of chiral catalytic enamine intermediates to forge stereocenters, and since the original report enamine catalysis, and other applications of aminocatalysis, attracted considerable attention of synthetic chemists.¹¹⁹ In following studies, the design and development of new non-natural chiral aminocatalysts were reported, which

¹¹⁶ Hajos, Z. G.; Parrish, D. R. Asymmetric synthesis of bicyclic intermediates of natural product chemistry. *J. Org. Chem.* **1974**, *39*, 1615-1621.

¹¹⁷ (a) Wagner, J.; Lerner, R. A.; Barbas, C. F., III Efficient Aldolase Catalytic Antibodies That Use the Enamine Mechanism of Natural Enzymes. *Science* **1995**, *270*, 1797-1800. (b) Barbas, C. F., III; Heine, A.; Zhong, G.; Hoffmann, T.; Gramatikova, S.; Bjo Ernestedt, R.; List, B.; Anderson, J.; Stura, E. A.; Wilson, E. A.; Lerner, R. A. Immune Versus Natural Selection: Antibody Aldolases with Enzymic Rates But Broader Scope *Science* **1997**, *278*, 2085-2092.

¹¹⁸ List, B.; Lerner, R. A.; Barbas III, C. F. "Proline-Catalyzed Direct Asymmetric Aldol Reactions" *J. Am. Chem. Soc.* **2000**, *122*, 2395-2396.

¹¹⁹ Melchiorre, P.; Marigo, M.; Carlone, A.; Bartoli, G. "Asymmetric aminocatalysis--gold rush in organic chemistry" *Angew. Chem. Int. Ed.* **2008**, *47*, 6138-6171.

demonstrated that structural variations on proline can lead to enhanced stereoselectivity by discriminating the facial approach of the electrophile either by electronic or steric interactions with the enamine (Figure 3.5). It was shown that the chiral aminocatalyst can infer stereochemical information by exploiting 1) bulky stereodirecting groups, which hinder the approach of an electrophile to one of the diastereotopic faces, or 2) specific functional groups, which lower the barrier to bond formation on one face through stabilizing non-covalent interactions with the electrophile.

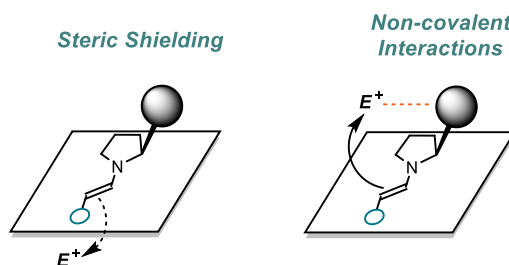


Figure 3.5. Different mode of actions of the aminocatalyst. *Left:* facial discrimination by steric shielding. *Right:* facial discrimination by non-covalent interactions.

Nowadays, aminocatalysis stands as an established and versatile tool to build complex chiral molecules for application in both total syntheses¹²⁰ and in the manufacturing of active pharmaceutical ingredients (APIs).¹²¹

3.3 The Principle of Vinylogy

3.3.1 General concept

In 1935, Reynold Fuson elegantly introduced the concept of vinylogy. This principle stated that “*in a molecule containing a system of conjugated double linkages, the influence of a functional group may sometimes be propagated along the chain and make itself apparent at a remote point in the molecule*”.¹²² Following this principle, we can exploit the presence of conjugated double bonds along a chain to activate a carbon in a remote position to the

¹²⁰ For a comprehensive review see: Marquez-Lopez, E.; Herrera, R. P.; Christmann, M. Asymmetric organocatalysis in total synthesis – a trial by fire. *Nat. Prod. Rep.*, **2010**, *27*, 1138-1167. For elegant examples and applications see: (a) Michrowska, A.; List, B. Concise synthesis of ricciolepin A and discovery of a more potent analogue. *Nat. Chem.* **2009**, *1*, 225-228. (b) Jones, B. S.; Simmons, B.; Mastracchio, A.; MacMillan, D. W. C. Collective synthesis of natural products by means of organocascade catalysis. *Nature*, **2011**, *475*, 183 – 188. (c) Coulthard, G.; Erb, W.; Aggarwal, V. K. Stereocontrolled organocatalytic synthesis of prostaglandin PGF2 α in seven steps *Nature*, **2012**, *489*, 278-281.

¹²¹ Han, B.; He, X.; Liu, Y.; He, G.; Peng, C.; Li, J. Asymmetric organocatalysis: an enabling technology for medicinal chemistry. *Chem. Soc. Rev.*, **2021**, *50*, 1522-1586.

¹²² Fuson, R. C. The Principle of Vinylogy *Chem. Rev.* **1935**, *16*, 1-27.

conjugated functional group (Figure 3.6a). Vinylogous silyl enol ethers, which found broad application in total synthesis, are one of the most noteworthy examples of this concept.¹²³ While classic enolate chemistry is used to activate the α -position of a carbonyl substrate, the application of vinylogous reactivity has fostered the use of extended enolates and silyl enol ethers to activate remote positions (Figure 3.6b) towards reactions with electrophiles.¹²⁴

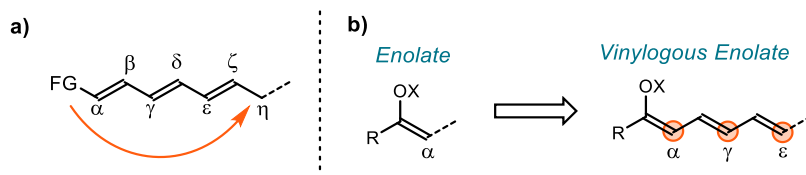


Figure 3.6. (a) Transmission of electronic effect to a general remote position. (b) Translation of enolate to vinylogous trienolate.

The great power of vinylogy lies in the fact that is general and can be applied not only to stoichiometric intermediates, but can also be merged with multiple catalytic platforms.¹²⁵ However, the main issue related to the use of vinylogous intermediates concerns regioselectivity. While the presence of the conjugated double bonds enables transmission of reactivity to other positions, reaction at the most remote position is not guaranteed, and mixtures of α -, γ -, or ϵ -functionalized products can be obtained (as highlighted in seminal examples using vinylogous dienolates).¹²⁶ The main factors governing the regiomic outcome are: 1) the distribution of electronic density between the reactive sites (electronic effects); 2) the presence of bulky substituents (steric effects); and 3) the thermodynamic stability of the reaction intermediates.¹²⁷ When dealing with vinylogous asymmetric processes, stereoselectivity is difficult to achieve due to the intrinsic low spatial proximity of the newly formed stereocenter to the functional group. In addition, the ability to control the various possible configurations of the double bond provides an additional challenge, since

¹²³ Denmark, S. E.; Heemstra, J. R.; Beutner, G. L. Catalytic, Enantioselective, Vinylogous Aldol Reactions. *Angew. Chem. Int. Ed.* **2005**, *44*, 4682-4689. (b) Kalesse, M.; Cordes, M.; Symkenberg, G.; Lu, H. The vinylogous Mukaiyama aldol reaction (VMAR) in natural product synthesis. *Nat. Prod. Rep.*, **2014**, *31*, 563-594.

¹²⁴ Oiarbide, M.; Paolomo, C. Extended Enolates: Versatile Intermediates for Asymmetric C-H Functionalization via Noncovalent Catalysis. *Chem. Eur. J.* **2021**, *27*, 10226-1024.

¹²⁵ Curti, C.; Battistini, L.; Sartori, A.; Zanardi F. New Developments of the Principle of Vinylogy as Applied to π -Extended Enolate-Type Donor Systems. *Chem. Rev.* **2020**, *120*, 2448-2612.

¹²⁶ (a) Rathke, M. W., Sullivan, D. The preparation and reactions of enolate anions derived from α,β -unsaturated esters. *Tetrahedron Lett.* **1972**, *13*, 4249-4252. (b) J. L. Herrmann, G. R. Kieczkowski, R. H. Schlessinger, "Deconjugative alkylation of the enolate anion derived from ethyl crotonate. *Tetrahedron Lett.* **1973**, *14*, 2433-2436.

¹²⁷ Bencivenni, G.; Galzerano, P.; Mazzanti, A.; Bartoli, G.; Melchiorre, P. Direct Asymmetric Vinylogous Michael Addition of Cyclic Enones to Nitroalkenes via Dienamine Catalysis. *Proc. Natl. Acad. Sci. U.S.A.* **2010**, *107*, 20642-20647.

this determines the stereochemical outcome of the process. Albeit far from a general answer to this problem, some strategies can be adopted to mitigate these issues and achieve high levels of regio- and stereocontrol.

In the next sections, I will highlight the progress made in merging the concept of vinylogy with asymmetric enamine catalysis, and the strategies used by chemists to tackle the significant challenges posed by stereocontrol.

3.3.2 Vinylogous enamine catalysis

The chemistry of vinylogous (or extended) enamines has a long history. The use of stoichiometric extended enamines was studied in 1939 by Snyder, who demonstrated their utility as dienes in [4+2]-cycloaddition reactions (Figure 3.7a) for the synthesis of complex structures such as **10**.¹²⁸ Many years later, Huisman and coworkers showed that steroid-derived extended enamine **11** could react also as a nucleophile in substitution reactions (Figure 3.7b). The study already highlighted how, depending on the reaction conditions, the alkylation could suffer from regioselectivity issues, producing mixtures of **12a** and **12b**.¹²⁹

¹²⁸ H. R. Snyder, R. B. Hasbrouck and J. F. Richardson Reactions of Anils. III.1 A New Type of Diels-Alder Reaction. *J. Am. Chem. Soc.*, **1939**, *61*, 3558.

¹²⁹ Huisman, H. O. Approaches to Total Synthesis of Heterocyclic Steroidal Systems. *Angew. Chem. Int. Ed.* **1971**, *10*, 450-459.

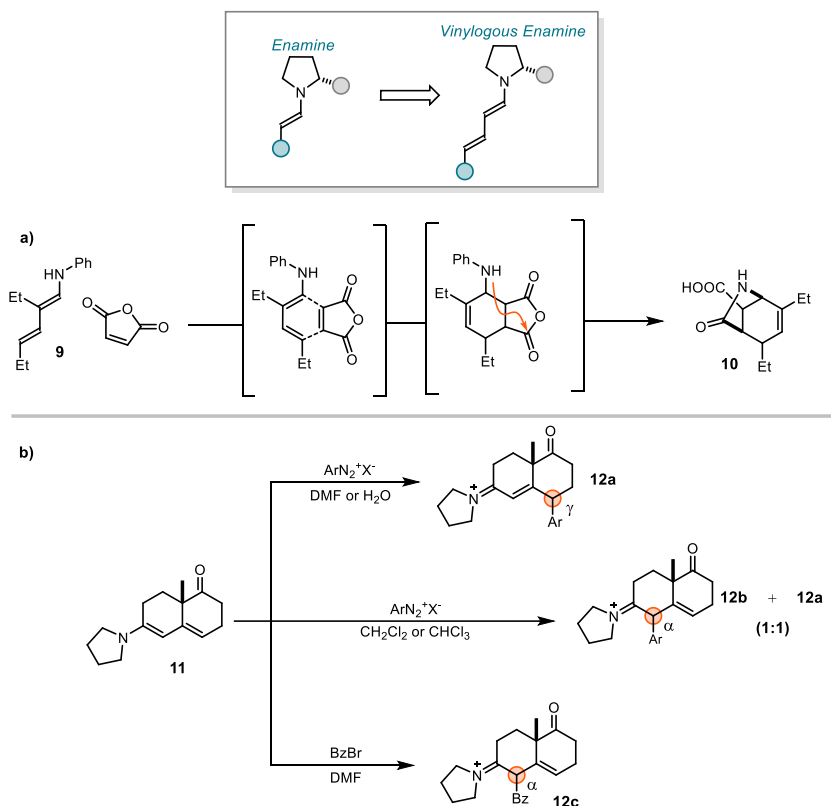


Figure 3.7. First examples of reactions involving stoichiometric dienamine intermediates

The translation of this reactivity to a catalytic system was reported for the first time in 1998 by Serebryakov, who exploited vinylogous enamine intermediates in the synthesis of polysubstituted cyclohexadienes (Figure 3.8a).¹³⁰ Nucleophilic dienamine **13** was shown to react efficiently with Michael acceptors **14** in a [4+2] cycloaddition to afford **15**. Interestingly, no further examples of this reactivity were disclosed until 2006, when the group of Jørgensen reported the first enantioselective γ -amination of enals (Figure 3.8b).¹³¹ In this report, it was demonstrated that linear enals **16** could react with diazo compounds **17** in the presence of a chiral secondary amine catalyst to generate enantioenriched γ -aminated products **18**.

¹³⁰ Serebryakov, E. P.; Nigmatov, A. G.; Shcherbakov, M. A.; Struchkova, M. I. The effects of the nature of catalyst and of the solvent on the stereoselectivity in amine-catalyzed asymmetric synthesis of substituted cyclohexa-1,3-dienes from prenal and monoesters of ylidene malonic acids. *Russ. Chem. Bull.*, **1998**, *47*, 82-90.

¹³¹ Bertelsen, S.; Marigo, M.; Brandes, S.; Diner, P.; Jørgensen, K. A. Dienamine Catalysis: Organocatalytic Asymmetric γ -Amination of α,β -Unsaturated Aldehydes. *J. Am. Chem. Soc.*, **2006**, *128*, 12973-12980.

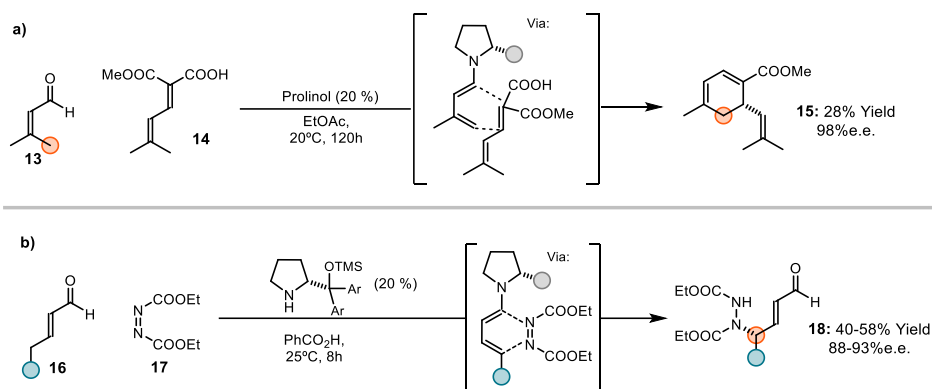


Figure 3.8. Early examples of reactions involving catalytic dienamine intermediates in cycloaddition manifolds

Both processes harness the dienamine's conjugated double bonds to perform [4+2] cycloadditions with a dienophile. The intrinsic stereospecificity of cycloaddition reactions,¹³² combined with the facial bias elicited by the chiral aminocatalyst, accounted for the high level of stereoselectivity. The report by Jørgensen is considered a significant milestone, not only because this sparked a flurry of reports into the use of dienamine as organocatalytic intermediates, but also for the mechanistic interrogation of the various equilibria that govern the conformation of the dienamine's double bonds and therefore the observed stereoselectivity. Nowadays, this reactivity has been leveraged by several groups to generate chemical complexity while controlling stereoselectivity with high fidelity.¹³³

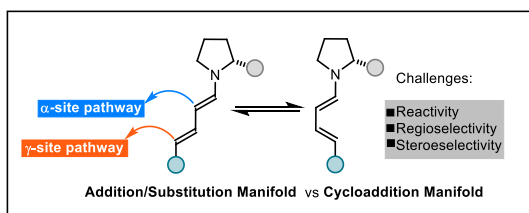


Figure 3.9. Challenges in the direct γ -functionalization of catalytic dienamine intermediates

When considering reactions that do not involve pericyclic processes, the direct functionalization of a remote position in a catalytic extended enamine becomes much more challenging. First of all, competitive α -functionalization is an undesired pathway which leads to mixtures of products. Second, the conjugated system can exist in solution with multiple *E/Z*

¹³² Hoffman, R.; Woodward, B. Conservation of orbital symmetry. *Acc. Chem. Res.* **1968**, *1*, 17-22. (b) Gleiter, R.; Bohm, M. C.; Regio- and Stereoselectivity in Diels-Alder reactions. Theoretical considerations. *Pure and App. Chem.* **1983**, *55*, 2, 237-244.

¹³³ Klier, L.; Tur, F.; Poulsen, P. H.; Jørgensen, K.A. Asymmetric cycloaddition reactions catalysed by diarylprolinol silyl ethers. *Chem. Soc. Rev.* **2017**, *46*, 1080-1102.

double bond isomers, thus decreasing the likelihood of stereocontrol over the forming stereogenic center (Figure 3.9).

The first step towards a general solution to these problems was reported almost simultaneously by the group of Christmann and the Melchiorre group. By investigating a series of substituted enals in an organocatalytic S_N1 reaction, it was found that substitution plays a significant role in influencing the regiomer outcome of α/γ products (Figure 3.10).¹³⁴ Linear and γ -branched enals delivered a mixture of regioisomeric products, with linear enals giving preferential γ -alkylation (20:80 α,γ) and γ -branched enals giving mostly α -alkylated product (75:25 α,γ). Intriguingly, a β -branched enal was reported to undergo exclusive γ -alkylation, albeit with lower stereocontrol. On the other hand, our group found that the use of α -substituted enals under similar reaction conditions delivered exclusively the γ -alkylated product with excellent levels of enantioselectivity.¹³⁵

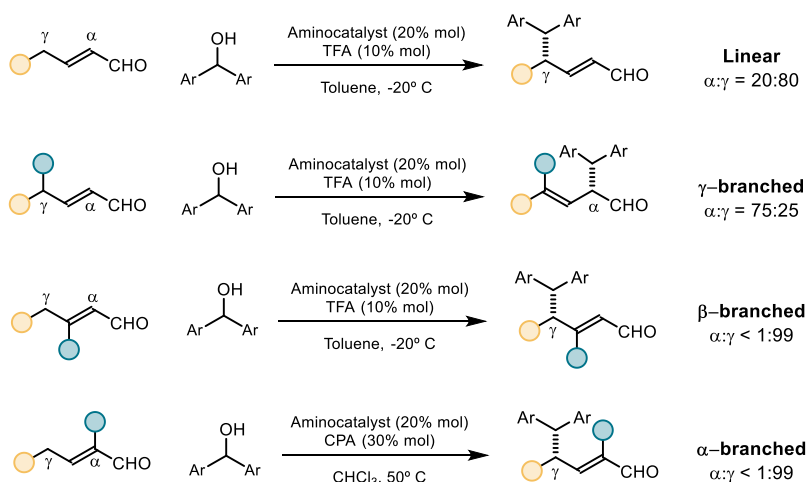


Figure 3.10. Systematic evaluation of the effect of substitution pattern on regioselectivity for the alkylation of enals.

From the previous studies, it appeared clear that the substitution pattern on the enal can have a dramatic impact on both the regioselectivity and enantioselectivity of the process. This empirical notion was later rationalized by the substituents effect on the equilibrium constants between the various conformations and double bond configurations of the proposed dienamine intermediates. Further studies made by our group confirmed this hypothesis.¹³⁶

¹³⁴ Stiller, L.; Marques-Lopez, E.; Herrera, R.; Frohlich, R.; Strohmam, C; Christmann, M. Enantioselective α - and γ -Alkylation of α,β -Unsaturated Aldehydes Using Dienamine Activation. *Org. Lett.*, **2011**, *13*, 70-73.

¹³⁵ Bergonzini, G.; Vera, S.; Melchiorre, P. Cooperative Organocatalysis for the Asymmetric γ Alkylation of α -Branched Enals. *Angew. Chem., Int. Ed.*, **2010**, *49*, 9685-9688.

¹³⁶ Silvi, M.; Cassani, C.; Moran, A.; Melchiorre, P. Secondary amine-catalyzed asymmetric gamma-alkylation of alpha-branched enals via dienamine activation. *Helv. Chim. Acta*, **2012**, *95*, 1985-2006.

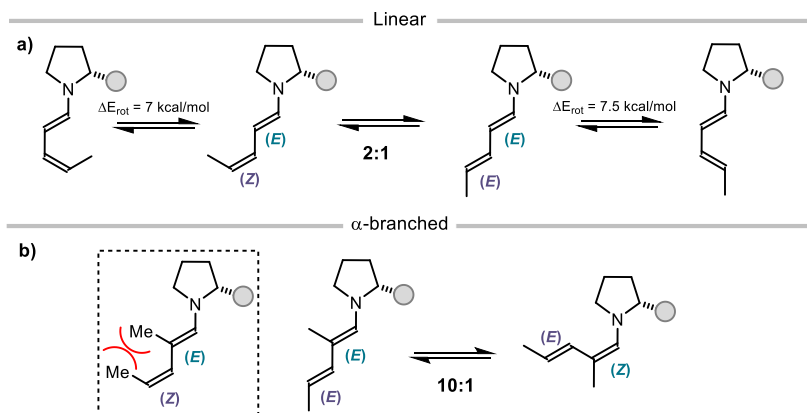


Figure 3.11. Different equilibrium distribution in the case of: *a)* linear dienamines and *b)* α -branched dienamines

Through the aid of NMR spectroscopy, the isomeric dienamine intermediates arising from the condensation of a chiral secondary amine catalyst with 2-methyl-pentenal were studied. The results highlighted interesting mechanistic considerations when compared with the spectroscopic analysis carried by the group of Jørgensen using linear enals (Figure 3.11a).¹³¹ In the case of linear unsaturated aldehydes, two prominent isomers were determined by NMR spectroscopy, differing in the configuration of the second double bond. The (1*E*,3*Z*) isomer was found to be dominant in solution, with a 2:1 preference over the (1*E*,*E*) isomer. DFT calculations confirmed that the relative stability of these intermediates differs by just 1.2 kcal/mol at room temperature. However, studies of an α -methyl substituted enal revealed a different constitution of the dynamic equilibrium of isomers. The steric clash provoked by the methyl substituent destabilizes the (1*E*,3*Z*) conformation of the dienamine, prompting a shift in the equilibria to an isomeric ratio of 10:1 (Figure 3.11b). This result highlights the importance of the α -substituent to direct the reactivity towards the γ position, but also to drastically bias the dienamine geometry, a crucial prerequisite to forge a stereocenter with high fidelity.

Despite these advances, the enantioselective γ -functionalization of enals has remained an underdeveloped synthetic goal. After the publication of S_N1 reactivity reported in 2010, our group reported that the same α -branched enals **19** could be employed in vinylogous aldol reactions with isatins **20** as electrophiles (Figure 3.12).¹³⁷ In this case, when an α -alkyl enal is used, the dienamine intermediate underwent remote attack to the isatin carbonyl in a stereocontrolled fashion, leading to γ -functionalised enals in good yields and with excellent enantioselectivities.

¹³⁷ Cassani, C.; Melchiorre, P. Direct Catalytic Enantioselective Vinylogous Aldol Reaction of α -Branched Enals with Isatins. *Org. Lett.*, **2012**, *14*, 5590-5593.

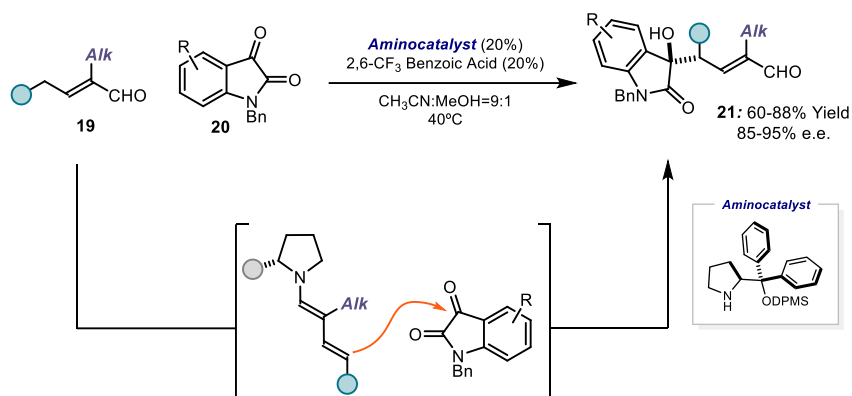


Figure 3.12. Direct enantioselective vinylogous aldol reaction

The vinylogous aldol manifold was also elegantly applied by Woogon and coworkers in the synthesis of α -tocopherol (Figure 3.13).¹³⁸ Through a vinylogous domino aldol/oxa-Michael reaction between *ortho*-hydroxyaldehyde **22** and phytenal **23**, the key stereocenters of the lactol's core **24** were set with excellent stereocontrol, providing a general access to several members of the vitamin E family

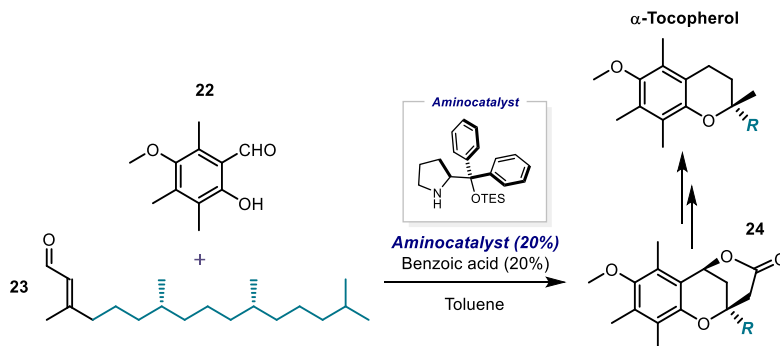


Figure 3.13. Direct enantioselective vinylogous aldol reaction: application in the synthesis of Tocopherol

In 2014, the Jørgensen group exploited β -branched enals **25** to perform a vinylogous Michael addition with vinyl phosphonates **26** (Figure 3.14).¹³⁹ The conformation of the dienamine formed under these conditions proved to be rigid enough to achieve good level of enantioselectivity. The products could be elaborated through intramolecular Wittig

¹³⁸ Liu, K.; Chogunette, A.; Woogon, W.-D. A Short Route to α -Tocopherol. *Angew. Chem. Int. Ed.* **2008**, *47*, 5827-5829.

¹³⁹ Donslud, B. S.; Halskov, K. S.; Leth, L. A.; Paz, B. M.; Jørgensen, K. A Organocatalytic asymmetric strategies to carbocyclic structures by γ -alkylation-annulation sequences. *Chem. Comm.* **2014**, *50*, 13676-13679.

olefination to produce enantioenriched carbocyclic scaffolds **27**, which constitute widespread cores in naturally occurring compounds.

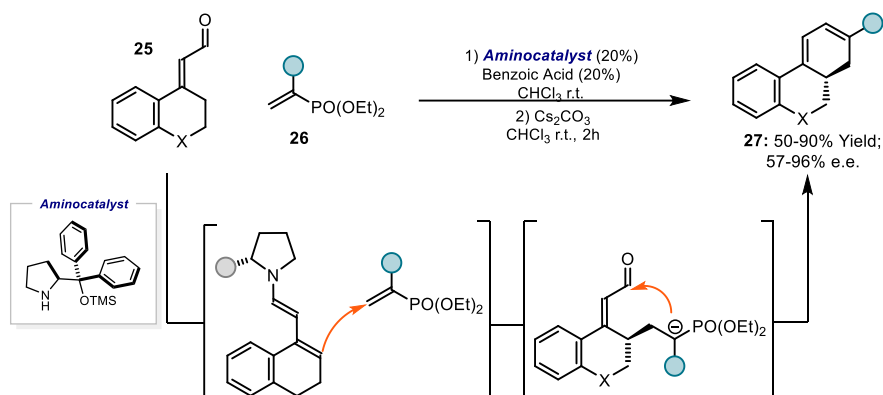


Figure 3.14. Direct enantioselective vinylogous Michael reaction

The same group subsequently disclosed a dual catalytic platform for the enantioselective γ -allylation of enals using allylic alcohols **28** (Figure 3.15).¹⁴⁰ The organocatalytic system was combined with iridium-catalyzed activation of allylic alcohols to generate electrophilic π -allyl complexes able to intercept the chiral dienamine intermediate.¹⁴¹ The reaction features high levels of enantioselectivity and diastereoselectivity, and is also highly regiodivergent with respect to the allylation step. Precisely, by a careful choice of the metal complex (iridium or palladium) is possible to achieve either the branched or the linear product (**29** or **30**) with excellent enantioselectivity.

¹⁴⁰ Næsborg, L.; Halskov, K. S.; Tur, F.; Mønsted S.; Jørgensen, K. A. Asymmetric γ -Allylation of α,β -Unsaturated Aldehydes by Combined Organocatalysis and Transition-Metal Catalysis. *Angew. Chem., Int. Ed.*, **2015**, *54*, 10193-10197.

¹⁴¹ (a) Trost, B. M.; Van Vranken, D. L. Asymmetric Transition Metal-Catalyzed Allylic Alkylations. *Chem. Rev.*, **1996**, *96*, 395-422. (b) Trost, B. M.; Crawley, M. L. Asymmetric Transition-Metal-Catalyzed Allylic Alkylations: Applications in Total Synthesis. *Chem. Rev.*; **2003**, *103*, 2921-2944.

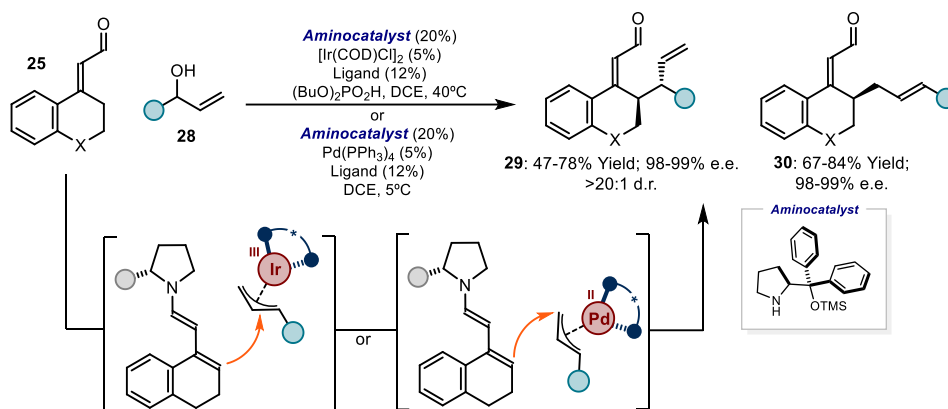


Figure 3.15. Direct enantioselective vinylogous allylation of enals

3.4 Enamines as radical traps

Enamine intermediates are generally recognized as useful carbon nucleophiles that can undergo several transformations in classical two-electron polar chemistry. The first decade of the 21st century experienced a blossoming of methodologies involving the catalytic use of enamines for the α -functionalization of carbonyls. To expand the repertoire of possible transformations using organocatalytic enamine intermediates, radical chemistry was soon envisaged as a possible solution to achieve diversity and orthogonality. While radicals were generally perceived as too reactive to be implemented with the impressive levels of efficiency and stereoselectivity reached in polar enamine catalysis, the recent advent of photocatalysis as a tool for radical formation under mild conditions grasped the attention of synthetic chemists.¹⁴²

¹⁴² (a) Silvi, M.; Melchiorre, P. Enhancing the potential of enantioselective organocatalysis with light. *Nature*, **2018**, *554*, 41-49. (b) Jiang, C.; Chen, W.; Zheng, W.-H.; Lu, H. Advances in asymmetric visible-light photocatalysis, 2015–2019. *Org. Biomol. Chem.* **2019**, *17*, 8673-8689. (c) Rigotti, T.; Alemán, J. Visible light photocatalysis – from racemic to asymmetric activation strategies. *Chem. Commun.*, **2020**, *56*, 11169-11190.

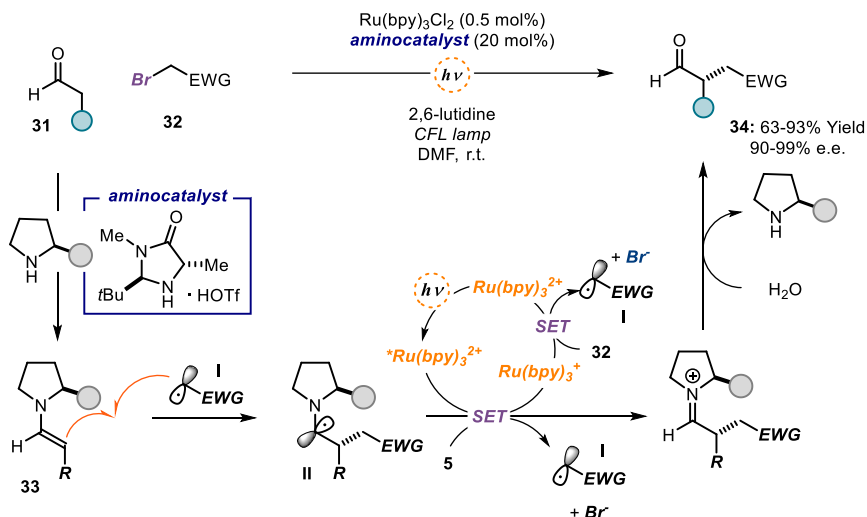


Figure 3.16. Enantioselective α -alkylation of aldehydes by merging organo- and photoredox catalysis

In 2008, pioneering work by Nicewicz and MacMillan on photoredox catalysis underlined how radical chemistry could be efficiently coupled with asymmetric enamine-based catalysis to provide a new way to forge stereocenters (Figure 3.16).¹⁴³ With the aid of a photocatalyst, electron-deficient radicals could be generated through single electron transfer (SET) to simple alkyl bromides **32**. These open-shell intermediates **I** could be efficiently trapped by the organocatalytic enamine **33**. Thanks to the chiral environment elicited by the aminocatalyst, the radical could be efficiently trapped in an enantioselective fashion. The incipient α -amino radical **II**, upon SET oxidation, regenerated an iminium ion, which was hydrolyzed to give enantioenriched aldehydes **34**. This seminal report has been recognized as the starting point of modern photoredox catalysis, which has since sparked significant interest in the enantioselective functionalization of carbonyls through radical chemistry.¹⁴⁴

While several radical-based methodologies for the α -functionalization of carbonyls have been reported, the application of this strategy to the vinylogous dienamine intermediate was barely reported. In this regard, our group studied the photochemical activity of extended enamines (and classical enamines) in the excited state (Figure 3.17).¹⁴⁵ The excitation of enamines with a compact fluorescent lamp (CFL) generates an electronically excited state that displays

¹⁴³ Nicewicz, D. A.; MacMillan, D. W. C. Merging photoredox catalysis with organocatalysis: the direct asymmetric alkylation of aldehydes. *Science*, **2008**, *322*, 77-80.

¹⁴⁴ Zou, Y.-Q.; Hörmann, F. M.; Bach, T. Iminium and enamine catalysis in enantioselective photochemical reactions. *Chem. Soc. Rev.*, **2018**, *47*, 278-290.

¹⁴⁵ Silvi, M.; Arceo, E.; Jurberg, I. D.; Cassani, C.; Melchiorre, P.; Enantioselective Organocatalytic Alkylation of Aldehydes and Enals Driven by the Direct Photoexcitation of Enamines. *J. Am. Chem. Soc.* **2015**, *137*, 6120-6123.

potent SET reducing properties. The photoexcited enamine could generate malonyl radicals **II** by SET reduction of bromomalonates **36**. The ensuing malonyl radicals were trapped by the ground-state chiral dienamines with high level of enantioselectivity and total γ -regioselectivity, generating products **38**.

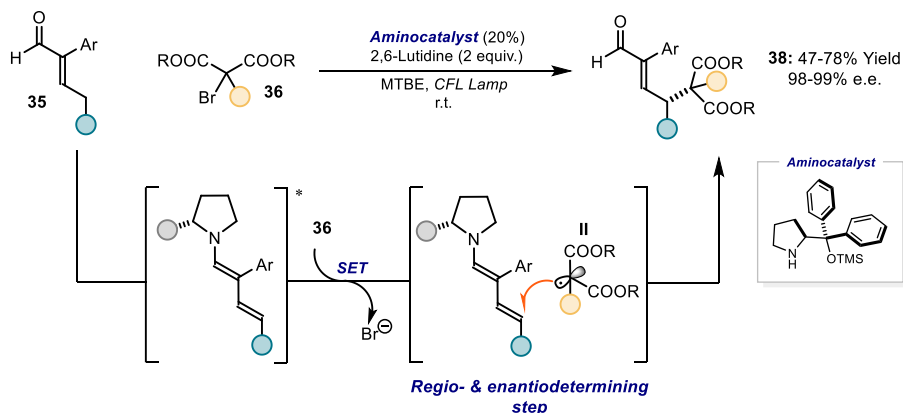


Figure 3.17. Direct enantioselective vinylogous alkylation of enals

An important feature of this radical process regards the regioselectivity of the reaction. While the substituent at the α -position was needed to fix the geometry of the dienamine to ensure sufficient stereocontrol, the regioselectivity was shown to be independent of the nature of the substrate. When linear enals were employed, the reaction still proceeded with exclusive regioselectivity for the remote position, albeit with poor stereocontrol over the newly formed stereocenter. The observed selectivity toward the γ -position is strictly related to the radical nature of the process and stands in contrast with the classical polar dienamine chemistry, which generally gives low levels of regioselectivity.¹³⁴

3.5 Target of the project

The work recently published by our group¹⁴⁵ disclosed the possibility to use organocatalytic dienamines as radical traps to generate new stereocenters at the γ -position of enals with good enantioselectivity and unique regioselectivity. Until now this chemistry has been restricted to the use of tertiary bromomalonates as radical precursors. To increase the synthetic applicability of this chemistry and expand the scope of radical precursors, we aimed to develop a general strategy for the synthesis of a wide array of enantioenriched γ -alkylated enals.

3.5.1 Design plan

To tackle this issue, we envisioned that the productive merger of the DTC catalytic platform (detailed in Chapter II) and dienamine catalysis could serve our purpose (Figure 3.18).

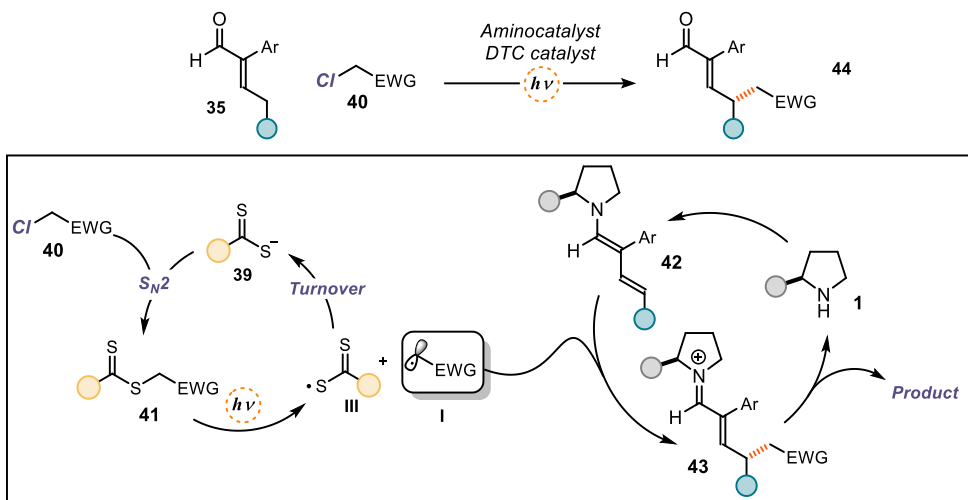


Figure 3.18. Design plan

As illustrated in Figure 3.17, the nucleophilic DTC catalyst **39** would undergo S_N2 reaction with simple alkyl chlorides to generate a photoactive intermediate **41**. Upon blue light irradiation, the intermediate **41** would undergo homolytic scission to deliver the target radical **I** and thyl radical **III**. Meanwhile, the presence of aminocatalyst **1** would guide the formation of dienamine **42** from an α -branched enal. In line with our previous investigation,⁵³ this catalytic intermediate should trap the electron-poor radicals generated by photolysis of **41** at the remote γ -carbon. Thanks to the radical nature of the process and the chiral environment provided by the aminocatalyst, we hypothesized that the C-C bond formation could proceed in a regio- and enantioselective fashion, generating the γ -alkylated iminium ion **43** from which product **44** is released upon hydrolysis.

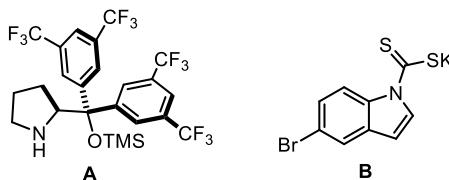
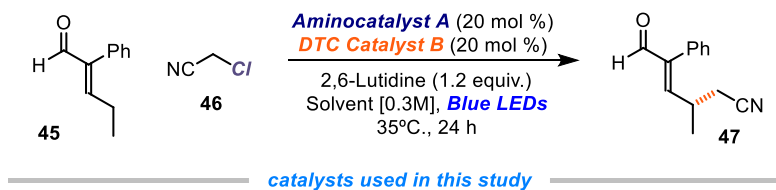
3.6 Results and discussion

3.6.1 Reaction optimization

We evaluated the feasibility of the blueprint described in Section 3.5.1 by reacting 2-phenyl-pentenal **45** with chloroacetonitrile **46** in the presence of 20 mol% of aminocatalyst **A**, 20 mol% of 5-bromoindole DTC catalyst **B**, 2,6-lutidine as a base and toluene as solvent (Table 1). We were pleased to find that after 24 hours under blue LED irradiation ($\lambda_{\text{max}} = 465 \text{ nm}$), the desired product **47** was formed in 40% yield and 77:23 enantiomeric ratio (e.r., entry 1).

Pleasingly, the reaction proceeded with total γ -regioselectivity, with no trace of α -alkylation product detected in the crude mixture. Preliminary screening of reaction media underlined that highly polar solvents, such as MeCN and DMF, were not suitable (entries 3 & 4), while optimal reactivity was found when ethereal solvents, such as THF and CPME, were employed (entries 5 & 6). The enantioselectivity was largely independent of solvent choice. The presence of a catalytic amount of benzoic acid, which is generally used to accelerate amine-aldehyde condensation,¹⁴⁶ was detrimental in this case (entry 7). Control experiments showed that the presence of both catalysts and the light were essential for reactivity (entries 8, 9, 10).

Table 3.1. Proof of concept and solvent optimization



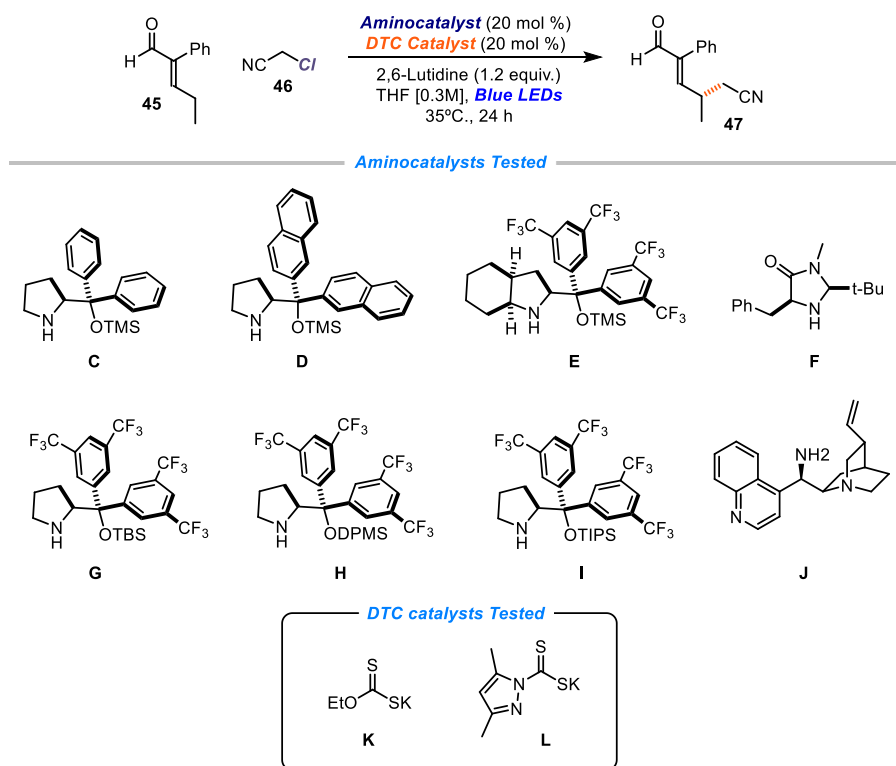
entry	solvent	yield 47 (%) ^a	e.r. 47 (%) ^b
1	Tol	40	77:23
2	MeCN	18	79:21
3	DMF	traces	/
4	THF	70	77:23
5	CPME	69	77:23
6	CHCl ₃	66	78:22
7 ^c	Tol	13	77:23
8 ^d	THF	0	/
9 ^e	THF	0	/
10 ^f	THF	0	/

- a) Reaction performed on a 0.2 mmol scale using 3 equiv. of **45**. Yields of **47** determined by ¹H NMR analysis of the crude mixture using trichloroethylene as the internal standard. b) Enantiomeric ratio (e.r.) of **47** determined by UPC² analysis. c) Reaction performed in the presence of 0.3 equiv. of benzoic acid. d) Performed in the absence of light. e) Performed in the absence of catalyst **A**. f) Performed in the absence of catalyst **B**.

¹⁴⁶ Hong, L.; Sun, W.; Yang, D.; Li, G.; Wang, R. Additive effects on Asymmetric Catalysis. *Chem. Rev.* **2016**, *116*, 4006-4123.

We next sought to explore the effect of the aminocatalyst's structure on yield and enantioselectivity (Table 3.2). When employing the less sterically demanding catalyst **C**, product **47** was obtained with the same yield but with a lower enantiomeric ratio (entry 1). Replacing the phenyl groups with bulkier naphthyl groups in the catalyst resulted in increased e.r. but at the expense of reactivity (entry 2). Bicyclic catalyst **E** didn't afford any product (entry 3), probably due to an increased steric clash with the branched enal, hampering enamine formation. In line with this observation, MacMillan-type catalyst **F** was also unable to promote the reaction (entry 4). Realizing that the trifluoromethylated phenyl prolinol scaffold is essential for satisfactory reactivity, we investigated the effect of the silylether protecting group embedded within catalyst **A**.

Table 3.2. Catalyst screening



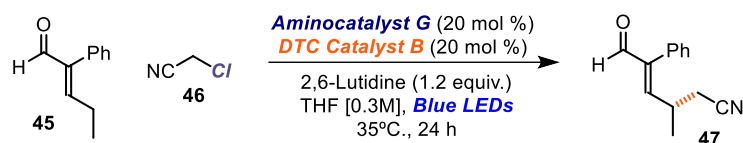
entry	aminocatalyst	DTC Catalyst	yield 47 (%) ^a	e.r. 47 (%) ^b
1	C	B	70	70:30
2	D	B	37	75:25
3	E	B	/	/
4	F	B	/	/
5	G	B	56	80:20
6	H	B	60	70:30
7	I	B	22	78:22
8	J	B	/	/
9	G	K	traces	/
10	G	L	traces	/

a) Reaction performed on a 0.2 mmol scale using 3 equiv. of **45**. Yields of **47** determined by ¹H NMR analysis of the crude mixture using trichloroethylene as the internal standard. b) Enantiomeric ratio of **47** determined by UPC².

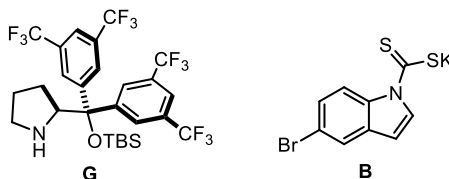
Between different silylated catalysts (**A**, **G–I**), we identified the tert-butyl silyl protected catalyst **G** as the one giving the best results (entry 5), while other derivatives gave either lower enantioselectivity (entry 6) or lower yields (entry 7). The employment of the cinchona-derivative primary amine catalyst **J**, which was previously shown to be a suitable catalyst to generate enamines,¹⁴⁷ did not afford any product (entry 8).

Finally, a screening of DTC catalyst was also performed to ensure an efficient radical generation process. When the commercially available ethyl xanthogenate catalyst **K** was employed, almost no reaction occurred within 24 hours (entry 9), probably due to the low absorption of the intermediate in the 460 nm region. Similarly, pyrazole based DTC catalyst **L** did not afford any desired product (entry 10).

¹⁴⁷ Melchiorre, P. Cinchona-based Primary Amine Catalysis in the Asymmetric Functionalization of Carbonyl Compounds *Angew. Chem. Int. Ed.* **2012**, *51*, 9748-9770.

Table 3.3. Screening of other reaction parameters


catalysts used in this study



entry	Deviation	yield 47 (%) ^a	e.r. 47 (%) ^b
1	10% of G	22	80:20
2	40% of G	59	80:20
3	30% of B	67	80:20
4	T = 10° C	traces	/
5	T = 60° C	58	50:50
6	60 h rxn	62	68:32
7	THF [0.7M]	75 (70)	80:20
8	4 equiv ald	71 (65)	80:20

a) Reaction performed on a 0.2 mmol scale using 3 equiv of **45**. Yields of **47** determined by ¹H NMR analysis of the crude mixture using trichloroethylene as the internal standard. b) enantiomeric ratio of **47** determined by direct injection in UPC². Numbers in parenthesis refers to the yields of product isolated after flash chromatography.

Once the best catalysts were identified, we performed a third round of optimization to evaluate the effect of standard reaction parameters. First, we investigated the possibility of using lower amounts of catalyst. While 10 mol% of aminocatalyst **G** offered in low conversion, increasing the amount to 40 mol% was not beneficial compared to 20 mol% (entries 1 & 2). However, increasing the loading of DTC catalyst **B** to 30 mol% led to an increased yield (67%, entry 3). We then evaluated the effect of the temperature. Cooling from ambient temperature to 10 °C had a detrimental effect on the yield of the product, probably due to inhibition of the S_N2 process required for effective radical generation (entry 4). When the temperature was increased to 60 °C, the reactivity was restored but enantioselectivity was totally lost, with the product formed as a racemate (entry 5). Variation of the reaction time revealed that partial racemization of the product occurred during the reaction, with a decrease from 80:20 to 68:32 e.r. observed after 60 hours (entry 6). We therefore set to keep the reaction time at 24 hours, so to preserve the stereo-integrity of the product. Modulation of the concentration to 0.7 M was found to elevate the yield to 75% (entry 7). Further screening of the components' stoichiometry, such as base or enal, did not provide any improvement.

3.6.2 Reaction scope & product functionalization

With optimized conditions in hand (Table 3.3, entry 7), we next evaluated the generality of the reaction by testing structural and electronic variations of the alkyl chloride radical precursor (Figure 3.19). We were pleased to find that the reaction could be applied to a broad range of primary alkyl chlorides. A variety of phenacyl chlorides participated smoothly to the reaction with moderate to good yields and enantiomeric ratios. Interestingly, thanks to the S_N2 manifold through which the DTC catalyst operates, phenacyl triflates could be activated toward the generation of the corresponding radical (**47a**). Both electron-donating (products **47b**, **47c**) and electron-withdrawing groups (**47i**, **47j**, **47k**) on the aryl moiety of the phenacyl scaffold were well-tolerated. Also, phenacyl chlorides bearing halogen atoms at the *ortho*-, *meta*-, and *para*- positions of the phenyl ring could be used with no dramatic erosion in yield (**47e**, **47f**, **47g**). Phenacyl groups bearing an aryl C-F bond, which is a useful bioisostere for aryl C-H bonds because of the imparted reduced metabolic consumption, could be effectively installed with our protocol maintaining good levels of enantioselectivity and reactivity (**47d**, **47h**). Aliphatic chlorinated ketones (and α -bromo-butylolactone were suitable radical precursors, generating the products with good enantioselectivity, albeit with diminished reactivity (products **47q** and **47o**, respectively). We also shown that benzyl chlorides are suitable radical precursors but strongly deactivating groups are needed for the reactivity (**47m**, **47n**). Finally, we also demonstrated that this strategy is suitable for the direct functionalization of a biorelevant compound, installing the *celestolide* scaffold within product **47r**.

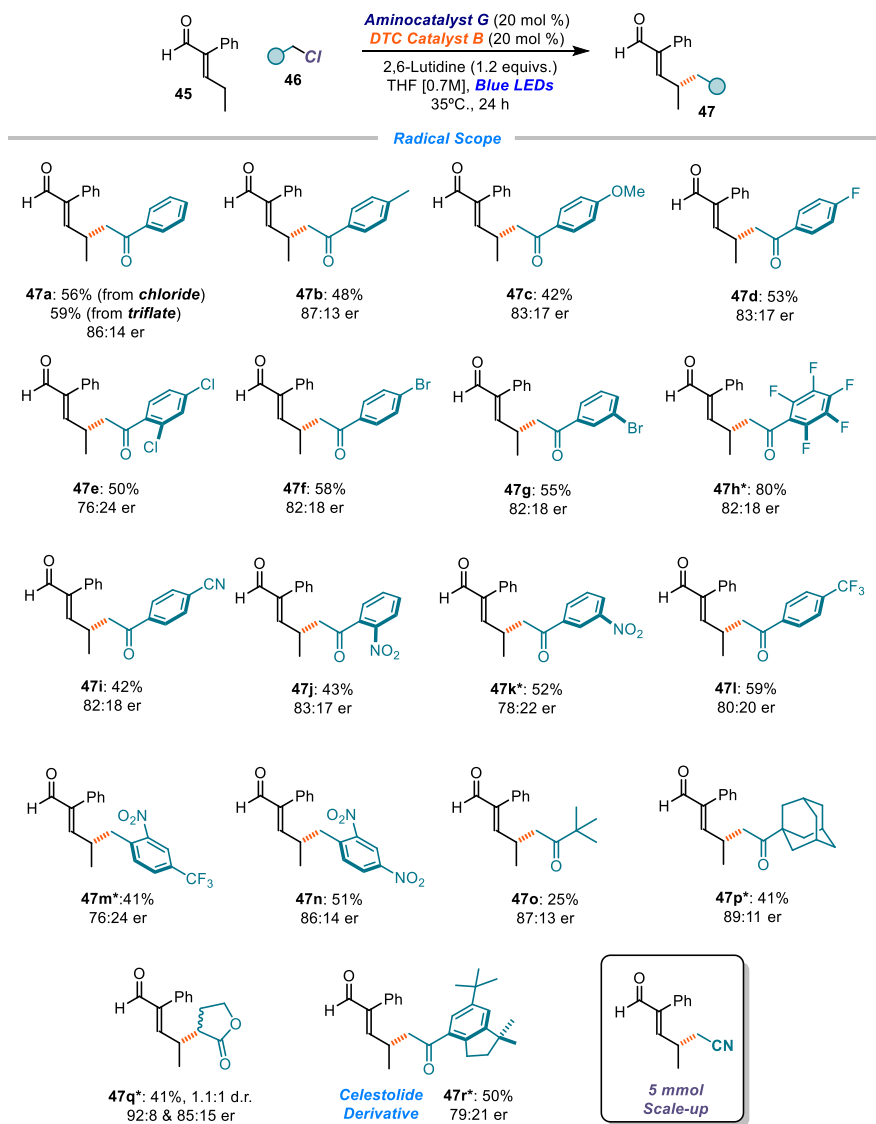


Figure 3.19. Survey of radical precursors that can participate in the γ -alkylation of enal. *Using the corresponding bromide as radical precursors

The usefulness of this synthetic protocol was also showcased by scaling-up the model reaction, using 5 mmol of **46** by using a simple round-bottom flask setup. The reaction smoothly generated the product in 67% yield and 80:20 e.r., in line with the standard protocol showing that the reactivity is maintained at larger scales.

Next, we evaluated whether variations of the enal substrate could be tolerated (Figure 3.20). Substituents of different electronic nature and in different positions of the α -aryl ring were

tolerated well, although they offered somewhat reduced reactivity (products **48a–e**). As for the substituents at the enal β position, branched and linear aliphatic chains could be included in the final products (**48f** and **48g**, respectively). As already highlighted in section 3.3.2, the substituent in α -position acts as a crucial stereocontrol element for achieving the desired enantioselectivities, enforcing a preferred conformation of the chiral dienamine intermediate. To showcase this concept, we performed an experiment using linear pentenal as substrate. The corresponding product **48h** was obtained with no control over the formed stereocenter but with excellent regioselectivity for the γ -position. The ability to control the site selectivity was further corroborated by subjecting hepta-2,4-dienal to our reaction conditions. This substrate may potentially react at the α - and γ -positions by forming a trienamine intermediate¹⁴⁸ but was exclusively alkylated at the more remote ϵ -carbon, albeit with no stereocontrol (product **48i**). We assessed also the reactivity of *citral*, which reacted with total γ -site selectivity, leading to the preferential formation of the more substituted regioisomer (**48j**).

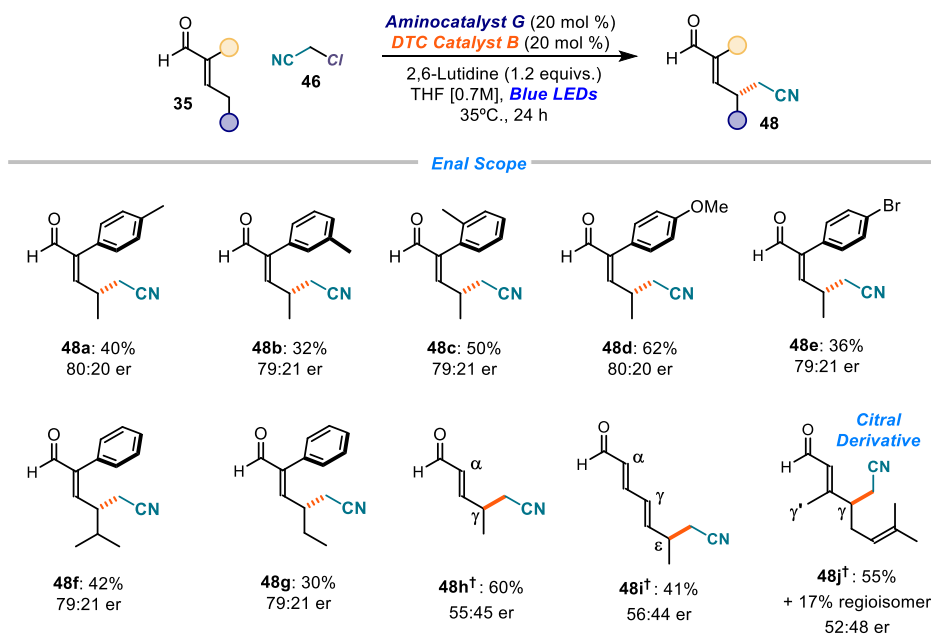


Figure 3.20. Scope of enals. * Product isolated as 1:1 atropisomeric ratio. † Using catalyst F

¹⁴⁸ Jia, Z.-J.; Jiang, H.; Li, J.-L.; Gschwend, B.; Li, Q.-Z.; Yin, X.; Grouleff, J.; Chen, Y.-C.; Jørgensen, K. A. Trienamines in Asymmetric Organocatalysis: Diels–Alder and Tandem Reactions. *J. Am. Chem. Soc.* **2011**, *133*, 5053–5061.

One synthetic benefit of this protocol lies in the possibility to directly install a stereocenter at the remote γ -carbon leaving α,β -unsaturated system amenable to further transformations (Figure 3.21). Simple reduction of the aldehyde with sodium borohydride afforded the allylic alcohol **49** (path *a*), which could then be employed as substrate for the Sharpless epoxidation¹⁴⁹ affording the chiral epoxy alcohol **50** (path *b*) featuring three contiguous stereocenters in good yield and enantiomeric ratio. Using the Eschenmoser-Claisen conditions, we could also convert **49** in the chiral dimethylamide **51** through a [3,3]-sigmatropic rearrangement (path *c*).¹⁵⁰ The coupling of **49** with ferrocenyl carboxylic acid smoothly produced the chiral ferrocenyl ester **52** in good yield and with no loss of enantiomeric purity (path *d*). Finally, the carbonyl moiety in **47** was subjected to a Wittig olefination, which afforded the ε -enantioenriched unsaturated ester **53** (path *e*).

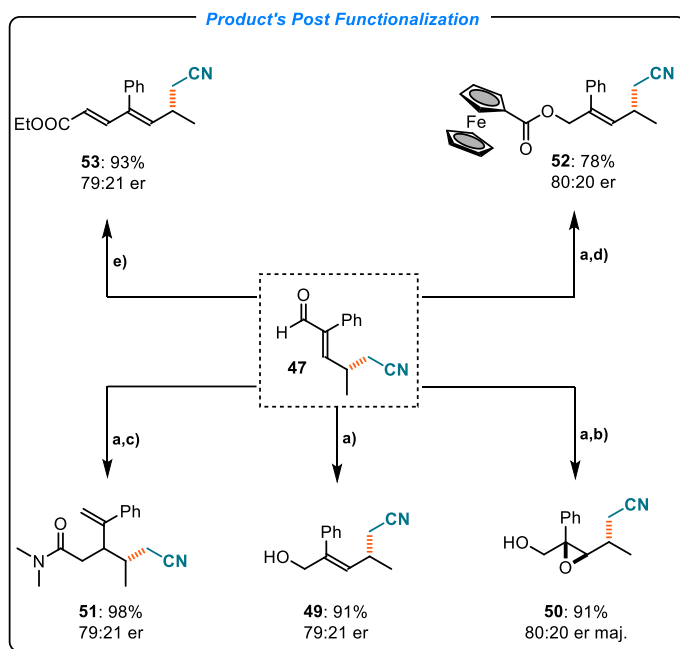


Figure 3.21. Derivatization of product **47**. Conditions: (a) NaBH₄, MeOH, 1h, 0° C; (b) (-)-diethyl-*D*-tartrate (23 mol %), Ti(OiPr)₄ (20 mol %), t-BuOOH, DCM, 20° C; (c) N,N-dimethylacetamide dimethyl acetal, xylene, 110° C; (d) ferrocenyl carboxylic acid, oxalyl chloride, DMF; (e) (carbethoxymethyl)triphenylphosphonium bromide, DCE

¹⁴⁹ Katsuki, T.; Sharpless, K. B. The first practical method for asymmetric epoxidation. *J. Am. Chem. Soc.* **1980**, *102*, 5974-5976.

¹⁵⁰ Wick, A. E.; Felix, D.; Steen, K.; Eschenmoser, A. CLAISEN'sche Umlagerungen bei Allyl- und Benzylalkoholen mit Hilfe von Acetalen des N, N-Dimethylacetamids. Vorläufige Mitteilung. *Helv. Chem. Acta*, **1964**, *47*, 2425-2429.

3.6.3 Mechanistic Proposal

Based on the previous literature reports on aminocatalysis and the knowledge collected by our group on dithiocarbamate-mediated catalysis, we propose that the transformation works through a cooperative dual catalysis, as detailed in Figure 3.22.

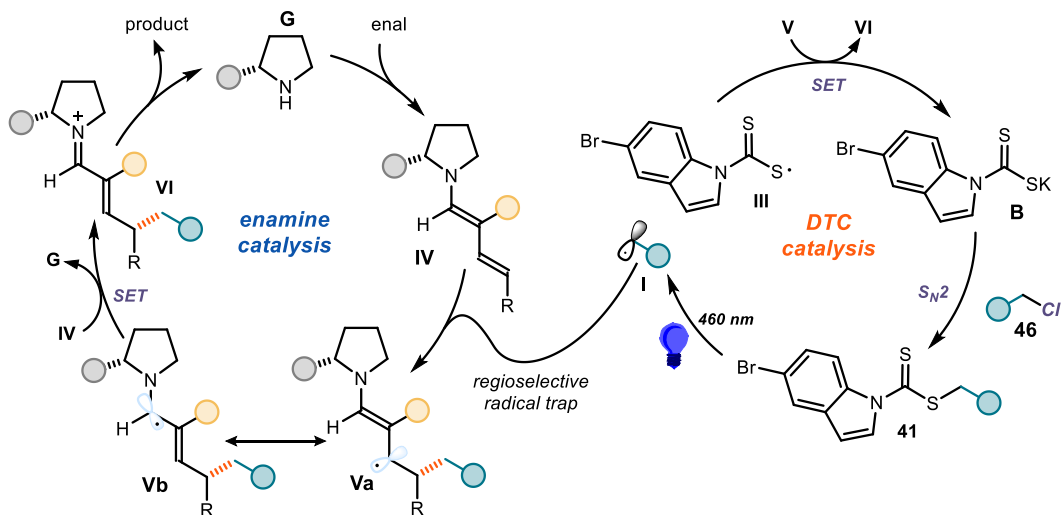


Figure 3.22. Mechanistic proposal

By harnessing the nucleophilic properties of the 5-bromoindole catalyst **B**, it is possible to generate the photoactive intermediate **41** by an S_N2 mechanism with alkyl chlorides **46**. Under blue LED irradiation, the catalytic intermediate **41** releases the target radical **I** and the thyl radical **III** via homolytic cleavage. At the same time, the aminocatalyst **G** triggers the formation of the dienamine **IV** by condensation with the enal substrate. This intermediate is capable of trapping electrophilic radicals with high regioselectivity for the γ -position, delivering the more stable 5π intermediate **Va**. The latter can be described as an α -amino radical **Vb** resonance form, which is readily prone to oxidation. Our first mechanistic hypothesis envisioned that a SET between this intermediate and the thyl radical **III** could provide a turnover event for both catalysts, generating the iminium ion **VI** (from which the product is released) and the DTC catalyst **B**.

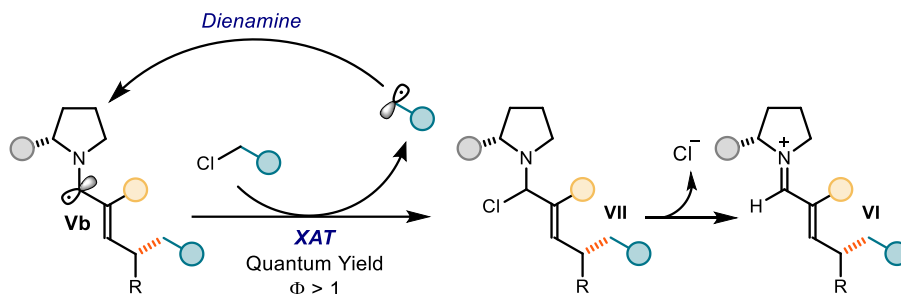


Figure 3.23. Alternative XAT mechanism turnover event

Whereas the redox potentials of the two intermediates show that this process is indeed exoergonic¹⁵¹, we considered a possible alternative turnover mechanism proceeding by a halogen atom transfer (XAT) path, depicted in Figure 3.22. This process is known to take place from α -amino radicals¹⁵² and, while alkyl chlorides are recalcitrant to undergo XAT, this remained another mechanistic possibility. Under this regime, more than one molecule of product would be formed per photon absorbed, since **Vb** can initiate a radical chain mechanism in which photons are not required for product formation. (Figure 3.23).¹⁵³ To exclude this pathway, we measured the quantum yield (ϕ) of the reaction to relate the number of photons arriving to the reaction vessel and the moles of product generated.¹⁵⁴ The quantum yield of the model reaction was measured to be as low as 0.002, therefore suggesting that a radical chain propagation, if present, is not a dominant path.

¹⁵¹ The parent ethyl xanthogenate anion, where the indole moiety in **B** is replaced by OEt, has an oxidation potential as low as +0.04 V vs. SCE, see: Dag, O.; Yaman, S. O.; Onal, A. M.; Isci, H. Spectroelectrochemistry of potassium ethylxanthate, bis(ethylxanthato)nickel(II) and tetraethylammonium tris(ethylxanthato)nickelate(II). *J. Chem. Soc., Dalton Trans.*, **2001**, 2819-2824. For the redox potentials of α -amino radicals see: Wayner, D. D. M.; Dannenberg, J. J.; Griller, D. Oxidation potentials of α -aminoalkyl radicals: bond dissociation energies for related radical cations *Chem. Phys. Lett.*, **1986**, *131*, 189-191.

¹⁵² (a) Constantin, T.; Zanini, M.; Regni, A.; Sheikh, N. E.; Julià, F.; Leonori, D. Aminoalkyl radicals as halogen-atom transfer agents for activation of alkyl and aryl halides *Science*, **2020**, *367*, 6481, 1021-1026. (b) Zhang, Z.; Görki, B.; Leonori, D.; Merging Halogen-Atom Transfer (XAT) and Copper Catalysis for the Modular Suzuki–Miyaura-Type Cross-Coupling of Alkyl Iodides and Organoborons. *J. Am. Chem. Soc.* **2022**, *144*, 1986-1992. (c) Zhao, H.; McMillan, A. J.; Constantin, T.; Mykura, R. C.; Julià, F.; Leonori, D. Merging Halogen-Atom Transfer (XAT) and Cobalt Catalysis to Override E₂-Selectivity in the Elimination of Alkyl Halides: A Mild Route toward contra-Thermodynamic Olefins. *J. Am. Chem. Soc.* **2021**, *143*, 14806-14813. (d) Julià, F.; Constantin, T.; Leonori, D.; Applications of Halogen-Atom Transfer (XAT) for the Generation of Carbon Radicals in Synthetic Photochemistry and Photocatalysis. *Chem. Rev.* **2022**, *122*, 2292-2352.

¹⁵³ Cismesia, M. A.; Yoon, T. P. Characterizing chain processes in visible light photoredox catalysis. *Chem. Sci.* **2015**, *6*, 5426-5434.

¹⁵⁴ Murov, S. L. Ed. *Handbook of Photochemistry* (Marcel Dekker, New York, 1973)

3.7 Conclusions

In summary, we have developed a dual organocatalytic platform for the regio- and enantioselective remote functionalization of enals by the merging of dienamine catalysis and DTC catalysis. While the former provides a tool for the activation of the γ -position of enals, the latter ensures the efficient generation of primary and secondary radicals. The protocol requires cheap and bench stable radical precursors and leads to the asymmetric γ -alkylation products with excellent regioselectivity and moderate to good enantioselectivity. Overall, the transformation provides a rare example of radical enantioselective γ -functionalization of branched enals. The synthetic usefulness of the process was underlined by a scale-up reaction and a variety of product manipulations.

3.8 Experimental section

3.8.1 General information

The NMR spectra and UPC2 traces of enantioenriched product can be found in the supporting information published on-line. The NMR spectra were recorded at 400 MHz and 500 MHz for ^1H and 100 or 125 MHz for ^{13}C . The chemical shift (δ) for ^1H and ^{13}C are given in ppm relative to residual signals of the solvents (CHCl_3 @ 7.26 ppm ^1H NMR and 77.16 ppm ^{13}C NMR, and tetramethylsilane @ 0 ppm). Coupling constants are given in Hertz. The following abbreviations are used to indicate the multiplicity: s, singlet; d, doublet; q, quartet; m, multiplet; bs, broad signal; app, apparent.

High resolution mass spectra (HRMS) were obtained from the ICIQ HRMS unit on MicroTOF Focus and Maxis Impact (Bruker Daltonics) with electrospray ionization. (ESI).

Yields refer to isolated materials of >95% purity as determined by ^1H NMR.

The authors are indebted to the team of the Research Support Area at ICIQ, particularly to the NMR and the High-Resolution Mass Spectrometry Units.

General Procedures. All reactions were set up under an argon atmosphere in oven-dried glassware. Synthesis grade solvents were used as purchased, anhydrous solvents were taken from a commercial SPS solvent dispenser. Chromatographic purification of products was accomplished using forced-flow chromatography (FC) on silica gel (35-70 mesh). For thin layer chromatography (TLC) analysis throughout this work, Merck pre-coated TLC plates (silica gel 60 GF₂₅₄, 0.25 mm) were employed, using UV light as the visualizing agent and an acidic mixture of vanillin or basic aqueous potassium permanganate (KMnO_4) stain solutions, and heat as developing agents. Organic solutions were concentrated under reduced pressure on a Büchi rotatory evaporator.

Determination of Enantiomeric Purity. UPC² analysis on chiral stationary phase was performed on a Waters Acquity instrument using ID3, IG, IA3, IC, IB and OJ chiral columns. The exact conditions for the analyses are specified within the characterization section.

Materials. The starting materials used in this study are commercial and were purchased in the highest purity available from Sigma-Aldrich, Fluka, Alfa Aesar, Fluorochem, and used as received, without further purifications. Phenacyl chlorides that are not commercially available were synthesized using known literature procedures¹⁵⁵ and their characterization matched with the literature reported data. The synthesis of Aldehydes substrates and the Celastrolide Bromide is described in the section **B**.

Experimental Setup

Our 3D printed photoreactor consisted of a 9 cm diameter crystallizing dish with a 3D printed support of 6 positions, and a hole of 22 mm in the middle to allow ventilation. A commercial 1-meter LED strip was wrapped around the crystallizing dish. In order to control the temperature, a fan was used to cool down the reactor. Reaction temperature was measured, through a vial containing a thermometer, and it stayed between 35-40 °C (Figure S1). Each of the positions could be used to fit a standard 16 mm diameter vial with a Teflon screw cap.

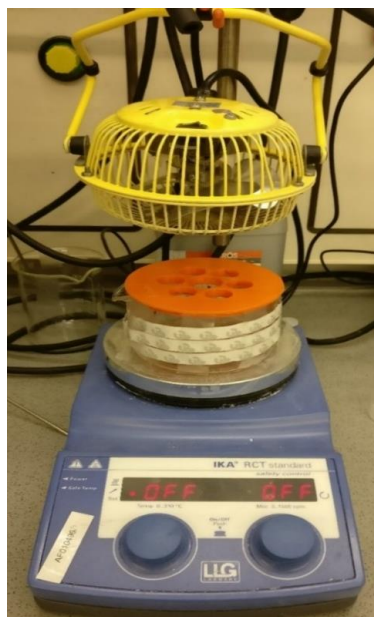


Figure 3.24 Photoreactor used for the catalytic reactions.

¹⁵⁵ (a) Zhu, Y.; Cai, Q.; Gao, Q.; Jia, F.; Liu, M.; Gao, M.; Wu, A. *Tetrahedron*, **2013**, *69*, 6392-6398. (b) Lee, J. C.; Bae, Y. H.; Chang, S.-K. *Bull. Korean. Chem. Soc.* **2003**, *24*, 407

Experiments at 465 nm were conducted using a 1m strip, 14.4W “LEDXON MODULAR 9009083 LED, SINGLE 5050” purchased from Farnell, catalog number 9009083. The emission spectrum of these LEDs was recorded (Figure S2). The emission maximum was determined as 465 nm with a spectral width of 30 nm (450-480 nm) at half peak intensity and a total spectral width of 120 nm (420-540 nm).

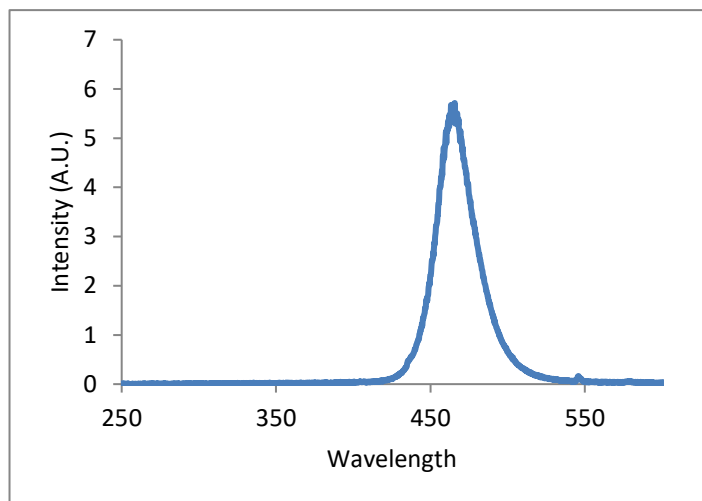


Figure 3.25: Emission spectrum of the 465 nm LED strip used in this study.

3.8.2. Substrate Synthesis

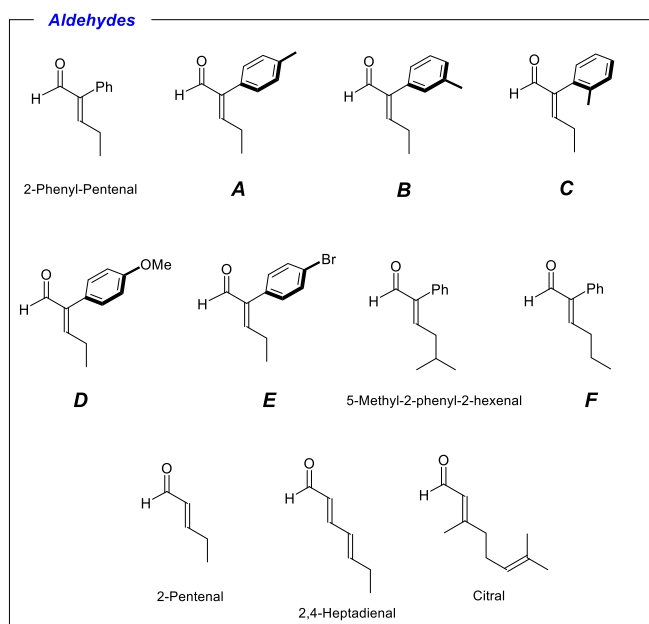
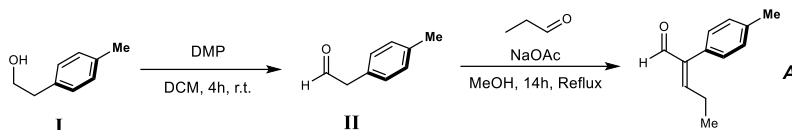


Figure 3.26: Aldehydes used for the reactions.

2-Phenyl-2-Pentenal, 2-Pentenal, 2,4-Heptadienal, 5-Methyl-2-phenyl-2-hexenal and Citral were commercially available and were used without further purifications. Aldehydes **A**, **B**, **C**, **D**, **E** and **G** and were synthesized through a two-step procedure using known and slightly modified protocols.¹⁵⁶

Synthesis of (*E*)-2-(*p*-tolyl)pent-2-enal (**A**):



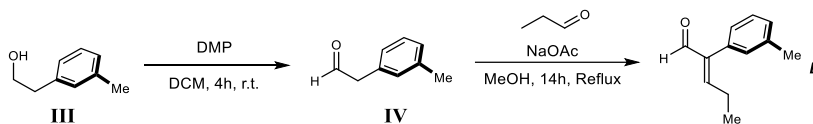
To a stirred solution of alcohol **I** (1.36 g, 10.0 mmol) in CH_2Cl_2 dry (60 mL), 6.4 g of Dess-Martin Periodinane (15 mmol) were added under argon. After 3h the reaction was quenched with saturated aqueous solutions of NaHCO_3 and $\text{Na}_2\text{S}_2\text{O}_3$ (20 mL). After 30 min, the resulting mixture was extracted with CH_2Cl_2 (2 x 25 mL). The combined organic layers were washed with brine (10 mL), dried over MgSO_4 , filtered, evaporated under reduced pressure, and purified by column chromatography (eluent: hexane/EtOAc 10:1) to give 631 mg of the corresponding aldehyde **II** (4.7 mmol, 47% yield) as a colorless oil.

To a stirred solution of **II** (631 mg, 4.7 mmol) in MeOH (9.5 mL), 1.01 mL of propionaldehyde (14.1 mmol) and 385 mg of NaOAc (4.7 mmol) were sequentially added. The resulting mixture was heated to reflux for 14h. Subsequently, the solvent was evaporated under vacuum and the resulting material was extracted with Et_2O (3 x 20 mL). The combined organic layers were washed with brine (10 mL), dried over MgSO_4 , filtered, evaporated under reduced pressure. The excess of propionaldehyde was removed by column chromatography (eluent: hexane/EtOAc 99:1) and then the residue (mixture of desired product and self-condensed by-product) purified by Kugelrohr distillation (2.1×10^{-1} bar, 90 °C) to afford 296 mg the corresponding enal **A** (1.7 mmol, 36% yield) as a colorless oil.

¹H NMR (500 MHz, CDCl_3) δ 9.63 (s, 1H), 7.24 (d, $J = 7.9$ Hz, 2H), 7.09 (d, $J = 8.1$ Hz, 2H), 6.71 (t, $J = 7.5$ Hz, 1H), 2.49 – 2.33 (m, 5H), 1.14 (t, $J = 7.5$ Hz 3H).

¹³C NMR (126 MHz, CDCl_3) δ 194.1, 157.7, 143.3, 137.7, 129.6, 129.3 (2C), 129.0 V, 23.3, 21.3, 13.3.

Synthesis of (*E*)-2-(*m*-tolyl)pent-2-enal (**B**):



¹⁵⁶ (a) Kolonko, K. J.; Reich, H. J. *J. Am. Chem. Soc.* **2008**, *130*, 9668-9669. (b) Schreiber, W. L.; Pittet, A. O., Vock, M.H. *J. Agric. Food Chem.* **1974**, *22*, 269-273.

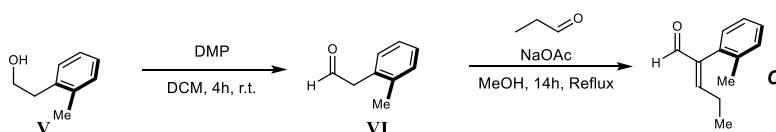
To a stirred solution of alcohol **III** (1.36 g, 10.0 mmol) in CH₂Cl₂ dry (60 mL), 6.4 g of Dess-Martin Periodinane (15 mmol) were added under argon. After 3h the reaction was quenched with saturated aqueous solutions of NaHCO₃ and Na₂S₂O₃ (20 mL). After 30 min, the resulting mixture was extracted with CH₂Cl₂ (2 x 25 mL). The combined organic layers were washed with brine (10 mL), dried over MgSO₄, filtered, evaporated under reduced pressure, and purified by column chromatography (eluent: hexane/EtOAc 10:1) to give 872 mg of the corresponding aldehyde **IV** (6.5 mmol, 65% yield) as a colorless oil.

To a stirred solution of **IV** (872 mg, 6.5 mmol) in MeOH (13 mL), 1.39 mL of propionaldehyde (19.5 mmol) and 540 mg of NaOAc (6.5 mmol) were sequentially added. The resulting mixture was heated to reflux for 14h. Subsequently, the solvent was evaporated under vacuum and the resulting material was extracted with Et₂O (3 x 20 mL). The combined organic layers were washed with brine (10 mL), dried over MgSO₄, filtered, evaporated under reduced pressure. The excess of propionaldehyde was removed by column chromatography (eluent: hexane/EtOAc 99:1) and then the residue (mixture of desired product and self-condensed by-product) purified by Kugelrohr distillation (2.1×10⁻¹ bar, 90 °C) to afford 362 mg the corresponding enal **B** (2.1 mmol, 32% yield) as a colorless oil.

¹H NMR (500 MHz, CDCl₃) δ 9.63 (s, 1H), 7.31 (t, *J* = 7.6 Hz, 1H), 7.21 – 7.15 (m, 1H), 7.03 – 6.94 (m, 2H), 6.71 (t, *J* = 7.5 Hz, 1H), 2.47 – 2.33 (m, 5H), 1.13 (t, *J* = 7.5 Hz, 3H).

¹³C NMR (126 MHz, CDCl₃) δ 193.9, 157.7, 143.6, 137.8, 132.5, 130.0, 128.7, 128.1, 126.4, 23.2, 21.5, 13.3.

Synthesis of (*E*)-2-(*o*-tolyl)pent-2-enal (**C**):



To a stirred solution of alcohol **V** (1.36 g, 10.0 mmol) in CH₂Cl₂ dry (60 mL), 6.4 g of Dess-Martin Periodinane (15 mmol) were added under argon. After 3h the reaction was quenched with saturated aqueous solutions of NaHCO₃ and Na₂S₂O₃ (20 mL). After 30 min, the resulting mixture was extracted with CH₂Cl₂ (2 x 25 mL). The combined organic layers were washed with brine (10 mL), dried over MgSO₄, filtered, evaporated under reduced pressure, and purified by column chromatography (eluent: hexane/EtOAc 10:1) to give 791 mg of the corresponding aldehyde **VI** (5.9 mmol, 59% yield) as a colorless oil.

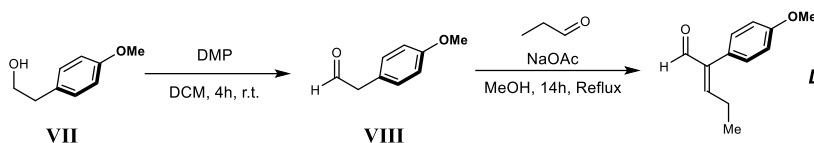
To a stirred solution of **VI** (591 mg, 5.9 mmol) in MeOH (12 mL), 1.26 mL of propionaldehyde (17.7 mmol) and 484 mg of NaOAc (5.9 mmol) were sequentially added. The resulting mixture was heated to reflux for 14h. Subsequently, the solvent was evaporated under vacuum and the resulting material was extracted with Et₂O (3 x 20 mL). The combined

organic layers were washed with brine (10 mL), dried over MgSO_4 , filtered, evaporated under reduced pressure, and purified by column chromatography (eluent: pentane/ Et_2O 9:1) to afford 452 mg the corresponding enal **C** (2.6 mmol, 44% yield) as a colorless oil.

$^1\text{H NMR}$ (300 MHz, CDCl_3) δ 9.64 (d, $J = 0.6$ Hz, 1H), 7.27 – 7.25 (m, 1H), 7.25 – 7.16 (m, 2H), 6.96 (d, $J = 7.1$ Hz, 1H), 6.84 (t, $J = 7.5$ Hz, 1H), 2.24 – 2.14 (m, 2H), 2.12 (s, 3H), 1.09 (t, $J = 7.5$ Hz, 3H).

$^{13}\text{C NMR}$ (126 MHz, CDCl_3) δ 194.10, 157.65, 143.33, 137.71, 129.30, 128.96, 23.25, 21.28, 13.31.

Synthesis of (*E*)-2-(4-methoxyphenyl)pent-2-enal (**D**):



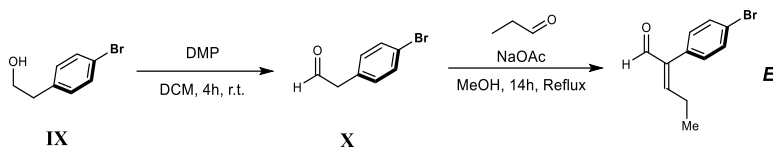
To a stirred solution of alcohol **VII** (1.5 g, 10.0 mmol) in CH_2Cl_2 dry (60 mL), 6.4 g of Dess-Martin Periodinane (15 mmol) were added under argon. After 3h the reaction was quenched with saturated aqueous solutions of NaHCO_3 and $\text{Na}_2\text{S}_2\text{O}_3$ (20 mL). After 30 min, the resulting mixture was extracted with CH_2Cl_2 (2 x 25 mL). The combined organic layers were washed with brine (10 mL), dried over MgSO_4 , filtered, evaporated under reduced pressure, and purified by column chromatography (eluent: hexane/ EtOAc 4:1) to give 795 mg of the corresponding aldehyde **VIII** (5.3 mmol, 53% yield) as a colorless oil.

To a stirred solution of **VIII** (795 mg, 5.3 mmol) in MeOH (10 mL), 1.13 mL of propionaldehyde (15.9 mmol) and 434 mg of NaOAc (5.3 mmol) were sequentially added. The resulting mixture was heated to reflux for 14h. Subsequently, the solvent was evaporated under vacuum and the resulting material was extracted with Et_2O (3 x 20 mL). The combined organic layers were washed with brine (10 mL), dried over MgSO_4 , filtered, evaporated under reduced pressure, and purified by column chromatography (eluent: hexane/ EtOAc 9:1) to afford 413 mg the corresponding enal **D** (2.2 mmol, 41% yield) as a pale-yellow oil.

$^1\text{H NMR}$ (500 MHz, CDCl_3) δ 9.62 (s, 1H), 7.13 (d, $J = 8.8$ Hz, 2H), 6.96 (d, $J = 8.9$ Hz, 2H), 6.68 (t, $J = 7.5$ Hz, 1H), 3.85 (s, 3H), 2.42 (p, $J = 7.5$ Hz, 2H), 1.14 (t, $J = 7.5$ Hz, 3H).

$^{13}\text{C NMR}$ (126 MHz, CDCl_3) δ 194.2, 159.3, 157.5, 142.9, 130.6 (2C), 124.7, 113.7 (2C), 55.3, 23.2.

Synthesis of (*E*)-2-(4-bromophenyl)pent-2-enal (**E**):



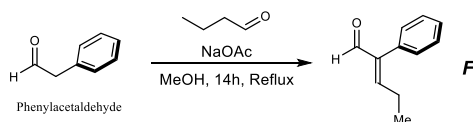
To a stirred solution of alcohol **IX** (2.0 g, 10.0 mmol) in CH_2Cl_2 dry (60 mL), 6.4 g of Dess-Martin Periodinane (15 mmol) were added under argon. After 3h the reaction was quenched with saturated aqueous solutions of NaHCO_3 and $\text{Na}_2\text{S}_2\text{O}_3$ (20 mL). After 30 min, the resulting mixture was extracted with CH_2Cl_2 (2 x 25 mL). The combined organic layers were washed with brine (10 mL), dried over MgSO_4 , filtered, evaporated under reduced pressure, and purified by column chromatography (eluent: hexane/EtOAc 3:1) to give 1.4 g the corresponding aldehyde **X** (7.1 mmol, 72% yield) as a pale-yellow oil.

To a stirred solution of **X** (1.4 g, 7.1 mmol) in MeOH (14 mL), 1.52 mL of propionaldehyde (21.3 mmol) and 582 mg of NaOAc (7.1 mmol) were sequentially added. The resulting mixture was heated to reflux for 14h. Subsequently, the solvent was evaporated under vacuum and the resulting material was extracted with Et_2O (3 x 20 mL). The combined organic layers were washed with brine (10 mL), dried over MgSO_4 , filtered, evaporated under reduced pressure, and purified by column chromatography (eluent: hexane/EtOAc 9:1) to afford 899 mg the corresponding enal **E** (3.7 mmol, 53% yield) as a colorless oil.

$^1\text{H NMR}$ (400 MHz, CDCl_3) 9.59 (s, 1H), 7.54 (d, $J = 8.6$ Hz, 2H), 7.05 (d, $J = 8.6$ Hz, 2H), 6.73 (t, $J = 7.6$ Hz, 1H), 2.37 (p, $J = 7.5$ Hz 2H), 1.12 (t, $J = 7.5$ Hz, 3H).

$^{13}\text{C NMR}$ (101 MHz, CDCl_3) δ 193.3, 158.2, 142.4, 131.5 (2C), 131.4, 131.1 (2C), 23.2, 13.2.

Synthesis of (*E*)-2-phenylhex-2-enal (**F**):

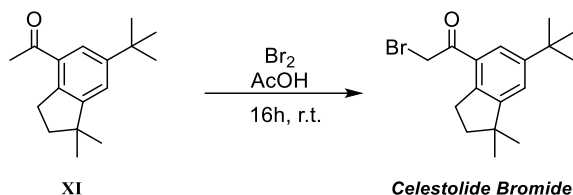


To a stirred solution of phenylacetaldehyde (1.0 g, 8.3 mmol) in MeOH (16 mL), 2.24 mL of butyraldehyde (24.9 mmol) and 680 mg of NaOAc (8.3 mmol) were sequentially added. The resulting mixture was heated to reflux for 14h. Subsequently, the solvent was evaporated under vacuum and the resulting material was extracted with Et_2O (3 x 20 mL). The combined organic layers were washed with brine (10 mL), dried over MgSO_4 , filtered, evaporated under reduced pressure, and purified by column chromatography (eluent: hexane/ Et_2O 97:3) to afford 709 mg the corresponding enal **F** (4.1 mmol, 49% yield) as a pale yellow oil.

$^1\text{H NMR}$ (400 MHz, CDCl_3) δ 9.64 (s, 1H), 7.45 – 7.34 (m, 3H), 7.20 – 7.16 (m, 2H), 6.75 (t, $J = 7.5$ Hz, 1H), 2.37 (q, $J = 7.5$ Hz, 2H), 1.56 (q, $J = 7.4$ Hz, 2H), 0.96 (t, $J = 7.4$ Hz, 3H).

^{13}C NMR (101 MHz, CDCl_3) δ 193.8, 156.4, 144.1, 132.7, 129.4 (2C), 128.2 (2C), 127.9, 31.7, 22.1, 13.8.

Synthesis of 2-bromo-1-(6-(tert-butyl)-1,1-dimethyl-2,3-dihydro-1H-inden-4-yl)ethan-1-one:



Ketone **XI** (1.95 g, 8.0 mmol) was dissolved in glacial AcOH (0.2M) and treated dropwise with Br_2 (0.411 mL, 17.7 mmol) in AcOH (1.3 M) at r.t. The mixture was stirred at r.t. for 16h and then the solvent was removed by rotary evaporation. The crude mixture was evaporated under reduced pressure, and purified by column chromatography (eluent: pentane/ Et_2O 8:2) to afford 1.50 g of the desired product (4.64 mmol, 58% yield) as a colorless oil.

^1H NMR (300 MHz, CDCl_3) δ 7.71 (s, 1H), 7.38 (s, 1H), 4.48 (s, 1H), 3.18 (td, $J = 7.3, 1.2$ Hz, 2H), 1.95 (td, $J = 7.3, 1.3$ Hz, 2H), 1.36 (s, 9H), 1.27 (s, 6H).

^{13}C NMR (101 MHz, CDCl_3) δ 192.88, 154.99, 150.24, 142.52, 130.41, 124.89, 124.40, 43.65, 41.47, 34.91, 33.13, 31.60, 30.93, 28.88.

3.8.3. Catalysts Synthesis

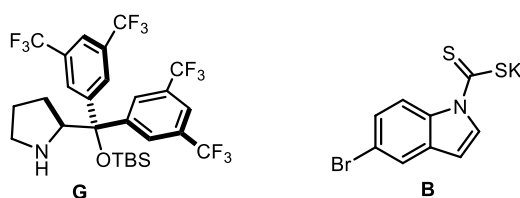


Figure 3.27: Catalysts used for the reactions.

Dithiocarbamate catalyst was synthesized from 5-bromoindole by a one-step synthesis previously reported by our group.¹⁵⁷

Aminocatalyst **G** was synthesized starting from L-Proline by a 5-step synthesis described below. All the product matched the spectroscopic characterization reported in literature.

¹⁵⁷ Schweitzer-Chapat, B.; Horwitz, M. A.; de Pedro Beato, E. and Melchiorre, P. *Nat. Chem.* **2019**, *11*, 129-135

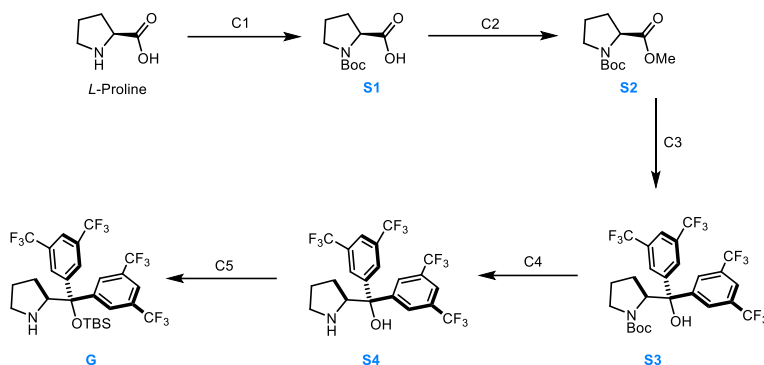
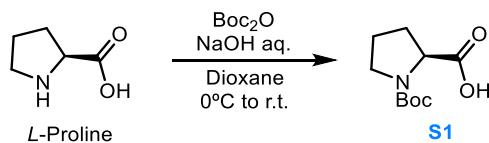


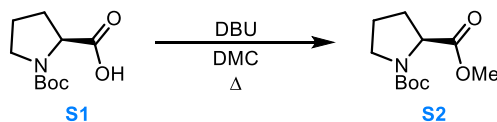
Figure 3.28: Synthesis route for the catalyst G.

Synthesis of (tert-butoxycarbonyl)-L-proline



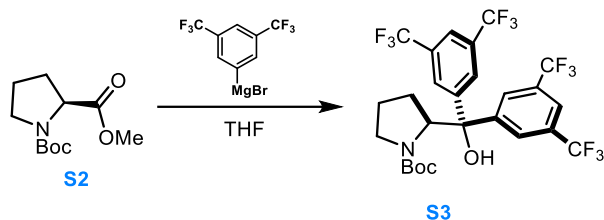
To a solution of (S)-proline (8.0 g, 69 mmol) in aq. NaOH (1M, 130 mL) and dioxane (33 mL) at 0 °C was added Boc₂O (18 g, 82 mmol) portionwise over 20 min. The resulting mixture was stirred at 0 °C for 30 min, then allowed to warm to 23 °C and stirred overnight. The organic solvent was removed under reduced pressure. The remaining aqueous solution was acidified to pH ~2 with aq. KHSO₄ (1 M). The aqueous solution was extracted with CHCl₃ (3 x 150 mL). The combined organic layers were washed with brine (200 mL), dried over Na₂SO₄, and concentrated by rotary evaporation to afford the target carbamate **S1** (14.2 g, 95% yield) as a white solid, which was sufficiently pure to be taken on to the next step.

Synthesis of 1-(tert-butyl) 2-methyl (S)-pyrrolidine-1,2-dicarboxylate



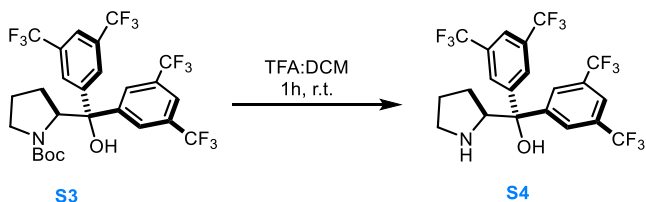
DBU (9.9 g, 9.8 mL equiv) was added to a solution of N-Boc Proline **S1** (14 g, 65 mmol) in DMC (250 mL 0.25M), and the resulting mixture was heated to reflux. Upon completion, the reaction mixture was cooled to room temperature and diluted with either EtOAc and H₂O. The aqueous layer was removed, and the organic layer was washed with H₂O, twice with 2 M HCl or 10% aqueous citric acid, twice with saturated aqueous NaHCO₃, and twice with H₂O. The organic layer was dried over Na₂SO₄, filtered, and concentrated under vacuum to afford the target ester **S2** (14,6 g, 98% yield) as a pale-yellow oil which was sufficiently pure to be taken on to the next step.

Synthesis of (S)-bis(3,5-bis(trifluoromethyl)phenyl)(pyrrolidin-2-yl)methanol



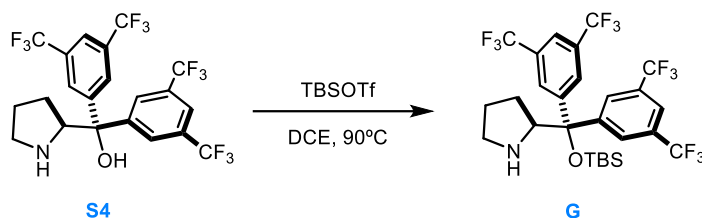
In a two-necked round bottom flask equipped with septum and condenser containing a stirring bar were added the Mg turnings (1,59 g, 65,4 mmol). The air was removed through vacuum air flaming for 30 minutes. To the Mg was added anhydrous THF (30 mL) and the reaction was stirred for 2 minutes after which a crystal of I₂ was added (the solution turns brownish). At this stage the aryl bromide (11,98 mL, 65,4 mmol) was added portion wise to the suspension of Mg. During the addition the solution turns gradually to grey (note: exothermic reaction). Once the addition of the aryl bromide was complete, the solution was refluxed for 1 hour at 65°C. After the indicated time the solution was cooled to 0°C and the Proline ester **S2** (as 1M solution in dry THF, 5 g, 21.8 mmol) was added via syringe. The reaction was stirred overnight and then slowly quenched with H₂O. The reaction crude was then filtered on cotton before being extracted 2 times with AcOEt (or DCM). The collected organic phase were then collected and anhydridified over MgSO₄, filtered and concentrated under vacuum to obtain a dark brown oil which contains the product. The oil was then purified by Flash Chromatography o silica gel (100%hexane to 95:5 hexane:AcOEt) to afford the Prolinol **S3** (10.1 g, 73% yield) as an orange and dense oil.

Synthesis of tert-butyl (S)-2-(bis(3,5bis(trifluoromethyl)phenyl)(hydroxy)methyl)pyrrolidine-1-carboxylate



Prolinol **S4** (9,4 g, 15,95 mmol) was dissolved in a 1:1 mixture of DCM:TFA and stirred for 1 hour at room temperature. The solution was then basified to pH 7 using a solution of NaHCO₃. The organic phase was then extracted with DCM 3 times. After anhydridification with NaSO₄ and removal of the solvent the free amine **S5** (7,3 g, 92% yield) was obtained as an orange oil.

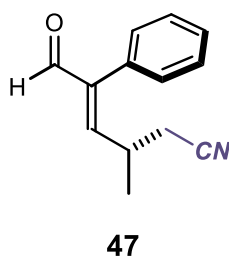
Synthesis of Catalyst 3e



In a two-necked round bottom flask equipped with condenser and a magnetic stirring bar was made a 0.4M solution of substrate **S4** (5.00 g, 9.5 mmol) in DCE. Triethylamine (5,97 mL, 42,8 mmol) and TBSOTf (4,38 mL, 19,04 mmol) were added sequentially while stirring. The reaction was then stirred under reflux overnight. After cooling the reaction mixture was quenched with brine. The organic phase was extracted with Et₂O 3 times and after anhydrication over MgSO₄ the crude was purified by Flash Chromatography on silica gel (2% Et₂O in Pentane) to afford the catalyst **C** (3,2 g, 50% yield) as a pale-yellow oil which solidifies at low temperature.

3.8.4. Experimental Procedures & characterization of products

General Procedure: Synthesis of (*S,E*)-3-methyl-6-oxo-5-phenylhex-4-enitrile [(+)-**3a**]



In an oven dried 5 mL vial equipped with a Teflon septum screw cap and a magnetic stirring bar, (*E*)-2-phenylpent-2-enal **45** (0.6 mmol, 96 mg, 3 equiv.) and aminocatalyst **G** (0.04 mmol, 25.6 mg, 0.2 equiv.) were dissolved in 250 μL of degassed THF. After 5 minutes 2,6-lutidine (0.24 mmol, 25.5 μL, 1.2 equiv.), α-chloroacetonitrile **46** (0.2 mmol, 12.6 μL) and dithiocarbamate catalyst **B** (0.04 mmol, 12.4 mg, 0.2 equiv.) were added. The reaction mixture was degassed

through Ar sparging for 20 seconds before closing the cap. The vial was then sealed with parafilm and placed in the 3D printed support photoreactor (Figure S1) and irradiated under stirring. After 20 hours, the solvent was evaporated under reduced pressure and the residue purified by column chromatography (eluent: hexane/EtOAc 8:2) to afford 27.9 mg of the corresponding product (0.14 mmol, 70%, 80:20 *er*) as a pale-orange oil. The enantiomeric excess of the product was determined to be 80:20 by UPC² analysis on a Daicel Chiralpak IA-3 column (eluent: CO₂/IPA = 90:10; flow rate 1 mL/min, λ = 300 nm. τ_{Major} = 3.54 min, τ_{Minor} = 3.66 min.

[α]_D²⁰ = +86.2 (c = 0.5 g/100 mL, CHCl₃)

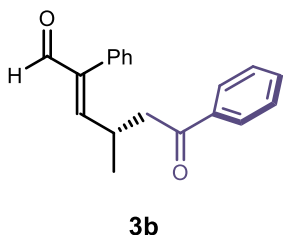
¹H NMR (500 MHz, CDCl₃) δ 9.67 (s, 1H), 7.49 – 7.37 (m, 3H), 7.20 – 7.11 (m, 2H), 6.54 (d, *J* = 10.3 Hz, 1H), 3.11 – 2.99 (m, 1H), 2.44 (d, *J* = 6.3 Hz, 2H), 1.28 (d, *J* = 6.7 Hz, 3H).

$^{13}\text{C NMR}$ (126 MHz, CDCl_3) δ 193.0, 153.9, 144.7, 131.9, 129.0 (2C), 128.6 (2C), 128.5, 117.3, 30.7, 24.1, 19.7.

HRMS (ESI) : m/z calculated for $[\text{C}_{18}\text{H}_{25}\text{NO}_4\text{Na}]^+$ $[\text{M}+\text{Na}]^+$: 222.0895; found: 222.0889.

Scope of Radical Precursors

Synthesis of (*S,E*)-4-methyl-6-oxo-2,6-diphenylhex-2-enal [(-)-**3b**]



Synthesized according to the general procedure using phenylpent-2-enal **1a** (0.6 mmol, 96 mg, 3 equiv.), 2-chloro-1-phenylethan-1-one (30.9 mg, 0.2 mmol), aminocatalyst **B** (0.04 mmol, 25.6 mg, 0.2 equiv.), dithiocarbamate catalyst **G** (0.04 mmol, 12.4 mg, 0.2 equiv.) and 2,6-lutidine (0.24 mmol, 25.5 μL , 1.2 equiv.). The crude mixture was purified by flash column chromatography on silica gel (eluent: hexane/EtOAc 8:2) to afford product **3b** (31.2 mg, 56% yield) as a Yellow Oil. The enantiomeric excess of the product was determined to be 84:16 by UPC² analysis on a Daicel Chiralpak IG column (eluent: $\text{CO}_2/\text{IPA} = 90:10$; flow rate 1 mL/min, $\lambda = 320$ nm. $\tau_{\text{Major}} = 3.17$ min, $\tau_{\text{Minor}} = 3.98$ min.

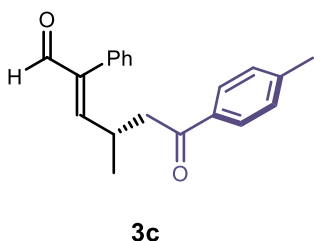
$[\alpha]_{\text{D}}^{20} = -76.4$ ($c = 0.5$ g/100 mL, CHCl_3)

$^1\text{H NMR}$ (500 MHz, CDCl_3) δ 9.61 (s, 1H), 7.93 – 7.81 (m, 2H), 7.57 (ddt, $J = 7.9, 6.9, 1.3$ Hz, 1H), 7.48 – 7.34 (m, 5H), 7.21 – 7.15 (m, 2H), 3.39 – 3.37 (m, 1H), 3.10 – 3.07 (m, 2H), 1.19 (d, $J = 6.7$ Hz, 3H).

$^{13}\text{C NMR}$ (126 MHz, CDCl_3) δ 197.9, 193.8, 159.2, 143.2, 136.6, 133.3, 132.6, 129.2 (2C), 128.7 (2C), 128.4 (2C), 128.1 (2C), 128.0, 45.0, 30.4, 20.1.

HRMS (ESI) : m/z calculated for $[\text{C}_{19}\text{H}_{18}\text{O}_2\text{Na}]^+$ $[\text{M}+\text{Na}]^+$: 301.1204; found: 301.1199.

Synthesis of (*S,E*)-4-methyl-6-oxo-2-phenyl-6-(*p*-tolyl)hex-2-enal [(-)-**3c**]



Synthesized according to the general procedure A using phenylpent-2-enal **1a** (0.6 mmol, 96 mg, 3 equiv.), 2-chloro-1-(*p*-tolyl)ethan-1-one (42.6 mg, 0.2 mmol), aminocatalyst **B** (0.04 mmol, 25.6 mg, 0.2 equiv.), dithiocarbamate catalyst **G** (0.04 mmol, 12.4 mg, 0.2 equiv.) and 2,6-lutidine (0.24 mmol, 25.5 μL , 1.2 equiv.). The crude mixture was purified by flash column chromatography on silica gel (eluent: hexane/EtOAc 8:2) to afford product **3c** (28.1 mg, 48% yield) as a pale yellow. The enantiomeric excess of the product was determined to be 85:15 by UPC² analysis on a Daicel

Chiralpak IG column (eluent: CO₂/IPA = 90:10; flow rate 1 mL/min, λ = 320 nm. τ_{Major} = 3.80 min, τ_{Minor} = 4.12 min.

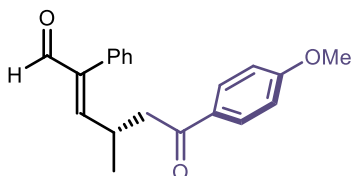
[α]_D²⁰ = -15.6 (c = 0.5 g/100 mL, CHCl₃)

¹H NMR (500 MHz, CDCl₃) δ 9.61 (s, 1H), 7.76 (d, *J* = 8.2 Hz, 2H), 7.45 – 7.32 (m, 3H), 7.25 – 7.21 (m, 2H), 7.20 – 7.15 (m, 2H), 6.61 (d, *J* = 10.2 Hz, 1H), 3.38 – 3.27 (m, 1H), 3.06 (dd, *J* = 6.8, 1.5 Hz, 2H), 2.42 (s, 3H), 1.17 (d, *J* = 6.7 Hz, 3H).

¹³C NMR (126 MHz, CDCl₃) δ 197.5, 193.8, 159.4, 144.1, 143.1, 134.2, 132.6, 129.4 (2C), 129.2 (2C), 128.4 (2C), 128.2 (2C), 128.0, 44.9, 30.5, 21.7, 20.0.

HRMS (ESI): *m/z* calculated for [C₂₀H₂₀O₂Na]⁺ [M+Na]⁺: 315.1361; found: 315.1356.

Synthesis of (*S,E*)-6-(4-methoxyphenyl)-4-methyl-6-oxo-2-phenylhex-2-enal [(-)-**3d**]



3d

Synthesized according to the general procedure A using phenylpent-2-enal **1a** (0.6 mmol, 96 mg, 3 equiv.), 2-chloro-1-(4-methoxy)ethan-1-one (45.8 mg, 0.2 mmol), aminocatalyst **B** (0.04 mmol, 25.6 mg, 0.2 equiv.), dithiocarbamate catalyst **G** (0.04 mmol, 12.4 mg, 0.2 equiv.) and 2,6-lutidine (0.24 mmol, 25.5 μL, 1.2 equiv.).

The crude mixture was purified by flash column chromatography on silica gel (eluent: hexane/EtOAc 7:3) to afford product **3d** (32.0 mg, 53% yield) as a colorless oil. The enantiomeric excess of the product was determined to be 83:17 by UPC² analysis on a Daicel Chiralpak IG column (eluent: CO₂/IPA=20:80; flow rate 1 mL/min, λ = 320 nm. τ_{Major} = 4.15 min, τ_{Minor} = 4.39 min.

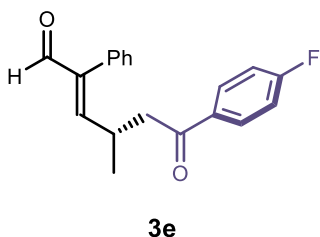
[α]_D²⁰ = -51.1 (c = 0.5 g/100 mL, CHCl₃)

¹H NMR (500 MHz, CDCl₃) δ 9.61 (s, 1H), 7.84 (d, *J* = 8.9 Hz, 2H), 7.43 – 7.32 (m, 3H), 7.17 (d, *J* = 8.0 Hz, 2H), 6.91 (d, *J* = 8.9 Hz, 2H), 6.61 (d, *J* = 10.1 Hz, 1H), 3.88 (s, 3H), 3.39 – 3.23 (m, 1H), 3.03 (d, *J* = 6.8 Hz, 2H), 1.17 (d, *J* = 6.7 Hz, 3H).

¹³C NMR (126 MHz, CDCl₃) δ 196.4, 193.8, 163.6, 159.4, 143.1, 132.6, 130.4 (2C), 129.7, 129.2 (2C), 128.4 (2C), 128.0, 113.8 (2C), 55.5, 44.7, 30.6, 20.1.

HRMS (ESI): *m/z* calculated for [C₂₀H₂₀O₃Na]⁺ [M+Na]⁺: 331.1310; found: 331.1305.

Synthesis of (*S,E*)-6-(4-fluorophenyl)-4-methyl-6-oxo-2-phenylhex-2-enal [(+)-**3e**]



Synthesized according to the general procedure A using phenylpent-2-enal **1a** (0.6 mmol, 96 mg, 3 equiv.), 2-chloro-1-(4-fluorophenyl)ethan-1-one (43.4 mg, 0.2 mmol), aminocatalyst **B** (0.04 mmol, 25.6 mg, 0.2 equiv.), dithiocarbamate catalyst **G** (0.04 mmol, 12.4 mg, 0.2 equiv.) and 2,6-lutidine (0.24 mmol, 25.5 μ L, 1.2 equiv.). The crude mixture was purified by flash column chromatography on silica gel (eluent: hexane/EtOAc 8:2) to afford product **3e** (31.4 mg, 53% yield) as a colorless oil. The enantiomeric excess of the product was determined to be 83:17 by UPC² analysis on a Daicel Chiralpak IG column (eluent: CO₂/IPA = 90:10; flow rate 1 mL/min, λ = 320 nm. τ Major = 3.30 min, τ Minor = 3.54 min.

$[\alpha]_D^{20} = +63.4$ (c = 0.5 g/100 mL, CHCl₃)

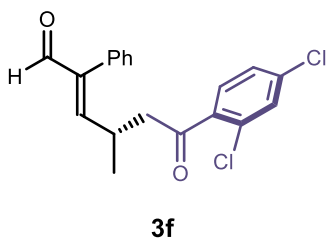
¹H NMR (500 MHz, CDCl₃) δ 9.61 (s, 1H), 7.87 (dd, J = 8.9, 5.4 Hz, 2H), 7.48 – 7.32 (m, 3H), 7.22 – 7.14 (m, 2H), 7.14 – 7.04 (m, 2H), 6.60 (d, J = 10.2 Hz, 1H), 3.39 – 3.24 (m, 1H), 3.04 (d, J = 6.8 Hz, 2H), 1.19 (d, J = 6.7 Hz, 3H).

¹⁹F NMR (471 MHz, CDCl₃) δ -104.87.

¹³C NMR (126 MHz, CDCl₃) δ 196.2, 193.7, 165.8 (d, ¹J_{C,F} = 255 Hz), 158.9, 143.2, 133.0 (d, ⁴J_{C,F} = 3 Hz), 132.6, 130.7 (d, ³J_{C,F} = 9 Hz, 2C), 129.2 (2C), 128.4 (2C), 128.1, 115.8 (d, ²J_{C,F} = 22 Hz, 2C), 44.9, 30.4, 20.0.

HRMS (ESI): m/z calculated for [C₁₉H₁₇FO₂Na]⁺ [M+Na]⁺: 319.1110; found: 319.1105.

Synthesis of (*S,E*)-6-(2,4-dichlorophenyl)-4-methyl-6-oxo-2-phenylhex-2-enal [(+)-**3f**]



Synthesized according to the general procedure A using phenylpent-2-enal **1a** (0.6 mmol, 96 mg, 3 equiv.), 2-chloro-1-(2,4-dichlorophenyl)ethan-1-one (53.6 mg, 0.2 mmol), aminocatalyst **B** (0.04 mmol, 25.6 mg, 0.2 equiv.), dithiocarbamate catalyst **G** (0.04 mmol, 12.4 mg, 0.2 equiv.) and 2,6-lutidine (0.24 mmol, 25.5 μ L, 1.2 equiv.). The crude mixture was purified by flash column chromatography on silica gel (eluent: hexane/EtOAc 75:25) to afford product **3f** (34.7 mg, 50% yield) as a yellowish oil. The enantiomeric excess of the product was determined to be 76:24 by UPC² analysis on a Daicel Chiralpak IG column (eluent: 85:15 CO₂/MeOH; flow rate 1.00 mL/min, λ = 240 nm. τ Major = 3.47 min, τ Minor = 3.79 min.

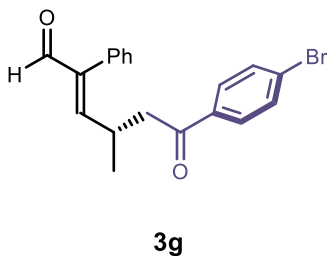
$[\alpha]_D^{20} = +87.0$ (c = 0.5 g/100 mL, CHCl₃)

¹H NMR (500 MHz, CDCl₃) δ 9.61 (s, 1H), 7.44 – 7.35 (m, 4H), 7.33 – 7.28 (m, 1H), 7.18 – 7.14 (m, 2H), 6.56 (d, J = 10.2 Hz, 1H), 3.35 – 3.23 (m, 1H), 3.07 (dd, J = 6.8, 1.7 Hz, 2H), 1.19 (d, J = 6.7 Hz, 3H).

¹³C NMR (126 MHz, CDCl₃) δ 199.6, 193.6, 158.2, 143.2, 137.7, 137.0, 132.4, 132.1, 130.5, 130.2, 129.1 (2C), 128.4 (2C), 128.1, 127.5, 49.1, 30.4, 20.1.

HRMS (ESI): m/z calculated for [C₁₉H₁₆Cl₂O₂Na]⁺ [M+Na]⁺: 369.0425; found: 369.0420.

Synthesis of (*S,E*)-6-(4-bromophenyl)-4-methyl-6-oxo-2-phenylhex-2-enal [(+)-**3g**]



Synthesized according to the general procedure A using phenylpent-2-enal **1a** (0.6 mmol, 96 mg, 3 equiv.), 2-chloro-1-(4-bromophenyl)ethan-1-one (55.6 mg, 0.2 mmol), aminocatalyst **B** (0.04 mmol, 25.6 mg, 0.2 equiv.), dithiocarbamate catalyst **G** (0.04 mmol, 12.4 mg, 0.2 equiv.) and 2,6-lutidine (0.24 mmol, 25.5 μL, 1.2 equiv.). The crude mixture was purified by flash column chromatography on silica gel (eluent: hexane/EtOAc 7:3) to afford product **3g** (42 mg, 58% yield) as a colorless oil. The enantiomeric excess of the product was determined to be 82:18 by UPC² analysis on a Daicel Chiralpak IE column (eluent: CO₂/IPA = 85:15; flow rate 1 mL/min, λ = 320 nm. τ_{Major} = 3.54 min, τ_{Minor} = 3.66 min.

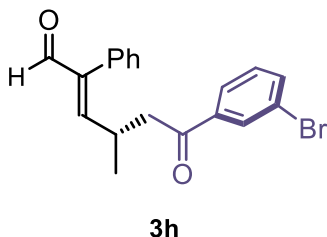
[α]_D²⁰ = +19.2 (c = 0.5 g/100 mL, CHCl₃)

¹H NMR (500 MHz, CDCl₃) δ 9.62 (s, 1H), 7.70 (d, J = 8.6 Hz, 2H), 7.58 (d, J = 8.6 Hz, 2H), 7.43 – 7.35 (m, 3H), 7.19 – 7.14 (m, 2H), 6.59 (d, J = 10.2 Hz, 1H), 3.32 (dq, J = 10.2, 6.8 Hz, 1H), 3.04 (d, J = 6.8 Hz, 2H), 1.19 (d, J = 6.7 Hz, 3H).

¹³C NMR (126 MHz, CDCl₃) δ 196.76, 193.58, 158.59, 143.26, 135.21, 132.53, 131.98, 129.55, 129.14, 128.50, 128.40, 128.07, 44.97, 30.39, 20.04.

HRMS (ESI): m/z calculated for [C₁₉H₁₇BrO₂Na]⁺ [M+Na]⁺: 379.0310; found: 379.0291.

Synthesis of (*S,E*)-6-(3-bromophenyl)-4-methyl-6-oxo-2-phenylhex-2-enal [(-)-**3h**]



Synthesized according to the general procedure A using phenylpent-2-enal **1a** (0.6 mmol, 96 mg, 3 equiv.), 2-bromo-1-(3-bromophenyl)ethan-1-one (55.6 mg, 0.2 mmol), aminocatalyst **B** (0.04 mmol, 25.6 mg, 0.2 equiv.), dithiocarbamate catalyst **G** (0.04 mmol, 12.4 mg, 0.2 equiv.) and 2,6-lutidine (0.24 mmol, 25.5 μL, 1.2 equiv.). The crude mixture was purified by flash column chromatography on silica gel (eluent: hexane/EtOAc 8:2) to afford product **3h** (39.3 mg, 52% yield) as a yellowish oil. The enantiomeric excess of the product was determined to be 82:18 by UPC² analysis on a Daicel Chiralpak IG column (eluent: 80:20 CO₂/MeCN; flow rate 1.00 mL/min, λ = 250 nm. τ_{Major} = 3.95 min, τ_{Minor} = 4.18 min.

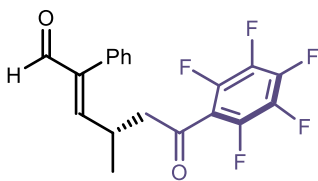
$[\alpha]_D^{20} = -30.7$ ($c = 0.5$ g/100 mL, CHCl_3)

$^1\text{H NMR}$ (500 MHz, CDCl_3) δ 9.61 (s, 1H), 8.01 (t, $J = 1.8$ Hz, 1H), 7.76 (d, $J = 7.8$ Hz, 1H), 7.71 – 7.68 (m, 1H), 7.45 – 7.34 (m, 3H), 7.32 (t, $J = 7.9$ Hz, 1H), 7.20 – 7.15 (m, 2H), 6.59 (d, $J = 10.2$ Hz, 1H), 3.38 – 3.25 (m, 1H), 3.06 (d, $J = 6.7$ Hz, 2H), 1.19 (d, $J = 6.7$ Hz, 3H).

$^{13}\text{C NMR}$ (126 MHz, CDCl_3) δ 196.4, 193.6, 158.6, 143.3, 138.3, 136.1, 132.5, 131.1, 130.3, 129.2 (2C), 128.4 (2C), 128.1, 126.5, 123.1, 45.0, 30.3, 20.1.

HRMS (ESI): m/z calculated for $[\text{C}_{19}\text{H}_{17}\text{BrO}_2\text{Na}]^+ [\text{M}+\text{Na}]^+$: 379.0310; found: 379.0304.

Synthesis of (*S,E*)-4-methyl-6-oxo-6-(perfluorophenyl)-2-phenylhex-2-enal [(-)-**3i**]



3i

Synthesized according to the general procedure A using phenylpent-2-enal **1a** (0.6 mmol, 96 mg, 3 equiv.), 2-bromo-1-(perfluorophenyl)ethan-1-one (57.8 mg, 0.2 mmol), aminocatalyst **B** (0.04 mmol, 25.6 mg, 0.2 equiv.), dithiocarbamate catalyst **G** (0.04 mmol, 12.4 mg, 0.2 equiv.) and 2,6-lutidine (0.24 mmol, 25.5 μL , 1.2 equiv.). The crude mixture was purified by flash column chromatography on silica gel (eluent: 85:15) to afford product **3i** (60.8 mg, 80% yield) as a yellowish oil. The enantiomeric excess of the product was determined to be 82:18 by UPC² analysis on a Daicel Chiralpak IA-3 column (eluent: 91:9 CO_2/MeCN ; flow rate 1.00 mL/min, $\lambda = 255$ nm. $\tau_{\text{Minor}} = 2.18$ min, $\tau_{\text{Major}} = 2.32$ min).

$[\alpha]_D^{20} = -57.3$ ($c = 0.5$ g/100 mL, CHCl_3)

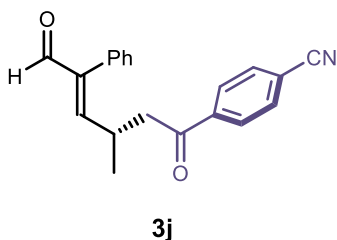
$^1\text{H NMR}$ (500 MHz, CDCl_3) δ 9.61 (s, 1H), 7.45 – 7.33 (m, 3H), 7.19 – 7.13 (m, 2H), 6.53 (d, $J = 10.2$, 1H), 3.34 – 3.22 (m, 1H), 2.98 (dt, $J = 7.0, 1.4, 1.4$, 2H), 1.22 (d, $J = 6.7$, 3H).

$^{19}\text{F NMR}$ (471 MHz, CDCl_3) δ -140.63 – -141.10 (m), -148.61 (t, $J = 20.7$ Hz), -159.26 – -159.84 (m).

$^{13}\text{C NMR}$ (126 MHz, CDCl_3) δ 193.4, 191.8, 157.0, 144.2 (d, $^1J_{\text{C,F}} = 255$ Hz), 143.4, 142.8 (d, $^1J_{\text{C,F}} = 260$ Hz), 137.5 (d, $^1J_{\text{C,F}} = 255$ Hz), 132.2, 129.0 (2C), 128.4 (2C), 128.2, 114.3 (t, $^2J_{\text{C,F}} = 18$ Hz), 51.2 (t, $^4J_{\text{C,F}} = 2$ Hz), 30.1, 20.0.

HRMS (ESI): m/z calculated for $[\text{C}_{19}\text{H}_{13}\text{F}_5\text{O}_2\text{Na}]^+ [\text{M}+\text{Na}]^+$: 391.0733; found: 391.0728.

Synthesis of (*S,E*)-4-(3-methyl-6-oxo-5-phenylhex-4-enoyl)benzointrile [(-)-**3j**]



Synthesized according to the general procedure A using phenylpent-2-enal **1a** (0.6 mmol, 96 mg, 3 equiv.), 4-(2-chloroacetyl)benzotrile (44.8 mg, 0.2 mmol), aminocatalyst **B** (0.04 mmol, 25.6 mg, 0.2 equiv.), dithiocarbamate catalyst **G** (0.04 mmol, 12.4 mg, 0.2 equiv.) and 2,6-lutidine (0.24 mmol, 25.5 μ L, 1.2 equiv.).

The crude mixture was purified by flash column chromatography on silica gel (eluent: hexane/EtOAc 7:3) to afford product **3j** (26.0 mg, 42% yield) as a colorless oil. The enantiomeric excess of the product was determined to be 82:18 by UPC² analysis on a Daicel Chiralpak IE column (eluent: 85:15 CO₂/MeCN; flow rate 1.00 mL/min, λ = 220 nm. τ Major = 3.54 min, τ Minor = 3.66 min.

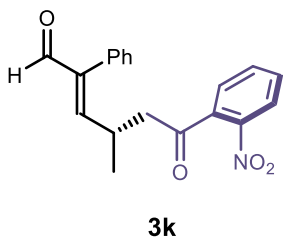
$[\alpha]_D^{20}$ = -46.2 (c = 0.5 g/100 mL, CHCl₃)

¹H NMR (400 MHz, CDCl₃) δ 9.60 (s, 1H), 7.94 – 7.83 (m, 2H), 7.77 – 7.63 (m, 2H), 7.43 – 7.31 (m, 3H), 7.19 – 7.10 (m, 2H), 6.56 (d, J = 10.1 Hz, 1H), 3.30 (dq, J = 10.1, 6.7 Hz, 1H), 3.12 – 3.01 (m, 2H), 1.19 (d, J = 6.7 Hz, 3H).

¹³C NMR (101 MHz, CDCl₃) δ 196.34, 193.44, 158.00, 143.35, 139.26, 132.50, 132.44, 129.09, 128.40, 128.12, 117.76, 116.51, 45.21, 30.17, 19.98.

HRMS (ESI): m/z calculated for [C₂₀H₁₇NO₂Na]⁺ [M+Na]⁺: 326.1157; found: 326.1151.

Synthesis of (*S,E*)-4-methyl-6-(2-nitrophenyl)-6-oxo-2-phenylhex-2-enal [(+)-**3k**]



Synthesized according to the general procedure A using phenylpent-2-enal **1a** (0.6 mmol, 96 mg, 3 equiv.), 2-chloro-1-(2-nitrophenyl)ethan-1-one (48.8 mg, 0.2 mmol), aminocatalyst **B** (0.04 mmol, 25.6 mg, 0.2 equiv.), dithiocarbamate catalyst **G** (0.04 mmol, 12.4 mg, 0.2 equiv.) and 2,6-lutidine (0.24 mmol, 25.5 μ L, 1.2 equiv.). The crude mixture was purified by flash column chromatography on silica gel (eluent: hexane/EtOAc

8:2) to afford product **3k** (27.8 mg, 43% yield) as a brownish oil. The enantiomeric excess of the product was determined to be 82:18 by UPC² analysis on a Daicel Chiralpak IC column (eluent: 90:10 CO₂/IPA; flow rate 1.00 mL/min, λ = 250 nm. τ Major = 4.17 min, τ Minor = 4.31 min.

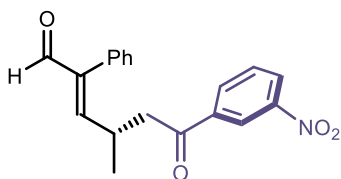
$[\alpha]_D^{20}$ = +15.3 (c = 0.5 g/100 mL, CHCl₃)

¹H NMR (500 MHz, CDCl₃) δ 9.65 (s, 1H), 8.15 (dd, J = 8.1, 1.2 Hz, 1H), 7.71 – 7.67 (m, 1H), 7.65 – 7.59 (m, 1H), 7.47 – 7.42 (m, 2H), 7.41 – 7.38 (m, 1H), 7.26 – 7.23 (m, 3H), 6.64 (d, J = 10.2 Hz, 1H), 3.40 – 3.29 (m, 1H), 2.99 – 2.85 (m, 2H), 1.23 (d, J = 6.7 Hz, 3H).

¹³C NMR (126 MHz, CDCl₃) δ 199.8, 193.8, 158.4, 143.3, 137.6, 134.4, 132.6, 130.6, 129.3, 129.2 (2C), 128.4 (2C), 128.1, 127.4, 124.5, 49.0, 29.8, 19.9.

HRMS (ESI): m/z calculated for $[C_{19}H_{17}NO_4Na]^+$ $[M+Na]^+$: 346.1055; found: 346.1050.

Synthesis of (*S,E*)-4-methyl-6-(3-nitrophenyl)-6-oxo-2-phenylhex-2-enal [(+)-**3I**]



3I

Synthesized according to the general procedure A using phenylpent-2-enal **1a** (0.6 mmol, 96 mg, 3 equiv.), 2-bromo-1-(3-nitrophenyl)ethan-1-one (48.8 mg, 0.2 mmol), aminocatalyst **B** (0.04 mmol, 25.6 mg, 0.2 equiv.), dithiocarbamate catalyst **G** (0.04 mmol, 12.4 mg, 0.2 equiv.) and 2,6-lutidine (0.24 mmol, 25.5 μ L, 1.2 equiv.).

The crude mixture was purified by flash column chromatography on silica gel (eluent: hexane/EtOAc 7:3) to afford product **3I** (33.6 mg, 52% yield) as a colorless oil. The enantiomeric excess of the product was determined to be 78:22 by UPC² analysis on a Daicel Chiralpak IG column (eluent: 85:15 CO₂/MeCN; flow rate 1.00 mL/min, λ = 220 nm. τ Major = 4.00 min, τ Minor = 4.12 min.

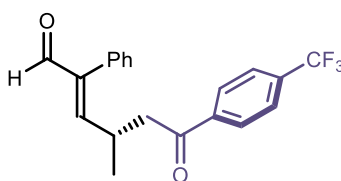
$[\alpha]_D^{20}$ = +21.0 (c = 0.5 g/100 mL, CHCl₃)

¹H NMR (500 MHz, CDCl₃) δ 9.63 (s, 1H), 8.68 (t, J = 1.9 Hz, 1H), 8.42 (ddd, J = 8.2, 2.3, 1.1 Hz, 1H), 8.18 (ddd, J = 7.7, 1.7, 1.1 Hz, 1H), 7.66 (t, J = 8.0 Hz, 1H), 7.43 – 7.34 (m, 3H), 7.19 – 7.15 (m, 2H), 6.60 (d, J = 10.2 Hz, 1H), 3.43 – 3.30 (m, 1H), 3.15 (d, J = 6.7 Hz, 2H), 1.24 (d, J = 6.7 Hz, 3H).

¹³C NMR (126 MHz, CDCl₃) δ 195.5, 193.5, 158.0, 143.4, 137.7, 133.5, 132.4, 130.0, 129.7, 129.1 (2C), 128.4 (2C), 128.2, 127.6, 122.9, 45.2, 30.2, 20.1.

HRMS (ESI): m/z calculated for $[C_{19}H_{17}NO_4Na]^+$ $[M+Na]^+$: 346.1055; found: 346.1050.

Synthesis of (*S,E*)-4-methyl-6-oxo-2-phenyl-6-(4-(trifluoromethyl)phenyl)hex-2-enal [(+)-**3m**]



3m

Synthesized according to the general procedure A using phenylpent-2-enal **1a** (0.6 mmol, 96 mg, 3 equiv.), 2-chloro-1-(4-trifluoromethyl)ethan-1-one (44.2 mg, 0.2 mmol), aminocatalyst **B** (0.04 mmol, 25.6 mg, 0.2 equiv.), dithiocarbamate catalyst **G** (0.04 mmol, 12.4 mg, 0.2 equiv.) and 2,6-lutidine (0.24 mmol, 25.5 μ L, 1.2 equiv.).

The crude mixture was purified by flash column chromatography on silica gel (eluent: hexane/EtOAc 8:2) to afford product **3m** (27.8 mg, 59% yield) as a brownish oil. The enantiomeric excess of the product was determined to be 81:19 by UPC² analysis on a Daicel Chiralpak OJ column (eluent: 90:10 CO₂/EtOH; flow rate 1.00 mL/min, λ = 250 nm. τ Major = 2.29 min, τ Minor = 2.83 min.

$[\alpha]_D^{20} = +58.7$ ($c = 0.5$ g/100 mL, CHCl_3)

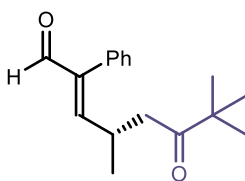
$^1\text{H NMR}$ (400 MHz, CDCl_3) δ 9.60 (s, 1H), 7.94 – 7.88 (m, 2H), 7.74 – 7.65 (m, 2H), 7.40 – 7.31 (m, 3H), 7.11 – 7.17 (m, 2H), 6.57 (d, $J = 10.1$ Hz, 1H), 3.25 – 3.38 (m, 1H), 3.08 (d, $J = 6.8$ Hz, 2H), 1.19 (d, $J = 6.7$ Hz, 3H).

$^{13}\text{C NMR}$ (126 MHz, CDCl_3) δ 196.80, 193.52, 158.25, 143.36, 139.09, 134.56 (q, $J = 32.7$ Hz), 132.50, 129.12, 128.39, 128.37, 128.11, 125.73 (q, $J = 3.8$ Hz), 123.50 (q, $J = 272.8$ Hz), 45.29, 30.30, 20.04.

$^{19}\text{F NMR}$ (376 MHz, CDCl_3) δ -63.27

HRMS (ESI): m/z calculated for $[\text{C}_{19}\text{H}_{17}\text{NO}_4\text{Na}]^+ [\text{M}+\text{Na}]^+$: 346.1055; found: 346.1050.

Synthesis of (*S,E*)-4,7,7-trimethyl-6-oxo-2-phenyloct-2-enal [(*-*)-**3n**]



3n

Synthesized according to the general procedure A using phenylpent-2-enal **1a** (0.6 mmol, 96 mg, 3 equiv.), 1-chloro-3,3-dimethylbutan-2-one (35.8 mg, 0.2 mmol), aminocatalyst **C** (0.04 mmol, 25.6 mg, 0.2 equiv.), dithiocarbamate catalyst **E** (0.04 mmol, 12.4 mg, 0.2 equiv.) and 2,6-lutidine (0.24 mmol, 25.5 μL , 1.2 equiv.). The crude mixture was purified by flash column chromatography on silica gel (eluent: hexane/EtOAc 9:1) to afford product **3n** (13.0 mg, 25% yield) as a colorless oil. The enantiomeric excess of the product was determined to be 87:13 by UPC² analysis on a Daicel Chiralpak IC column (eluent: 93:7 CO_2/MeCN ; flow rate 1.00 mL/min, $\lambda = 250$ nm. $\tau_{\text{Minor}} = 2.73$ min, $\tau_{\text{Major}} = 2.85$ min).

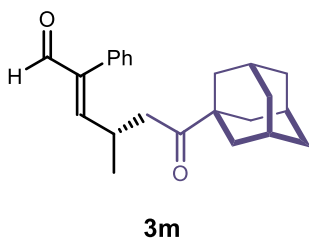
$[\alpha]_D^{20} = -11.2$ ($c = 0.5$ g/100 mL, CHCl_3)

$^1\text{H NMR}$ (500 MHz, CDCl_3) δ 9.60 (s, 1H), 7.46 – 7.39 (m, 2H), 7.38 – 7.33 (m, 1H), 7.23 – 7.19 (m, 2H), 6.53 (d, $J = 10.2$ Hz, 1H), 3.25 – 3.12 (m, 1H), 2.61 (ABq, $J = 17.3, 6.5$ Hz, 2H), 1.12 (s, 9H), 1.07 (d, $J = 6.6$ Hz, 3H).

$^{13}\text{C NMR}$ (126 MHz, CDCl_3) δ 213.3, 193.9, 159.7, 142.9, 132.6, 129.2 (2C), 128.4 (2C), 128.0, 42.8, 31.6, 29.7, 26.2, 19.9.

HRMS (ESI): m/z calculated for $[\text{C}_{17}\text{H}_{22}\text{O}_2\text{Na}]^+ [\text{M}+\text{Na}]^+$: 281.1518; found: 281.1512.

Synthesis of (*S,E*)-6-((*3R,5R,7R*)-adamantan-1-yl)-4-methyl-6-oxo-2-phenylhex-2-enal [(*+*)-**3m**]



Synthesized according to the general procedure A using phenylpent-2-enal **1a** (0.6 mmol, 96 mg, 3 equiv.), 1-((3*r*,5*r*,7*r*)-adamantan-1-yl)-2-bromoethan-1-one (51.4 mg, 0.2 mmol), aminocatalyst **B** (0.04 mmol, 25.6 mg, 0.2 equiv.), dithiocarbamate catalyst **G** (0.04 mmol, 12.4 mg, 0.2 equiv.) and 2,6-lutidine (0.24 mmol, 25.5 μ L, 1.2 equiv.). The crude mixture was purified by flash column chromatography on silica gel (eluent: hexane/EtOAc 9:1) to afford product **3m** (17 mg, 41% yield) as a colorless oil. The enantiomeric excess of the product was determined to be 89:11 by UPC² analysis on a Daicel Chiralpak OJ column (eluent: 90:10 CO₂/MeCN; flow rate 1.00 mL/min, λ = 220 nm. τ Minor = 2.43 min, τ Major = 2.90 min.

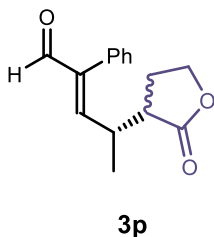
$[\alpha]_D^{20} = +23.1$ ($c = 0.5$ g/100 mL, CHCl₃)

¹H NMR (500 MHz, CDCl₃) δ 9.59 (s, 1H), 7.45 – 7.40 (m, 2H), 7.38 – 7.33 (m, 1H), 7.24 – 7.19 (m, 2H), 6.52 (d, $J = 10.2$ Hz, 1H), 3.23 – 3.11 (m, 1H), 2.57 (ABq, $J = 17.2, 6.5$ Hz, 2H), 2.09 – 2.01 (m, 2H), 1.79 – 1.74 (m, 8H), 1.71 – 1.65 (m, 3H), 1.58 (s, 2H), 1.06 (d, $J = 6.7$ Hz, 3H).

¹³C NMR (126 MHz, CDCl₃) δ 213.1, 193.9, 160.0, 142.8, 132.7, 129.2 (2C), 128.3 (2C), 128.0, 42.4, 38.1, 36.5, 29.6, 27.9, 20.0.

HRMS (ESI): m/z calculated for [C₂₃H₂₈O₂Na]⁺ [M+Na]⁺: 359.1987; found: 359.1982.

Synthesis of (*E*)-4-(2-oxotetrahydrofuran-3-yl)-2-phenylpent-2-enal [(-)-**3p**]



Synthesized according to the general procedure A using phenylpent-2-enal **1a** (0.6 mmol, 96 mg, 3 equiv.), 3-bromodihydrofuran-2(3*H*)-one (33.0 mg, 0.2 mmol), aminocatalyst **B** (0.04 mmol, 25.6 mg, 0.2 equiv.), dithiocarbamate catalyst **G** (0.04 mmol, 12.4 mg, 0.2 equiv.) and 2,6-lutidine (0.24 mmol, 25.5 μ L, 1.2 equiv.). The crude mixture was purified by flash column chromatography on silica gel (eluent: hexane/EtOAc 8:2) to afford product **3p** as a mixture 1.2:1 of the two diastereoisomers (20.0 mg, 41% yield) as a colorless oil. The enantiomeric excess of the diastereoisomeric products was determined to be 91:9 for diastereoisomer 1 and 86:14 for diastereoisomer 2 by UPC² analysis on a Daicel Chiralpak IC column (eluent: 87:13 CO₂/IPA; flow rate 1.00 mL/min, λ = 250 nm. τ Major_{dias1} = 4.91 min, τ Minor_{dias1} = 5.04 min; τ Minor_{dias2} = 5.39 min, τ Major_{dias2} = 5.83 min.

$[\alpha]_D^{20} = -8.2$ ($c = 0.5$ g/100 mL, CHCl₃)

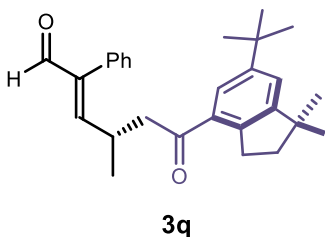
¹H NMR (500 MHz, CDCl₃) δ 9.66 (s, 1H_{dias1} + 1H_{dias2}), 7.46 – 7.35 (m, 3H_{dias1} + 3H_{dias2}), 7.18 – 7.13 (m, 2H_{dias1} + 2H_{dias2}), 6.75 (d, $J = 10.6$ Hz, 1H_{dias1}), 6.64 (d, $J = 10.5$ Hz, 1H_{dias2}), 4.33 (td, $J = 8.9, 8.8, 2.8$ Hz, 1H_{dias1}), 4.28 – 4.22 (m, 1H_{dias2}), 4.22 – 4.16 (m, 1H_{dias1} + 1H_{dias2}),

3.10 – 2.97 (m, 1H_{dias1} + 1H_{dias2}), 2.70 – 2.58 (m, 1H_{dias1} + 1H_{dias2}), 2.38 – 2.27 (m, 1H_{dias1} + 1H_{dias2}), 2.11 – 1.95 (m, 1H_{dias1} + 1H_{dias2}), 1.29 (d, $J = 6.7$ Hz, 1H_{dias1}), 1.21 (d, $J = 6.9$ Hz, 1H_{dias2}).

¹³C NMR (126 MHz, CDCl₃) [signals of both diastereoisomers] δ 193.5, 193.4, 176.9, 176.8, 155.8, 155.2, 144.3, 144.0, 132.4, 132.3, 129.1 (4C), 128.6 (4C), 128.3, 128.2, 66.3 (2C), 43.9, 43.4, 34.0, 33.9, 26.5, 26.0, 17.6, 17.0.

HRMS (ESI): m/z calculated for [C₁₅H₁₆O₃Na]⁺ [M+Na]⁺: 267.0997; found: 267.0992.

Synthesis of (*S,E*)-6-(6-(*tert*-butyl)-1,1-dimethyl-2,3-dihydro-1*H*-inden-4-yl)-4-methyl-6-oxo-2-phenylhex-2-enal [(+)-**3q**]



Synthesized according to the general procedure A using phenylpent-2-enal **1a** (0.6 mmol, 96 mg, 3 equiv.), 2-bromo-1-(6-(*tert*-butyl)-1,1-dimethyl-2,3-dihydro-1*H*-inden-4-yl)ethan-1-one (64.6 mg, 0.2 mmol), aminocatalyst **B** (0.04 mmol, 25.6 mg, 0.2 equiv.), dithiocarbamate catalyst **G** (0.04 mmol, 12.4 mg, 0.2 equiv.) and 2,6-lutidine (0.24 mmol, 25.5 μ L, 1.2 equiv.). The crude mixture was purified

by flash column chromatography on silica gel (eluent: hexane/EtOAc 9:1) to afford product **3q** (40.0 mg, 50% yield) as a pale-yellow oil. The enantiomeric excess of the product was determined to be 79:21 by UPC² analysis on a Daicel Chiralpak IA-3 column (eluent: 92:8 CO₂/IPA; flow rate 1.00 mL/min, $\lambda = 250$ nm. $\tau_{\text{Major}} = 3.82$ min, $\tau_{\text{Minor}} = 3.73$ min.

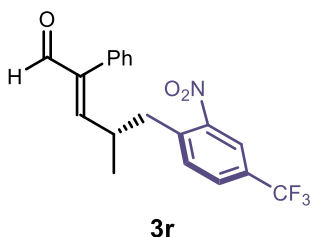
$[\alpha]_{\text{D}}^{20} = +51.4$ ($c = 0.5$ g/100 mL, CHCl₃)

¹H NMR (500 MHz, CDCl₃) δ 9.59 (s, 1H), 7.56 (d, $J = 1.8$ Hz, 1H), 7.38 – 7.27 (m, 4H), 7.14 – 7.07 (m, 2H), 6.61 (d, $J = 10.3$ Hz, 1H), 3.31 (dq, $J = 10.3, 6.7$ Hz, 1H), 3.11 (m, 2H), 3.05 (m, 2H), 1.91 (t, $J = 7.2$ Hz, 2H), 1.32 (s, 9H), 1.25 (d, $J = 3.3$ Hz, 6H), 1.17 (d, $J = 6.7$ Hz, 3H).

¹³C NMR (126 MHz, CDCl₃) δ 199.97, 193.82, 159.45, 154.58, 149.97, 142.85, 141.17, 133.16, 132.50, 129.14, 128.29, 127.96, 123.80, 123.42, 46.55, 43.40, 41.39, 34.70, 31.48, 30.78, 30.58, 28.74, 28.72, 20.16.

HRMS (ESI): m/z calculated for [C₂₈H₃₄O₂Na]⁺ [M+Na]⁺: 425.2456; found: 425.2451.

Synthesis of (*S,E*)-4-methyl-5-(2-nitro-4-(trifluoromethyl)phenyl)-2-phenylpent-2-enal [(+)-**3r**]



Synthesized according to the general procedure A using phenylpent-2-enal **1a** (0.6 mmol, 96 mg, 3 equiv.), 1-(bromomethyl)-2-nitro-4-(trifluoromethyl)benzene (56.8 mg, 0.2 mmol), aminocatalyst **B** (0.04 mmol, 25.6 mg, 0.2 equiv.), dithiocarbamate catalyst **G** (0.04 mmol, 12.4 mg, 0.2 equiv.) and 2,6-lutidine (0.24 mmol, 25.5 μ L, 1.2 equiv.). The crude mixture was purified by flash column chromatography on silica gel (eluent: hexane/EtOAc 8:2) to afford product **3r** (29.1 mg, 41% yield) as a pale orange oil. The enantiomeric excess of the product was determined after reduction to the corresponding alcohol by adding 2 eq. of NaBH₄ to a 1:1=MeOH:DCM solution of the product (cooled at 0°C through ice bath). The enantiomeric ratio of the corresponding alcohol was measured to be 76:24 by UPC² analysis on a Daicel Chiralpak IA-3 column (eluent: 90:10 CO₂/IPA; flow rate 1.00 mL/min, λ = 250 nm. τ Major = 2.87 min, τ Minor = 3.12 min.

$[\alpha]_D^{20} = +69.8$ (c = 0.5 g/100 mL, CHCl₃)

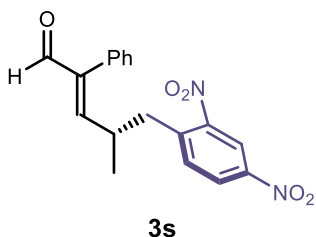
¹H NMR (500 MHz, CDCl₃) δ 9.58 (s, 1H), 8.11 – 8.08 (m, 1H), 7.70 – 7.63 (m, 1H), 7.34 – 7.21 (m, 4H), 6.67 (dd, J = 8.0, 1.6 Hz, 2H), 6.50 (d, J = 10.4 Hz, 1H), 3.19 (dd, J = 12.8, 4.6 Hz, 1H), 3.14 – 3.06 (m, 1H), 3.02 (dd, J = 12.8, 9.3 Hz, 1H), 1.27 (d, J = 6.4 Hz, 3H).

¹⁹F NMR (471 MHz, CDCl₃) δ -62.89.

¹³C NMR (126 MHz, CDCl₃) δ 193.2, 157.2, 144.2, 138.3, 133.4, 131.9, 130.4 (q, ⁴ $J_{C,F}$ = 34 Hz), 129.1 (q, ³ $J_{C,F}$ = 4 Hz), 128.8 (d, ² $J_{C,F}$ = 80 Hz) 128.7 (2C), 128.2 (2C), 128.1, 122.7 (q, ¹ $J_{C,F}$ = 273 Hz), 122.2 (d, ³ $J_{C,F}$ = 4 Hz), 39.4, 35.2, 20.4.

HRMS (ESI): m/z calculated for [C₁₉H₁₆F₃NO₃Na]⁺ [M+Na]⁺: 386.0979; found: 386.0974.

Synthesis of (*S,E*)-5-(2,4-dinitrophenyl)-4-methyl-2-phenylpent-2-enal [(-)-**3s**]



Synthesized according to the general procedure A using phenylpent-2-enal **1a** (0.6 mmol, 96 mg, 3 equiv.), 1-(chloromethyl)-2,4-dinitrobenzene (52.2 mg, 0.2 mmol), aminocatalyst **B** (0.04 mmol, 25.6 mg, 0.2 equiv.), dithiocarbamate catalyst **G** (0.04 mmol, 12.4 mg, 0.2 equiv.) and 2,6-lutidine (0.24 mmol, 25.5 μ L, 1.2 equiv.). The crude mixture was purified by flash column chromatography on silica gel (eluent: hexane/EtOAc 8:2) to afford product **3s** (34.7 mg, 51% yield) as an orange oil. The enantiomeric excess of the product was determined to be 76:24 by UPC² analysis on a Daicel Chiralpak IC column (eluent: 90:10 CO₂/IPA; flow rate 1.00 mL/min, λ = 255 nm. τ Major = 5.36 min, τ Minor = 5.38 min.

$[\alpha]_D^{20} = -91.1$ (c = 0.5 g/100 mL, CHCl₃)

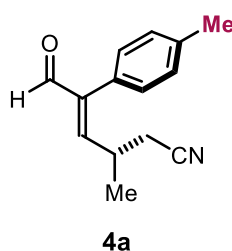
¹H NMR (500 MHz, CDCl₃) δ 9.58 (s, 1H), 8.67 (d, *J* = 2.3 Hz, 1H), 8.25 (dd, *J* = 8.5, 2.4 Hz, 1H), 7.38 – 7.22 (m, 5H), 6.77 – 6.71 (m, 2H), 6.50 (d, *J* = 10.2 Hz, 1H), 3.22 (1/2 ABq, *J* = 12.7, 4.7 Hz, 1H), 3.18 – 3.10 (m, 1H), 3.07 (1/2 ABq, *J* = 12.7, 9.0 Hz, 1H), 1.29 (d, *J* = 6.4 Hz, 3H).

¹³C NMR (126 MHz, CDCl₃) δ 193.0, 156.6, 149.2, 146.6, 144.2, 141.2, 133.7, 131.9, 128.7 (2C), 128.3 (2C), 128.2, 126.6, 120.3, 39.4, 35.1, 20.5.

HRMS (ESI): *m/z* calculated for [C₁₈H₁₆N₂O₅Na]⁺ [M+Na]⁺: 363.0957; found: 363.0961.

Enal Scope

Synthesis of (*S,E*)-3-methyl-6-oxo-5-(*p*-tolyl)hex-4-enenitrile [(+)-4a]



Synthesized according to the general procedure A using (*E*)-2-(*p*-tolyl)pent-2-enal **A** (0.6 mmol, 104 mg, 3 equiv.), α-chloroacetonitrile **2a** (0.2 mmol, 12.6 μL), aminocatalyst **B** (0.04 mmol, 25.6 mg, 0.2 equiv.), dithiocarbamate catalyst **G** (0.04 mmol, 12.4 mg, 0.2 equiv.) and 2,6-lutidine (0.24 mmol, 25.5 μL, 1.2 equiv.). The crude mixture was purified by flash column chromatography on silica gel (eluent: hexane/EtOAc 9:1) to afford

product **4a** (17.1 mg, 40% yield) as a colorless oil. The enantiomeric excess of the product was determined to be 80:20 by UPC² analysis on a Daicel Chiralpak IC column (eluent: 90:10 CO₂/IPA; flow rate 1.00 mL/min, λ = 250 nm. τ_{Minor} = 4.02 min, τ_{Major} = 4.18 min.

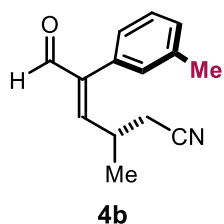
[α]_D²⁰ = +45.0 (c = 0.5 g/100 mL, CHCl₃)

¹H NMR (500 MHz, CDCl₃) δ 9.66 (s, 1H), 7.25 (d, *J* = 7.7 Hz, 2H), 7.05 (d, *J* = 8.1 Hz, 2H), 6.51 (d, *J* = 10.3 Hz, 1H), 3.14 – 3.01 (m, 1H), 2.44 (d, *J* = 6.3 Hz, 2H), 2.40 (s, 3H), 1.28 (d, *J* = 6.7 Hz, 3H).

¹³C NMR (126 MHz, CDCl₃) δ 193.3, 153.8, 144.6, 138.4, 129.4 (2C), 128.9 (3C), 117.4, 30.6, 24.1, 21.3, 19.7.

HRMS (ESI): *m/z* calculated for [C₁₄H₁₅NONa]⁺ [M+Na]⁺: 236.1051; found: 236.1046.

Synthesis of (*R,E*)-3-methyl-6-oxo-5-(*m*-tolyl)hex-4-enenitrile [(-)-4b]



Synthesized according to the general procedure A using (*E*)-2-(*m*-tolyl)pent-2-enal **B** (0.6 mmol, 104 mg, 3 equiv.), α-chloroacetonitrile **2a** (0.2 mmol, 12.6 μL), aminocatalyst **B** (0.04 mmol, 25.6 mg, 0.2 equiv.), dithiocarbamate catalyst **G** (0.04 mmol, 12.4 mg, 0.2 equiv.) and 2,6-lutidine (0.24 mmol, 25.5 μL, 1.2 equiv.). The crude mixture was purified by flash column chromatography on silica gel (eluent:

hexane/EtOAc 9:1) to afford product **4b** (13.6 mg, 40% yield) as a colorless oil. The

enantiomeric excess of the product was determined to be 80:20 by UPC² analysis on a Daicel Chiralpak IC column (eluent: 90:10 CO₂/MeCN; flow rate 1.00 mL/min, λ = 225 nm. τ_{Minor} = 3.08 min, τ_{Major} = 3.20 min.

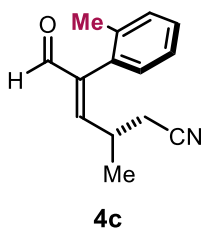
[α]_D²⁰ = -19.7 (c = 0.5 g/100 mL, CHCl₃)

¹H NMR (500 MHz, CDCl₃) δ 9.66 (s, 1H), 7.37 – 7.31 (m, 1H), 7.24 – 7.20 (m, 1H), 6.98 – 6.92 (m, 2H), 6.52 (d, *J* = 10.3 Hz, 1H), 3.11 – 2.99 (m, 1H), 2.45 (d, *J* = 6.3 Hz, 2H), 2.42 – 2.36 (m, 3H), 1.29 (d, *J* = 6.7 Hz, 3H).

¹³C NMR (126 MHz, CDCl₃) δ 193.1, 153.8, 144.9, 138.4, 131.9, 129.6, 129.3, 128.5, 126.7, 126.0, 117.4, 30.6, 24.1, 19.7.

HRMS (ESI): *m/z* calculated for [C₁₄H₁₅NONa]⁺ [M+Na]⁺: 236.1051; found: 236.1041.

Synthesis of (*R,E*)- 3-methyl-6-oxo-5-(*o*-tolyl)hex-4-enitrile [(+ *o* -)-5fa]



Synthesized according to the general procedure A using (*E*)-2-(*o*-tolyl)pent-2-enal **C** (0.6 mmol, 104 mg, 3 equiv.), α-chloroacetonitrile **2a** (0.2 mmol, 12.6 μL), aminocatalyst **B** (0.04 mmol, 25.6 mg, 0.2 equiv.), dithiocarbamate catalyst **G** (0.04 mmol, 12.4 mg, 0.2 equiv.) and 2,6-lutidine (0.24 mmol, 25.5 μL, 1.2 equiv.). The crude mixture was purified by flash column chromatography on silica gel (eluent:

hexane/EtOAc 9:1) to afford product **4c** as a mixture 1:1 of the two rotamers (21.3 mg, 50% yield) as a colorless oil. The enantiomeric excess of the product was determined to be 80:20 for both rotamers by UPC² analysis on a Daicel Chiralpak IC column (eluent: 90:10 CO₂/MeCN; flow rate 1.00 mL/min, λ = 225 nm. τ_{Minor_{rot1}} = 3.21 min, τ_{Major_{rot1}} = 3.38 min; τ_{Minor_{rot2}} = 3.71 min, τ_{Major_{rot2}} = 3.89 min.

[α]_D²⁰ = -44.1 (c = 0.5 g/100 mL, CHCl₃)

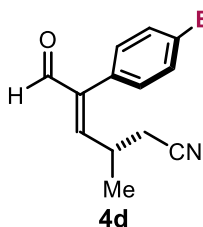
¹H NMR (500 MHz, CDCl₃, 25 °C) δ 9.70 – 9.66 (m, 1H_{rot1} + 1H_{rot2}), 7.35 – 7.17 (m, 3H_{rot1} + 3H_{rot2}), 7.02 (d, *J* = 7.4 Hz, 1H_{rot1}), 6.94 (d, *J* = 7.5 Hz, 1H_{rot2}), 6.69 – 6.63 (m, 1H_{rot1} + 1H_{rot2}), 2.85 – 2.74 (m, 1H_{rot1} + 1H_{rot2}), 2.45 (d, *J* = 6.3 Hz, 2H_{rot1}), 2.39 (d, *J* = 6.3 Hz, 2H_{rot2}), 2.16 (s, 3H_{rot1}), 2.12 (s, 3H_{rot2}), 1.28 (d, *J* = 6.8 Hz, 3H_{rot1}), 1.20 (d, *J* = 6.7 Hz, 3H_{rot2}).

¹H NMR (500 MHz, CDCl₃, 60 °C) δ 9.67 (s, 1H), 7.33 – 7.27 (m, 2H), 7.26 – 7.18 (m, 1H), 7.03 – 6.93 (m, 1H), 6.63 (d, *J* = 9.9 Hz, 1H), 2.86 – 2.74 (m, 1H), 2.44 – 2.36 (m, 2H), 2.15 (s, 3H), 1.29 – 1.19 (m, 3H).

¹³C NMR (101 MHz, CDCl₃) [signals of both rotamers] δ 192.7, 192.6, 154.3, 154.2, 145.5 (2C), 136.4, 136.1, 132.0 (2C), 130.5, 130.3, 129.2, 129.0, 128.8 (2C) 126.1, 126.0, 117.4 (2C), 31.0, 30.9, 24.1, 23.7, 19.9, 19.8, 19.7, 19.6.

HRMS (ESI): *m/z* calculated for [C₁₄H₁₅NOH]⁺ [M+H]⁺: 214.1231; found: 214.1224.

Synthesis of (*R,E*)-5-(4-methoxyphenyl)-3-methyl-6-oxohex-4-enenitrile [(-)-**4d**]



Synthesized according to the general procedure A using (*E*)-2-(4-methoxyphenyl)pent-2-enal **D** (0.6 mmol, 114 mg, 3 equiv.), α -chloroacetonitrile **2a** (0.2 mmol, 12.6 μ L), aminocatalyst **B** (0.04 mmol, 25.6 mg, 0.2 equiv.), dithiocarbamate catalyst **G** (0.04 mmol, 12.4 mg, 0.2 equiv.) and 2,6-lutidine (0.24 mmol, 25.5 μ L, 1.2 equiv.).

The crude mixture was purified by flash column chromatography on silica gel (eluent: hexane/EtOAc 7:3) to afford product **4d** (28.4 mg, 62% yield) as a colorless oil. The enantiomeric excess of the product was determined to be 80:20 by UPC² analysis on a Daicel Chiralpak IC column (eluent: 85:15 CO₂/IPA; flow rate 1.00 mL/min, λ = 250 nm. τ_{Minor} = 4.30 min, τ_{Major} = 4.47 min.

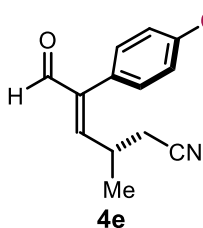
$[\alpha]_{\text{D}}^{20}$ = -96.1 (c = 0.5 g/100 mL, CHCl₃)

¹H NMR (500 MHz, CDCl₃) δ 9.66 (s, 1H), 7.10 (d, *J* = 8.7 Hz, 2H), 6.98 (d, *J* = 8.7 Hz, 2H), 6.49 (d, *J* = 10.3 Hz, 1H), 3.85 (s, 3H), 3.15 – 3.05 (m, 1H), 2.45 (d, *J* = 6.3 Hz, 2H), 1.29 (d, *J* = 6.8 Hz, 3H).

¹³C NMR (126 MHz, CDCl₃) δ 193.4, 159.7, 153.8, 144.2, 130.3 (2C), 123.9, 117.4, 114.2 (2C), 55.3, 30.7, 24.1, 19.7.

HRMS (ESI): *m/z* calculated for [C₁₄H₁₅NO₂Na]⁺ [M+Na]⁺: 252.1000; found: 252.0995.

Synthesis of (*S,E*)-5-(4-bromophenyl)-3-methyl-6-oxohex-4-enenitrile [(-)-**4e**]



Synthesized according to the general procedure A using (*E*)-2-(4-bromophenyl)pent-2-enal **E** (0.6 mmol, 143 mg, 3 equiv.), α -chloroacetonitrile **2a** (0.2 mmol, 12.6 μ L), aminocatalyst **B** (0.04 mmol, 25.6 mg, 0.2 equiv.), dithiocarbamate catalyst **G** (0.04 mmol, 12.4 mg, 0.2 equiv.) and 2,6-lutidine (0.24 mmol, 25.5 μ L, 1.2 equiv.). The crude mixture was purified by flash column

chromatography on silica gel (eluent: hexane/EtOAc 8:2) to afford product **4e** (20.0 mg, 36% yield) as a colorless oil. The enantiomeric excess of the product was determined to be 82:18 by UPC² analysis on a Daicel Chiralpak IC column (eluent: 80:20 CO₂/IPA; flow rate 1.00 mL/min, λ = 250 nm. τ_{Minor} = 4.09 min, τ_{Major} = 4.29 min.

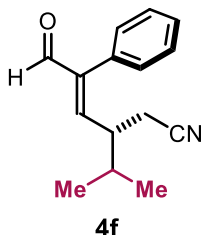
$[\alpha]_{\text{D}}^{20}$ = -33.9 (c = 0.5 g/100 mL, CHCl₃)

¹H NMR (500 MHz, CDCl₃) δ 9.66 (s, 1H), 7.59 (d, *J* = 8.2 Hz, 2H), 7.05 (d, *J* = 8.3 Hz, 2H), 6.56 (d, *J* = 10.4 Hz, 1H), 3.13 – 2.93 (m, 1H), 2.46 (d, *J* = 6.0 Hz, 2H), 1.28 (d, *J* = 6.7 Hz, 3H).

¹³C NMR (126 MHz, CDCl₃) δ 192.5, 154.4, 143.8, 131.9 (2C), 130.8 (2C), 130.7, 123.0, 117.2, 30.8, 24.1, 19.7.

HRMS (ESI): m/z calculated for $[C_{13}H_{12}BrNONa]^+ [M+Na]^+$: 299.9999; found: 299.9987.

Synthesis of (*S,E*)-3-isopropyl-6-oxo-5-phenylhex-4-enenitrile [(+)-**4f**]



Synthesized according to the general procedure A using (*E*)-5-methyl-2-phenylhex-2-enal (0.6 mmol, 113 mg, 3 equiv.), α -chloroacetonitrile **2a** (0.2 mmol, 12.6 μ L), aminocatalyst **B** (0.04 mmol, 25.6 mg, 0.2 equiv.), dithiocarbamate catalyst **G** (0.04 mmol, 12.4 mg, 0.2 equiv.) and 2,6-lutidine (0.24 mmol, 25.5 μ L, 1.2 equiv.). The crude mixture was purified by flash column chromatography on silica gel (eluent: hexane/EtOAc 8:2) to afford product **4f** (19.1 mg, 42% yield) as a colorless oil. The enantiomeric excess of the product was determined to be 79:21 by UPC² analysis on a Daicel Chiralpak IB column (eluent: 90:10 CO₂/MeCN; flow rate 1 mL/min, λ = 320 nm. τ_{Minor} = 2.61 min, τ_{Major} = 2.73 min.

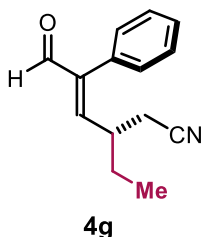
$[\alpha]_D^{20}$ = +35.3 (c = 1 g/100 mL, CHCl₃)

¹H NMR (500 MHz, CDCl₃) δ 9.71 (s, 1H), 7.55 – 7.31 (m, 3H), 7.20 – 7.13 (m, 2H), 6.59 (d, J = 10.8 Hz, 1H), 2.75 – 2.62 (m, 1H), 2.52 – 2.49 (m, 2H), 1.96 – 1.83 (m, 1H), 0.95 (t, J = 7.0 Hz, 6H).

¹³C NMR (126 MHz, CDCl₃) δ 192.9, 152.3, 146.8, 132.1, 129.2 (2C), 128.6 (2C), 128.4, 117.6, 41.7, 31.4, 20.7, 20.1, 19.6.

HRMS (ESI): m/z calculated for $[C_{15}H_{17}NONa]^+ [M+Na]^+$: 250.1208; found: 250.1202.

Synthesis of (*S,E*)-3-ethyl-6-oxo-5-phenylhex-4-enenitrile [(+)-**4g**]



Synthesized according to the general procedure A using (*E*)-2-phenylhex-2-enal **F** (0.6 mmol, 104 mg, 3 equiv.), α -chloroacetonitrile **2a** (0.2 mmol, 12.6 μ L), aminocatalyst **B** (0.04 mmol, 25.6 mg, 0.2 equiv.), dithiocarbamate catalyst **G** (0.04 mmol, 12.4 mg, 0.2 equiv.) and 2,6-lutidine (0.24 mmol, 25.5 μ L, 1.2 equiv.). The crude mixture was purified by flash column chromatography on silica gel (eluent: hexane/EtOAc 8:2) to afford product **4g** (12.8 mg, 30% yield) as a colorless oil. The enantiomeric excess of the product was determined to be 79:21 by UPC² analysis on a Daicel Chiralpak IB column (eluent: 90:10 CO₂/MeCN; flow rate 1.00 mL/min, λ = 250 nm. τ_{Minor} = 2.50 min, τ_{Major} = 2.59 min.

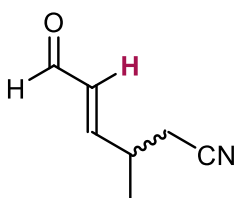
$[\alpha]_D^{20}$ = +12.1 (c = 0.5 g/100 mL, CHCl₃)

¹H NMR (500 MHz, CDCl₃) δ 9.70 (s, 1H), 7.48 – 7.38 (m, 3H), 7.20 – 7.13 (m, 2H), 6.51 (d, J = 10.6 Hz, 1H), 2.89 – 2.77 (m, 1H), 2.47 (d, J = 6.2 Hz, 2H), 1.75 – 1.59 (m, 2H), 0.92 (t, J = 7.4 Hz, 3H).

$^{13}\text{C NMR}$ (126 MHz, CDCl_3) δ 192.89, 153.20, 146.22, 132.00, 129.08, 128.55, 128.38, 117.38, 37.03, 27.08, 22.29, 11.39.

HRMS (ESI): m/z calculated for $[\text{C}_{14}\text{H}_{15}\text{NOH}]^+$ $[\text{M}+\text{H}]^+$: 214.1226; found: 214.1226.

Synthesis of Rac-(E)-6-methyl-3-(4-oxobut-2-en-2-yl)hept-5-enitrile [4h]



4h

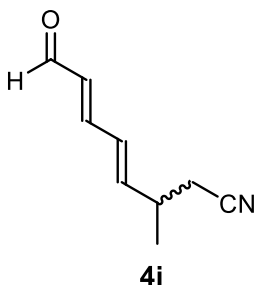
Synthesized according to the general procedure A using *trans*-2-Pentenal (0.6 mmol, 50.5 mg, 3 equiv.), α -chloroacetonitrile **2a** (0.2 mmol, 12.6 μL), aminocatalyst **D** (0.04 mmol, 25.6 mg, 0.2 equiv.), dithiocarbamate catalyst **G** (0.04 mmol, 12.4 mg, 0.2 equiv.) and 2,6-lutidine (0.24 mmol, 25.5 μL , 1.2 equiv.). The crude mixture was purified by flash column chromatography on silica gel (eluent: hexane/EtOAc 7:3) to afford product **4h** (14.5 mg, 59% yield) as a colorless oil.

$^1\text{H NMR}$ (500 MHz, CDCl_3) δ 9.56 (d, $J = 7.6$ Hz, 1H), 6.76 (dd, $J = 15.8, 6.9$ Hz, 1H), 6.18 (ddd, $J = 15.8, 7.6, 1.3$ Hz, 1H), 2.89 (m, 1H), 2.51 (dd, $J = 6.5, 1.4$ Hz, 2H), 1.31 (d, $J = 6.8$ Hz, 3H).

$^{13}\text{C NMR}$ (126 MHz, CDCl_3) δ 193.15, 156.78, 132.66, 117.27, 33.44, 23.64, 18.63.

HRMS (ESI): m/z calculated for $[\text{C}_7\text{H}_{10}\text{NO}]^+$ $[\text{M}+\text{H}]^+$: 124.0762; found: 124.0757.

Synthesis of Rac-(4E,6E)-3-methyl-8-oxoocta-4,6-dienitrile



4i

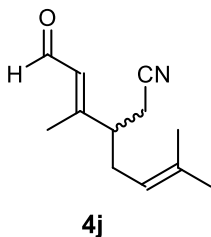
Synthesized according to the general procedure A using 2,4-Heptadienal (0.6 mmol, 66 mg, 3 equiv.), α -chloroacetonitrile **2a** (0.2 mmol, 12.6 μL), aminocatalyst **D** (0.04 mmol, 25.6 mg, 0.2 equiv.), dithiocarbamate catalyst **G** (0.04 mmol, 12.4 mg, 0.2 equiv.) and 2,6-lutidine (0.24 mmol, 25.5 μL , 1.2 equiv.). The crude mixture was purified by flash column chromatography on silica gel (eluent: hexane/EtOAc 85:15) to afford product **4i** (13 mg, 43% yield) as a colorless oil.

$^1\text{H NMR}$ (500 MHz, CDCl_3) δ 9.57 (d, $J = 7.9$ Hz, 1H), 7.13 – 7.02 (m, 1H), 6.47 – 6.34 (m, 1H), 6.17 (dt, $J = 15.2, 7.5$ Hz, 2H), 2.77 (m, 1H), 2.45 (d, $J = 6.5$ Hz, 2H), 1.27 (d, $J = 6.8$ Hz, 3H).

$^{13}\text{C NMR}$ (126 MHz, CDCl_3) δ 193.52, 150.82, 145.63, 132.03, 129.00, 117.67, 33.97, 24.28, 19.15.

HRMS (ESI): m/z calculated for $[\text{C}_9\text{H}_{10}\text{NO}]^+$ $[\text{M}]^+$: 148.0762; found: 148.0757.

Synthesis of Rac-(E)-6-methyl-3-(4-oxobut-2-en-2-yl)hept-5-enitrile [4j]



Synthesized according to the general procedure A using *Citral* (0.6 mmol, 91 mg, 3 equiv.), α -chloroacetonitrile **2a** (0.2 mmol, 12.6 μ L), aminocatalyst **D** (0.04 mmol, 25.6 mg, 0.2 equiv.), dithiocarbamate catalyst **G** (0.04 mmol, 12.4 mg, 0.2 equiv.) and 2,6-lutidine (0.24 mmol, 25.5 μ L, 1.2 equiv.). The crude mixture was purified by flash column chromatography on silica gel (eluent: hexane/EtOAc 8:2) to afford product **4g** (21 mg, 55% yield) as a yellowish oil.

¹H NMR (500 MHz, CDCl₃) δ 10.04 (d, J = 7.5 Hz, 1H), 5.92 (d, J = 7.5 Hz, 1H), 5.00 – 4.94 (m, 1H), 2.62 – 2.41 (m, 3H), 2.29 (t, J = 6.9 Hz, 2H), 2.19 (d, J = 1.2 Hz, 3H), 1.70 (s, 3H), 1.62 (s, 3H).

¹³C NMR (126 MHz, CDCl₃) δ 190.79, 160.77, 136.13, 128.59, 119.21, 117.92, 45.90, 31.09, 25.90, 20.78, 18.11, 15.57.

HRMS (ESI): m/z calculated for [C₁₅H₁₇NONa]⁺ [M+Na]⁺: 146.0581; found: 146.0585.

3.8.5. Scaled up reaction

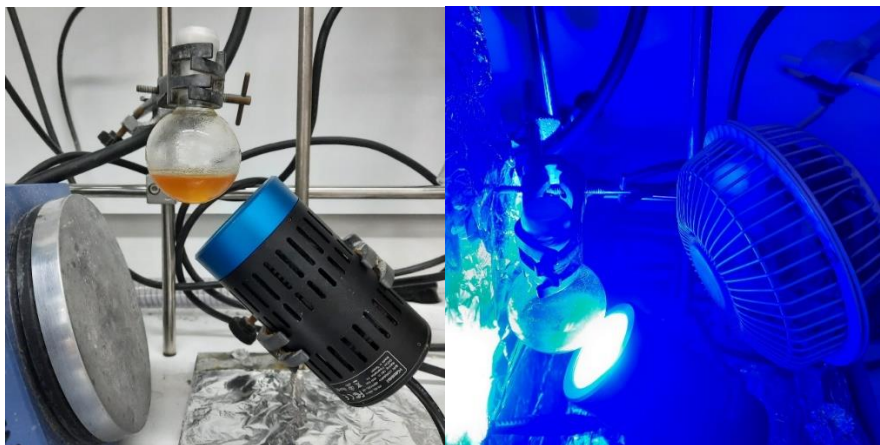


Figure 3.29: Setup used for the Scaled-Up reaction

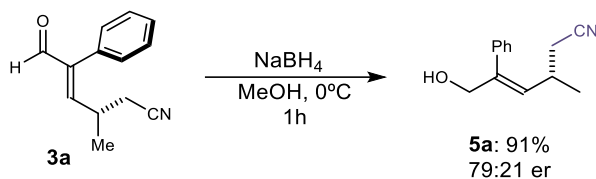
The experimental setup for the scaled-up reaction consisted of 50ml round bottom flask placed on a stirring plate. The light source was provided by a 456nm Kessil Lamp placed under the reactor; to avoid over heating the reactor was cooled using a cooling fan placed on the side of the reactor as illustrated in figure S6.

General Procedure

In a 50ml round-bottom flask charged with a stirring bar were added sequentially the aminocatalyst **B** (1 mmol, 640 mg, 0.2 eq.), THF (3.5 mL) and phenylpent-2-enal **1a** (15 mmol, 2.40 mL, 3 eq.). The reaction was stirred for 5 minutes before the addition of 2,6-Lutidine (6 mmol, 395 μ L, 1.2 eq.) and Chloroacetonitrile **2a** (5 mmol, 317 μ L, 1 eq.). Finally, Dithiocarbamate **G** (1 mmol, 310 mg, 0.2 eq.) was added and the reactor was closed with a rubber septum. The solution was degassed through Ar bubbling for 5 minutes while stirring and then the reactor capped with a septum and sealed with parafilm. A 456nm Kessil Lamp was placed approximately 3 cm from the reactor and switched on at 100% intensity. The solution was irradiated under vigorous stirring overnight. After 20 hours the lamp was turned off and the solvent was removed through rotary evaporation. The product was purified by flash column chromatography on silica gel (eluent: hexane/EtOAc 8:2) to afford the product **5a** as a pale-orange oil in a 67% yield (average yield on 2 different runs). The enantiomeric excess of the product was determined to be 80:20 by UPC² analysis on a Daicel Chiralpak IA-3 column (eluent: CO₂/IPA = 90:10; flow rate 1 mL/min, λ = 300 nm. τ Major = 3.54 min, τ Minor = 3.66 min.

3.8.6. Product derivatization

Aldehyde Reduction



In a 10 mL round bottom flask charged with a magnetic stirring bar the substrate **3a** (60.0 mg, 0.3 mmol) was dissolved in MeOH (0.5M). The solution was placed in an ice bath and cooled to 0°C before the addition of NaBH₄ (34.0 mg, 0.9 mmol). The reaction was stirred at 0°C for 1 hour and then removed from the ice bath. Distilled water (2ml) was then slowly added to the solution while stirring. The organic phase was extracted two times with EtOAc and dried over anhydrous Magnesium Sulfate. After filtration, the solution was concentrated under vacuum to afford the title compound **5a** in 91% yield as pale-yellow oil. The enantiomeric excess of the product was determined to be 79:21 by UPC² analysis on a Daicel Chiralpak IA-3 column (eluent: 80:20 CO₂/IPA; flow rate 1.00 mL/min, λ = 220 nm. τ Major = 3.54 min, τ Minor = 3.66 min.

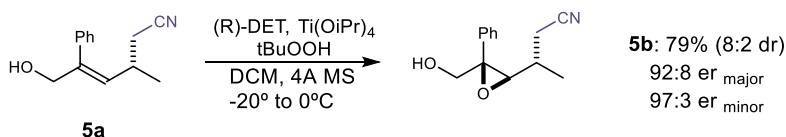
$$[\alpha]_{\text{D}}^{20} = -17.2 \text{ (c = 0.5 g/100 mL, CHCl}_3\text{)}$$

¹H NMR (500 MHz, CDCl₃) δ 7.39 (m, 2H), 7.33 (m, 1H), 7.19 (m, 2H), 5.58 (d, J = 10.1 Hz, 1H), 4.31 (d, J = 1.4 Hz, 2H), 2.65 (m, 1H), 2.27 (d, J = 6.6 Hz, 2H), 1.13 (d, J = 6.7 Hz, 3H).

¹³C NMR (101 MHz, CDCl₃) δ 142.79, 137.92, 129.19, 128.87, 128.53, 127.90, 118.60, 67.60, 30.15, 25.17, 20.80

HRMS (ESI): m/z calculated for [C₁₄H₁₆NO]⁺ [M+H]⁺: 202,1232; found: 202,1226.

Sharpless Epoxidation



Diethyl L-(+)-tartrate (7.9 μL, 0.046 mmol) and titanium tetraisopropoxide (12 μL, 0.04 mmol) were added sequentially to a mixture of powdered activated 4 Å molecular sieves and dichloromethane (200 mL) at 0 °C with stirring. The reaction mixture was cooled to -20 °C, tert-butyl hydroperoxide (6 M in hexane, 87 μL, 0.520 mmol) was added dropwise over 0.2 h, and the resulting mixture was stirred at -20 °C for 1 h. A 1.1M solution of **5a** (40.25 mg, 0.200 mmol) in dry DCM was then added dropwise over 0.2 h. After stirring for 15 h at -20 °C, the reaction mixture was poured into 7ml of a freshly prepared ferrous sulfate solution (66 g of FeSO₄ · 7H₂O and 22 g of citric acid in 200 mL of H₂O) at -20 °C and stirred for 1 h. The organic layer was separated, and the aqueous layer was extracted with Et₂O. The combined organic layer was dried, filtered, and concentrated in vacuo. To the residue in Et₂O (300 mL) was added 30% NaOH (3 mL), and the resultant mixture was stirred at 0 °C for 1 h. The two phases were separated, and the aqueous phase was extracted twice with Et₂O. The combined organic phases were washed with brine, dried, filtered, and then concentrated in vacuo. The product was purified by Flash Chromatography on silica gel (7:3 Hex:EtOAc) to afford the title compound **5b** as a colorless oil in 79% yield (8:2 mixture of both diastereoisomers). The enantiomeric excess of the two diastereoisomers of the product was determined to be 97:3 and 92:8 by UPC² analysis on a Daicel Chiralpak IE column (eluent: 80:20 CO₂/IPA; flow rate 1.00 mL/min, λ = 250 nm τ_{Major}^{dias1} = 4.13 min, τ_{Minor}^{dias1} = 4.06 min; τ_{Minor}^{dias2} = 4.32 min, τ_{Major}^{dias2} = 4.40 min.

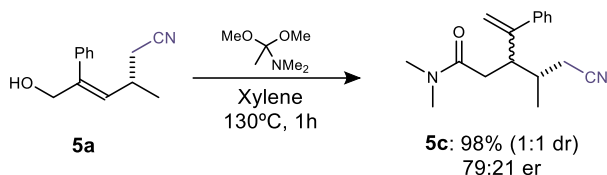
[α]_D²⁰ = +40.9 (c = 0.5 g/100 mL, CHCl₃)

¹H NMR (500 MHz, CDCl₃) δ 7.40 – 7.32 (m, 10H *diast1* + *diast2*), 4.00 (d, J = 1.7 Hz, 1H *diast1*), 3.97 (d, J = 1.3 Hz, 1H *diast2*), 3.26 (m, 4H *diast1* + *diast2*) 1.43 – 1.24 (m, 2H *diast1* + *diast2*) 1.21 (d, J = 6.7 Hz, 3H *diast1*), 1.00 (d, J = 6.9 Hz, 3H *diast2*).

¹³C NMR (126 MHz, CDCl₃) δ 134.78, 134.75, 128.92, 128.59, 128.56, 128.34, 126.66, 126.55, 117.90, 117.50, 67.55, 66.88, 66.63, 64.13, 63.65, 63.13, 29.97, 29.02, 22.12, 20.75, 17.05, 15.00.

HRMS (ESI): m/z calculated for [C₂₀H₂₃N₂] [M+H]⁺: 291.1861; found: 291.1856

Eshenmoser-Claisen Rearrangement



In an oven dried Shlenk tube charged with a magnetic stirring bar, the aldehyde **5aa** (2 eq.) was dissolved in Xylene (0.3M). *N,N*-dimethylacetamide dimethyl acetal (3 eq.) was subsequently added and the solution was then stirred for 1 hour at 130°C . After the indicated time the starting material was totally consumed (checked by TLC) and the reaction was removed from the oil bath. After the reaction cooled down the solution was concentrated through rotary evaporation and the product was purified by Flash Chromatography on silica gel (1:1 Hex:EtOAc) to afford the title compound **5c** as a brownish oil in quantitative yield. The enantiomeric excess of the product was determined to be 79:21 by UPC² analysis on a Daicel Chiralpak IE column (eluent: 90:10 CO_2/EtOH ; flow rate 1.00 mL/min, $\lambda = 250$ nm. $\tau_{\text{Major}}^{\text{dias1}} = 6.85$ min, $\tau_{\text{Minor}}^{\text{dias1}} = 7.12$ min; $\tau_{\text{Minor}}^{\text{dias2}} = 7.84$ min, $\tau_{\text{Major}}^{\text{dias2}} = 8.35$ min.

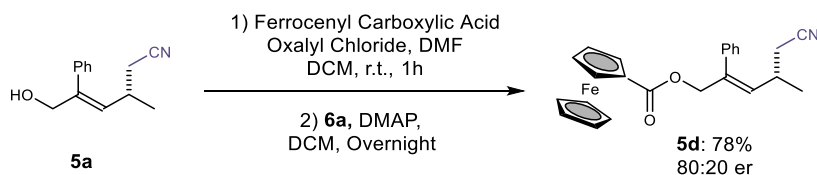
$[\alpha]_{\text{D}}^{20} = -88.3$ ($c = 0.5$ g/100 mL, CHCl_3)

¹H NMR (500 MHz, CDCl_3) δ 7.48 (m, 4H *diast1* + *diast2*), 7.34 (m, 6H *diast1* + *diast2*), 5.38 (s, 1H, *diast1*), 5.34 (s, 1H, *diast2*), 5.06 (s, 1H, *diast1*), 4.99 (s, 1H, *diast2*), 3.47 (m, 1H, *diast2*), 3.37 (m, 1H, *diast1*), 3.07 (s, 3H, *diast2*), 3.03 (s, 3H, *diast1*), 2.97 (s, 3H, *diast2*), 2.94 (s, 3H, *diast1*), 2.80-2.65 (m, 2H *diast1* + *diast2*), 2.60-2.00 (m, 8H *diast1* + *diast2*), 1.13 (d, $J = 6.7$ Hz, 3H, *diast2*), 1.09 (d, $J = 6.8$ Hz, 3H, *diast1*).

¹³C NMR (126 MHz, CDCl_3) δ 171.09, 170.99, 150.88, 150.19, 142.76, 142.39, 128.56, 128.53, 127.80, 126.89, 126.88, 119.26, 119.16, 113.72, 113.65, 44.48, 44.13, 37.39, 37.35, 35.69, 34.45, 34.26, 33.90, 33.37, 22.97, 22.00, 17.17, 16.98.

HRMS (ESI): m/z calculated for $[\text{C}_{17}\text{H}_{23}\text{N}_2\text{O}]$ $[\text{M}+\text{H}]^+$: 271.1810; found: 271.1805

Esterification



To a suspension of ferrocenecarboxylic acid (104 mg, 0.450 mmol) in DCM (1 mL) were added oxalyl chloride (0.036 mL, 0.420 mmol) and three drops of dry DMF at 0 C. After the gas evolution ceased and the reaction mixture turned into a clear solution, it was stirred for 0.5 h at rt. Next, a solution of **5a** (65 mg, 0.32 mmol) and DMAP (106 mg, 0.870 mmol) in

DCM (1 mL) was added and the reaction mixture was stirred for 16 h at rt. The reaction mixture was quenched by adding a small amount of silica gel and concentrating to dryness. The crude product was purified by flash chromatography on silica gel (70:30 Hexane:EtOAc) to afford the title product **5d** as an orange oil in 78% yield. The enantiomeric excess of the product was determined to be 79:21 by UPC² analysis on a Daicel Chiralpak IB column (eluent: 85:15 CO₂/MeCN; flow rate 1.00 mL/min, $\lambda = 250$ nm. $\tau_{\text{Minor}} = 3.47$ min, $\tau_{\text{Major}} = 3.67$ min.

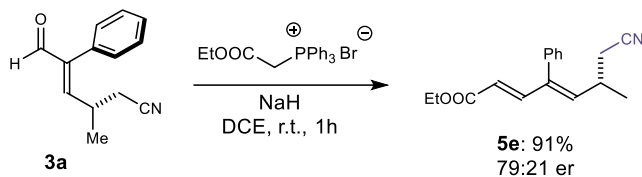
$[\alpha]_{\text{D}}^{20} = -54.7$ ($c = 0.5$ g/100 mL, CHCl₃)

¹H NMR (500 MHz, CDCl₃) δ 7.42 (m, 2H), 7.34 (m, 1H), 7.28 (m, 2H), 5.69 (d, $J = 10.2$ Hz, 1H), 4.89 (qd, $J = 13.0, 1.1$ Hz, 2H), 4.74 (bs, 2H), 4.28 (bs, 2H), 2.72 (m, 1H), 2.31 (d, $J = 6.5$ Hz, 2H), 1.16 (d, $J = 6.7$ Hz, 3H)

¹³C NMR (101 MHz, CDCl₃) δ 171.40, 138.57, 137.60, 132.30, 128.75, 128.45, 127.95, 118.29, 71.62, 70.35, 69.98, 68.12, 30.18, 24.97, 20.55

HRMS (ESI): m/z calculated for [C₂₄H₂₃NNaO₂Fe]⁺ [M+Na]⁺: 436.0975; found: 436.0970

Wittig Olefination



In an oven dried Shlenk tube the Wittig reagent (2 eq.) was dissolved in DCE (0.1M respect to the substrate). Sodium Hydride (2.2 eq.) was subsequently added to the solution which was then stirred for 10 minutes. The substrate was added and the reaction was stirred 1h. After total consumption of the starting material (checked by TLC) the reaction was quenched with water and the organic phase was extracted twice with EtOAc, dried over anhydrous MgSO₄ and concentrated by rotary evaporation. The product was purified by Flash Chromatography on silica gel (85:15 Hex:EtOAc) to afford the title compound **5e** as a brownish oil in 93% yield. The enantiomeric excess of the product was determined to be 79:21 by UPC² analysis on a Daicel Chiralpak IG column (eluent: 90:10 CO₂/IPA; flow rate 1.00 mL/min, $\lambda = 250$ nm. $\tau_{\text{Minor,rot1}} = 5.31$ min, $\tau_{\text{Major,rot1}} = 4.02$ min.

$[\alpha]_{\text{D}}^{20} = +65.9$ ($c = 0.5$ g/100 mL, CHCl₃)

¹H NMR (500 MHz, CDCl₃) δ 7.47 (d, $J = 15.6$ Hz 1H), 7.41 (m, 2H), 7.36 (m, 1H), 7.11 (m, 2H), 5.92 (d, $J = 10.2$ Hz, 2H), 5.40 (d, $J = 15.6$ Hz, 2H), 4.16 (q, $J = 7.1$ Hz, 2H), 2.59 (m, 1H), 2.29 (d, $J = 6.5$ Hz, 2H), 1.25 (t, $J = 7.1$ Hz, 3H), 1.13 (d, $J = 6.7$ Hz, 3H).

¹³C NMR (101 MHz, CDCl₃) δ 167.03, 147.49, 141.78, 141.40, 135.82, 128.96, 128.88, 128.02, 121.47, 117.97, 60.48, 30.99, 24.56, 20.16, 14.35.

HRMS (ESI): m/z calculated for $[C_{17}H_{19}NO_2Na]^+$ $[M+Na]^+$: 292.1313; found: 292.1883

3.8.7. Determination of the absolute configuration

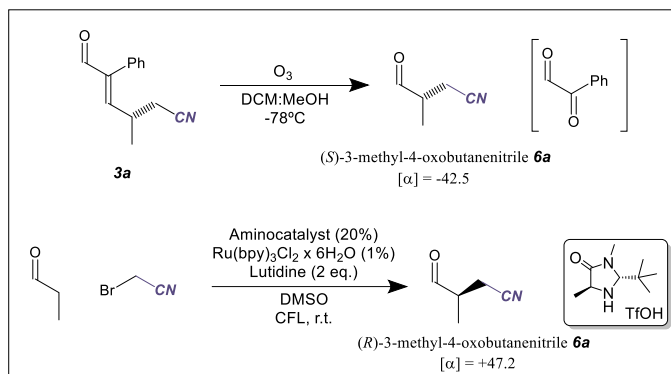


Figure 3.28: Determination of the absolute configuration by correlation.

The absolute configuration was obtained by correlation with known compound. The model product **3a** was subjected to ozonolysis reaction to achieve the corresponding α -branched aldehyde **6a** which optical rotation was measured to be $[\alpha]_D^{20} = -42.5$ ($c = 1$ g/100 mL, $CHCl_3$). The same compound was obtained subjecting Propanal to MacMillan's conditions for the α -cyanomethylation of aldehydes.¹⁵⁸ Although this compound (**6a**) was not synthesized by MacMillan group, the same reaction using Octanal produced the (*R*)-configuration for the same stereocenter. An original sample of **6a** was prepared using MacMillan's conditions; the optical rotation was measured to be $[\alpha]_D^{20} = +47.2$ ($c = 1$ g/100 mL, $CHCl_3$).

We therefore assign the (*S*)-configuration to the stereocenter produced with our protocol. The different nature of the two stereocenters was also corroborated by UPC² analysis as shown by the chromatograms reported below:

¹⁵⁸ Welin, E. R.; Warkentin, A.; Conrad, J. C.; MacMillan, D. W. C. *Angew. Chem. Int. Ed.* **2015**, *54*, 1-6

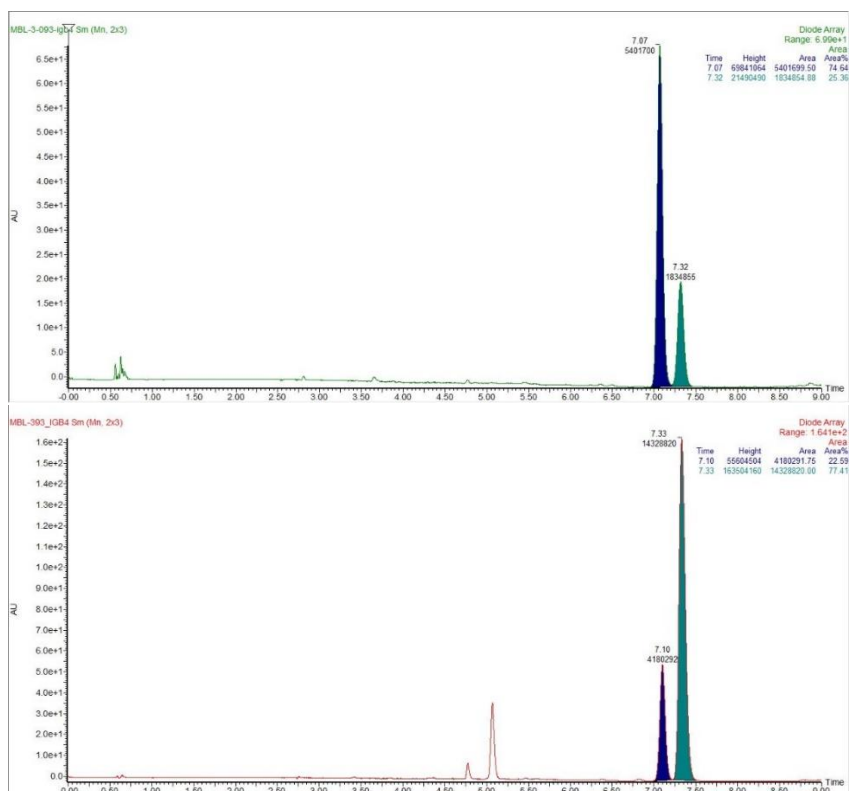


Figure 3.29: Upper Chromatogram: **6f** synthesized through ozonolysis
 Lower Chromatogram: **6f** synthesized through MacMillan protocol

3.8.8. Failed Substrates

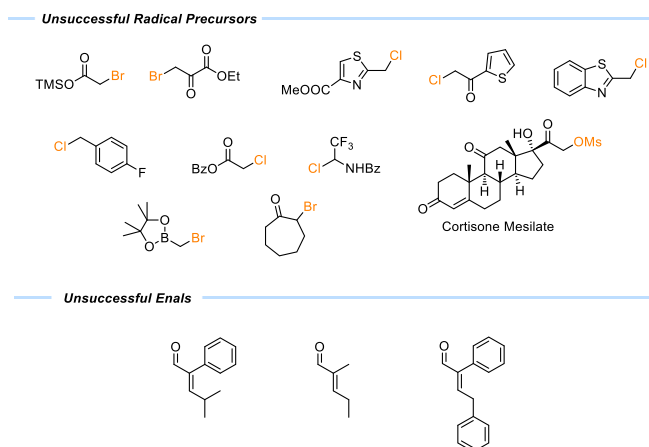


Figure 3.30: Survey of substrates which failed to produce the expected product under our conditions.

UNIVERSITAT ROVIRA I VIRGILI

EXCITATION OF ORGANOCATALYTIC INTERMEDIATES AND APPLICATION IN NEW RADICAL PROCESSES

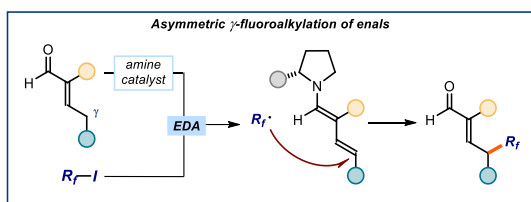
Matteo Balletti

Chapter IV

Asymmetric γ -perfluoroalkylation of α -branched enals driven by the photoactivity of dienamine-based EDA complex

Target

Developing a photochemical radical strategy for the regio- and enantioselective γ -perfluoroalkylation of α -branched enals.



Tool

Exploiting the photophysical properties of extended enamines to form electron donor-acceptor (EDA) complexes with electron-poor perfluoroalkyl iodides. The visible light excitation of such complexes can promote redox events to generate perfluoroalkyl radicals, which are trapped by the chiral dienamines in a regio- and enantio-selective fashion.¹⁵⁹

4.1 Introduction

The introduction of fluorinated groups into pharmacologically active scaffolds dramatically affects the physical and pharmacokinetic properties of a drug molecule.¹⁶⁰ The functionalization of a drug candidate with fluorine or fluoroalkyl motifs provides higher metabolic stability, bioavailability, and increased protein–ligand interactions (Figure 4.1).¹⁶¹ For this reason, methodologies that can supply a straightforward installation of fluoroalkyl groups are useful. The majority of available strategies focuses on the fluoroalkylation of (hetero)aromatic scaffolds by harnessing metal-catalyzed cross-coupling processes.¹⁶² In contrast, the direct installation of such groups into aliphatic sp^3 -carbons is less explored. The

¹⁵⁹ The project discussed in this chapter has been conducted in collaboration with Tommy Wachsmuth, who performed part of the reaction scope and helped with the reaction optimization. I was involved in the discovery of the reaction, its optimization, and evaluation of part of the reaction scope. This work is presently under consideration for publication.

¹⁶⁰ (a) Yale, H. L., "The Trifluoromethyl Group in Medical Chemistry" *J. Med. Chem.* **1958**, *1*, 121–133. (b) Filler, R.; Kobayashi, Y.; Yagupolskii, L. M. (Eds.) "Organofluorine Compounds in Medicinal Chemistry and Biomedical Applications" (Elsevier, 1993).

¹⁶¹ (a) Purser, S.; Moore, P. R.; Swallow, S.; Gouverneur, V. "Fluorine in medicinal chemistry" *Chem. Soc. Rev.*, **2008**, *37*, 320–330. (b) Inoue, M.; Sumii, Y.; Shibata, N. "Contribution of Organofluorine Compounds to Pharmaceuticals" *ACS Omega* **2020**, *5*, 10633–10640. (c) Smart B E. "Fluorine substituent effects on bioactivity" *J. Fluor. Chem.* **2001**, *109*, 3–11. (d) Hagmann W. K. "The many roles for fluorine in medicinal chemistry" *J. Med. Chem.* **2008**, *51*, 4359–4369.

¹⁶² Tomashenko, O. A.; Grushin, V. V. "Aromatic trifluoromethylation with metal complexes" *Chem. Rev.* **2011**, *111*, 4475–4521.

challenge becomes more complex when a precise control over the newly formed stereogenic center is needed.

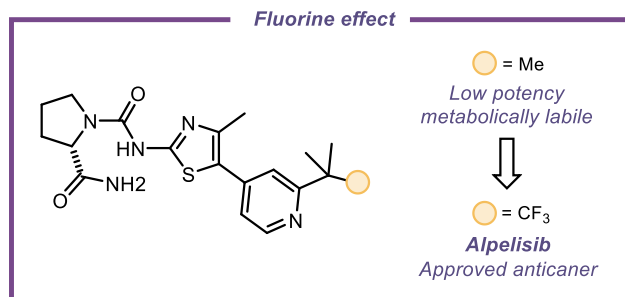


Figure 4.1. Fluorine effect in drug design

Whereas significant steps have been made in the area of nucleophilic 1,2-trifluoromethylation of carbonyl compounds, the enantioselective α -fluoroalkylation of carbonyl-derived enolates (or enolate equivalents) remained elusive for a long time.¹⁶³ Recently, it was possible to tackle this issue successfully by merging the power of radical intermediates with asymmetric organocatalysis. Concomitantly to the advent of photoredox catalysis, radical fluoroalkylation strategies experienced a renaissance due to the mild conditions in which these radicals are generated.¹⁶⁴

For example, it has been shown that organocatalytic chiral enamines can trap photo-generated perfluoroalkyl radicals inferring high levels of enantioselectivity, typical of polar organocatalysis. The group of MacMillan was the first to pioneer this concept by using chiral enamines for the enantioselective capture of fluoroalkyl radicals generated by the action of a photocatalyst (Figure 4.2a).¹⁶⁵ Excitation of the Ru(bpy)₃²⁺ photocatalyst and subsequent reductive quenching generated the highly reducing Ru(bpy)₃⁺ species, which was capable of reducing the perfluoroalkyl iodide **2**. Upon fragmentation, the perfluoroalkyl radical **II** was trapped by the SOMO-philic enamine **4**. The addition of **II** occurred in a stereocontrolled fashion due to the chiral environment provided by the aminocatalyst **3**. The incipient α -amino radical **I** then reduced the excited photocatalyst regenerating the reducing Ru(bpy)₃⁺. Final hydrolysis of the iminium ion **III** delivered the enantioenriched aldehydes **4**, which were

¹⁶³ (a) Yang, X.; Wu, T.; Phipps, R. J.; Toste, F. D.; Advances in Catalytic Enantioselective Fluorination, Mono-, Di-, and Trifluoromethylation, and Trifluoromethylthiolation Reactions *Chem. Rev.* **2015**, *115*, 826–870. (b) Ma, J.; Cahard, D. Update 1 of: Asymmetric Fluorination, Trifluoromethylation, and Perfluoroalkylation Reactions *Chem. Rev.* **2008**, *108*, 9, PR1–PR43. (c) Billard, T. Langlois, B. R. “How to Reach Stereogenic Trifluoromethylated Carbon? En Route to the “Grail” of the Asymmetric Trifluoromethylation Reaction *Eur. J. Org. Chem.* **2007**, 2007, 891–897.

¹⁶⁴ (a) Studer, A. A “Renaissance” in Radical Trifluoromethylation. *Angew. Chem. Int. Ed.* **2012**, *51*, 8950–8958. (b) Chatterjee, T.; Iqbal, N.; You, Y.; Cho, E. J. Controlled Fluoroalkylation Reactions by Visible-Light Photoredox Catalysis. *Acc. Chem. Res.* **2016**, *49*, 2284–2294.

¹⁶⁵ Nagib, D. A.; Scott, N. E.; MacMillan, D.W.C. Enantioselective α -Trifluoromethylation of Aldehydes via Photoredox Organocatalysis *J. Am. Chem. Soc.* **2009**, *131*, 10875–10877.

typically reduced to the corresponding β -trifluoromethyl alcohols to avoid racemization of the stereocenter (not shown in the figure).

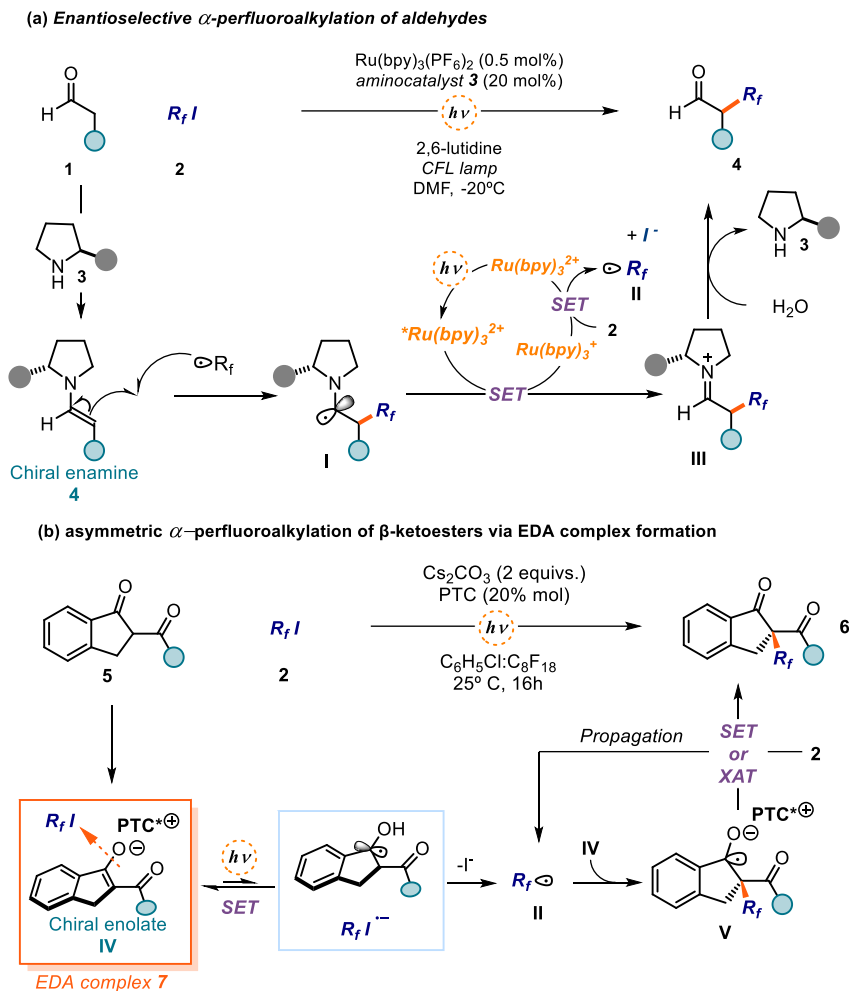


Figure 4.2. (a) enantioselective α -perfluoroalkylation of aldehydes and (b) asymmetric perfluoroalkylation of β -ketoesters via EDA complex formation; SET: single-electron transfer.

Few years later, Melchiorre and coworkers also contributed to this field by harnessing the ability of chiral enolates, derived from β -ketoesters, to trap fluoroalkyl radicals with high efficiency (Figure 4.2b).¹⁶⁶ In this study, it was found that chiral enolates were also responsible for the generation of these radicals by eliciting the formation of photoactive electron donor-acceptor (EDA) complexes upon aggregation with fluoroalkyl iodides. In

¹⁶⁶ Wozniak, L.; Murphy, J. J.; Melchiorre, P. Photo-organocatalytic Enantioselective Perfluoroalkylation of β -Ketoesters. *J. Am. Chem. Soc.* **2015**, *137*, 5678–5681.

general, EDA complexes are formed by the pre-association of two (or more) molecules, which led to the formation of new molecular orbitals. Whereas the two partners, the acceptor (A) and the donor (D), may not absorb visible light, the resulting EDA complex generally does. As a result, irradiation of such ground-state EDA complexes results in a single-electron transfer (SET) from the electron-rich (D) to the electron-poor (A) molecule of the complex. This SET delivers a radical pair, which can generate reactive radicals suitable for chemical processes.¹⁶⁷ Our group showed that, upon deprotonation of β -ketoesters **5**, the corresponding enolate formed a colored EDA complex with perfluoroalkyl iodides **2** at the surface of Cs_2CO_3 (Figure 4.2b). The presence of a catalytic amount of chiral phase transfer catalyst (PTC), which facilitated solubility of the enolate in the organic phase, led to the EDA complex **7** upon association of the chiral enolate **IV** and **2**. Visible light excitation of **7** triggered the formation of perfluoroalkyl radicals **II** by reductive fragmentation of the iodide. The perfluoroalkyl radicals **II** were then intercepted by the chiral enolate **IV** under stereocontrol of the PTC. The incipient α -oxo radical then performed an SET or XAT on **2**, thereby regenerating **II** in a chain manifold.

Despite the progresses in enantioselective α -perfluoroalkylation of carbonyls, the catalytic installation of such groups at a remote position of carbonyl substrates has remained elusive. To tackle this problem, we sought to exploit the organocatalytic dienamine activation strategy described in chapter III. Here, I will discuss how dienamines **VI** and perfluoroalkyl iodides **2** can aggregate to form a photoactive EDA complex (Figure 4.3). Visible light excitation of this complex triggered the generation of perfluoroalkyl radicals **II** under mild conditions. Exploiting the nucleophilic properties of chiral dienamines, perfluoroalkyl radicals could be efficiently trapped in γ -position with exquisite regio- and enantio-selectivity. This strategy served to develop a photo-organocatalytic route for the synthesis of enantioenriched γ -perfluoroalkyl enals. In the following section, I will briefly highlight the photophysical basis of EDA complexes before discussing how the project was developed.

¹⁶⁷ Lima, C. G. S.; Lima, T. d. M.; Duarte, M.; Jurberg, I. D.; Paixao, M. W. Organic Synthesis Enabled by Light-Irradiation of EDA Complexes: Theoretical Background and Synthetic Applications. *ACS Catal.* **2016**, *6*, 1389–1407.

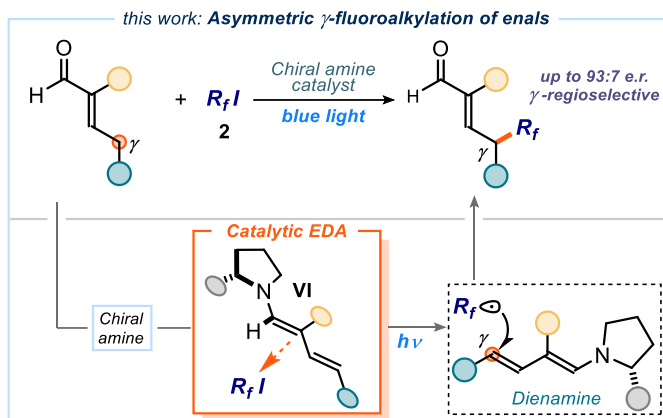


Figure 4.3. Nature of the project: regio- and enantioselective γ -perfluoroalkylation of enals.

4.2 Electron donor-acceptor complexes

4.2.1 General concepts

Electron donor-acceptor (EDA) complexes have a long history. In 1949, Benesi and Hildebrand were the first to observe and report the formation of an EDA complex between arenes and iodine.¹⁶⁸ This study suggested that the color change observed when mixing the two partners was the result of a ground-state association between the donor (the aromatic hydrocarbon) and the acceptor (iodine), which formed a “new entity” featuring new physicochemical properties. This pioneering study fostered the development of a theory that provided a model to rationalize the observed properties of the EDA complex. Mulliken,¹⁶⁹ among others,¹⁷⁰ developed a quantum mechanical theory which described the association between a donor (D) and an acceptor (A) forming a new complex in the ground state (the EDA complex, Figure 4.4). In this complex, new molecular orbitals are formed, emerging from the frontier orbitals of D and A (HOMO/LUMO, respectively), which confer diverse physical properties to the EDA complex with respect to the separated substrates. Generally, an EDA complex features a new charge-transfer band in the absorption spectrum ($h\nu_{CT}$),

¹⁶⁸ Benesi, H. A.; Hildebrand, J. H., A Spectrophotometric Investigation of the Interaction of Iodine with Aromatic Hydrocarbons. *J. Am. Chem. Soc.* **1949**, *71*, 2703–2707.

¹⁶⁹ (a) Mulliken, R. S., Structures of Complexes Formed by Halogen Molecules with Aromatic and with Oxygenated Solvents. *J. Am. Chem. Soc.* **1950**, *72*, 600–608. (b) Mulliken, R. S. “Molecular Compounds and their Spectra. II” *J. Am. Chem. Soc.* **1952**, *74*, 811 – 824. (c) Mulliken, R. S. “Molecular Compounds and their Spectra. III. The Interaction of Electron Donors and Acceptors.” *J. Phys. Chem.* **1952**, *56*, 801–822.

¹⁷⁰ (a) Lewis, G. N. Acids and Bases. *J. Franklin Inst.* **1938**, *226*, 293–313. (b) Winstein, S.; Lucas, H. J. The Coordination of Silver Ion with Unsaturated Compounds. *J. Am. Chem. Soc.* **1938**, *60*, 836–847. (c) Dewar, M. J. S. Mechanism of the Benzidine and Related Rearrangements. *Nature* **1945**, *156*, 784.

associated with an $\Psi_{GS} \rightarrow \Psi_{ES}$ electronic transition (Ψ = wave-function, associated with ground and excited states).

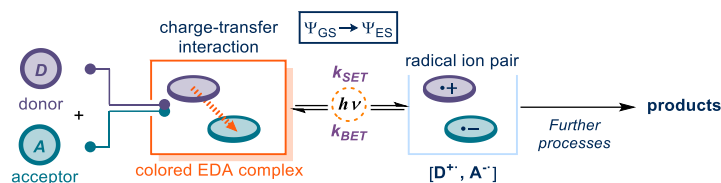


Figure 4.4. EDA complex formation and photoinduced intra-complex SET.

Upon photoexcitation of the EDA complex (orange box in Figure 4.4), the Ψ_{ES} is populated, which translates in an intra-complex SET from D to A to generate a radical ion pair characterized by a net charge separation (light blue box).

Within the context of radical generation strategies, the photoactivity of EDA complexes recently emerged as a cutting-edge technology for the generation of open-shell intermediates and the development of radical-based methodologies. Albeit the physicochemical properties of such complexes were already studied during the second half of the 20th century, it was not until recently that their use in organic synthesis has found fruitful applications.¹⁷¹ This is likely due to the challenges arising from the intrinsic properties of EDA complexes. Precisely, after visible-light excitation of the EDA complex, the ensuing SET event can be followed by a reverse back electron transfer (BET) process, which restores the ground-state EDA complex while hampering productive radical formation (Figure 4.5). When the kinetics of radical formation are not competitive with the kinetics of the BET, the EDA complex excitation is unproductive. A useful approach to mitigate this issue relies on the presence of a suitable leaving group (LG) within the acceptor (or the donor). After the SET event, the presence of such leaving group triggers the irreversible fragmentation of the formed radical anion. When this process is fast enough to compete with the BET event, the target radical **R**• is generated efficiently and can be engaged in synthetically useful transformations.

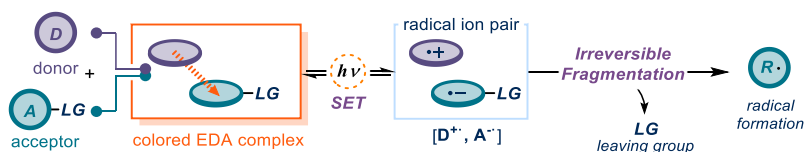


Figure 4.5. Installation of a leaving group in the acceptor leads to irreversible fragmentation, generating the target radical.

¹⁷¹ Crisenza, G. E. M.; Mazzarella, D.; Melchiorre, P. Synthetic Methods Driven by the Photoactivity of Electron Donor– Acceptor Complexes. *J. Am. Chem. Soc.* **2020**, *142*, 5461–5476.

In 1977, Cantacuzene and coworkers demonstrated an elegant application of this approach.¹⁷² The authors showed that stoichiometric enamines **8** could participate in the EDA complex formation with perfluoroalkyl iodide **2** (Figure 4.6). The association of the two partners resulted in a colored EDA complex **9**, which could be excited using visible light. Upon excitation, an SET event generated the perfluoroalkyl radical **II**. The native iodide functionality, embedded within the acceptor core, served as a suitable leaving group to promote a quick fragmentation while avoiding an unproductive BET. The perfluoroalkyl radical **II** could be efficiently trapped by the ground state enamine **8**. It was proposed that the ensuing α -amino radical **IV** could then reduce another molecule of **2**, propagating the formation of another perfluoroalkyl radical **II** through a chain mechanism. The iminium ion **10** formed after SET reduction of **2** was hydrolyzed to deliver the alkylated ketone **11**. The net reaction was a formal α -perfluoroalkylation of ketones.

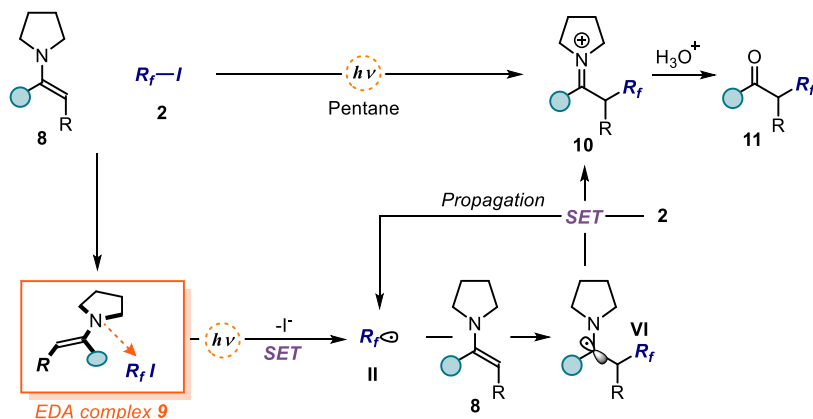


Figure 4.6. Radical alkylation of enolates promoted by the light excitation of an EDA complex.

Concomitant studies by Kornblum,¹⁷³ Russell,¹⁷⁴ and Kochi,¹⁷⁵ among others,¹⁷⁶ reported other donor-acceptor partners and their photoactivities, underlining the strength of EDA

¹⁷² Cantacuzene, D.; Wakselman, C.; Dorme, R. Condensation of Perfluoroalkyl Iodides with Unsaturated Nitrogen Compounds *J. Chem. Soc., Perkin Trans. 1* **1977**, 1365–1371.

¹⁷³ Wade, P. A.; Morrison, H. A.; Kornblum, N. The Effect of Light on Electron-Transfer Substitution at a Saturated Carbon Atom. *J. Org. Chem.* **1987**, *52*, 3102–3107.

¹⁷⁴ Russell, G. A.; Wang, K. Homolytic Alkylation of Enamines by Electrophilic Radicals. *J. Org. Chem.* **1991**, *56*, 3475–3479.

¹⁷⁵ (a) Sankararaman, S.; Haney, W. A.; Kochi, J. K. Annihilation of Aromatic Cation Radicals by Ion-Pair and Radical-Pair Collapse. Unusual Solvent and Salt Effects in the Competition for Aromatic Substitution. *J. Am. Chem. Soc.* **1987**, *109*, 7824–7838. (b) Fukuzumi, S.; Mochida, K.; Kochi, J. K. A Unified Mechanism for Thermal and Photochemical Activation of Charge-Transfer Processes with Organometals. Steric Effects in the Insertion of Tetracyanoethylene. *J. Am. Chem. Soc.* **1979**, *101*, 5961–5972.

¹⁷⁶ (a) Gotoh, T.; Padias, A. B.; Hall, J. H. K. An Electron Donor Acceptor Complex and Thermal Triplex as Intermediates in the Cycloaddition Reaction of N-Vinylcarbazole with Dimethyl 2,2-Dicyanoethylene-1,1-dicarboxylate. *J. Am. Chem. Soc.* **1991**, *113*, 1308–1312. (b) Bunnett, J. F.; Sundberg, J. E.

complex photochemistry as a general radical generation strategy useful for synthetic transformations. Synthetic photochemistry was regarded at that time as a specialized scientific area, requiring specific experimental expertise. This may explain why, until the second decade of the 21st century, the EDA complex strategy was not fully recognized as an independent field of organic chemistry, which could provide effective benefits in the synthesis of molecules. The advent of photocatalysis shed light on how such manifold could provide an overarching and powerful platform in visible-light-driven radical synthesis.

4.2.2 Organocatalytic intermediates as EDA partners

The first reports on the photoactivity of EDA complexes featured the use of both acceptors and donors in stoichiometric amounts. The realization of an EDA complex using one of the two partners in a catalytic amount was as an important achievement. Organocatalytic enamines are not just excellent radical traps, as demonstrated by the pioneering work of MacMillan,¹⁶⁵ but can also contribute to the radical generation by acting as donors for EDA complex formation with different acceptors. The first example of this concept was reported by our group in 2013, showing that enamines, formed by condensation between the aminocatalyst **13** and aldehydes **1** (mechanism detailed in Chapter III, Figure 3.3), could effectively participate as donors in EDA complex association with electron-poor bromides **12** (Figure 4.7).¹⁷⁷ Visible-light excitation of the EDA complex **9** triggered the SET event that ultimately generated the radical **VIII** upon fragmentation of the radical anion **VII**.

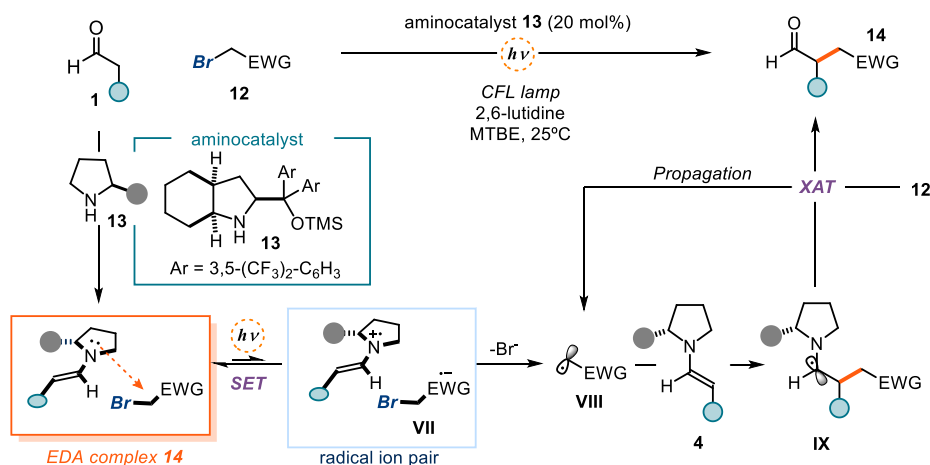


Figure 4.7. Organocatalytic EDA complex: enamines as donors.

¹⁶⁵Photostimulated arylation of ketone enolate ions by the S_{RN}1 mechanism. *J. Org. Chem.* **1976**, *41*, 1702–1706.

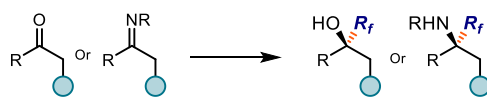
¹⁷⁷Arceo, E.; Jurberg, I. D.; Álvarez-Fernández, A.; Melchiorre, P. Photochemical activity of a key donor–acceptor complex can drive stereoselective catalytic α -alkylation of aldehydes. *Nat. Chem.* **2013**, *5*, 750–756.

The generated radicals were effectively trapped by the ground-state enamine **4** in an enantioselective fashion to deliver alkylated products **14** with high efficiency. Mechanistic studies, by means of quantum yield measurement, revealed that the radical generation arising from the excitation of the EDA complex serves as an initiation process, while the main reaction followed a chain mechanism where the α -amino radical **IX** was responsible for the propagation step by halogen atom transfer (XAT) mechanism from **12**.¹⁷⁸ As in the case of β -ketoesters derived enolates (discussed in Section 4.1), this example highlighted how chiral organocatalytic intermediates can behave simultaneously as radical traps and as donor partners in EDA complex manifolds, being directly involved in the generation of open-shell intermediates under mild reaction conditions.

4.3 Enantioselective perfluoroalkylation of carbonyls

The enantiocontrolled installation of a perfluoroalkyl group within an aliphatic carbon chain is not an easy task. While the asymmetric 1,2-fluoroalkylation of carbonyl compounds has been successfully achieved using various methods (Figure 4.8a),¹⁷⁹ the simple substitution of a hydrogen atom with a perfluoroalkyl group is more difficult (Figure 4.8b).

(a) Asymmetric 1,2-fluoroalkylation of carbonyls: several reports



(b) Asymmetric α -fluoroalkylation of carbonyls: few reports

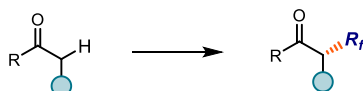


Figure 4.8. Perfluoroalkylation of carbonyls: state of the art.

¹⁷⁸ Bahamonde, A.; Melchiorre, P. Mechanism of the Stereoselective α -Alkylation of Aldehydes Driven by the Photochemical Activity of Enamines. *J. Am. Chem. Soc.* **2016**, *138*, 80198030.

¹⁷⁹ For representative example see: (a) Iseki, K.; Nagai, T.; Kobayashi, Y. Asymmetric trifluoromethylation of aldehydes and ketones with trifluoromethyltrimethylsilane catalyzed by chiral quaternary ammonium fluorides. *Tetrahedron Lett.* **1994**, *35*, 3137–3138. (b) Kuroki, Y.; Iseki, K. A chiral triaminosulfonium salt: design and application to catalytic asymmetric synthesis. *Tetrahedron Lett.* **1999**, *40*, 8231–8234. (c) Nagao, H.; Yamane, Y.; Mukaiyama, T. Asymmetric Trifluoromethylation of Ketones with (Trifluoromethyl)trimethylsilane Catalyzed by Chiral Quaternary Ammonium Phenoxides. *Chem. Lett.* **2007**, *36*, 666–667. (d) Nagao, H.; Kawano, Y.; Mukaiyama, T. Enantioselective Trifluoromethylation of Ketones with (Trifluoromethyl)trimethylsilane Catalyzed by Chiral Quaternary Ammonium Phenoxides. *Bull. Chem. Soc. Jpn.* **2007**, *80*, 2406–2412. (e) Mizuta, S.; Shibata, N.; Akita, S.; Fujimoto, H.; Nakamura, S.; Toru, T. Cinchona Alkaloids/TMAF Combination-Catalyzed Nucleophilic Enantioselective Trifluoromethylation of Aryl Ketones. *Org. Lett.* **2007**, *9*, 3707–3710. (f) Caron, S.; Do, N. M.; Arpin, P.; Larivee, A. Enantioselective Addition of a Trifluoromethyl Anion to Aryl Ketones and Aldehydes. *Synthesis* **2003**, 1693–1694. (g) Kawai, H.; Kusuda, A.; Nakamura, S.; Shiro, M.; Shibata, N. Catalytic Enantioselective Trifluoromethylation of Azomethine Imines with Trimethyl(trifluoromethyl)silane. *Angew. Chem. Int. Ed.* **2009**, *48*, 6324–6327.

The first methodologies to achieve this transformation involved the use of chiral auxiliaries, therefore suffering from harsh conditions and additional steps to install and remove the auxiliary. The advent of organocatalysis and photoredox catalysis fostered the development of more efficient routes towards the enantioselective α -perfluoroalkylation of carbonyls by use of radical manifolds.

4.3.1 Early approaches: chiral auxiliaries

The earliest example of asymmetric perfluoroalkylation of enolate derivatives is dated 1987. In this seminal work, Kitazume and co-workers demonstrated that stoichiometric chiral enamines could be used to obtain enantioenriched α -trifluoromethylated ketones.¹⁸⁰ Treatment of enamine **15** with a preformed fluoroalkylzinc reagent in the presence of Cp_2TiCl_2 , afforded the corresponding α -perfluoroalkyl ketones **16**, albeit with moderate stereoselectivity (Figure 4.9a). Later, in the early 1990s, the group of Kobayashi showed that Evans oxazolidinones could be used efficiently as chiral auxiliaries (Figure 4.9b).¹⁸¹ Interestingly, this approach involved the formation of perfluoroalkyl radicals **II** by treatment of the iodide precursors with triethylborane under oxygen.¹⁸² Radical **II** was then trapped by the *in situ* formed chiral lithium enolate **18** in a stereocontrolled fashion. Also in this case, the incipient α -oxo radical **X** was proposed to feed a radical chain mechanism by XAT mechanism from **2** and concomitant release of product **19**. The reaction proceeded with good yield and diastereoselectivity to afford α -trifluoromethyl carboximides **19**, which were treated with LiBH_4 to provide the corresponding enantioenriched β -trifluoromethyl alcohols without racemization of the newly formed stereogenic center (not shown in figure).

¹⁸⁰ Kitazume, T.; Ishikawa, N. Ultrasound-promoted selective perfluoroalkylation on the desired position of organic molecules. *J. Am. Chem. Soc.* **1985**, *107*, 5186–5191.

¹⁸¹ (a) Iseki, K.; Nagai, T.; Kobayashi, Y. “Diastereoselective trifluoromethylation of chiral imide enolates with iodotrifluoromethane mediated by Triethylborane” *Tetrahedron Lett.* **1993**, *34*, 2169–2170. (b) Iseki, K.; Nagai, T.; Kobayashi, Y. “Diastereoselective trifluoromethylation of chiral imide enolates with iodotrifluoromethane mediated by Triethylborane” *Tetrahedron: Asymmetry* **1994**, 961–974.

¹⁸² Yorimitsu, H.; Oshima, K. Radical Chain Reactions: Organoborane Initiators. In “Radicals in organic synthesis” Renaud, P.; Sibi, M. Eds. WILEY-VCH Verlag, Weinheim, **2001**, pp: 11-27. For a detailed mechanistic investigation of the radical generation using triethylborane and oxygen see: Curran, D.; McFadden, T. R. Understanding Initiation with Triethylboron and Oxygen: The Differences between Low-Oxygen and High-Oxygen Regimes. *J. Am. Chem. Soc.* **2016**, *138*, 7741–7752.

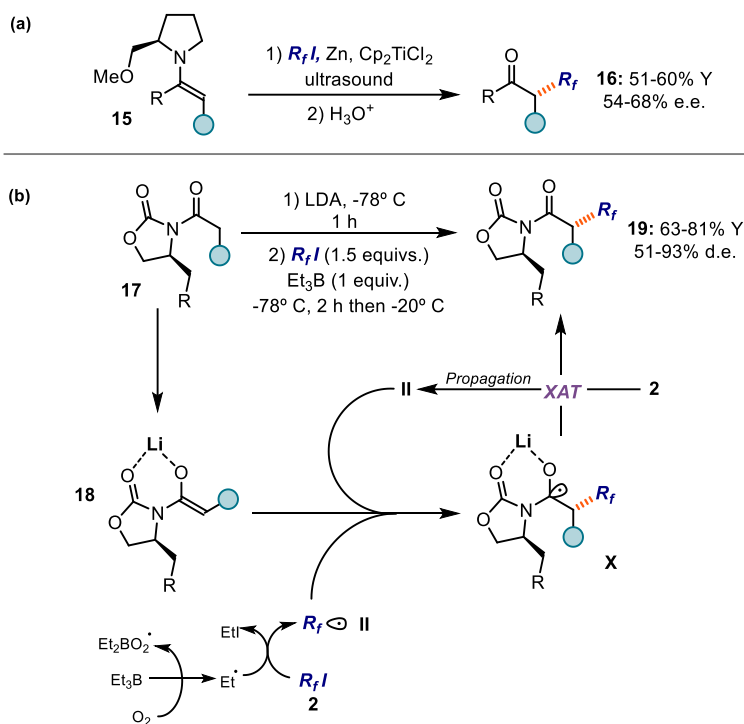


Figure 4.9. Perfluoroalkylation of carbonyls: state of the art.

4.3.2 Improved routes: organocatalysis

Methodologies for the catalytic enantioselective α -perfluoroalkylation of carbonyls remained underexplored until the first decade of the new century. In 2008, the pioneering work of MacMillan and Nicewicz¹⁸³ spurred the development of methodologies based on photoredox and organocatalysis, opening new strategies for chiral molecule synthesis. The merger of these two catalytic platforms was quickly exploited in 2009 by the group of MacMillan to develop the first catalytic system for the enantioselective α -fluoroalkylation of aldehydes (Figure 4.2a).⁷ MacMillan and coworkers also disclosed that the combination of organocatalysis and Lewis acid catalysis could provide a non-photocatalytic approach to the enantioselective α -trifluoromethylation of aldehydes (Figure 4.10).¹⁸⁴ In line with the mechanism reported by the

¹⁸³ Nicewicz, D. A.; MacMillan, D. W. C. Merging Photoredox Catalysis with Organocatalysis: The Direct Asymmetric Alkylation of Aldehydes *Science*, **2008**, 322, 77-80.

¹⁸⁴ Allen, A. E.; MacMillan, D. W. C. The Productive Merger of Iodonium Salts and Organocatalysis: A Non-photolytic Approach to the Enantioselective α -Trifluoromethylation of Aldehydes. *J. Am. Chem. Soc.* **2010**, 132, 4986–4987.

group of Baran¹⁸⁵ and Togni,¹⁸⁶ activation of the electrophilic trifluoromethylating reagent **21** by a copper salt triggered the attack of the organocatalytic enamine **4** on the iodine atom, generating a λ^3 -iodane species **XI**. The latter quickly underwent stereo-retentive alkyl transfer forging the desired C-CF₃ bond with good efficiency and high enantiomeric excess. Final hydrolysis of the iminium ion **XII** provided catalyst turnover and delivered product **22**.

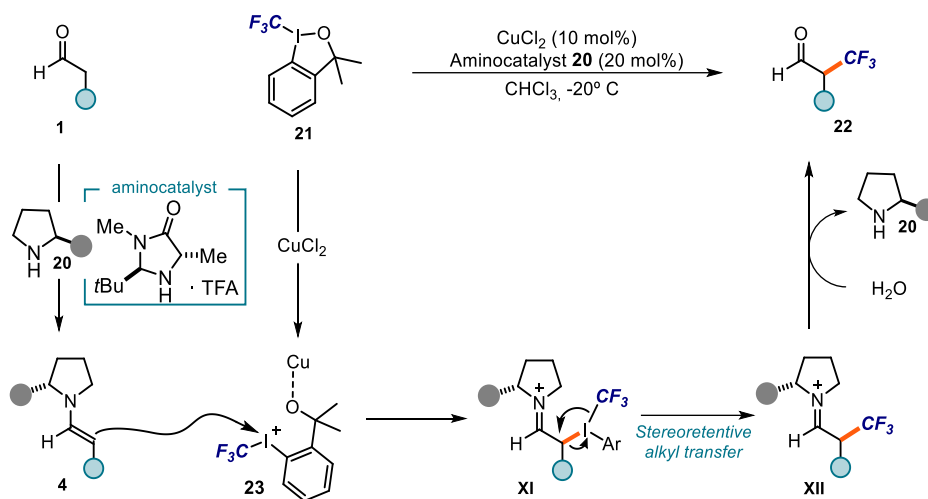


Figure 4.10. Enantioselective α -trifluoromethylation of aldehydes via the combination of Lewis acid and organocatalysis.

4.4 Target of the project

Considering the challenges related to the enantiocontrolled installation of fluoroalkyl moieties and the few reports on the topic, we believed that a route leading to enantioenriched γ -perfluoroalkyl enals would be a significant advance to the field. Furthermore, as discussed in the previous chapter, the remote asymmetric functionalization of carbonyl is still a limited transformation. Despite the advances in the α -functionalization of aldehydes, a more distal γ -functionalization is hampered by regioselectivity and enantioselectivity issues. To fill this gap in asymmetric methodology and achieve an asymmetric γ -perfluoroalkylation of enals, we sought to leverage on the ability of dienamine intermediates (described in chapter III) to trap electron-deficient perfluoroalkyl radicals at the most remote position.

¹⁸⁵ Eastman, K.; Baran, P. S. Simple Method for the Direct Arylation of Indoles. *Tetrahedron* **2009**, *65*, 3149–3151.

¹⁸⁶ Koller, R.; Stanek, K.; Stolz, D.; Aardoom, R.; Niedermann, K.; Togni, A. Zinc-mediated formation of trifluoromethyl ethers from alcohols and hypervalent iodine trifluoromethylation reagents. *Angew. Chem. Int. Ed.* **2009**, *48*, 4332–4336.

The blueprint of our design plan is depicted in Figure 4.11. By harnessing the ability of organocatalytic enamine intermediates and perfluoroalkyl iodides (R_fI) to form photoactive EDA complexes acting as donors^{172,187} and acceptors,^{166,174,188} respectively, we envisioned that it would be possible to translate this concept into a vinylogous manifold. Specifically, we sought to use the dienamine **25**, formed upon condensation of an aminocatalyst with enal **24**, to form an EDA complex **26** with perfluoroalkyl iodides. Light excitation of **26** would trigger the SET leading to the perfluoroalkyl radical **II**. In analogy to the chemistry discussed in Chapter III, we hypothesized that the dienamine **25** could trap radical **II** with perfect γ -site selectivity and high stereocontrol. Final propagation through SET or XAT would then deliver another radical **II** while releasing the γ -alkylated product **27**. In the following sections, I will detail the successful realization of this idea.

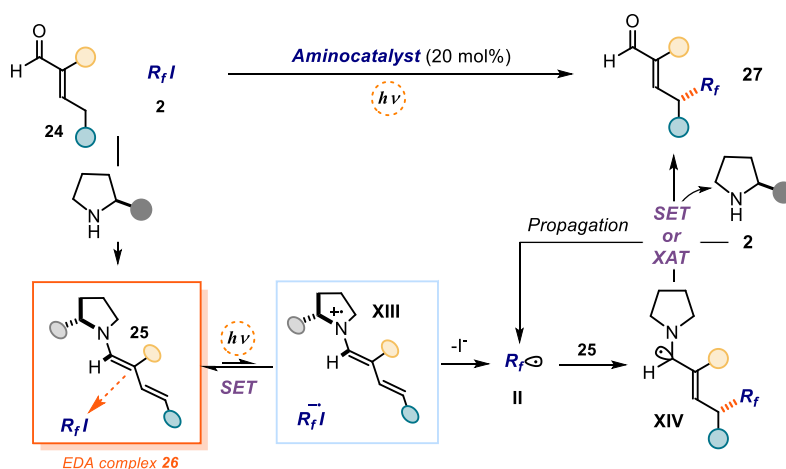


Figure 4.11. Design plan for the enantioselective γ -perfluoroalkylation of branched enals.

4.5 Results and discussion

4.5.1 Reaction optimization

To assess the possible reactivity between the dienamine and the perfluoroalkyl iodide, we tested the reaction between α -branched enal **28** and nonafluoro-1-iodobutane **29** in the presence of Hayashi-Jorgensen catalyst **A**, 2,6-lutidine as a base, and THF as solvent. After

¹⁸⁷ James, M.J.; Strieth-Kalthoff, F.; Sandfort, F.; Klauk, F. J. R.; Wagener, F.; Glorius, F. Visible-Light-Mediated Charge Transfer Enables C-C Bond Formation with Traceless Acceptor Groups. *Chem. Eur. J.* **2019**, *25*, 8240–8244.

¹⁸⁸ (a) Ma, L.; Feng, W.; Xi, Y.; Chen, X.; Lin, X. Mechanistic Insights into Visible-Light-Driven Dearomative Fluoroalkylation Mediated by an Electron Donor–Acceptor Complex. *J. Org. Chem.* **2022**, *87*, 944–951. (b) Liu, Y.; Chen, X.-L.; Sun, K.; Li, X.-Y.; Zeng, F.-L.; Liu, X.-C.; Qu, L.-B.; Zhao, Y.-F.; Yu, B. Visible Light Induced Radical Perfluoroalkylation/Cyclization Strategy to Access 2-Perfluoroalkyl benzothiazoles/Benzoselenazoles by EDA Complex. *Org. Lett.* **2019**, *21*, 4019–4024. (c) Li, L.; Chen, X.; Pei, C.; Li, J.; Zou, D.; Wu, Y.; Wu, Y. Visible-light-mediated direct C-H perfluoroalkylation of imidazoheterocycles. *Tetrahedron Lett.* **2021**, *83*, 153407–153410.

addition of all the components, the reaction mixture appeared slightly yellow (Figure 4.12), and the UV-Vis spectra of the reaction mixture showed the appearance of a new absorption band tailing at 460 nm (Figure 4.13), which we ascribed to a new ground-state aggregation. We therefore used a 460 nm light-emitting diode (LED) as the light source to conduct our initial test reactions (Table 4.1).

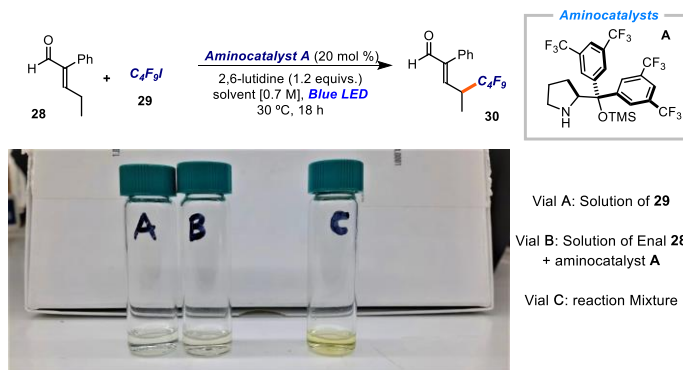


Figure 4.12. UV-Vis absorption spectra of the reaction component and the reaction mixture.

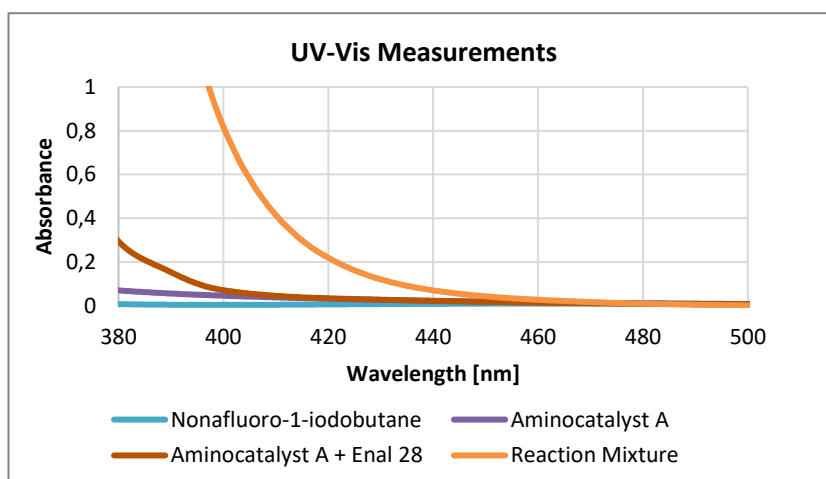
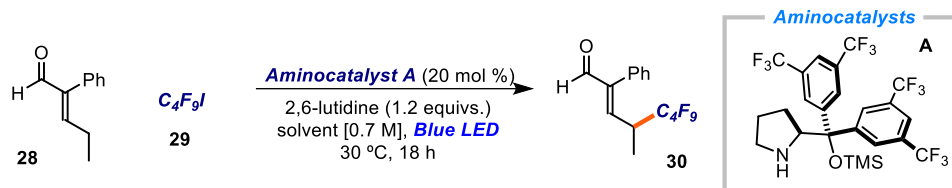


Figure 4.13. UV-Vis absorption spectra of the reaction component and the reaction mixture.

After 18 hours, we were pleased to find that the target γ -perfluoroalkylated product **30** was formed in 63% yield and 83:17 enantiomeric ratio, with no trace of α -alkylated product (entry 1). Control experiments showed that both light and the aminocatalyst were essential for reactivity (entry 2 & 3). Screening of solvents highlighted that non-protic solvents were crucial for reactivity, with diethyl ether being most beneficial (entries 4-6). A polar solvent (DMF) had a negative effect on the reaction outcome (entry 7). Interestingly, the choice of solvent did not alter the enantiomeric ratio of the product in any case. We also noticed that

the reaction features a fast kinetic profile at 30 °C, since the product was formed quantitatively (95% yield) in 2 hours (entry 8).

Table 4.1. Initial studies and solvent optimization



entry	solvent	yield 30 (%) ^a	e.r. 30 (%) ^b
1	THF	63	83:17
2 ^d	Et ₂ O	0	/
3 ^e	Et ₂ O	0	/
4	Et ₂ O	96	83:17
5	Tol	77	84:16
6	DCM	60	83:17
7	DMF	0	/
8 ^c	Et ₂ O	95	83:17

a) Reaction performed on a 0.2 mmol scale using 3 equiv. of **28**. Yields of **30** determined by ¹H NMR analysis of the crude mixture using trimethyl orthoformate as the internal standard. b) Enantiomeric ratio (e.r.) of **30** determined by derivatization to the corresponding 2,4-dinitrophenyl hydrazone prior to chiral UPC² analysis. c) Reaction time: 2.5 hours. d) Reaction conducted in the absence of the aminocatalyst. e) Reaction conducted in the absence of light

Since the aminocatalyst is directly involved in the enantioinduction of the process, we screened a variety of chiral secondary amines as catalysts (Table 4.2). The nature of the aryl rings on the diphenyl prolinol scaffold was of paramount importance for the catalytic activity. Catalyst **B**, which features unfunctionalized aryl rings, displayed a worse efficiency than catalyst **A**, delivering product **30** with considerably diminished yield (37%, entry 1). Also, the silyl ether protection played an important role. Replacement of the trimethylsilyl (TMS) group with a bulky thexydimethylsilyl (TDS) group in catalyst **C** lowered both the yield and enantiomeric ratio of **30** (entry 2). We rationalized these results considering that both the CF₃ groups on the aryl rings and the TMS protection on the catalyst structure **A** were somehow important *i*) to achieve the photophysical properties necessary to supply an effective radical generation, thus affecting reactivity, and *ii*) to infer good levels of enantiocontrol during the radical trapping event. This is because the organocatalytic intermediate is directly involved in both the radical generation process and the radical trapping event.¹⁸⁹ For this reason, we

¹⁸⁹ (a) Bergmann, K.; Davis, R. L. The Tunable Photophysical Properties of Enamine Intermediates Involved in Light-Driven Aminocatalysis. *Org. Lett.* **2021**, *23*, 7033–7037. (b) Vega-Peñaloza, A.; Paria, S.;

carefully tune the structure of the best-performing catalyst **A**, mainly focusing on the 4-position of the pyrrolidine ring. Previous reports highlighted that 4-hydroxy-proline derivatives can impart increased stereocontrol in polar chemistry of both enamines¹⁹⁰ and iminium ions.¹⁹¹ We were delighted to see that the *O*-silylated 4-hydroxyproline-derived catalyst **D**, when applied to our model reaction, offered good yield of product **30** with an increased enantioselectivity (88:12 e.r., entry 3). Finally, using a bulkier hexyldimethylsilyl protecting group in catalyst structure **E** delivered the product in a 90:10 enantiomeric ratio (entry 4). Lowering the temperature to -10 °C allowed the isolation of the perfluoralkyl product **30** in 72% yield and 93:7 enantiomeric ratio (entry 7), while further decrease in temperature shut down the reactivity (entry 8). It is noteworthy that imidazolidinone **F** and primary amine **G**, which are common catalyst in enamine activation,¹⁹² were completely ineffective in this chemistry (entries 5 & 6).

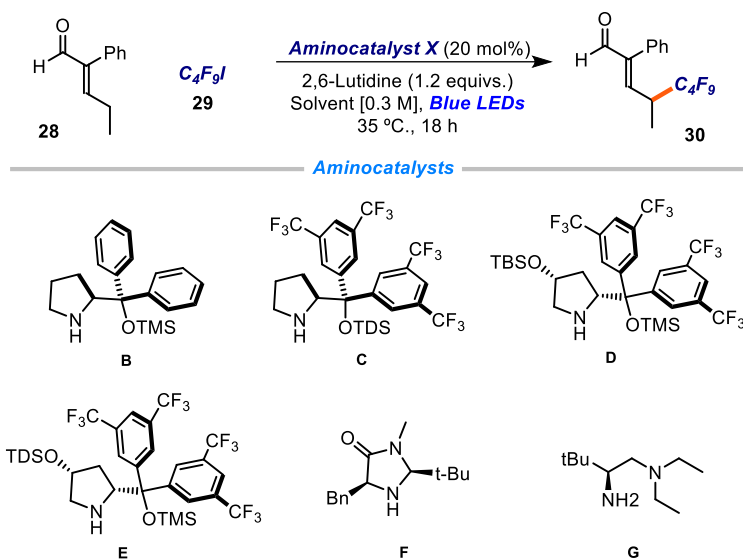
Bonchio, M.; Dell'Amico, L.; Companyó X. Profiling the Privileges of Pyrrolidine-Based Catalysts in Asymmetric Synthesis: From Polar to Light-Driven Radical Chemistry *ACS Catal.* **2019**, *9*, 6058–6072.

¹⁹⁰ Caruana, L.; Kniep, F.; Küllerich Johansen, T.; Poulsen, P. H.; Jørgensen, K. A. A New Organocatalytic Concept for Asymmetric α -Alkylation of Aldehydes. *J. Am. Chem. Soc.* **2014**, *136*, 15929–15932.

¹⁹¹ Arenas, I.; Ferrali, A.; Rodríguez-Esrich, C.; Bravo, F.; Pericas, M. A. cis-4-Alkoxydialkyl- and cis-4-Alkoxydiarylprolinol Organocatalysts: High Throughput Experimentation (HTE)-Based and Design of Experiments (DoE)-Guided Development of a Highly Enantioselective aza-Michael Addition of Cyclic Imides to α,β Unsaturated Aldehydes. *Adv. Synth. Catal.* **2017**, *359*, 2414–2424.

¹⁹² (a) Brochu, M. P.; Brown, S. P.; MacMillan, D. W. C. Direct and Enantioselective Organocatalytic α -Chlorination of Aldehydes. *J. Am. Chem. Soc.* **2004**, *126*, 4108–4109. (b) Zhu, Y.; Zhang, L.; Luo, S. Asymmetric α -Photoalkylation of β -Ketocarbonyls by Primary Amine Catalysis: Facile Access to Acyclic All-Carbon Quaternary Stereocenters *J. Am. Chem. Soc.* **2014**, *136*, 14642–14645.

Table 4.2. Catalyst optimization



entry	Temperature	Aminocatalyst	yield 30 (%) ^a	e.r. 30 (%) ^b
1	30 °C	B	37	82:18
2	30 °C	C	51	81:19
3	30 °C	D	78	88:12
4	30 °C	E	86	90:10
5	30 °C	F	0	/
6	30 °C	G	0	/
7	-10 °C	E	92 (72)	93:7
8	-40 °C	E	0	/

- a) Reaction performed on a 0.2 mmol scale using 3 equivs of **28**. Yields of **30** determined by ¹H NMR analysis of the crude mixture using trimethyl orthoformate as the internal standard. b) enantiomeric ratio of **30** determined by derivatization to the corresponding 2,4-dinitrophenyl hydrazine prior to injection in UPC². Numbers in parenthesis refer to the yields of product isolated after flash chromatography.

4.5.2 Reaction scope

Once we found the best condition for the photochemical dienamine-catalyzed γ -perfluoroalkylation reaction (Table 4.1 entry 7), we explored the generality of the system. A wide array of perfluoroalkyl iodides smoothly reacted under our reaction conditions (Figure 4.14).

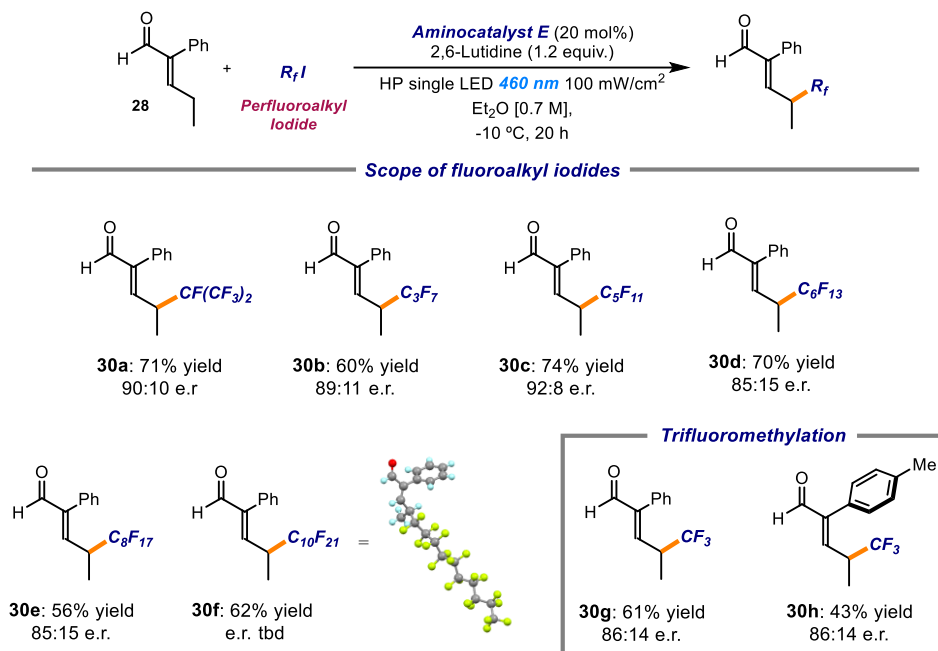


Figure 4.14. Perfluoroalkyl iodides that can participate in the reaction.

While the model compound (nonafluorobutyl iodide) gave the best result, other radical precursors afforded products **30** with similar yields and enantiomeric ratios in the range of 85:15 and 92:8 (**30a-30e**). Noteworthy, this protocol is also suitable to install CF₃ groups on different enals using simple and commercially available trifluoromethyl iodide. The small and highly reactive trifluoromethyl radical could be trapped efficiently by the chiral dienamine with good enantiomeric ratio (products **30g**, **30h**).

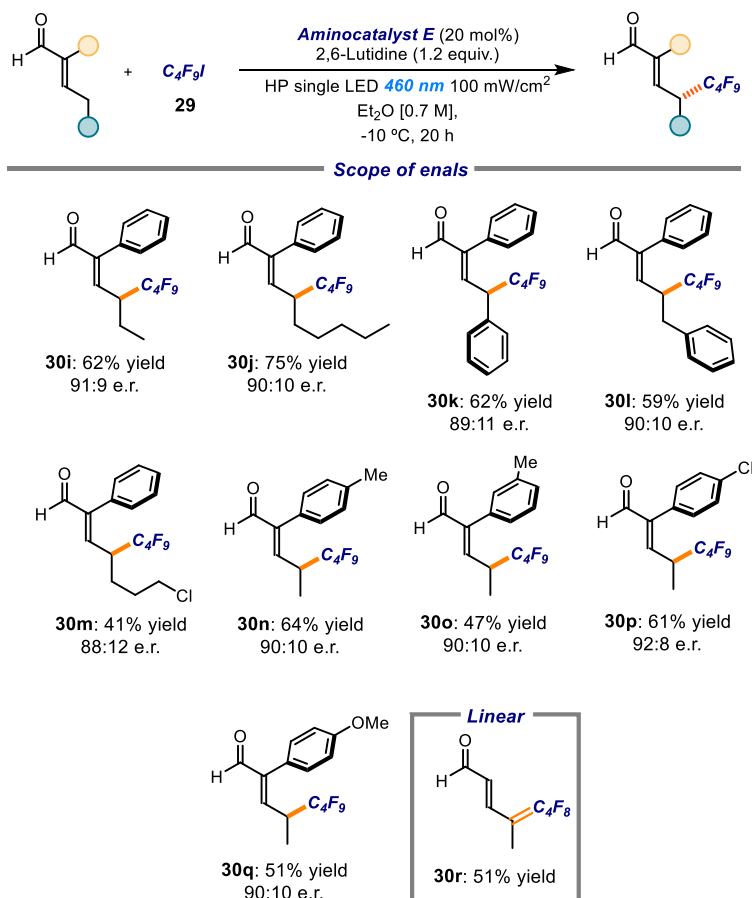


Figure 4.15. Scope of enals that can participate in the reaction.

We next evaluated the α -branched enals that could participate in the γ -perfluoroalkylation process (Figure 4.15). The introduction in γ -position of longer alkyl chains (products **30i** and **30j**), as well as the presence of a phenyl ring (**30k**), did not affect the reactivity. The enantioenriched hydrocinnamaldehyde derivative **30l** could also be synthesized with analogous efficiency. A chlorine atom in the alkyl chain was also tolerated, albeit the product **30m** was produced with a lower yield and slightly lower enantiomeric ratio. We continued our studies by exploring the versatility in the substitution pattern of the α -aryl moiety. Enals bearing electron-withdrawing or electron-donating groups at different positions of the arene also reacted well to afford the corresponding products **30n**, **30o**, **30p**, **30q** in good yields and enantiomeric ratios. In analogy with the chemistry discussed in Chapter III, the aromatic ring in the α -position acts as a crucial stereo-controlling element, enforcing a preferred conformation of the chiral dienamine, which is important for stereocontrol. Nevertheless, the absence of this substituent does not influence the regioselectivity of the process. This is highlighted by the result obtained with 2-pentalen, since the product of the reaction was

formed as a single regioisomer albeit isolation through column chromatography produced the corresponding unsaturated product **30r** upon HF elimination.

To expand the synthetic utility of the reaction, we also tested different radical precursors and aldehydes (Figure 4.16) using the standard conditions (reaction performed at ambient temperature). Regarding the radical precursors, we noticed that both the perfluorinated pattern on the alkyl chain and the native iodide functionality are strictly necessary to achieve the desired reactivity. When different electron-poor functional groups, including sulfones (**31**) and phosphonates (**32**), were introduced in the radical precursor structure, the reaction did not take place. Also trifluoro-2-iodoethane (**33**) and 1,2-dibromo-perfluoroethane (**34**) failed to react. These results likely define the strict structural and electronic properties required by the radical precursors to form a productive EDA complex with the dienamine, albeit the lack of reactivity could be a consequence of a reduced electrophilicity of the ensuing radical too. Some limitations could also be found on the enal counterpart. The substitution of the phenyl ring with a methyl substituent in α -position resulted in a complete shutdown of the reactivity. Presently, we have no suitable explanation for the negative outcome of this reaction, in particular considering that these substrates can readily form dienamines by condensation with a secondary amine.¹⁹³ In addition, while δ -branched enals such as **36** delivered the product with consistently reduced yields, the use of hepta-2,4-dienal **35** resulted in a complex reaction mixture.

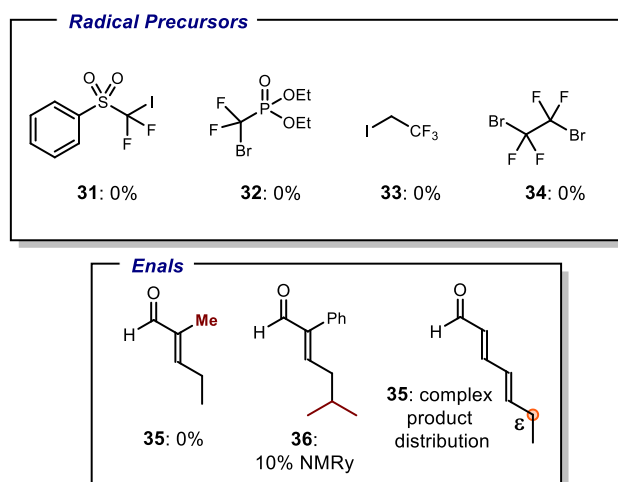


Figure 4.16: Survey of substrates that failed to give the perfluoroalkylation products under the optimized reaction conditions.

¹⁹³ Silvi, M.; Cassani, C.; Moran, A.; Melchiorre, P. Secondary amine-catalyzed asymmetric gamma-alkylation of alpha-branched enals via dienamine activation. *Helv. Chim. Acta*, **2012**, *95*, 1985-2006.

4.5.3 Mechanistic considerations

Mechanistically, we propose that the photochemical organocatalytic perfluoroalkylation of α -branched enals follows the mechanism depicted in Figure 4.17. The UV-Vis spectrum of the reaction mixture shows a new band (red-shifted, different from the single components) tailing at 460 nm (Figure 4.13), which is diagnostic of the formation of an EDA complex **26** between the dienamine **25** and the perfluoroalkyl iodide. Excitation of **26** with visible light would trigger the SET responsible for the generation of the radical **II**. The latter is then intercepted by the chiral organocatalytic dienamine formed *in situ* by the condensation of catalyst **E** with the enal **28**.

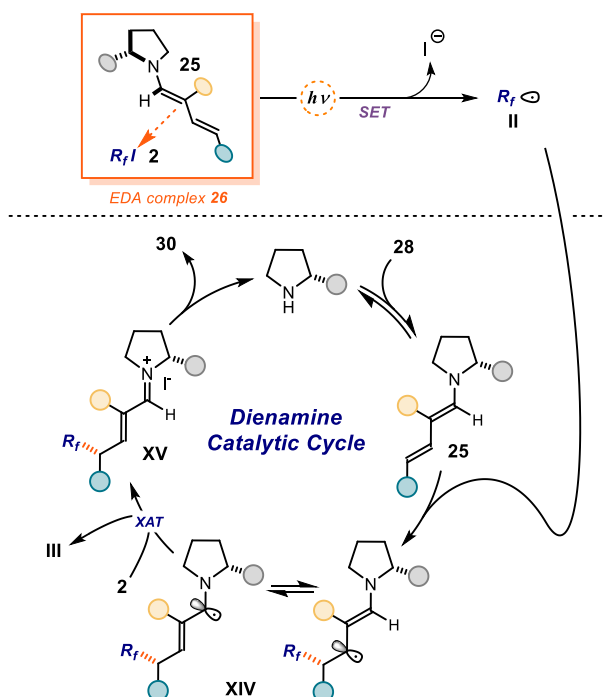


Figure 4.17. Mechanistic proposal for the enantioselective γ -perfluoroalkylation of enals

The incipient α -amino radical **XIV** is responsible for the generation of another perfluoroalkyl radical **II** by XAT mechanism from the iodide.¹⁹⁴ Based on the reported electrochemical potentials for α -amino radicals ($E_{1/2}^{\text{red}} = -0.92$ to -1.12 V vs SCE)¹⁹⁵ and for perfluoroalkyl iodides ($E_{1/2}^{\text{red}} \text{CF}_3\text{I} = -1.22$ V vs SCE in DMF; $E_{1/2}^{\text{red}} \text{C}_6\text{F}_{13}\text{I} = -1.32$ V vs SCE in DMF),¹⁹⁶ a

¹⁹⁴ Julià, F.; Constantin, T.; Leonori, D. Applications of Halogen-Atom Transfer (XAT) for the Generation of Carbon Radicals in Synthetic Photochemistry and Photocatalysis *Chem. Rev.* **2022**, *122*, 2292–2352.

¹⁹⁵ D. D. M. Wayner, J. J. Dannenberg, D. Griller Oxidation potentials of α -aminoalkyl radicals: bond dissociation energies for related radical cations. *Chem. Phys. Lett.*, **1986**, *131*, 189–191.

¹⁹⁶ (a) Andrieux, C. P.; Gelis, L.; Me´debielle, M.; Pinson, J.; Saveant, J. M. Outer-sphere dissociative electron transfer to organic molecules: a source of radicals or carbanions? Direct and indirect electrochemistry of perfluoroalkyl bromides and iodides *J. Am. Chem. Soc.* **1990**, *112*, 3509–3520. (b) Bonesi, S. M.; Erra-Balsells,

SET pathway that generates **III** from **2** should be thermodynamically unfavorable. Regardless of the nature of the chain propagation step, measurement of the quantum yield (ϕ) using a 460 nm single LED with power fixed at 100 mW/cm² provided a value of 1.14. This result is congruent with a chain mechanism being operative under our reaction conditions.

4.6 Conclusions

In summary, based on our previous knowledge on vinylogous radical reactivity and dienamine catalysis, we developed a radical generation strategy for the elusive asymmetric γ -perfluoroalkylation of enals. This photochemical protocol does not rely on any external photocatalyst to generate perfluoroalkyl radicals but exploits the ability of dienamines to engage in EDA complexes with perfluoroalkyl iodides. We demonstrated that chiral dienamines can trap radicals at the distal γ -position while inferring high degrees of enantioselectivity. The generality of the process was showcased with the synthesis of different enantioenriched γ -perfluoroalkyl enals. Importantly, this strategy also provides an entry into chiral γ -trifluoromethylated enals. UV-Vis experiments provided elucidation on the nature of the EDA complex, while we established that a chain mechanism is operative by means of quantum yield determination, highlighting the role of the dienamine-based EDA complex as a photo-initiating complex. Expansion of the reaction scope and further manipulation of the products are ongoing in our laboratories.

4.7 Experimental section

4.7.1 General information

The NMR spectra were recorded at 400 MHz and 500 MHz for ¹H, 101 or 126 MHz for ¹³C, and 282 MHz or 376 MHz for ¹⁹F. Copies are provided in the final section of the Experimental Part. The chemical shift (δ) for ¹H and ¹³C are given in ppm relative to residual signals of the solvents (CHCl₃ @ 7.26 ppm ¹H NMR and 77.16 ppm ¹³C NMR). Coupling constants are given in Hertz. The following abbreviations are used to indicate the multiplicity: s, singlet; d, doublet; q, quartet; m, multiplet; bs, broad signal; app, apparent.

High resolution mass spectra (HRMS) were obtained from the ICIQ HRMS unit on MicroTOF Focus and Maxis Impact (Bruker Daltonics) with electrospray ionization. (ESI). Isolated yields refer to materials of >95% purity as determined by ¹H NMR.

R. J. Outer-sphere electron transfer from carbazoles to halomethanes. Reduction potentials of halomethanes measured by fluorescence quenching experiments *Chem. Soc., Perkin Trans. 2* **2000**, 7, 1583–1595.

The authors are indebted to the team of the Research Support Area at ICIQ, particularly to the NMR and the High-Resolution Mass Spectrometry Units.

General Procedures. All reactions were set up under an argon atmosphere in oven-dried glassware using standard Schlenk techniques, unless otherwise stated. Synthesis grade solvents were used as purchased, anhydrous solvents were taken from a commercial SPS solvent dispenser. Chromatographic purification of products was accomplished using force-flow chromatography (FC) on silica gel (35-70 mesh). For thin layer chromatography (TLC) analysis throughout this work, Merck pre-coated TLC plates (silica gel 60 GF254, 0.25 mm) were employed, using UV light as the visualizing agent and basic aqueous potassium permanganate (KMnO_4) stain solution and heat as developing agents. Organic solutions were concentrated under reduced pressure on a Büchi rotary evaporator (in vacuo at 40 °C, ~5 mbar).

Determination of Enantiomeric Purity. UPC2 analysis on chiral stationary phase was performed on a Waters Acquity instrument using IA, IB, IC, OJ and IE chiral columns. The exact conditions for the analyses are specified within the characterization section.

Materials. The starting materials used in this study are commercial and were purchased in the highest purity available from Sigma-Aldrich, Fluka, Alfa Aesar, Fluorochem, Apollo and CarboSynth, and used as received, without further purifications. The synthesis of Aldehydes substrates is described in the section B.

4.7.2 Experimental Setup

The reaction setup used in this study consists of an aluminium supported single-LED connected to a power supply to control the intensity of the light (Figure 4.18). The single LED is provided of a plastic 3D-printed support above which is placed an aluminium fitter for the reaction vials. The latter is provided with inlet and outlet holes through which the refrigerating liquid flows. The setup is connected by rubber tubes to a Huber minichiller set to -12 °C, which cools the aluminium plate and the reaction (the temperature of the reaction mixture was measured to be -10 °C). The setup is finally inserted in a homemade plastic cover to provide a closed space in which an argon/nitrogen atmosphere is created to prevent any water condensation during the reaction. The irradiance of the single LED is measured before every reaction through the aid of a photodiode and is generally stable on 115 mW/cm².

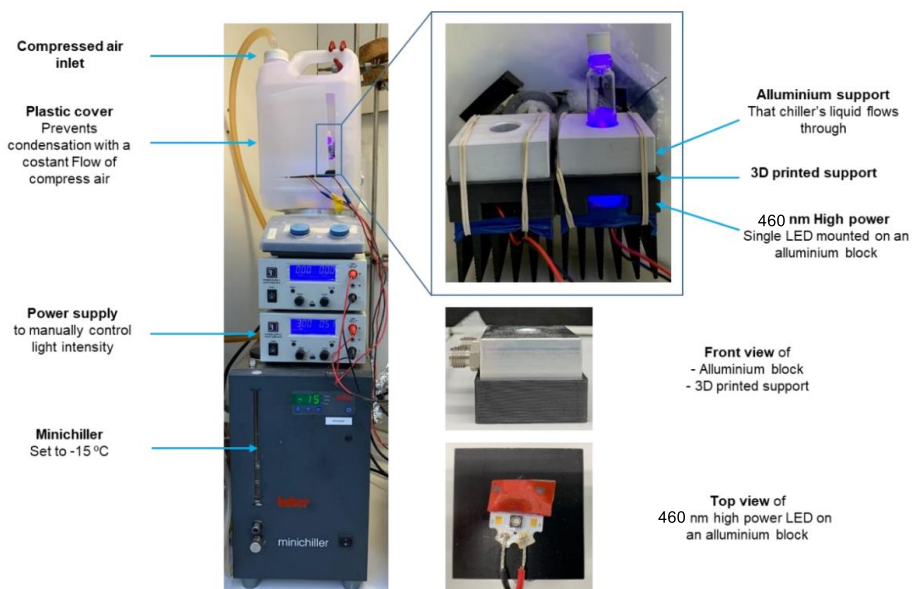


Figure 4.18: Photoreactor used for the catalytic reactions.

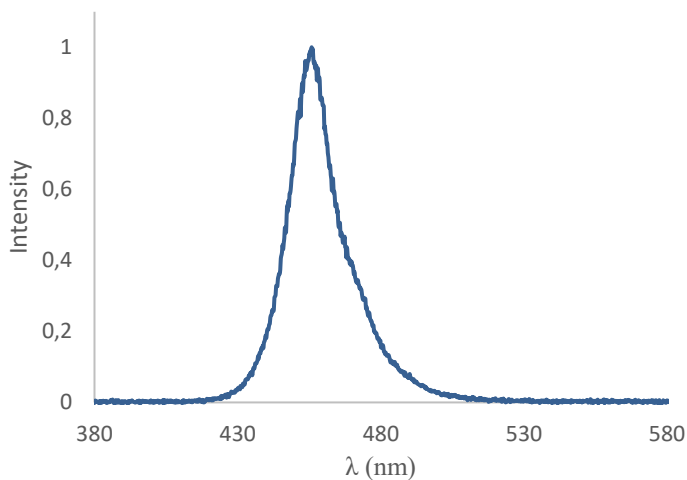


Figure 4.19: Emission spectrum of the 465 nm single LED used in this study.

4.7.3 Substrate synthesis

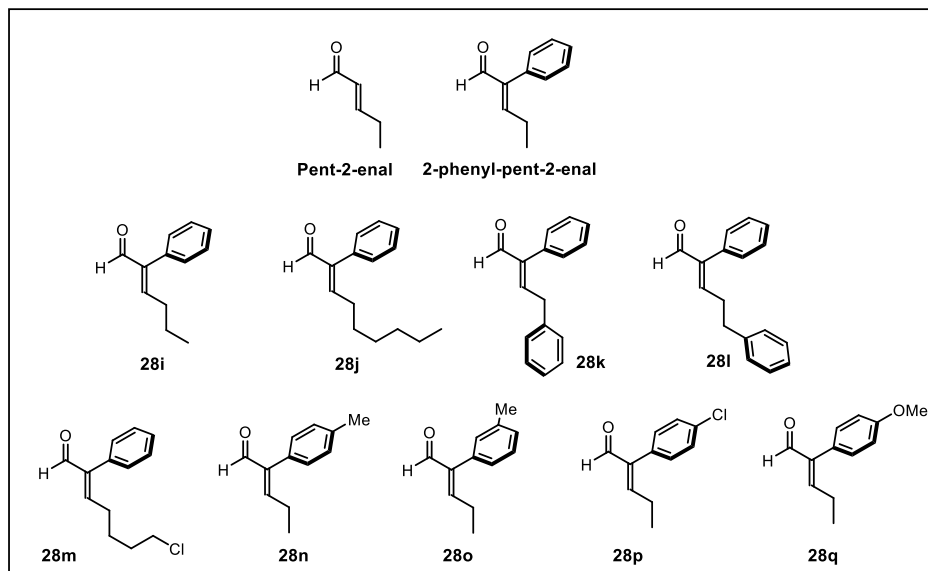
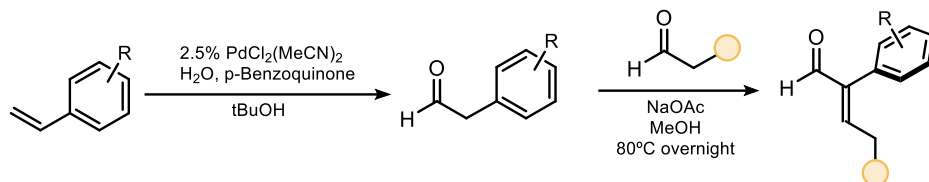


Figure 4.20: Survey of the enal substrates used in this study.

Pent-2-enal and 2-phenyl-pent-2-enal are commercially available and were used without prior purification. Enals **28i**, **28j**, **28k**, **28l** and **28m** were prepared by aldol condensation from 2-phenyl acetaldehyde and butanal, heptenal, 2-phenyl acetaldehyde, hydrocinnamaldehyde and 5-chloro-pentanal respectively. Substrates **28n**, **28o**, **28q** were prepared by a two-step sequence synthesis following slightly modified literature procedures.¹⁹⁷ Enal **28p** was prepared with general procedure **B**. All products matched the spectroscopic characterization reported in literature.¹⁹⁸

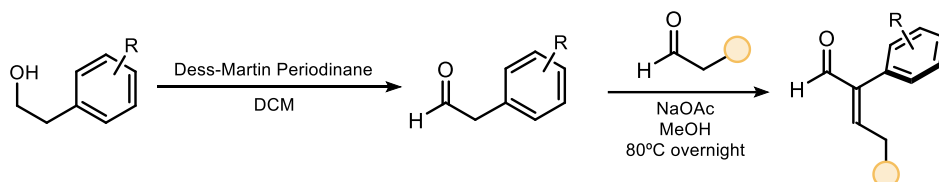
¹⁹⁷ Wacker oxidation: Teo, P.; Wickens, Z. K.; Dong, G.; Grubbs, Efficient and Highly Aldehyde Selective Wacker Oxidation R. H. *Org. Lett.* **2012**, *14*, 3237 – 3239. Alcohol Oxidation: Kolonko, K. J.; Reich, H. J. *J. Am. Chem. Soc.* **2008**, *130*, 9668–9669. Aldol Condensation: Schreiber, W. L., Pittet A. O.; Vock M. H. Flavor properties of phenylpentenals. *J. Agric. Food Chem.* **1974**, *22*, 269 – 273.

¹⁹⁸ (a) Silvi, M.; Arceo, E.; Jurberg, I. D.; Cassani, C.; Melchiorre, P. Enantioselective Organocatalytic Alkylation of Aldehydes and Enals Driven by the Direct Photoexcitation of Enamines. *J. Am. Chem. Soc.* **2015**, *137*, 6120–6123 (b) Balletti, M.; Marcantonio, E.; Melchiorre, P. Photochemical organocatalytic enantioselective radical γ -functionalization of α -branched enals. *Chem. Commun.* **2022**, *58*, 6072 – 6075.

General Procedure A: Wacker Oxidation + Aldol Condensation

To a stirring solution of $\text{PdCl}_2(\text{MeCN})_2$ (0.025 equiv.) and benzoquinone (1.15 equivs.) were added distilled H_2O (1 equiv.) and styrene derivative (1 equiv.) at 85°C . The resulting mixture was stirred for 45-60 minutes (until consumption of starting material, as judged by TLC analysis) at the same temperature. Most of the solvent was removed under reduced pressure and the residue was dissolved in DCM. The organic layer was washed with distilled water, brine, dried over MgSO_4 , and the solvent was removed under reduced pressure. Vacuum distillation afforded the aldehyde that was sufficiently pure for use in the next step.

To a stirring solution of 2-phenyl acetaldehyde (1 equivs.) in MeOH (0.3M), propionaldehyde (3 equiv.) and NaOAc (2 equivs.) were added and the resulting mixture was heated to reflux overnight. The MeOH was evaporated under reduced pressure and the resulting material was diluted in a minimal amount of Et_2O . The organic phase was washed twice with brine, dried over MgSO_4 , and the solvent was evaporated under reduced pressure. The residue was purified by column chromatography on silica (2% EtOAc in hexane) to afford 2-phenylpent-2-enal as colorless oil (yields ranging from 25% to 30%).

General Procedure B: Alcohol Oxidation + Aldol Condensation

To a stirring solution of alcohol (1 equivs.) in DCM (0.1M), Dess-Martin periodinane (1.2 equivs.) was added under argon. After 3h stirring, the reaction was quenched with saturated aqueous solutions of NaHCO_3 and $\text{Na}_2\text{S}_2\text{O}_3$ (20 mL). After 30 min, the resulting mixture was extracted with DCM (2 x 25 mL). The combined organic layers were washed with brine, dried over MgSO_4 , filtered, evaporated under reduced pressure, and purified by column chromatography (eluent: hexane/EtOAc 10:1) to give the corresponding aldehyde (yields ranging from 40% to 60%) as a colorless oil. The crude aldehyde was of sufficient purity and used for the next step without further purification.

To a stirred solution of 2-phenyl acetaldehyde (1 equivs.) in MeOH (0.3M), propionaldehyde (3 equiv.) and NaOAc (2 equivs.) were added and the resulting mixture was heated to reflux overnight. The MeOH was evaporated under reduced pressure and the resulting material was diluted in a minimal amount of Et₂O. The organic phase was washed twice with brine, dried over MgSO₄, and the solvent was evaporated under reduced pressure. The residue was purified by column chromatography on silica (2% EtOAc in hexane) to afford 2-phenylpent-2-enal as colorless oil (yields ranging from 25% to 30%).

4.7.4 Catalyst synthesis

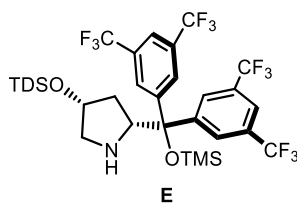


Figure 4.21: Best performing catalyst

Aminocatalyst **E** was synthesized starting from commercially available *trans*-4-hydroxy-*L*-proline by a 5-step synthesis described below. All the products matched the spectroscopic characterization reported in literature.¹⁹⁹

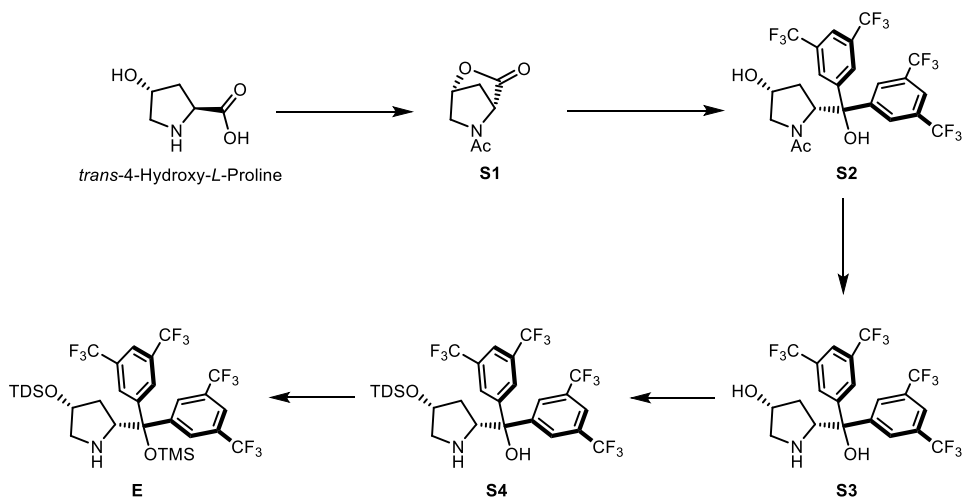
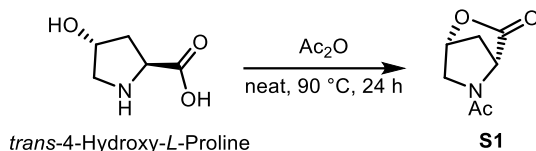
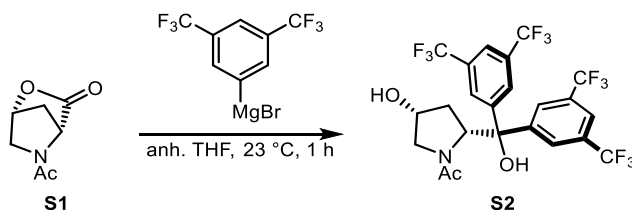


Figure 4.22: General synthetic sequence for the enal synthesis.

¹⁹⁹ Arenas, I.; Ferrali, A.; Rodríguez-Esrich, C.; Bravo, F.; Pericas, M. A. *cis*-4-Alkoxydialkyl- and *cis*-4-Alkoxydiarylprolinol Organocatalysts: High Throughput Experimentation (HTE)-Based and Design of Experiments (DoE)-Guided Development of a Highly Enantioselective aza-Michael Addition of Cyclic Imides to α,β -Unsaturated Aldehydes. *Adv. Synth. Catal.* **2017**, *359*, 2414–2424.

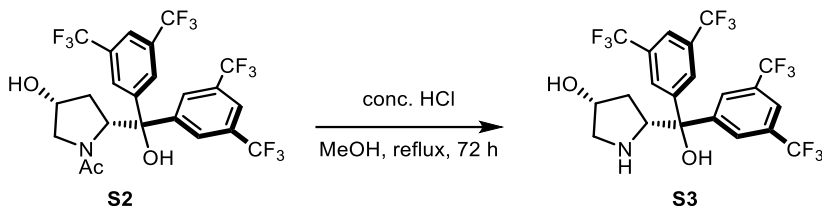
S1. Synthesis of (1*R*,4*R*)-5-acetyl-2-oxa-5-azabicyclo[2.2.1]heptan-3-one (S1)

A suspension of commercially available *trans*-4-hydroxy-L-proline (10.0 g, 76 mmol) in acetic anhydride (50 mL, 534 mmol) was stirred at 90 °C for 24 h. Upon completion, the reaction mixture was cooled to room temperature and concentrated under reduced pressure. *i*PrOH (50 mL) was added under rapid stirring and the resulting mixture was kept at -20 °C for 16 h. The resulting white precipitate was filtered off and washed with hexane (3 x 25 mL). Drying under vacuum afforded lactone S1 (7.1 g, 60% yield) as a white solid, which was sufficiently pure to be taken on to the next step.

S2. Synthesis of 1-((2*R*,4*R*)-2-(bis(3,5-bis(trifluoromethyl)phenyl)(hydroxy)methyl)-4-hydroxypyrrolidin-1-yl)ethan-1-one (S2)

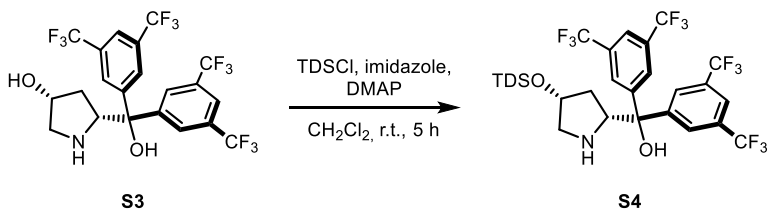
In a two-necked round bottom flask equipped with a septum and condenser containing a stirring bar were added Mg turnings (3.3 g, 137 mmol). The air and residual moisture were removed through vacuum air flaming for 30 minutes. To the Mg was added anhydrous THF (2M) and a crystal of I₂. 1-Bromo-3,5-bis(trifluoromethyl)benzene (25.2 mL, 137 mmol) was added portion wise to the suspension and the color changes gradually from red-brown to grey (exothermic reaction). After the resulting solution cooled back to room temperature, lactone S1 (7.1 g, 46 mmol) was added as solid in one portion. The reaction was stirred for 1 h and then slowly quenched with 1M HCl at 0 °C. The reaction was extracted with DCM (3 x 50 mL). The organic layer washed with brine, dried over MgSO₄ and concentrated under reduced pressure to afford prolinol S2 (65% yield) as a dark brown oil which was sufficiently pure to be taken on to the next step.

S3. *Synthesis of (3R,5R)-5-(bis(3,5-bis(trifluoromethyl)phenyl)(hydroxy)methyl)-pyrrolidin-3-ol (S3)*



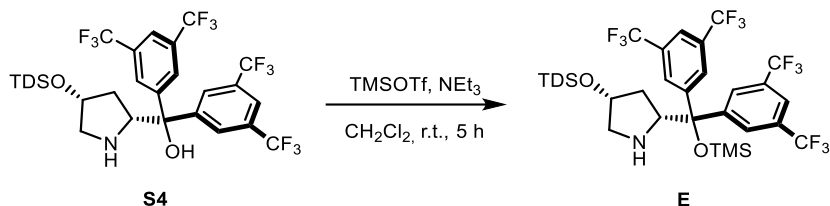
A suspension of prolinol S2 (2.8 g, 4.8 mmol) and conc. HCl (37% in water, ca. 12 M, 15 mL) in MeOH (30 mL) was heated to reflux for 72 h. The excess of MeOH was evaporated in the rotavapor and the acid was neutralized carefully with aq. Na₂CO₃ to reach a pH of 10. The mixture was extracted with DCM (3 x 25 mL). The organic layer was washed with brine, dried over MgSO₄, and concentrated under reduced pressure to afford a brownish foam. The crude product was purified by column chromatography on silica (50% EtOAc in hexane) to afford prolinol S3 (1.9 g, 72% yield) as a light brown foam.

S4. *Synthesis of bis(3,5-bis(trifluoromethyl)phenyl)((2R,4R)-4-(((2,3-dimethylbutan-2-yl)dimethylsilyl)oxy)pyrrolidin-2-yl)methanol (S4)*



To a solution of prolinol S3 (3.30 g, 6.10 mmol), imidazole (1.04 g, 15.24 mmol), and DMAP (112 mg, 0.91 mmol) in DCM (40 mL) was added TDSiCl (2.94 g, 15.24 mmol) dropwise under strong stirring. The resulting solution was stirred at 23 °C for 5 h. The reaction was quenched with H₂O and extracted with DCM (3 x 50 mL). The organic layer was washed with brine, dried over MgSO₄, and concentrated under reduced pressure to afford crude prolinol S4 as a light brown oil which was sufficiently pure to be taken on to the next step.

S5. Synthesis of (2*R*,4*R*)-2-(bis(3,5-bis(trifluoromethyl)phenyl)((trimethylsilyl)oxy)-methyl)-4-(((2,3-dimethylbutan-2-yl)dimethylsilyl)oxy)pyrrolidine (**E**)



To a solution of prolinol **S4** (4.17 g, 6.10 mmol) and triethylamine (2.6 mL, 18.29 mmol) in DCM (40 mL) was added TMSOTf (3.3 mL, 18.29 mmol) dropwise at 0 °C under strong stirring. The resulting solution was stirred at 23 °C for 5 h. The reaction was quenched with H₂O and extracted with DCM (3 x 50 mL). The organic layer was washed with brine, dried over MgSO₄, and concentrated under reduced pressure to afford a light brown oil. The oil was purified by column chromatography on silica (2% Et₂O in hexane) to afford catalyst **E** (3.46 g, 75% yield over two steps) as a pale-yellow oil.

HRMS: calculated for [C₃₂H₄₂F₁₂NO₂Si₂]⁺ [M+H]⁺: 756.2557; found: 756.2588.

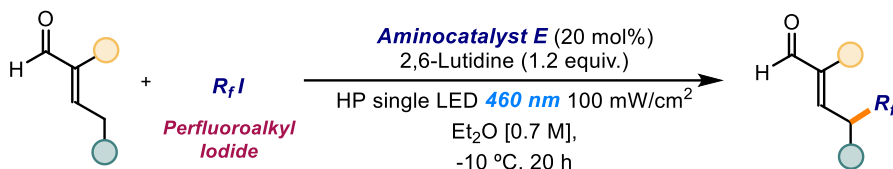
¹H NMR (500 MHz, CDCl₃) δ 7.98 (s, 2H), 7.84 (s, 2H), 7.80 (s, 2H), 4.21 (ddd, J = 7.0, 4.0, 1.1 Hz, 1H), 3.99 (dd, J = 9.4, 7.4 Hz, 1H), 2.90 (dd, J = 11.7, 5.9 Hz, 1H), 2.42 (dd, J = 11.7, 4.8 Hz, 1H), 1.88 (dt, J = 13.8, 7.2 Hz, 1H), 1.49 (p, J = 6.9 Hz, 1H), 1.30 (ddd, J = 13.1, 9.5, 5.9 Hz, 1H), 0.77 (d, J = 6.9 Hz, 6H), 0.71 (d, J = 2.9 Hz, 6H), -0.02 (d, J = 1.8 Hz, 6H), -0.07 (s, 9H).

¹³C NMR (126 MHz, CDCl₃) 148.25, 146.24, 131.54 (q, J_{C,F} = 33.4 Hz), 131.19 (q, J_{C,F} = 33.2 Hz), 129.61 (broad s), 128.55 (broad s), 124.45 (d, J_{C,F} = 14.4 Hz), 122.28 (d, J_{C,F} = 14.4 Hz), 121.96 (overlapped signals, m), 82.07, 72.24, 64.49, 55.78, 37.87, 34.23, 24.84, 20.28 (d, J = 8.2 Hz), 18.53 (d, J = 3.8 Hz), 2.00, -2.71.

¹⁹F NMR (471 MHz, CDCl₃) δ -62.83 (s, 6F), -62.89 (s, 6F).

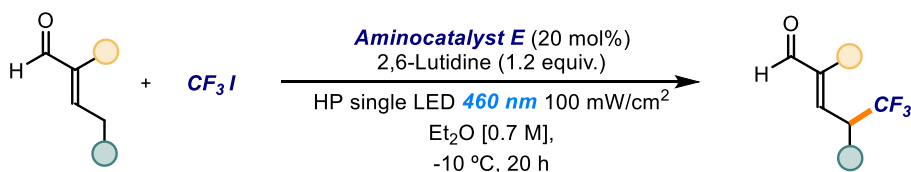
4.7.5 General procedures for the organocatalytic fluoroalkylation

General Procedure C: γ -fluoroalkylation using liquid or solid perfluoroalkyl iodides



In an oven dried 5 mL vial equipped with a Teflon septum screw cap and a magnetic stirring bar, aminocatalyst **E** (0.04 mmol, 0.2 eq) was dissolved in freshly degassed Et₂O (300 μ L). To this solution was added the enal (0.6 mmol, 3 eq) followed by 2,6-lutidine (0.24 mmol, 1.2 eq), and the perfluoroalkyl iodide (0.2 mmol, 1 eq). The vial was filled with argon then closed and sealed with parafilm. The reaction was finally placed in the 3D printed support single-LED photoreactor (Figure 4.17) and with irradiance fixed at 100 mW/cm² (as controlled by an external power supply and measured using a photodiode light detector at the start of each reaction). This setup secured a reliable irradiation while keeping a distance of 1 cm between the reaction vessel and the light source. The reaction was stirred at -10 $^\circ$ C with a chiller connected to the irradiation plate (the setup is detailed in Figure 4.18). After 20 hours, the reaction mixture was directly charged on silica gel and purified by column chromatography*. In order to determine the enantiomeric excess of the products conversion to the corresponding hydrazone (condensation with 2,4-dinitrophenyl hydrazine) is performed prior to the UPC² analysis.

General Procedure B: γ -trifluoromethylation (gas reagent)



An argon purged Schlenk tube equipped with a Teflon septum screw cap and a magnetic stirring bar was cooled with a dry-ice/acetone bath to -78 $^\circ$ C. Under a gentle flow of Argon, the trifluoromethyl iodide (1 eq.) was condensed in the tared Schlenk tube using a rubber tube fitted with a 18-gauge needle (see figure 4.22). At this stage diethylether (300 μ L) was added, followed by 2,6-lutidine (0.24 mmol, 1.2 eq), the enal (0.6 mmol, 3 eq) and aminocatalyst **E** (0.04 mmol, 0.2 eq). Finally, DMSO was added (25 μ L) and the septum sealed with parafilm. The Schlenk tube was removed from the cooling bath and quickly transferred to the pre-cooled photoreactor (the setup is detailed in Figure 4.23, the same used in general procedure A). The reaction is stirred at -10 $^\circ$ C under 460 nm irradiation (irradiance fixed at 100 mW/cm²) for

24 h. The mixture is then directly charged on silica gel and purified by column chromatography* to afford the trifluoromethylated compound in the stated yield and optical purity. In order to determine the enantiomeric excess of the products conversion to the corresponding hydrazone (condensation with 2,4-dinitrophenyl hydrazine) is performed prior to the UPC² analysis.

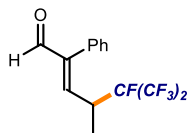
***Note:** To avoid partial racemization of the products, pre-neutralized silica was used in combination with a cold and fast elution during the chromatography purification (solvents pre-cooled to 0 °C in the freezer). Neutralization of the silica: in a 500 mL round-bottom flask 150 g of silica were added followed by 200 mL of hexane and 3 mL of triethylamine. The mixture was stirred for 5 minutes before drying the silica under vacuum.



Figure 4.23: Set-up for the trifluoromethylation reaction. *Left:* general setup used to condense CF₃I gas in the Schlenk tube. *Right:* zoom of the reactor cooled to condense the CF₃I.

4.7.6 Characterization of the products

(*S,E*)-4-(perfluoroisopropyl)-2-phenylpent-2-enal



Synthesized according to general procedure **C** using phenylpent-2-enal (0.6 mmol, 96 mg, 3 eq.) and heptafluoro-2-iodopropane (28.5 μ L, 0.2 mmol) as reaction partners. The crude mixture was purified by flash column chromatography on silica gel (eluent: hexane/CH₂Cl₂ 8:2) to afford product **30a** (47 mg, 71% yield) as a colorless oil. The enantiomeric ratio of the product was determined to be 90:10 by UPC² analysis on a Daicel Chiralpak IE column (eluent: CO₂/IPA = 90:10; flow rate 2 mL/min, λ = 360 nm. τ Major = 4.72 min, τ Minor = 4.53 min

$[\alpha]_D^{26} = -17.0$ ($c = 0.5$, CHCl_3)

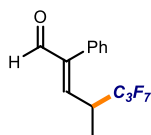
HRMS (ESI): m/z calculated for $[\text{C}_{14}\text{H}_{11}\text{OF}_7\text{Na}]^+ [\text{M}+\text{Na}]^+$: 351.0590; found: 351.0581.

$^1\text{H NMR}$ (500 MHz, CDCl_3) δ 9.68 (s, 1H), 7.52 – 7.37 (m, 3H), 7.13 – 7.06 (m, 2H), 6.68 (d, $J = 10.8$, 1H), 3.59 – 3.45 (m, 1H), 1.33 (d, $J = 8.3$ Hz, 3H).

$^{13}\text{C NMR}$ (126 MHz, CDCl_3) δ 192.71, 146.79, 146.19, 131.20, 128.75, 128.72, 128.31, 35.42, 14.49.

$^{19}\text{F NMR}$ (471 MHz, CDCl_3) δ -73.09 (m, 6F), -178.42 (m, 1F).

(*S,E*)-4-(perfluoropropyl)-2-phenylpent-2-enal



Synthesized according to general procedure **C** using phenylpent-2-enal (0.6 mmol, 96 mg, 3 eq.) and heptafluoro-1-iodopropane (28.5 μL , 0.2 mmol) as reaction partners. The crude mixture was purified by flash column chromatography on silica gel (eluent: hexane/ CH_2Cl_2 8:2) to afford product **30b** (39 mg, 60% yield) as a colorless oil. The enantiomeric ratio of the product was determined to be 89:11 by UPC² analysis on a Daicel Chiralpak IE column (eluent: $\text{CO}_2/\text{IPA} = 90:10$; flow rate 2 mL/min, $\lambda = 360$ nm. $\tau_{\text{Major}} = 6.55$ min, $\tau_{\text{Minor}} = 6.29$ min.

$[\alpha]_D^{26} = +11.3$ ($c = 0.5$, CHCl_3)

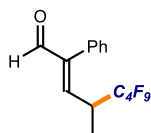
HRMS: calculated for $[\text{C}_{14}\text{H}_{11}\text{OF}_7\text{Na}]^+ [\text{M}+\text{Na}]^+$: 351.0590; found: 351.0592

$^1\text{H NMR}$ (500 MHz, CDCl_3) δ 9.68 (s, 1H), 7.52 – 7.34 (m, 3H), 7.14 – 7.07 (m, 2H), 6.63 (d, $J = 10.4$ Hz, 1H), 3.53 – 3.33 (m, 1H), 1.30 (d, $J = 6.9$ Hz, 3H).

$^{13}\text{C NMR}$ (126 MHz, CDCl_3) δ 192.65, 146.39, 145.93, 131.39, 128.75, 128.71, 128.69, 36.66, 12.95.

$^{19}\text{F NMR}$ (471 MHz, CDCl_3) δ -80.8 (m, 3F), -116.1 – -120.9 (m, 2F), -123.5 – -126.8 (m, 2F).

(*S,E*)-4-(perfluorobutyl)-2-phenylpent-2-enal



Synthesized according to general procedure **C** using phenylpent-2-enal (0.6 mmol, 96 mg, 3 eq.) and nonafluoro-1-iodobutane (34.6 μL , 0.2 mmol) as reaction partners. The crude mixture was purified by flash column chromatography on silica gel (eluent: hexane/ CH_2Cl_2 8:2) to afford product **30** (54 mg, 72% yield) as a colorless oil. The enantiomeric ratio of the product was determined to be 93:7 by UPC² analysis on a Daicel Chiralpak IE column (eluent: $\text{CO}_2/\text{IPA} = 90:10$; flow rate 2 mL/min, $\lambda = 360$ nm. $\tau_{\text{Major}} = 4.46$ min, $\tau_{\text{Minor}} = 4.33$ min.

$$[\alpha]_D^{26} = -56.1 \text{ (} c = 0.5, \text{CHCl}_3 \text{)}$$

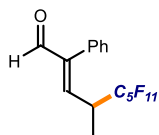
HRMS: m/z calculated for $[\text{C}_{15}\text{H}_{11}\text{OF}_9\text{Na}]^+ [\text{M}+\text{Na}]^+$: 401.0558; found: 401.0553..

$^1\text{H NMR}$ (500 MHz, CDCl_3) δ 9.68 (s, 1H), 7.55 – 7.35 (m, 3H), 7.13 – 7.08 (m, 2H), 6.64 (d, $J = 10.4$ Hz, 1H), 3.44 (m, 1H), 1.30 (d, $J = 6.9$ Hz, 3H).

$^{13}\text{C NMR}$ (126 MHz, CDCl_3) δ 192.64, 146.39, 145.88, 131.37, 128.73 (2C), 128.71, 36.85, 13.02.

$^{19}\text{F NMR}$ (471 MHz, CDCl_3) δ -81.0 (t, $J = 10.3$ Hz, 3F), -115.5 – -120.0 (m, 2F), -120.3 – -122.8 (m, 2F), -124.6 – -127.1 (m, 2F).

(*S,E*)-4-(perfluoropentyl)-2-phenylpent-2-enal



Synthesized according to general procedure **C** using phenylpent-2-enal (0.6 mmol, 96 mg, 3 eq.) and undecafluoro-1-iodopentane (37.5 μL , 0.2 mmol) as reaction partners. The crude mixture was purified by flash column chromatography on silica gel (eluent: hexane/ CH_2Cl_2 8:2) to afford product **30c** (63.5 mg, 74% yield) as a colorless oil. The enantiomeric ratio of the product was determined to be 92:8 by UPC² analysis on a Daicel Chiralpak IE column (eluent: $\text{CO}_2/\text{IPA} = 90:10$; flow rate 2 mL/min, $\lambda = 360$ nm. $\tau_{\text{Major}} = 5.98$ min, $\tau_{\text{Minor}} = 5.79$ min).

$$[\alpha]_D^{26} = -40.7 \text{ (} c = 0.5, \text{CHCl}_3 \text{)}$$

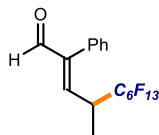
HRMS: m/z calculated for $[\text{C}_{16}\text{H}_{11}\text{OF}_{11}\text{Na}]^+ [\text{M}+\text{Na}]^+$: 451.0526; found: 451.0511

$^1\text{H NMR}$ (500 MHz, CDCl_3) δ 9.68 (s, 1H), 7.52 – 7.35 (m, 3H), 7.13 – 7.08 (m, 2H), 6.64 (d, $J = 10.5$ Hz, 1H), 3.52 – 3.40 (m, 1H), 1.30 (d, $J = 6.9$ Hz, 3H).

$^{13}\text{C NMR}$ (126 MHz, CDCl_3) δ 192.64, 146.42, 145.88, 131.39, 128.73, 128.71, 128.70, 36.95, 13.02.

$^{19}\text{F NMR}$ (471 MHz, CDCl_3) δ -80.8 (m, 3F), -115.4 – -119.5 (m, 2F), -119.7 – -121.8 (m, 2F), -122.8 (m, 2F), -125.4 – -127.0 (m, 2F).

(*S,E*)-4-(perfluorohexyl)-2-phenylpent-2-enal



Synthesized according to general procedure **C** using phenylpent-2-enal (0.6 mmol, 96 mg, 3 eq.) and tridecafluoro-1-iodohexane (44.6 μL , 0.2 mmol) as reaction partners. The crude mixture was purified by flash column chromatography on silica gel (eluent: hexane/ CH_2Cl_2 8:2) to afford product **30d** (67 mg, 70% yield) as a colorless oil. The enantiomeric ratio of the product was

determined to be 85:15 by UPC² analysis on a Daicel Chiralpak IE column (eluent: CO₂/IPA = 90:10; flow rate 2 mL/min, λ = 360 nm. τ_{Major} = 5.33 min, τ_{Minor} = 5.03 min.

[α]_D²⁶ = +22.3 (c = 0.5, CHCl₃)

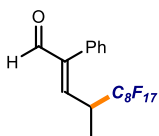
HRMS (ESI): m/z calculated for [C₁₇H₁₂OF₁₃]⁺ [M]⁺: 479.0675; found: 479.0685.

¹H NMR (500 MHz, CDCl₃) δ 9.68 (s, 1H), 7.47 – 7.37 (m, 3H), 7.13 – 7.07 (m, 2H), 6.64 (dd, *J* = 10.5 Hz, 1H), 3.47 – 3.38 (m, 1H), 1.30 (d, *J* = 7.0 Hz, 3H).

¹³C NMR (126 MHz, CDCl₃) δ 192.64, 146.42, 145.88, 131.39, 128.73, 128.71, 128.70, 36.96, 13.04.

¹⁹F NMR (471 MHz, CDCl₃) δ -80.8 (m, 3F), -115.1 – -119.4 (m, 2F), -119.6 – -121.6 (m, 2F), -122.0 (m, 2F), -122.8 (m, 2F), -126.0 – -126.3 (m, 2F).

(*S,E*)-4-(perfluorooctyl)-2-phenylpent-2-enal



Synthesized according to general procedure C using phenylpent-2-enal (0.6 mmol, 96 mg, 3 eq.) and heptadecafluoro-1-iodooctane (53.5 μL, 0.2 mmol) as reaction partners. The crude mixture was purified by flash column chromatography on silica gel (eluent: hexane/CH₂Cl₂ 85:15) to

afford product **30e** (65 mg, 56% yield) as a colorless oil. The enantiomeric ratio of the product was determined to be 85:15 by UPC² analysis on a Daicel Chiralpak IB column (eluent: CO₂/IPA = 92:8; flow rate 2 mL/min, λ = 360 nm. τ_{Major} = 3.53 min, τ_{Minor} = 3.33 min.

[α]_D²⁶ = +5.0 (c = 0.5, CHCl₃)

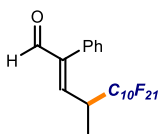
HRMS (ESI): m/z calculated for [C₁₉H₁₁F₁₇NaO]⁺ [M+Na]⁺: 601.0427; found: 601.0431.

¹H NMR (500 MHz, CDCl₃) δ 9.68 (s, 1H), 7.55 – 7.36 (m, 3H), 7.15 – 7.05 (m, 2H), 6.64 (d, *J* = 10.5 Hz, 1H), 3.51 – 3.38 (m, 1H), 1.30 (d, *J* = 7.0 Hz, 3H).

¹³C NMR (126 MHz, CDCl₃) δ 192.63, 146.43, 145.88, 131.39, 128.73, 128.71, 128.69, 36.95, 13.02.

¹⁹F NMR (471 MHz, CDCl₃) δ -80.8 (t, *J* = 10.3 Hz, 3F), -115.3 – -119.3 (m, 2F), -119.4 – -121.5 (m, 2F), -121.6 – -122.0 (m, 6F), -122.7 (m, 2F), -126.1 (m, 2F).

(*S,E*)-4-(perfluorodecyl)-2-phenylpent-2-enal



Synthesized according to general procedure C using phenylpent-2-enal (0.6 mmol, 96 mg, 3 eq.) and hencosafluoro-1-iododecane (129 mg, 0.2 mmol) as reaction partners. The crude mixture was purified by flash

column chromatography on silica gel (eluent: hexane/CH₂Cl₂ 9:1) to afford product **30f** (84 mg, 62% yield) as a white solid.

$[\alpha]_D^{26} = -81.1$ (c = 0.5, CHCl₃)

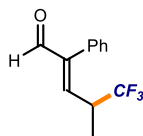
HRMS (ESI): m/z calculated for [C₂₁H₁₁O₂Na]⁺ [M+Na]⁺: 701.0367; found: 701.0374.

¹H NMR (500 MHz, CDCl₃) δ 9.69 (s, 1H), 7.51 – 7.35 (m, 3H), 7.10 (m, 2H), 6.64 (d, *J* = 10.4 Hz, 1H), 3.52 – 3.40 (m, 1H), 1.30 (d, *J* = 6.8 Hz, 3H).

¹³C NMR (126 MHz, CDCl₃) δ 192.64, 146.44, 145.87, 131.39, 128.73, 128.71, 128.70, 36.98, 13.05.

¹⁹F NMR (471 MHz, CDCl₃) δ -80.8 (t, *J* = 9.5 Hz, 3F), -115.6 – -119.2 (m, 2F), -119.6 – -121.5 (m, 2F), -121.9 (m, 10F), -122.7 (m, 2F), -126.2 (m, 2F).

(*S,E*)-4-(trifluoromethyl)-2-phenylpent-2-enal



Synthesized according to general procedure **D** using phenylpent-2-enal **1a** (0.6 mmol, 96 mg, 3 eq.) and trifluoromethyl iodide (39.8 mg, 0.2 mmol) as reaction partners. The crude mixture was purified by flash column chromatography on silica gel (eluent: hexane/CH₂Cl₂ 8:2) to afford product

3b (31.2 mg, 56% yield) as a colorless oil. The enantiomeric excess of the product was determined to be 86:14 by UPC² analysis on a Daicel Chiralpak IE column (eluent: CO₂/IPA = 90:10; flow rate 2 mL/min, λ = 360 nm. τ_{Major} = 5.49 min, τ_{Minor} = 5.25 min.

$[\alpha]_D^{26} = -12.3$ (c = 0.5, CHCl₃)

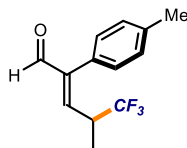
HRMS: calculated for [C₁₂H₁₁F₃NaO]⁺ [M+Na]⁺: 251.0659, found: 251.0654.

¹H NMR (400 MHz, CDCl₃) δ 9.69 (s, 1H), 7.50 – 7.38 (m, 3H), 7.14 (m, 2H), 6.57 (d, *J* = 10.4 Hz, 1H), 3.43 – 3.24 (m, 1H), 1.26 (d, *J* = 7.0 Hz, 3H).

¹³C NMR (126 MHz, CDCl₃) δ 192.71, 146.71, 146.41, 131.39, 128.99, 128.69, 127.81, 38.71, 13.78.

¹⁹F NMR (376 MHz, CDCl₃) δ -71.6 (d, *J* = 8.1 Hz, 3F).

(*S,E*)-4-(trifluoromethyl)-2-(4-methylphenyl)pent-2-enal



Synthesized according to general procedure **D** using phenylpent-2-enal **1a** (0.6 mmol, 96 mg, 3 eq.) and trifluoromethyl iodide (39.8 mg, 0.2 mmol) as reaction partners. The crude mixture was purified by flash column chromatography on silica gel (eluent: hexane/CH₂Cl₂ 8:2) to afford product

3b (21 mg, 43% yield) as a colorless oil. The enantiomeric excess of the

product was determined to be 86:14 by UPC² analysis on a Daicel Chiralpak IE column (eluent: CO₂/IPA = 90:10; flow rate 2 mL/min, λ = 360 nm. τ_{Major} = 5.66 min, τ_{Minor} = 5.40 min.

HRMS: calculated for [C₁₃H₁₃F₃NaO]⁺ [M+Na]⁺: 265.0815, found: 265.0811.

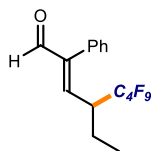
[α]_D²⁶ = +19.4 (c = 0.5, CHCl₃)

¹H NMR (400 MHz, CDCl₃) δ 9.68 (s, 1H), 7.25 – 7.22 (m, 2H), 7.03 (m, 2H), 6.54 (d, J = 10.4 Hz, 1H), 3.42 – 3.28 (m, 1H), 2.39 (s, 3H), 1.26 (d, J = 6.9 Hz, 3H).

¹³CNMR (126 MHz, CDCl₃) δ 192.9, 146.7, 146.2, 146.2, 138.6, 129.4, 128.9, 38.9, 21.3, 13.8, 13.8.

¹⁹F NMR (376 MHz, CDCl₃) δ -71.5 (d, J = 8.1 Hz, 3F).

(*S,E*)-2-phenyl-4-(perfluorobutyl)hex-2-enal



Synthesized according to general procedure **C** using phenylhex-2-enal **1a** (0.6 mmol, 102 mg, 3 eq.) and nonafluoro-1-iodobutane (34.6 μL, 0.2 mmol) as reaction partners. The crude mixture was purified by flash column chromatography on silica gel (eluent: hexane/CH₂Cl₂ 8:2) to afford product

30i (49 mg, 62% yield) as a colorless oil. The enantiomeric excess of the product was determined to be 91:9 by UPC² analysis on a Daicel Chiralpak IE column (eluent: CO₂/IPA = 90:10; flow rate 2 mL/min, λ = 360 nm. τ_{Major} = 6.24 min, τ_{Minor} = 6.06 min.

[α]_D²⁶ = -8.0 (c = 0.5, CHCl₃)

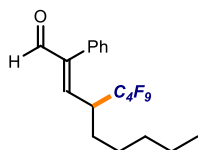
HRMS: calculated for [C₁₆H₁₃F₃NaO]⁺ [M+Na]⁺: 415.0706, found: 415.0715.

¹H NMR (400 MHz, CDCl₃) δ 9.72 (s, 1H), 7.48 – 7.35 (m, 3H), 7.11 (m, 2H), 6.54 (dd, J = 10.8, 2.0 Hz, 1H), 3.37 – 3.20 (m, 1H), 1.94 (m, 1H), 1.65 (m, 1H), 0.86 (t, J = 7.5 Hz, 3H).

¹³CNMR (126 MHz, CDCl₃) δ 192.8, 148.0, 145.4, 131.7, 129.2, 128.7, 77.4, 43.4, 20.6, 11.3

¹⁹F NMR (376 MHz, CDCl₃) δ -81.1 (m, 3F), -113.9 – -116.5 (m, 2F), -119.4 – -123.0 (m, 2F), -126.0 (m, 2F).

(*S,E*)-2-phenyl-4-(perfluorobutyl)non-2-enal



Synthesized according to general procedure **C** using phenylnon-2-enal (0.6 mmol, 130 mg, 3 eq.) and nonafluoro-1-iodobutane (34.6 μL, 0.2 mmol) as reaction partners. The crude mixture was purified by flash column chromatography on silica gel (eluent: hexane/CH₂Cl₂ 9:1) to

afford product **30j** (65 mg, 75% yield) as a colorless oil. The enantiomeric excess of the product was determined to be 90:10 by UPC² analysis on a Daicel Chiralpak IE column (eluent: CO₂/IPA = 90:10; flow rate 2 mL/min, λ = 360 nm. τ_{Major} = 4.70 min, τ_{Minor} = 4.37 min.

$[\alpha]_{\text{D}}^{26}$ = -13.1 (c = 0.5, CHCl₃)

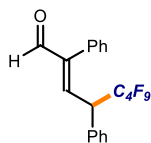
HRMS: calculated for [C₁₆H₁₃F₃NaO]⁺ [M+Na]⁺: 415.0706, found: 415.0715.

¹H NMR (500 MHz, CDCl₃) δ 9.71 (s, 1H), 7.48 – 7.34 (m, 3H), 7.19 – 7.04 (m, 2H), 6.54 (dd, J = 10.8, 1.8 Hz, 1H), 3.43 – 3.30 (m, 1H), 3.46 – 3.32 (m, 1H), 1.91 – 1.80 (m, 1H), 1.62 (m, 1H), 1.38 – 1.01 (m, 6H), 0.84 (t, J = 7.3 Hz, 3H).

¹³C NMR (126 MHz, CDCl₃) δ 192.9, 147.6, 145.9, 131.7, 129.2, 128.7 (2C), 42.0, 31.5, 27.2, 26.2, 22.5, 14.0.

¹⁹F NMR (376 MHz, CDCl₃) δ -81.1 (m, 3F), -113.9 – -116.5 (m, 2F), -119.4 – -123.0 (m, 2F), -126.0 (m, 2F).

(*S,E*)-2-phenyl-4-(phenyl)-4-(perfluorobutyl)but-2-enal



Synthesized according to general procedure **C** using 2,4-diphenylbut-2-enal (0.6 mmol, 133 mg, 3 eq.) and nonafluoro-1-iodobutane (34.6 μ L, 0.2 mmol) as reaction partners. The crude mixture was purified by flash column chromatography on silica gel (eluent: hexane/CH₂Cl₂ 8:2) to afford product

30k (55 mg, 62% yield) as a colorless oil. The enantiomeric excess of the product was determined to be 89:11 by UPC² analysis on a Daicel Chiralpak OJ column (eluent: CO₂/MeCN = 90:10; flow rate 2 mL/min, λ = 360 nm. τ_{Major} = 2.91 min, τ_{Minor} = 2.70 min.

$[\alpha]_{\text{D}}^{26}$ = +44.5 (c = 0.5, CHCl₃)

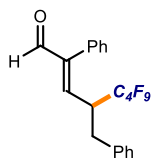
HRMS: calculated for [C₂₀H₁₃F₉NaO]⁺ [M+Na]⁺: 463.0727, found: 463.0715.

¹H NMR (500 MHz, CDCl₃) δ 9.74 (s, 1H), 7.44 – 7.36 (m, 6H), 7.24 – 7.19 (m, 2H), 7.13 – 7.03 (m, 2H), 7.02 – 6.96 (d, 10.5 Hz, 1H), 4.44 (m, 1H).

¹³C NMR (126 MHz, CDCl₃) δ 192.50, 146.33, 143.65, 131.21, 129.33, 129.25, 128.95, 128.89, 128.85, 128.60, 127.78, 47.7

¹⁹F NMR (376 MHz, CDCl₃) δ -81.1 (m, 3F), -111.8 – -115.9 (m, 2F), -121.0 (m, 2F), -126.04 (m, 2F).

(*S,E*)-2-phenyl-5-(phenyl)-4-(perfluorobutyl)pent-2-enal



Synthesized according to general procedure **C** using 2,5-diphenylpent-2-enal (0.6 mmol, 142 mg, 3 eq.) and nonafluoro-1-iodobutane (34.6 μ L, 0.2 mmol) as reaction partners. The crude mixture was purified by flash column chromatography on silica gel (eluent: hexane/ CH_2Cl_2 8:2) to afford product **30l** (54 mg, 59% yield) as a colorless oil. The enantiomeric excess of the product was determined to be 90:10 by UPC² analysis on a Daicel Chiralpak IE column (eluent: CO_2 /IPA = 90:10; flow rate 2 mL/min, λ = 360 nm. τ_{Major} = 4.73 min, τ_{Minor} = 4.91 min.

$[\alpha]_{\text{D}}^{26} = +31.2$ (c = 0.5, CHCl_3)

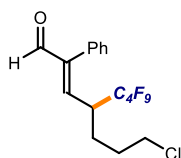
HRMS: calculated for $[\text{C}_{21}\text{H}_{15}\text{F}_9\text{NaO}]^+ [\text{M}+\text{Na}]^+$: 477.0871, found: 477.0871.

¹H NMR (500 MHz, CDCl_3) δ 9.63 (s, 1H), 7.27 – 7.23 (m, 4H), 7.22 – 7.10 (m, 2H), 7.00 – 6.93 (m, 2H), 6.54 (dd, J = 10.9, 2.1 Hz, 1H), 6.35 – 6.29 (m, 2H), 3.60 – 3.46 (m, 1H), 3.30 (dd, J = 13.6, 3.2 Hz, 1H), 2.78 (dd, J = 13.6, 10.8 Hz, 1H).

¹³C NMR (126 MHz, CDCl_3) δ 192.6, 148.2, 143.9, 135.9, 131.0, 129.7, 128.9, 128.7, 128.4, 128.2, 127.4, 44.6, 33.5.

¹⁹F NMR (376 MHz, CDCl_3) δ -81.0 (m, 3F), -112.5 – -117.6 (m, 2F), -118.6 – -123.2 (m, 2F), -125.7 – -126.3 (m, 2F).

(*S,E*)-2-phenyl-4-(perfluorobutyl)-7-chloro-hept-2-enal



Synthesized according to general procedure **C** using 2-phenyl-7-chloro-hept-2-enal (0.6 mmol, 134 mg, 3 eq.) and nonafluoro-1-iodobutane (34.6 μ L, 0.2 mmol) as reaction partners. The crude mixture was purified by flash column chromatography on silica gel (eluent: hexane/ CH_2Cl_2 8:2) to afford product **30m** (36 mg, 41% yield) as a colorless oil. The enantiomeric excess of the product was determined to be 88:12 by UPC² analysis on a Daicel Chiralpak IE column (eluent: CO_2 /MeCN = 90:10; flow rate 2 mL/min, λ = 360 nm. τ_{Major} = 4.80 min, τ_{Minor} = 4.64 min.

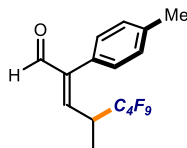
$[\alpha]_{\text{D}}^{26} = -4.1$ (c = 0.5, CHCl_3)

HRMS: calculated for $[\text{C}_{20}\text{H}_{13}\text{F}_9\text{NaO}]^+ [\text{M}+\text{Na}]^+$: 463.0727, found: 463.0715.

¹H NMR (500 MHz, CDCl_3) δ 9.72 (s, 1H), 7.51 – 7.35 (m, 3H), 7.13 – 7.08 (m, 2H), 6.56 (dd, J = 10.7, 1.5 Hz, 1H), 3.45 – 3.27 (m, 3H), 2.05 (m, 1H), 1.82 – 1.70 (m, 2H), 1.60 – 1.48 (m, 1H).

¹³C NMR (126 MHz, CDCl_3) δ 192.5, 147.8, 144.6, 131.4, 129.04, 128.9 (2C), 43.9, 41.5, 29.4, 24.8

¹⁹F NMR (376 MHz, CDCl_3) δ -81.0 (m, 3F), -112.9 – -116.6 (m, 2F), -118.9 – -122.7 (m, 2F), -125.0 – -127.1 (m, 2F).

(*S,E*)-4-(perfluorobutyl)-2-(*p*-methylphenyl)pent-2-enal

Synthesized according to general procedure **C** using (*p*-methylphenyl)pent-2-enal (0.6 mmol, 104 mg, 3 eq.) and nonafluoro-1-iodobutane (34.6 μ L, 0.2 mmol) as reaction partners. The crude mixture was purified by flash column chromatography on silica gel (eluent: hexane/ CH_2Cl_2 85:15) to afford product **30n** (50 mg, 64% yield) as a colorless oil. The enantiomeric excess of the product was determined to be 90:10 by UPC² analysis on a Daicel Chiralpak IE column (eluent: CO_2/IPA = 92:8; flow rate 2 mL/min, λ = 360 nm. τ_{Major} = 4.60 min, τ_{Minor} = 4.40 min).

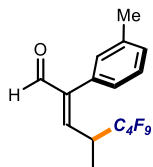
$[\alpha]_{\text{D}}^{26}$ = +21.0 (c = 0.5, CHCl_3)

HRMS: calculated for $[\text{C}_{16}\text{H}_{13}\text{F}_9\text{NaO}]^+ [\text{M}+\text{Na}]^+$: 415.0731, found: 415.0715.

¹H NMR (500 MHz, CDCl_3) δ 9.67 (s, 1H), 7.26 – 7.21 (m, 2H), 7.02 – 6.96 (m, 2H), 6.61 (dd, J = 10.4, 2.1 Hz, 1H), 3.51 – 3.42 (m, 1H), 2.39 (s, 3H), 1.29 (d, J = 7.0 Hz, 3H).

¹³C NMR (126 MHz, CDCl_3) δ 192.89, 146.21, 145.86, 138.61, 129.45, 128.61, 128.32, 36.88, 36.86, 21.28, 13.03

¹⁹F NMR (282 MHz, CDCl_3) δ -81.0 (m, 3F), -115.2 – -119.9 (m, 2F), -120.3 – -122.9 (m, 2F), -126.1 (m, 2F).

(*S,E*)-4-(perfluorobutyl)-2-(*m*-methylphenyl)pent-2-enal

Synthesized according to general procedure **C** using (*m*-methylphenyl)pent-2-enal (0.6 mmol, 104 mg, 3 eq.) and nonafluoro-1-iodobutane (34.6 μ L, 0.2 mmol) as reaction partners. The crude mixture was purified by flash column chromatography on silica gel (eluent: hexane/ CH_2Cl_2 85:15) to afford product **30o** (37 mg, 47% yield) as a colorless oil. The enantiomeric excess of the product was determined to be 90:10 by UPC² analysis on a Daicel Chiralpak IE column (eluent: CO_2/IPA = 92:8; flow rate 2 mL/min, λ = 360 nm. τ_{Major} = 4.43 min, τ_{Minor} = 4.27 min).

$[\alpha]_{\text{D}}^{26}$ = -15.9 (c = 0.5, CHCl_3)

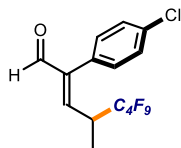
HRMS: calculated for $[\text{C}_{16}\text{H}_{13}\text{F}_9\text{NaO}]^+ [\text{M}+\text{Na}]^+$: 415.0731, found: 415.0715.

¹H NMR (500 MHz, CDCl_3) δ 9.67 (s, 1H), 7.32 (t, J = 7.5 Hz, 1H), 7.21 (d, J = 7.7 Hz, 1H), 6.92 – 6.87 (m, 2H), 6.62 (dd, J = 10.4, 2.2 Hz, 1H), 3.52 – 3.38 (m, 1H), 2.38 (s, 3H), 1.29 (d, J = 6.9 Hz, 3H).

¹³C NMR (126 MHz, CDCl₃) δ 192.9, 146.4, 146.2, 138.6, 131.5, 129.6, 129.5, 128.8, 125.9, 37.0, 21.6, 13.2

¹⁹F NMR (282 MHz, CDCl₃) δ -81.0 (m, 3F), -115.5 – -119.7 (m, 2F), -120.2 – -123.1 (m, 2F), -126.1 (m, 2F).

(*S,E*)-4-(perfluorobutyl)-2-(*p*-chlorophenyl)pent-2-enal



Synthesized according to general procedure **C** using (*p*-chlorophenyl)pent-2-enal (0.6 mmol, 117 mg, 3 eq.) and nonafluoro-1-iodobutane (34.6 μL, 0.2 mmol) as reaction partners. The crude mixture was purified by flash column chromatography on silica gel (eluent: hexane/CH₂Cl₂ 8:2) to afford product **30p** (50 mg, 61% yield) as a colorless oil. The enantiomeric excess of the product was determined to be 92:8 by UPC² analysis on a Daicel Chiralpak IE column (eluent: CO₂/IPA = 90:10; flow rate 2 mL/min, λ = 360 nm. τ_{Major} = 4.60 min, τ_{Minor} = 4.84 min.

[α]_D²⁶ = -46.3 (c = 0.5, CHCl₃)

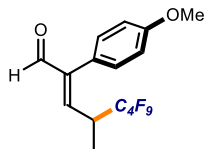
HRMS: calculated for [C₁₅H₁₀ClF₉NaO]⁺ [M+Na]⁺: 435.0165, found: 435.0169.

¹H NMR (500 MHz, CDCl₃) δ 9.66 (s, 1H), 7.42 (d, *J* = 8.7 Hz, 2H), 7.05 (d, *J* = 8.6 Hz, 2H), 6.65 (dd, *J* = 10.5, 2.2 Hz, 1H), 3.41 (m, 1H), 1.30 (d, *J* = 6.9 Hz, 3H).

¹³C NMR (126 MHz, CDCl₃) δ 192.4, 147.1, 145.0, 135.1, 130.3, 129.8, 129.2, 37.1, 13.2.

¹⁹F NMR (282 MHz, CDCl₃) δ -80.4 – -81.1 (m, 3F), -115.4 – -119.8 (m, 2F), -119.9 – -123.1 (m, 2F), -126.05 (m, 2F).

(*S,E*)-4-(perfluorobutyl)-2-(*p*-methoxyphenyl)pent-2-enal



Synthesized according to general procedure **C** using (*p*-methoxyphenyl)pent-2-enal (0.6 mmol, 114 mg, 3 eq.) and nonafluoro-1-iodobutane (34.6 μL, 0.2 mmol) as reaction partners. The crude mixture was purified by flash column chromatography on silica gel (eluent: hexane/CH₂Cl₂ 7:3) to afford product **30q** (42 mg, 51% yield) as a colorless oil. The enantiomeric excess of the product was determined to be 90:10 by UPC² analysis on a Daicel Chiralpak IE column (eluent: CO₂/IPA = 90:10; flow rate 2 mL/min, λ = 360 nm. τ_{Major} = 4.78 min, τ_{Minor} = 4.54 min.

[α]_D²⁶ = -40.1 (c = 0.5, CHCl₃)

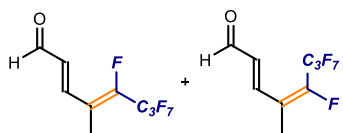
HRMS: calculated for [C₁₆H₁₃F₉NaO₂]⁺ [M+Na]⁺: 408.0771, found: 408.0783.

¹H NMR (400 MHz, CDCl₃) δ 9.66 (s, 1H), 7.07 – 7.00 (m, 2H), 7.00 – 6.90 (m, 2H), 6.59 (dd, *J* = 10.5, 2.1 Hz, 1H), 3.84 (s, 3H), 3.56 – 3.44 (m, 1H), 1.30 (d, *J* = 7.1 Hz, 3H).

$^{13}\text{C NMR}$ (101 MHz, CDCl_3) δ 193.2, 160.0, 146.3, 145.6, 130.2, 123.5, 114.4, 54.9, 37.2, 13.2.

$^{19}\text{F NMR}$ (376 MHz, CDCl_3) δ -81.0 (m, 3F), -115.4 – -119.5 (m, 2F), -119.9 – -123.1 (m, 2F), -126.2 (m, 2F).

(2E)-octafluoro-4-methylocta-2,4-dienal



Synthesized according to general procedure **C** using pent-2-enal (0.6 mmol, 51 mg, 3 eq.) and nonafluoro-1-iodobutane (34.6 μL , 0.2 mmol) as reaction partners. The crude mixture was purified by flash column chromatography on silica gel (eluent: hexane/ CH_2Cl_2 8:2) to afford product **30r** (31 mg, 51% yield) as a colorless oil as a mixture of conformational isomers.

$^1\text{H NMR}$ (500 MHz, CDCl_3) δ 9.74 (d, $J = 7.5$ Hz, 1H *isomer1*), 9.68 (d, $J = 7.5$ Hz, 1H *isomer2*), 7.65 (dd, $J = 16.0, 1.8$ Hz, 1H *isomer1*), 7.49 (dd, $J = 15.6, 1.2$ Hz, 1H *isomer2*), 6.48 – 6.41 (m, 2H *isomer1+2*), 2.10 (dt, $J = 4.6, 2.3$ Hz, 3H *isomer1*), 2.04 (q, $J = 3.1$ Hz, 3H *isomer2*).

$^{13}\text{C NMR}$ (101 MHz, CDCl_3) δ 193.02, 192.77, 143.38, 143.29, 134.11, 134.02, 133.12, 133.07, 29.85 (2C).

$^{19}\text{F NMR}$ (376 MHz, CDCl_3) δ -80.61 (td, $J = 9.1, 2.6$ Hz), -80.71 (td, $J = 9.1, 2.4$ Hz), -110.50 – -110.74 (m), -112.50 (m), -114.14 (m), -115.64 (m), -127.51 (d, $J = 6.8$ Hz), -127.56 (d, $J = 6.5$ Hz).

4.7.7 Quantum yield measurements

A ferrioxalate actinometer solution was prepared by following the Hammond variation of the Hatchard and Parker procedure outlined in the Handbook of Photochemistry²⁰⁰. The ferrioxalate actinometer solution measures the decomposition of ferric ions to ferrous ions, which are complexed by 1,10-phenanthroline and monitored by UV/Vis absorbance at 510 nm. The moles of iron-phenanthroline complex formed are related to moles of photons absorbed.

The following solutions were prepared and stored in a dark laboratory (red light):

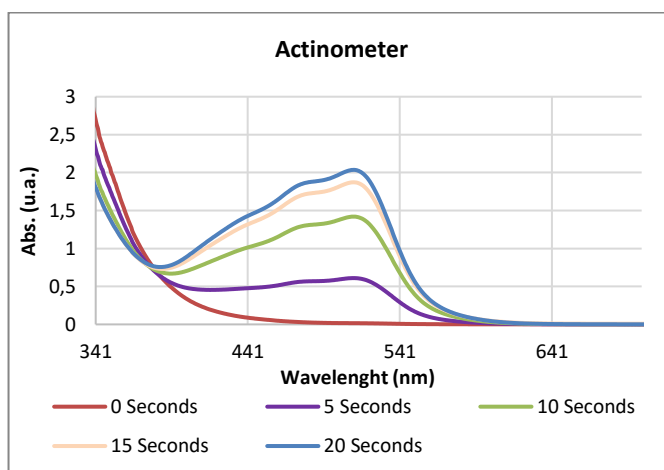
1. Potassium ferrioxalate solution: 294.8 mg of potassium ferrioxalate (commercially available from Alfa Aesar) and 139 μL of sulfuric acid (96%) were added to a 50 mL volumetric flask, and filled to the mark with water (HPLC grade).

²⁰⁰ Murov, S. L. Ed. Handbook of Photochemistry (Marcel Dekker, New York, 1973)

2. Phenanthroline solution: 0.2% by weight of 1,10-phenanthroline in water (100 mg in 50 mL volumetric flask).
3. Buffer solution: 2.47 g of NaOAc and 0.5 mL of sulfuric acid (96%) were added to a 50 mL volumetric flask, and filled to the mark with water (HPLC grade).

The actinometry measurements were done as follows:

1. 1 mL of the actinometer solution was added to a vial. The vial was placed in the reactor.
2. The solution was irradiated at 460 nm (irradiance 238 mW/cm²). This procedure was repeated 4 times, quenching the solutions after different time intervals: 5 sec, 10 sec, 15 sec, and 20 sec. Then a model reaction using perfluorodecyl iodide²⁰¹ was set following the general procedure C (differently from the general procedure, for this experiment the reaction was conducted at room temperature), placed in the irradiation set up and it has been irradiated for 30 minutes. This procedure has been performed other two times with different irradiation times (45 min and 60 min).
3. After irradiation, the actinometer solutions were removed and placed in a 10 mL volumetric flask containing 0.5 mL of 1,10-phenanthroline solution and 2 mL of buffer solution. These flasks were filled to the mark with water (HPLC grade).
4. The UV-Vis spectra of the complexed actinometer samples were recorded for each time interval. The absorbance of the complexed actinometer solution was monitored at 510 nm.



The moles of Fe²⁺ formed for each sample is determined using Beers' Law (Eq. 1):

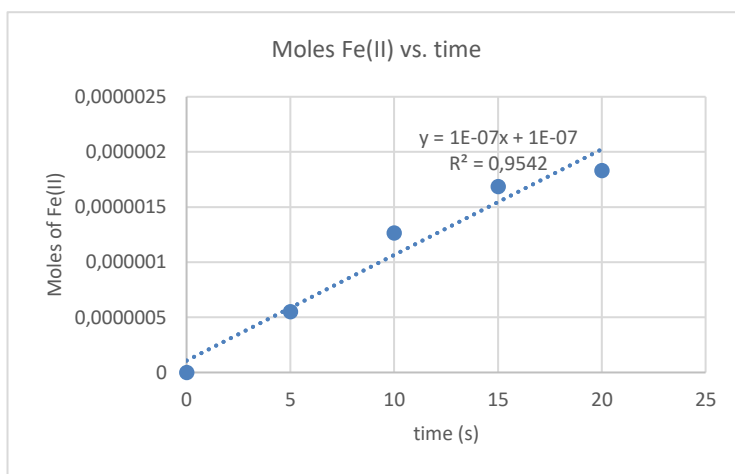
²⁰¹ To avoid the use of volatiles perfluorinated compounds for the GC-FID calibration, we conducted the experiment with perfluorodecyl iodide since the corresponding product **30f** is solid with low melting point

$$\text{Mols of Fe(II)} = V1 \times V3 \times \Delta A(510 \text{ nm}) / 10^3 \times V2 \times l \times \epsilon(510 \text{ nm}) \quad (\text{Eq. 1})$$

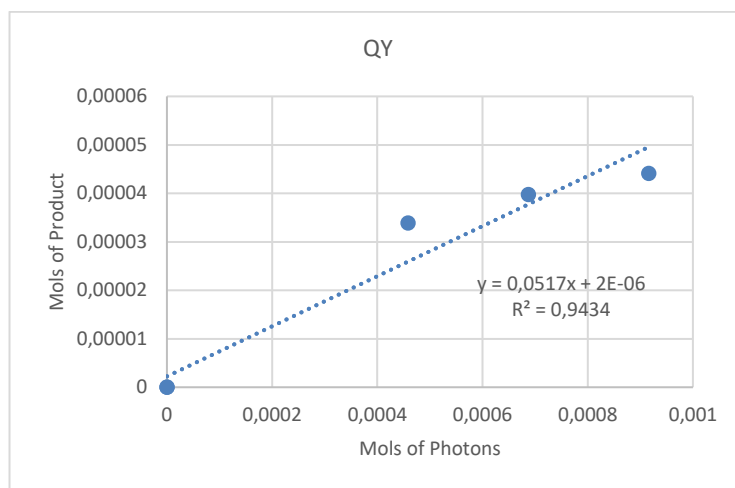
where V1 is the irradiated volume (1 mL), V2 is the aliquot of the irradiated solution taken for the determination of the ferrous ions (1 mL), V3 is the final volume after complexation with phenanthroline (10 mL), l is the optical path-length of the irradiation cell (1 cm), $\Delta A(510 \text{ nm})$ is the optical difference in absorbance between the irradiated solution and the one stored in the dark, $\epsilon(510 \text{ nm})$ is the extinction coefficient the complex $\text{Fe}(\text{phen})_3^{2+}$ at 510 nm ($11100 \text{ L mol}^{-1} \text{ cm}^{-1}$). The moles of Fe^{2+} formed (x) are plotted as a function of time (t). The slope of this line was correlated to the moles of incident photons by unit of time ($q_{n,p}^0$) by the use of the following Equation 2:

$$\Phi(\lambda) = dx/dt q_{n,p}^0 [1 - 10^{-A(\lambda)}] \quad (\text{Eq. 2})$$

where dx/dt is the rate of change of a measurable quantity (spectral or any other property), the quantum yield (Φ) for Fe^{2+} at 458 nm is 1.2, $[1 - 10^{-A(\lambda)}]$ is the ratio of absorbed photons by the solution, and $A(\lambda)$ is the absorbance of the actinometer at the wavelength used to carry out the experiments (460 nm). The absorbance at 460 nm $A(460 \text{ nm})$ was measured using a Shimadzu 2401PC UV-Vis spectrophotometer in a 10 mm path quartz cuvette, obtaining an absorbance of 0.142. $q_{n,p}^0$, which is the photon flux, was determined to be $2,54 \times 10^{-07}$.



The moles of product **30f** formed for the model reaction were determined by GC measurement (FID detector) using 1,3,5-trimethoxybenzene as internal standard. The moles of product per unit of time are related to the number of photons absorbed. The photons absorbed are correlated to the number of incident photons by the use of Equation 1. According to this, if we plot the moles of product (x) versus the moles of incident photons ($q_{n,p}^0 \cdot dt$), the slope is equal to: $\Phi \cdot (1 - 10^{-A(460 \text{ nm})})$, where Φ is the quantum yield to be determined and $A(460 \text{ nm})$ is the absorption of the reaction under study. $A(460 \text{ nm})$ was measured using a Shimadzu 2401PC UV-Vis spectrophotometer in 10 mm path quartz. An absorbance of 0.2 was determined for the model reaction mixture.

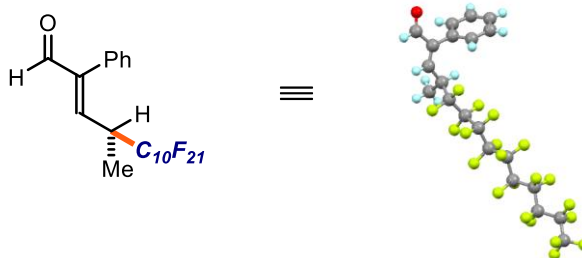


The quantum yield (ϕ) of the reaction at 460nm irradiation has been measured to be **1.14**.

4.7.8 Crystal Structure

Single Crystal X-ray Diffraction Data for compound 30f

Crystals of the compound 30f were obtained by slow evaporation of a diethyl ether / n-hexane solution (1:1). Data Collection. Measurements were made on a Bruker-Nonius diffractometer equipped with an APPEX 2 4K CCD area detector, a FR591 rotating anode with MoK α radiation. Montel mirrors and a Cryostream Plus low temperature device (T = 100K). Full-sphere data collection was used with ω and ϕ scans



Empirical formula: C₂₁H₁₁F₂₁O

Formula weight: 678,05

Temperature: 100(2)K

Wavelength: 1.54178 Å

Crystal system: monoclinic

Space group: P21

Cell lengths dimensions: $a = 5.6498(2) \text{ \AA}$. $b = 9.6522(3) \text{ \AA}$. $c = 22.2488(6) \text{ \AA}$.

Cell angles dimensions: $\alpha = 90^\circ$; $\beta = 92.285(2)^\circ$; $\gamma = 90^\circ$

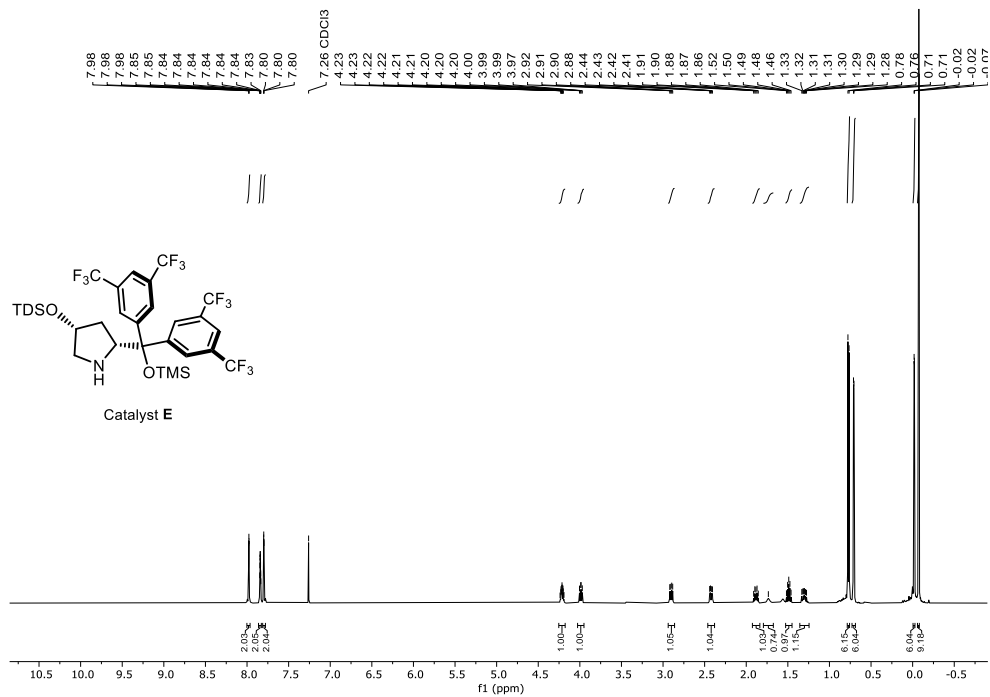
Volume: 1212.33 \AA^3

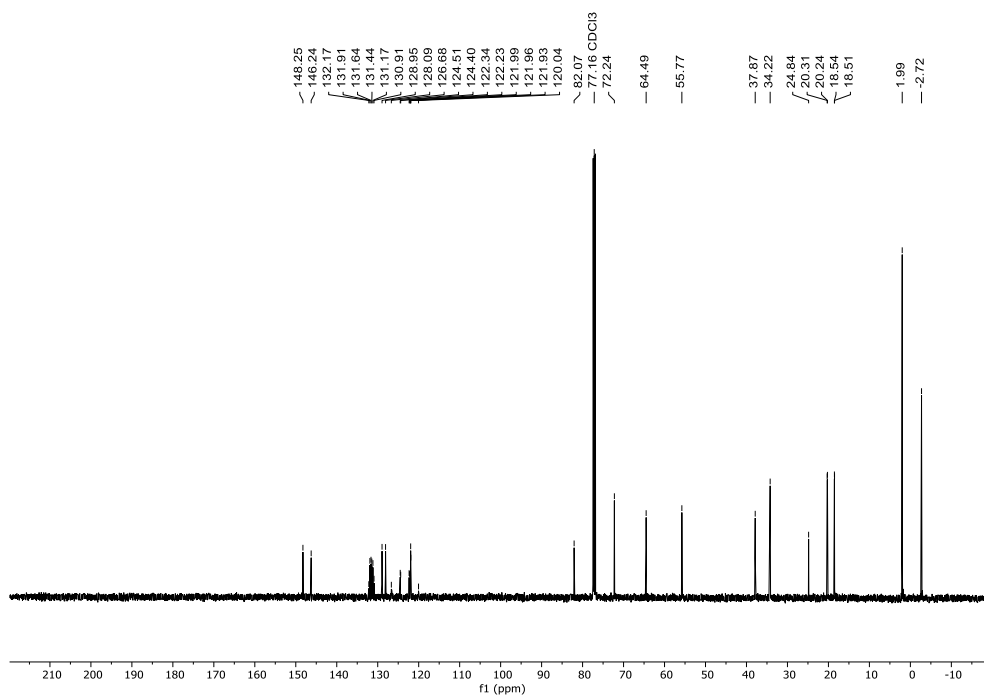
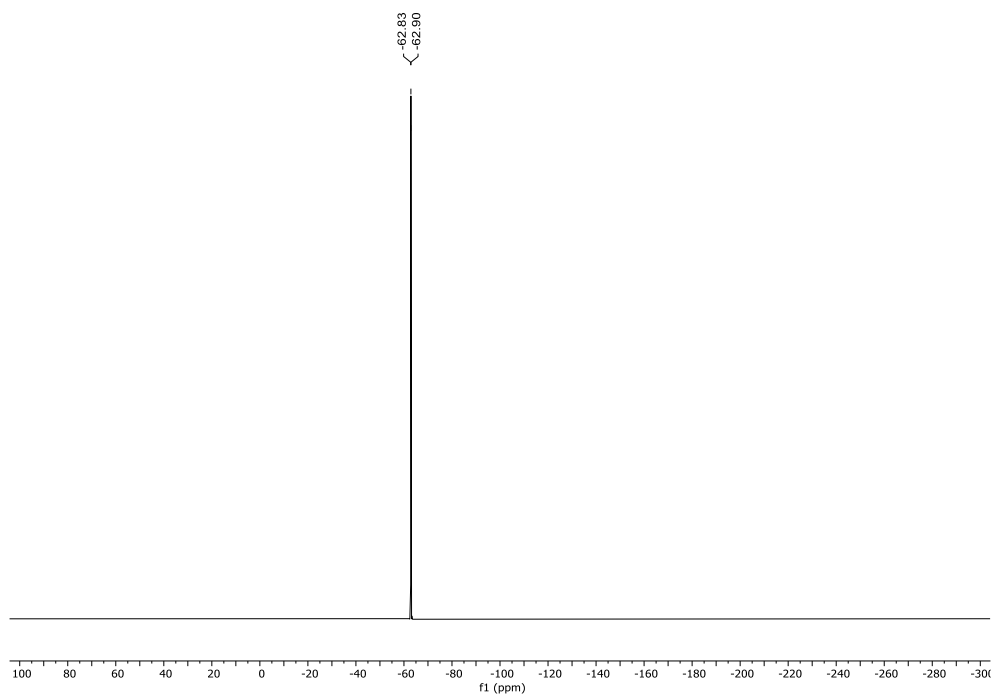
Z: 0; Z': 0

4.7.9 NMR Traces

Catalyst E

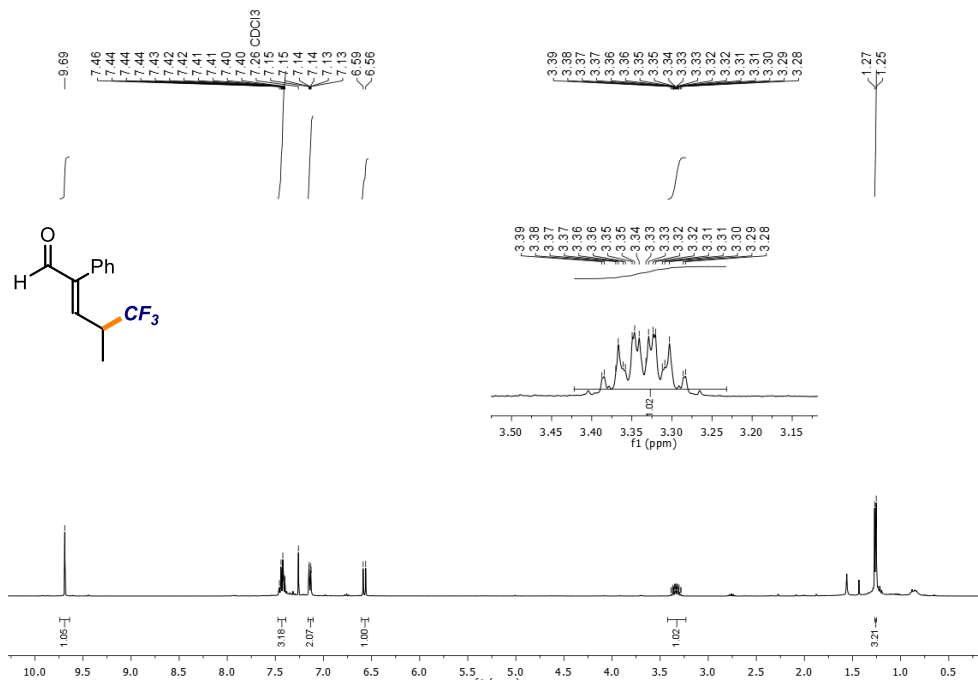
^1H NMR (500 MHz, CDCl_3)



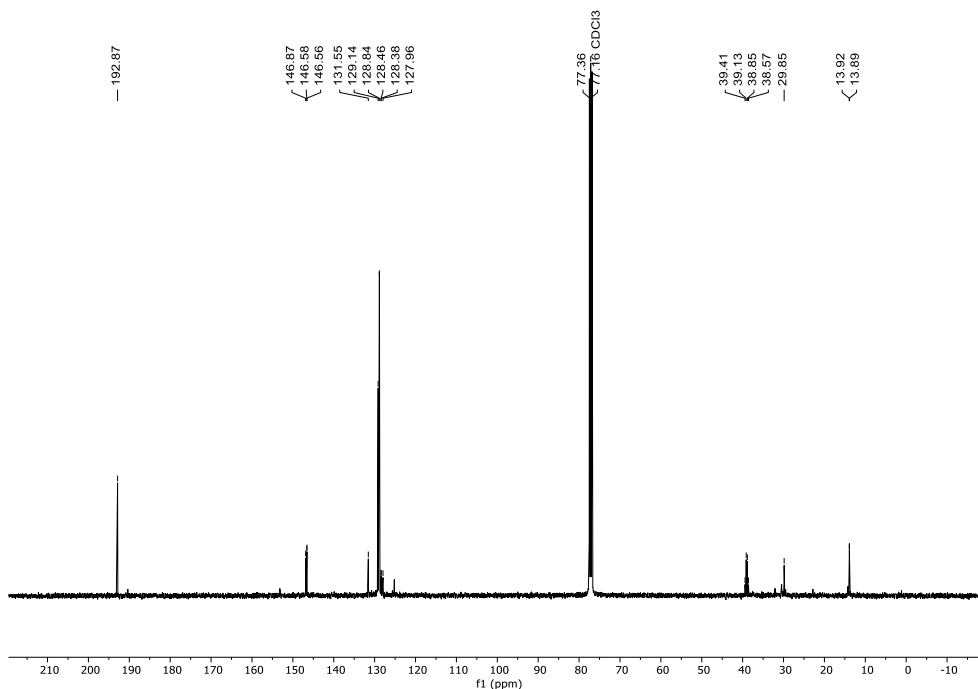
^{13}C NMR (126 MHz, CDCl_3) ^{19}F NMR (471 MHz, CDCl_3)

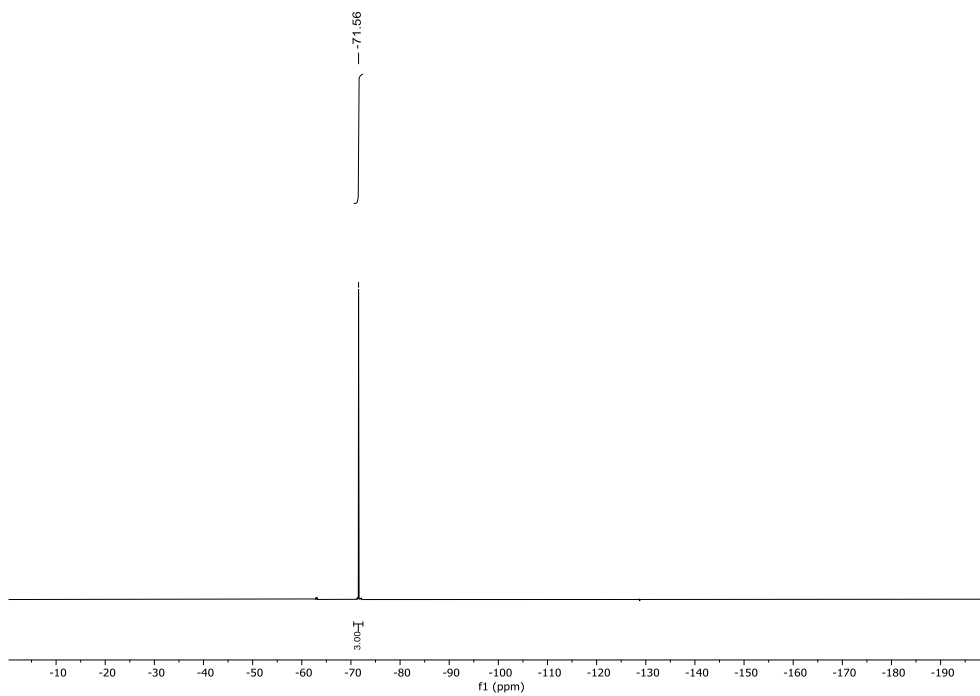
(*S,E*)-4-(trifluoromethyl)-2-phenylpent-2-enal

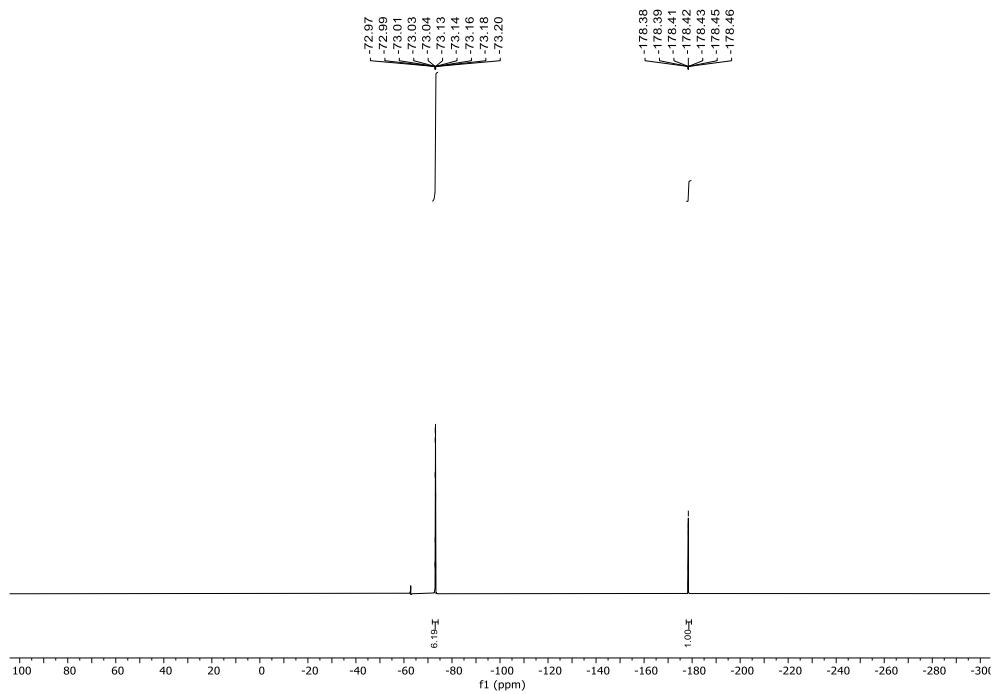
¹H NMR (500 MHz, CDCl₃):



¹³C NMR (126 MHz, CDCl₃):

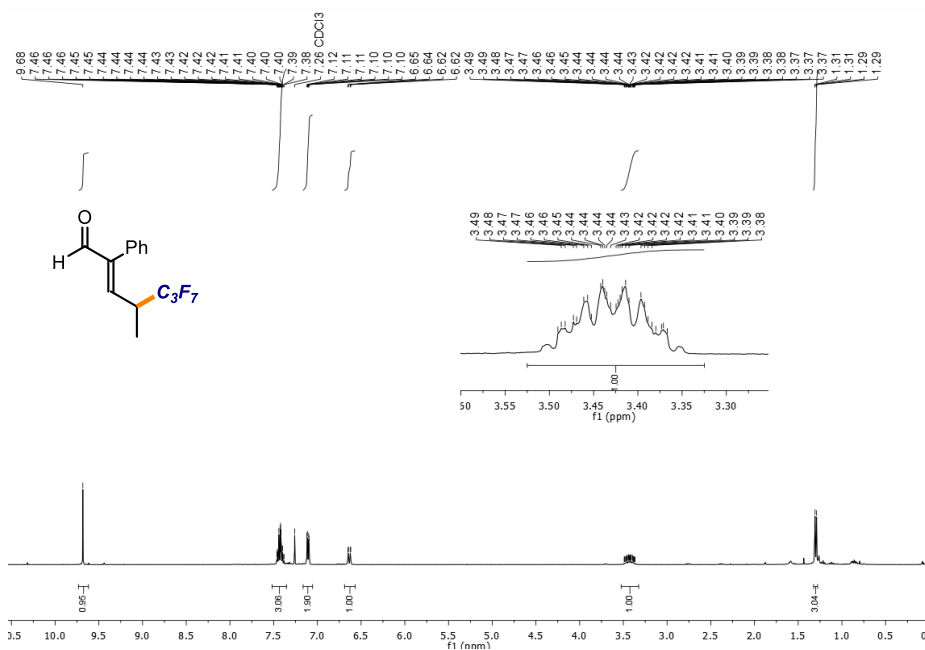


^{19}F NMR (471 MHz, CDCl_3)

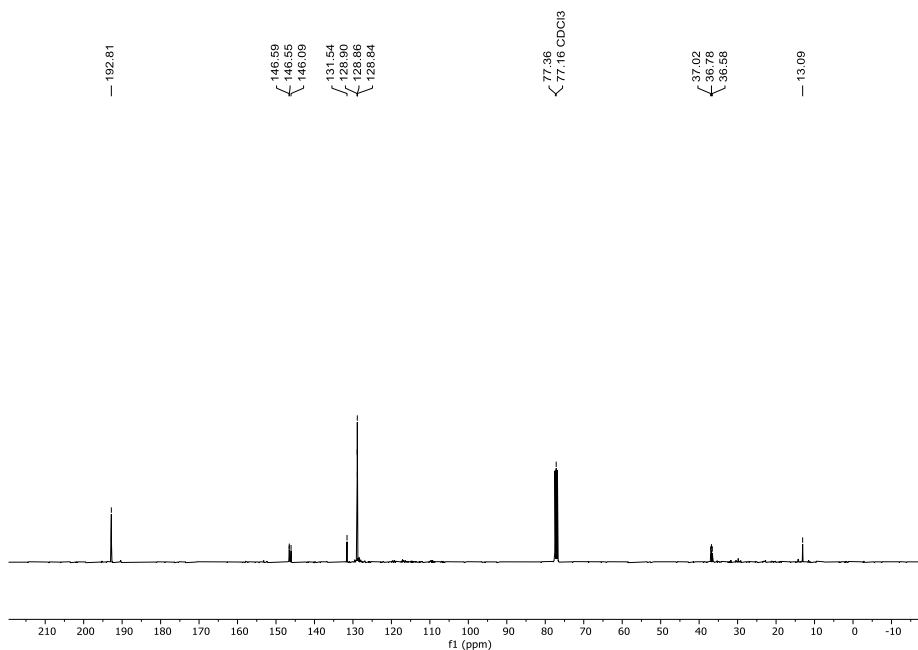
^{19}F NMR (471 MHz, CDCl_3)

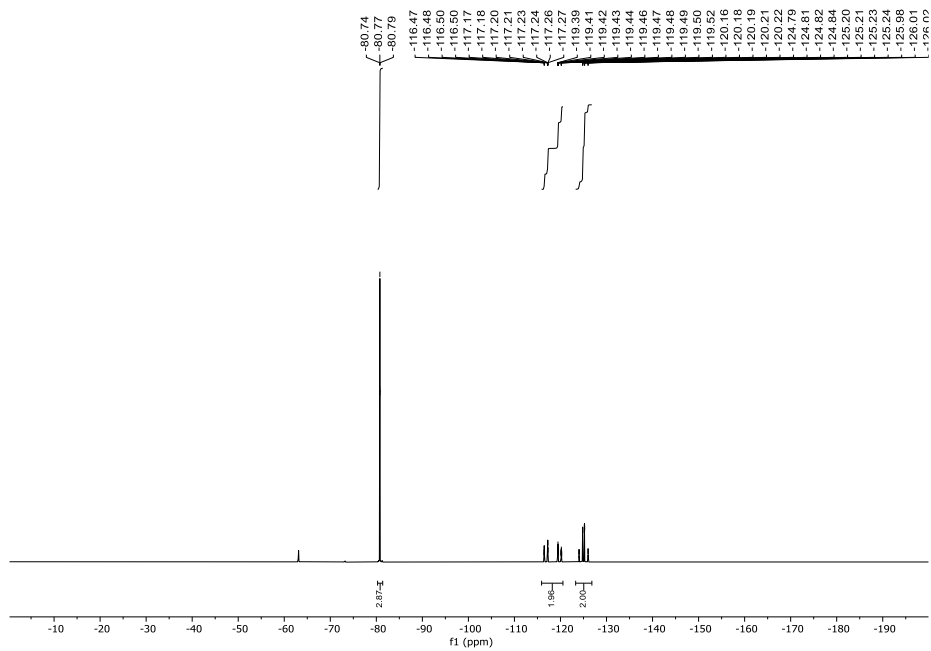
(S,E)-4-(perfluoropropyl)-2-phenylpent-2-enal

^1H NMR (500 MHz, CDCl_3) C3:



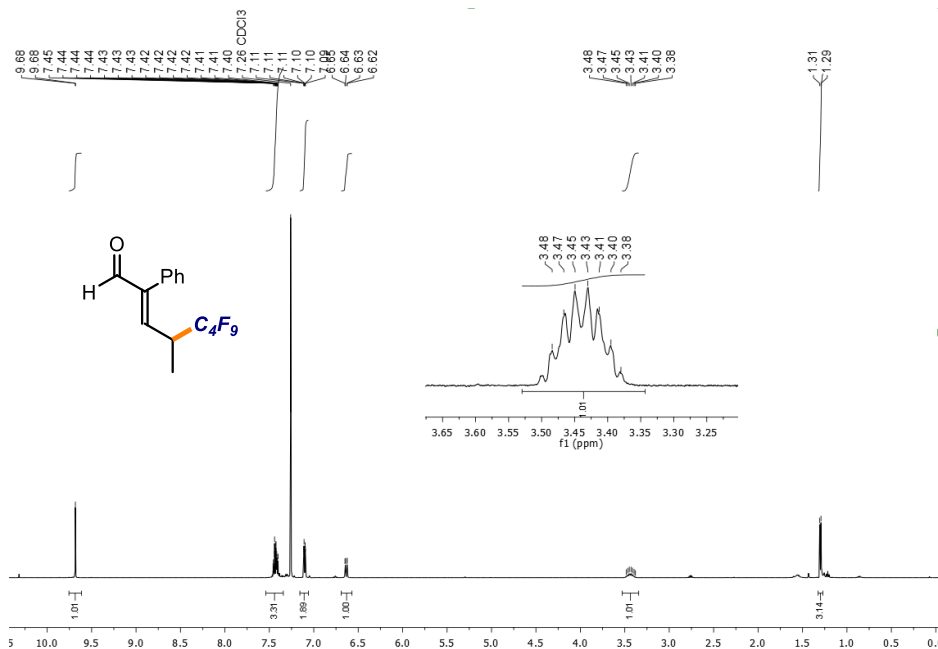
^{13}C NMR (126 MHz, CDCl_3)



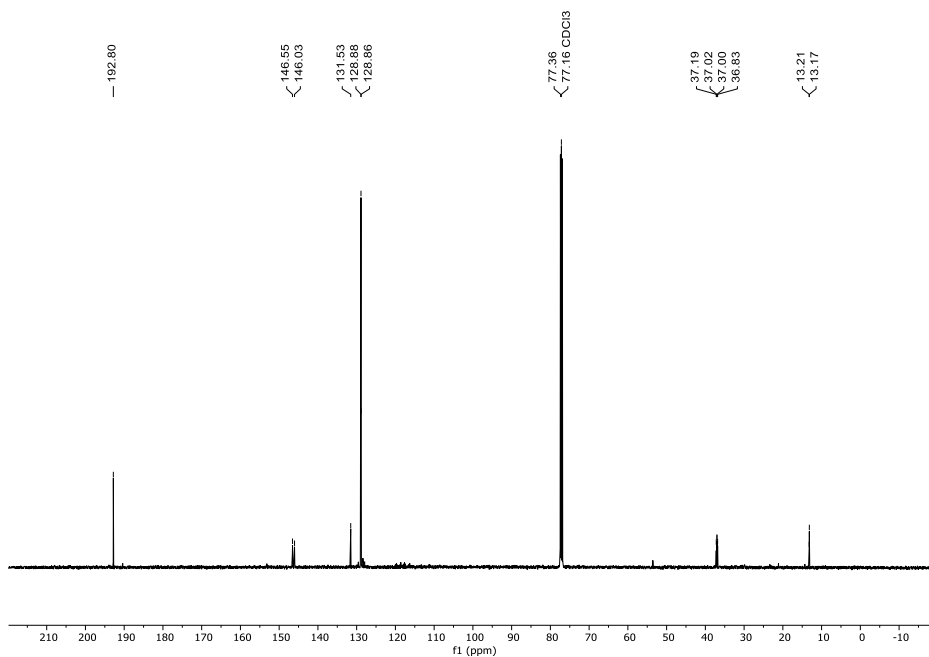
^{19}F NMR (471 MHz, CDCl_3)

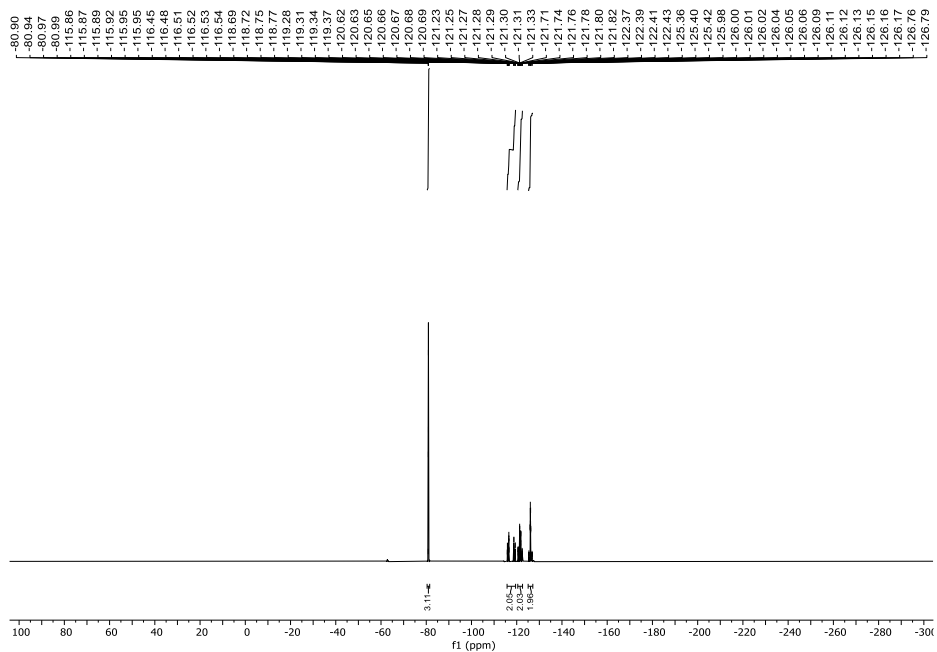
(*S,E*)-4-(perfluorobutyl)-2-phenylpent-2-enal

^1H NMR (500 MHz, CDCl_3) C4:



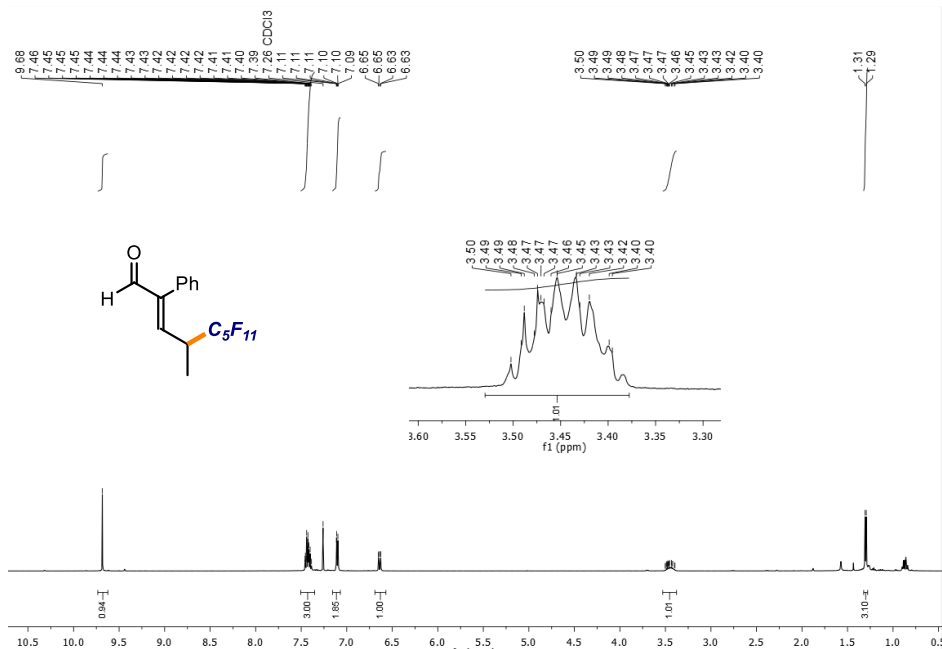
^{13}C NMR (126 MHz, CDCl_3)



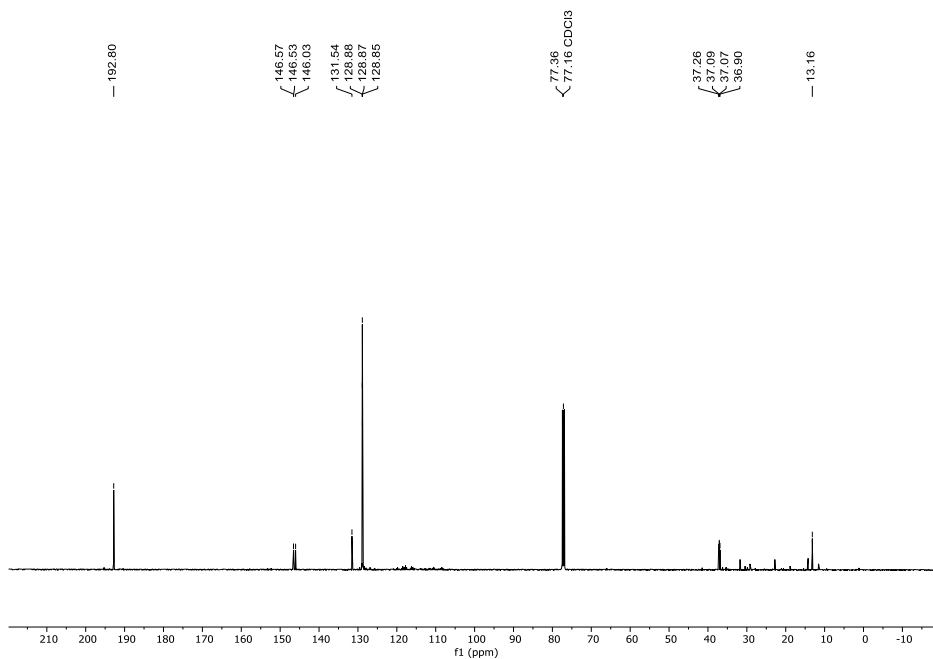
^{19}F NMR (471 MHz, CDCl_3)

(S,E)-4-(perfluoropentyl)-2-phenylpent-2-enal

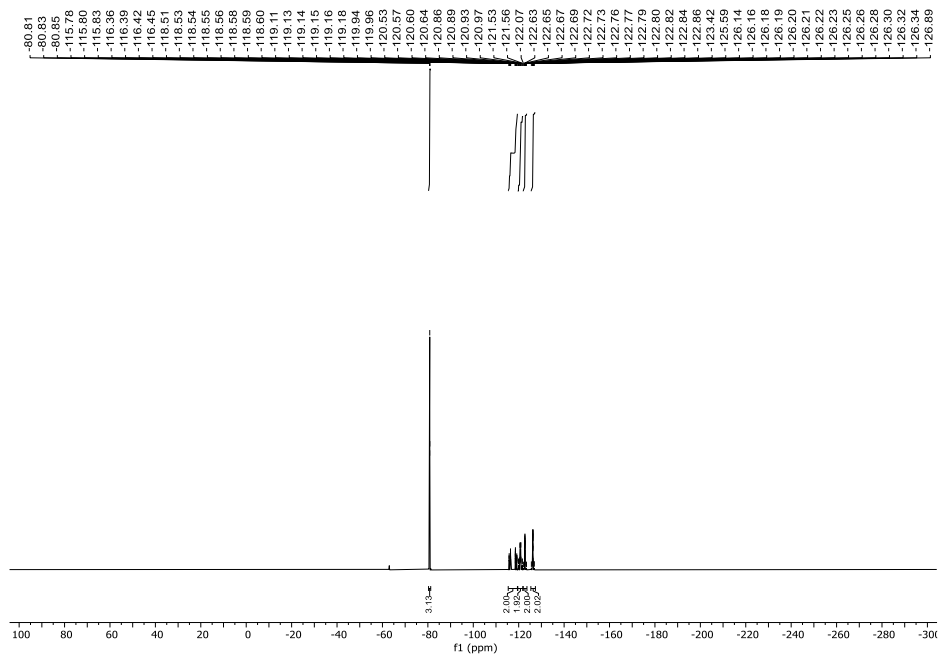
¹H NMR (500 MHz, CDCl₃):



¹³C NMR (126 MHz, CDCl₃)

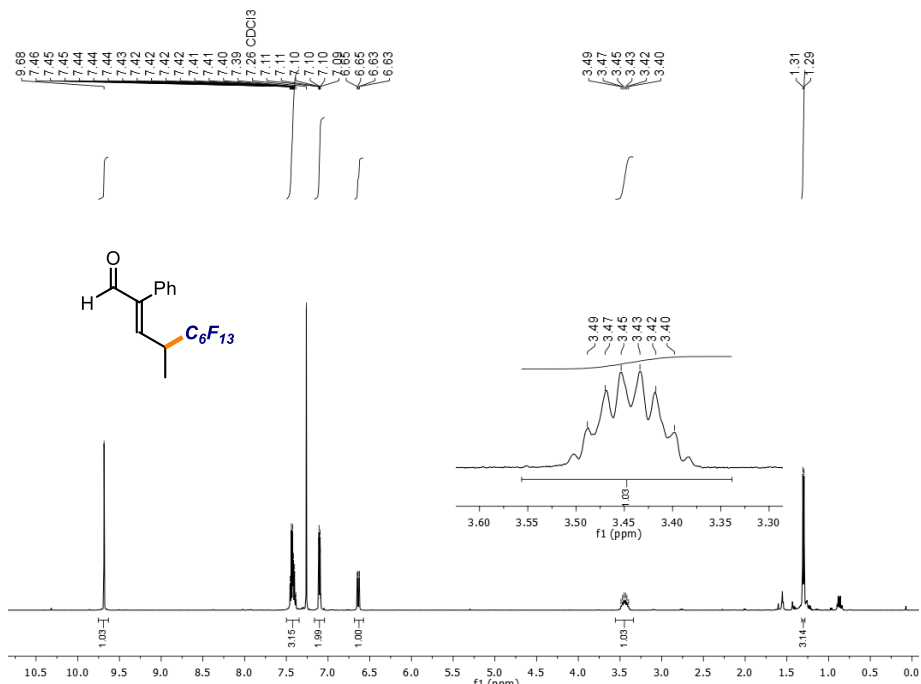


^{19}F NMR (471 MHz, CDCl_3)

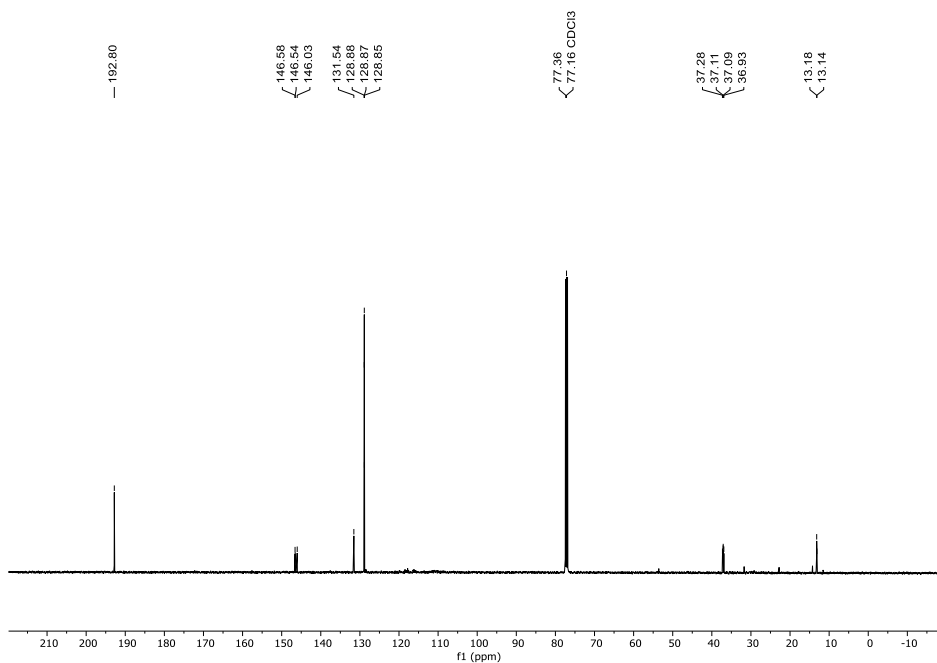


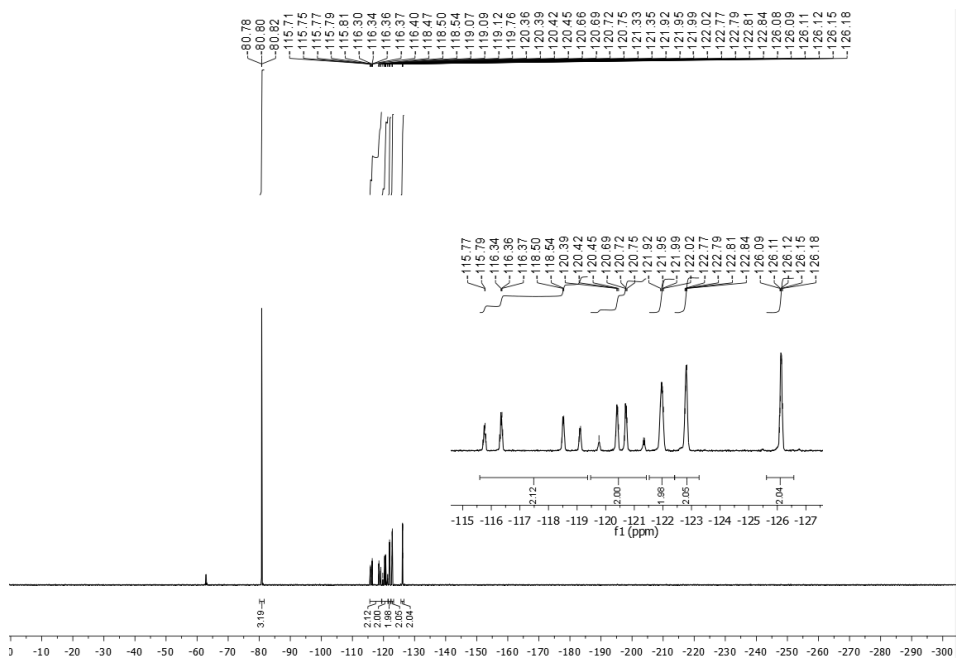
(S,E)-4-(perfluorohexyl)-2-phenylpent-2-enal

^1H NMR (500 MHz, CDCl_3):



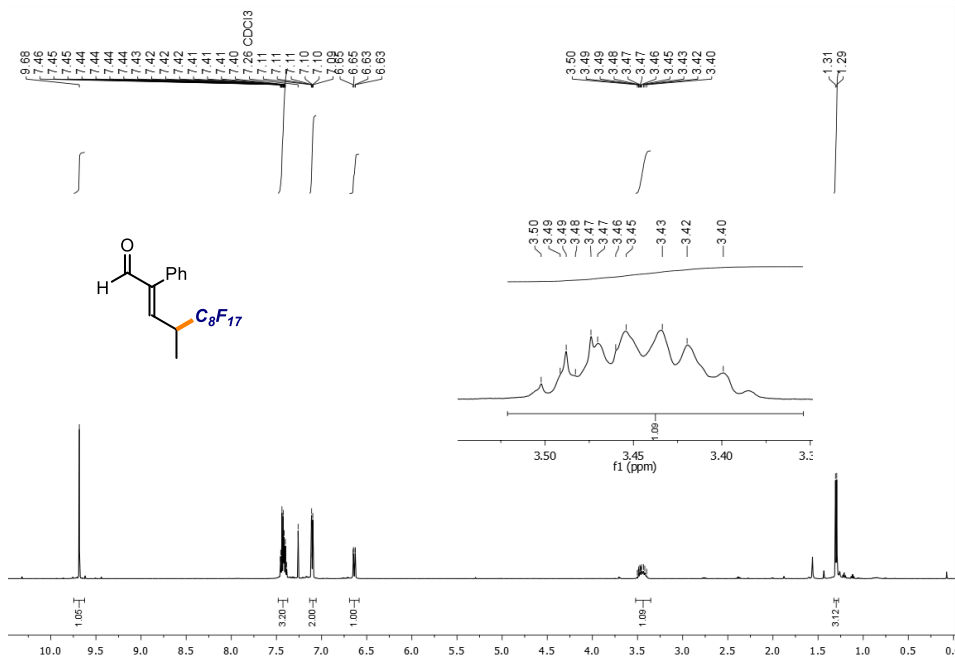
^{13}C NMR (126 MHz, CDCl_3)



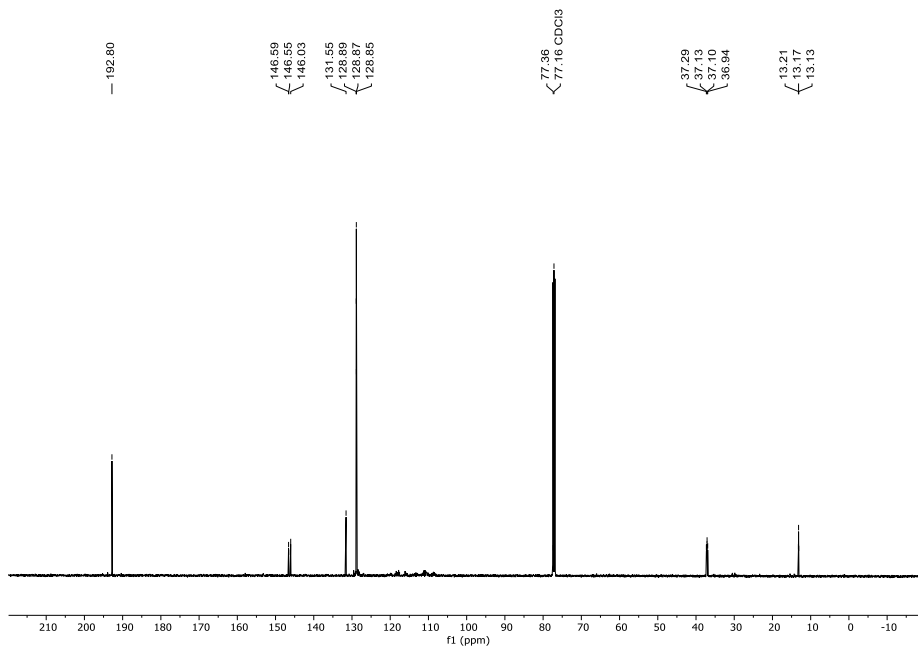
^{19}F NMR (471 MHz, CDCl_3)

(S,E)-4-(perfluorooctyl)-2-phenylpent-2-enal

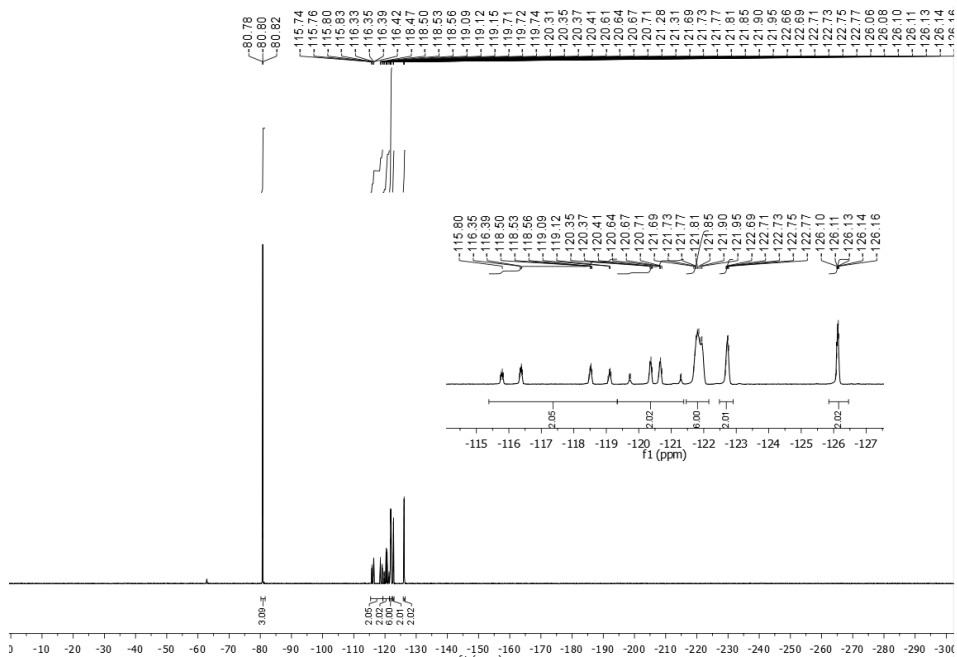
^1H NMR (500 MHz, CDCl_3):



^{13}C NMR (126 MHz, CDCl_3)

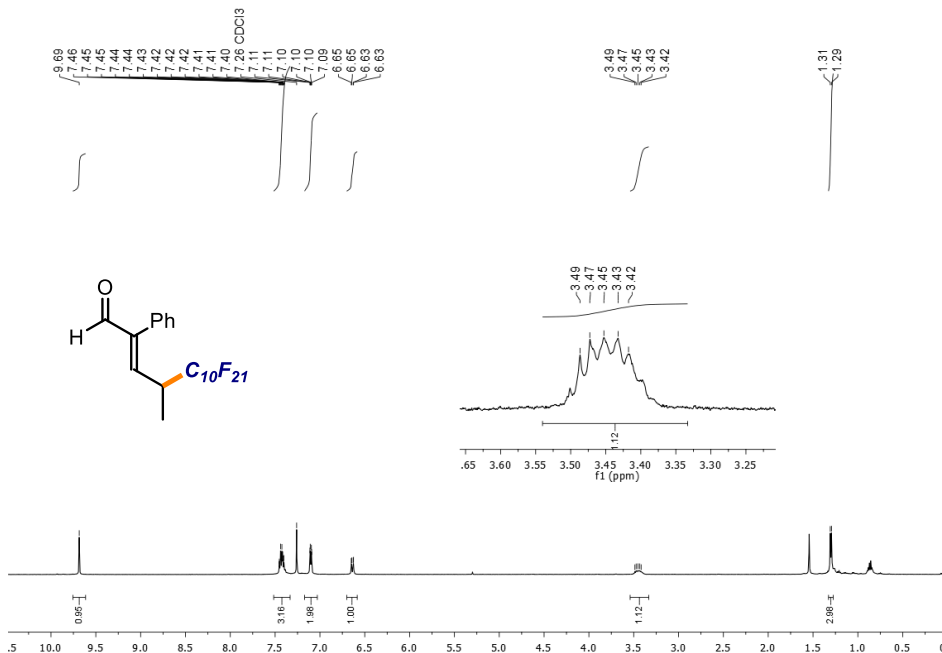


^{19}F NMR (471 MHz, CDCl_3)

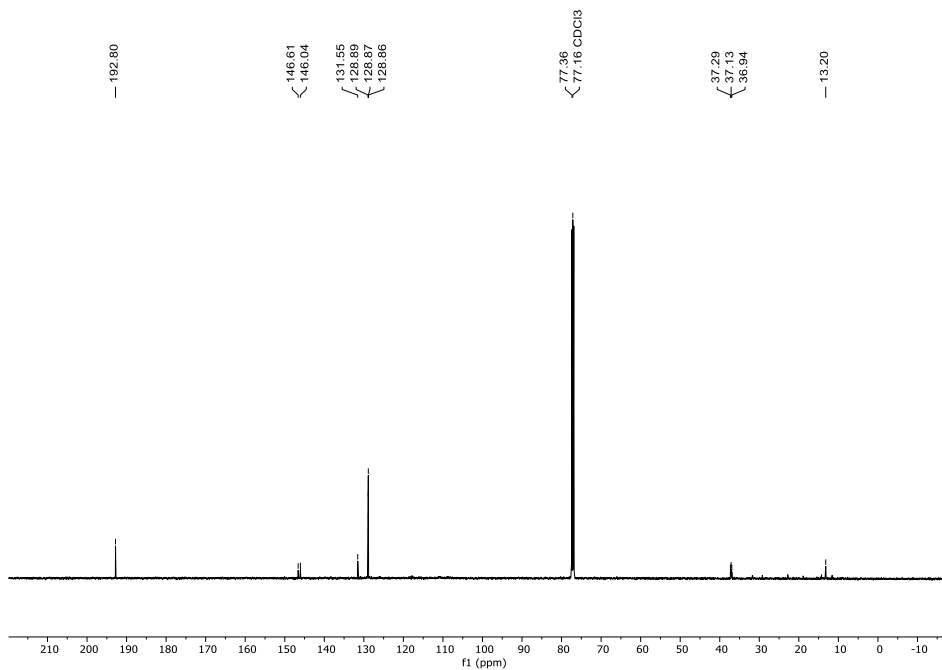


(S,E)-4-(perfluorodecyl)-2-phenylpent-2-enal

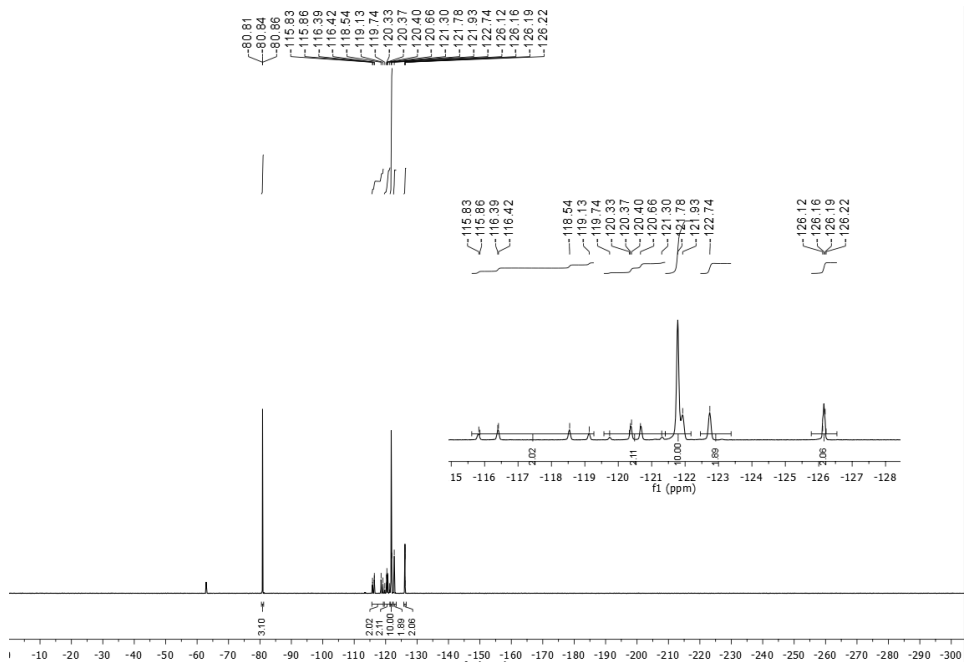
¹H NMR (500 MHz, CDCl₃):



¹³C NMR (126 MHz, CDCl₃)

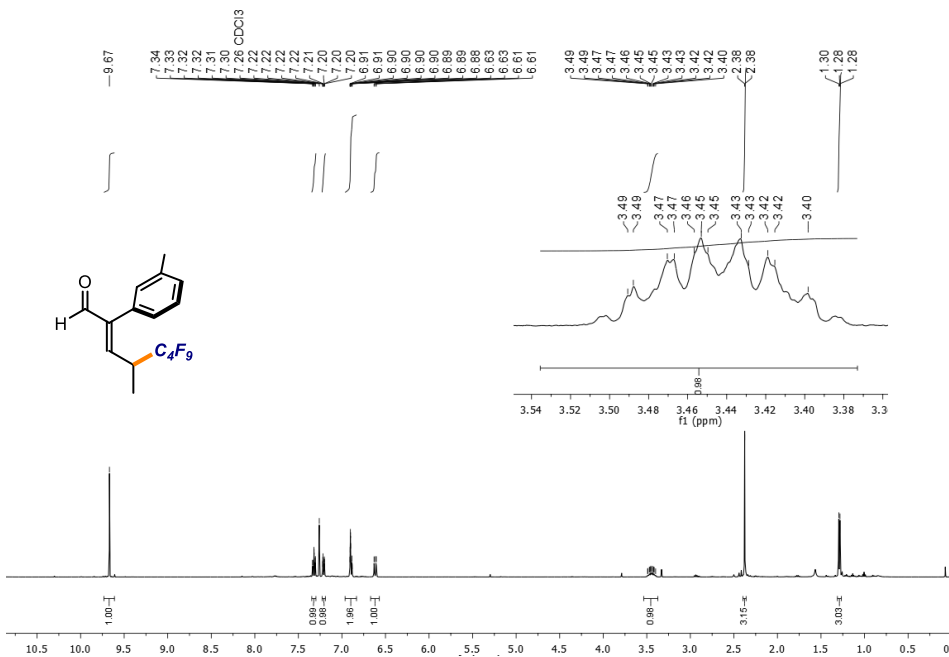


^{19}F NMR (471 MHz, CDCl_3)

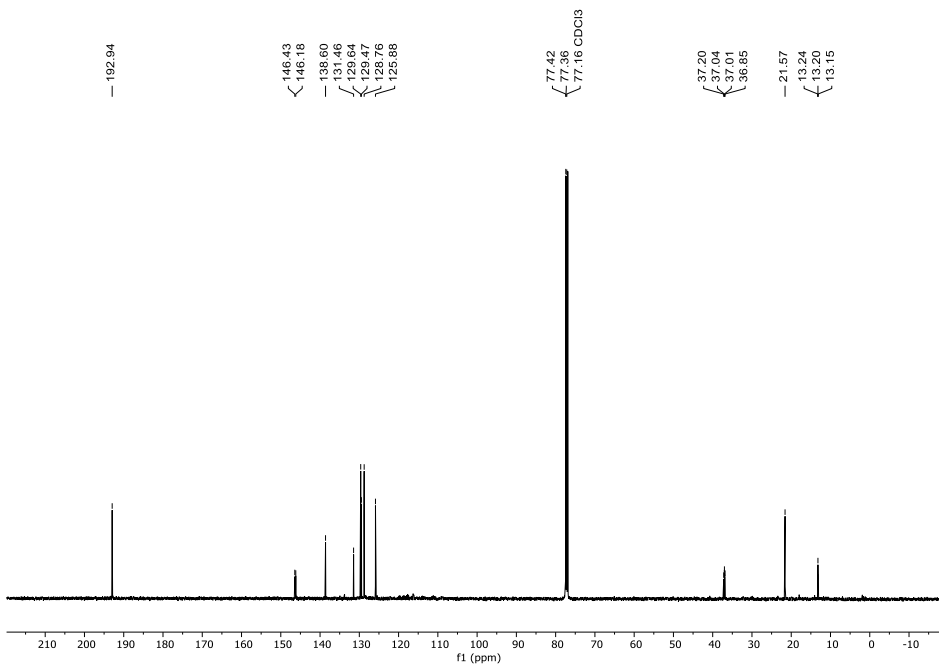


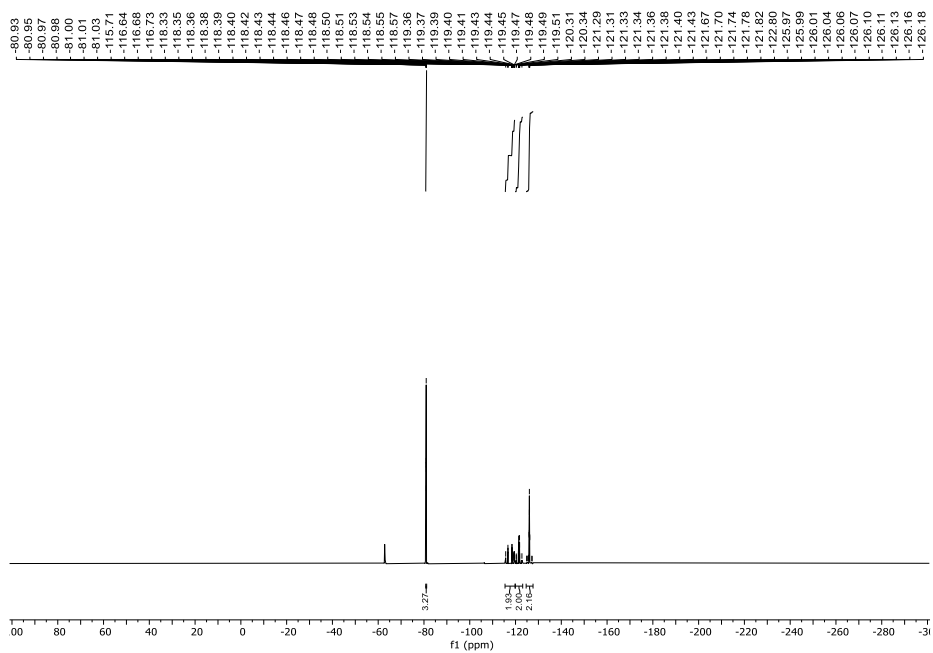
(*S,E*)-4-(perfluorobutyl)-2-(3-methylphenyl)pent-2-enal

^1H NMR (500 MHz, CDCl_3):



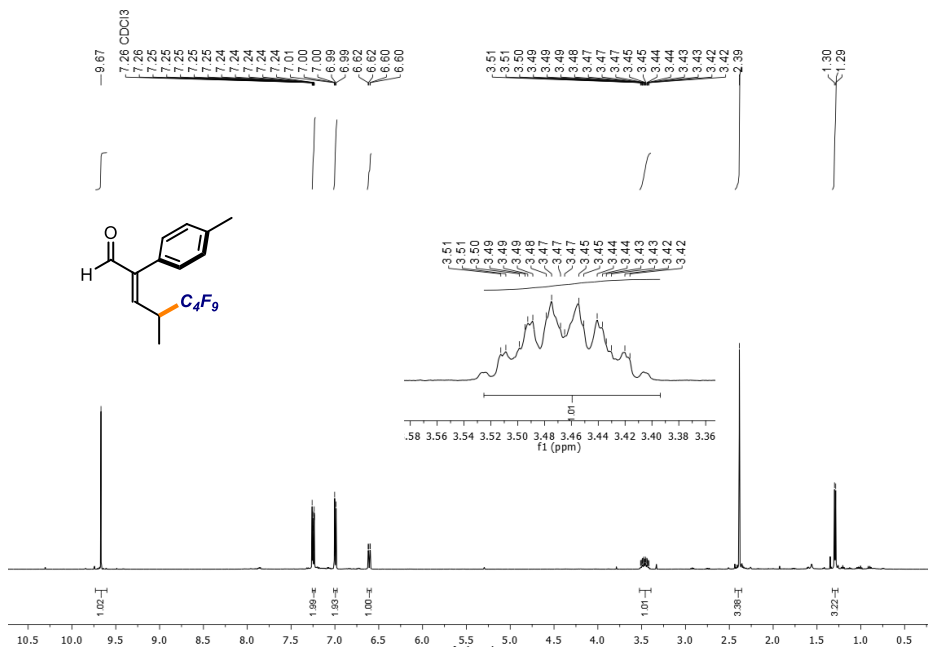
^{13}C NMR (126 MHz, CDCl_3)



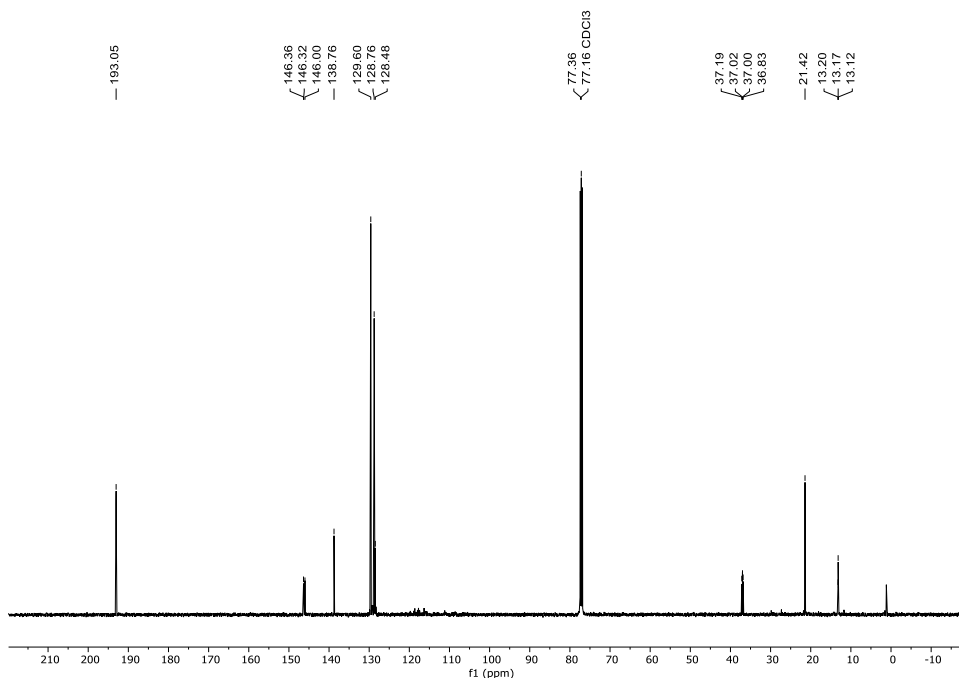
^{19}F NMR (471 MHz, CDCl_3)

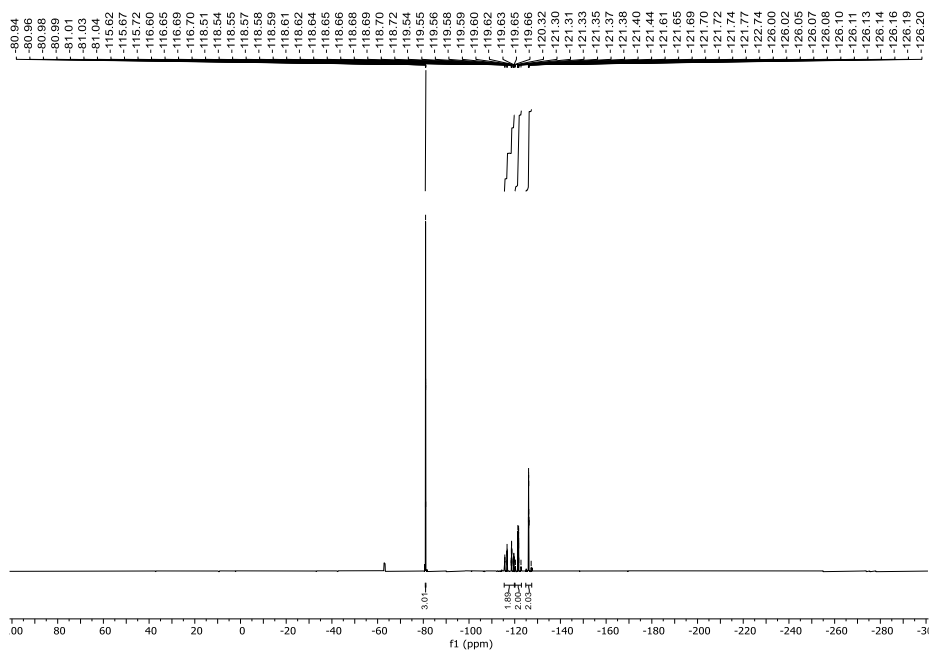
(*S,E*)-4-(perfluorobutyl)-2-(4-methylphenyl)pent-2-enal

¹H NMR (500 MHz, CDCl₃):



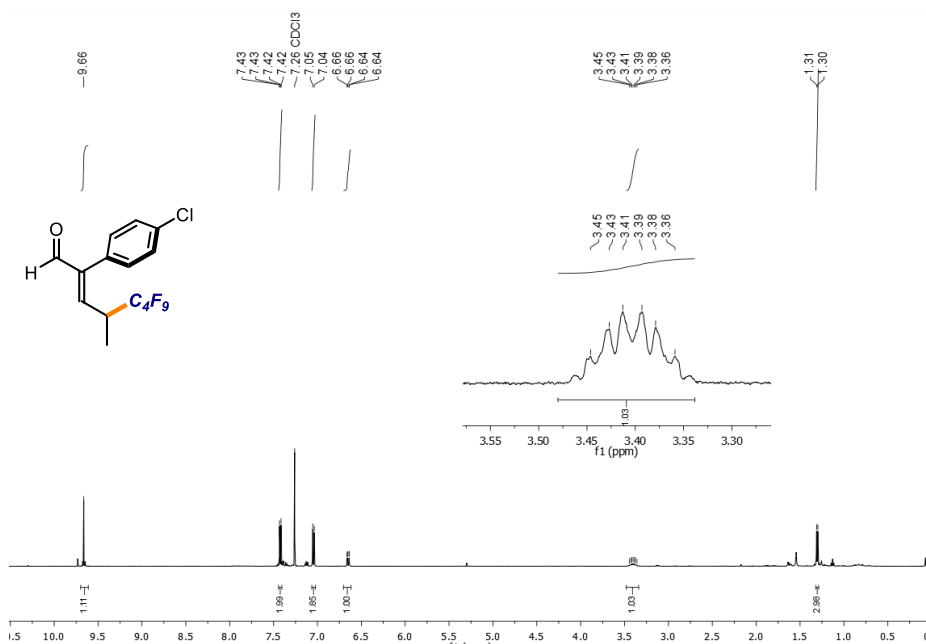
¹³C NMR (126 MHz, CDCl₃)



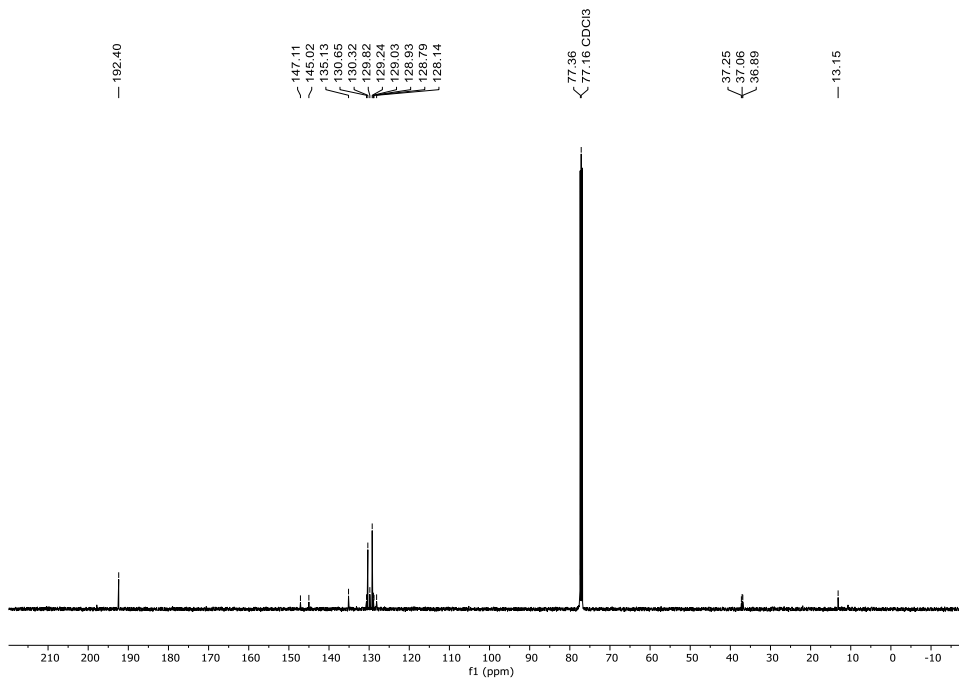
^{19}F NMR (471 MHz, CDCl_3)

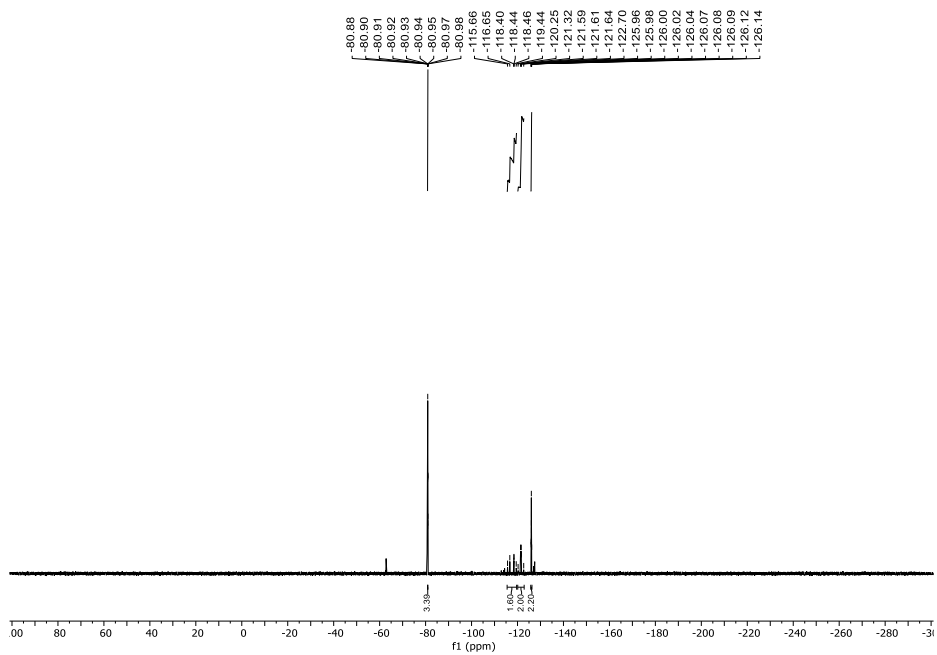
(*S,E*)-4-(perfluorobutyl)-2-(4-chlorophenyl)pent-2-enal

^1H NMR (500 MHz, CDCl_3):



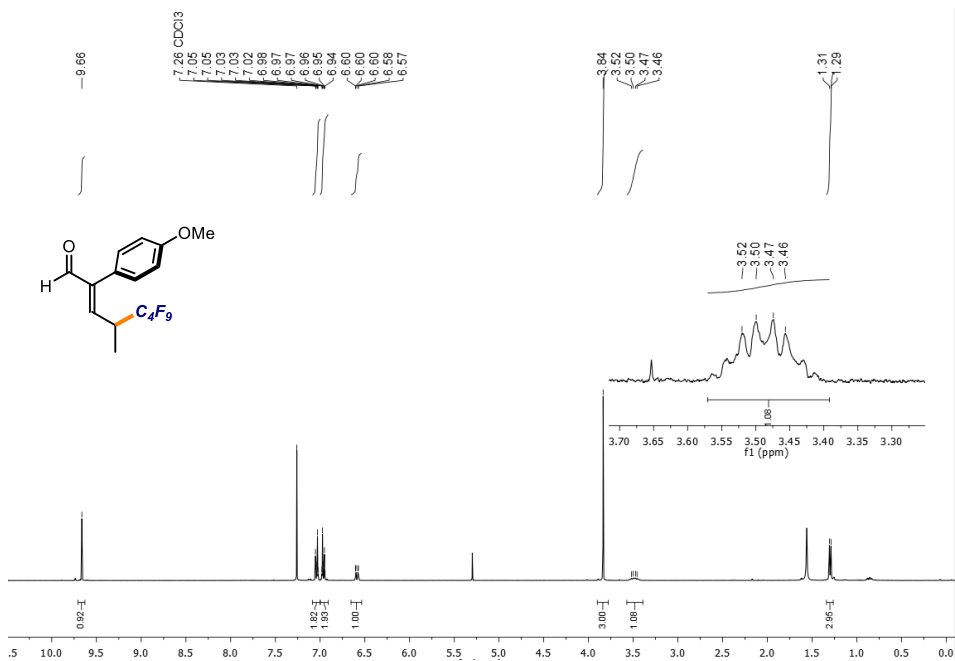
^{13}C NMR (126 MHz, CDCl_3)



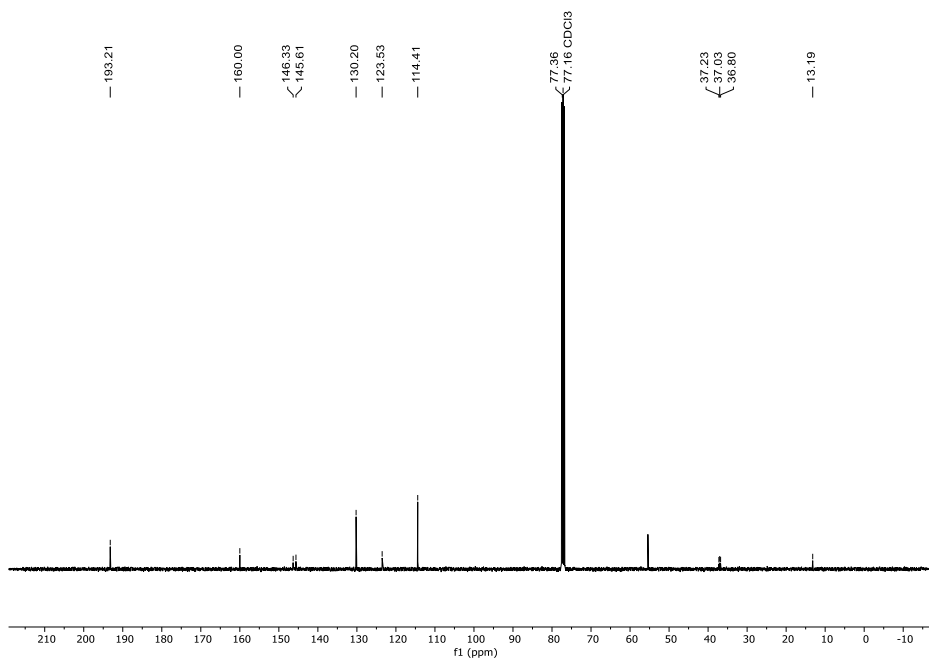
^{19}F NMR (471 MHz, CDCl_3)

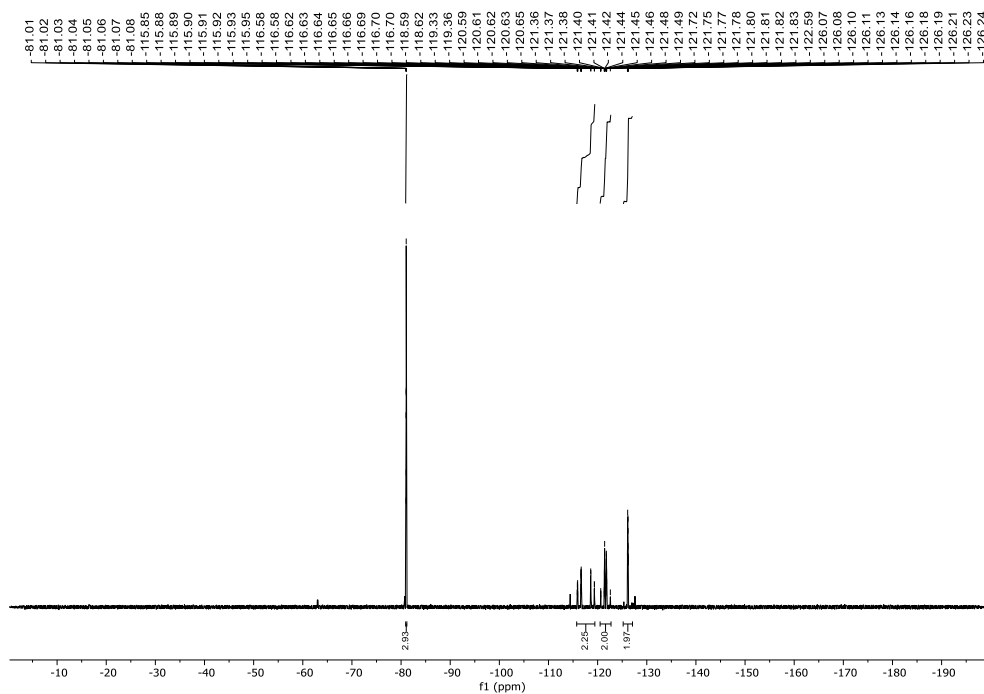
(*S,E*)-4-(perfluorobutyl)-2-(4-methoxyphenyl)pent-2-enal

^1H NMR (500 MHz, CDCl_3):



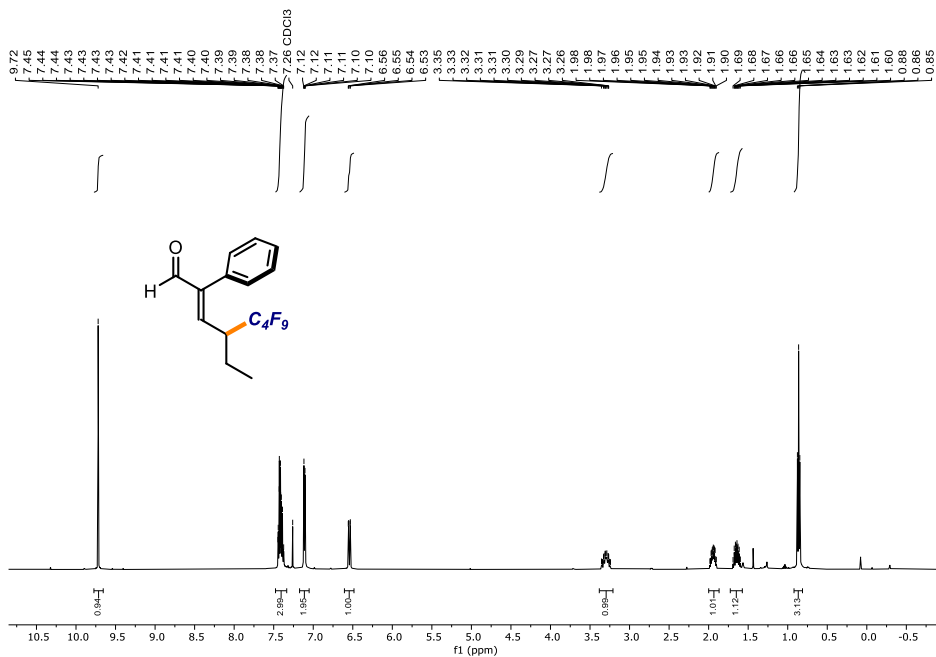
^{13}C NMR (126 MHz, CDCl_3):



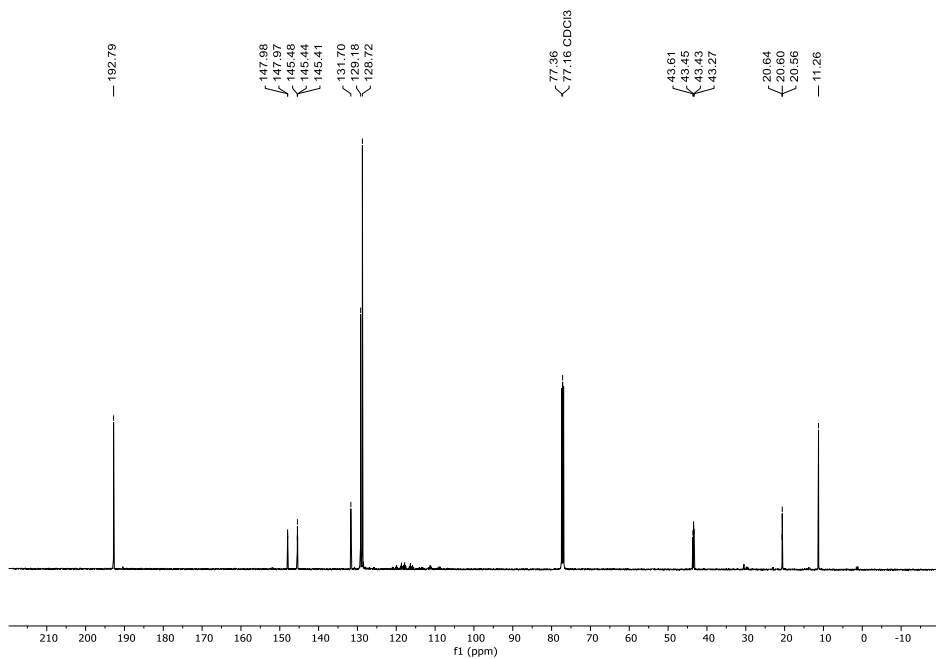
^{19}F NMR (471 MHz, CDCl_3)

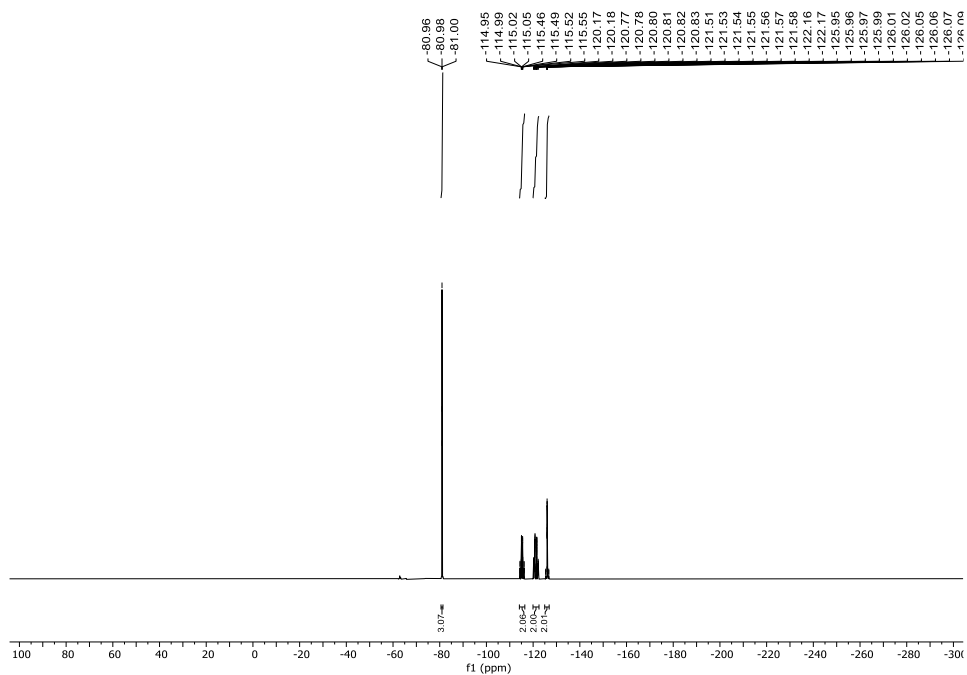
(*S,E*)-4-(perfluorobutyl)-2-phenylhex-2-enal

^1H NMR (500 MHz, CDCl_3):



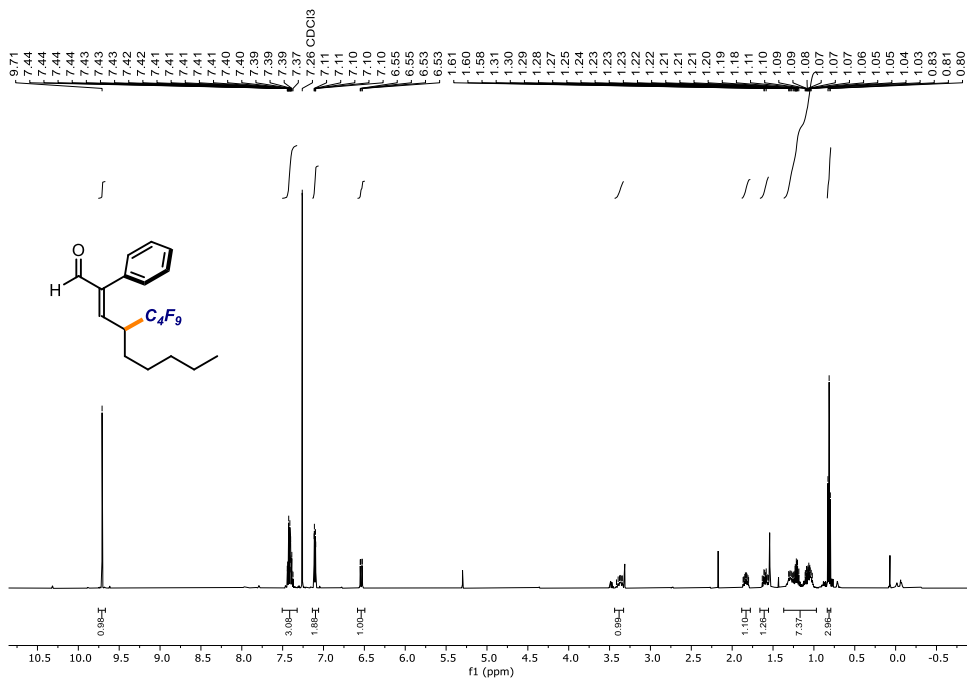
^{13}C NMR (126 MHz, CDCl_3)



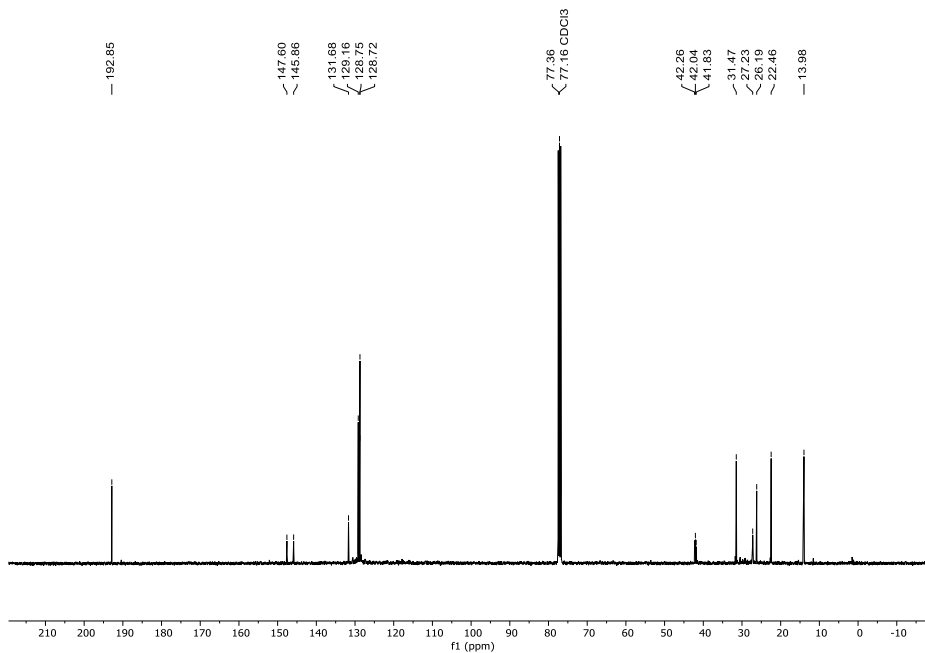
^{19}F NMR (471 MHz, CDCl_3)

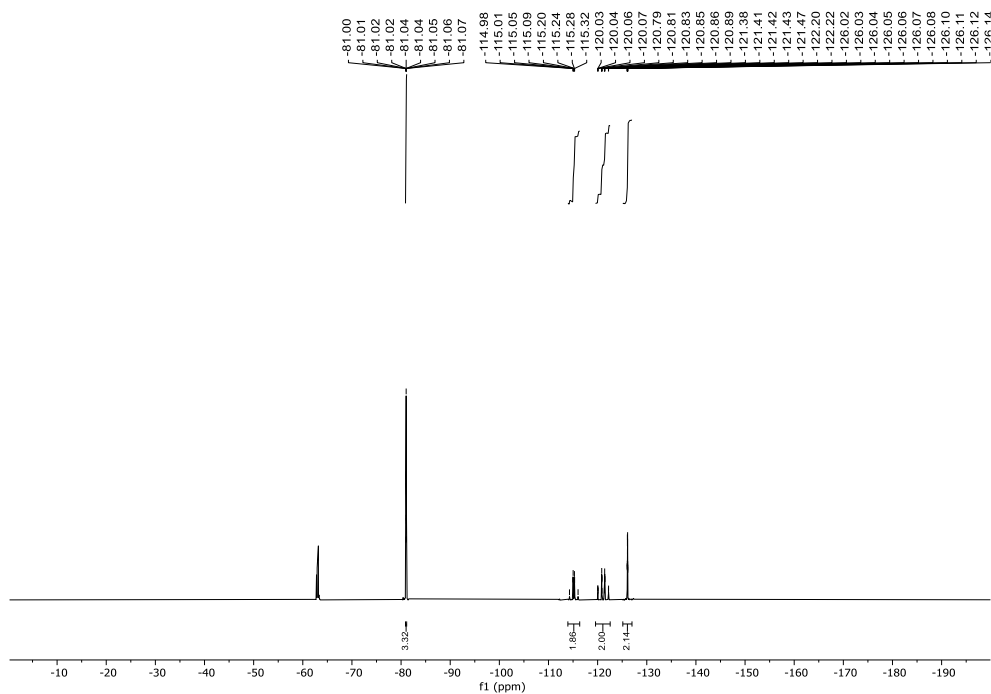
(*S,E*)-4-(perfluorobutyl)-2-phenylnon-2-enal

¹H NMR (500 MHz, CDCl₃):



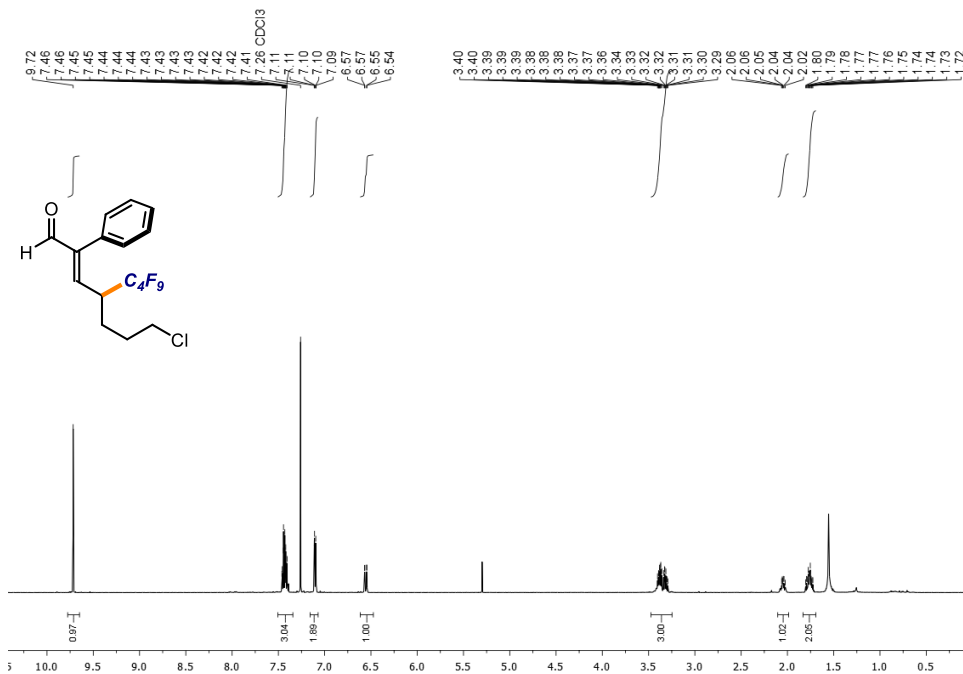
¹³C NMR (126 MHz, CDCl₃)



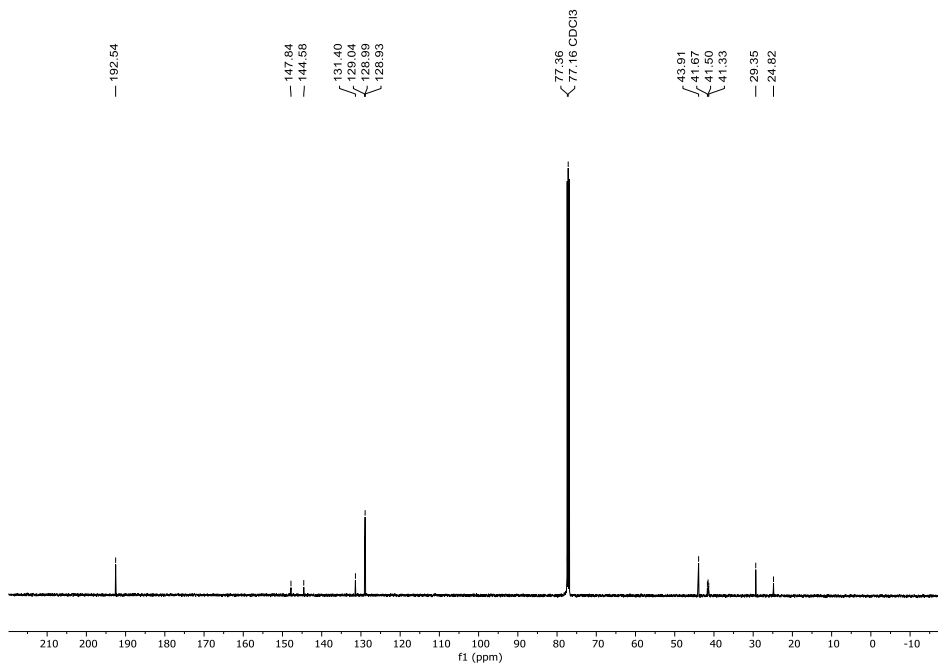
^{19}F NMR (471 MHz, CDCl_3)

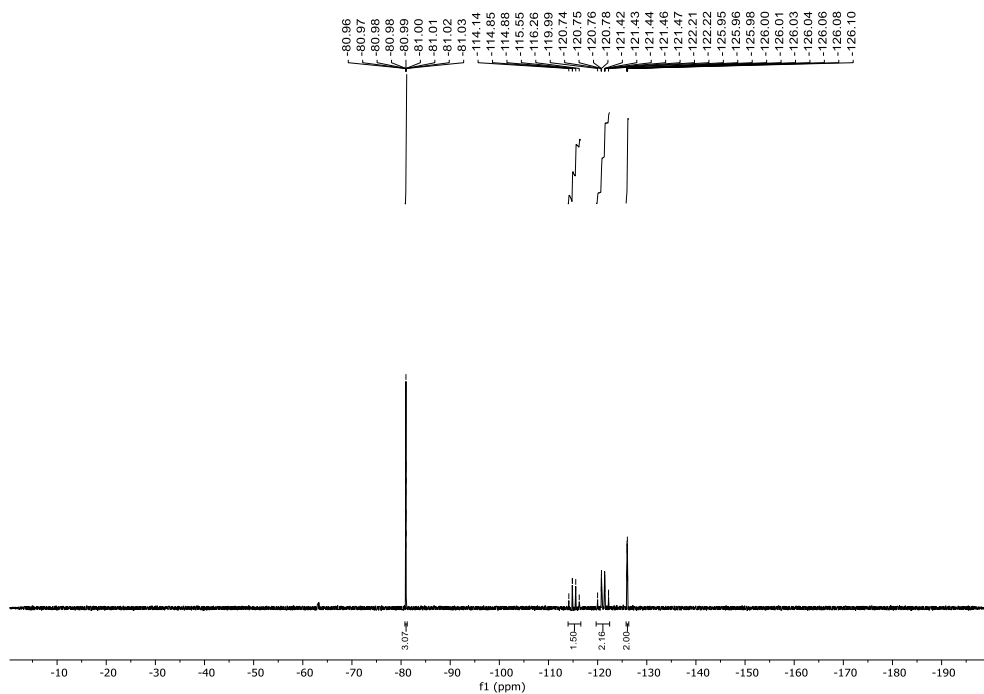
(*S,E*)-7-chloro-4-(perfluorobutyl)-2-phenylhept-2-enal

^1H NMR (500 MHz, CDCl_3):



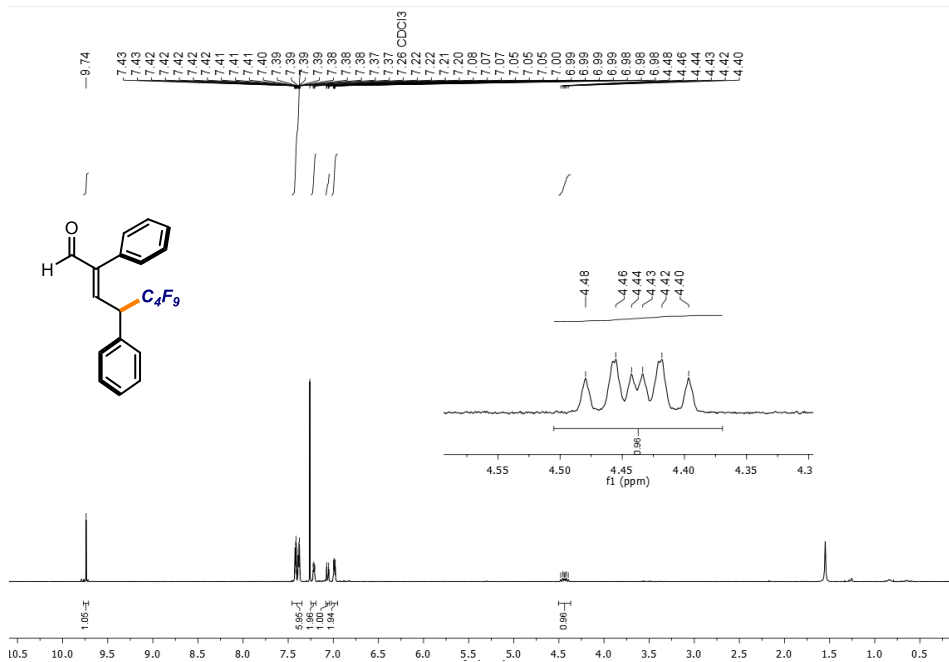
^{13}C NMR (126 MHz, CDCl_3):



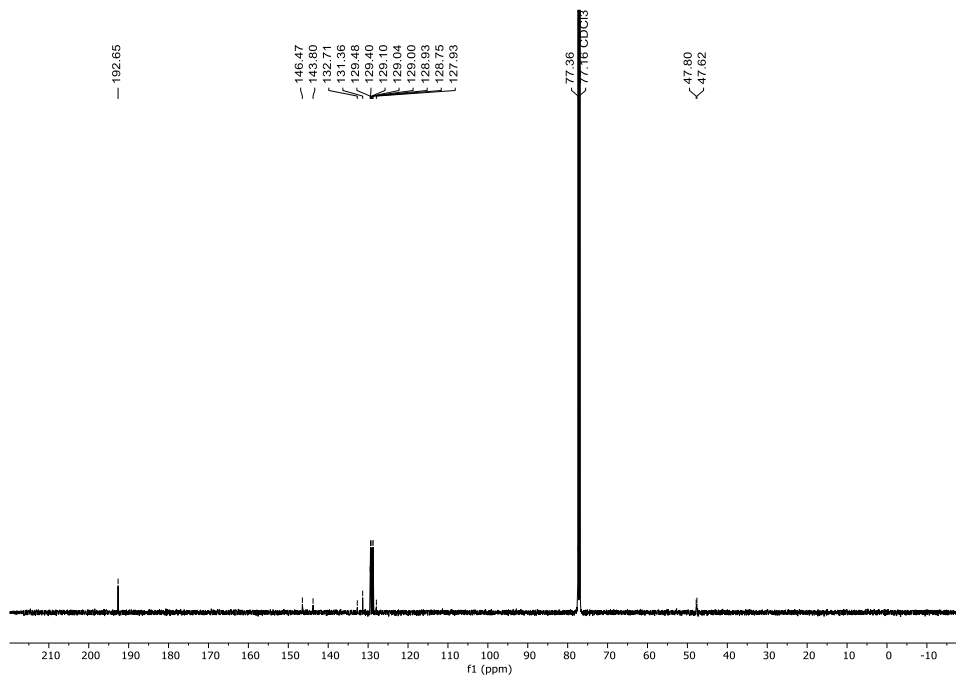
^{19}F NMR (471 MHz, CDCl_3)

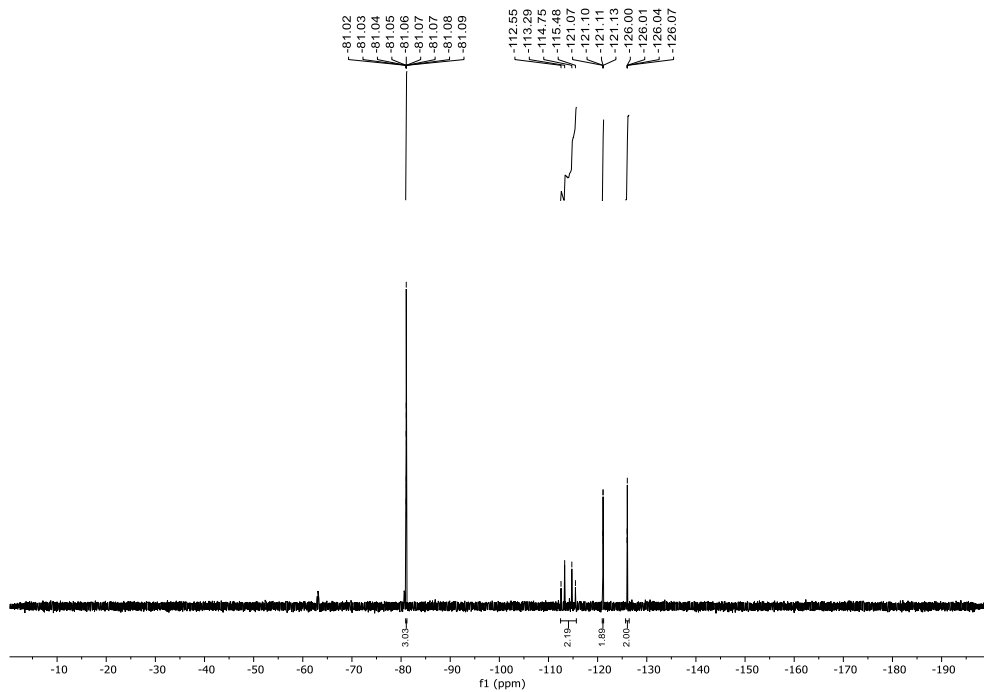
(S,E)-4-phenyl-4-(perfluorobutyl)-2-phenylbut-2-enal

¹H NMR (500 MHz, CDCl₃):



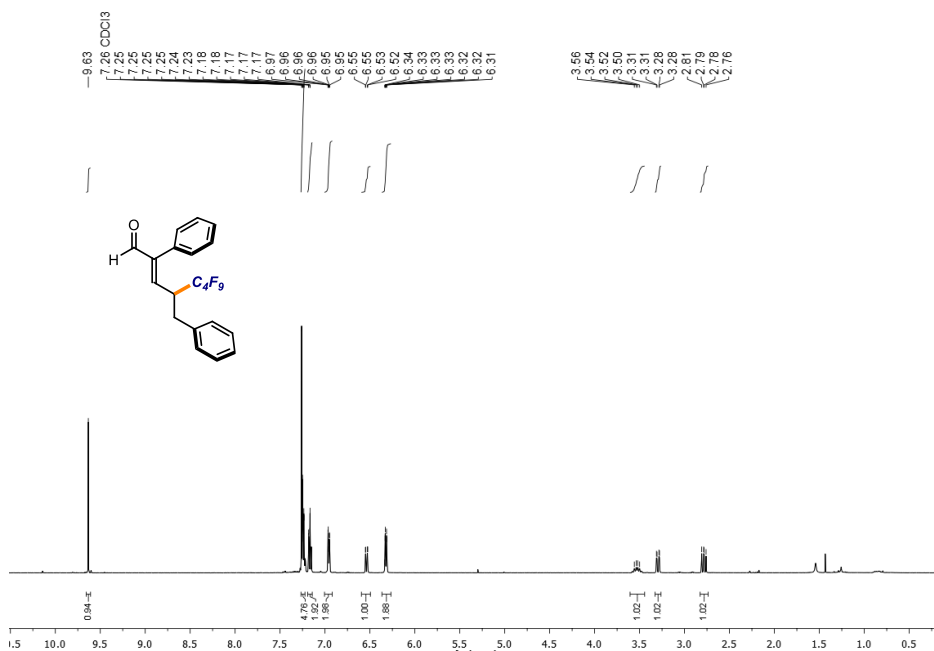
¹³C NMR (126 MHz, CDCl₃)



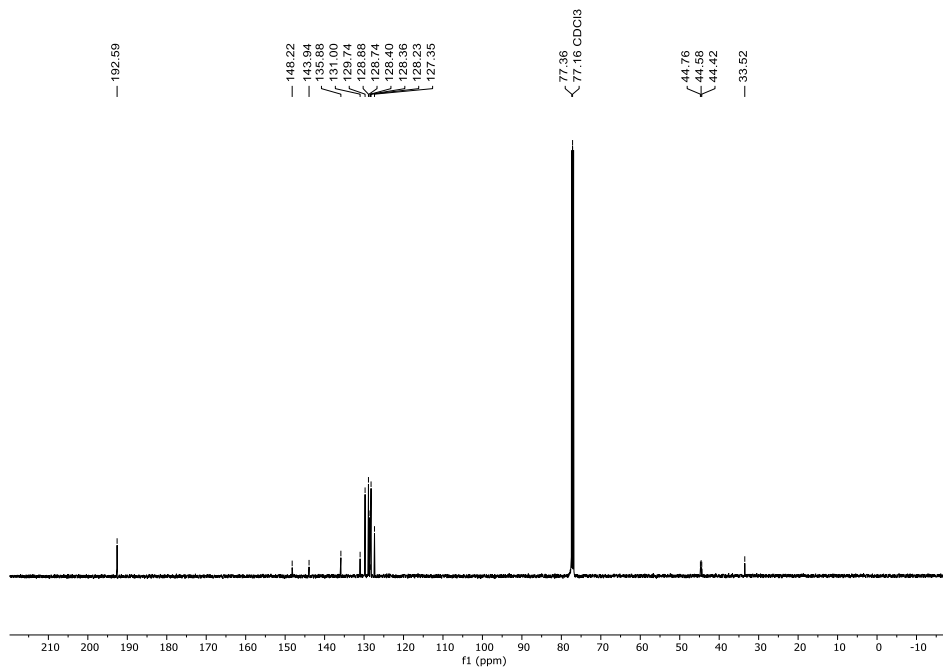
^{19}F NMR (471 MHz, CDCl_3)

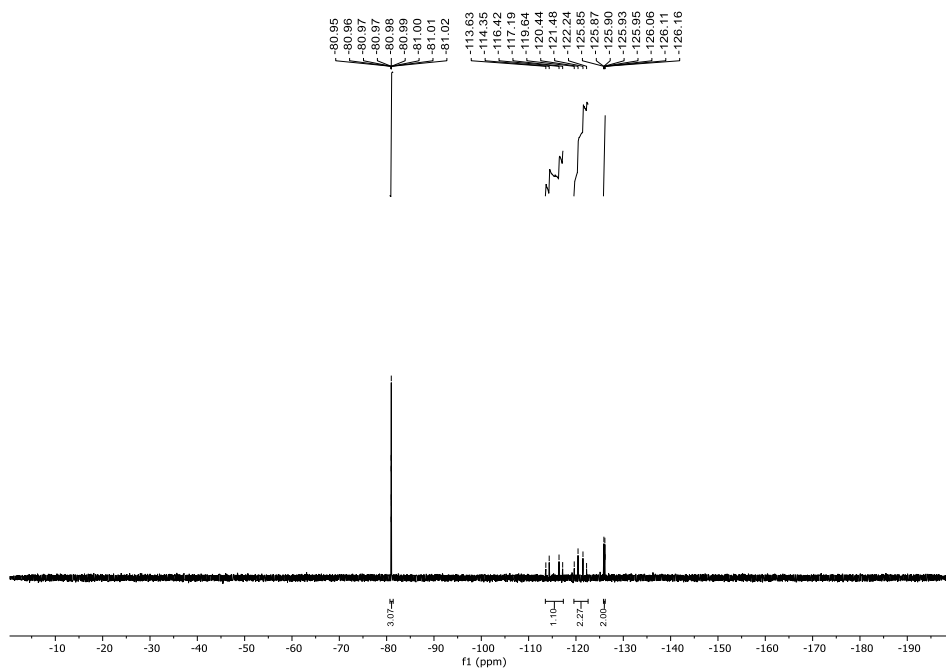
(*S,E*)-5-phenyl-4-(perfluorobutyl)-2-phenylpent-2-enal

¹H NMR (500 MHz, CDCl₃):



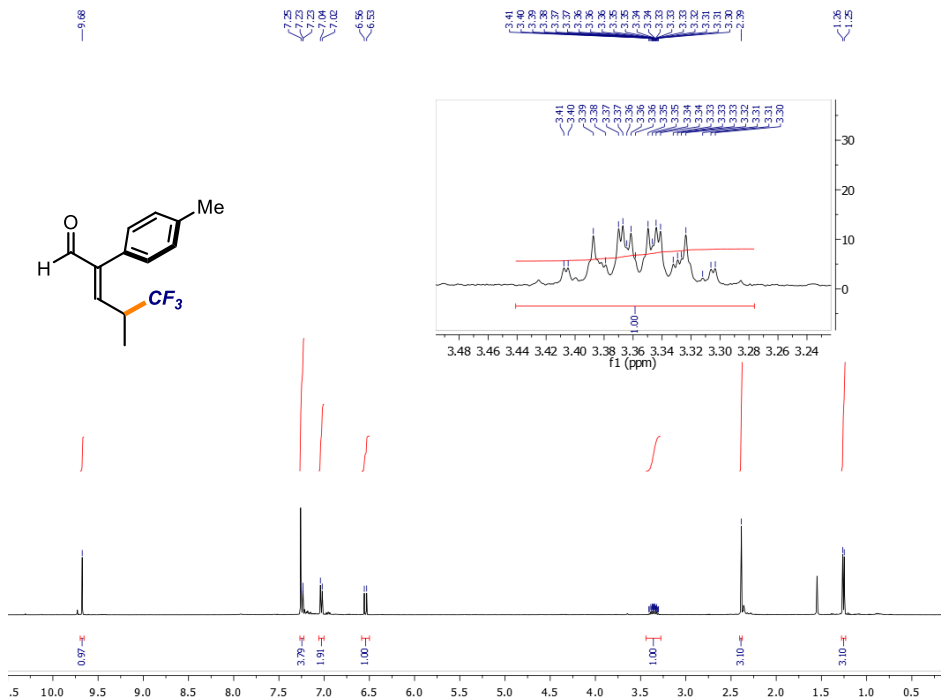
¹³C NMR (126 MHz, CDCl₃)



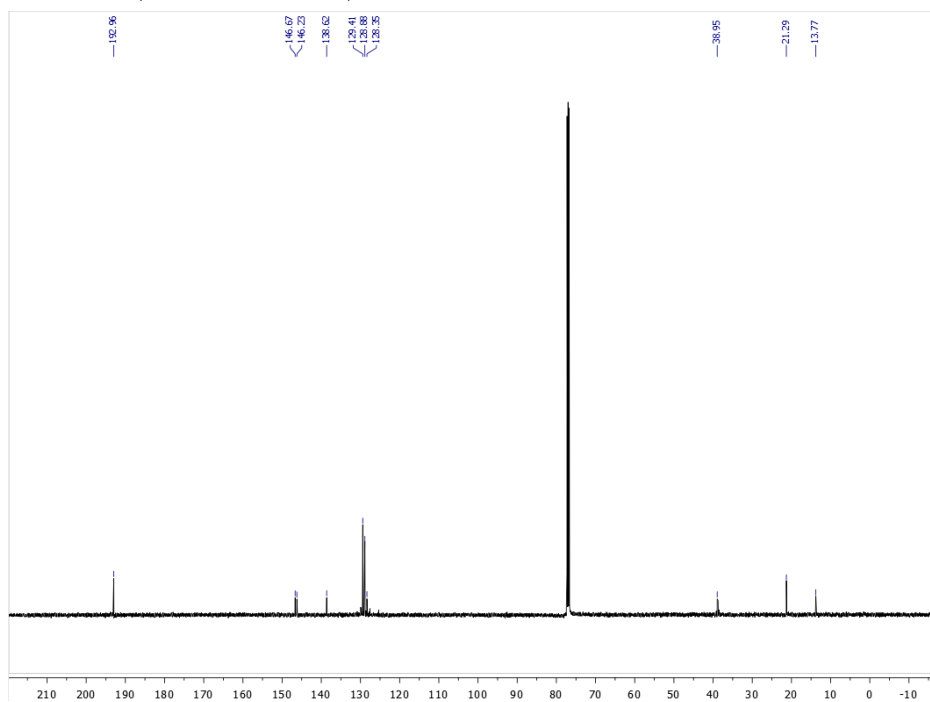
^{19}F NMR (471 MHz, CDCl_3)

(*S,E*)-4-(trifluoromethyl)-2-(4-methylphenyl)pent-2-enal

^1H NMR (500 MHz, CDCl_3):

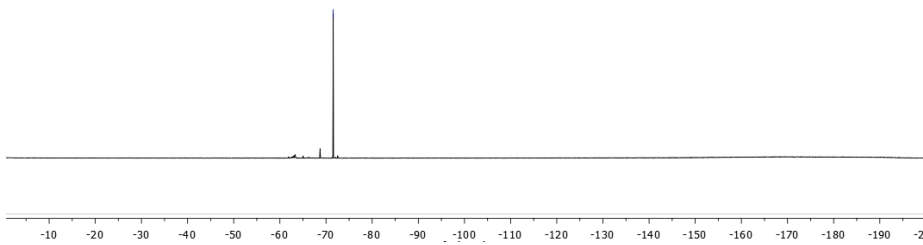


^{13}C NMR (126 MHz, CDCl_3):



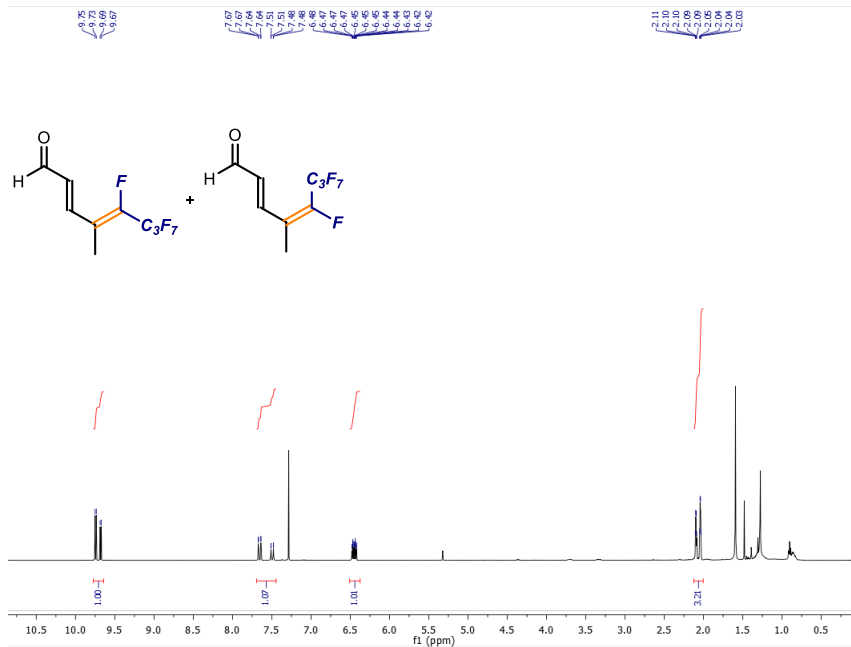
^{19}F NMR (471 MHz, CDCl_3)

88
77
75

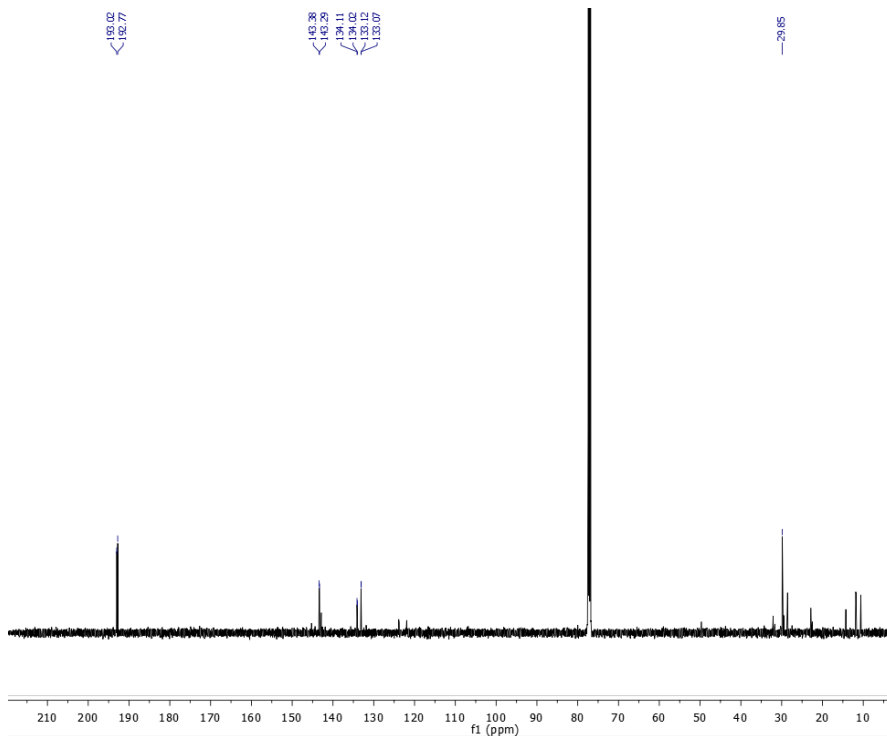


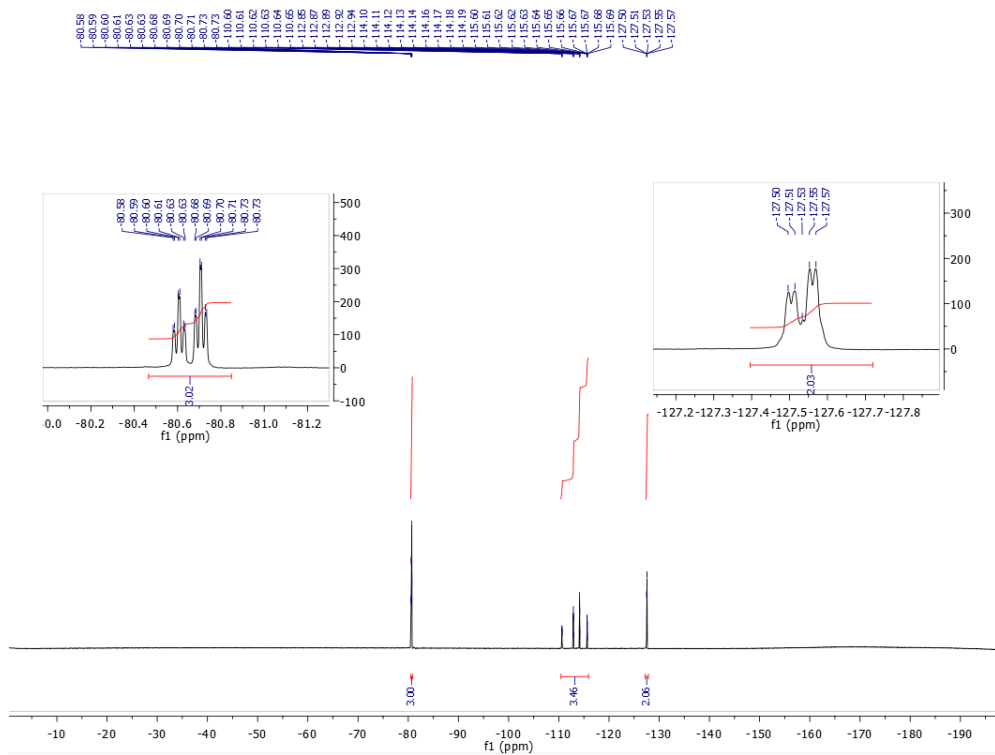
(2E)-octafluoro-4-methylocta-2,4-dienal

^1H NMR (500 MHz, CDCl_3):



^{13}C NMR (126 MHz, CDCl_3)

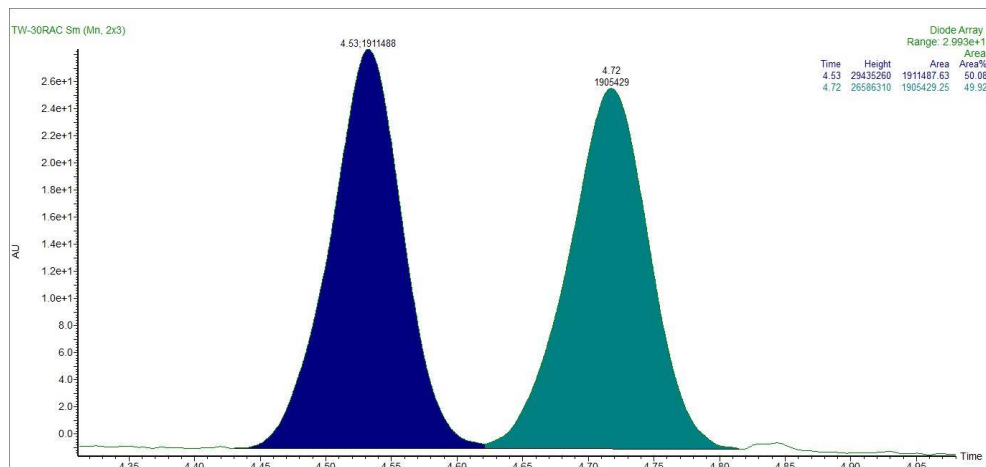


^{19}F NMR (471 MHz, CDCl_3)

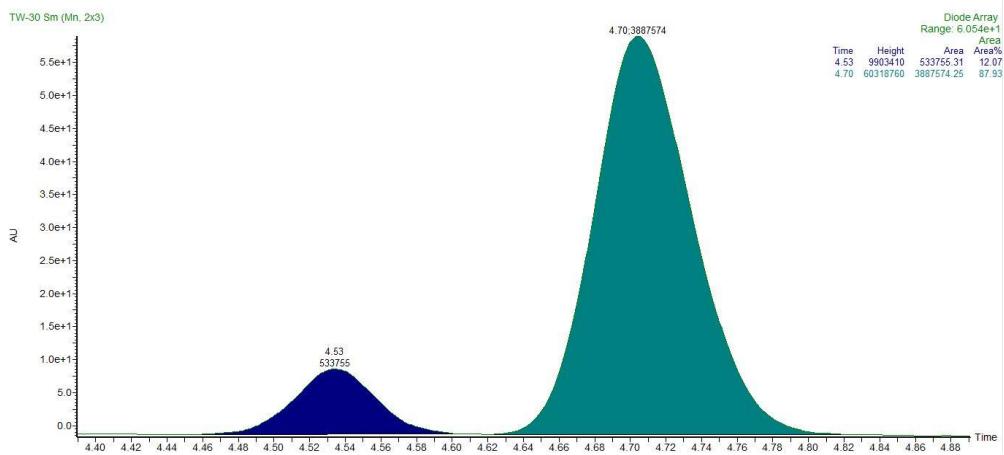
4.7.10 UPC² Traces

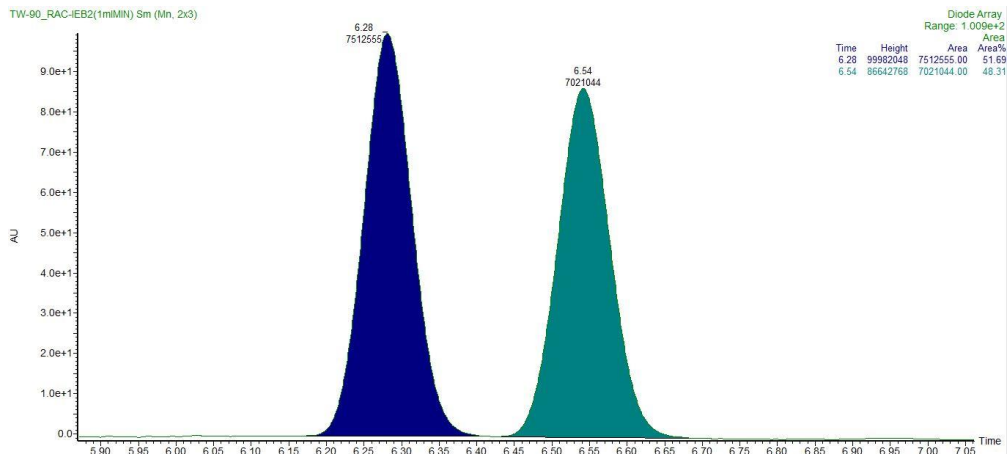
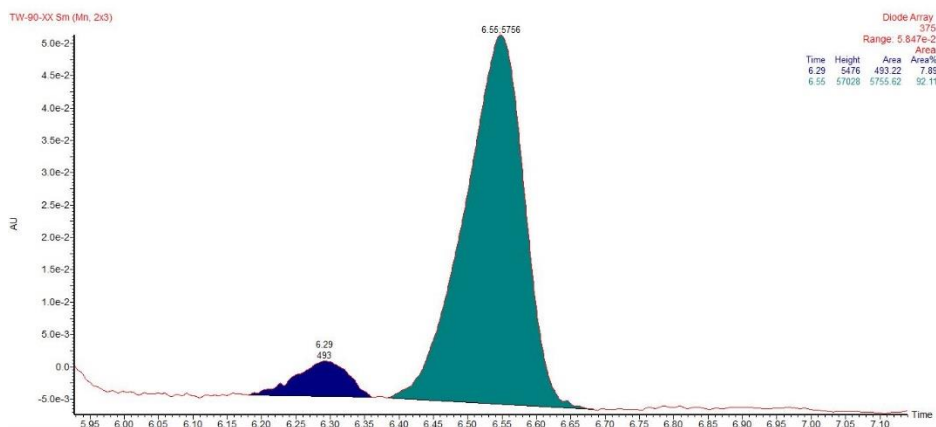
(*S,E*)-4-(perfluoroisopropyl)-2-phenylpent-2-enal (30a)

Racemic



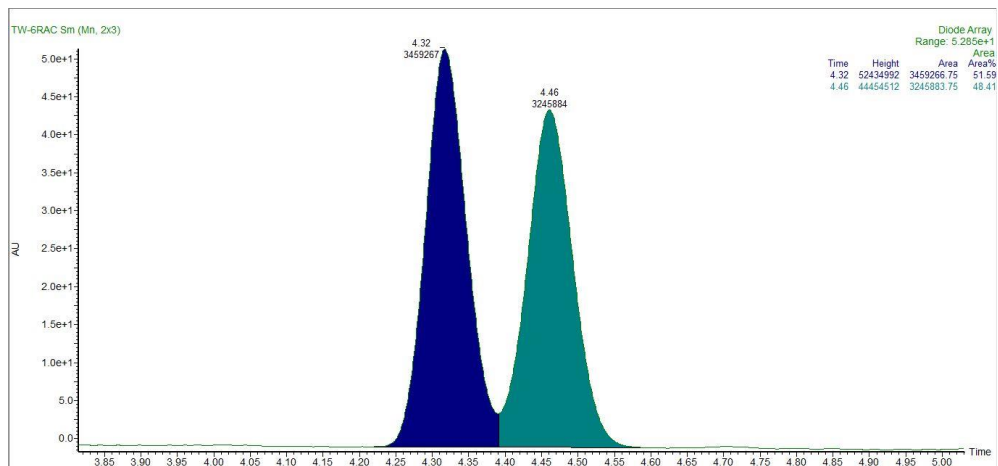
Enantioenriched



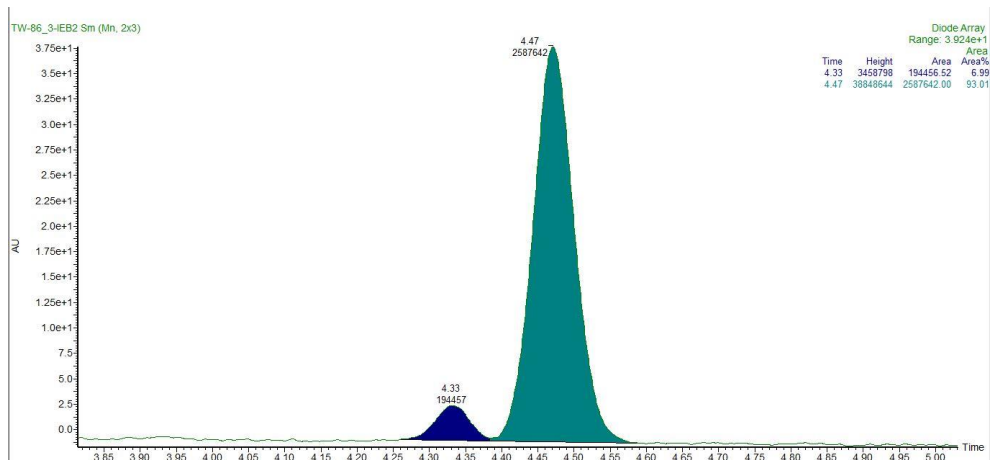
(*S,E*)-4-(perfluoropropyl)-2-phenylpent-2-enal (30b)**Racemic****Enantioenriched**

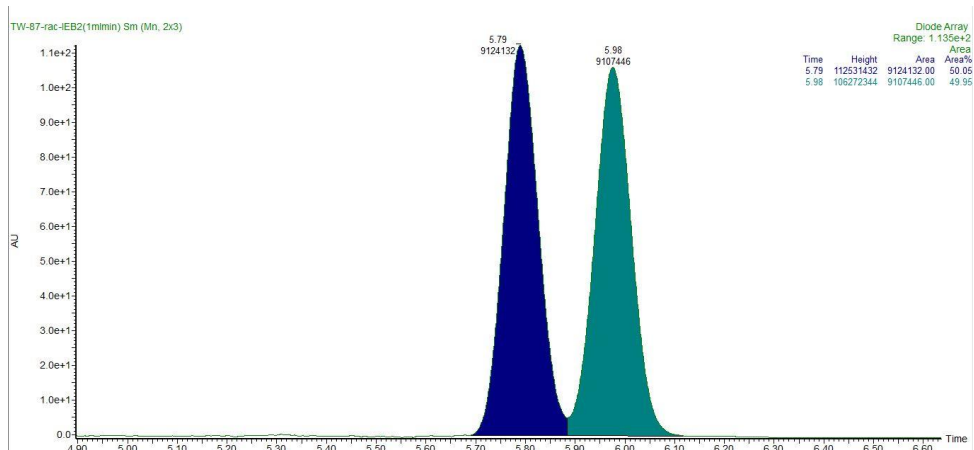
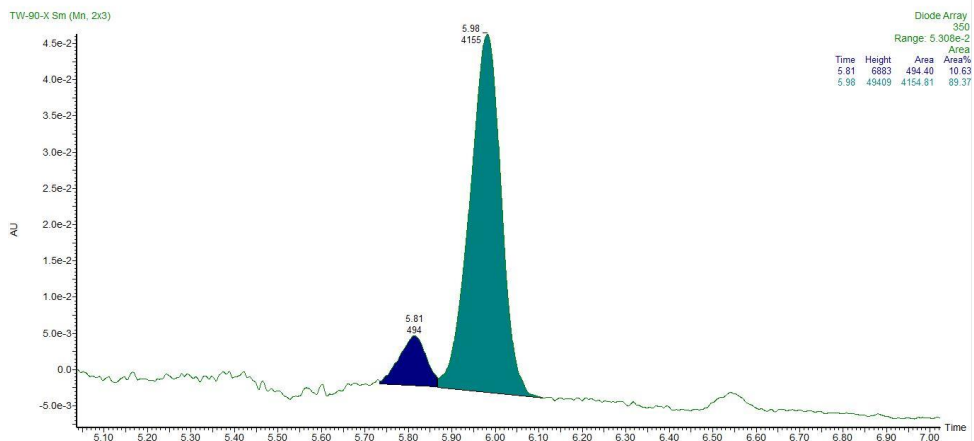
(*S,E*)-4-(perfluorobutyl)-2-phenylpent-2-enal (30)

Racemic



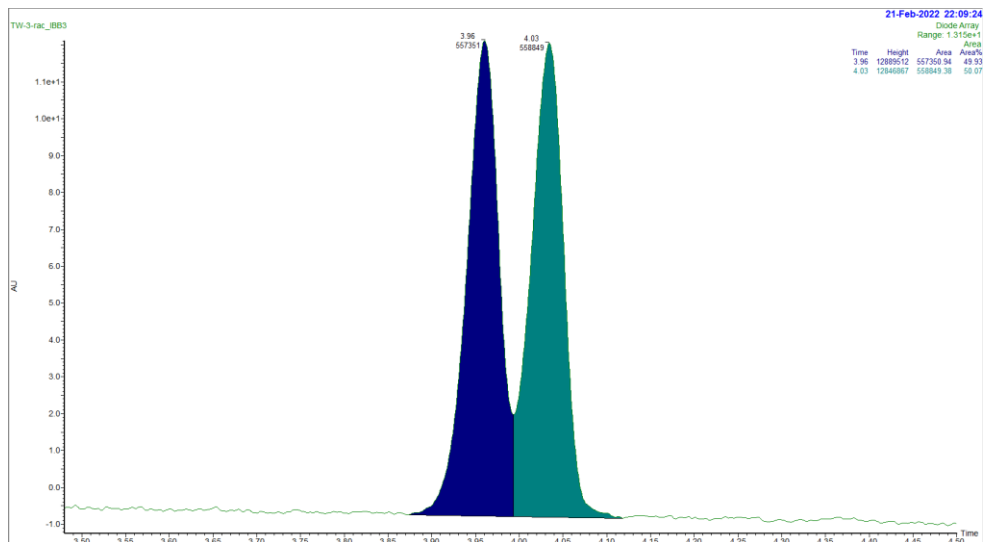
Enantioenriched



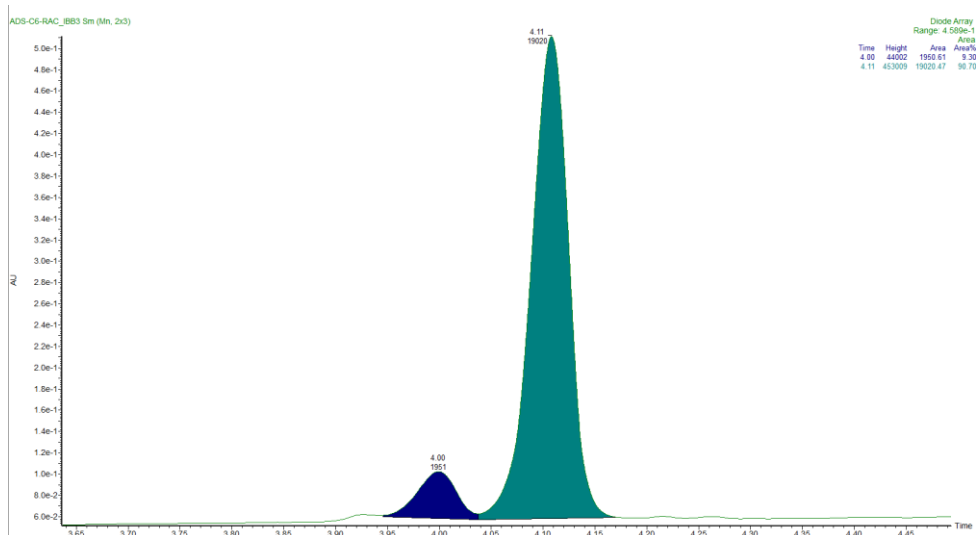
(S,E)-4-(perfluoropentyl)-2-phenylpent-2-enal (30c)**Racemic****Enantioenriched**

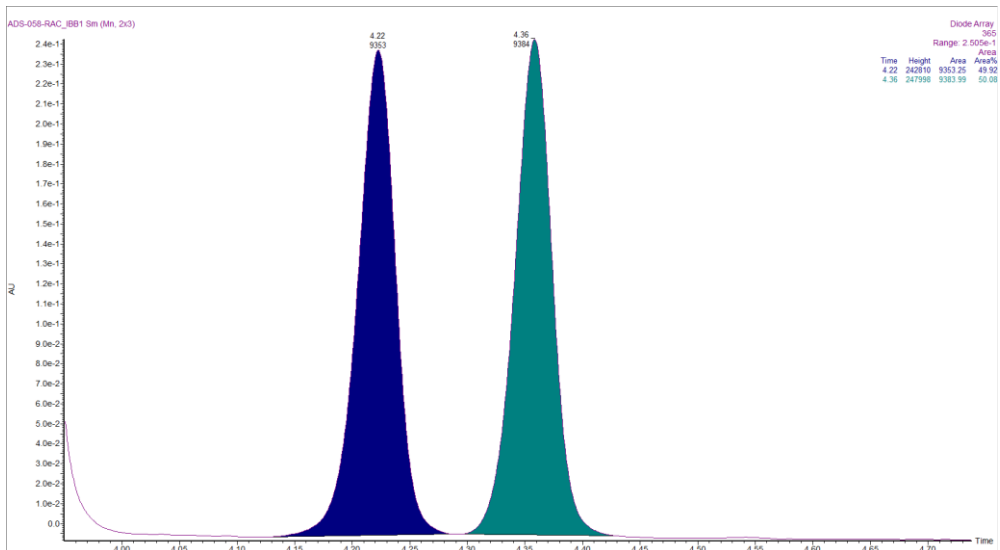
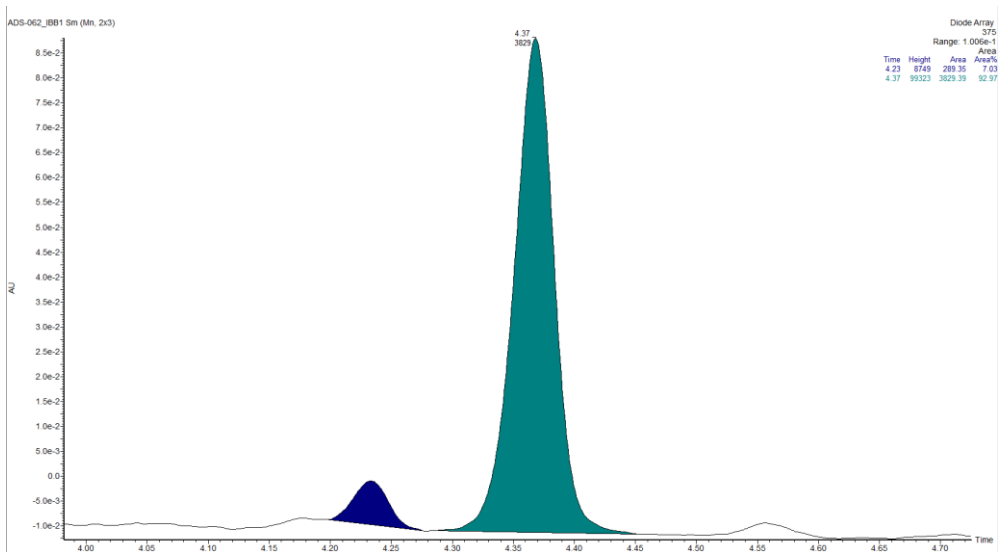
(*S,E*)-4-(perfluorohexyl)-2-phenylpent-2-enal (30d)

Racemic



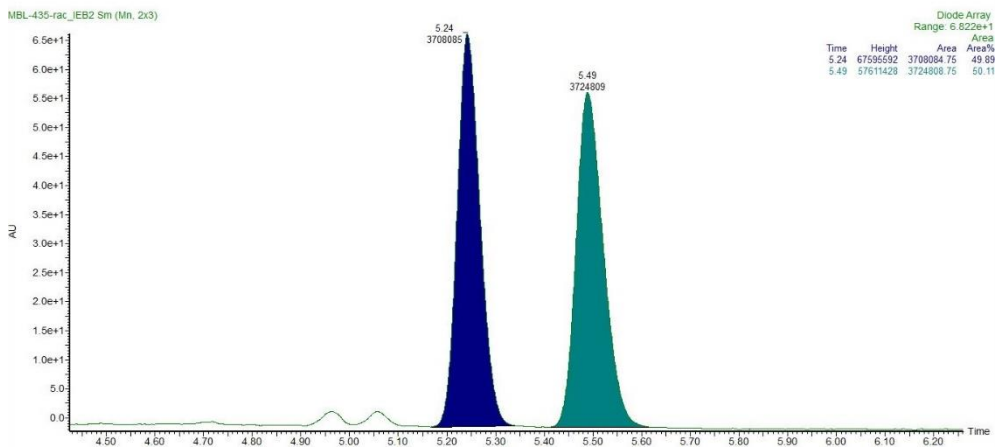
Enantioenriched



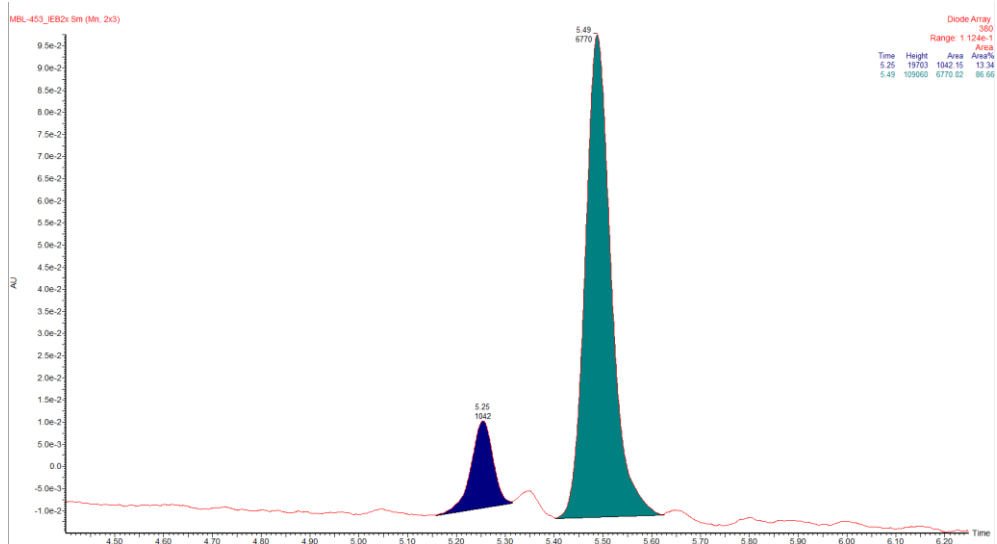
(*S,E*)-4-(perfluorooctyl)-2-phenylpent-2-enal (30e)**Racemic****Enantioeriched**

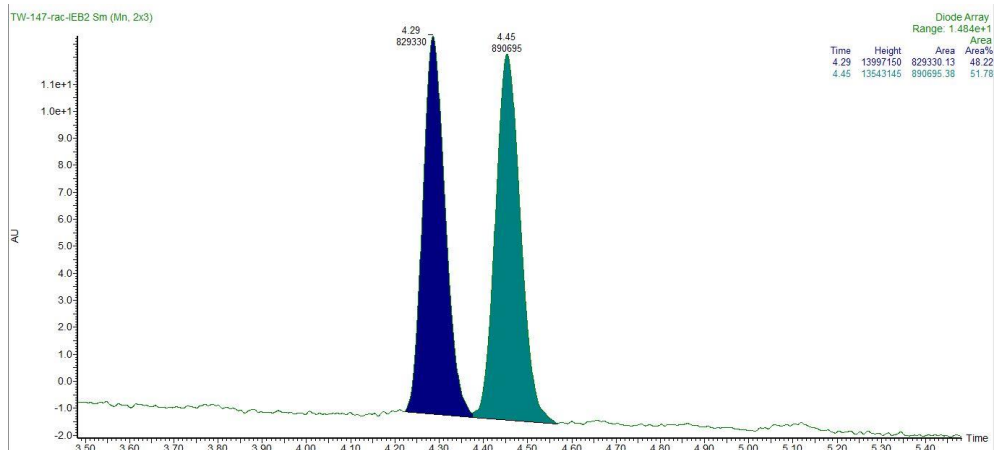
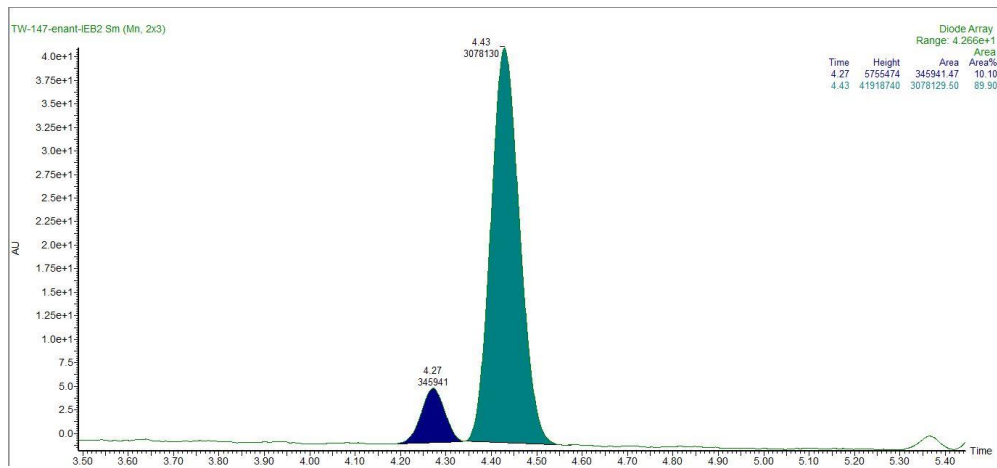
(*S,E*)-4-(trifluoromethyl)-2-phenylpent-2-enal (30g)

Racemic



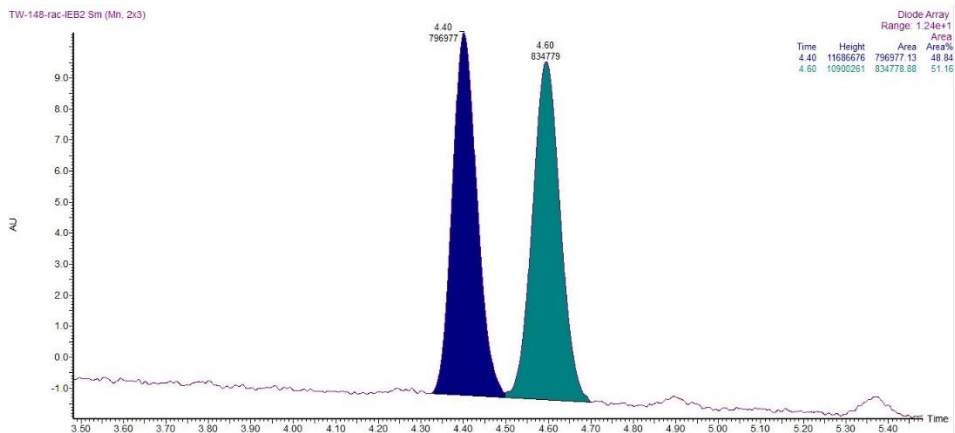
Enantioenriched



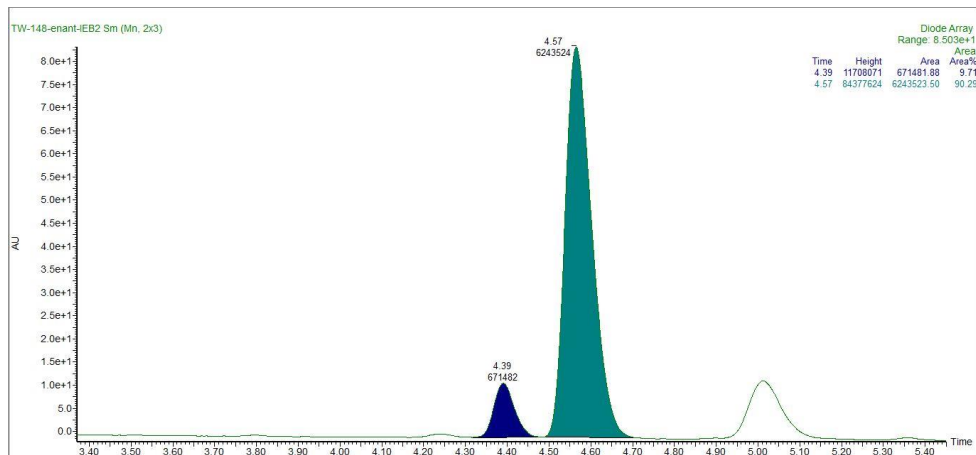
(*S,E*)-4-(perfluorobutyl)-2-(3-methylphenyl)pent-2-enal (30o)**Racemic****Enantioenriched**

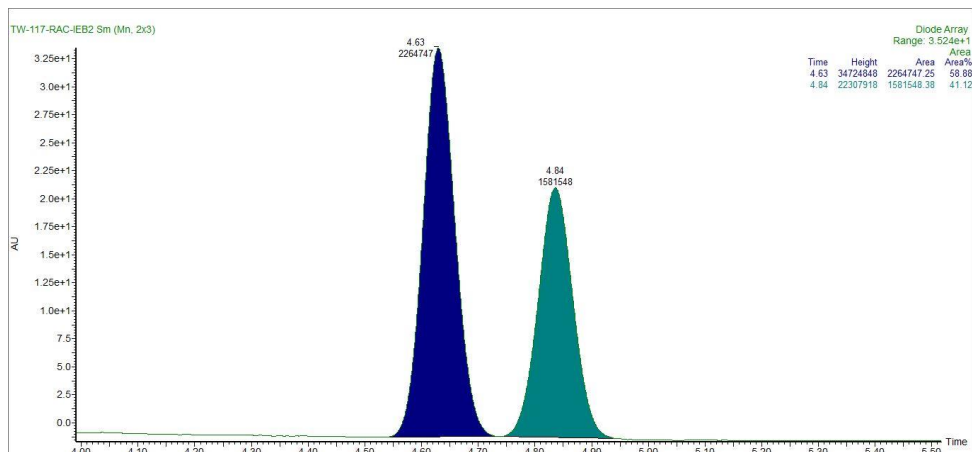
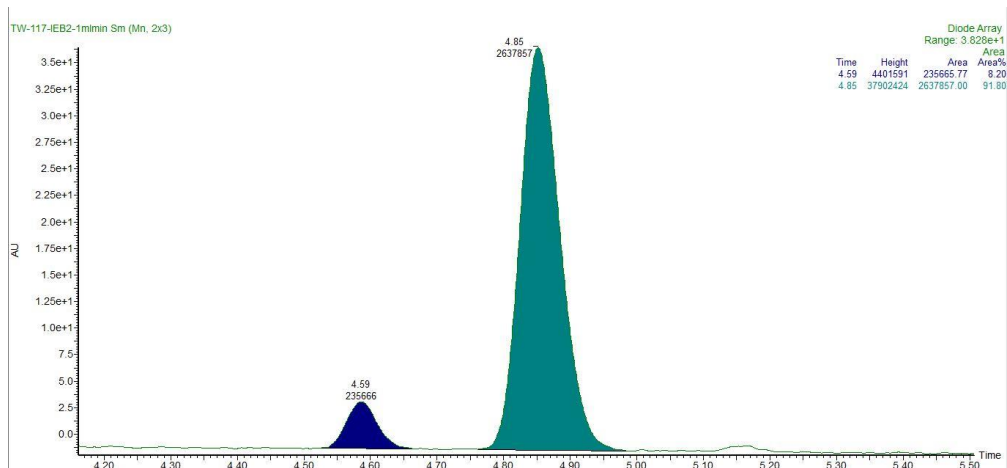
(*S,E*)-4-(perfluorobutyl)-2-(4-methylphenyl)pent-2-enal (30n)

Racemic



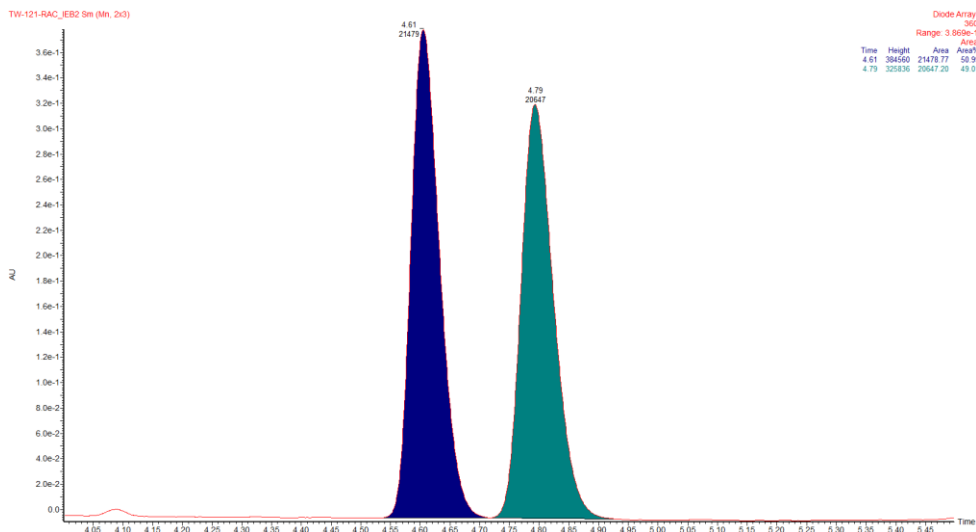
Enantioenriched



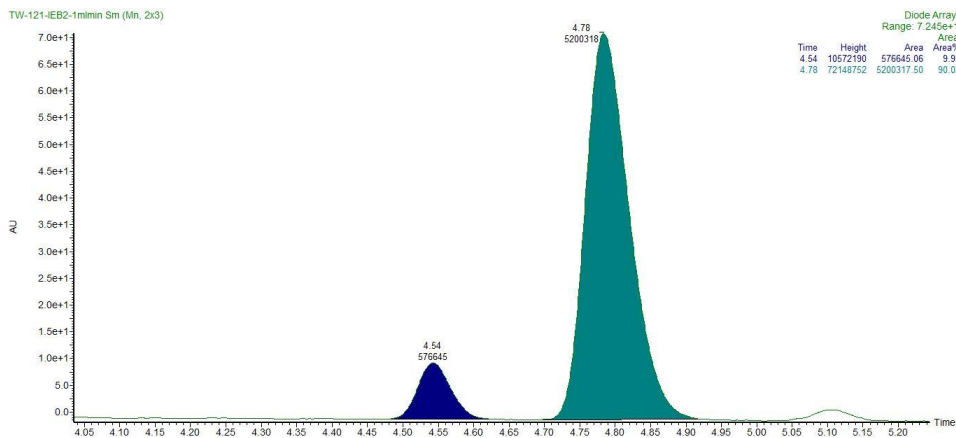
(*S,E*)-4-(perfluorobutyl)-2-(4-chlorophenyl)pent-2-enal (30p)**Racemic****Enantioenriched**

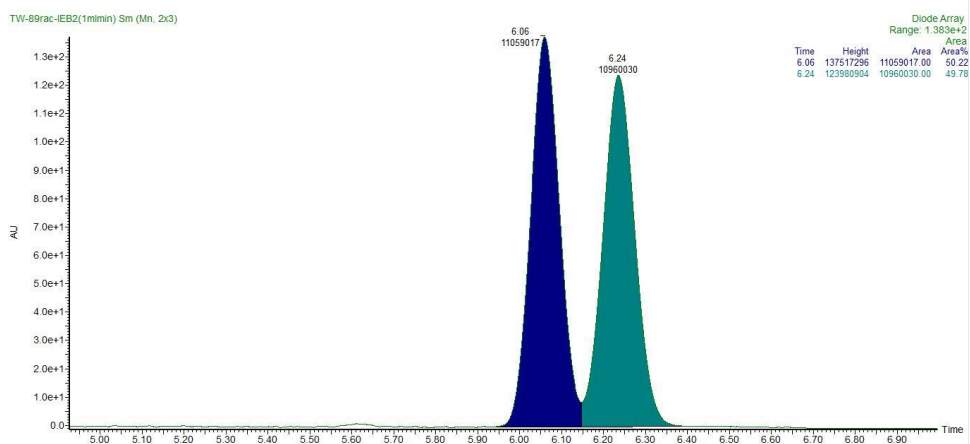
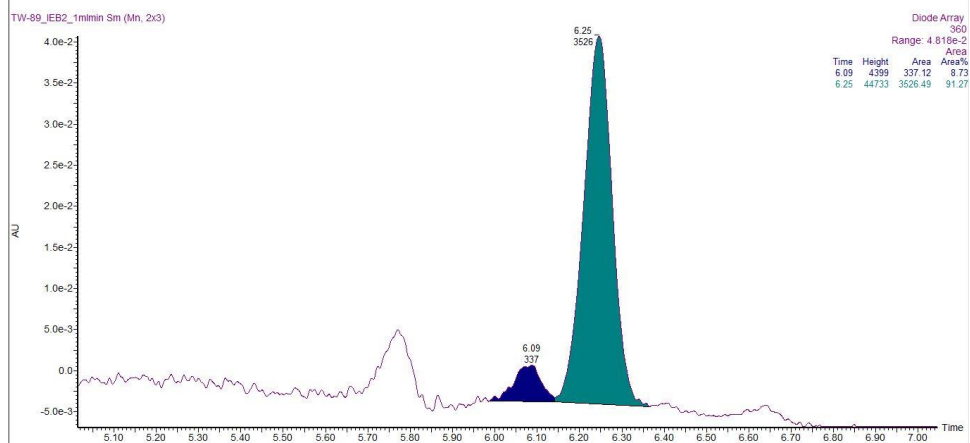
(S,E)-4-(perfluorobutyl)-2-(4-methoxyphenyl)pent-2-enal (30q)

Racemic



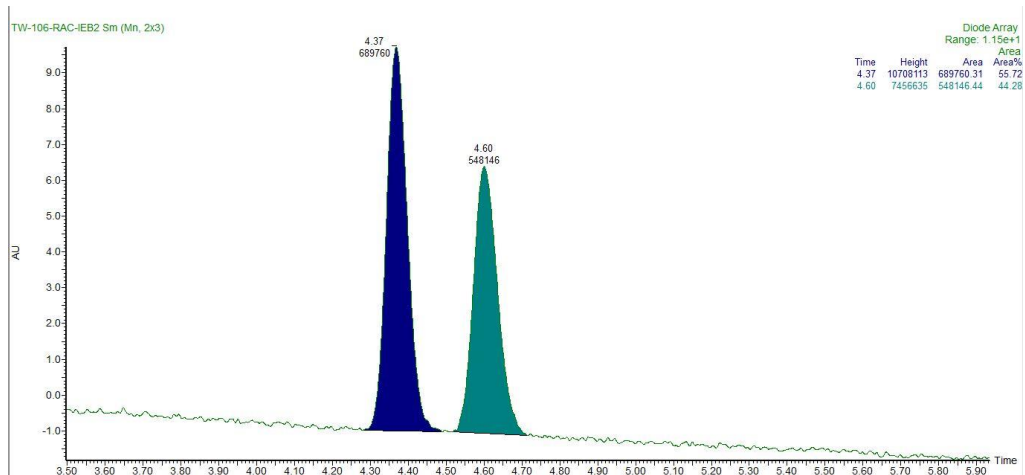
Enantioenriched



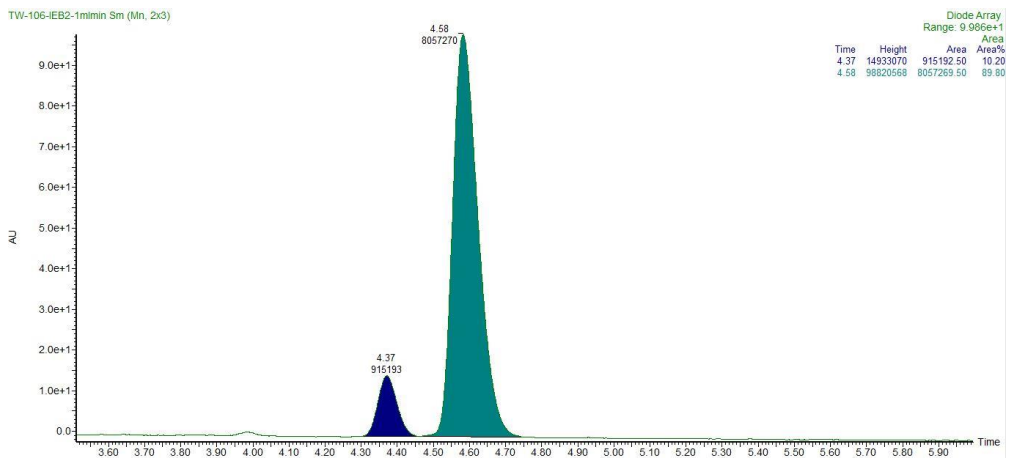
(*S,E*)-4-(perfluorobutyl)-2-phenylhex-2-enal (30i)**Racemic****Enantioenriched**

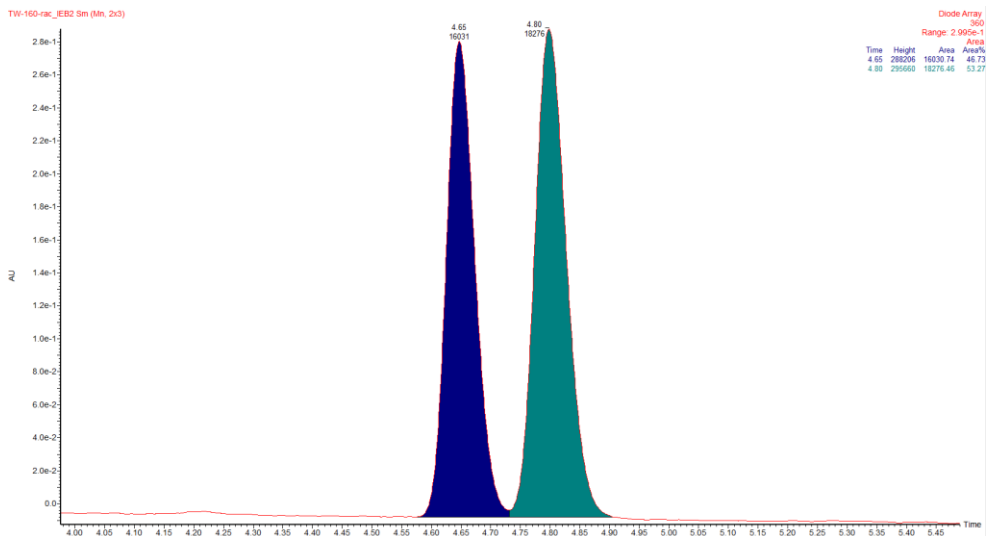
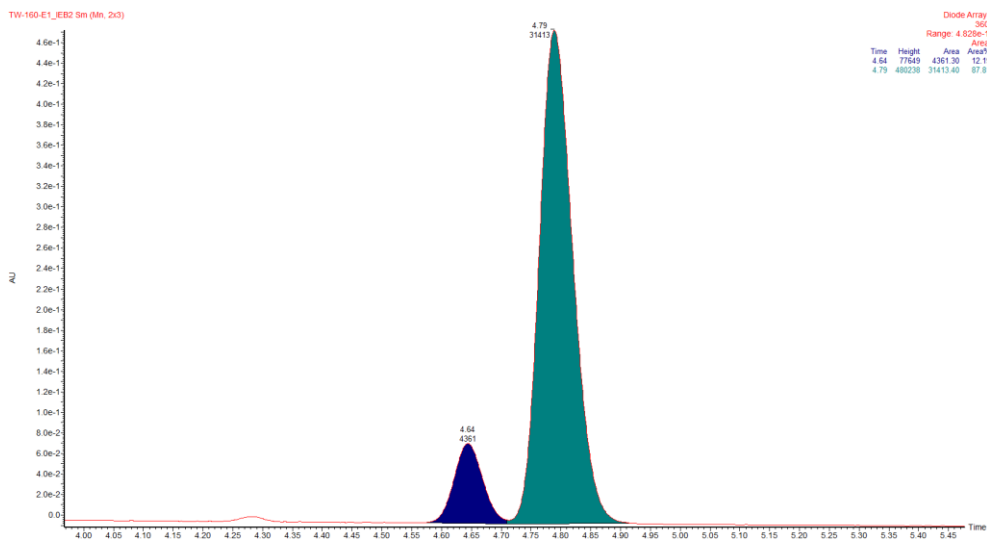
(*S,E*)-4-(perfluorobutyl)-2-phenylhex-2-enal (30j)

Racemic



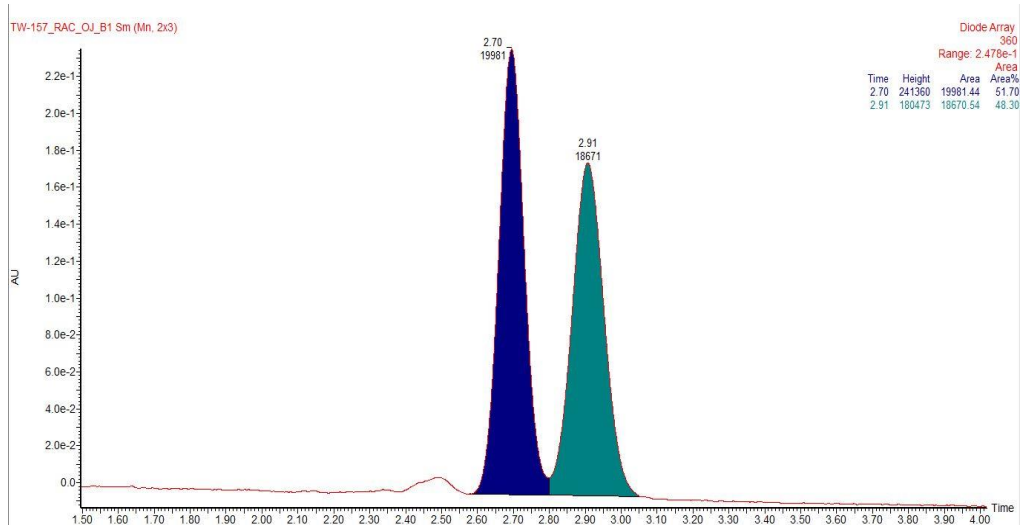
Enantioenriched



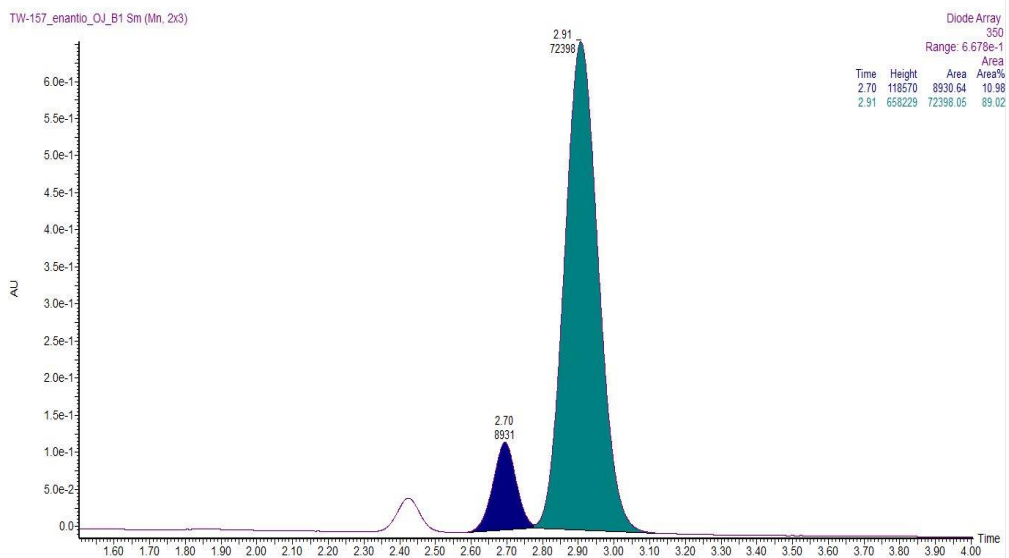
(*S,E*)-7-chloro-4-(perfluorobutyl)-2-phenylhept-2-enal (30m)**Racemic****Enantioenriched**

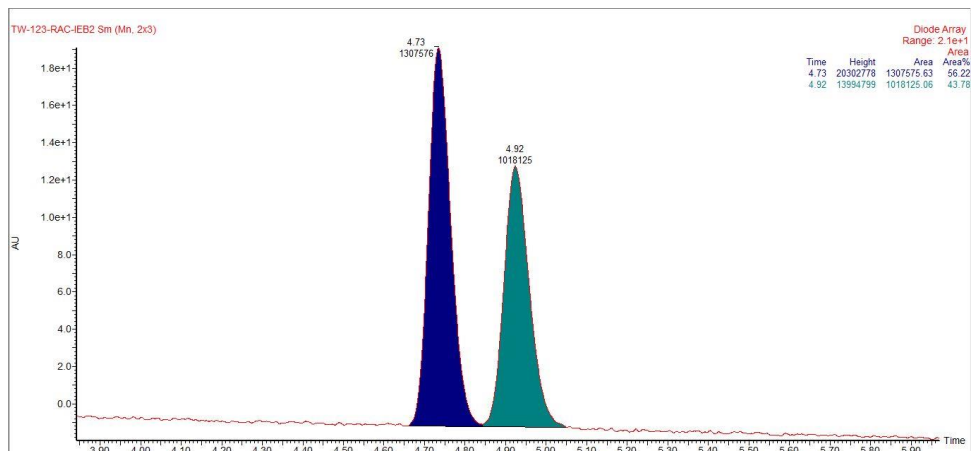
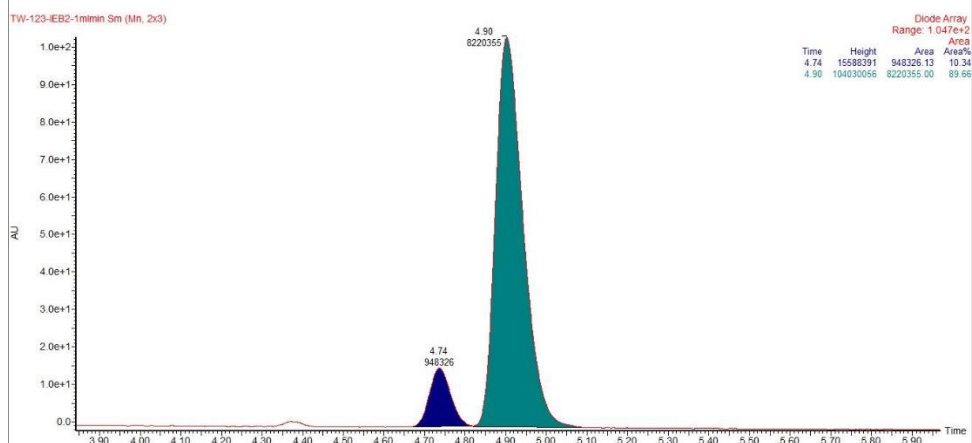
(*S,E*)-4-phenyl-4-(perfluorobutyl)-2-phenylbut-2-enal (30k)

Racemic



Enantioenriched



(*S,E*)-5-phenyl-4-(perfluorobutyl)-2-phenylpent-2-enal (30l)**Racemic****Enantioenriched**

Chapter V

General Conclusions

During my doctoral studies, I focused on the development of new radical organocatalytic reactions promoted by visible light. By exploiting the excitation of organocatalytic intermediates, I have shown how it is possible to generate radical intermediates under mild conditions while unlocking new reactivity. The development of a new class of dithiocarbamate catalysts (DTC) led to the development of a catalytic platform which generates acyl and crabmoyl radicals through acyl nucleophilic substitution. The corresponding C(sp²) radicals, could be trapped by electron-poor olefins in a Giese-type addition to provide a wide array of building blocks and functionalized complex scaffolds. Mechanistic studies, by means of transient absorption spectroscopy, electron paramagnetic resonance (EPR), cyclic voltammetry, and quantum yield determination, allowed us to elucidate the main steps of the catalytic cycle and of relevant off-cycle equilibria.

In this thesis I also showed how the excitation of organocatalytic intermediates can serve as a strategy to promote the asymmetric C-C bond forming event. Thanks to the knowledge gathered on the DTC photochemical activation strategy, we were able to couple this photochemical activation with asymmetric aminocatalysis to develop a regio- and enantioselective remote functionalization of enals. Due to the mild conditions under which both catalysts work, we could achieve the regioselective formation of γ -alkylated products starting from simple alkyl chlorides and triflates. The following step was to remove the DTC catalyst from the system and try to generate radicals exploiting dienamines as donor partners for EDA complex formation with perfluoroalkyl iodides. Visible-light excitation of such complexes have shown promising potentials in organic synthesis. The perfluoroalkyl radicals generated in this way could be intercepted by the chiral dienamines with high levels of regio- and enantio-selectivity. Overall, the transformations provided in this thesis highlighted how organic intermediates can participate in the formation of open-shell species, and how visible-light mediated radical process might spur the development of novel processes in asymmetric catalysis.

UNIVERSITAT ROVIRA I VIRGILI
EXCITATION OF ORGANOCATALYTIC INTERMEDIATES AND APPLICATION IN NEW RADICAL PROCESSES
Matteo Balletti



UNIVERSITAT
ROVIRA i VIRGILI